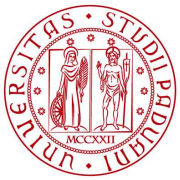

UNIVERSITÀ
DEGLI STUDI
DI PADOVA

Sede Amministrativa: Università degli Studi di Padova

Dipartimento di Biologia

CORSO DI DOTTORATO DI RICERCA IN: Bioscienze
CURRICOLO: Biochimica e Biotecnologie
CICLO: XXXVI

DECIPHERING THE ROLE OF RESPIRATION IN BIOENERGETICS AND METABOLISM OF PLANTS USING THE MODEL *PHYSCOMITRIUM PATENS*

Coordinatore: Ch.ma Prof.ssa Chiara Romualdi
Supervisore: Ch.mo Prof. Tomas Morosinotto

Dottorando : Antoni Mateu Vera Vives

A mun pare i mumare,
que tot ho fan possible.

TABLE OF CONTENTS

SUMMARY

This thesis delves into the intricate relationship between mitochondrial respiration and plant metabolism, unraveling the pivotal role played by respiration in orchestrating metabolic processes. Over four chapters, it traces the historical progression of research in this field, from the early investigation of cytoplasmic male sterility to the contemporary utilization of genetic manipulation techniques in various plant models. These models have been instrumental in studying the physiological consequences of altering respiratory efficiency, paving the way for a deeper understanding of the interconnectedness of respiration and metabolism.

CHAPTER I, the introductory chapter, describes the main components of the respiratory machinery in plants, provides a historical perspective on plant mitochondrial respiration research and sets the stage for understanding the subsequent chapters' experimental findings. It highlights the evolution of experimental techniques and models used to investigate respiratory complexes' roles in metabolic regulation.

CHAPTER II presents a newly isolated respiratory mutant in *P. patens*, *cox11*, which is completely depleted in Complex IV activity. This mutant was characterized by a different set of experiments, including transcriptomics and metabolomics, that show the metabolic consequences of the depletion of Complex IV in a plant model. The mutants displayed altered growth patterns and strong metabolic disruptions, shedding light on the critical role of respiration in energy mobilization and metabolic homeostasis.

CHAPTER III explores the metabolic repercussions of Complex I depletion in the *ndufa5* mutant. It uncovers metabolic alterations that are however different from those described for the Complex IV mutant *cox11*. In this chapter we also study, by exploiting transcrtipomics data, the candidate signaling pathways involved in mitochondrial retrogrdade signaling in *P. patens*. We propose that the induction of one or more mitochondrial retrograde signaling pathways is at the root of the unique phenotypic characteristics of Complex I-deficient *ndufa5* plants.

CHAPTER IV investigates subcellular ATP dynamics in response to light in the moss *Physcomitrium patens*. It underscores the interplay between photosynthesis and mitochondrial respiration in energy provision, even in fully photoautotrophic organisms. We present reporter lines that express a genetically-encoded ATP sensor, both in WT or in Complex I-deficiency backgrounds. This chapter, which is the result of a collaboration with the group of Prof. Markus Scwarzländer, illuminates the dynamic nature of ATP synthesis and highlights the central role of respiration in maintaining metabolic stability.

Besides the four main chapters, we also included a series of appendices that are either manuscripts ready for submission or articles that have already been published in peer-reviewed journals.

Appendices I and II show different experiments using *P. patens* as a model. APPENDIX I explores the roles of photosynthetic alternative electron transport mechanisms, such as cyclic electron transport (CET) and pseudo-cyclic electron transport (PCET), in modulating photosynthetic electron transport in response to varying light intensities. It demonstrates how these mechanisms effectively adjust electron transport to prevent over-reduction of carriers, safeguarding plant cells from light-induced damage. APPENDIX II shows previous work done to characterize the mutant *ndufa5*, which is the main line used in chapters III and IV.

Appendices III, IV and V instead have microalgae as a model organism, and validate the use of a novel, high-resolution system for quantifying the rate of oxygen consumption and evolution of microalgae. Appendices III and IV investigate how photosynthesis in microalgae, in particular in the species *Nannochloropsis gaditana*, responds to the complex light environments of photobioreactors, crucial for sustainable biomass production. We optimized this system to assess photosynthetic functionality in fluctuating light conditions, offering insights into optimizing microalgae cultures for biomass production. APPENDIX V shows the characterization of a particular species of red alga, *Dixoniella giordanoi*, which includes the monitoring of photosynthesis-irradiance curves.

In conclusion, this thesis constitutes a comprehensive investigation into the intricate interplay of mitochondrial respiration and photosynthesis in plant metabolism. By

integrating historical context, experimental discoveries, and metabolic insights, it enhances our understanding of how plants adapt to dynamic environmental conditions and optimize their energy utilization.

CHAPTER I

The impact of defective mitochondrial respiratory complexes in plants

Authorship statement

This introductory chapter consists in a literature review. Original conception, research of literature, outline of ideas and writing process has been conducted by me, with critical inputs during the revision process from my supervisor prof. Tomas Morosinotto.

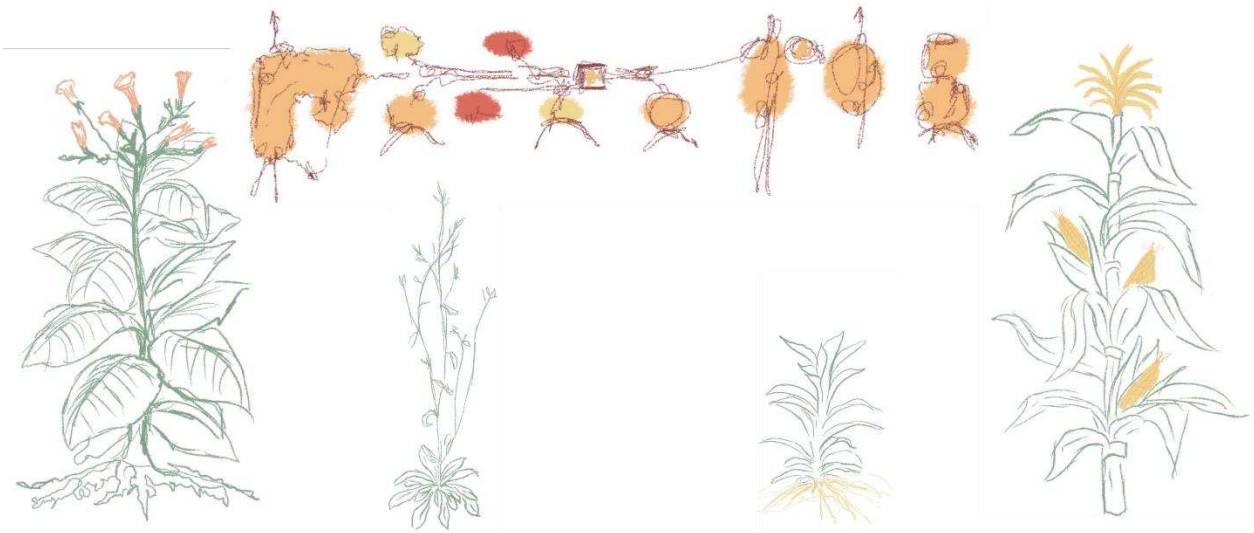

Abstract

This thesis aims to enhance the current comprehension of the pivotal role played by mitochondrial respiration in orchestrating and regulating plant metabolism. The historical progression of research in this area traces its origins to the 1950s when naturally occurring plants afflicted with cytoplasmic male sterility served as the initial model systems for understanding mitochondrial function. Subsequent advancements in DNA screening and editing techniques enabled the generation of several plant lines with altered mitochondrial function using both forward and reverse genetics methodologies. Presently, a multitude of plant models spanning various species exhibit modifications in one of the five principal respiratory complexes, which have been used to investigate the metabolic consequences of alterations in the respiratory efficiency. Although a large body of experimental observations is available, the heterogeneity of experiments and the variety of models used makes it complex to withdraw general conclusions from all these observations. This introductory chapter offers a comprehensive overview of the existing literature regarding the physiological consequences of alterations in the respiration efficiency across various plant species.

1. Respiration in plants

1.1. Molecular basis of respiration

1.1.1. Definition of respiration

Respiration is a set of biochemical processes that enables cells to convert reducing power from organic compounds and molecular oxygen into free, usable energy in the form of adenosine triphosphate (ATP). Respiration in eukaryotes is composed by several steps taking place in the cytosol and mitochondria. We can conceptually divide the whole process into simpler reactions. First, a molecule of glucose is cleaved onto two molecules of pyruvate. Each of these molecules is converted to acetyl-CoA, releasing a CO_2 molecule. Acetyl-CoA enters then the tricarboxylic acid (TCA) cycle, that generates reductant power exploited by the mitochondrial electron transport chain (mETC), or respiratory chain, to sustain a proton gradient across the inner mitochondrial membrane. This proton gradient powers the ATP synthase, which synthesizes ATP via oxidative phosphorylation. In this section we will describe the molecular basis of these processes, paying special attention to the most relevant component for this thesis: the respiratory chain.

1.1.2. Extraction of reducing equivalents: from glucose to NADH

1.1.2.1. The Embden-Meyerhof-Parnas pathway

The first step of respiration takes place in the cytosol, and it is the glycolysis or Embden-Meyerhof-Parnas (EMP) pathway (Kresge et al., 2005), by which one molecule of glucose (six carbon atoms) yields two molecules of pyruvic acid (three carbon atoms) in a process that generates a net gain of 2 NADH and 2 ATP molecules per glucose molecule (Figure 1.1). The free energy released in this ten-step process is used to synthesize ATP and NADH.

Most monosaccharides, like fructose or galactose, can be converted to one of the intermediates of the EMP pathway, thus fuelling it. Unlike animal mitochondria, where both fatty acids and glycolytically derived pyruvate are important respiratory substrates, plant mitochondria rarely respire fatty acids (Plaxton, 1996). Consequently, the EMP

pathway becomes pivotal in plants as it is the main pathway that sustains plant respiration. The EMP pathway also holds a pivotal role in central metabolism as some of its intermediates also substrates of other catabolic and anabolic reactions.

The EMP pathway is oxygen-independent and in fact it is common in both anaerobic and aerobic organisms; indeed, it is almost universal in all living organisms (Kierans & Taylor, 2021). Instead, an important divergence point is defined by the fate of the pyruvic acid generated by the EMP pathway. On one side, anaerobic organisms use the pyruvic acid as a substrate for fermentation reactions that serves mainly to restore the pool of the cofactor NAD^+ so glycolysis can continue. On the other side, aerobic organisms use molecular oxygen to completely oxidize the pyruvic acid to CO_2, strongly increasing the energetic yield per glucose. Thanks to these metabolic pathways, aerobic organisms can produce up to 32 ATP molecules per glucose (Flurkey, 2010).

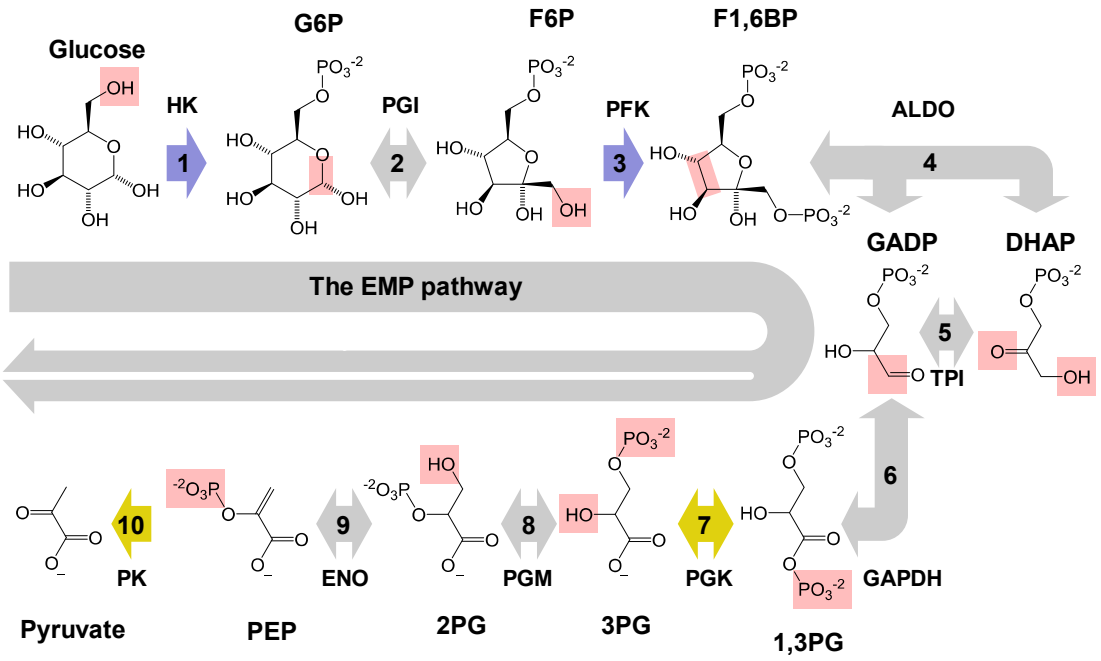

Figure 1.1 | The Embden-Meyerhof-Parnas (EMP) pathway, its intermediates and the enzymes involved. Reversible reactions are represented with a double-headed arrow. Each chemical modification is highlighted in pink. Steps 1 and 3 (purple) consume ATP, and steps 7 and 10 (yellow) produce ATP. Since steps 6-10 occur twice per glucose molecule, there is a net production of ATP. Intermediates abbreviations: G6P, glucose 6-phosphate; F6P, fructose 6-phosphate; F1,6BP, fructose 1,6-bisphosphate; GADP, glyceraldehyde 3-phosphate; DHAP, dihydroxyacetone phosphate; 1,3PG, 1,3-bisphosphoglyceric acid; 3PG, 3-phosphoglyceric acid; 2PG, 2-phosphoglyceric acid; PEP, phosphoenolpyruvate. Enzymes abbreviations: HK, hexokinase; PGI, phosphoglucose isomerase; PFK, phosphofructokinase; ALDO, aldolase; TPI, triose-phosphate isomerase; GAPDH, glyceraldehyde-3-phosphate dehydrogenase; PGK, phosphoglycerate kinase; PGM, phosphoglycerate mutase; ENO, enolase; PK, pyruvate kinase. Adapted from Thomas Shafee (CC BY 4.0, Wikimedia Commons).

In aerobic respiration, pyruvic acid is the substrate of a single step reaction that generates the two-carbon molecule acetyl-coenzyme A (acetyl-CoA) and yields the first CO_2 molecule of the process. Different catabolic reactions, and not only the EMP pathway, produce acetyl-CoA, like the β–oxidation of fatty acids (Jallet et al., 2020) or the degradation of ketogenic amino acids (Hildebrandt et al., 2015). In plants, acetyl-CoA is produced mainly through the EMP pathway or as a product of the mitochondrial NAD-malic enzyme (Plaxton, 1996; Tronconi et al., 2008).

1.1.2.2. The tricarboxylic acid (TCA) cycle

Acetyl-CoA can be the substrate of different reactions. For its use in respiration, acetyl-CoA is the substrate of the enzyme citrate synthase, that catalyses the following reaction:

$$\text{acetyl-CoA} + \text{oxaloacetate} + H_2O \longrightarrow \text{citrate} + \text{CoA-SH}$$

This reaction represents the entry point of acetyl-CoA into the tricarboxylic acid cycle (TCA cycle), or Krebs cycle, which is a common cyclic pathway used by all aerobic organisms in catabolism. In aerobic prokaryotes the TCA cycle takes place in the cytosol, whilst in eukaryotes it is localized in the mitochondrial matrix. After condensation of acetyl-CoA and oxaloacetate, the cycle proceeds through a set of oxidative steps that release two carbon atoms in form of CO_2 and ends with the regeneration of oxaloacetate. One round of the cycle also generates 1 GTP molecule, 3 NADH molecules and a reduced equivalent of ubiquinol. The main steps and players of the TCA cycle are summarised in Figure 1.2.

NADH molecules and ubiquinol equivalents provide the reductant power fuelling the next component of the process, the mitochondrial electron transport chain (mETC). In the classical model, acetyl-CoA from the EMP pathway sustains a cyclic flow through the TCA cycle that produces reductant power used by the mETC. As mentioned above for glycolysis and acetyl-CoA, however, these metabolites can be synthetized or consumed by other cellular pathways. The TCA cycle is known to play other relevant functions in plants: it provides carbon skeletons for anabolic processes of secondary metabolites, isoprenoids, amino acids, nucleic acids or fatty acids (Plaxton, 1996), or it

oxidises organic acids coming from other pathways such as the glyoxylate cycle during lipid mobilization (Wiskich & Dry, 1985; Y. Zhang & Fernie, 2018). These other functions need non-cyclic flux modes and an input of a TCA intermediate to compensate for the loss of carbon from the cycle. In the specific case of plants, different experiments showed that a variety of non-cyclic flux modes occur in specific instances, such as the illuminated leaf, developing oilseeds and tissues under anoxia (Sweetlove et al., 2010). Non-cyclic flux modes might be dominant in some tissues but not others and vary depending on the metabolic state of the cell at a specific moment. Therefore, the TCA cycle in plants must be seen as a dynamic pathway that is modulated according to the cell needs, and the scheme shown in Figure 1.2 is not always representative of its activity.

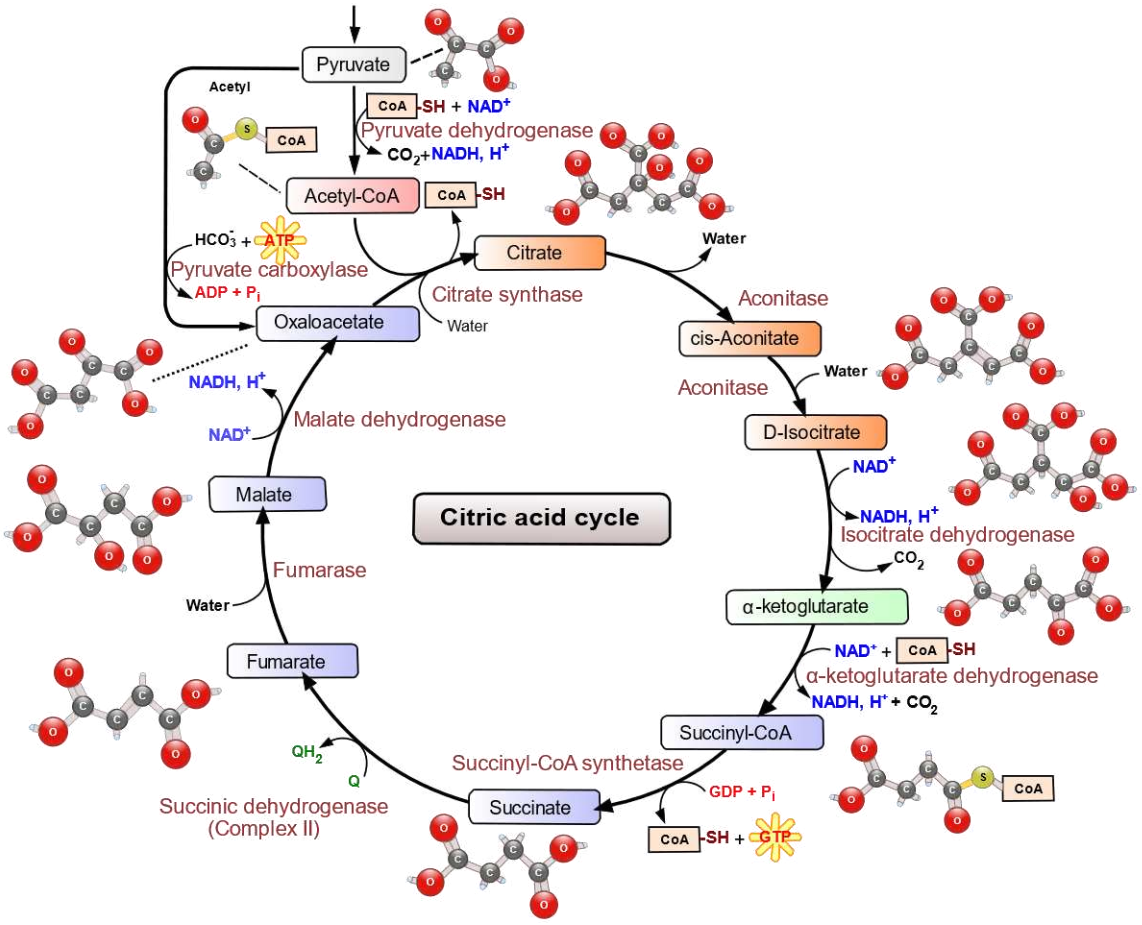

Figure 1.2 | **Overview of the tricarboxylic acid (TCA) cycle**. The colour of the intermediates represents the number of carbon atoms in the molecule: two (red), three (white), four (purple), five (green) or six (orange). CoA stands for Coenzyme A. Q and QH_2 stands for ubiquinone and ubiquinol, respectively. Adapted from Narayanese, WikiUserPedia, YassineMrabet and TotoBaggins (CC BY-SA 3.0, Wikimedia Commons).

1.1.3. The respiratory chain and oxidative phosphorylation

The reductant power extracted by the TCA cycle or other catabolic pathways fuels the next component of the process: the mitochondrial electron transport chain (mETC) or respiratory chain. A flow of electrons is used to sustain a proton gradient across the inner mitochondrial membrane, and this gradient is exploited by the ATP synthase to synthetise ATP through oxidative phosphorylation.

The main structure and function of mETC is conserved among all eukaryotes. However, there are some significant differences between animal and plant cells. In the following subsections we will describe the components of the plant mETCs. The classical view of the mETC describes a lineal electron flow from reductant agents towards the final electron acceptor, O_2, via a set of membrane-bound complexes and mobile carriers. Each component of the mETC has a redox potential more positive than the previous one, and with each transfer electrons lose additional free energy (Alberts et al., 2002). The free energy released by the electron transfer process is used to generate a proton gradient, eventually used for endergonic synthesis of ATP. A detailed depiction of plant mETC and interacting dehydrogenases is shown in Figure 1.3.

1.1.3.1. Electron entry: complexes I, II and alternative dehydrogenases

There are multiple ways for electrons to enter the mETC. The main electron input site is the NADH:ubiquinone oxidoreductase or Complex I, one of the classical oxidoreductase complexes (Wirth et al., 2016). Compared to its homologs from bacteria and other eukaryotes, Complex I in plants is especially large (Braun et al., 2014). It is composed of more than 50 subunits and has a plant-specific extra domain which includes carbonic anhydrase-like proteins (Braun, 2020). Complex I couples the oxidation of NADH from the matrix with the reduction of the Coenzyme Q. This redox reaction is coupled with proton translocation from the matrix towards the intermembrane space. Complex I is strongly inhibited by rotenone (Darrouzet et al., 1998; Palmer et al., 1968), so the pathway of input of electrons that uses the Complex I can be referred to as the rotenone-sensitive pathway.

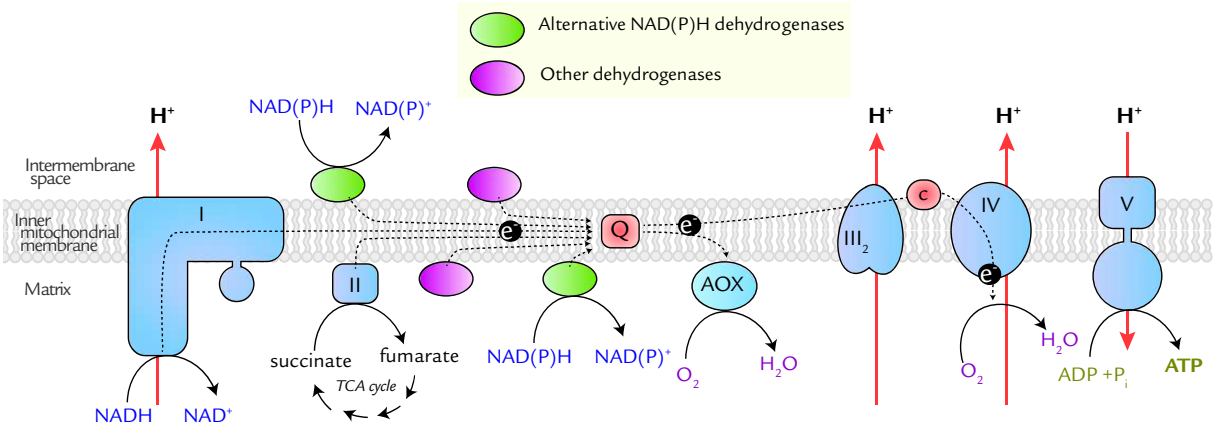

Figure 1.3 | **Mitochondrial dehydrogenases and the respiratory chain**. The NADH produced in the matrix by numerous dehydrogenases is re-oxidised at the inner mitochondrial membrane by the mitochondrial electron transport chain (mETC), either by Complex I, Complex II or alternative NAD(P)H-dehydrogenases. In the intermembrane space, electrons from NAD(P)H generated in the cytoplasm can enter the mETC via alternative NAD(P)H dehydrogenases. Electrons can enter the mETC also through other dehydrogenases that oxidise different carbon compounds at either side of the membrane. A series of redox reactions through the other mETC components are used for generating a proton gradient used for oxidative phosphorylation. Electrons are ultimately exploited for O_2 reduction, either by the Complex IV or the AOX. Adapted from Schertl & Braun, 2014.

There are other electron entry mechanisms that do not depend on Complex I and are therefore called rotenone-insensitive pathways. One of the rotenone-insensitive pathways relies on the smallest of the classical oxidoreductase complexes, the succinate dehydrogenase or Complex II, located at the matricial side of the membrane (Millar et al., 2011) and whose presence in plants was first demonstrated by Price & Thimann, 1951. Complex II catalyses the transfer of electrons from succinate to the Coenzyme Q, through an internal redox system that relies on FAD as a prosthetic group and Fe-S clusters as electron relays (Gnaiger, 2023). It is a particular component of the respiratory chain, as it is also part of the TCA cycle (Hederstedt, 2003; Zhang & Fernie, 2023). The structure, subunits and assembly factors needed for Complex II biogenesis in plants have been recently reviewed by Huang et al., 2019. In Arabidopsis, Complex II is composed by eight different subunits (Figure 1.4). Four of them are conserved through all eukaryotes (SDH1-4), while the other four are plant-specific (SDH5-8). In Arabidopsis, subunits SDH1, SDH2, SDH3 and SDH7 are encoded by more than one gene. Interestingly, Complex II in plants can bind and be directly activated by ATP, independently of the membrane potential. This has been demonstrated for both Arabidopsis and rice, although the activation was much stronger in Arabidopsis (Huang et al., 2010). The activity of Complex

II can be regulated by light (Popov et al., 2010). The abundance ratio of Complexes I and II differs strongly in various organs of Arabidopsis, suggesting that Complex II is more relevant in heterotrophic tissues such as roots (Peters et al., 2012).

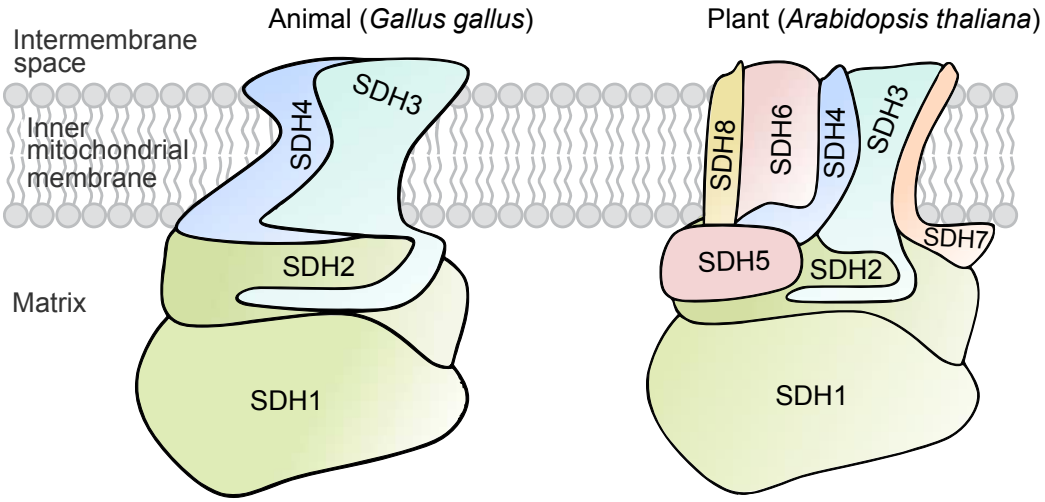

Figure 1.4 | **Topological model of Complex II in animals (*Gallus gallus)* and plants *(Arabidopsis thaliana)***. Subunits SDH1-4 are conserved among plants and animals. Plants have four additional subunits, SDH5-8. The lower part of the complex, which protrudes into the mitochondrial matrix, includes SDH1 and SDH2. The upper part of the complex anchors SDH1 and SDH2 to the inner mitochondrial membrane. Besides SDH3 and SDH4, it includes the plant-specific subunits SDH6 and SDH7. SDH7 is suggested to interact with SDH3 and SDH6 is suggested to interact with SDH4, based on biochemical and evolutionary considerations. SDH5 is probably localised at the interface between the matrixial and the membrane domain but could also be found in another position. The localization of SDH8 is unknown. Adapted from Huang et al., 2019.

Besides Complexes I and II, which are conserved across eukaryotes (Cardol, 2011; Karavaeva & Sousa, 2023), some organisms including plants have additional "alternative" pathways for electrons to enter the mETC. On one hand, a set of alternative NAD(P)H dehydrogenases exist at both sides of the mitochondrial inner membrane (Ian Menz & Day, 1996; Rasmusson et al., 2008). These enzymes catalyse the same reaction than Complex I, i.e. the electron transfer from NAD(P)H to the Coenzyme Q, with the difference that the process is not coupled with proton translocation (Rasmusson et al., 2008; Xu et al., 2013). Some of them are calcium-dependent (Geisler et al., 2007; Michalecka et al., 2004). These alternative NAD(P)H dehydrogenases are thought to play a protective role in electron overflow situations, e.g. under high light or during drought stress, when they enable to consume excess reducing power (Jethva et al., 2023; Sweetman et al., 2019; Wallström, Florez-Sarasa, Araújo, Aidemark, et al., 2014; Wallström, Florez-Sarasa, Araújo, Escobar, et al., 2014). On the other hand, other

FAD/FMN-containing dehydrogenases exist, located at either sides of the inner mitochondrial membrane, that can transfer electrons from different substrates directly to the Coenzyme Q, such as the proline dehydrogenase (Elthon & Stewart, 1981) or the glyceraldehyde-3-phosphate dehydrogenase (Shen et al., 2003, 2006), or to the cytochrome c, such as the D-lactate dehydrogenase (Atlante et al., 2005).

The existence of this variety of oxidoreductase complexes, with their diversity in terms of cofactors and localization, defines multiple possible pathways for the entry of electrons: i) the matrix NAD(P)H pathway, ii) the matrix $FADH_2$ pathway, iii) the intermembrane space NAD(P)H pathway and iv) the intermembrane space $FADH_2$/$FMNH_2$ pathway (Schertl & Braun, 2014). The relative contribution of each of the four pathways to the overall electron entry depends on the metabolic state of the cell, the light conditions, and environmental stress factors (Schertl & Braun, 2014; Sweetlove et al., 2010).

1.1.3.2. Electron flow: coenzyme Q, complex III and cytochrome c

The electron entry pathways are many and diverse, but they mostly converge in a singular electron transporting molecule: the Coenzyme Q. One exception is the D-lactate dehydrogenase, which directly reduces the cytochrome c instead (Atlante et al., 2005; Bari et al., 2004; Engqvist et al., 2009). The Coenzyme Q, also called ubiquinone when oxidized or ubiquinol when reduced by two electrons, is a mobile lipidic electron carrier formed by a benzoquinone bound to different units of isoprene (Nowicka & Kruk, 2010). The hydrophobic isoprenoid tail allows its fast diffusion through the inner mitochondrial membrane (Nowicka & Kruk, 2010). Since the oxidoreduction of the Coenzyme Q works one electron at a time, through an intermediate called semiquinone, the Coenzyme Q provides a connexion interphase between the two-electron transporters (classical or alternative NADH dehydrogenases) and the single-electron acceptor cytochrome c (Mathews et al., 1999; Y. Wang & Hekimi, 2016).

In the classical model, the Coenzyme Q gives electrons directly to the cytochrome bc_1 complex or Complex III. This complex has ubiquinol-cytochrome c oxidoreductase activity and couples the transfer of two electrons with the pumping of two protons across the inner mitochondrial membrane, in the so-called Q cycle (Crofts, 2004). The structure

of the Complex III is highly conserved among eukaryotes. It functions as a homodimer, each unit being composed by 10 or 11 subunits (Welchen et al., 2011). The two largest subunits, considered core subunits, are homologous to the two subunits of the mitochondrial processing peptidase (MPP), a metallo-endopeptidase that specifically cleaves off presequences from several hundreds of mitochondrial precursor proteins (Braun & Schmitz, 1997; Majsec et al., 2017). The core subunits do not have a proteolytic activity in animal mitochondria, but they retain intact active sites in plants (Braun et al., 1992; Glaser et al., 1994).

The cytochrome c is a small haemoprotein found loosely associated with the mitochondrial inner membrane. Its primary role is to facilitate electron transfer between Complex III and Complex IV. In mammals, the transfer of electrons mediated by cytochrome c is considered the rate-limiting step in the electron transport process (Hüttemann et al., 2011) and it can be regulated by ATP, which binds to the cytochrome c and slows down the electron transfer process, aligning the respiratory chain's activity with the cell's energy status (Tuominen et al., 2001). In plants, cytochrome c has additional binding sites for the cytochrome c1 subunit of Complex III, which enhances the electron transport rate between Complex III and Complex IV (Acín-Pérez et al., 2008; Moreno-Beltrán et al., 2014; Vempati et al., 2009). The presence of cytochrome c also contributes to the stabilization of Complex IV assembly in plants (Welchen et al., 2012). Beyond its role in energy metabolism, cytochrome c serves as a signalling molecule in mitochondria, triggering programmed cell death (PCD) when released into the cytosol (Van Hautegem et al., 2015). This PCD mechanism is crucial for various biological processes, from embryogenesis to responding to pathogen attacks (Van Hautegem et al., 2015). Additionally, cytochrome c plays a vital role in the synthesis of antioxidant molecules, detoxification of cytotoxic byproducts, and electron flow regulation in stressful environments, making it a multifunctional protein essential for mitochondrial function and cellular adaptation to environmental cues (Bartoli et al., 2000; Millar et al., 2004; Welchen & Gonzalez, 2016).

1.1.3.3. Electron exit from mETC: complex IV and alternative oxidase

The protein complex that catalyses the last oxidoreduction step, i.e. the transfer of electrons to the final electron acceptor, O_2, in the classical pathway is the cytochrome c oxidase or Complex IV, which couples its cytochrome-c:oxygen oxidoreductase activity with proton pumping (Schmidt-Rohr, 2020; Wikström & Sharma, 2018).

The Complex IV is present in all aerobic organisms, from prokaryotes to humans. The first systematic study that demonstrated the presence of cytochrome c oxidase activity in plants was published in the mid-forties (Goddard, 1944). In bacteria, this complex is formed by solely three subunits that form the catalytic core, which are called COX1, COX2 and COX3. The eukaryotic complex is formed by the catalytic core and 10 to 14 additional subunits that have been likely acquired after endosymbiosis and act as a protecting structural scaffold that stabilises the core of the enzyme (Kadenbach, 2017; Soto & Barrientos, 2016).

The detailed composition of the Complex IV in plants has been described (Mansilla et al., 2018; Millar et al., 2004). The general rule for eukaryotes is that the three core subunits are encoded in the mitochondrial DNA, while all the additional subunits are instead encoded in the nuclear genome, translated in the cytosol, and imported to the mitochondria (Khalimonchuk & Rödel, 2005). Some exceptions have been described in plants: in leguminoses, the subunit COX2 is encoded in the nucleus and has been lost in the mtDNA (Daley et al., 2002); in Arabidopsis, the gene that encodes the subunit COX3 is found in both the mitochondrial and the nuclear genomes, but the protein encoded by nuclear DNA is thought not to be imported to the mitochondrion after translation (Mansilla et al., 2018). Whilst the core subunits are quite conserved between organisms, the number and properties of the additional subunits present diversity across the tree of life, and several plant-specific specific subunits have been described (Mansilla et al., 2018).

Besides the polypeptidic components, the Complex IV also harbours redox cofactors involved in reactions of electron transfer. A di-copper centre, Cu_A, present in COX2, receives electrons from reduced cytochrome c (Tsukihara et al., 1995). These electrons are then transferred to a haem *a* group present in COX1, to a binuclear haem a_3-Cu_B centre in the same subunit, and finally to O_2 (Blomberg, 2016). The assembly of

these cofactors requires the participation of a set of assembly factors and chaperones, that are conserved from prokaryotes to mammals (Figure 1.5). These are involved in haem *a* synthesis (COX10, COX15), haem *a* insertion into COX1 (presumably SURF1) and copper insertion (COX11, COX17, HCC1) (Meyer et al., 2019).

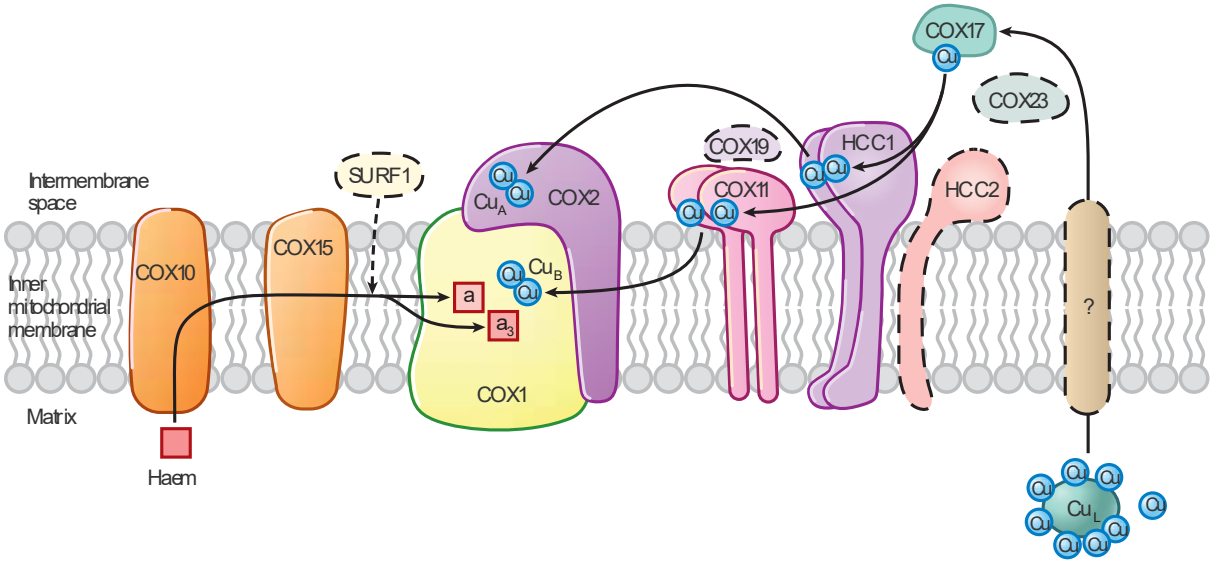

Figure 1.5 | Pathways for cofactor delivery into COX1 and COX2 in land plants during Complex IV biogenesis. Copper (Cu) is bound on the metal chaperone COX17 in the intermembrane space. COX17 transfers copper to COX11 and HCC1. HCC1 delivers copper to COX2, forming the Cu_A centre, and COX11 delivers copper to COX1, forming the Cu_B centre. Haem is modified by COX10 and COX15 to form haem a (a) and haem a_3 (a_3), subsequently delivered to COX1. Dashed outlines indicate conserved assembly factors with unconfirmed function in plants. The question mark indicates that the transporter responsible for the transfer of copper from the matrix to the intermembrane space remains unknown. *Cu_L* represents an unidentified copper ligand. Modified from Meyer et al., 2019.

In addition to Complex IV, the respiratory chain of plants possesses another electron exit site: the alternative oxidase, AOX. This component is found also in several fungi and protists and has also been described in a broad range of animal species (Moore et al., 2013; Pennisi et al., 2016). Since the activity of the Complex IV is inhibited by cyanide but the AOX is not, these two pathways are defined as cyanide-sensitive and cyanide-insensitive, respectively.

The AOX transfers electrons directly from Coenzyme Q to O_2 (Vanlerberghe & McIntosh, 1997). It thus constitutes an alternative exit point of the mETC that bypasses two of the three proton pumping sites (complexes III and IV). The AOX is encoded in the nuclear genome and is highly conserved in all plant lineages (Pennisi et al., 2016); five isoforms have been described in Arabidopsis, the most abundant being AtAOX1a (Clifton

et al., 2006). The alternative oxidase represents a conserved mechanism for dissipation of excess of reducing power in mitochondria, being able to reduce the production of reactive oxygen species (ROS) by the respiratory chain, as reviewed by Vanlerberghe et al., 2020. It can be activated when the classical cyanide-sensitive pathway is saturated with electrons due to an impaired transport of electrons under stress conditions such as low temperature, drought or excessive light (Vanlerberghe & McIntosh, 1997; Vanlerberghe & Ordog, 2002).

Several levels of regulation of AOX expression and activity have been described (Garmash, 2022). At the transcript level, the promoter of AtAox1a contains several cis-regulatory elements, which can be recognized by transcription factors including, but not limited to, ABI4, ANAC017 (Ng et al., 2013) or WRKY40 (Dojcinovic et al., 2005; Van Aken et al., 2013), as well as light sensitive elements (Ho et al., 2008; D. W. Zhang et al., 2010). The AOX can also be post-translationally regulated. Most AOX isoforms have two highly conserved Cys residues towards the N-terminus of the protein (*CysI* and *CysII*), and some organisms possess a less conserved third Cys residue (*CysIII*) (Albury et al., 2009; Andersson & Nordlund, 1999). The formation of an intermolecular disulfide bond between *CysI* of each monomer causes the inactivation of AtAOX1a under oxidizing conditions, but reducing conditions lead to a noncovalently linked dimer that is the active form of AtAOX1a (Figure 1.6). This system, called the disulfide/thiol switch, can be modulated by the action of thioredoxins, which rely on the redox state of the mitochondrial NADPH pool that in turn depends on the isocitrate dehydrogenase activity (Garmash, 2022; Rhoads et al., 1998). The reduced, active forms of AtAOX1a can be further activated by 2-oxo acids (e.g. pyruvate) through the formation of a thiohemiacetal bond with the cysteine residues (Figure 1.6) (Rhoads et al., 1998; Selinski et al., 2017). Due to their multiple levels of regulation, higher transcript levels do not necessarily correspond to higher protein levels, and higher protein levels might not translate in increased AOX activity (Del-Saz et al., 2018).

The capacity of the cyanide-insensitive (AOX-mediated) pathway is usually measured *in vitro* on isolated mitochondria by inducing the maximal transfer of electrons in the presence of cyanide or other inhibitors of Complex IV and activator of the

AOX (Lyu et al., 2018). A method that has been widely used is based on quantification of the ATP synthesis efficiency through the ADP/O ratio, i.e. the ratio between the amount of ADP used for ATP synthesis and the amount of oxygen that is consumed in the process, in the presence of inhibitors (Estabrook, 1967). Comparison of the ADP/O ratio with or without blocking the AOX-mediated pathway allows to infer the capacity of the AOX pathway (Sluse & Jarmuszkiewicz, 2000).

However, due to the multiple levels of regulation of AOX, the *in vitro* capacity is not suitable for inferring the relative contribution of the cyanide-sensitive (Complex IV-mediated) and cyanide-insensitive to the electron flow *in vivo*. The latter can instead be quantified by the ($^{18}O/^{16}O$) oxygen-isotope-fractionation technique (Day et al., 1996; Millar et al., 1998; Ribas-Carbo et al., 2005; Robinson et al., 1992).

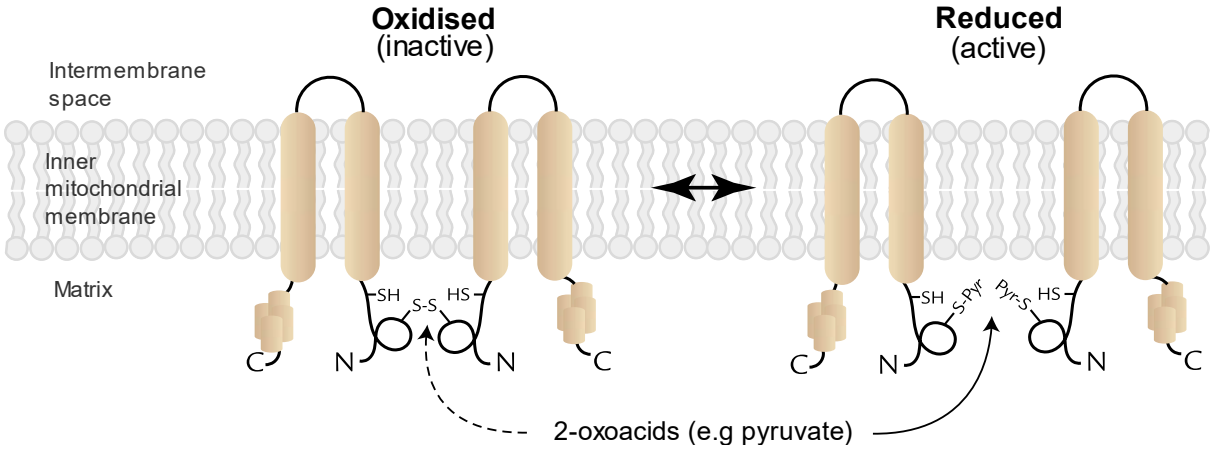

Figure 1.6 | **Schematic diagram of the *Arabidopsis thaliana* alternative oxidase (AOX) regulation**. In the oxidised state (inactive), the AOX dimer is linked by an intersubunit disulfide bond, which blocks the 2-oxo acid site of action at *CysI* residue (dashed arrow). The disulfide bond is reduced by added reductant or by reduced endogenous thioredoxin. The free *CysI* sulfhydryls can then interact with pyruvate or other 2-oxo acids to form a thioacetal, with a resulting increase in enzyme activity. *CysII* does not appear to be involved in either of these regulatory features. S-Pyr indicates the thiohemiacetal. Adapted from Rhoads et al., 1998.

1.1.3.4. Oxidative phosphorylation: complex V

The Complex V is a membrane-bound F_1F_O type H^+-ATP synthase, a member of the larger group of rotary ATPases, that catalyses the terminal step in oxidative phosphorylation. It converts the electrochemical gradient across the inner membrane generated by proton translocation into ATP.

The structure of F_1F_O-ATP synthases (Figure 1.7) is highly conserved across various biological domains, encompassing prokaryotes, eukaryotes, and photosynthetic bioenergetic membranes like the thylakoid F_1F_O -ATP synthase (Millar et al., 2011). This structure comprises a F_O domain, integrated into the inner mitochondrial membrane, and the hydrophilic F_1 domain, responsible for ATP synthesis (Zancani et al., 2020). The F_O domain was named after its sensitivity to the antibiotic oligomycin (Kagawa & Racker, 1966), which blocks oxidative phosphorylation and ATPase activity of Complex V (Lardy et al., 1958).

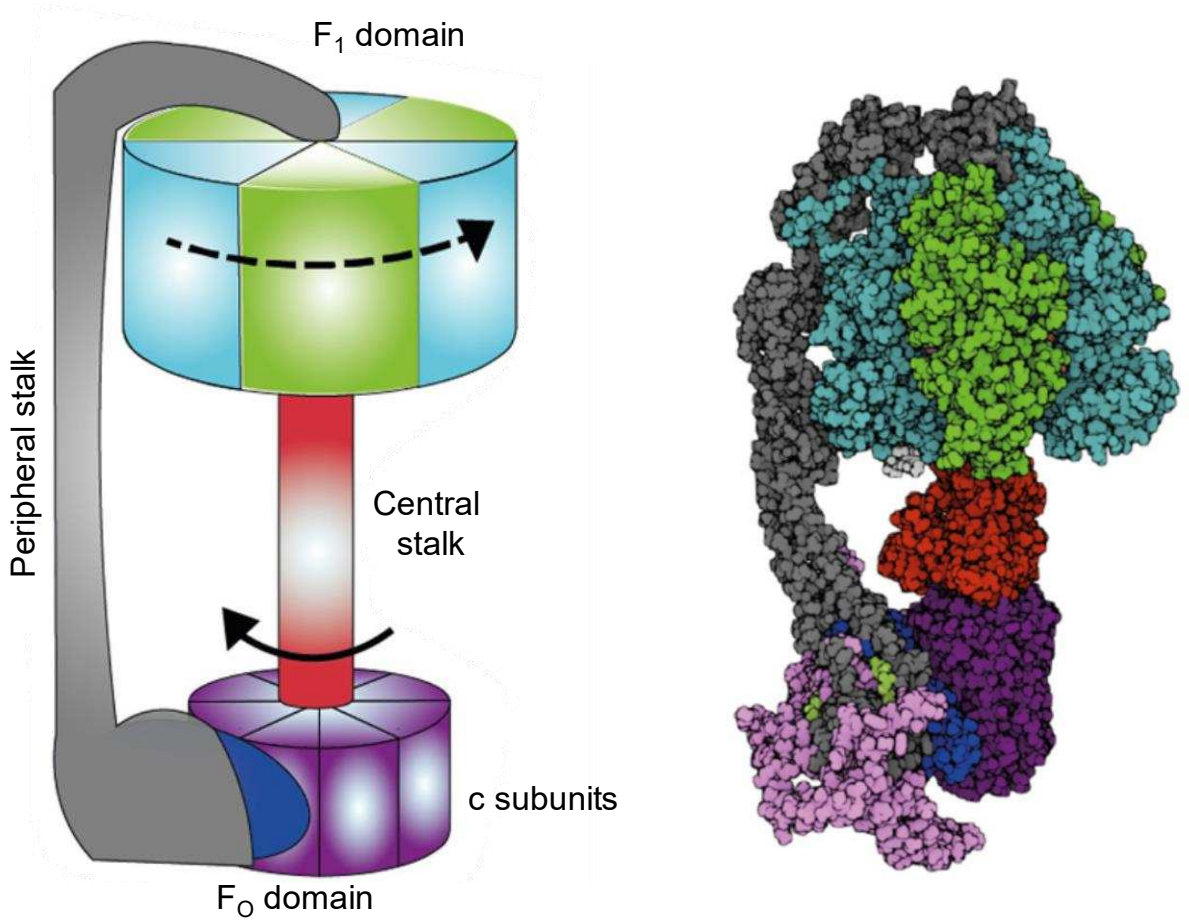

Figure 1.7 | **Schematic structure and model of a Complex V monomer**. Left: Overall scheme of a Complex V. Catalytic core or F_1 domain, which is a trimer of dimers αβ. Central stalk, which is composed by subunits γ, δ and ε. The rotor or F_O domain, which is made by subunits a, b, c, 8, f and g. Multiple c subunits form the c-ring; the number of c subunits in plants is still debated and should change among species. Peripheral stalk, which consists of subunits b, d, and OSCP. From Zancani et al., 2020 and Miranda-Astudillo et al., 2022. Right: structural model of Complex V monomer from *Bos taurus* (PDB 6ZPO, Spikes et al., 2020). Modified from Miranda-Astudillo et al., 2022.

These two domains are interconnected by a central stalk that transmits the rotational energy from F_O to the catalytic F_1 subunit (Zancani et al., 2020). The rotation of the F_O domain is driven by proton translocation, and a full 360° rotation causes the complete turnover of the F_1 domain, leading to the generation of three ATP molecules (Kubo et al., 2023). The structure also includes a peripheral stalk, which stabilizes the stationary components of both domains during the catalytic rotation (Liu et al., 2021; Zancani et al., 2020). The native Complex V is a dimer connected via F_O that forms an angled structure which induces the folding of the mitochondrial inner membrane (Dudkina et al., 2006).

Most of the Complex V subunits are highly conserved among yeast, animals, and plants (Braun, 2020). The core of the subunit F_O in plants is composed of three nuclear-encoded subunits, including the beta subunit, and nine mtDNA-encoded components (Millar et al., 2011). Out of the five subunits of the F_1 structure, four are encoded in the nucleus and one is encoded in the mtDNA, in Arabidopsis (Unseld et al., 1997). In plants, two additional plant-specific subunits of the F_O portion have been identified, named F_Ad and 6kDa-subunit (Liu et al., 2021; Senkler et al., 2017). Although these subunits have been associated with the F_O moiety in various plant species (Zancani et al., 2020), the precise role of these proteins in the assembly, stability, and activity of the complex remains unclear, primarily due to the lack of direct biochemical and structural evidence.

Besides the conserved subunits, there is a relatively high variety of stator structures across eukaryotic lineages (Miranda-Astudillo et al., 2022). This variety results also in different levels of aggregation to form dimers, tetramers or higher oligomers, which can assemble into larger associations forming higher complexity structures. Complex V oligomers define the shape of mitochondrial cristae, and therefore the variety of oligomers translates in a variety of mitochondrial cristae shapes across eukaryotic lineages (Miranda-Astudillo et al., 2022). From single-mitochondrion proteomics data it was proposed that Arabidopsis mitochondria might contain approximately 3,000 dimers of Complex V, involved in the formation of 18 cristae sheets. Alternatively, monomers or tetramers could be also relevant, decreasing the number of cristae sheets (Fuchs et al., 2020). Remarkably, Complex V also interacts with other respiratory complexes to form a

functional unit of the oxidative phosphorylation system called the oxphosome (Miranda-Astudillo et al., 2022; Ukolova et al., 2020).

1.2. The biological role of respiration in plants

As we have discussed, the main structure and function of mETC is conserved among all eukaryotes, but there are some significant differences between animal and plant cells. The unique features of the respiratory chain of plants allow the existence of alternative pathways for electron transfer, which are thought to play an important role in optimizing photosynthetic performance in the light (Michalecka et al., 2004; Selinski et al., 2018; Wallström, Florez-Sarasa, Araújo, Aidemark, et al., 2014). In plants another organelle is involved in energy supply: the chloroplast. In chloroplasts, energy from light is used to sustain an electron flow through the plastid electron transport chain (pETC), which produces reducing equivalents in form of NADPH and generates a transmembrane proton gradient that is exploited by the plastidial ATP-synthase (M. Qi et al., 2023). The NADPH and ATP generated this way can be used for carbon fixation and anabolic reactions inside the chloroplast or can be exported to the cytosol to sustain cell growth (Krämer & Kunz, 2021; Moreno-García et al., 2022; Voon & Lim, 2019).

Plants are obligatory photoautotrophs and thus all energy supporting their metabolism ultimately comes from light thanks to photosynthesis. Plants rely on mitochondrial respiration particularly when light is not present or in tissues that are not photosynthetically active (e.g. roots or during seed germination). However, there is evidence that mitochondria are active in photosynthetic tissues during the day, and that they act synergically with chloroplasts to ensure an optimal photosynthetic performance (Hurry et al., 2005; Raghavendra et al., 1994; Shameer et al., 2019; Tcherkez et al., 2017; Vanlerberghe et al., 2020). Studies in different photosynthetic models confirmed the reciprocal influence of respiration and photosynthesis. For example, mutants of the green alga *Chlamydomonas reinhardtii* with impaired dark respiration showed a significant decrease in photosynthetic efficiency under phototrophic conditions, and others with altered photosynthetic electron transport had alterations in respiration (Cardol et al., 2003).

Despite their relevance, the identity of the key players and the precise pathways that connect mitochondria and chloroplasts are far from clear, especially in land plants. One main reason for this incomplete knowledge has been the difficulty in generating plant mutant lines with defects in mitochondrial respiration. As we review in this chapter, mutations that compromise respiration are mostly embryo lethal in seed plants, which hampers the isolation of respiratory mutants through reverse genetics approaches. The only exception is the mitochondrial Complex I, for which multiple plant lines with null activity have been isolated, as they can survive thanks to the partially overlapping function of rotenone-insensitive pathways. For the other complexes, only lines with reduced activity have been isolated, that in most cases present severe growth defects and do not produce viable seeds, strongly suggesting that the knockouts were not isolable because of their lethality.

2. The first land plant models that remarked the metabolic relevance of respiration

Historically, the first identified lines of embryophytes with genetic alterations that caused dysfunction of one or more components of the respiratory chain were either naturally occurring variants or the result of mutagenesis events. In several cases mutants selected for a specific phenotypic trait were later discovered to be affected in a locus related to mitochondrial function. This is the case of mutants showing cytoplasmic male sterility (CMS), some lines of maize with a particular phenotype in leaves termed nonchromosomal stripe (NCS) or some lines in cucumber that presented mosaic-like (MSC) spots in leaves. These three families of mutants will be described as they have been an important source of information regarding the role of respiration in plants.

2.1. Plants suffering of cytoplasmic male sterility

2.1.1. Definition and discovery of cytoplasmic male sterility

Chronologically, the first described plants with altered levels of respiration due to their genetics were cytoplasmic male sterile plants, including many different plant species. Cytoplasmic male sterility (CMS) is defined as the abortion of the male gametophyte driven by cytoplasmically inherited factors, i.e. the inheritance is not nuclear. CMS was first described in 1931 in flax and maize (Rhoades, 1931), and we now know that it is a relatively common phenomenon, as it has been described in more than 140 plant species (Hanson & Conde, 1985).

The molecular basis behind CMS in plants always involves a rearrangement of the mitochondrial genome (mtDNA) that causes either the appearance of a new protein (gain-of-function hypothesis) or the alteration of an existing protein (loss-of-function hypothesis) (Newton et al., 2004). The gain-of-function hypothesis has been recently validated by novel techniques that allow fine gene editing in plant mtDNA: the knockout of the CMS-associated mtDNA-encoded gene in rice could eliminate the CMS phenotype (Kazama et al., 2019). Many CMS-causing proteins form pores in the inner mitochondrial membrane, disturbing the proton gradient and impairing energy production (Horn et al., 2014). For

example, in petunia, CMS appears after the recombination of different segments of the atp9, cox2 and urfS genes in mtDNA, with the resulting recombinant gene encoding the novel protein PCF (Young & Hanson, 1987). The genetic bases were confirmed by showing that reduction of PCF levels restores fertility (Nivison & Hanson, 1989).

2.1.2. Cytoplasmic male sterility in maize: one well studied case

The first detailed studies on the genetic bases of CMS were conducted in maize, with the remarkable initial contribution of Marcus M. Rhoades and Warren H. Gabelman in the context of their respective PhD theses. Gabelman concluded that the cytosolic factor causing CMS had to act as a whole unit, and it must have many characteristics in common with chromosomes, although he did not discard this factor to be a virus (Gabelman, 1949). Rhoades went one step further and suggested that the cytosolic factor could be mitochondria (Rhoades, 1950). At that time, plastids were already proposed to be carriers of genetic information (Rhoades, 1943), but that had not been seen yet for mitochondria. Also, it was still believed that plastids derived from mitochondria (DuBuy et al., 1950; Guilliermond, 1941; Newcomer, 1946; Zirkle, 1929).

Both nuclear- and cytoplasmic-driven male sterilities were the object of many works at that time (Schwartz, 1951) because of the commercial interest in having sterile maize hybrids, as they did not need to be emasculated to avoid cross-fertilization (Edwardson & Corbett, 1961; Rogers & Edwardson, 1952). One case was the “Texas” line of maize, a common variety used for decades in agriculture until it was found to be particularly susceptible to the pathogen *Bipolaris maydis* (Levings, 1990; Peterson et al., 1975; Ullstrup, 1972). The Texas line was also more susceptible to the fungus *Phylosticta maydis* (Rhoads et al., 1995). Both pathogens would produce pathotoxins, BmT and BmP, respectively, collectively referred to as “T-toxin” (Laughnan & Gabay, 1973; Lim & Hooker, 1972). Different studies were carried out to find the subcellular site of the susceptibility to the pathogens. Some of them focused on mitochondria and found that the T-toxin would uncouple oxidative phosphorylation, inhibit oxoglutarate oxidation and cause the irreversible swelling of mitochondria in Texas plants, but would have no effect on other mitochondria from other maize lines (Miller & Koeppe, 1971). At the time, the identity of the cytoplasmic particle responsible for the CMS information remained

unknown. In the mid-70s, (Peterson et al., 1975) already suggested that the carrier of the CMS information could be mitochondrial DNA, and this was proposed again, this time with supporting evidence, by (Levings & Pring, 1976). By comparing the DNA band pattern resulting from treating mtDNA with a set of restriction enzymes -a novel technique at the time (Nathans & Smith, 1975)-, they confirmed that mitochondria from normal and Texas lines were genetically different, thus supporting the hypothesis that this was at the origin of the resistant phenotype (Levings & Pring, 1976).

Currently, three different types of CMS in maize are known, named CMS-T, CMS-S and CMS-C (Gabay-Laughnan & Laughnan, 1994), and all three appeared after recombination events in the mtDNA. CMS-T mtDNA contains a chimeric gene, T-*urf13*, which is transcribed (Dewey, 1986). The T-*urf13* transcript encodes a protein that is an integral membrane of the inner mitochondrial membrane which can form a pore through the membrane in the presence of the T-toxin (Hack et al., 1991; Korth et al., 1991; Rhoads et al., 1995). However, whether the pore formation is also the mechanism of male sterility has not been confirmed. In CMS-S, a nuclear-encoded transcription factor induces the transcription of the mitochondrial orf355 specifically in microspores, causing sterility (Xiao et al., 2020). In CMS-C, a defective atp6 gene causes suboptimal assembly of Complex V and premature programmed cell death in developing pollen (Yang et al., 2022). Studies showed that respiration is altered in all three types of CMS (-C, -S, -T), since they all show increased levels of Complex IV activity during the seedling stage, but undetectable activity levels in sterile anthers (Bino et al., 1986; Watson et al., 1977).

2.1.3. CMS in tobacco: the first model for studying the metabolic impact of altered respiration in plants

Two CMS plants have been isolated in *Nicotiana sylvestris*. They both appeared during propagation of protoplast cultures and were named CMSI and CMSII (Lonsdale, 1987). CMSI and CMSII showed the same abnormal phenotype, characterized by decreased growth rate, altered leaf shape and male sterility (X. Q. Li et al., 1988). It was later found that both lines carry alterations at the mtDNA level; in CMSI, two recombination events, rec1 and rec2, caused the reorganization of mtDNA (Chetrit et al., 1992), while in CMSII only rec1 occurred. In both cases, rec1 caused the deletion of a

16.2 kb region in mtDNA (Chetrit et al., 1992). Consequently, both lines are deficient for the CI subunit NAD7 (Lelandais et al., 1998; Pla et al., 1995), which is at the base of the observed phenotype. Accordingly, a complete phenotypic rescue was achieved by re-inserting nad7 as transgene (Pineau et al., 2005). Besides nad7, CMSI and CMSII also lack the proteins NAD9 (Gutierres et al., 1997) and NAD1 (Gutierres et al., 1999), likely because of the destabilization of the complex.

Besides these two cytoplasmic male sterile mutants, a third relevant mitochondrial mutant, NMS1 (for Nuclear Male Sterile 1), has been described in tobacco. It was also identified for being male sterile, although in this case the inheritance was nuclear (De Paepe et al., 1990). NMS1 carries defects in the processing of the Complex I structural gene nad4, which causes the loss of several Complex I subunits including NAD7 and NAD9 (Brangeon et al., 2000).

2.1.4. CMS mutants in different species involve alterations of mtDNA

Other studies have been performed on different plant species known to present lines with cytoplasmic male sterility, although with less detail than maize and tobacco (Nivison & Hanson, 1989; Pla et al., 1995; Young & Hanson, 1987). In CMS petunia the levels of Complex IV activity in sterile anthers are strongly reduced (Bino et al., 1986), as it has been described for maize CMS (Bino et al., 1986; Watson et al., 1977). Phenotype is caused by the appearance of a region in mtDNA after recombination of three gene segments (atp9, cox2 and urfS), which is transcribed and translated into a new protein PCF (Petunia CMS-associated fused locus) that likely alters mitochondrial activity (Young & Hanson, 1987). The fertility can be restored by the nuclear locus Rf (Restorer of fertility) (Nivison & Hanson, 1989), which encodes a pentatricopeptide (PPR) protein that forms part of a large protein complex attached to the inner mitochondrial membrane capable of interacting with Pcf mRNA and blocking its translation (Gillman et al., 2007).

The presence of nuclear restorers of fertility that act post-translationally is common among CMS plants. There are other examples of CMS in plants that involve alteration of mitochondrial genes. *Sorghum bicolor* CMS present a larger version of the cox1 gene (Dixon & Leaver, 1982). In Brassica it was observed that CMS occurred along with the

translation of the novel putative mtDNA gene orf138 (Grelon et al., 1994), and a restorer of fertility worked by post-translationally downregulating the protein (Bellaoui et al., 1999). In sunflower, CMS is caused by a novel orf522 in mtDNA that encodes a 15 kDa polypeptide, which is destabilized by the expression of a nuclear fertility restoring factor (Moneger et al., 1994). A reduction in mitochondrial redox activity has been observed also in CMS lines of wheat, rye, rice and lucerne, as discussed in (Bino et al., 1986).

In summary, despite the different molecular determinants, CMS mutants all share an alteration in mitochondrial activity. To note, the system CMS-Rf is currently being exploited in the production of hybrid seeds (Kitazaki et al., 2023).

2.2. Maize non-chromosomal stripe (NCS) mutants

Another set of cytoplasmically-transmitted mutations in maize are non-chromosomal stripe (NCS) mutations, which are also maternally inherited as CMS. NCS plants were first described by (Shumway & Bauman, 1967) as having leaves with light-green striping and showing a growth deficit, although the first detailed characterization of NCS lines were published in the mid-80s, at a time when CMS was already known to be usually associated with rearrangements of the mitochondrial DNA and was indeed the main phenomenon of study related to mitochondrial variability in plants.

The first NCS mutant derived from a CMS-T maize line, and it was maternally inherited; this NCS1 line got lost (Shumway & Bauman, 1967). Two other NCS lines were discovered, named NCS2 and NCS3, also in CMS-T lines (Coe, 1983). The phenotypes of NCS2 and NCS3 were slightly different, suggesting different genetic basis. Both NCS2 and NCS3 had abnormalities in mtDNA (seen by digestion with restriction enzymes) but not in plastid DNA, and the lines were characterized by having heterogenous mitochondria, containing either normal or altered mtDNA (Newton & Coe, 1986). NCS2 had alterations in mtDNA, and germ cells containing mutant mitochondria only would give no viable progeny (Newton & Coe, 1986). The altered region in NCS2 mitochondria was found to encode a 24,000 Mr polypeptide (Feiler & Newton, 1987) that was the consequence of a fusion between intron 3 of *nad4* gene and intron 2 of *nad7* gene (Marienfeld & Newton, 1994). In affected NCS2 mitochondria there is a partially

assembled version of the Complex I, which lacks the subunit NAD4 and the membrane arm, becoming more loosely attached to the membrane (Karpova & Newton, 1999). This partially assembled complex, however, retains the NADH dehydrogenase activity (Karpova & Newton, 1999). NCS3 was later found to have altered mitochondria translation (Hunt & Newton, 1991), as was the case of another mutant, NCS4 (Karpova et al., 2002; Newton et al., 1996).

Two other NCS mutant, named NCS5 and NCS6, were found to contain both normal and cox2-defective mitochondria (Lauer et al., 1990). The NCS5 mutant lacks part of the first exon of cox2, and therefore the Complex IV; however, the altered mitochondria are found in heteroplasmy, ensuring the viability of NCS5 cells (Newton et al., 1990). In NCS6, a recombination between 36 bp repeats causes a partial deletion of cox2, with consequent reduced levels of both cox2 mRNA and protein (Lauer et al., 1990). Although initially defined as homoplasmic (Gu et al., 1993), yellow stripes of NCS6 leaves were later shown to also contain a reduced proportion of healthy mitochondria (Jiao et al., 2005).

Two other NCS lines have been obtained, carrying mitochondrial defects in a background different than CMS-T. These are NCS-C, with a CMS-C cytoplasm, and NCS-RU, with a male fertile RU cytoplasm (Newton et al., 1989). We are not aware of detailed molecular analyses on these lines.

2.3. Cucumber mosaic family (MSC)

Another interesting family of mitochondrial mutants in seed plants is the mosaic (MSC) family in cucumber. Different MSC lines have appeared through passing *in vitro* cultures, by the process called somaclonal variation first described by (Larkin & Scowcroft, 1981). The first MSC lines (MSC19, MSC16 and MSC22) were described by (Malepszy et al., 1996). Since the phenotype was transmitted paternally, mitochondria and not chloroplasts were suggested to be the carriers of the genotype (Malepszy et al., 1996), and indeed now it has been verified that mitochondrial inheritance in cucumber is paternal (Park et al., 2021).

The most well studied MSC mutant is MSC16, which have a slight reduction in Complex I activity (Juszczuk & Rychter, 2009). The transcript levels of Complex I subunits are not reduced in MSC16 (Del Valle-Echevarria et al., 2015), although protein levels are (Juszczuk & Rychter, 2009). This could be due to impairment of mitochondrial ribosomes (Del Valle-Echevarria et al., 2015). Another line, MSC3, showed reduced transcripts of mitochondrially encoded genes *nad5* and *atp4*, although their protein levels did not change (Del Valle-Echevarria et al., 2015). MSC3 showed increased levels of AOX (Mróz et al., 2015).

2.4. Beyond naturally occurring variants

Up to now we described lines that appeared spontaneously and were identified for their phenotype, i.e. male sterility that follows cytoplasmic inheritance, variegated leaves, or mosaic-like spots in leaves, and that were later found to carry genetic variations affecting mitochondria and respiratory complexes. More recently, the approaches for specifically studying the role of respiration in plants have been based on the screening of randomly mutagenized plants for a desired phenotype, which sometimes lead to the discovery of respiratory mutants, or targeting either direct subunits of the complexes or genes involved in complex assembly or maturation by reverse genetics.

When discussing the first studies aimed to analyse the impact of depleting respiration in plants, we must acknowledge the studies conducted using mutants of the unicellular model alga *Chlamydomonas reinhardtii*. Genetic manipulation in *C. reinhardtii* is straightforward, as nuclear genes can be targeted by RNA interference (RNAi) or interrupted by insertional mutagenesis (Mussgnug, 2015). In addition, random or site-directed mutagenesis can be performed in the mitochondrial genome of this alga (Mussgnug, 2015; Remacle et al., 2006). The first nuclear respiratory mutants were isolated in 1977 after random mutagenesis using nitrosoguanidine (Wiseman et al., 1977). Between 1989 and 2002, a series of mitochondrial mutants were generated, either by direct or reverse genetics approaches (Salinas et al., 2014). All these lines showed very slow or null growth under heterotrophic conditions (i.e. at dark and in media containing acetic acid) while they maintained growth in photoautotrophic conditions

(Salinas et al., 2014). The mitochondrial mutants were called dark uniparental minus inheritance (dum) mutants. In the following years, other respiratory mutants were isolated targeting nuclear-encoded genes via RNAi.

In the collection of respiratory mutants in *C. reinhardtii*, reviewed by Salinas et al., 2014, there are mutants lacking the Complex I (*dum5*, *dum17*, *dum20* and *dum25*), the Complex III (*dum1* and *dum21*), the Complex IV (*dum18* and *dum19*, *cox3-RNAi*, *cox17-RNAi*), the Complex V and different combinations of them (*dum19/25*, *dum22*). A mutant lacking an alternative NADH dehydrogenase has also been isolated (*nda1-RNAi*). These mutants have been extensively characterised and have yield valuable information on the role of respiration in photosynthetic organisms. However, *C. reinhardtii* is a unicellular organism with specific features and thus not a suitable model for studying the impact of respiration from a systemic point of view. Also, the chlorophyte ancestor diverged from the embryophyte ancestor very early during evolution of viridiplantae (see Figure 1.8) and therefore it is not the optimal candidate to model vascular plants.

Most respiratory complexes are multiunit protein complexes with some subunits, usually the bigger and catalytic ones, encoded by mtDNA, whilst most of subunits are nuclear encoded and imported into mitochondria. Since reverse genetics on mtDNA in plants has not been available as a tool until very recently (Arimura et al., 2020; Kazama et al., 2019; Nakazato et al., 2022), the nuclear encoded subunits have been the common target for reverse genetics-base approaches. In most cases, the complete inactivation of a given respiratory complex was lethal and the plant would not survive. This prompted the development of alternative approaches for generating partially depleted plants, using RNA interference, or knocking out assembly factors or pentatrico peptide (PPR) proteins involved in RNA splicing, as we will see in the following subsections. Several RNA editing proteins that target subunits of the respiratory complexes have been identified in different plant models, and the resulting mutants are called surrogate mutants.

In the following sections, we will go through the available body of embryophytes reported to have altered capacities of the pathways most directly linked to oxidative phosphorylation, i.e. the rotenone-sensitive pathway, the Complex II-mediated rotenone-insensitive pathway, the cyanide-sensitive pathway (including mutants with either altered

Complex III, cytochrome c, or Complex IV) or the Complex V. We did not include in this review mutants of the alternative pathways or surrogate mutants; the latter have been reviewed by Colas Des Francs-Small & Small, 2014.

3. Land plants with reduced capacity of the rotenone-sensitive pathway

3.1. Complex I: the most frequent target in respiratory mutants

For most of the reported plant mutants with reduced or depleted respiration, the affected complex is Complex I. As we discussed earlier, we can justify this because plant mitochondria have alternative pathways that allow electrons to enter the mETC even if Complex I is impaired. Although these alternative pathways are not proton-pumping, therefore decreasing the efficiency of ATP production by oxidative phosphorylation, they consume reducing power and can maintain —at least partially— the redox balance of mitochondria and the connected cell compartments.

We have already presented three families of mutants that are deficient in Complex I: CMS in tobacco, NCS in maize and MSC in cucumber. In addition to these, a supplementary set of Complex I mutants has been produced in the last decades, which allowed a relatively detailed understanding of the metabolic and physiological consequences of the reduction or depletion of the rotenone-sensitive pathway.

3.2. CMSII and NMS1 in tobacco

Different to CMS lines in maize, tobacco CMSI and CMSII lines showed a phenotype also in vegetative tissues, that was related to the Complex I deficiency (Gutierres et al., 1997). CMSI and CMSII plants grew slower but reached the same biomass than the WT, and male sterility could be overcome depending on the growth conditions such as the photoperiod (De Paepe et al., 1990; X. Q. Li et al., 1988).

Mitochondria isolated from CMSII plants had reduced respiration when glycine was used as a substrate, outlining that the activity of the glycine decarboxylase complex depended on a functioning Complex I (Gutierres et al., 1997). Mitochondria retained almost WT levels of succinate-dependent respiration, normal values of malate-linked respiration and increased capacity for oxidation of exogenous NADH, suggesting a higher activity of both matrix-facing and intermembrane space-facing alternative NADH

dehydrogenases (Gutierres et al., 1997; Sabar et al., 2000). The AOX protein levels were increased in CMSII (Gutierres et al., 1997). While there is contrasting evidence regarding the AOX capacity of CMSII mutants, with different reports showing that it was either unaltered (Priault et al., 2007) or increased (Gutierres et al., 1997; Vidal et al., 2007), there is agreement in showing no increased *in vivo* AOX activity in CMSII plants (Priault et al., 2007; Vidal et al., 2007). (Vidal et al., 2007) reported the transcription of a different isoform of the AOX, called AOX1.2, which resembles what has also been observed in maize NCS2 mutants (Karpova et al., 2002). Vidal et al., 2007 also showed that AOX accumulated in both the reduced (more active) and oxidized (less active) forms. Respiration of CMSII plants, quantified either as O_2 consumption or CO_2 evolution in the dark, was found to be up to 70 % higher than WT (Dutilleul, Driscoll, et al., 2003; Vidal et al., 2007). Contrasting reports support that light respiration was either unchanged (Priault, Tcherkez, et al., 2006) or increased (Lothier et al., 2019) in CMSII.

The photosynthetic capacity of CMSII was not reduced, but photosynthesis induction under physiological conditions was slower and net CO_2 fixation was lower. The reduction of net CO_2 fixation, which was not observed under control but not under low light intensities (Dutilleul, Driscoll, et al., 2003), could be explained in part due to an increased rate of carbohydrate oxidation (i.e. respiration), but also due to lowered carbon fixation that could not be explained by a reduced ATP availability for sucrose synthesis (Dutilleul, Driscoll, et al., 2003). CMSII plants could not efficiently acclimate to hight light, showing lower net C assimilation and lower initial RuBisCO activity (Priault, Fresneau, et al., 2006), i.e. having a higher rate of excess electron transport compared to the WT in the same conditions. CMSII showed slightly higher chloroplast-specific NADP-dependent malate dehydrogenase (NADP-MDH) activity under control conditions (Dutilleul, Driscoll, et al., 2003) but not under high light conditions (Priault, Fresneau, et al., 2006), meaning that the malate valve was not dissipating the excessive reduction of the mutant stroma.

Although the glycine metabolism was impaired in darkened leaves (Gutierres et al., 1997), the glycine:serine ratio in the light was not different, suggesting that extramitochondrial enzymes such as the hydroxypyruvate reductase or the nitrate reductase could be oxidizing the NADH produced by the glycine decarboxylase complex

(Dutilleul, Driscoll, et al., 2003). However, even though the glycine:serine ratio was maintained, the cellular redox equilibrium was disturbed, reducing the efficiency of photosynthesis (Dutilleul, Driscoll, et al., 2003). It was therefore proposed that the Complex I is an important sink of electrons during the day, when mitochondria must oxidize both respiratory and photorespiratory substrates (Dutilleul, Driscoll, et al., 2003). The phenotype of growth in CMSII was largely due to alterations in enzymatic functions of RuBisCO and sucrose phosphate synthase that impacted photorespiration (Dutilleul, Driscoll, et al., 2003), as growth under elevated CO_2 could rescue the phenotype almost completely (Priault, Tcherkez, et al., 2006). Interestingly, CMSII had lower stomatal conductance and were therefore more resistant to drought than WT (Djebbar et al., 2012).

The metabolome of CMSII plants under different conditions has been studied, including control conditions (Dutilleul et al., 2005), low nitrogen availability (Hager et al., 2010), increased CO_2 availability (Hager et al., 2010) or drought stress (Djebbar et al., 2012). CMSII leaves contained more total free amino acids, some of them at different relative proportions (Dutilleul et al., 2005; Hager et al., 2010). Levels of glycine or serine were unchanged, with a strong decrease in aspartate or glutamate and the accumulation of asparagine, arginine or glutamine (Dutilleul et al., 2005; Lothier et al., 2019). CMSII extracts contained more soluble proteins when normalized to the amount of chlorophylls (Dutilleul et al., 2005). Regarding the carbon metabolism, CMSII had less starch, free hexoses or 2-oxoglutarate; the ratio starch:solube sugars and transcript levels of the key enzyme in starch biosynthesis, ADP glucose pyrophosphorylase (AGPase), were also lower (Dutilleul et al., 2005). The levels of the TCA intermediates malate and citrate were both increased, as was the amount and activity of the phosphoenolpyruvate carboxylase (PEPc) enzyme (Dutilleul et al., 2005), an enzyme involved in anaplerotic reactions that replenish TCA intermediates during nitrogen assimilation or other biosynthetic pathways (Izui et al., 2004; Masumoto et al., 2010). The major isoform of the cytosolic isocitrate dehydrogenase, which is NADP-dependent (NADP-ICDH), was unaltered at transcript, protein, or activity levels, while the mitochondrial, NAD-dependent version (NAD-ICDH) was upregulated at all three levels (Dutilleul et al., 2005). The NADPH, but not the NADP, pool was increased, and both NAD and NADH pools were doubled, although the NAD/NADH ratio remained unchanged (Dutilleul et al., 2005), suggesting that NADH-

consuming mechanisms, like nitrogen assimilation, maintained a normal NAD/NADH ratio, consistent with previous observations (Dutilleul, Driscoll, et al., 2003).

CMSII plants accumulated glutathione (Vidal et al., 2007) and showed an increase in glutathione reductase protein levels and activity (Dutilleul, Garmier, et al., 2003). CMSII also had increased protein levels and activity of ascorbate peroxidases (Dutilleul, Garmier, et al., 2003), although the ascorbate levels were unchanged (Vidal et al., 2007). Catalase was instead not induced (Dutilleul, Garmier, et al., 2003). Both the transcript levels and activity of the mitochondria-specific ROS-detoxifying superoxide dismutase (MnSOD) were increased in CMSII (Priault et al., 2007; Vidal et al., 2007). However, the levels of H_2O_2 were lower in CMSII (Dutilleul, Garmier, et al., 2003). These results show that CMSII had a general induction of the antioxidant system but did not suffer of oxidative stress. Indeed, CMSII plants had increased resistance to both biotic and abiotic stresses (Dutilleul, Garmier, et al., 2003), which suggests that CMSII were stress acclimated. It was proposed that in CMSII some kind of mitochondrial retrograde signalling mechanism was active, which the authors attributed to the emission of ROS, that caused the acclimation and avoidance of oxidative stress, indeed scavenging ROS accumulation (Dutilleul, Garmier, et al., 2003; Vidal et al., 2007).

Another Complex I-defective mutant in tobacco is the nuclear encoded NMS1, which in general showed a growth phenotype more severe than CMSII (Brangeon et al., 2000), likely due to a different composition of partial Complex I assemblies: NMS1 retains a smaller Complex I which does not stimulate a metabolic adaption as in CMSII (Lothier et al., 2019). The activity of matrix-facing but not of intermembrane space-facing alternative NADH dehydrogenases, as well as AOX protein levels and capacity were increased in NMS1, but to a less extent than in CMSII plants (Sabar et al., 2000). In both CMSII and NMS1, net CO_2 assimilation was 25% lower than WT (Lothier et al., 2019), partially explained by lower stomatal conductance (Lothier et al., 2019; Sabar et al., 2000). The carboxylase activity of RuBisCO was reduced and ribulose-1,5-bisphosphate oxygenation-to-carboxylation ratio was 40 % higher in both CMSII and NMS1 (Lothier et al., 2019).

3.3. NCS2 in maize

Plants of one of the maize non-chromosomal stripes mutant lines, NCS2, carried a partially assembled version of the Complex I which lacked the subunit NAD4 and the membrane arm, becoming more loosely attached to the membrane (Karpova & Newton, 1999). This partially assembled complex, however, retained the NADH dehydrogenase activity (Karpova & Newton, 1999).

The stripes in NCS2 leaves were either homoplasmic or near-homoplasmic for the mutant version of nad4 (Baker & Newton, 1995) and were not completely chlorotic, but pale green (Newton & Coe, 1986). The growth of NCS2 plants varied between plants showing either low or moderate growth phenotypes (Newton & Coe, 1986). The variability of severity was true also for the kernels, with either sectors of small kernels or sectors of aborted kernels on NCS2 ears (Newton & Coe, 1986). Aborted kernels of NCS2 were homoplasmic, and embryos would stop developing at stage 3-4, point at which Complex I activity is assumed to become essential for kernel maturation (Baker & Newton, 1995).

Mitochondria of NCS2 plants exhibited reduced cristae (Roussell et al., 1991). O_2 consumption of isolated mitochondria was reduced when malate was used as substrate but showed no differences when succinate or NADH was supplied (Marienfeld & Newton, 1994). Malate fuels the production of NADH in the matrix through the TCA cycle, while externally supplied NADH is the substrate of the external NADH dehydrogenases, suggesting that the latter were active in NCS2 mitochondria while confirming that the rotenone-sensitive pathway capacity was reduced. The amount of the alternative NAD(P)H dehydrogenases was found not to be different (Karpova & Newton, 1999). The transcript and protein levels of AOX and the transcript of different heat-shock proteins (HSPs) were increased in different tissues of NCS2, despite not showing evident molecular signs of oxidative stress (Karpova et al., 2002; Kuzmin et al., 2004). Interestingly, the AOX protein induced in NCS2 had a larger apparent molecular weight, suggesting that it could be a singular AOX variant (Karpova et al., 2002). Kuzmin et al., 2004 proposed that the induction of AOX and HSPs could be the result of the accumulation of mitochondrial protein precursors in the cytosol rather than a response to oxidative stress signalling.

Chloroplasts of NCS2 plants suffered of abnormal development that resulted in fewer thylakoids, altered protein composition and the absence of starch granules (Roussell et al., 1991). Exposure to low light conditions did not alter the appearance of stripes, and therefore photodamage was discarded as the cause of the pale-green phenotype (Roussell et al., 1991). CO_2 fixation was reduced and processes downstream of photosystem II (e.g. PSI, electron transport, NADP reduction, proton gradient formation) were altered (Roussell et al., 1991).

From homoplasmic cell cultures of NCS2, Complex I was proposed to be necessary for a correct development of endosperm, but it could not be essential for germination (Yamato & Newton, 1999). A single NCS2 homoplasmic plant could be isolated, with uniformly pale green leaves, that was both male and female sterile and was shorter and smaller than heteroplasmic NCS2 (Yamato & Newton, 1999). Further studies did not follow to our knowledge.

3.4. MSC16 in cucumber

MSC16 lines in cucumber have a mild reduction in Complex I abundance and activity, which are approximately 20 % less than the WT (Juszczuk et al., 2007; Juszczuk & Rychter, 2009). These plants showed slower growth and leafspots that follow a mosaic pattern (Malepszy et al., 1996). MSC16 had increased levels and capacity of external NADH dehydrogenases (Juszczuk et al., 2007; Juszczuk & Rychter, 2009) and increased AOX levels (Juszczuk et al., 2007), although the AOX capacity and activity was not different from the WT (Florez-Sarasa et al., 2009). MSC16 mitochondria showed increased capacity for NADH oxidation and reduced capacity for exploiting malate to fuel the respiratory chain (Juszczuk et al., 2007), confirming the reduced Complex I activity. In the presence of the Complex IV inhibitor KCN, oxidation of NADH largely decreased in WT while not in MSC16. In the same experiment, oxidation of succinate and malate decreased in both genotypes, indicating that the AOX capacity was substrate-dependent (Juszczuk et al., 2007).

MSC16 plants showed a increased rate of photorespiration (Juszczuk et al., 2007). There is a small decrease of net photosynthesis. There is a large decrease in stomatal

and mesophyll conductance to CO_2, causing a lower CO_2 concentration in the chloroplasts. In general, there is lower ATP availability and slower plant growth, with strong reduction in biomass (Juszczuk et al., 2007). MSC16 had more soluble carbohydrates (Florez-Sarasa et al., 2009).

Comparing the whole cell, MSC16 protoplasts had a smaller adenylate (ATP+ADP) pool (Szal et al., 2008); this is in contrast with CMSII plants, that had a higher adenylate pool, more pronounced at night than day (Szal et al., 2008). Whilst there were no differences in the NAD(H) pool, the NADP(H) pool was smaller and more reduced (Szal et al., 2008). Through sub-compartment fractionation, chloroplasts of MSC16 were found to have less ATP and a more reduced NADP(H) pool (Szal et al., 2008). The mitochondrial NAD(H) pool was more oxidized, and cytosolic NAD(H) and NADP(H) pools were more reduced and more oxidized, respectively (Szal et al., 2008).

Cold stress would increase the antioxidant defence systems in WT but not in CMS16, where antioxidants were already high (Szal et al., 2009). MSC16 leaf extracts had less total H_2O_2 compared to the WT, but mitochondrial superoxide generation in the direction of the intermembrane space was increased (Szal et al., 2009). The authors proposed that the increase of H_2O_2 in the intermembrane space might act as a signal for induction of AOX and other protective genes through retrograde signalling (Szal et al., 2009).

3.5. Main Complex I-deficient mutants in Arabidopsis

3.5.1. *ndufs4*

During a forward genetics experiment where Arabidopsis plants were screened for a defective induction of stress markers after cold stress, the mutant *frostbite1* (fro1) was identified (Lee et al., 2002). The locus fro1 encodes the 18-kDa Fe-S subunit of Complex I NDUFS4, and the finding established a link between mitochondria and cold induction of nuclear gene expression (Lee et al., 2002). *ndufs4* plants (the alternative names *ndufs4* and *fro1* are used in different publications) carry a point mutation that result in mis-splicing

and premature stop (Lee et al., 2002), which translates in a disassembled and completely non-functional Complex I (Meyer et al., 2009; Podgórska et al., 2015).

Although Complex I activity is completely lost, dark respiration rate was unaltered in *ndufs4* plants (Meyer et al., 2009), showing that the flow of electrons through the chain was the same than the WT despite the loss of one proton-pumping site (the Complex I); accordingly, *ndufs4* plants had reduced capacity for ATP synthesis (Meyer et al., 2009) and a lower ATP/ADP ratio (Podgórska et al., 2015). Isolated *ndufs4* mitochondria showed increased capacity of the external NADH dehydrogenases but not higher capacity of the AOX, despite accumulating more AOX protein (Meyer et al., 2009). An increase in cyanide-insensitive respiration was instead reported from experiments done on cut leaves (McCollum et al., 2019). Both the NAD(H) and the NADP(H) pools were more than doubled in *ndufs4* plants (McCollum et al., 2019). The NAD(H) pool was always more oxidized, while the NADP(H) pool was more oxidized at the end of the day and more reduced at the end of the night (McCollum et al., 2019).

A microarray experiment on samples harvested at the middle of the day showed that the photosynthetic machinery, but not the Calvin cycle components, was transcriptionally induced in *fro1* (Meyer et al., 2009), although the protein levels of photosynthetic machinery were unaltered (Meyer et al., 2009). *ndufs4* plants showed reduced efficiency of photosynthesis, as both the electron transport rate (ETR) and the photochemical energy dissipation (ψ_{PSII}) were significantly lower (Meyer et al., 2009).

ndufs4 plants had general alterations of central catabolism, accumulating amino acids and organic acids (Meyer et al., 2009; Pétriacq et al., 2017) in a pattern mostly consistent with what has been described for tobacco CMSII and NMS1 (Dutilleul et al., 2005; Lothier et al., 2019). However, metabolic fluxes through glycolysis and the TCA cycle were described as barely altered in *ndufs4* (Kühn et al., 2015). When *ndufs4* plants were grown using nitrate as the only source of nitrogen, sugars were directed towards nitrogen assimilation and energy production, and the integration of cellulose into the cell wall was restricted (Podgórska et al., 2018). When reduced NH_4^+ was used as the sole source of nitrogen instead, which caused growth defects on the WT, the growth of *ndufs4* improved and the cell wall assembly was restored (Podgórska et al., 2015, 2018). In these

conditions, *ndufs4* had increased capacity of both the rotenone-insensitive NADH dehydrogenases and the Complex IV-mediated cyanide-sensitive pathway (Podgórska et al., 2015). The authors described a tight connection between the mitochondrial redox system and the apoplastic levels of pH and ROS, which in turn could alter the plasticity of the wall and modulate the growth (Podgórska et al., 2015, 2018).

3.5.2. Targeting the carbonic anhydrase domain

In plants, Complex I contains a spherical extra-domain located facing the matrix defined as an heterotrimer of three carbonic anhydrase (CA) subunits (Sunderhaus et al., 2006). The genome of Arabidopsis encodes five structurally related subunits representing γ-type carbonic anhydrases, which are termed CA1, CA2, CA3, CAL1 and CAL2 (Peters et al., 2013), but only three copies of this group of proteins form an individual extra domain (Fromm, Senkler, Zabaleta, et al., 2016).

An Arabidopsis mutant lacking CA2 showed an 80% reduction in Complex I levels, although it had normal growth rate and fertility (Perales et al., 2005). Cell cultures from this *ca2* mutants had reduced rate of cyanide-sensitive respiration and reduced growth (Perales et al., 2005). The overexpression of CA2 caused a decrease in Complex I activity, verified by reduced respiration of leaves, which was rotenone-insensitive (Villarreal et al., 2009). CA2-overexpressors were male sterile, likely to a defective production of ROS for H_2O_2-dependent polymerization of lignin, which is required for proper anther development (Villarreal et al., 2009).

The targeting of the carbonic anhydrase domain to achieve Complex I depleted lines in Arabidopsis was pursued in parallel by two independent groups, by generating *ca1ca2* double knockouts. One group reported that seeds of *ca1ca2* mutants were able to germinate with a delay of 12 days compared to WT seeds, but they would die immediately due to oxidative stress (Córdoba et al., 2016). The other group crossed the homozygous *ca1/ca1* and *ca2/ca2* plants and obtained all the possible combinations but the double KO, as seeds would not germinate (Fromm, Braun, et al., 2016). However, this same group reported an embryo rescue method in the presence of high sucrose, so

double homozygous *ca1ca2* plants could be eventually obtained, that completely missed Complex I (Fromm, Braun, et al., 2016).

ca1ca2 embryos showed impaired mitochondrial membrane potential and accumulated ROS in mitochondria (Córdoba et al., 2016). *ca1ca2* plants obtained through the embryo rescue method had increased levels of Complexes II, IV and AOX, as well as increased rate of oxidation of organic substrates (Fromm, Senkler, Eubel, et al., 2016). The rate of respiration of isolated mitochondria was significantly increased (Fromm, Braun, et al., 2016). Proteomics experiments showed an increase in proteins involved in respiration, such as enzymes involved in glycolysis or the TCA cycle, and branched-chain amino acid catabolism, as well as a reduction in proteins involved in photosynthesis affecting the light reactions, carbon fixation and photorespiration (Fromm, Senkler, Eubel, et al., 2016). The growth delay in *ca1ca2* plants was in part attributed to a reduction in photosynthesis (Fromm, Senkler, Eubel, et al., 2016). The protein levels of ROS-protective antioxidants were strongly increased in *ca1ca2* (Fromm, Senkler, Eubel, et al., 2016).

The role of proteins CAL1 and CAL2 has also been assessed. The single homozygous mutants *cal1* and *cal2* showed no phenotype, but the double homozygous mutants *cal1cal2* failed to germinate (Q. Wang et al., 2012). By following a knockdown approach, cal2 was silenced in a cal1 KO background, yielding Δcal1/cal2i plants (Q. Wang et al., 2012). These plants had up to a 95 % reduction in Complex I and a strong reduction in malate-dependent O_2 consumption of isolated mitochondria (Fromm, Göing, et al., 2016). Proteomics experiments suggested that these plants had a reduced capacity for glycine-serine conversion during photorespiration, enhanced capacity for glutamate and pyruvate breakdown and induction of biosynthesis of several stress-related proteins was clearly induced in the mutant (Fromm, Göing, et al., 2016).

3.5.3. *ndufs8* and *ndufv1*

Another mutant line in Arabidopsis with undetectable levels of Complex I is a double knockout that misses the two isogenes encoding for the Complex I subunit NDUFS8 (Pétriacq et al., 2017). *ndufs8* plants showed a significant growth retardation,

described as similar to that of *ndufs4* plants (Pétriacq et al., 2017). Both the AOX content and *in vivo* activity were higher in *ndufs8*, as were the levels of H_2O_2 and transcripts of antioxidants in *ndufs8* illuminated leaves, although there were photoperiod-dependent differences (Pétriacq et al., 2017). Monitoring of the metabolome showed that metabolism was less responsive to the short-to-long day transition in the mutants (Pétriacq et al., 2017). Net CO2 fixation was reduced at high light intensities, but not different at mid and low intensities (Pétriacq et al., 2017). The authors proposed that alterations in redox homeostasis and NAD/NADH ratio had an impact on the phenotype of *ndufs8* mutants and their capacity to adapt to different photoperiods and suggested mitochondrial ROS to trigger retrograde signalling in the mutants (Pétriacq et al., 2017).

Kühn et al., 2015 described another Arabidopsis line with reduced Complex I activity, *ndufv1*, and compared it to the already mentioned line *ndufs4*, with complete loss of Complex I activity. *ndufv1* had a more severely impacted growth than *ndufs4* and increased metabolic fluxes through glycolysis and the TCA cycle, compared to both WT and *ndufs4*. In both mutants, the NAD(H) pool increased but the NAD/NADH ratio did not change. Transcriptomics experiments found increased expression of the genes of the respiratory pathways (glycolysis, TCA cycle, respiratory chain) and specific catabolic pathways like amino acid degradation. A reduction was seen in the expression of genes encoding components of pathways that are particularly energy demanding such as cell wall biosynthesis and synthesis pathways for secondary metabolites and storage proteins.

3.6. Other Complex I deficient mutants

The mutants reported so far are the ones for which the largest set of molecular characterization has been produced. Other mutants with altered Complex I levels have been described, although with less detail in terms of their molecular and metabolic profile. Most of them have been obtained not targeting structural subunits, but key players in the biogenesis of complex. One example are mutants depleted in the enzyme L-Galactono-1,4-lactone dehydrogenase (GLDH), which were found to lack a functional

Table 1 | **Most relevant Complex I mutants obtained by targeting PPR proteins or maturases**. For a detailed review, see Colas Des Francs-Small & Small, 2014.

		Target	Affected subunit	Consequences	Ref
Arabidopsis	**PPR**	OTP43	NAD1	Undetectable CI AOX induction Growth defects	De Longevialle et al., 2007
		BIR6	NAD7	Decreased CI AOX induction Mild growth defects	Koprivova et al., 2010
		RUG3	NAD1	Decreased CI Increased protein import in mitochondria	Kühn et al., 2011
		SLG1	NAD3	Decreased CI Lowered ATP production	Yuan et al., 2012
		MTSF3	NAD2	Less CI assembly AOX induction	C. Wang et al., 2022
		MSP1	NAD1	Seed abortion	Best et al., 2022
		mTERF15	NAD2	Undetectable CI Altered mitochondria Growth retardation	Hsu et al., 2014
	Maturases	nMAT1	NAD1, NAD2, NAD4	Decreased CI activity Altered respiration AOX induction Growth defects	Keren et al., 2012; Nakagawa & Sakurai, 2006
		nMAT2	NAD1, NAD7, COX2	Decreased CI activity	Keren et al., 2009
		nMAT3	NAD1	Complex I defects Altered respiration	Shevtsov-Tal et al., 2021
		nMAT4	NAD1	Decreased CI activity Development defects Altered mitochondria AOX induction	Cohen et al., 2014
Maize	**PPR**	DEK10	NAD3, COX2	Decreased CI activity Less CIV abundance	W. Qi et al., 2017
	Maturases	nMAT1	NAD1, NAD4	Decreased CI activity	Fan et al., 2022
		nMAT3	NAD1	Decreased CI activity	Chen et al., 2021

Complex I (Schimmeyer et al., 2016); physiological studies have not been performed on them to our knowledge. A common approach has been the generation of surrogate mutants by targeting either pentatrico peptide repeat (PPR) proteins involved in RNA editing during mRNA maturation, or maturases, nuclear-encoded proteins that play a crucial role in the splicing and maturation of group-II introns in Arabidopsis mitochondria (Keren et al., 2009; Table 1). Arabidopsis contains four maturase-related nuclear genes,

which reside within mitochondria and act in trans to facilitate the splicing of organellar-encoded introns (Keren et al., 2009). Mutants defective in all form isoforms have been isolated, and all of them have defects in Complex I subunits. However, we must take into consideration that PPR proteins or maturases do not always have a unique target, and therefore their depletion can lead to defects in multiple transcripts and proteins.

4. Land plants with altered levels of Complex II

4.1. Complete depletion of Complex II is incompatible with life

In contrast with the large number of Complex I mutants, land plants completely depleted in Complex II activity have not been isolated so far. Complex II, despite having a partially overlapping function with Complex I, holds the unique property of being a component of the TCA cycle, and this is likely the cause by which its depletion is lethal. Also, Complex II seems to be the main pathway to fuel the respiratory chain in heterotrophic tissues (Peters et al., 2012), making its depletion even more detrimental during energy-demanding life stages where photosynthesis is not active, such as germinating seeds (Bentsink & Koornneef, 2008). However, different mutants with reduced levels of Complex II have been isolated in different plant models, as we will now review.

4.2. Heterozygous *sdh1* mutants

The Complex II subunit SDH1 is a flavoprotein that holds the succinate-binding site, and therefore it is essential for the enzymatic activity of the complex. SDH1 in Arabidopsis is encoded by two nuclear genes, sdh1-1 and sdh1-2, the first showing higher transcript levels than the second (Figueroa et al., 2002). Accordingly, *sdh1-2* homozygous plants did not show any growth defects (León et al., 2007). Oppositely, *sdh1-1* homozygous plants were not viable and only heterozygous SDH1-1/*sdh1-1* could be isolated, showing that SDH1-1, and Complex II, are essential for gametophyte development in Arabidopsis (León et al., 2007).

To our knowledge, the expected decrease of succinate dehydrogenase activity in SDH1-1/*sdh1-1* plants has not been quantified. SDH1-1/*sdh1-1* plants showed a normal sporophyte development, but pollen development was altered (León et al., 2007). SDH1-1/*sdh1-1* plants had 30% higher CO_2 assimilation rates, that could be explained by an increase of stomatal conductance (Fuentes et al., 2011). The mutants showed 1.7 to 2.3-fold increase of shoot biomass under short-day conditions, with the differences with the WT disappearing under long-day conditions (Fuentes et al., 2011). Furthermore, when

grown under nitrogen-limiting conditions, the mutants grew better and had a greater uptake of nitrate (Fuentes et al., 2011).

4.3. An altered version of SDH1-1: *dsr1*

Another mutant altered in Complex II was identified during the screening of a collection of mutagenized seedlings, looking for mutants that had lost the ability to induce the stress marker GSTF8 after treatment with salicylic acid (Gleason et al., 2011). A mutant was identified, *dsr1*, that carried a point mutation in the sequence of SDH1-1 which caused an Ala-to-Thr substitution (Gleason et al., 2011). This mutant had 80 % less succinate dehydrogenase activity than WT but did not show any of the defects previously described on the heterozygous SDH1-1/*sdh1-1* mutants (Gleason et al., 2011). *dsr1* plants had lowered levels of mitochondrial ROS (Gleason et al., 2011). Experiments on *dsr1* and another line deficient in Complex II, *sdhaf2* (described below), confirmed that the Complex II has an important role in the production of ROS for signalling, particularly for salicylic acid-dependent stress signalling (Belt et al., 2017; Gleason et al., 2011).

4.4. SDH2 mutants in Arabidopsis

Another essential subunit of Complex II is SDH2. In Arabidopsis, it is encoded by three nuclear genes (sdh2-1, sdh2-2, sdh2-3). sdh2-1 and sdh2-2 are the main expressed isoforms during most of the life cycle of Arabidopsis, while sdh2-3 is the dominant isoform during embryo development (Elorza et al., 2004, 2006; Figueroa et al., 2001, 2002). SDH2-3 was not detected in the adult mitochondrial proteome (Heazlewood et al., 2004); accordingly, s*dh2-3* homozygous mutants showed a delay in germination but did not have phenotypic defects during vegetative nor reproductive growth (Roschzttardtz et al., 2009). *sdh2-1* homozygous mutants did not show any observable phenotypes, which suggests functional redundance between sdh2-1 and sdh2-2 genes (Elorza et al., 2004). We are not aware of mutants of the sdh2-2 gene.

Respirometry on cut leaves showed reduced dark respiration and increased cyanide-resistant respiration in *sdh2-1* plants (McCollum et al., 2019). The NADP(H) pool was more oxidized at the end of the day and more reduced at the end of the night

(McCollum et al., 2019). A three-fold accumulation of succinate was reported (McCollum et al., 2019), supporting a reduced Complex II activity in these plants.

4.5. *sdh2-2* knockdown in tomato

For the SDH2 subunit, we have additional information coming from knockdown mutants in tomato, where it is encoded by two nuclear genes, sdh2-1 and sdh2-2. Araújo et al., 2011 used an *A. tumefaciens*-based RNA silencing approach to target the sdh2-2 gene, which in WT is near-constitutively expressed. sdh2 knockdown (*sdh2*^{KD}) lines in tomato, with up to 75 % less succinate-dependent O_2 consumption, had a reduced flux through the TCA cycle and increased photosynthetic rates, that translated in increased biomass (Araújo et al., 2011). The mutants showed increased stomatal conductance, which was depicted as the main cause of the increase in biomass (Araújo et al., 2011). From this study, the authors concluded that the reduction of Complex II activity caused changes in the levels of organic acids in mesophyll cells, with consequences in guard cells that caused an eventual increase of stomata conductance (Araújo et al., 2011). The study provided evidence for the importance of mitochondrial metabolism, specifically the TCA cycle, in regulating stomatal function and influencing photosynthesis and growth in plants.

4.6. The assembly factors SDHAF1 and SDHAF2

Huang et al., 2009 described a previously uncharacterized peptide from the mitochondrial proteome of Arabidopsis which was later identified as SDHAF2 (Succinate Dehydrogenase Assembly Factor 2) by similarity to its human homolog (Huang et al., 2013), which is responsible of FAD insertion into SDH1 (Hao et al., 2009). The same authors studied two Arabidopsis T-DNA lines with a disrupted sdhaf2 gene (Huang et al., 2013). One of them, affected in one intron, could not be isolated in homozygosity, and it was postulated to be lethal during early development (Huang et al., 2013). The second line had an insertion in amino acid 17, within an exon in the predicted presequence, and could be isolated in homozygosity (Huang et al., 2013).

Homozygous *sdhaf2* lines accumulated 50 % less SDHAF2 and 70 % less SDH1-1 in mitochondria, and had a reduction in Complex II of 60-70 %, measured by *in vitro* activity, in gel activity and respirometry (Huang et al., 2013). *sdhaf2* plants did not show any growth defects in shoots under either long- or short-day conditions, and authors could not find differences in terms of photosynthetic efficiency or stomatal conductance (Huang et al., 2013). A strong phenotype was instead observed in roots, as the rate of primary root elongation in seedlings was strongly reduced in *sdhaf2* lines (Huang et al., 2013). A decrease of approximately 50% of total respiration was reported in roots, and the root defects could be replicated in WT plants treated with the Complex II inhibitor malonate (Huang et al., 2013). Metabolite analyses showed a more than 6-fold accumulation of succinate in the mutants, that was even higher in roots (Huang et al., 2013). Leaves accumulated different organic acids and amino acids, while in roots these metabolites remained unchanged or lower (Huang et al., 2013). The root phenotype in *sdhaf2* lines was strongly dependent on pH, as root elongation was not different than WT at pH 7.0 but dropped rapidly with a slight decrease in pH (Tivendale et al., 2021). SDH activity in roots was found to be dependent on the pH, being lower at pH and increasing with lower pH values, whilst *sdhaf2* mutants had a constant SDH activity regardless of pH that was the same for the WT at pH 7 (Tivendale et al., 2021). Therefore, *sdhaf2* roots could not adapt their SDH activity upon acidification of the media. Transcriptomics of roots at acidic pH showed a reprogramming of H_2O_2-related metabolism, highlighting a complex interplay between mitochondrial function, ROS levels, auxin signalling, and root growth in response to pH changes (Tivendale et al., 2021).

More recently, knockdown lines of the related SDHAF1 protein, required for SDH2 biogenesis, have been generated (Y. Li et al., 2022), as knock-out lines were not available. Knockdown lines have approx. 25 % less SDH activity measured as succinate-dependent O_2 consumption (Y. Li et al., 2022). Further physiological analysis on the plants did not follow.

(Belt et al., 2018) studied another assembly factor of Complex II, called SDHAF4. In other eukaryotes, this protein is involved in the assembly of SDH1 and SDH2. They used a T-DNA insertion line, *sdhaf4*, that retained 40% of transcript levels but completely

lost protein levels and was considered a knockout for SDHAF4. Complex II activity levels were significantly reduced, with halved succinate-dependent respiration and doubled accumulation of succinate in total extracts. However, the homozygous *sdhaf4* knockout lines showed no growth defects in shoots or roots.

5. Land plants with reduced capacity of the cyanide-sensitive pathway

5.1. Targeting Complex III or Cytochrome c

Alterations in Complex III, Cytochrome c or Complex IV have the same impact on the mETC, i.e. the depletion of the cyanide-sensitive pathway. However, the phenotypes of the single KO can be different due to the specific roles of each individual component. Cytochrome c is required for the stability of Complex IV in yeast and mammals (Barrientos et al., 2003; Vempati et al., 2009) and, accordingly, mutants with altered levels of Cytochrome c also showed reduced levels of complexes IV (Welchen et al., 2012).

Until recently, the only mutant in Arabidopsis with reduced activity of Complex III was the mutant of the pentatricopeptide protein PPR40 (Zsigmond et al., 2008). While levels of Complex III were normal, cyanide-sensitive respiration was reduced in *ppr40* isolated mitochondria (Zsigmond et al., 2008). *ppr40* plants were smaller than WT and were more sensitive to different types of stress, including ABA treatment, salt stress or oxidative stress (Zsigmond et al., 2008). Respiration rate of isolated mitochondria was reduced when fuelled with NADH or succinate, but increased when fuelled by ascorbate, which can donate electrons directly to cytochrome c (Zsigmond et al., 2008). The AOX capacity was higher, as were the transcript levels of Aox1d (Zsigmond et al., 2008). The expression levels of Aox1a have not been reported. Isolated mitochondria showed increased superoxide dismutase activity and H_2O_2 accumulation, and leave extracts had higher lipid peroxidation (Zsigmond et al., 2008), suggesting that *ppr40* suffered of moderate oxidative stress.

More recently, another line has been described in Arabidopsis, *ucr8*, carrying an insertion in an intron of the gene ucr8 that encodes subunit 8 of Complex III (McCollum et al., 2019). *ucr8* are knockdown lines where the transcripts are reduced a 90 % compared to the WT (McCollum et al., 2019). Total respiration in *ucr8* leaves was reduced by 40 %, and AOX capacity was increased (McCollum et al., 2019). At the end of the night, the NADPH/NADP+ ratio was higher and the NADH/NAD+ ratio was lower (McCollum et al., 2019).

Other groups managed to generate lines with highly reduced levels of cytochrome c. In Arabidopsis, there are two redundant genes that encode cytochrome c: cytc1 and cytc2. Single homozygous *cyt1* and *cyt2* knockout mutants could be obtained, but the double knockout *cyt1cyt2* could not be isolated, suggesting that cytochrome c is essential for life (Welchen et al., 2012). By knocking out cyt2 in a silenced cytc1 background, *cytc1^{KD}cyt2^{KO}* mutants were obtained which had very low levels of cytochrome c and lower levels of Complex IV subunits (Welchen et al., 2012). *cytc1^{KD}cyt2^{KO}* lines presented a delay in development, although the final growth was unaltered (Racca et al., 2018; Welchen et al., 2012).

Although a significant decrease in cytochrome c oxidase (Complex IV) activity was reported in *cytc1^{KD}cyt2^{KO}* mitochondrial extracts (Welchen et al., 2012), the cyanide-sensitive pathway was not strongly impaired in *cytc1^{KD}cyt2^{KO}* lines (Florez-Sarasa et al., 2021). Total respiration was slightly reduced in *cytc1^{KD}cyt2^{KO}* lines (Florez-Sarasa et al., 2021; Racca et al., 2018). The Aox1a transcript levels were slightly reduced in *cytc1^{KD}cyt2^{KO}* lines, while protein levels were not different from the WT (Florez-Sarasa et al., 2021). *In vivo* partitioning showed that the cyanide-sensitive pathway activity was reduced by only a 10 % in *cytc1^{KD}cyt2^{KO}* lines, with a similarly low increase of the cyanide-insensitive pathway activity (Florez-Sarasa et al., 2021). An increased expression of ascorbate peroxidase, ascorbate oxidase and peroxisomal catalase was reported, although a general increase in ROS was not detected in *cytc1^{KD}cyt2^{KO}* plants (Welchen et al., 2012).

Photosynthesis did not have major alterations in *cytc1^{KD}cyt2^{KO}* (Racca et al., 2018; Welchen et al., 2012). At the beginning of the day, mutants accumulated more soluble sugars (glucose, fructose), fumarate and some amino acids (phenylalanine, leucine, valine, isoleucine) (Racca et al., 2018). Accordingly, the expression of sugar-induced and sugar-repressed genes were higher and lower in C lines, respectively (Racca et al., 2018). The plants had increased rate of starch synthesis during day that caused starch accumulation at the end of the day; however, the starch was totally degraded during the night (Racca et al., 2018). Interestingly, *cytc1^{KD}cyt2^{KO}* plants showed increased starch accumulation during the light period but also an increased degradation during the night.

Interestingly, gibberellic acid (GA) homeostasis was altered in plants, and treatment with GA reduced the glucose levels and abolished the growth delay (Racca et al., 2018).

There are other examples of lines with reduced cytochrome c levels. One of them lacks WTF9, a mitochondrial protein required for splicing of pre-mRNA of ccmFc, a component of the cytochrome c maturation system (des Francs-Small et al., 2012). The mutants have severely reduced proteins levels of Cytochrome C, Cytochrome C1 (a subunit of Complex III) and COX2 (a core subunit of Complex IV) (des Francs-Small et al., 2012). Complexes III or IV were not detected by BN-PAGE, and a strong increase in AOX protein levels was reported (des Francs-Small et al., 2012). *wtf9* mutants grew with severe developmental defects and developed anormal flowers that did not yield any viable seeds (des Francs-Small et al., 2012).

One group targeted the protein OXA2A, which is required for the synthesis of c-type cytochromes in mitochondria, for depleting the Cytochrome c. Since oxa2a homozygous knockout (KO) plants were not available, a system was designed so oxa2a KO were complemented with a version of oxa2a controlled by an embryo-specific ABI3 promoter (Kolli et al., 2020). This allowed the plants to grow, but they were much smaller and showed important growth defects (Kolli et al., 2020). The mutants presented a strong reduction in Complex III activity, as well as in Complex III dimer and Complex I-III supercomplex abundances (Kolli et al., 2020).

Surrogate mutants have also been obtained by targeting PPR proteins, as described previously for Complex I mutants. This is the case of a knockout mutant in the moss *Physcomitrium patens* lacking PPR protein PPR_65, involved in editing of ccmFc mRNA (Schallenberg-Rüdinger et al., 2013). *ppr65* lines in *P. patens* showed a severe developmental delay, as mosses had to be incubated for several months to have enough material for downstream experimentation (Schallenberg-Rüdinger et al., 2013); detailed physiological analyses of this plants are not reported.

There are also some reported attempts to generate mutants with altered levels of cytochrome c in Arabidopsis which failed. One of these attempts targeted an essential component of the c-type cytochrome maturation pathway, CCMH, but homozygous KO plants could not be isolated, as embryos would arrest development (Meyer et al., 2005).

Another group successfully knocked out RPF3, an RNA processing factor which was thought to be required for cytochrome c biogenesis, but the KO mutants did not have any growth phenotype or defects in the respiratory chain, and therefore it was concluded that RPF3 was not essential for cytochrome c biogenesis (Jonietz et al., 2012).

5.2. Land plants with altered levels of Complex IV

5.2.1. Non-chromosomal stripe (NCS-) -5 and -6 mutants in maize

The first mutants with reduced or depleted Complex IV were probably the family of non-chromosomal stripe (NCS) mutants in maize, including NCS5 and NCS6, and some cytoplasmic male sterile (CMS) plants (Dixon & Leaver, 1982). The NCS5 mutant showed yellow stripes in the leaves, which was linked to a deficiency of Complex IV (Newton et al., 1990). However, we did not find any further works describing NCS5.

NCS6 mitochondria had reduced cristae and little intermembrane space but were not different in size (Gu et al., 1993). *In vitro* homoplasmic lines of NCS6 (*cox2*) could be obtained and studied, which were unable to regenerate any roots or shoots from calli (Gu et al., 1994). NCS6 chloroplasts were less in number, with a less well-developed membrane system, less thylakoids, less chlorophyll, and less chlorophyll-protein I complex of PSI (CPI) (Gu et al., 1993). There were no differences in protein composition of PSII, but there was a reduction of several PSI proteins, as well as of transcript levels of chloroplast-encoded PSI subunits (which were reduced more than 50%) (Jiao et al., 2005). Some nuclear-encoded subunits were also reduced at different extent, and ferredoxin and FNR transcripts were lower (Jiao et al., 2005). CO_2 fixation was found to be extremely reduced in the yellow stripes (Gu et al., 1993). CO_2 assimilation rate was reduced by 85 % and O_2 respiration rate was decreased by 67 % in yellow sectors, with green sectors not being different to WT (Jiao et al., 2005). Because of these structural alterations in chloroplasts, NCS6 is not the best model to study the impact of Complex IV deficiency.

5.2.2. The assembly factors HCC1 and HCC2

SCO (for Synthesis of Cytochrome c Oxidase) proteins were first identified in the yeast *Saccharomyces cerevisiae* as an essential component for the biogenesis of the Complex IV. Arabidopsis genome encodes two orthologs of SCO, named HCC1 and HCC2 (Attallah et al., 2011). Homozygous *hcc2* knockouts could be isolated, with no apparent growth defects (Attallah et al., 2011), suggesting that HCC2 is likely not involved in the biogenesis of Complex IV in Arabidopsis. On the other hand, homozygous *hcc1* plants could not be isolated: *hcc1* embryos aborted at the torpedo stage, where cytochrome c oxidase (Complex IV) activity was very low (Attallah et al., 2011; Steinebrunner et al., 2011). HCC1 localizes in mitochondria and is required for the delivery of Cu^{2+} during the assembly of Complex IV (Steinebrunner et al., 2011). Complementation of lethal *hcc1* homozygosity with a version of hcc1 controlled by an embryo-specific promoter allowed embryos to develop, but seedlings did not grow into mature plants (Steinebrunner et al., 2014), remarking the importance of Complex IV for plant development.

5.2.3. The assembly factor COX11

Another assembly factor that has been targeted is COX11, a protein with an evolutionary conserved role in the biogenesis of Complex IV (see Figure 1.5). In 2013, research on cytoplasmic male sterile (CMS) lines of rice identified COX11 as the interactor of another protein in a mechanism that caused CMS (Luo et al., 2013). The authors suggested that COX11 in rice might have a role in degradation of H_2O_2 (Luo et al., 2013), as it had already been described for the COX11 homolog in *Saccharomyces cerevisiae* (Veniamin et al., 2011). In Arabidopsis, COX11 was shown to have an antioxidative role independent of its role as an assembly factor of the Complex IV (Radin et al., 2021). Arabidopsis homozygous *cox11* lines could not be isolated, but both knockdown and overexpressing lines have been reported (Radin et al., 2015). Both lines showed a decreased cytochrome c oxidase activity, between 45 % and 80 % of the WT levels, and a 2-4-fold increase in Aox1a transcripts (Radin et al., 2015). Silenced lines showed root growth inhibition, smaller rosettes, and curled leaves (Radin et al., 2015).

5.2.4. The PPR protein COD1

The approach of targeting PPR proteins required for the maturation of transcripts encoding for mitochondrial proteins, described earlier for Complex I mutants, has also been applied for isolating surrogate mutants of the Complex IV. Following this approach, Dahan et al., 2014 targeted the gene cod1 (cytochrome c oxidase deficient 1), which encodes a PPR protein needed for cytosine-to-uracil editing of Cox2 mRNA. Homozygous *cod1* seeds were not able to germinate *in vitro* on a mineral growth medium, but *cod1* mutants could be germinated from immature seeds by plating them successively on a high- and low-sugar medium supplemented with cofactors and nutrients (Dahan et al., 2014). Only after several weeks in a growth chamber homozygous *cod1* seeds could germinate, and their subsequent growth was retarded, very slow and associated with anarchical development (Dahan et al., 2014). *cod1* plants showed particularly compromised root development, altered respiratory electron flow partitioning and a re-orchestrated carbon and nitrogen primary metabolism (Dahan et al., 2014). The activity levels of Complex IV were undetectable (Dahan et al., 2014). However, as happens for surrogate mutants in general, one cannot exclude the mutation of the PPR protein-encoding gene *Cod1* to affect the maturation of other mRNAs, causing pleiotropic effects. Moreover, the strong phenotype of the plants made it difficult to identify specific consequences of Complex IV loss.

5.2.5. Other plants with altered Complex IV levels

Besides HCC1/2, COD1 and COX11, other mutants with reduced levels of Complex IV activity have been reported, but we have little or no information about their physiology or metabolism.

There are some examples in Arabidopsis, where proteins have been targeted for their putative homology with assembly factors of Complex IV in other organisms. For example, Mansilla et al., 2015 studied the protein AtCOX10. Homozygous *cox10* KO plants could not be isolated, and heterozygous COX10/*cox10* mutants plants presented seeds with aborted embryos that lacked Complex IV activity. Heterozygous COX10/*cox10* plants had lower levels of Complex IV activity; total respiration was unaltered, although

plants showed increased cyanide-insensitive and reduced cyanide-sensitive capacities (Mansilla et al., 2015). These plants had accelerated senescence-related processes (Mansilla et al., 2015).

Another example is COX17, encoded by two genes in Arabidopsis. Silencing both genes produced plants that had growth defects but normal levels of Complex IV (Garcia et al., 2016). The authors claimed that some plants aborted before developing, and they suggest that those could be lines where the strong silencing of the genes caused a severe reduction in Complex IV activity that was not compatible with life.

A more recent example regards the assembly factor OXA2B in Arabidopsis, which is required for membrane insertion of the Complex IV core subunit COX2 into the inner mitochondrial membrane (Kolli et al., 2019). OXA2B homozygous plants were embryo lethal, but Kolli et al., 2019 could complement them with a truncated version of OXA2b that misses a tetratricopeptide repeat (TPR) domain. These truncated-OXA2b-complemented plants had very low levels of Complex IV activity and showed a strong growth retardation at all live stages. To our knowledge, these plants have not been further studied from a physiological point of view.

As another case, homozygous KO plants of the gene AtSurfeit1a, which is likely involved in Complex IV biogenesis, could not be isolated (Gras et al., 2020). Aborted homozygous *surfeit1a* embryos had very low Complex IV activity, suggesting that this might be the cause of embryo lethality (Gras et al., 2020).

6. Land plants with altered levels of Complex V

Several of the reported cytoplasmic male sterile plant lines are reported to carry defects that cause alteration in the levels of Complex V, as reviewed by Zancani et al., 2020. However, we found few examples of phenotypic characterization of plants with altered Complex V activity.

One example comes from the generation of Arabidopsis plants with reduced levels of two structural subunits, whose complete depletion was not viable, which showed impaired vegetative development, stunted growth, and abnormalities in leaf morphology (Robison et al., 2009). Leaves of these plants showed increased respiration and accumulated amino acids mostly at night (Robison et al., 2009). The transcript levels of Aox1a were increased (Robison et al., 2009).

By using a custom-designed PPR protein, Yang et al., 2022 generated Arabidopsis plants with reduced levels of the Complex V subunit ATP1 and of the overall Complex V. These plants showed delayed vegetative growth, reduced fertility, and lowered rates of ATP synthesis in mitochondria, although the energy charge was not altered (Yang et al., 2022).

7. *Physcomitrium patens*: a model for respiratory mutants

We reviewed the most relevant embryophyte mutants available with altered levels of respiration. In the following chapters, we will describe the characterization of three mutant lines depleted in Complex I, Complex IV or Complex V in the model organism *Physcomitrium patens*. *P. patens* is a bryophyte, and within bryophytes it is a moss of the Funariaceae family. The relationship among these groups is summarised in Figure 1.8. Bryophytes are the closest extant relatives of early terrestrial plants. Unlike their vascular relatives (the tracheophytes), the bryophytes are characterised by an ontogenetic cycle with an haploid dominant phase (Figure 1.9). The diploid phase, represented by the sporophyte, is reduced and grows at the expense of the gametophytic generation.

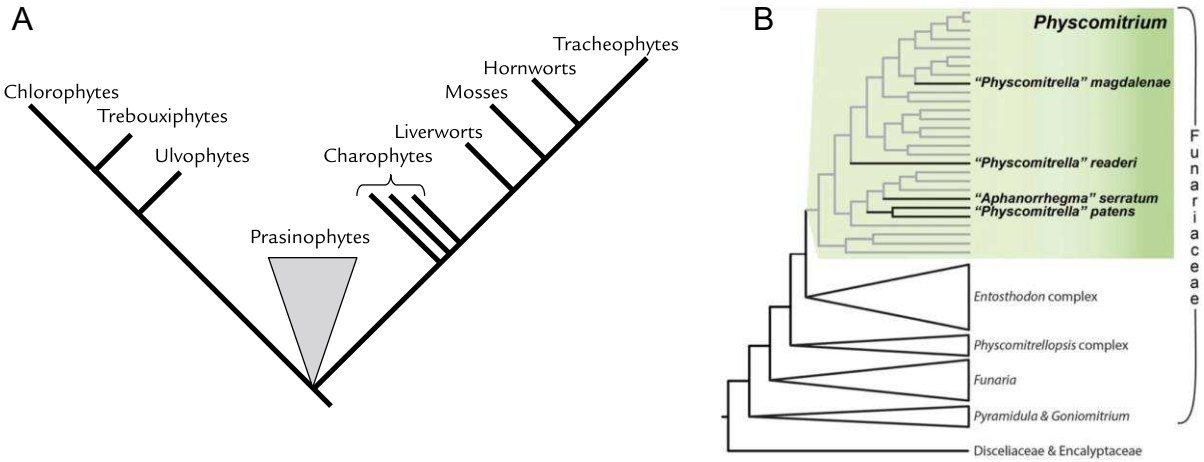

Figure 1.8 | **The taxonomic position of *Physcomitrella patens***. (A) Summation of the currently hypothesised cladistic relationships of green plants. *Chlamydomonas* and *Volvox* are members of the farthest left clade, while flowering plants are nested well up in the farthest right clade. The marine green algae are in the Ulvophytes. The Prasinophytes are a residual group of unicells whose relationships are not yet clear. The Charophytes are a paraphyletic assemblage of land plant relatives that include *Chara*, *Coleochaete* and *Spirogyra*. Within mosses, *P. patens* is a member of the Funariaceae. Adapted from Mishler & Oliver, 2009. B) Summarised phylogeny of Funariaceae, from Rensing et al., 2020.

The Gransden ecotype of the moss *P. patens* was established as a model species based on cultures derived from a single spore of a sample collected by the botanist Harold Whitehouse from a site in Gransden Wood (Huntingdonshire, United Kingdom) in 1962. Until the 1980s, this organism was mainly used as a genetic system to isolate and study mutants in different processes such as hormone biology, plant morphology or gravitropism (Ashton et al., 1979; Ashton & Cove, 1977; Engel, 1968; Steere & Schuster, 1984). In 1997, it was found that gene targeting via homologous recombination was

feasible in this moss (Schaefer & Zrÿd, 1997) and today we know that the rate of site-specific homologous recombination in *P. patens* is the highest among all the plant models, reaching levels comparable to *Saccharomyces cerevisiae* (Rensing et al., 2020). These features, along with its position in the life tree close to other established model species, converted *P. patens* in a functional genomic model. The plastidic, mitochondrial and nuclear genomes have been sequenced (Rensing et al., 2008; Sugiura et al., 2003; Terasawa et al., 2007).

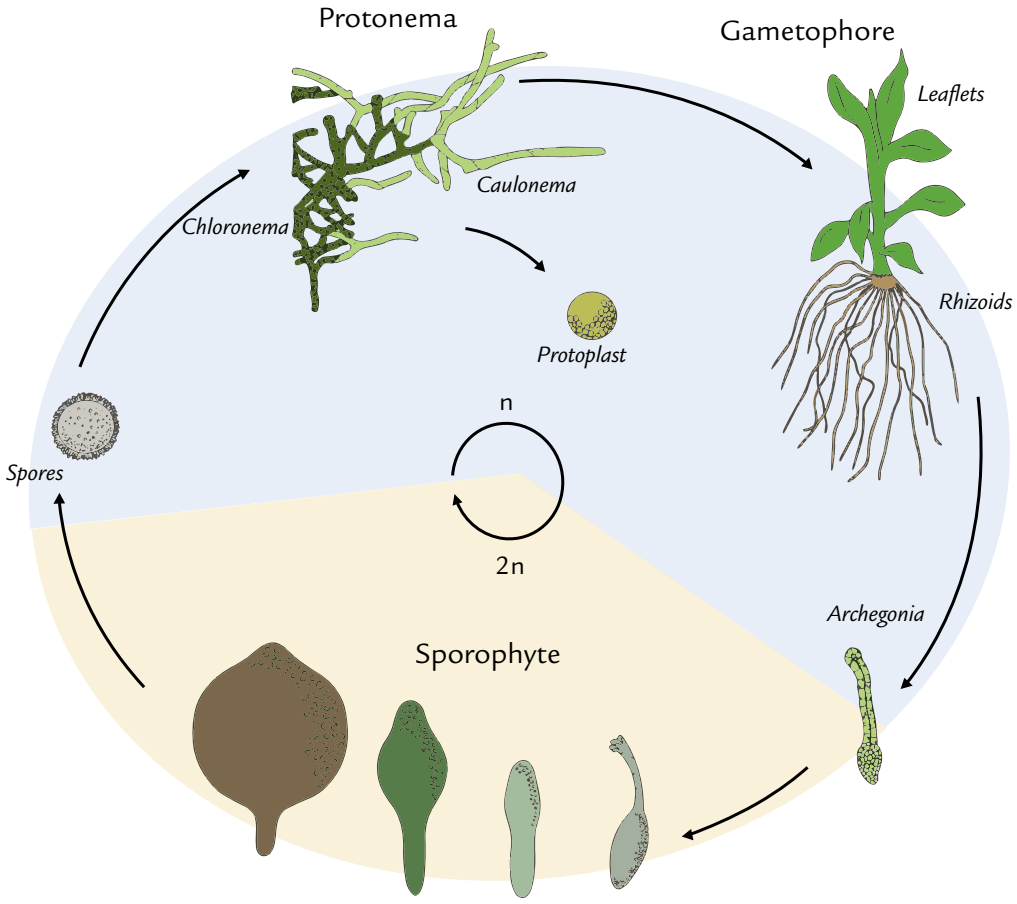

Figure 1.9 | **Life cycle of *Physcomitrella patens***. It takes about 3 months to complete the cycle. A spore (n) can divide by mitosis and produce the protonema (n), the first tissue after germination. Protonema is distinguished in chloronema, formed by small cells that contain many chloroplasts, and caulonema, formed by elongated cells with few chloroplasts and a big mitochondrial network. These cells form buds that are the transition point between the two-dimensional and the three-dimensional development, represented by the gametophore (n). In lab, the protonema can be treated to produce isolated protoplasts. The gametophore holds the reproductive organs (antheridia and archegonia) and it is formed by a non-vascularised, photosynthetic stem that has leaflets and rhizoids. *P. patens* is monoicous, and self-fertilization is a common phenomenon. The presence of water is needed for fertilization, so spermatids can reach the egg cell inside the archegonium. From the embryo (2n) it develops the sporophyte (2n), composed by a capsule inside of which the meiotic division that gives rise to spores (n) takes place. Modified from Ortiz-Ramírez et al., 2016.

P. patens is a good model for studying respiratory mutants in land plants. First, it is an established model organism for genetic studies in plants, with a sequenced genome and a very efficient site-specific homologous recombination. *P. patens* can be easily cultured in lab using culture media containing inorganic salts. Thanks to its great regenerative potential, we can obtain high amounts of material through vegetative propagation. After tissue homogenisation, a single cell coming from any tissue can regenerate protonema genetically identical to the previous generation.

The analysis of phenotypes in *P. patens* mutants is fast. The life cycle of *P. patens* can be completed in laboratory conditions in about 3 months, although the mutant phenotype can be usually observed before the completion of the cycle. The dominant phase of the life cycle is haploid, so mutant phenotypes can be observed directly with no need of crossing to produce homozygotes. In the specific case of respiratory deficiencies, *P. patens* has yet a further advantage in front of their vascular relatives: genetic transformation can be done under fully phototrophic conditions. The process of transformation and mutagenesis in *P. patens* is done through vegetative propagation and does not involve any strictly heterotrophic stage. This can be done under continuous illumination that, in the case of respiratory mutants, represents a further advantage since photosynthesis will be able to sustain cell growth and plant development.

We previously described mutants of *P. patens* deficient in the respiratory Complex I (Mellon et al., 2021). In this thesis, we further characterize one of these Complex I mutants and we present and characterize two novel respiratory mutants in *P. patens*, completely depleted in Complex IV (CHAPTER II) or Complex V (CHAPTER IV). These lines represent a significant step forward in the understanding of the role of respiration in land plants and establish *P. patens* as a model for this kind of analyses.

8. References

Acín-Pérez, R., Fernández-Silva, P., Peleato, M. L., Pérez-Martos, A., & Enriquez, J. A. (2008). Respiratory Active Mitochondrial Supercomplexes. *Molecular Cell*, *32*(4), 529–539. https://doi.org/10.1016/J.MOLCEL.2008.10.021

Alberts, B., Johnson, A., Lewis, J., Raff, M., Roberts, K., & Walter, P. (2002). *Electron-Transport Chains and Their Proton Pumps*. https://www.ncbi.nlm.nih.gov/books/NBK26904/

Albury, M. S., Elliott, C., & Moore, A. L. (2009). Towards a structural elucidation of the alternative oxidase in plants. *Physiologia Plantarum*, *137*(4), 316–327. https://doi.org/10.1111/J.1399-3054.2009.01270.X

Andersson, M. E., & Nordlund, P. (1999). A revised model of the active site of alternative oxidase. *FEBS Letters*, *449*(1), 17–22. https://doi.org/10.1016/S0014-5793(99)00376-2

Araújo, W. L., Nunes-Nesi, A., Osorio, S., Usadel, B., Fuentes, D., Nagy, R., Balbo, I., Lehmann, M., Studart-Witkowski, C., Tohge, T., Martinoia, E., Jordana, X., DaMatta, F. M., & Fernie, A. R. (2011). Antisense Inhibition of the Iron-Sulphur Subunit of Succinate Dehydrogenase Enhances Photosynthesis and Growth in Tomato via an Organic Acid–Mediated Effect on Stomatal Aperture. *The Plant Cell*, *23*(2), 600–627. https://doi.org/10.1105/TPC.110.081224

Arimura, S. ichi, Ayabe, H., Sugaya, H., Okuno, M., Tamura, Y., Tsuruta, Y., Watari, Y., Yanase, S., Yamauchi, T., Itoh, T., Toyoda, A., Takanashi, H., & Tsutsumi, N. (2020). Targeted gene disruption of ATP synthases 6-1 and 6-2 in the mitochondrial genome of Arabidopsis thaliana by mitoTALENs. *The Plant Journal*, *104*(6), 1459–1471. https://doi.org/10.1111/TPJ.15041

Ashton, N. W., & Cove, D. J. (1977). The isolation and preliminary characterisation of auxotrophic and analogue resistant mutants of the moss, Physcomitrella patens. *MGG Molecular & General Genetics*, *154*(1), 87–95. https://doi.org/10.1007/BF00265581

Ashton, N. W., Grimsley, N. H., & Cove, D. J. (1979). Analysis of gametophytic development in the moss, Physcomitrella patens, using auxin and cytokinin resistant mutants. *Planta*, *144*(5), 427–435. https://doi.org/10.1007/BF00380118/METRICS

Atlante, A., de Bari, L., Valenti, D., Pizzuto, R., Paventi, G., & Passarella, S. (2005). Transport and metabolism of d-lactate in Jerusalem artichoke mitochondria. *Biochimica et Biophysica Acta (BBA) - Bioenergetics*, *1708*(1), 13–22. https://doi.org/10.1016/j.bbabio.2005.03.003

Attallah, C. V., Welchen, E., Martin, A. P., Spinelli, S. V., Bonnard, G., Palatnik, J. F., & Gonzalez, D. H. (2011). Plants contain two SCO proteins that are differentially involved in cytochrome c oxidase function and copper and redox homeostasis. *Journal of Experimental Botany*, *62*(12), 4281–4294. https://doi.org/10.1093/JXB/ERR138

Baker, R., & Newton, K. (1995). Analysis of defective leaf sectors and aborted kernels in NCS2 mutant maize plants. *Maydica*, *40*(1), 89–98. https://agris.fao.org/agris-search/search.do?recordID=IT9561185

Bari, R., Kebeish, R., Kalamajka, R., Rademacher, T., & Peterhänsel, C. (2004). A glycolate dehydrogenase in the mitochondria of Arabidopsis thaliana. *Journal of Experimental Botany*, *55*(397), 623–630. https://doi.org/10.1093/JXB/ERH079

Barrientos, A., Pierre, D., Lee, J., & Tzagoloff, A. (2003). Cytochrome oxidase assembly does not require catalytically active cytochrome C. *The Journal of Biological Chemistry*, *278*(11), 8881–8887. https://doi.org/10.1074/JBC.M212427200

Bartoli, C. G., Pastori, G. M., & Foyer, C. H. (2000). Ascorbate biosynthesis in mitochondria is linked to the electron transport chain between complexes III and IV. *Plant Physiology*, *123*(1), 335–343. https://doi.org/10.1104/PP.123.1.335

Bellaoui, M., Grelon, M., Pelletier, G., & Budar, F. (1999). The restorer Rfo gene acts post-translationally on the stability of the ORF138 Ogura CMS-associated protein in reproductive tissues of rapeseed cybrids. *Plant Molecular Biology 1999 40:5*, *40*(5), 893–902. https://doi.org/10.1023/A:1006223908044

Belt, K., Huang, S., Thatcher, L. F., Casarotto, H., Singh, K. B., Van Aken, O., & Millar, A. H. (2017). Salicylic Acid-Dependent Plant Stress Signaling via Mitochondrial Succinate Dehydrogenase. *Plant Physiology*, *173*(4), 2029–2040. https://doi.org/10.1104/PP.16.00060

Belt, K., van Aken, O., Murcha, M., Millar, A. H., & Huang, S. (2018). An Assembly Factor Promotes Assembly of Flavinated SDH1 into the Succinate Dehydrogenase Complex. *Plant Physiology*, *177*(4), 1439–1452. https://doi.org/10.1104/PP.18.00320

Bentsink, L., & Koornneef, M. (2008). Seed Dormancy and Germination. *The Arabidopsis Book / American Society of Plant Biologists*, *6*, e0119. https://doi.org/10.1199/TAB.0119

Best, C., Mizrahi, R., Edris, R., Tang, H., Zer, H., Francs-Small, C. C. des, Finkel, O. M., Zhu, H., Small, I. D., & Ostersetzer-Biran, O. (2022). MSP1 encodes an essential RNA-binding PPR factor required for nad1 maturation and complex I biogenesis in Arabidopsis mitochondria. *BioRxiv*, 2022.11.12.516219. https://doi.org/10.1101/2022.11.12.516219

Bino, R. J., Suurs, L. C. J. M., de Hoop, S. J., Van Der Neut, A., Van Went, J. L., & Van Marrewijk, G. A. M. (1986). Characterization of cytoplasmic male sterility in Petunia hybrida and Zea mays. Localization and activity of cytochrome c oxidase. *Euphytica 1986 35:3*, *35*(3), 905–918. https://doi.org/10.1007/BF00028599

Blomberg, M. R. A. (2016). Mechanism of Oxygen Reduction in Cytochrome c Oxidase and the Role of the Active Site Tyrosine. *Biochemistry*, *55*(3), 489–500. https://doi.org/10.1021/ACS.BIOCHEM.5B01205/ASSET/IMAGES/LARGE/BI-2015-01205H_0007.JPEG

Brangeon, J., Sabar, M., Gutierres, S., Combettes, B., Bove, J., Gendy, C., Chétrit, P., Colas Des Francs-Small, C., Pla, M., Vedel, F., & De Paepe, R. (2000). Defective splicing of the first nad4 intron is associated with lack of several complex I subunits in the Nicotiana sylvestris NMS1 nuclear mutant. *The Plant Journal : For Cell and Molecular Biology*, *21*(3), 269–280. https://doi.org/10.1046/J.1365-313X.2000.00679.X

Braun, H. P. (2020). The Oxidative Phosphorylation system of the mitochondria in plants. *Mitochondrion*, *53*, 66–75. https://doi.org/10.1016/J.MITO.2020.04.007

Braun, H. P., Binder, S., Brennicke, A., Eubel, H., Fernie, A. R., Finkemeier, I., Klodmann, J., König, A. C., Kühn, K., Meyer, E., Obata, T., Schwarzländer, M., Takenaka, M., & Zehrmann, A. (2014). The life of plant mitochondrial complex I. *Mitochondrion*, *19*(PB), 295–313. https://doi.org/10.1016/j.mito.2014.02.006

Braun, H. P., Emmermann, M., Kruft, V., & Schmitz, U. K. (1992). The general mitochondrial processing peptidase from potato is an integral part of cytochrome c reductase of the respiratory chain. *The EMBO Journal*, *11*(9), 3219–3227. https://doi.org/10.1002/J.1460-2075.1992.TB05399.X

Braun, H. P., & Schmitz, U. K. (1997). The mitochondrial processing peptidase. *The International Journal of Biochemistry & Cell Biology*, *29*(8–9), 1043–1045. https://doi.org/10.1016/S1357-2725(97)00032-0

Cardol, P. (2011). Mitochondrial NADH:ubiquinone oxidoreductase (complex I) in eukaryotes: a highly conserved subunit composition highlighted by mining of protein databases. *Biochimica et Biophysica Acta*, *1807*(11), 1390–1397. https://doi.org/10.1016/J.BBABIO.2011.06.015

Cardol, P., Gloire, G., Havaux, M., Remacle, C., Matagne, R., & Franck, F. (2003). Photosynthesis and state transitions in mitochondrial mutants of Chlamydomonas reinhardtii affected in respiration. *Plant Physiology*, *133*(4), 2010–2020. https://doi.org/10.1104/pp.103.028076

Chen, W., Cui, Y., Wang, Z., Chen, R., He, C., Liu, Y., Du, X., Liu, Y., Fu, J., Wang, G., Wang, J., & Gu, R. (2021). Nuclear-Encoded Maturase Protein 3 Is Required for the Splicing of Various Group II Introns in Mitochondria during Maize (Zea mays L.) Seed Development. *Plant and Cell Physiology*, *62*(2), 293–305. https://doi.org/10.1093/PCP/PCAA161

Chetrit, P., Rios, R., de Paepe, R., Vitart, V., Gutierres, S., & Vedel, F. (1992). Cytoplasmic male sterility is associated with large deletions in the mitochondrial DNA of two Nicotiana sylvestris protoclones. *Current Genetics 1992 21:2*, *21*(2), 131–137. https://doi.org/10.1007/BF00318472

Clifton, R., Millar, A. H., & Whelan, J. (2006). Alternative oxidases in Arabidopsis: A comparative analysis of differential expression in the gene family provides new insights into function of non-phosphorylating bypasses. *Biochimica et Biophysica Acta (BBA) - Bioenergetics*, *1757*(7), 730–741. https://doi.org/10.1016/J.BBABIO.2006.03.009

Coe, E. H. J. (1983). Maternally inherited abnormal plants in maize. *Maydica*, *28*, 151–167.

Cohen, S., Zmudjak, M., Colas des Francs-Small, C., Malik, S., Shaya, F., Keren, I., Belausov, E., Many, Y., Brown, G. G., Small, I., & Ostersetzer-Biran, O. (2014). nMAT4, a maturase factor required for *nad1* pre-mRNA processing and maturation, is essential for holocomplex I biogenesis in Arabidopsis mitochondria. *The Plant Journal*, *78*(2), 253–268. https://doi.org/10.1111/tpj.12466

Colas Des Francs-Small, C., & Small, I. (2014). Surrogate mutants for studying mitochondrially encoded functions. *Biochimie*, *100*(1), 234–242. https://doi.org/10.1016/J.BIOCHI.2013.08.019

Córdoba, J. P., Marchetti, F., Soto, D., Martin, M. V., Pagnussat, G. C., & Zabaleta, E. (2016). The CA domain of the respiratory complex I is required for normal embryogenesis in *Arabidopsis thaliana*. *Journal of Experimental Botany*, *67*(5), 1589–1603. https://doi.org/10.1093/jxb/erv556

Crofts, A. R. (2004). The Cytochrome *bc* $_1$ Complex: Function in the Context of Structure. *Annual Review of Physiology*, *66*(1), 689–733. https://doi.org/10.1146/annurev.physiol.66.032102.150251

Dahan, J., Tcherkez, G., Macherel, D., Benamar, A., Belcram, K., Quadrado, M., Arnal, N., & Mireau, H. (2014). Disruption of the *CYTOCHROME C OXIDASE DEFICIENT1* Gene Leads to Cytochrome c Oxidase Depletion and Reorchestrated Respiratory Metabolism in Arabidopsis . *Plant Physiology*, *166*(4), 1788–1802. https://doi.org/10.1104/pp.114.248526

Daley, D. O., Adams, K. L., Clifton, R., Qualmann, S., Millar, A. H., Palmer, J. D., Pratje, E., & Whelan, J. (2002). Gene transfer from mitochondrion to nucleus: novel mechanisms for gene activation from Cox2. *The Plant Journal*, *30*(1), 11–21. https://doi.org/10.1046/J.1365-313X.2002.01263.X

Darrouzet, E., Issartel, J. P., Lunardi, J., & Dupuis, A. (1998). The 49-kDa subunit of NADH-ubiquinone oxidoreductase (Complex I) is involved in the binding of piericidin and rotenone, two quinone-related inhibitors. *FEBS Letters*, *431*(1), 34–38. https://doi.org/10.1016/S0014-5793(98)00719-4

Day, D. A., Krab, K., Lambers, H., Moore, A. L., Siedow, J. N., Wagner, A. M., & Wiskich, J. T. (1996). The Cyanide-Resistant Oxidase: To Inhibit or Not to Inhibit, That Is the Question. *Plant Physiology*, *110*(1), 1–2. https://doi.org/10.1104/pp.110.1.1

De Longevialle, A. F., Meyer, E. H., Andrés, C., Taylor, N. L., Lurin, C., Millar, A. H., & Smalla, I. D. (2007). The Pentatricopeptide Repeat Gene OTP43 Is Required for trans-Splicing of the Mitochondrial nad1 Intron 1 in Arabidopsis thaliana. *The Plant Cell*, *19*(10), 3256. https://doi.org/10.1105/TPC.107.054841

De Paepe, R., Chétrit, P., Vitart, V., Ambard-Bretteville, F., Prat, D., & Vedel, F. (1990). Several nuclear genes control both male sterility and mitochondrial protein synthesis in Nicotiana sylvestris protoclones. *MGG Molecular & General Genetics*, *222*(2–3), 206–210. https://doi.org/10.1007/BF00633819/METRICS

Del Valle-Echevarria, A. R., Kielkowska, A., Bartoszewski, G., & Havey, M. J. (2015). The mosaic mutants of cucumber: A method to produce knock-downs of mitochondrial transcripts. *G3: Genes, Genomes, Genetics*, *5*(6), 1211–1221. https://doi.org/10.1534/G3.115.017053/-/DC1

Del-Saz, N. F., Ribas-Carbo, M., McDonald, A. E., Lambers, H., Fernie, A. R., & Florez-Sarasa, I. (2018). An In Vivo Perspective of the Role(s) of the Alternative Oxidase Pathway. In *Trends in Plant Science* (Vol. 23, Issue 3, pp. 206–219). Elsevier Ltd. https://doi.org/10.1016/j.tplants.2017.11.006

des Francs-Small, C. C., Kroeger, T., Zmudjak, M., Ostersetzer-Biran, O., Rahimi, N., Small, I., & Barkan, A. (2012). A PORR domain protein required for rpl2 and ccmFC intron splicing and for the biogenesis of c-type cytochromes in Arabidopsis mitochondria. *The Plant Journal*, *69*(6), 996–1005. https://doi.org/10.1111/J.1365-313X.2011.04849.X

Dewey, R. (1986). Novel recombinations in the maize mitochondrial genome produce a unique transcriptional unit in the texas male-sterile cytoplasm. *Cell*, *44*(3), 439–449. https://doi.org/10.1016/0092-8674(86)90465-4

Dixon, L. K., & Leaver, C. J. (1982). Mitochondrial gene expression and cytoplasmic male sterility in sorghum. *Plant Molecular Biology*, *1*(2), 89–102. https://doi.org/10.1007/BF00024973

Djebbar, R., Rzigui, T., Pétriacq, P., Mauve, C., Priault, P., Fresneau, C., de Paepe, M., Florez-Sarasa, I., Benhassaine-Kesri, G., Streb, P., Gakière, B., Cornic, G., & de Paepe, R. (2012). Respiratory complex I deficiency induces drought tolerance by impacting leaf stomatal and hydraulic conductances. *Planta*, *235*(3), 603–614. https://doi.org/10.1007/S00425-011-1524-7/FIGURES/7

Dojcinovic, D., Krosting, J., Harris, A. J., Wagner, D. J., & Rhoads, D. M. (2005). Identification of a region of the Arabidopsis AtAOX1a promoter necessary for mitochondrial retrograde regulation of expression. *Plant Molecular Biology 2005 58:2*, *58*(2), 159–175. https://doi.org/10.1007/S11103-005-5390-1

DuBuy, H. G., Woods, M. W., & Lackey, M. D. (1950). Enzymatic activities of isolated normal and mutant mitochondria and plastids of higher plants. *Science*, *111*(2891), 572–574. https://doi.org/10.1126/SCIENCE.111.2891.572/ASSET/BF27F55A-BD4D-434A-ACF4-D46CAC65AD24/ASSETS/SCIENCE.111.2891.572.FP.PNG

Dudkina, N. V., Sunderhaus, S., Braun, H. P., & Boekema, E. J. (2006). Characterization of dimeric ATP synthase and cristae membrane ultrastructure from Saccharomyces and Polytomella mitochondria. *FEBS Letters*, *580*(14), 3427–3432. https://doi.org/10.1016/J.FEBSLET.2006.04.097

Dutilleul, C., Driscoll, S., Cornic, G., de Paepe, R., Foyer, C. H., & Noctor, G. (2003). Functional mitochondrial complex I is required by tobacco leaves for optimal photosynthetic performance in photorespiratory conditions and during transients. *Plant Physiology*, *131*(1), 264–275. https://doi.org/10.1104/pp.011155

Dutilleul, C., Garmier, M., Noctor, G., Mathieu, C., Chétrit, P., Foyer, C. H., & De Paepe, R. (2003). Leaf Mitochondria Modulate Whole Cell Redox Homeostasis, Set Antioxidant Capacity, and Determine Stress Resistance through Altered Signaling and Diurnal Regulation. *The Plant Cell*, *15*(5), 1212–1226. https://doi.org/10.1105/TPC.009464

Dutilleul, C., Lelarge, C., Prioul, J. L., De Paepe, R., Foyer, C. H., & Noctor, G. (2005). Mitochondria-Driven Changes in Leaf NAD Status Exert a Crucial Influence on the Control of Nitrate Assimilation and the Integration of Carbon and Nitrogen Metabolism. *Plant Physiology*, *139*(1), 64–78. https://doi.org/10.1104/PP.105.066399

Edwardson, J. R., & Corbett, M. K. (1961). ASEXUAL TRANSMISSION OF CYTOPLASMIC MALE STERILITY. *Proceedings of the National Academy of Sciences*, *47*(3), 390–396. https://doi.org/10.1073/pnas.47.3.390

Elorza, A., León, G., Gómez, I., Mouras, A., Holuigue, L., Araya, A., & Jordana, X. (2004). Nuclear SDH2-1 and SDH2-2 Genes, Encoding the Iron-Sulfur Subunit of Mitochondrial Complex II in Arabidopsis,

Have Distinct Cell-Specific Expression Patterns and Promoter Activities. *Plant Physiology*, *136*(4), 4072–4087. https://doi.org/10.1104/PP.104.049528

Elorza, A., Roschzttardtz, H., Gómez, I., Mouras, A., Holuigue, L., Araya, A., & Jordana, X. (2006). A Nuclear Gene for the Iron–Sulfur Subunit of Mitochondrial Complex II is Specifically Expressed During Arabidopsis Seed Development and Germination. *Plant and Cell Physiology*, *47*(1), 14–21. https://doi.org/10.1093/PCP/PCI218

Elthon, T. E., & Stewart, C. R. (1981). Submitochondrial Location and Electron Transport Characteristics of Enzymes Involved in Proline Oxidation. *Plant Physiology*, *67*(4), 780–784. https://doi.org/10.1104/PP.67.4.780

Engel, P. P. (1968). THE INDUCTION OF BIOCHEMICAL AND MORPHOLOGICAL MUTANTS IN THE MOSS PHYSCOMITRELLA PATENS. *American Journal of Botany*, *55*(4), 438–446. https://doi.org/10.1002/J.1537-2197.1968.TB07397.X

Engqvist, M., Drincovich, M. F., Flügge, U.-I., & Maurino, V. G. (2009). Two d-2-Hydroxy-acid Dehydrogenases in Arabidopsis thaliana with Catalytic Capacities to Participate in the Last Reactions of the Methylglyoxal and β-Oxidation Pathways. *Journal of Biological Chemistry*, *284*(37), 25026–25037. https://doi.org/10.1074/jbc.M109.021253

Estabrook, R. W. (1967). [7] Mitochondrial respiratory control and the polarographic measurement of ADP : O ratios. *Methods in Enzymology*, *10*(C), 41–47. https://doi.org/10.1016/0076-6879(67)10010-4

Fan, K., Fu, Q., Wei, Q., Jia, S., Zhao, A., Wang, T., Cao, J., Liu, Y., Ren, Z., & Liu, Y. (2022). ZmnMAT1, a nuclear-encoded type I maturase, is required for the splicing of mitochondrial Nad1 intron 1 and Nad4 intron 2. *Frontiers in Plant Science*, *13*, 4778. https://doi.org/10.3389/FPLS.2022.1033869/BIBTEX

Feiler, H., & Newton, K. (1987). Altered mitochondrial gene expression in the nonchromosomal stripe 2 mutant of maize. *The EMBO Journal*, *6*(6), 1535–1539. https://doi.org/10.1002/J.1460-2075.1987.TB02397.X

Figueroa, P., Léon, G., Elorza, A., Holuigue, L., Araya, A., & Jordana, X. (2002). The four subunits of mitochondrial respiratory complex II are encoded by multiple nuclear genes and targeted to mitochondria in Arabidopsis thaliana. *Plant Molecular Biology 2002 50:4*, *50*(4), 725–734. https://doi.org/10.1023/A:1019926301981

Figueroa, P., León, G., Elorza, A., Holuigue, L., & Jordana, X. (2001). Three different genes encode the iron-sulfur subunit of succinate dehydrogenase in Arabidopsis thaliana. *Plant Molecular Biology 2001 46:2*, *46*(2), 241–250. https://doi.org/10.1023/A:1010612506070

Florez-Sarasa, I., Ostaszewska, M., Galle, A., Flexas, J., Rychter, A. M., & Ribas-Carbo, M. (2009). Changes of alternative oxidase activity, capacity and protein content in leaves of Cucumis sativus wild-type and MSC16 mutant grown under different light intensities. *Physiologia Plantarum*, *137*(4), 419–426. https://doi.org/10.1111/J.1399-3054.2009.01244.X

Florez-Sarasa, I., Welchen, E., Racca, S., Gonzalez, D. H., Vallarino, J. G., Fernie, A. R., Ribas-Carbo, M., & Del-Saz, N. F. (2021). Cytochrome c Deficiency Differentially Affects the In Vivo Mitochondrial Electron Partitioning and Primary Metabolism Depending on the Photoperiod. *Plants 2021, Vol. 10, Page 444*, *10*(3), 444. https://doi.org/10.3390/PLANTS10030444

Flurkey, W. H. (2010). Yield of ATP Molecules per Glucose Molecule. *Journal of Chemical Education*, *87*(3), 271. https://doi.org/10.1021/ED800102G

Fromm, S., Braun, H. P., & Peterhansel, C. (2016). Mitochondrial gamma carbonic anhydrases are required for complex I assembly and plant reproductive development. *New Phytologist*, *211*(1), 194–207. https://doi.org/10.1111/NPH.13886

Fromm, S., Göing, J., Lorenz, C., Peterhänsel, C., & Braun, H. P. (2016). Depletion of the “gamma-type carbonic anhydrase-like” subunits of complex I affects central mitochondrial metabolism in Arabidopsis thaliana. *Biochimica et Biophysica Acta (BBA) - Bioenergetics*, *1857*(1), 60–71. https://doi.org/10.1016/J.BBABIO.2015.10.006

Fromm, S., Senkler, J., Eubel, H., Peterhänsel, C., & Braun, H. P. (2016). Life without complex I: proteome analyses of an Arabidopsis mutant lacking the mitochondrial NADH dehydrogenase complex. *Journal of Experimental Botany*, *67*(10), 3079–3093. https://doi.org/10.1093/JXB/ERW165

Fromm, S., Senkler, J., Zabaleta, E., Peterhänsel, C., & Braun, H. P. (2016). The carbonic anhydrase domain of plant mitochondrial complex I. *Physiologia Plantarum*, *157*(3), 289–296. https://doi.org/10.1111/PPL.12424

Fuchs, P., Rugen, N., Carrie, C., Elsässer, M., Finkemeier, I., Giese, J., Hildebrandt, T. M., Kühn, K., Maurino, V. G., Ruberti, C., Schallenberg-Rüdinger, M., Steinbeck, J., Braun, H. P., Eubel, H., Meyer, E. H., Müller-Schüssele, S. J., & Schwarzländer, M. (2020). Single organelle function and organization as estimated from Arabidopsis mitochondrial proteomics. *The Plant Journal*, *101*(2), 420–441. https://doi.org/10.1111/TPJ.14534

Fuentes, D., Meneses, M., Nunes-Nesi, A., Araújo, W. L., Tapia, R., Gómez, I., Holuigue, L., Gutiérrez, R. A., Fernie, A. R., & Jordana, X. (2011). A Deficiency in the Flavoprotein of Arabidopsis Mitochondrial Complex II Results in Elevated Photosynthesis and Better Growth in Nitrogen-Limiting Conditions. *Plant Physiology*, *157*(3), 1114–1127. https://doi.org/10.1104/PP.111.183939

Gabay-Laughnan, S., & Laughnan, J. R. (1994). Male Sterility and Restorer Genes in Maize. *The Maize Handbook*, 418–423. https://doi.org/10.1007/978-1-4612-2694-9_64

Gabelman, W. H. (1949). Reproduction and distribution of the cytoplasmic factor for male sterility in maize. *Proceedings of the National Academy of Sciences of the United States of America*, *35*(11), 634–640. https://doi.org/10.1073/PNAS.35.11.634

Garcia, L., Welchen, E., Gey, U., Arce, A. L., Steinebrunner, I., & Gonzalez, D. H. (2016). The cytochrome c oxidase biogenesis factor AtCOX17 modulates stress responses in Arabidopsis. *Plant, Cell & Environment*, *39*(3), 628–644. https://doi.org/10.1111/PCE.12647

Garmash, E. V. (2022). Signal Pathways for Regulation of Plant Alternative Oxidase Genes’ Expression. *Russian Journal of Plant Physiology*, *69*(1), 1–16. https://doi.org/10.1134/S1021443722010058/FIGURES/1

Geisler, D. A., Broselid, C., Hederstedt, L., & Rasmusson, A. G. (2007). Ca2+-binding and Ca2+-independent respiratory NADH and NADPH dehydrogenases of Arabidopsis thaliana. *Journal of Biological Chemistry*, *282*(39), 28455–28464. https://doi.org/10.1074/jbc.M704674200

Gillman, J. D., Bentolila, S., & Hanson, M. R. (2007). The petunia restorer of fertility protein is part of a large mitochondrial complex that interacts with transcripts of the CMS-associated locus. *The Plant Journal*, *49*(2), 217–227. https://doi.org/10.1111/J.1365-313X.2006.02953.X

Glaser, E., Eriksson, A. C., & Sjöling, S. (1994). Bifunctional role of the bc1 complex in plants. Mitochondrial bc1 complex catalyses both electron transport and protein processing. *FEBS Letters*, *346*(1), 83–87. https://doi.org/10.1016/0014-5793(94)00312-2

Gleason, C., Huang, S., Thatcher, L. F., Foley, R. C., Anderson, C. R., Carroll, A. J., Millar, A. H., & Singh, K. B. (2011). Mitochondrial complex II has a key role in mitochondrial-derived reactive oxygen species influence on plant stress gene regulation and defense. *Proceedings of the National Academy of Sciences of the United States of America*, *108*(26), 10768–10773. https://doi.org/10.1073/PNAS.1016060108/SUPPL_FILE/SD01.XLS

Gnaiger, E. (2023). Complex II ambiguities — FADH2 in the electron transfer system. *MitoFit Preprints*.

Goddard, D. R. (1944). CYTOCHROME C AND CYTOCHROME OXIDASE FROM WHEAT GERM. *American Journal of Botany*, *31*(5), 270–276. https://doi.org/10.1002/J.1537-2197.1944.TB08032.X

Gras, D. E., Mansilla, N., Rodríguez, C., Welchen, E., & Gonzalez, D. H. (2020). Arabidopsis thaliana SURFEIT1-like genes link mitochondrial function to early plant development and hormonal growth responses. *The Plant Journal*, *103*(2), 690–704. https://doi.org/10.1111/TPJ.14762

Grelon, M., Budar, F., Bonhomme, S., & Pelletier, G. (1994). Ogura cytoplasmic male-sterility (CMS)-associated orf138 is translated into a mitochondrial membrane polypeptide in male-sterile Brassica cybrids. *Molecular & General Genetics : MGG*, *243*(5), 540–547. https://doi.org/10.1007/BF00284202

Gu, J., Dempsey, S., & Newton, K. (1994). Rescue of a maize mitochondrial cytochrome oxidase mutant by tissue culture+. *The Plant Journal*, *6*(6), 787–794. https://doi.org/10.1046/j.1365-313X.1994.6060787.x

Gu, J., Miles, D., & Newton, K. (1993). Analysis of leaf sectors in the NCS6 mitochondrial mutant of maize. *The Plant Cell*, *5*(8), 963–971. https://doi.org/10.1105/tpc.5.8.963

Guilliermond, A. (1941). *The cytoplasm of the plant cell* (L. R. Atkinson, Ed.) [Book]. Chronica Botanica Company.

Gutierres, S., Combettes, B., de Paepe, R., Mirande, M., Lelandais, C., Vedel, F., & Chetrit, P. (1999). In the Nicotiana sylvestris CMSII mutant, a recombination-mediated change 5' to the first exon of the mitochondrial nad1 gene is associated with lack of the NADH:ubiquinone oxidoreductase (complex I) NAD1 subunit. *European Journal of Biochemistry*, *261*(2), 361–370. https://doi.org/10.1046/j.1432-1327.1999.00310.x

Gutierres, S., Sabar, M., Lelandais, C., Chetrit, P., Diolez, P., Degand, H., Boutry, M., Vedel, F., De Kouchkovsky, Y., & De Paepe, R. (1997). Lack of mitochondrial and nuclear-encoded subunits of complex I and alteration of the respiratory chain in Nicotiana sylvestris mitochondrial deletion mutants. *Proceedings of the National Academy of Sciences of the United States of America*, *94*(7), 3436–3441. https://doi.org/10.1073/PNAS.94.7.3436/ASSET/79B34D09-839C-41AD-B6EC-EC75A01880A5/ASSETS/GRAPHIC/PQ0670012008.JPEG

Hack, E., Lin, C., Yang, H., & Horner, H. T. (1991). T-URF 13 Protein from Mitochondria of Texas Male-Sterile Maize (Zea mays L.) Its Purification and Submitochondrial Localization, and Immunogold Labeling in Anther Tapetum during Microsporogenesis. *Plant Physiology*, *95*(3), 861–870. https://doi.org/10.1104/PP.95.3.861

Hager, J., Pellny, T. K., Mauve, C., Lelarge-Trouverie, C., de Paepe, R., Foyer, C. H., & Noctor, G. (2010). Conditional modulation of NAD levels and metabolite profiles in Nicotiana sylvestris by mitochondrial electron transport and carbon/nitrogen supply. *Planta*, *231*(5), 1145–1157. https://doi.org/10.1007/S00425-010-1117-X/FIGURES/6

Hanson, M. R., & Conde, M. F. (1985). Functioning and Variation of Cytoplasmic Genomes: Lessons from Cytoplasmic–Nuclear Interactions Affecting Male Fertility in Plants. *International Review of Cytology*, *94*(C), 213–267. https://doi.org/10.1016/S0074-7696(08)60398-8

Hao, H. X., Khalimonchuk, O., Schraders, M., Dephoure, N., Bayley, J. P., Kunst, H., Devilee, P., Cremers, C. W. R. J., Schiffman, J. D., Bentz, B. G., Gygi, S. P., Winge, D. R., Kremer, H., & Rutter, J. (2009). SDH5, a gene required for flavination of succinate dehydrogenase, is mutated in paraganglioma. *Science (New York, N.Y.)*, *325*(5944), 1139–1142. https://doi.org/10.1126/SCIENCE.1175689

Heazlewood, J. L., Tonti-Filippini, J. S., Gout, A. M., Day, D. A., Whelan, J., & Millar, A. H. (2004). Experimental analysis of the Arabidopsis mitochondrial proteome highlights signaling and regulatory components, provides assessment of targeting prediction programs, and indicates plant-specific mitochondrial proteins. *The Plant Cell*, *16*(1), 241–256. https://doi.org/10.1105/TPC.016055

Hederstedt, L. (2003). Structural biology: Complex II is complex too. *Science*, *299*(5607), 671–672. https://doi.org/10.1126/SCIENCE.1081821/ASSET/92B59819-A538-4B6A-88DC-57756E061B6E/ASSETS/SCIENCE.1081821.FP.PNG

Hildebrandt, T. M., Nunes Nesi, A., Araújo, W. L., & Braun, H.-P. (2015). Amino Acid Catabolism in Plants. *Molecular Plant*, *8*(11), 1563–1579. https://doi.org/10.1016/j.molp.2015.09.005

Ho, L. H. M., Giraud, E., Uggalla, V., Lister, R., Clifton, R., Glen, A., Thirkettle-Watts, D., Van Aken, O., & Whelan, J. (2008). Identification of Regulatory Pathways Controlling Gene Expression of Stress-Responsive Mitochondrial Proteins in Arabidopsis. *Plant Physiology*, *147*(4), 1858–1873. https://doi.org/10.1104/PP.108.121384

Horn, R., Gupta, K. J., & Colombo, N. (2014). Mitochondrion role in molecular basis of cytoplasmic male sterility. *Mitochondrion*, *19 Pt B*(PB), 198–205. https://doi.org/10.1016/J.MITO.2014.04.004

Hsu, Y. W., Wang, H. J., Hsieh, M. H., Hsieh, H. L., & Jauh, G. Y. (2014). Arabidopsis mTERF15 Is Required for Mitochondrial nad2 Intron 3 Splicing and Functional Complex I Activity. *PLOS ONE*, *9*(11), e112360. https://doi.org/10.1371/JOURNAL.PONE.0112360

Huang, S., Braun, H., Gawryluk, R. M. R., & Millar, A. H. (2019). Mitochondrial complex II of plants: subunit composition, assembly, and function in respiration and signaling. *The Plant Journal*, *98*(3), 405–417. https://doi.org/10.1111/tpj.14227

Huang, S., Taylor, N. L., Narsai, R., Eubel, H., Whelan, J., & Millar, A. H. (2010). Functional and composition differences between mitochondrial complex II in Arabidopsis and rice are correlated with the complex genetic history of the enzyme. *Plant Molecular Biology*, *72*(3), 331–342. https://doi.org/10.1007/S11103-009-9573-Z/FIGURES/4

Huang, S., Taylor, N. L., Ströher, E., Fenske, R., & Millar, A. H. (2013). Succinate dehydrogenase assembly factor 2 is needed for assembly and activity of mitochondrial complex II and for normal root elongation in Arabidopsis. *The Plant Journal*, *73*(3), 429–441. https://doi.org/10.1111/TPJ.12041

Huang, S., Taylor, N. L., Whelan, J., & Millar, A. H. (2009). Refining the Definition of Plant Mitochondrial Presequences through Analysis of Sorting Signals, N-Terminal Modifications, and Cleavage Motifs. *Plant Physiology*, *150*(3), 1272–1285. https://doi.org/10.1104/PP.109.137885

Hunt, M., & Newton, K. (1991). The NCS3 mutation: genetic evidence for the expression of ribosomal protein genes in Zea mays mitochondria. *The EMBO Journal*, *10*(5), 1045–1052. https://doi.org/10.1002/J.1460-2075.1991.TB08043.X

Hurry, V., Igamberdiev, A. U., Keerberg, O., Pärnik, T., Atkin, O. K., Zaragoza-Castells, J., & Gardeström, P. (2005). Respiration in Photosynthetic Cells: Gas Exchange Components, Interactions with Photorespiration and the Operation of Mitochondria in the Light. In *Plant Respiration* (pp. 43–61). Springer-Verlag. https://doi.org/10.1007/1-4020-3589-6_4

Hüttemann, M., Pecina, P., Rainbolt, M., Sanderson, T. H., Kagan, V. E., Samavati, L., Doan, J. W., & Lee, I. (2011). The multiple functions of cytochrome c and their regulation in life and death decisions of the mammalian cell: From respiration to apoptosis. *Mitochondrion*, *11*(3), 369–381. https://doi.org/10.1016/J.MITO.2011.01.010

Ian Menz, R., & Day, D. A. (1996). Purification and characterization of a 43-kDa rotenone-insensitive NADH dehydrogenase from plant mitochondria. *The Journal of Biological Chemistry*, *271*(38), 23117–23120. https://doi.org/10.1074/JBC.271.38.23117

Izui, K., Matsumura, H., Furumoto, T., & Kai, Y. (2004). Phosphoenolpyruvate carboxylase: A new era of structural biology. *Annual Review of Plant Biology*, *55*, 69–84. https://doi.org/10.1146/ANNUREV.ARPLANT.55.031903.141619

Jallet, D., Xing, D., Hughes, A., Moosburner, M., Simmons, M. P., Allen, A. E., & Peers, G. (2020). Mitochondrial fatty acid β-oxidation is required for storage-lipid catabolism in a marine diatom. *New Phytologist*, *228*(3), 946–958. https://doi.org/10.1111/nph.16744

Jethva, J., Lichtenauer, S., Schmidt-Schippers, R., Steffen-Heins, A., Poschet, G., Wirtz, M., van Dongen, J. T., Eirich, J., Finkemeier, I., Bilger, W., Schwarzländer, M., & Sauter, M. (2023). Mitochondrial alternative NADH dehydrogenases NDA1 and NDA2 promote survival of reoxygenation stress in Arabidopsis by safeguarding photosynthesis and limiting ROS generation. *The New Phytologist*, *238*(1), 96–112. https://doi.org/10.1111/nph.18657

Jiao, S., Thornsberry, J. M., Elthon, T. E., & Newton, K. (2005). Biochemical and molecular characterization of photosystem I deficiency in the NCS6 mitochondrial mutant of maize. *Plant Molecular Biology 2005 57:2*, *57*(2), 303–313. https://doi.org/10.1007/S11103-004-7792-X

Jonietz, C., Forner, J., Hölzle, A., Thuss, S., & Binder, S. (2012). RNA PROCESSING FACTOR2 Is Required for 5′ End Processing of nad9 and cox3 mRNAs in Mitochondria of Arabidopsis thaliana. *The Plant Cell*, *22*(2), 443–453. https://doi.org/10.1105/TPC.109.066944

Juszczuk, I. M., Flexas, J., Szal, B., Dąbrowska, Z., Ribas-Carbo, M., & Rychter, A. M. (2007). Effect of mitochondrial genome rearrangement on respiratory activity, photosynthesis, photorespiration and energy status of MSC16 cucumber (Cucumis sativus) mutant. *Physiologia Plantarum*, *131*(4), 527–541. https://doi.org/10.1111/j.1399-3054.2007.00984.x

Juszczuk, I. M., & Rychter, A. M. (2009). BN-PAGE analysis of the respiratory chain complexes in mitochondria of cucumber MSC16 mutant. *Plant Physiology and Biochemistry*, *47*(5), 397–406. https://doi.org/10.1016/j.plaphy.2008.12.022

Kadenbach, B. (2017). Regulation of Mammalian 13-Subunit Cytochrome c Oxidase and Binding of other Proteins: Role of NDUFA4. *Trends in Endocrinology and Metabolism*, *28*(11), 761–770. https://doi.org/10.1016/j.tem.2017.09.003

Kagawa, Y., & Racker, E. (1966). Partial Resolution of the Enzymes Catalyzing Oxidative Phosphorylation: VIII. PROPERTIES OF A FACTOR CONFERRING OLIGOMYCIN SENSITIVITY ON MITOCHONDRIAL ADENOSINE TRIPHOSPHATASE. *Journal of Biological Chemistry*, *241*(10), 2461–2466. https://doi.org/10.1016/S0021-9258(18)96640-8

Karavaeva, V., & Sousa, F. L. (2023). Modular structure of complex II: An evolutionary perspective. *Biochimica et Biophysica Acta (BBA) - Bioenergetics*, *1864*(1), 148916. https://doi.org/10.1016/J.BBABIO.2022.148916

Karpova, O., & Newton, K. (1999). A partially assembled complex I in NAD4-deficient mitochondria of maize. *The Plant Journal*, *17*(5), 511–521. https://doi.org/10.1046/j.1365-313X.1999.00401.x

Karpova, O. V., Kuzmin, E. V., Elthon, T. E., & Newton, K. (2002). Differential Expression of Alternative Oxidase Genes in Maize Mitochondrial Mutants. *The Plant Cell*, *14*(12), 3271–3284. https://doi.org/10.1105/tpc.005603

Kazama, T., Okuno, M., Watari, Y., Yanase, S., Koizuka, C., Tsuruta, Y., Sugaya, H., Toyoda, A., Itoh, T., Tsutsumi, N., Toriyama, K., Koizuka, N., & Arimura, S. ichi. (2019). Curing cytoplasmic male sterility via TALEN-mediated mitochondrial genome editing. *Nature Plants 2019 5:7*, *5*(7), 722–730. https://doi.org/10.1038/s41477-019-0459-z

Keren, I., Bezawork-Geleta, A., Kolton, M., Maayan, I., Belausov, E., Levy, M., Mett, A., Gidoni, D., Shaya, F., & Ostersetzer-Biran, O. (2009). AtnMat2, a nuclear-encoded maturase required for splicing of group-II introns in Arabidopsis mitochondria. *RNA*, *15*(12), 2299–2311. https://doi.org/10.1261/RNA.1776409

Keren, I., Tal, L., des Francs-Small, C. C., Araújo, W. L., Shevtsov, S., Shaya, F., Fernie, A. R., Small, I., & Ostersetzer-Biran, O. (2012). nMAT1, a nuclear-encoded maturase involved in the trans-splicing of

nad1 intron 1, is essential for mitochondrial complex I assembly and function. *The Plant Journal*, *71*(3), 413–426. https://doi.org/10.1111/J.1365-313X.2012.04998.X

Khalimonchuk, O., & Rödel, G. (2005). Biogenesis of cytochrome c oxidase. *Mitochondrion*, *5*(6), 363–388. https://doi.org/10.1016/j.mito.2005.08.002

Kierans, S. J., & Taylor, C. T. (2021). Regulation of glycolysis by the hypoxia-inducible factor (HIF): implications for cellular physiology. *The Journal of Physiology*, *599*(1), 23–37. https://doi.org/10.1113/JP280572

Kitazaki, K., Oda, K., Akazawa, A., & Iwahori, R. (2023). Molecular genetics of cytoplasmic male sterility and restorer-of-fertility for the fine tuning of pollen production in crops. *Theoretical and Applied Genetics 2023 136:7*, *136*(7), 1–16. https://doi.org/10.1007/S00122-023-04398-8

Kolli, R., Engstler, C., Akbas, S., Mower, J. P., Soll, J., & Carrie, C. (2020). The OXA2a Insertase of Arabidopsis Is Required for Cytochrome c Maturation. *Plant Physiology*, *184*(2), 1042–1055. https://doi.org/10.1104/PP.19.01248

Kolli, R., Soll, J., & Carrie, C. (2019). OXA2b is Crucial for Proper Membrane Insertion of COX2 during Biogenesis of Complex IV in Plant Mitochondria. *Plant Physiology*, *179*(2), 601–615. https://doi.org/10.1104/PP.18.01286

Koprivova, A., Francs-Small, C. C. Des, Calder, G., Mugford, S. T., Tanz, S., Lee, B. R., Zechmann, B., Small, I., & Kopriva, S. (2010). Identification of a pentatricopeptide repeat protein implicated in splicing of intron 1 of mitochondrial nad7 transcripts. *Journal of Biological Chemistry*, *285*(42), 32192–32199. https://doi.org/10.1074/jbc.M110.147603

Korth, K. L., Kaspi, C. I., Siedow, J. N., & Levings, C. S. (1991). URF13, a maize mitochondrial pore-forming protein, is oligomeric and has a mixed orientation in Escherichia coli plasma membranes. *Proceedings of the National Academy of Sciences*, *88*(23), 10865–10869. https://doi.org/10.1073/PNAS.88.23.10865

Krämer, M., & Kunz, H. H. (2021). Indirect Export of Reducing Equivalents From the Chloroplast to Resupply NADP for C3 Photosynthesis—Growing Importance for Stromal NAD(H)? *Frontiers in Plant Science*, *12*, 719003. https://doi.org/10.3389/FPLS.2021.719003/BIBTEX

Kresge, N., Simoni, R. D., & Hill, R. L. (2005). Otto Fritz Meyerhof and the elucidation of the glycolytic pathway. *The Journal of Biological Chemistry*, *280*(4), e3. https://doi.org/10.1016/s0021-9258(20)76366-0

Kubo, S., Niina, T., & Takada, S. (2023). FO-F1 coupling and symmetry mismatch in ATP synthase resolved in every FO rotation step. *Biophysical Journal*, *122*(14), 2898–2909. https://doi.org/10.1016/J.BPJ.2022.09.034

Kühn, K., Carrie, C., Giraud, E., Wang, Y., Meyer, E. H., Narsai, R., Colas Des Francs-Small, C., Zhang, B., Murcha, M. W., & Whelan, J. (2011). The RCC1 family protein RUG3 is required for splicing of nad2 and complex I biogenesis in mitochondria of Arabidopsis thaliana. *Wiley Online Library*, *67*(6), 1067–1080. https://doi.org/10.1111/j.1365-313X.2011.04658.x

Kühn, K., Obata, T., Feher, K., Bock, R., Fernie, A. R., & Meyer, E. H. (2015). Complete Mitochondrial Complex I Deficiency Induces an Up-Regulation of Respiratory Fluxes That Is Abolished by Traces of Functional Complex I. *Plant Physiology*, *168*(4), 1537–1549. https://doi.org/10.1104/PP.15.00589

Kuzmin, E. V., Karpova, O. V., Elthon, T. E., & Newton, K. (2004). Mitochondrial Respiratory Deficiencies Signal Up-regulation of Genes for Heat Shock Proteins. *Journal of Biological Chemistry*, *279*(20), 20672–20677. https://doi.org/10.1074/jbc.M400640200

Lardy, H. A., Johnson, D., & McMurray, W. C. (1958). Antibiotics as tools for metabolic studies. I. A survey of toxic antibiotics in respiratory, phosphorylative and glycolytic systems. *Archives of Biochemistry and Biophysics*, *78*(2), 587–597. https://doi.org/10.1016/0003-9861(58)90383-7

Larkin, P. J., & Scowcroft, W. R. (1981). Somaclonal variation - a novel source of variability from cell cultures for plant improvement. *TAG. Theoretical and Applied Genetics. Theoretische Und Angewandte Genetik*, *60*(4), 197–214. https://doi.org/10.1007/BF02342540

Lauer, M., Knudsen, C., Newton, K., Gabay-Laughnan, S., & Laughnan, J. R. (1990). A partially deleted mitochondrial cytochrome oxidase gene in the NCS6 abnormal growth mutant of maize. *The New Biologist*, *2*(2), 179–186. http://www.ncbi.nlm.nih.gov/pubmed/1964592

Laughnan, J. R., & Gabay, S. J. (1973). Reaction of Germinating Maize Pollen to Helminthosporium maydis Pathotoxins1. *Crop Science*, *13*(6), 681–684. https://doi.org/10.2135/CROPSCI1973.0011183X001300060028X

Lee, B. H., Lee, H., Xiong, L., & Zhu, J. K. (2002). A Mitochondrial Complex I Defect Impairs Cold-Regulated Nuclear Gene Expression. *The Plant Cell*, *14*(6), 1235–1251. https://doi.org/10.1105/TPC.010433

Lelandais, C., Albert, B., Gutierres, S., de Paepe, R., Godelle, B., Vedel, F., & Chétrit, P. (1998). Organization and expression of the mitochondrial genome in the Nicotiana sylvestris CMSII mutant. *Genetics*, *150*(2), 873–882. https://doi.org/10.1093/GENETICS/150.2.873

León, G., Holuigue, L., & Jordana, X. (2007). Mitochondrial Complex II Is Essential for Gametophyte Development in Arabidopsis. *Plant Physiology*, *143*(4), 1534–1546. https://doi.org/10.1104/PP.106.095158

Levings, C. S. (1990). The Texas Cytoplasm of Maize: Cytoplasmic Male Sterility and Disease Susceptibility. *Science*, *250*(4983), 942–947. https://doi.org/10.1126/SCIENCE.250.4983.942

Levings, C. S., & Pring, D. R. (1976). Restriction endonuclease analysis of mitochondrial DNA from normal and Texas cytoplasmic male-sterile maize. *Science (New York, N.Y.)*, *193*(4248), 158–160. https://doi.org/10.1126/SCIENCE.193.4248.158

Li, X. Q., Chetrit, P., Mathieu, C., Vedel, F., De Paepe, R., Remy, R., & Ambard-Bretteville, F. (1988). Regeneration of cytoplasmic male sterile protoclones of Nicotiana sylvestris with mitochondrial variations. *Current Genetics 1988 13:3*, *13*(3), 261–266. https://doi.org/10.1007/BF00387773

Li, Y., Belt, K., Alqahtani, S. F., Saha, S., Fenske, R., Van Aken, O., Whelan, J., Millar, A. H., Murcha, M. W., & Huang, S. (2022). The mitochondrial <scp>LYR</scp> protein <scp>SDHAF1</scp> is required for succinate dehydrogenase activity in Arabidopsis. *The Plant Journal*, *110*(2), 499–512. https://doi.org/10.1111/tpj.15684

Lim, S. M., & Hooker, A. L. (1972). Disease Determinant of Helminthosporium maydis Race T. *Phytopathology*, *62*, 968–971.

Liu, T., Arsenault, J., Vierling, E., & Kim, M. (2021). Mitochondrial ATP synthase subunit d, a component of the peripheral stalk, is essential for growth and heat stress tolerance in Arabidopsis thaliana. *The Plant Journal*, *107*(3), 713–726. https://doi.org/10.1111/TPJ.15317

Lonsdale, D. (1987). Cytoplasmic male sterility: a molecular perspective [mitochondrial DNA; a review]. In *Plant Physiology and Biochemistry (France)* (Vol. 25, Issue 3, pp. 265–271). https://www.worldcat.org/title/427363607

Lothier, J., De Paepe, R., & Tcherkez, G. (2019). Mitochondrial complex I dysfunction increases CO2 efflux and reconfigures metabolic fluxes of day respiration in tobacco leaves. *New Phytologist*, *221*(2), 750–763. https://doi.org/10.1111/NPH.15393

Luo, D., Xu, H., Liu, Z., Guo, J., Li, H., Chen, L., Fang, C., Zhang, Q., Bai, M., Yao, N., Wu, H., Wu, H., Ji, C., Zheng, H., Chen, Y., Ye, S., Li, X., Zhao, X., Li, R., & Liu, Y. G. (2013). A detrimental mitochondrial-nuclear interaction causes cytoplasmic male sterility in rice. *Nature Genetics 2013 45:5*, *45*(5), 573–577. https://doi.org/10.1038/ng.2570

Lyu, W., Selinski, J., Li, L., Day, D. A., Murcha, M. W., Whelan, J., & Wang, Y. (2018). Isolation and Respiratory Measurements of Mitochondria from Arabidopsis thaliana *Journal of Visualized Experiments*, *131*. https://doi.org/10.3791/56627

Majsec, K., Bhuiyan, N. H., Sun, Q., Kumari, S., Kumar, V., Ware, D., & Van Wijk, K. J. (2017). The Plastid and Mitochondrial Peptidase Network in Arabidopsis thaliana: A Foundation for Testing Genetic Interactions and Functions in Organellar Proteostasis. *The Plant Cell*, *29*(11), 2687. https://doi.org/10.1105/TPC.17.00481

Malepszy, S., Burza, W., & Smiech, M. (1996). Characterization of a cucumber (Cucumis sativus L.) somaclonal variant with paternal inheritance. *Journal of Applied Genetics*, *37*(1), 65–78.

Mansilla, N., Garcia, L., Gonzalez, D. H., & Welchen, E. (2015). AtCOX10, a protein involved in haem o synthesis during cytochrome c oxidase biogenesis, is essential for plant embryogenesis and modulates the progression of senescence. *Journal of Experimental Botany*, *66*(21), 6761–6775. https://doi.org/10.1093/JXB/ERV381

Mansilla, N., Racca, S., Gras, D., Gonzalez, D., & Welchen, E. (2018). The Complexity of Mitochondrial Complex IV: An Update of Cytochrome c Oxidase Biogenesis in Plants. *International Journal of Molecular Sciences*, *19*(3), 662. https://doi.org/10.3390/ijms19030662

Marienfeld, J., & Newton, K. (1994). The maize NCS2 abnormal growth mutant has a chimeric nad4-nad7 mitochondrial gene and is associated with reduced complex I function. *Genetics*, *138*(3), 855–863. https://doi.org/10.1093/GENETICS/138.3.855

Masumoto, C., Miyazawa, S. I., Ohkawa, H., Fukuda, T., Taniguchi, Y., Murayama, S., Kusano, M., Saito, K., Fukayama, H., & Miyao, M. (2010). Phosphoenolpyruvate carboxylase intrinsically located in the chloroplast of rice plays a crucial role in ammonium assimilation. *Proceedings of the National Academy of Sciences of the United States of America*, *107*(11), 5226–5231. https://doi.org/10.1073/PNAS.0913127107/SUPPL_FILE/PNAS.200913127SI.PDF

Mathews, C. K., van Holde, K. E., & Ahern, K. G. (1999). Electron transport, oxidative phosphorylation and oxygen metabolism. In B. Roberts, J. Marsh, & L. Weber (Eds.), *Biochemistry* (3rd ed.). Pearson Education.

McCollum, C., Geißelsöder, S., Engelsdorf, T., Voitsik, A. M., & Voll, L. M. (2019). Deficiencies in the Mitochondrial Electron Transport Chain Affect Redox Poise and Resistance Toward Colletotrichum higginsianum. *Frontiers in Plant Science*, *10*, 435622. https://doi.org/10.3389/FPLS.2019.01262/BIBTEX

Mellon, M., Storti, M., Vera-Vives, A. M., Kramer, D. M., Alboresi, A., & Morosinotto, T. (2021). Inactivation of mitochondrial Complex I stimulates chloroplast ATPase in Physcomitrium patens . *Plant Physiology*. https://doi.org/10.1093/plphys/kiab276

Meyer, E. H., Giegé, P., Gelhaye, E., Rayapuram, N., Ahuja, U., Thöny-Meyer, L., Grienenberger, J. M., & Bonnard, G. (2005). AtCCMH, an essential component of the c-type cytochrome maturation pathway in Arabidopsis mitochondria, interacts with apocytochrome c. *Proceedings of the National Academy of Sciences of the United States of America*, *102*(44), 16113–16118. https://doi.org/10.1073/PNAS.0503473102/SUPPL_FILE/03473FIG6.JPG

Meyer, E. H., Tomaz, T., Carroll, A. J., Estavillo, G., Delannoy, E., Tanz, S. K., Small, I. D., Pogson, B. J., & Millar, A. H. (2009). Remodeled Respiration in ndufs4 with Low Phosphorylation Efficiency Suppresses Arabidopsis Germination and Growth and Alters Control of Metabolism at Night. *Plant Physiology*, *151*(2), 603–619. https://doi.org/10.1104/PP.109.141770

Meyer, E. H., Welchen, E., & Carrie, C. (2019). Assembly of the Complexes of the Oxidative Phosphorylation System in Land Plant Mitochondria. *Annual Review of Plant Biology*, *70*(1), 23–50. https://doi.org/10.1146/annurev-arplant-050718-100412

Michalecka, A. M., Agius, S. C., Møller, I. M., & Rasmusson, A. G. (2004). Identification of a mitochondrial external NADPH dehydrogenase by overexpression in transgenic Nicotiana sylvestris. *The Plant Journal : For Cell and Molecular Biology*, *37*(3), 415–425. https://doi.org/10.1046/J.1365-313X.2003.01970.X

Millar, A. H., Atkin, O. K., Ian Menz, R., Henry, B., Farquhar, G., & Day, D. A. (1998). Analysis of Respiratory Chain Regulation in Roots of Soybean Seedlings1. *Plant Physiology*, *117*(3), 1083–1093. https://doi.org/10.1104/pp.117.3.1083

Millar, A. H., Eubel, H., Jänsch, L., Kruft, V., Heazlewood, J. L., & Braun, H. P. (2004). Mitochondrial cytochrome c oxidase and succinate dehydrogenase complexes contain plant specific subunits. *Plant Molecular Biology 2004 56:1*, *56*(1), 77–90. https://doi.org/10.1007/S11103-004-2316-2

Millar, A. H., Whelan, J., Soole, K. L., & Day, D. A. (2011). Organization and Regulation of Mitochondrial Respiration in Plants. *Annual Review of Plant Biology*, *62*(1), 79–104. https://doi.org/10.1146/annurev-arplant-042110-103857

Miller, R. J., & Koeppe, D. E. (1971). Southern corn leaf blight: susceptible and resistant mitochondria. *Science (New York, N.Y.)*, *173*(3991), 67–69. https://doi.org/10.1126/SCIENCE.173.3991.67

Miranda-Astudillo, H., Ostolga-Chavarría, M., Cardol, P., & González-Halphen, D. (2022). Beyond being an energy supplier, ATP synthase is a sculptor of mitochondrial cristae. *Biochimica et Biophysica Acta (BBA) - Bioenergetics*, *1863*(6), 148569. https://doi.org/10.1016/J.BBABIO.2022.148569

Mishler, B. D., & Oliver, M. J. (2009). Putting Physcomitrella patens on the Tree of Life: The Evolution and Ecology of Mosses. In *Annual Plant Reviews Volume 36: The Moss Physcomitrella patens* (pp. 1–15). John Wiley & Sons, Ltd. https://doi.org/https://doi.org/10.1002/9781444316070.ch1

Moneger, F., Smart, C. J., & Leaver, C. J. (1994). Nuclear restoration of cytoplasmic male sterility in sunflower is associated with the tissue-specific regulation of a novel mitochondrial gene. *The EMBO Journal*, *13*(1), 8–17. https://doi.org/10.1002/J.1460-2075.1994.TB06230.X

Moore, A. L., Shiba, T., Young, L., Harada, S., Kita, K., & Ito, K. (2013). Unraveling the Heater: New Insights into the Structure of the Alternative Oxidase. *Https://Doi.Org/10.1146/Annurev-Arplant-042811-105432*, *64*, 637–663. https://doi.org/10.1146/ANNUREV-ARPLANT-042811-105432

Moreno-Beltrán, B., Díaz-Quintana, A., González-Arzola, K., Velázquez-Campoy, A., De La Rosa, M. A., & Díaz-Moreno, I. (2014). Cytochrome c1 exhibits two binding sites for cytochrome c in plants. *Biochimica et Biophysica Acta (BBA) - Bioenergetics*, *1837*(10), 1717–1729. https://doi.org/10.1016/J.BBABIO.2014.07.017

Moreno-García, B., López-Calcagno, P. E., Raines, C. A., & Sweetlove, L. J. (2022). Suppression of metabolite shuttles for export of chloroplast and mitochondrial ATP and NADPH increases the cytosolic NADH:NAD+ ratio in tobacco leaves in the dark. *Journal of Plant Physiology*, *268*, 153578. https://doi.org/10.1016/J.JPLPH.2021.153578

Mróz, T. L., Havey, M. J., & Bartoszewski, G. (2015). Cucumber Possesses a Single Terminal Alternative Oxidase Gene That is Upregulated by Cold Stress and in the Mosaic (MSC) Mitochondrial Mutants. *Plant Molecular Biology Reporter*, *33*(6), 1893–1906. https://doi.org/10.1007/S11105-015-0883-9/FIGURES/7

Mussgnug, J. H. (2015). Genetic tools and techniques for Chlamydomonas reinhardtii. *Applied Microbiology and Biotechnology*, *99*(13), 5407–5418. https://doi.org/10.1007/S00253-015-6698-7

Nakagawa, N., & Sakurai, N. (2006). A Mutation in At-nMat1a, Which Encodes a Nuclear Gene Having High Similarity to Group II Intron Maturase, Causes Impaired Splicing of Mitochondrial NAD4 Transcript and Altered Carbon Metabolism in Arabidopsisthaliana. *Plant and Cell Physiology*, *47*(6), 772–783. https://doi.org/10.1093/PCP/PCJ051

Nakazato, I., Okuno, M., Zhou, C., Itoh, T., Tsutsumi, N., Takenaka, M., & Arimura, S. I. (2022). Targeted base editing in the mitochondrial genome of Arabidopsis thaliana. *Proceedings of the National Academy of Sciences of the United States of America*, *119*(20). https://doi.org/10.1073/PNAS.2121177119/-/DCSUPPLEMENTAL

Nathans, D., & Smith, H. O. (1975). Restriction endonucleases in the analysis and restructuring of dna molecules. *Annual Review of Biochemistry*, *44*, 273–293. https://doi.org/10.1146/ANNUREV.BI.44.070175.001421

Newcomer, E. H. (1946). Concerning the Duality of the Mitochondria and the Validity of the Osmiophilic Platelets in Plants. *American Journal of Botany*, *33*(8), 684. https://doi.org/10.2307/2437349

Newton, K., Coe, E., Gabay-Laughnan, S., & Laughnan, J. (1989). Abnormal growth phenotypes and mitochondrial mutations in maize. *Maydica*, *34*(3), 291–296.

Newton, K., & Coe, E. J. (1986). Mitochondrial DNA changes in abnormal growth (nonchromosomal stripe) mutants of maize. *Proceedings of the National Academy of Sciences*, *83*(19), 7363–7366. https://doi.org/10.1073/PNAS.83.19.7363

Newton, K., Gabay-Laughnan, S., & De Paepe, R. (2004). *Mitochondrial Mutations in Plants* (pp. 121–141). https://doi.org/10.1007/978-1-4020-2400-9_7

Newton, K., Knudsen, C., Gabay-Laughnan, S., & Laughnan, J. R. (1990). An abnormal growth mutant in maize has a defective mitochondrial cytochrome oxidase gene. *The Plant Cell*, *2*(2), 107–113. https://doi.org/10.1105/TPC.2.2.107

Newton, K., Mariano, J. M., Gibson, C. M., Kuzmin, E., & Gabay-Laughnan, S. (1996). Involvement of S2 Episomal Sequences in the Generation of NCS4 Deletion Mutation in Maize Mitochondria. *DEVELOPMENTAL GENETICS*, 19277–19286. https://doi.org/10.1002/(SICI)1520-6408(1996)19:3

Ng, S., Ivanova, A., Duncan, O., Law, S. R., Van Aken, O., De Clercq, I., Wang, Y., Carrie, C., Xu, L., Kmiec, B., Walker, H., Van Breusegem, F., Whelan, J., & Giraud, E. (2013). A Membrane-Bound NAC Transcription Factor, ANAC017, Mediates Mitochondrial Retrograde Signaling in Arabidopsis. *The Plant Cell*, *25*(9), 3450–3471. https://doi.org/10.1105/TPC.113.113985

Nivison, H. T., & Hanson, M. R. (1989). Identification of a mitochondrial protein associated with cytoplasmic male sterility in petunia. *The Plant Cell*, *1*(11), 1121–1130. https://doi.org/10.1105/TPC.1.11.1121

Nowicka, B., & Kruk, J. (2010). Occurrence, biosynthesis and function of isoprenoid quinones. *Biochimica et Biophysica Acta*, *1797*(9), 1587–1605. https://doi.org/10.1016/J.BBABIO.2010.06.007

Ortiz-Ramírez, C., Hernandez-Coronado, M., Thamm, A., Catarino, B., Wang, M., Dolan, L., Feijó, J. A., & Becker, J. D. (2016). A Transcriptome Atlas of Physcomitrella patens Provides Insights into the Evolution and Development of Land Plants. *Molecular Plant*, *9*(2), 205–220. https://doi.org/10.1016/j.molp.2015.12.002

Palmer, G., Horgan, D., Tisdale, H., … T. S.-J. of B., & 1968, undefined. (1968). Studies on the respiratory chain-linked reduced nicotinamide adenine dinucleotide dehydrogenase: XIV. Location of the sites of inhibition of rotenone, barbiturates. *ASBMB*, *243*(4), 844–847. https://doi.org/10.1016/S0021-9258(19)81742-8

Park, H. S., Lee, W. K., Lee, S. C., Lee, H. O., Joh, H. J., Park, J. Y., Kim, S., Song, K., & Yang, T. J. (2021). Inheritance of chloroplast and mitochondrial genomes in cucumber revealed by four reciprocal F1 hybrid combinations. *Scientific Reports 2021 11:1*, *11*(1), 1–11. https://doi.org/10.1038/s41598-021-81988-w

Pennisi, R., Salvi, D., Brandi, V., Angelini, R., Ascenzi, P., & Polticelli, F. (2016). Molecular Evolution of Alternative Oxidase Proteins: A Phylogenetic and Structure Modeling Approach. *Journal of Molecular Evolution*, *82*(4–5), 207–218. https://doi.org/10.1007/S00239-016-9738-8/FIGURES/6

Perales, M., Eubel, H., Heinemeyer, J., Colaneri, A., Zabaleta, E., & Braun, H.-P. (2005). Disruption of a Nuclear Gene Encoding a Mitochondrial Gamma Carbonic Anhydrase Reduces Complex I and Supercomplex I+III2 Levels and Alters Mitochondrial Physiology in Arabidopsis. *Journal of Molecular Biology*, *350*(2), 263–277. https://doi.org/10.1016/j.jmb.2005.04.062

Peters, K., Belt, K., & Braun, H.-P. (2013). 3D Gel Map of Arabidopsis Complex I. *Frontiers in Plant Science*, *4*. https://doi.org/10.3389/fpls.2013.00153

Peters, K., Nießen, M., Peterhänsel, C., Späth, B., Hölzle, A., Binder, S., Marchfelder, A., & Braun, H. P. (2012). Complex I-complex II ratio strongly differs in various organs of Arabidopsis thaliana. *Plant Molecular Biology*, *79*(3), 273–284. https://doi.org/10.1007/S11103-012-9911-4/FIGURES/8

Peterson, P. A., Flavell, R. B., & Barratt, D. H. P. (1975). Altered mitochondrial membrane activities associated with cytoplasmically-inherited disease sensitivity in maize. *TAG. Theoretical and Applied Genetics. Theoretische Und Angewandte Genetik*, *45*(7), 309–314. https://doi.org/10.1007/BF00276685

Pétriacq, P., De Bont, L., Genestout, L., Hao, J., Laureau, C., Florez-Sarasa, I., Rzigui, T., Queval, G., Gilard, F., Mauve, C., Guérard, F., Lamothe-Sibold, M., Marion, J., Fresneau, C., Brown, S., Danon, A., Krieger-Liszkay, A., Berthomé, R., Ribas-Carbo, M., … De Paepe, R. (2017). Photoperiod Affects the Phenotype of Mitochondrial Complex I Mutants. *Plant Physiology*, *173*(1), 434–455. https://doi.org/10.1104/PP.16.01484

Pineau, B., Mathieu, C., Gérard-Hirne, C., de Paepe, R., & Chétrit, P. (2005). Targeting the NAD7 subunit to mitochondria restores a functional complex I and a wild type phenotype in the Nicotiana sylvestris CMS II mutant lacking nad7. *Journal of Biological Chemistry*, *280*(28), 25994–26001. https://doi.org/10.1074/jbc.M500508200

Pla, M., Mathieu, C., de Paepe, R., Chétrit, P., & Vedel, F. (1995). Deletion of the last two exons of the mitochondrialnad7 gene results in lack of the NAD7 polypeptide in aNicotiana sylvestris CMS mutant. *Molecular and General Genetics MGG 1995 248:1*, *248*(1), 79–88. https://doi.org/10.1007/BF02456616

Plaxton, W. C. (1996). THE ORGANIZATION AND REGULATION OF PLANT GLYCOLYSIS. *Annual Review of Plant Physiology and Plant Molecular Biology*, *47*(1), 185–214. https://doi.org/10.1146/ANNUREV.ARPLANT.47.1.185

Podgórska, A., Ostaszewska, M., Gardeström, P., Rasmusson, A. G., & Szal, B. (2015). In comparison with nitrate nutrition, ammonium nutrition increases growth of the frostbite1 Arabidopsis mutant. *Plant, Cell and Environment*, *38*(1), 224–237. https://doi.org/10.1111/PCE.12404/SUPPINFO

Podgórska, A., Ostaszewska-Bugajska, M., Tarnowska, A., Burian, M., Borysiuk, K., Gardeström, P., & Szal, B. (2018). Nitrogen Source Dependent Changes in Central Sugar Metabolism Maintain Cell Wall Assembly in Mitochondrial Complex I-Defective frostbite1 and Secondarily Affect Programmed Cell Death. *International Journal of Molecular Sciences 2018, Vol. 19, Page 2206*, *19*(8), 2206. https://doi.org/10.3390/IJMS19082206

Popov, V. N., Eprintsev, A. T., Fedorin, D. N., & Igamberdiev, A. U. (2010). Succinate dehydrogenase in Arabidopsis thaliana is regulated by light via phytochrome A. *FEBS Letters*, *584*(1), 199–202. https://doi.org/10.1016/J.FEBSLET.2009.11.057

Priault, P., Fresneau, C., Noctor, G., De Paepe, R., Cornic, G., & Streb, P. (2006). The mitochondrial CMSII mutation of Nicotiana sylvestris impairs adjustment of photosynthetic carbon assimilation to higher growth irradiance. *Journal of Experimental Botany*, *57*(9), 2075–2085. https://doi.org/10.1093/jxb/erj161

Priault, P., Tcherkez, G., Cornic, G., de Paepe, R., Naik, R., Ghashghaie, J., & Streb, P. (2006). The lack of mitochondrial complex I in a CMSII mutant of Nicotiana sylvestris increases photorespiration through an increased internal resistance to CO2 diffusion. *Journal of Experimental Botany*, *57*(12), 3195–3207. https://doi.org/10.1093/JXB/ERL083

Priault, P., Vidal, G., De Paepe, R., & Ribas-Carbo, M. (2007). Leaf age-related changes in respiratory pathways are dependent on complex I activity in Nicotiana sylvestris. *Physiologia Plantarum*, *129*(1), 152–162. https://doi.org/10.1111/J.1399-3054.2006.00836.X

Price, C. A., & Thimann, K. v. (1951). The succinic dehydrogenase of seedlings. *Archives of Biochemistry and Biophysics*, *33*(1), 170–171. https://doi.org/10.1016/0003-9861(51)90093-8

Qi, M., Zhao, Z., & Nixon, P. J. (2023). The Photosynthetic Electron Transport Chain of Oxygenic Photosynthesis. *Https://Home.Liebertpub.Com/Bioe*, *5*(1), 31–38. https://doi.org/10.1089/BIOE.2023.0003

Qi, W., Tian, Z., Lu, L., Chen, X., Chen, X., Zhang, W., & Song, R. (2017). Editing of mitochondrial transcripts nad3 and cox2 by dek10 is essential for mitochondrial function and maize plant development. *Genetics*, *205*(4), 1489–1501. https://doi.org/10.1534/GENETICS.116.199331/-/DC1

Racca, S., Welchen, E., Gras, D. E., Tarkowská, D., Turečková, V., Maurino, V. G., & Gonzalez, D. H. (2018). Interplay between cytochrome c and gibberellins during Arabidopsis vegetative development. *The Plant Journal*, *94*(1), 105–121. https://doi.org/10.1111/TPJ.13845

Radin, I., Kost, L., Gey, U., Steinebrunner, I., & Rödel, G. (2021). The mitochondrial copper chaperone COX11 has an additional role in cellular redox homeostasis. *PLOS ONE*, *16*(12), e0261465. https://doi.org/10.1371/JOURNAL.PONE.0261465

Radin, I., Mansilla, N., Rödel, G., & Steinebrunner, I. (2015). The Arabidopsis COX11 Homolog is Essential for Cytochrome c Oxidase Activity. *Frontiers in Plant Science*, *6*(DEC), 1–17. https://doi.org/10.3389/fpls.2015.01091

Raghavendra, A. S., Padmasree, K., & Saradadevi, K. (1994). Interdependence of photosynthesis and respiration in plant cells: interactions between chloroplasts and mitochondria. *Plant Science*, *97*(1), 1–14.

Rasmusson, A. G., Geisler, D. A., & Møller, I. M. (2008). The multiplicity of dehydrogenases in the electron transport chain of plant mitochondria. *Mitochondrion*, *8*(1), 47–60. https://doi.org/10.1016/J.MITO.2007.10.004

Remacle, C., Cardol, P., Coosemans, N., Gaisne, M., & Bonnefoy, N. (2006). High-efficiency biolistic transformation of *Chlamydomonas* mitochondria can be used to insert mutations in complex I genes. *Proceedings of the National Academy of Sciences*, *103*(12), 4771–4776. https://doi.org/10.1073/pnas.0509501103

Rensing, S. A., Goffinet, B., Meyberg, R., Wu, S. Z., & Bezanilla, M. (2020). The Moss Physcomitrium (Physcomitrella) patens: A Model Organism for Non-Seed Plants. *The Plant Cell*, *32*(5), 1361–1376. https://doi.org/10.1105/TPC.19.00828

Rensing, S. A., Lang, D., Zimmer, A. D., Terry, A., Salamov, A., Shapiro, H., Nishiyama, T., Perroud, P. F., Lindquist, E. A., Kamisugi, Y., Tanahashi, T., Sakakibara, K., Fujita, T., Oishi, K., Shin-I, T., Kuroki, Y., Toyoda, A., Suzuki, Y., Hashimoto, S. I., … Boore, J. L. (2008). The Physcomitrella genome reveals evolutionary insights into the conquest of land by plants. *Science*, *319*(5859), 64–69. https://doi.org/10.1126/SCIENCE.1150646/SUPPL_FILE/RENSING_SOM.PDF

Rhoades, M. M. (1931). Cytoplasmic inheritance of male sterility in zea mays. *Science*, *73*(1891), 340–341. https://doi.org/10.1126/SCIENCE.73.1891.340/ASSET/7B0FA880-5702-4ED1-88A0-82D62D7D7008/ASSETS/SCIENCE.73.1891.340.FP.PNG

Rhoades, M. M. (1943). Genic Induction of an Inherited Cytoplasmic Difference. *Proceedings of the National Academy of Sciences*, *29*(11), 327–329. https://doi.org/10.1073/PNAS.29.11.327

Rhoades, M. M. (1950). Gene induced mutation of a heritable cytoplasmic factor producing male sterility in maize. *Proceedings of the National Academy of Sciences of the United States of America*, *36*(11), 634–635. https://doi.org/10.1073/PNAS.36.11.634

Rhoads, D. M., Levings, C. S., & Siedow, J. N. (1995). URF13, a Ligand-Gated, Pore-Forming Receptor for T-toxin in the Inner Membrane of cms.T Mitochondria. *Journal of Bioenergetics and Biomembranes*, *27*(4).

Rhoads, D. M., Umbach, A. L., Sweet, C. R., Lennon, A. M., Rauch, G. S., & Siedow, J. N. (1998). Regulation of the cyanide-resistant alternative oxidase of plant mitochondria. Identification of the cysteine residue involved in alpha-keto acid stimulation and intersubunit disulfide bond formation. *The Journal of Biological Chemistry*, *273*(46), 30750–30756. https://doi.org/10.1074/JBC.273.46.30750

Ribas-Carbo, M., Taylor, N. L., Giles, L., Busquets, S., Finnegan, P. M., Day, D. A., Lambers, H., Medrano, H., Berry, J. A., & Flexas, J. (2005). Effects of Water Stress on Respiration in Soybean Leaves. *Plant Physiology*, *139*(1), 466–473. https://doi.org/10.1104/pp.105.065565

Robinson, S. A., Yakir, D., Ribas-Carbo, M., Giles, L., Osmond, C. B., Siedow, J. N., & Berry, J. A. (1992). Measurements of the Engagement of Cyanide-Resistant Respiration in the Crassulacean Acid Metabolism Plant *Kalanchoë daigremontiana* with the Use of On-Line Oxygen Isotope Discrimination. *Plant Physiology*, *100*(3), 1087–1091. https://doi.org/10.1104/pp.100.3.1087

Robison, M. M., Ling, X., Smid, M. P. L., Zarei, A., & Wolyn, D. J. (2009). Antisense expression of mitochondrial ATP synthase subunits OSCP (ATP5) and gamma (ATP3) alters leaf morphology, metabolism and gene expression in Arabidopsis. *Plant & Cell Physiology*, *50*(10), 1840–1850. https://doi.org/10.1093/PCP/PCP125

Rogers, J. S., & Edwardson, J. R. (1952). The Utilization of Cytoplasmic Male-Sterile Inbreds in the Production of Corn Hybrids 1 . *Agronomy Journal*, *44*(1), 8–13. https://doi.org/10.2134/AGRONJ1952.00021962004400010004X

Roschzttardtz, H., Fuentes, I., Vásquez, M., Corvalán, C., León, G., Gómez, I., Araya, A., Holuigue, L., Vicente-Carbajosa, J., & Jordana, X. (2009). A Nuclear Gene Encoding the Iron-Sulfur Subunit of Mitochondrial Complex II Is Regulated by B3 Domain Transcription Factors during Seed Development in Arabidopsis. *Plant Physiology*, *150*(1), 84–95. https://doi.org/10.1104/PP.109.136531

Roussell, D. L., Thompson, D. L., Pallardy, S. G., Miles, D., & Newton, K. (1991). Chloroplast Structure and Function Is Altered in the NCS2 Maize Mitochondrial Mutant. *Plant Physiology*, *96*(1), 232. https://doi.org/10.1104/PP.96.1.232

Sabar, M., De Paepe, R., & De Kouchkovsky, Y. (2000). Complex I Impairment, Respiratory Compensations, and Photosynthetic Decrease in Nuclear and Mitochondrial Male Sterile Mutants of Nicotiana sylvestris. *Plant Physiology*, *124*(3), 1239–1250. https://doi.org/10.1104/PP.124.3.1239

Salinas, T., Larosa, V., Cardol, P., Maréchal-Drouard, L., & Remacle, C. (2014). Respiratory-deficient mutants of the unicellular green alga *Chlamydomonas*: A review. *Biochimie*, *100*(1), 207–218. https://doi.org/10.1016/j.biochi.2013.10.006

Schaefer, D. G., & Zrÿd, J. P. (1997). Efficient gene targeting in the moss Physcomitrella patens. *The Plant Journal*, *11*(6), 1195–1206. https://doi.org/10.1046/J.1365-313X.1997.11061195.X

Schallenberg-Rüdinger, M., Kindgren, P., Zehrmann, A., Small, I., & Knoop, V. (2013). A DYW-protein knockout in Physcomitrella affects two closely spaced mitochondrial editing sites and causes a severe developmental phenotype. *The Plant Journal*, *76*(3), 420–432. https://doi.org/10.1111/TPJ.12304

Schertl, P., & Braun, H.-P. (2014). Respiratory electron transfer pathways in plant mitochondria. *Frontiers in Plant Science*, *5*(APR), 1–11. https://doi.org/10.3389/fpls.2014.00163

Schimmeyer, J., Bock, R., & Meyer, E. H. (2016). l-Galactono-1,4-lactone dehydrogenase is an assembly factor of the membrane arm of mitochondrial complex I in Arabidopsis. *Plant Molecular Biology*, *90*(1–2), 117–126. https://doi.org/10.1007/S11103-015-0400-4/FIGURES/5

Schmidt-Rohr, K. (2020). Oxygen Is the High-Energy Molecule Powering Complex Multicellular Life: Fundamental Corrections to Traditional Bioenergetics. *ACS Omega*, *5*(5), 2221–2233. https://doi.org/10.1021/acsomega.9b03352

Schwartz, D. (1951). The Interaction of Nuclear and Cytoplasmic Factors in the Inheritance of Male Sterility in Maize. *Genetics*, *36*(6), 676–696. https://doi.org/10.1093/genetics/36.6.676

Selinski, J., Hartmann, A., Kordes, A., Deckers-Hebestreit, G., Whelan, J., & Scheibe, R. (2017). Analysis of posttranslational activation of alternative oxidase isoforms. *Plant Physiology*, *174*(4), 2113–2127. https://doi.org/10.1104/pp.17.00681

Selinski, J., Scheibe, R., Day, D. A., & Whelan, J. (2018). Alternative Oxidase Is Positive for Plant Performance. In *Trends in Plant Science* (Vol. 23, Issue 7, pp. 588–597). Elsevier Ltd. https://doi.org/10.1016/j.tplants.2018.03.012

Senkler, J., Senkler, M., Eubel, H., Hildebrandt, T., Lengwenus, C., Schertl, P., Schwarzländer, M., Wagner, S., Wittig, I., & Braun, H. P. (2017). The mitochondrial complexome of Arabidopsis thaliana. *The Plant Journal*, *89*(6), 1079–1092. https://doi.org/10.1111/TPJ.13448

Shameer, S., Ratcliffe, R. G., & Sweetlove, L. J. (2019). Leaf energy balance requires mitochondrial respiration and export of chloroplast NADPH in the light. *Plant Physiology*, *180*(4), 1947–1961. https://doi.org/10.1104/pp.19.00624

Shen, W., Wei, Y., Dauk, M., Tan, Y., Taylor, D. C., Selvaraj, G., & Zou, J. (2006). Involvement of a Glycerol-3-Phosphate Dehydrogenase in Modulating the NADH/NAD+ Ratio Provides Evidence of a Mitochondrial Glycerol-3-Phosphate Shuttle in Arabidopsis. *The Plant Cell*, *18*(2), 422–441. https://doi.org/10.1105/TPC.105.039750

Shen, W., Wei, Y., Dauk, M., Zheng, Z., & Zou, J. (2003). Identification of a mitochondrial glycerol-3-phosphate dehydrogenase from Arabidopsis thaliana: Evidence for a mitochondrial glycerol-3-phosphate shuttle in plants. *FEBS Letters*, *536*(1–3), 92–96. https://doi.org/10.1016/S0014-5793(03)00033-4

Shevtsov-Tal, S., Best, C., Matan, R., Chandran, S. A., Brown, G. G., & Ostersetzer-Biran, O. (2021). nMAT3 is an essential maturase splicing factor required for holo-complex I biogenesis and embryo development in Arabidopsis thaliana plants. *The Plant Journal*, *106*(4), 1128–1147. https://doi.org/10.1111/TPJ.15225

Shumway, L. K., & Bauman, L. F. (1967). Nonchromosomal Stripe of Maize. *Genetics*, *55*(1), 33. https://doi.org/10.1093/GENETICS/55.1.33

Sluse, F. E., & Jarmuszkiewicz, W. (2000). Activity and functional interaction of alternative oxidase and uncoupling protein in mitochondria from tomato fruit. *Brazilian Journal of Medical and Biological Research*, *33*(3), 259–268. https://doi.org/10.1590/S0100-879X2000000300002

Soto, I. C., & Barrientos, A. (2016). Mitochondrial Cytochrome c Oxidase Biogenesis Is Regulated by the Redox State of a Heme-Binding Translational Activator. *Https://Home.Liebertpub.Com/Ars*, *24*(6), 281–298. https://doi.org/10.1089/ARS.2015.6429

Spikes, T. E., Montgomery, M. G., & Walker, J. E. (2020). Structure of the dimeric ATP synthase from bovine mitochondria. *Proceedings of the National Academy of Sciences of the United States of America*, *117*(38), 23519–23526. https://doi.org/10.1073/PNAS.2013998117/SUPPL_FILE/PNAS.2013998117.SM03.MP4

Steere, W. C., & Schuster, R. M. (1984). New Manual of Bryology. *The Bryologist*, *87*(3), 288. https://doi.org/10.2307/3242815

Steinebrunner, I., Gey, U., Andres, M., Garcia, L., & Gonzalez, D. H. (2014). Divergent functions of the Arabidopsis mitochondrial SCO proteins: HCC1 is essential for COX activity while HCC2 is involved

in the UV-B stress response. *Frontiers in Plant Science*, *5*(MAR). https://doi.org/10.3389/FPLS.2014.00087

Steinebrunner, I., Landschreiber, M., Krause-Buchholz, U., Teichmann, J., & Rödel, G. (2011). HCC1, the Arabidopsis homologue of the yeast mitochondrial copper chaperone SCO1, is essential for embryonic development. *Journal of Experimental Botany*, *62*(1), 319–330. https://doi.org/10.1093/JXB/ERQ269

Sugiura, C., Kobayashi, Y., Aoki, S., Sugita, C., & Sugita, M. (2003). Complete chloroplast DNA sequence of the moss Physcomitrella patens : evidence for the loss and relocation of rpoA from the chloroplast to the nucleus. *Nucleic Acids Research*, *31*(18), 5324–5331. https://doi.org/10.1093/NAR/GKG726

Sunderhaus, S., Dudkina, N. V, Jänsch, L., Klodmann, J., Heinemeyer, J., Perales, M., Zabaleta, E., Boekema, E. J., & Braun, H.-P. (2006). Carbonic Anhydrase Subunits Form a Matrix-Exposed Domain Attached to the Membrane Arm of Mitochondrial Complex I in Plants. *Journal of Biological Chemistry*. https://doi.org/10.1074/jbc.m511542200

Sweetlove, L. J., Beard, K. F. M., Nunes-Nesi, A., Fernie, A. R., & Ratcliffe, R. G. (2010). Not just a circle: Flux modes in the plant TCA cycle. *Trends in Plant Science*, *15*(8), 462–470. https://doi.org/10.1016/j.tplants.2010.05.006

Sweetman, C., Waterman, C. D., Rainbird, B. M., Smith, P. M. C., Jenkins, C. D., Day, D. A., & Soole, K. L. (2019). AtNDB2 Is the Main External NADH Dehydrogenase in Mitochondria and Is Important for Tolerance to Environmental Stress. *Plant Physiology*, *181*(2), 774–788. https://doi.org/10.1104/pp.19.00877

Szal, B., Dąbrowska, Z., Malmberg, G., Gardeström, P., & Rychter, A. M. (2008). Changes in energy status of leaf cells as a consequence of mitochondrial genome rearrangement. *Planta*, *227*(3), 697–706. https://doi.org/10.1007/S00425-007-0652-6/TABLES/5

Szal, B., Łukawska, K., Zdolińska, I., & Rychter, A. M. (2009). Chilling stress and mitochondrial genome rearrangement in the MSC16 cucumber mutant affect the alternative oxidase and antioxidant defense system to a similar extent. *Physiologia Plantarum*, *137*(4), 435–445. https://doi.org/10.1111/J.1399-3054.2009.01255.X

Tcherkez, G., Gauthier, P., Buckley, T. N., Busch, F. A., Barbour, M. M., Bruhn, D., Heskel, M. A., Gong, X. Y., Crous, K. Y., Griffin, K., Way, D., Turnbull, M., Adams, M. A., Atkin, O. K., Farquhar, G. D., & Cornic, G. (2017). Leaf day respiration: low CO2 flux but high significance for metabolism and carbon balance. *New Phytologist*, *216*(4), 986–1001. https://doi.org/10.1111/NPH.14816

Terasawa, K., Odahara, M., Kabeya, Y., Kikugawa, T., Sekine, Y., Fujiwara, M., & Sato, N. (2007). The Mitochondrial Genome of the Moss Physcomitrella patens Sheds New Light on Mitochondrial Evolution in Land Plants. *Molecular Biology and Evolution*, *24*(3), 699–709. https://doi.org/10.1093/MOLBEV/MSL198

Tivendale, N. D., Belt, K., Berkowitz, O., Whelan, J., Millar, A. H., & Huang, S. (2021). Knockdown of Succinate Dehydrogenase Assembly Factor 2 Induces Reactive Oxygen Species–Mediated Auxin Hypersensitivity Causing pH-Dependent Root Elongation. *Plant and Cell Physiology*, *62*(7), 1185–1198. https://doi.org/10.1093/PCP/PCAB061

Tronconi, M. A., Fahnenstich, H., Gerrard Weehler, M. C., Andreo, C. S., Flügge, U. I., Drincovich, M. F., & Maurino, V. G. (2008). Arabidopsis NAD-Malic Enzyme Functions As a Homodimer and Heterodimer and Has a Major Impact on Nocturnal Metabolism. *Plant Physiology*, *146*(4), 1540. https://doi.org/10.1104/PP.107.114975

Tsukihara, T., Aoyama, H., Yamashita, E., Tomizaki, T., Yamaguchi, H., Shinzawa-Itoh, K., Nakashima, R., Yaono, R., & Yoshikawa, S. (1995). Structures of metal sites of oxidized bovine heart cytochrome c oxidase at 2.8 A. *Science (New York, N.Y.)*, *269*(5227), 1069–1074. https://doi.org/10.1126/SCIENCE.7652554

Tuominen, E. K. J., Zhu, K., Wallace, C. J. A., Clark-Lewis, I., Craig, D. B., Rytömaa, M., & Kinnunen, P. K. J. (2001). ATP induces a conformational change in lipid-bound cytochrome c. *The Journal of Biological Chemistry*, *276*(22), 19356–19362. https://doi.org/10.1074/JBC.M100853200

Ukolova, I. V., Kondakova, M. A., Kondratov, I. G., Sidorov, A. V., Borovskii, G. B., & Voinikov, V. K. (2020). New insights into the organisation of the oxidative phosphorylation system in the example of pea shoot mitochondria. *Biochimica et Biophysica Acta (BBA) - Bioenergetics*, *1861*(11), 148264. https://doi.org/10.1016/J.BBABIO.2020.148264

Ullstrup, A. J. (1972). The Impacts of the Southern Corn Leaf Blight Epidemics of 1970-1971. *Annual Review of Phytopathology*, *10*(1), 37–50. https://doi.org/10.1146/ANNUREV.PY.10.090172.000345

Unseld, M., Marienfeld, J. R., Brandt, P., & Brennicke, A. (1997). The mitochondrial genome of Arabidopsis thaliana contains 57 genes in 366,924 nucleotides. *Nature Genetics 1997 15:1*, *15*(1), 57–61. https://doi.org/10.1038/ng0197-57

Van Aken, O., Zhang, B., Law, S., Narsai, R., & Whelan, J. (2013). AtWRKY40 and AtWRKY63 Modulate the Expression of Stress-Responsive Nuclear Genes Encoding Mitochondrial and Chloroplast Proteins. *Plant Physiology*, *162*(1), 254–271. https://doi.org/10.1104/PP.113.215996

Van Hautegem, T., Waters, A. J., Goodrich, J., & Nowack, M. K. (2015). Only in dying, life: programmed cell death during plant development. *Trends in Plant Science*, *20*(2), 102–113. https://doi.org/10.1016/J.TPLANTS.2014.10.003

Vanlerberghe, G. C., Dahal, K., Alber, N. A., & Chadee, A. (2020). Photosynthesis, respiration and growth: A carbon and energy balancing act for alternative oxidase. *Mitochondrion*, *52*, 197–211. https://doi.org/10.1016/j.mito.2020.04.001

Vanlerberghe, G. C., & McIntosh, L. (1997). ALTERNATIVE OXIDASE: From Gene to Function. *Annual Review of Plant Physiology and Plant Molecular Biology*, *48*, 703–734. https://doi.org/10.1146/ANNUREV.ARPLANT.48.1.703

Vanlerberghe, G. C., & Ordog, S. H. (2002). *Alternative Oxidase: Integrating Carbon Metabolism and Electron Transport in Plant Respiration*. 173–191. https://doi.org/10.1007/0-306-48138-3_11

Vempati, U. D., Han, X., & Moraes, C. T. (2009). Lack of Cytochrome c in Mouse Fibroblasts Disrupts Assembly/Stability of Respiratory Complexes I and IV. *The Journal of Biological Chemistry*, *284*(7), 4383. https://doi.org/10.1074/JBC.M805972200

Veniamin, S., Sawatzky, L. G., Banting, G. S., & Glerum, D. M. (2011). Characterization of the peroxide sensitivity of COX-deficient yeast strains reveals unexpected relationships between COX assembly proteins. *Free Radical Biology & Medicine*, *51*(8), 1589–1600. https://doi.org/10.1016/J.FREERADBIOMED.2011.06.024

Vidal, G., Ribas-Carbo, M., Garmier, M., Dubertret, G., Rasmusson, A. G., Mathieu, C., Foyer, C. H., & De Paepe, R. (2007). Lack of Respiratory Chain Complex I Impairs Alternative Oxidase Engagement and Modulates Redox Signaling during Elicitor-Induced Cell Death in Tobacco. *The Plant Cell*, *19*(2), 640–655. https://doi.org/10.1105/tpc.106.044461

Villarreal, F., Martín, V., Colaneri, A., González-Schain, N., Perales, M., Martín, M., Lombardo, C., Braun, H.-P., Bartoli, C., & Zabaleta, E. (2009). Ectopic expression of mitochondrial gamma carbonic anhydrase 2 causes male sterility by anther indehiscence. *Plant Molecular Biology*, *70*(4), 471–485. https://doi.org/10.1007/s11103-009-9484-z

Voon, C. P., & Lim, B. L. (2019). ATP translocation and chloroplast biology. *National Science Review*, *6*(6), 1073–1076. https://doi.org/10.1093/NSR/NWZ089

Wallström, S. V., Florez-Sarasa, I., Araújo, W. L., Aidemark, M., Fernández-Fernández, M., Fernie, A. R., Ribas-Carbó, M., & Rasmusson, A. G. (2014). Suppression of the external mitochondrial NADPH

dehydrogenase, NDB1, in arabidopsis thaliana affects central metabolism and vegetative growth. *Molecular Plant*, *7*(2), 356–368. https://doi.org/10.1093/mp/sst115

Wallström, S. V., Florez-Sarasa, I., Araújo, W. L., Escobar, M. A., Geisler, D. A., Aidemark, M., Lager, I., Fernie, A. R., Ribas-Carbó, M., & Rasmusson, A. G. (2014). Suppression of NDA-Type Alternative Mitochondrial NAD(P)H Dehydrogenases in Arabidopsis thaliana Modifies Growth and Metabolism, but not High Light Stimulation of Mitochondrial Electron Transport. *Plant and Cell Physiology*, *55*(5), 881–896. https://doi.org/10.1093/PCP/PCU021

Wang, C., Blondel, L., Quadrado, M., Dargel-Graffin, C., & Mireau, H. (2022). The pentatricopeptide repeat protein MTSF3 is required for nad2 mRNA stability and embryogenesis in Arabidopsis. *BioRxiv*, 2022.05.20.492872. https://doi.org/10.1101/2022.05.20.492872

Wang, Q., Fristedt, R., Yu, X., Chen, Z., Liu, H., Lee, Y., Guo, H., Merchant, S. S., & Lin, C. (2012). The γ-Carbonic Anhydrase Subcomplex of Mitochondrial Complex I Is Essential for Development and Important for Photomorphogenesis of Arabidopsis. *Plant Physiology*, *160*(3), 1373. https://doi.org/10.1104/PP.112.204339

Wang, Y., & Hekimi, S. (2016). Understanding Ubiquinone. *Trends in Cell Biology*, *26*(5), 367–378. https://doi.org/10.1016/j.tcb.2015.12.007

Watson, C. V., Nath, J., & Nanda, D. (1977). Possible mitochondrial involvement in mechanism of cytoplasmic male sterility in maize (Zea mays L.). *Biochemical Genetics 1977 15:11*, *15*(11), 1113–1124. https://doi.org/10.1007/BF00484501

Welchen, E., & Gonzalez, D. H. (2016). Cytochrome c, a hub linking energy, redox, stress and signaling pathways in mitochondria and other cell compartments. *Physiologia Plantarum*, *157*(3), 310–321. https://doi.org/10.1111/ppl.12449

Welchen, E., Hildebrandt, T. M., Lewejohann, D., Gonzalez, D. H., & Braun, H. P. (2012). Lack of cytochrome c in Arabidopsis decreases stability of Complex IV and modifies redox metabolism without affecting Complexes I and III. *Biochimica et Biophysica Acta (BBA) - Bioenergetics*, *1817*(7), 990–1001. https://doi.org/10.1016/J.BBABIO.2012.04.008

Welchen, E., Klodmann, J., & Braun, H. P. (2011). Biogenesis and supramolecular organization of the oxidative phosphorylation system in plants. In *Plant Mitochondria* (pp. 327–355). Springer New York. https://doi.org/10.1007/978-0-387-89781-3_13

Wikström, M., & Sharma, V. (2018). Proton pumping by cytochrome c oxidase – A 40 year anniversary. *Biochimica et Biophysica Acta (BBA) - Bioenergetics*, *1859*(9), 692–698. https://doi.org/10.1016/J.BBABIO.2018.03.009

Wirth, C., Brandt, U., Hunte, C., & Zickermann, V. (2016). Structure and function of mitochondrial complex I. *Biochimica et Biophysica Acta (BBA) - Bioenergetics*, *1857*(7), 902–914. https://doi.org/10.1016/J.BBABIO.2016.02.013

Wiseman, A., Gillham, N. W., & Boynton, J. E. (1977). The mitochondrial genome ofChlamydomonas. *Molecular and General Genetics MGG*, *150*(2), 109–118. https://doi.org/10.1007/BF00695390

Wiskich, J. T., & Dry, I. B. (1985). The Tricarboxylic Acid Cycle in Plant Mitochondria: Its Operation and Regulation. *Higher Plant Cell Respiration*, 281–313. https://doi.org/10.1007/978-3-642-70101-6_11

Xiao, S., Zang, J., Pei, Y., Liu, J., Liu, J., Song, W., Shi, Z., Su, A., Zhao, J., & Chen, H. (2020). Activation of Mitochondrial orf355 Gene Expression by a Nuclear-Encoded DREB Transcription Factor Causes Cytoplasmic Male Sterility in Maize. *Molecular Plant*, *13*(9), 1270–1283. https://doi.org/10.1016/J.MOLP.2020.07.002

Xu, L., Law, S. R., Murcha, M. W., Whelan, J., & Carrie, C. (2013). The dual targeting ability of type II NAD(P)H dehydrogenases arose early in land plant evolution. *BMC Plant Biology*, *13*(1), 100. https://doi.org/10.1186/1471-2229-13-100

Yamato, K., & Newton, K. (1999). Heteroplasmy and homoplasmy for maize mitochondrial mutants: a rare homoplasmic nad4 deletion mutant plant. *Journal of Heredity*, *90*(3), 369–373. https://doi.org/10.1093/JHERED/90.3.369

Yang, H., Xue, Y., Li, B., Lin, Y., Li, H., Guo, Z., Li, W., Fu, Z., Ding, D., & Tang, J. (2022). The chimeric gene atp6c confers cytoplasmic male sterility in maize by impairing the assembly of the mitochondrial ATP synthase complex. *Molecular Plant*, *15*(5), 872–886. https://doi.org/10.1016/J.MOLP.2022.03.002

Young, E. G., & Hanson, M. R. (1987). A fused mitochondrial gene associated with cytoplasmic male sterility is developmentally regulated. *Cell*, *50*(1), 41–49. https://doi.org/10.1016/0092-8674(87)90660-X

Yuan, H., Journal, D. L.-T. P., & 2012, undefined. (2012). Functional disruption of the pentatricopeptide protein SLG1 affects mitochondrial RNA editing, plant development, and responses to abiotic stresses in Arabidopsis. *Wiley Online Library*, *70*(3), 432–444. https://doi.org/10.1111/j.1365-313X.2011.04883.x

Zancani, M., Braidot, E., Filippi, A., & Lippe, G. (2020). Structural and functional properties of plant mitochondrial F-ATP synthase. *Mitochondrion*, *53*, 178–193. https://doi.org/10.1016/j.mito.2020.06.001

Zhang, D. W., Xu, F., Zhang, Z. W., Chen, Y. E., Du, J. B., Jia, S. D., Yuan, S., & Lin, H. H. (2010). Effects of light on cyanide-resistant respiration and alternative oxidase function in Arabidopsis seedlings. *Plant, Cell & Environment*, *33*(12), 2121–2131. https://doi.org/10.1111/J.1365-3040.2010.02211.X

Zhang, Y., & Fernie, A. R. (2018). On the role of the tricarboxylic acid cycle in plant productivity. *Journal of Integrative Plant Biology*, *60*(12), 1199–1216. https://doi.org/10.1111/JIPB.12690

Zhang, Y., & Fernie, A. R. (2023). The Role of TCA Cycle Enzymes in Plants. *Advanced Biology*, 2200238. https://doi.org/10.1002/ADBI.202200238

Zirkle, C. (1929). Development of Normal and Divergent Plastid Types in Zea Mays. *Https://Doi.Org/10.1086/333989*, *88*(2), 186–203. https://doi.org/10.1086/333989

Zsigmond, L., Rigó, G., Szarka, A., Székely, G., Ötvös, K., Darula, Z., Medzihradszky, K. F., Koncz, C., Koncz, Z., & Szabados, L. (2008). Arabidopsis PPR40 connects abiotic stress responses to mitochondrial electron transport. *Plant Physiology*, *146*(4), 1721–1737. https://doi.org/10.1104/PP.107.111260

CHAPTER II

Genetic inactivation of mitochondrial complex IV in *Physcomitrium patens* unveils the relevance of respiration for efficient carbon and nitrogen metabolisms in plants

Antoni M. Vera-Vives[1], Marco Mellon[1], Libero Gurrieri[2], Anna Segalla[1], Edoardo Bizzotto[1], Matteo Soldera[1], Stefano Campanaro[1], Francesca Sparla[2], Alessandro Alboresi[1] and Tomas Morosinotto[1]

1. Department of Biology, University of Padova, Italy
2. Department of Pharmacy and Biotechnology (FABIT), University of Bologna, Italy

Authorship statement:

The general research question was proposed by Prof. Tomas Morosinotto and Prof. Alessandro Alboresi and redefined with my contribution through the experimental process. I delineated the experimental design, with critical input from my supervisor and collaborators. Construct and mutant lines were produced by PhD student Marco Mellon. I designed and conducted all the experiments reported, with the collaboration of: the MSc student Matteo Soldera, who did his internship under my supervision and collected part of the respirometry data; Dr. Anna Segalla, who aided in sample harvesting for omics experiments; Prof. Francesca Sparla and Dr. Libero Gurrieri, who aided designing and performed experiments of starch quantification and amylolytic activity. I conducted all the data analysis, except for the alignment of RNAseq reads onto the reference genome, which was done with the aid of PhD student Edoardo Bizzotto and Prof. Stefano Campanaro. I wrote the manuscript, designed the graphs and revised the text after the comments of my supervisor.

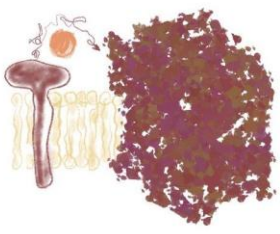

Abstract

In photosynthetic organisms, respiration is needed to support metabolism during the night and in non-photosynthetic tissues, but it also plays a fundamental metabolic role in the light. To gain information on the role of respiration in the light in plants we isolated the first plant model completely depleted cytochrome c oxidase complex (Complex IV), exploiting the ability of the moss *Physcomitrium patens* to perform homologous recombination and the possibility of generating knockout lines through vegetative propagation of photoautotrophic tissues. Mutants showed strongly impaired growth, with altered composition of the respiratory apparatus and increased electron transfer through the alternative oxidase. The light phase of photosynthesis remained substantially unaffected, and the efficiency of carbon fixation was reduced. Transcriptomics and metabolomics analyses showed that the disruption of the cytochrome pathway had general consequences on central carbon and nitrogen metabolism. Mutant plants accumulated starch that could not be efficiently mobilized during the night, causing a blockade of glycolysis during the night and a general reduction in amino acid abundance. We hypothesize that this metabolic switch could be modulated by the SnRK1 complex. A partial rescue of the growth could be obtained by growing the plants with an external apport of glucose and ammonia or by the addition of amino acids. We demonstrate that *Physcomitrium patens* is a good model for studying the impact of metabolic alterations that are lethal in other plant models, and that an alteration of the respiratory chain in plants has general consequences in the cell, altering the correct regulation of energy storage and mobilization in response to the cycles of night and day.

1. Introduction

Mitochondria are essential organelles found in eukaryotic cells, including plants, which are integral to diverse processes, such as cellular redox regulation, reactive oxygen species (ROS) management, and the synthesis of key metabolic intermediates. Moreover, they play an indispensable role in plant stress responses, including abiotic stress tolerance and the orchestration of programmed cell death. This multifaceted involvement of mitochondria in various cellular processes underscores their significance in plant growth, development, and adaptation to a dynamic environment.

Oxidative phosphorylation (OXPHOS), the main metabolic pathway responsible for generation of ATP in heterotrophic cells, is also localized in mitochondria. As we described in CHAPTER I, this process is fed by reducing power originating from the oxidation of organic acids and leads to the release of CO_2 and to the reduction of O_2 into water. OXPHOS is catalysed by five main large multi-subunit complexes embedded in the inner mitochondrial membrane: the NADH dehydrogenase complex (complex I, CI), the succinate dehydrogenase complex (CII), the cytochrome c reductase complex (CIII), the cytochrome c oxidase complex (CIV) and the ATP synthase (CV). Together, complexes I to IV form the mitochondrial electron transfer chain (mETC) or respiratory chain, which catalyses the electron transfer from NADH or $FADH_2$ to molecular oxygen. Complexes I, III and IV of the respiratory chain are proton translocators and the mETC activity drives the generation of an electrochemical gradient across the inner mitochondrial membrane which is subsequently exploited by Complex V to catalyse phosphorylation of ADP to ATP.

Photosynthetic organisms use light energy as their primary source of energy to synthetize the ATP and the reducing power (NADPH) needed to support all their metabolism and particularly the CO_2 fixation into organic molecules. This metabolic reaction is responsible of most of the Earth primary production, providing chemical energy to support largest majority of lifeforms. Photosynthetic organisms, however, also rely on respiration during the night (i.e., when light is absent) or in tissues that are not photosynthetically active (e.g., roots or during seed germination).

In addition to its role in supporting energetic metabolism in the dark, OXPHOS in plants has been shown to influence photosynthesis by acting as a sink for excess

of electrons coming from the chloroplasts thanks to the action of the malate-oxaloacetate valve that involves a redox-shuttling machinery between organelles (Alric & Johnson, 2017; Igamberdiev, 2020; Igamberdiev & Bykova, 2022). OXPHOS activity was shown to increase under illumination (De Col et al., 2017) and to directly influence photosynthetic electron transport (Larosa et al., 2018) and chloroplast ATPase activity (Mellon et al., 2021). In diatoms, a group of marine algae, the energetic coupling between plastids and mitochondria is essential to drive CO2 assimilation (Bailleul et al., 2015). An increasing body of evidence suggests that respiration in plants plays a major biological role also under illumination and that its activity is tightly interconnected with photosynthesis. Mitochondrial respiration has also a key role in supplying ATP to the cytosol, as we show in CHAPTER IV.

Despite its biological relevance, the role of mitochondrial respiration in plants under illumination is far from being understood. A major limitation for the advancement of knowledge in this field has been the lack of viable mutants with depleted respiration, as already discussed in CHAPTER I. We showed that complete knockout mutants are available only of Complex I in the model plant Arabidopsis thaliana, while the Complex IV activity is required for embryo development and only plants with a decreased accumulation of specific subunits of Complex IV have been isolated. Even if they retain a significant fraction of their activity, these plants with altered content of respiratory complexes showed severe phenotypes with decreased viability and developmental inhibition, sterility, and impairment of seed germination, consistent with the energetic depletion of non-photosynthetic tissues. A *cod1* mutant in Arabidopsis was reported with undetectable levels of Complex IV activity (Dahan et al., 2014). However, *cod1* seeds could not germinate, and plants could be obtained only by rescuing the embryo *in vitro*, that presented altered development which did not allow a full assessment of the metabolic impact of respiration deficiency in photosynthetic tissues.

In this work this limitation was addressed using the moss *Physcomitrium patens*. In *P. patens*, KO mutants can be generated by homologous recombination in vegetatively propagated tissues cultivated under continuous light. Most *P. patens* tissues are haploid, making the eventual phenotype related to any genetic modification directly assessable by-passing sexual reproduction and respiration dependent fertilization and seed/spore germination stages. Most of *P. patens* life cycle is constituted by photosynthetically active cells, and even rhizoids still contain a few

active chloroplasts (Sakakibara et al., 2003), making it a suitable model for isolating mutants with potentially altered mitochondrial functions.

In the past, we exploited *P. patens* to generate mutants depleted in mitochondrial Complex I, which were viable but showed significant growth defects (Mellon et al., 2021) Here, we present the generation and characterization of novel *P. patens* plants depleted in COX11, a conserved assembly factor required for the biogenesis and activity of Complex IV (Radin et al., 2015). We performed transcriptomics and metabolomics on these plants, providing a novel view on the metabolic rearrangement derived from the depletion of Complex IV in a plant model.

2. Results

2.1. Depletion of *cox11* causes loss of Complex IV activity and growth defects in *P. patens*

For targeting the activity of Complex IV, we chose the protein COX11, which is an assembly factor that is not present in the complete holoenzyme but is required for the insertion of two copper ions into the COX1 subunit that form the Cu_B centre of the catalytic core (Meyer et al., 2019, Figure 2.1A). COX11 activity is required for the functionality of Complex IV, and its mutation led to null respiratory mutants in yeast (Banting & Glerum, 2006). Complete knockout plants could not be obtained in Arabidopsis, and reduction of COX11 levels through knockdown approaches resulted in defective embryo development (Radin et al., 2015).

In *P. patens*, COX11 is encoded by a single nuclear gene (Pp3c16_1230). By using the tool MitoFates (Fukasawa et al., 2015), we predicted the PpCOX11 presequence to include a mitochondrial targeting peptide with a probability of 0.763 (Supplementary Figure 2.3). For COX11 to carry its role as a copper chaperone, three cysteine residues involved in Cu-binding have been identified (Carr et al., 2002), that are indeed conserved also in PpCOX11 (Supplementary Figure 2.3), showing that its activity is conserved also in P. patens. COX11 is quite spread in the tree of life (Esposti, 2020; Timón-Gómez et al., 2018). We built a phylogenetic tree comparing the COX11 sequences from 46 different organisms (Supplementary Figure 2.4). Most of the sequences clustered in expected taxonomic groups, except that we found two groups of green algae and that the eudicot plant *Rhodamnia argentea* clusters with mammals instead of with other plants. From the results of this tree, we can also conclude that diatoms, which are the result of a secondary endosymbiotic event (S. R. Smith et al., 2012), acquired the Cox11 gene in the secondary endosymbiosis from the photosynthetic rather than from the heterotrophic parent.

By using publicly available transcriptomics data, we found the Cox11 gene to be expressed at relatively low levels in *P. patens*, which are higher in germinating spores compared to other developing stages (Supplementary Figure 2.5). This is consistent with previous observations of Arabidopsis, where Cox11 was found to be

more expressed in metabolically active tissues such as young leaves, shoot and root meristems or vascular tissues of source and sink organs (Radin et al., 2015).

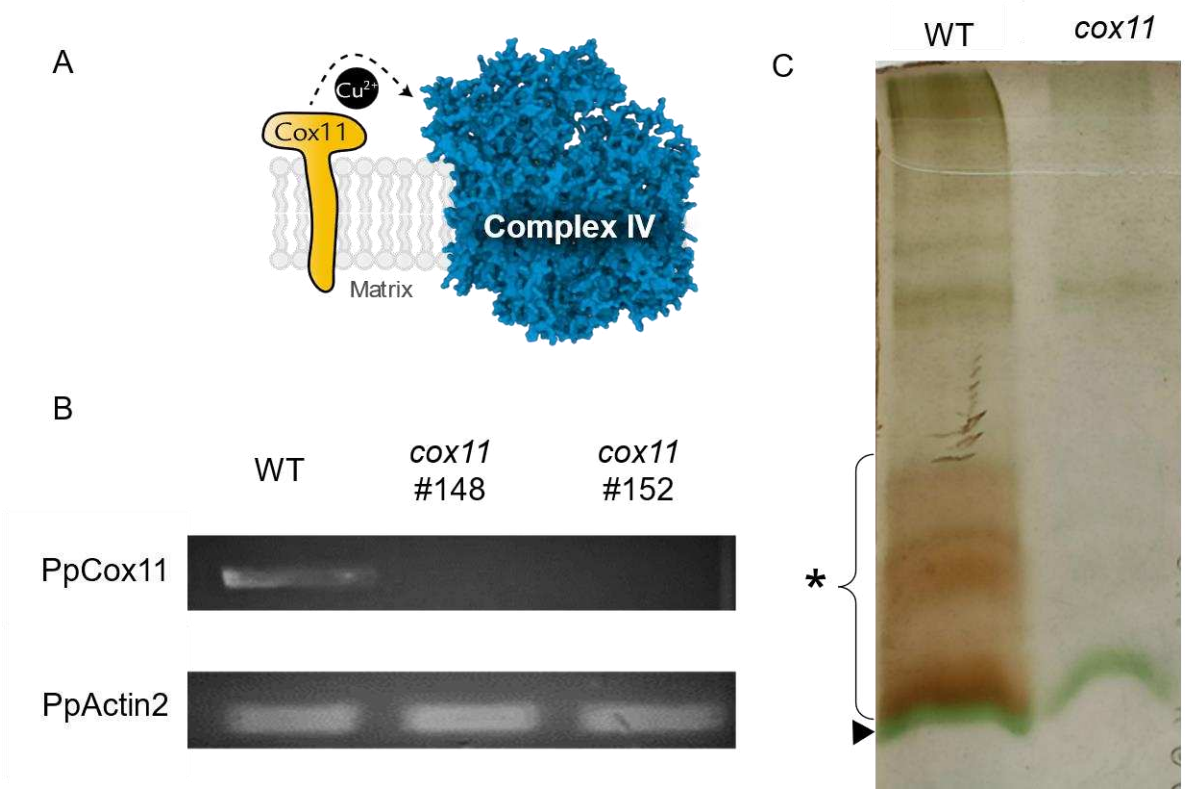

Figure 2.1 | **Isolation of knockout mutants for the gene *cox11* in *P. patens***. (A) Diagram showing the topology and function of COX11, which delivers Cu^{2+} into the active site of Complex IV, essential for activity. The model of Complex IV was retrieved from Maldonado et al., 2021, PDB entry 7JRO. (B) RT- PCR verification of the expression of the mRNA encoding for COX11. (C) In-gel activity staining after separation of crude membrane extracts by BN-PAGE. Green bands correspond to chlorophyll-containing complexes, and brown bands correspond to proteins with cytochrome c oxidase activity.

Once we verified the presence and conserved role of COX11 also in *P. patens*, we generated Cox11 knockout mutants by polyethylene glycol (PEG)-mediated transformation, exploiting the organism's ability to efficiently perform homologous recombination, as schematized in Supplementary Figure 2.6. The lines stably resistant to hygromycin were validated using PCR to confirm the insertion in the expected genomic region (Supplementary Figure 2.6B). The absence of the cox11 mRNA was confirmed by RNA extraction and RT-PCR (Figure 2.1B).

To verify that the loss of *cox11* led to a deficiency on Complex IV activity, crude membrane extracts, enriched in mitochondria proteins, were separated by blue native polyacrylamide gel electrophoresis (BN-PAGE). After separation, in-gel activity assay for the cytochrome c oxidase showed no detectable activity in *cox11* plants, which was instead detected in WT plants (Figure 2.1C).

All the validated *cox11* lines showed a strongly impaired growth and delay in developmental phases (Figure 2.2). *cox11* plants remained in the protonemal phase longer compared to the WT and first gametophores could be observed only after 21 days, while they are visible in WT after 10 days (Figure 2.2; Supplementary Figure 2.7). The production of spores could not be induced in the conditions normally used for WT plants.

The growth phenotype of *cox11* was verified under different growth conditions, considering the addition of external sources of reduced carbon and nitrogen (glucose and ammonia tartrate), increasing the CO_2 availability (atmospheric or 1%) or modifying the photoperiod (long day or continuous illumination) (Figure 2.2).

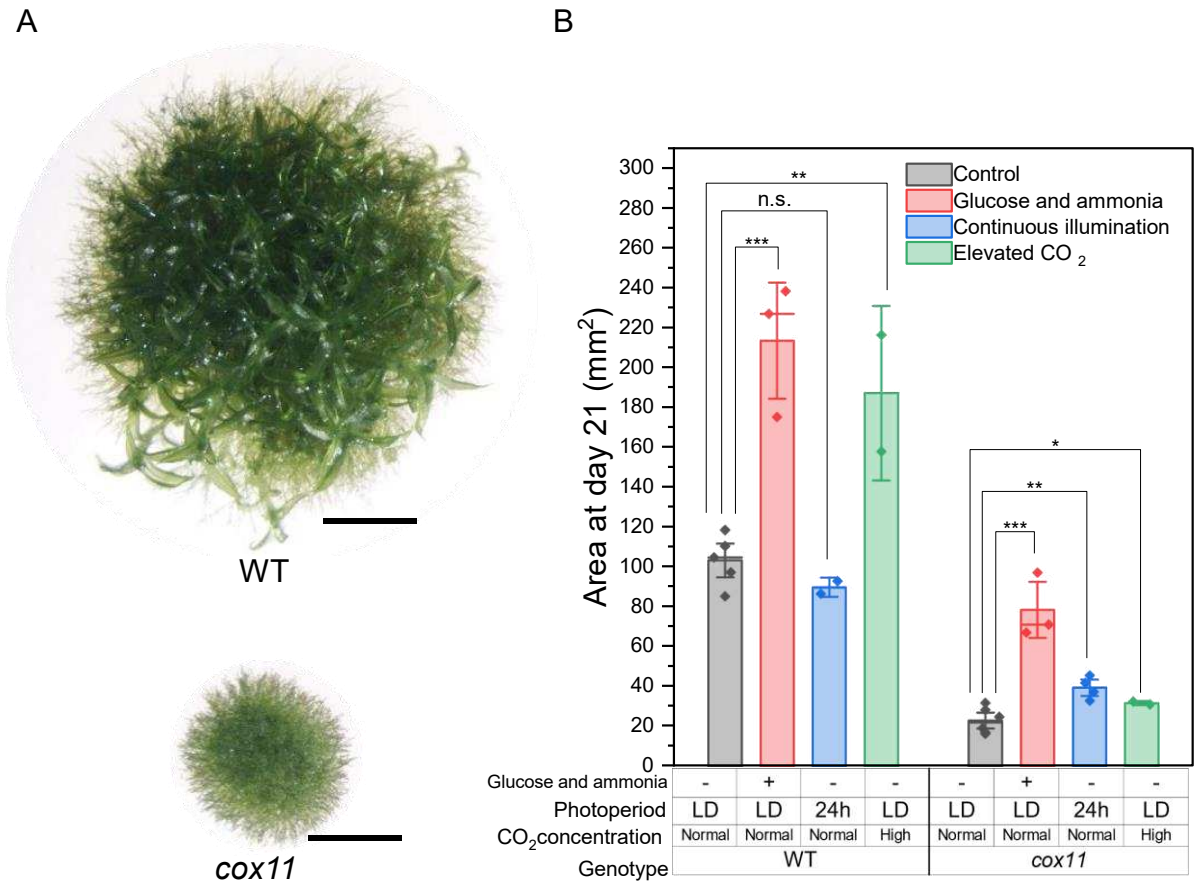

Figure 2.2 | Growth phenotype of *cox11* mutants under different growth conditions. (A) Image of a representative colony of WT and *cox11* after 21 days of growth on solid $PpNH_4$ medium. Scale bar is 1 mm. (B) Area quantification at day 21 of colonies grown under control conditions. LD, long day; 24 h, continuous illumination. Statistics: two-sample t-test, (***) $p<0.001$; (**) $p<0.01$; (*) $p<0.05$; (n. s.) $p>0.05$.

Addition of glucose and ammonia in the media showed a positive effect on *cox11* growth, as it had on WT plants, and the respective difference remained (Figure

2.2B). When compared to the control in long day conditions, growth under continuous illumination caused a small but significant improvement in *cox11* that was not observed in the WT plants. Finally, growth under an elevated CO_2 atmosphere, which removes the effect of photorespiration, represented only a small advantage to *cox11*, while it had a very positive effect on the WT plants.

2.2. Composition and activity of the respiratory apparatus are altered in *cox11*

The impact of *cox11* depletion on the respiratory apparatus composition was verified through immunoblotting, using antibodies against core proteins of the respiratory complexes (Figure 2.3A). Antibodies showed increased levels in the Complex I core subunit NAD9, the Complex II core subunit SDH2, and the ß-subunit of Complex V. Interestingly, the levels of MPP subunit of Complex III were lower. The protein levels of the alternative oxidase (AOX), which allows electrons to bypass the cytochrome pathway, were also lower.

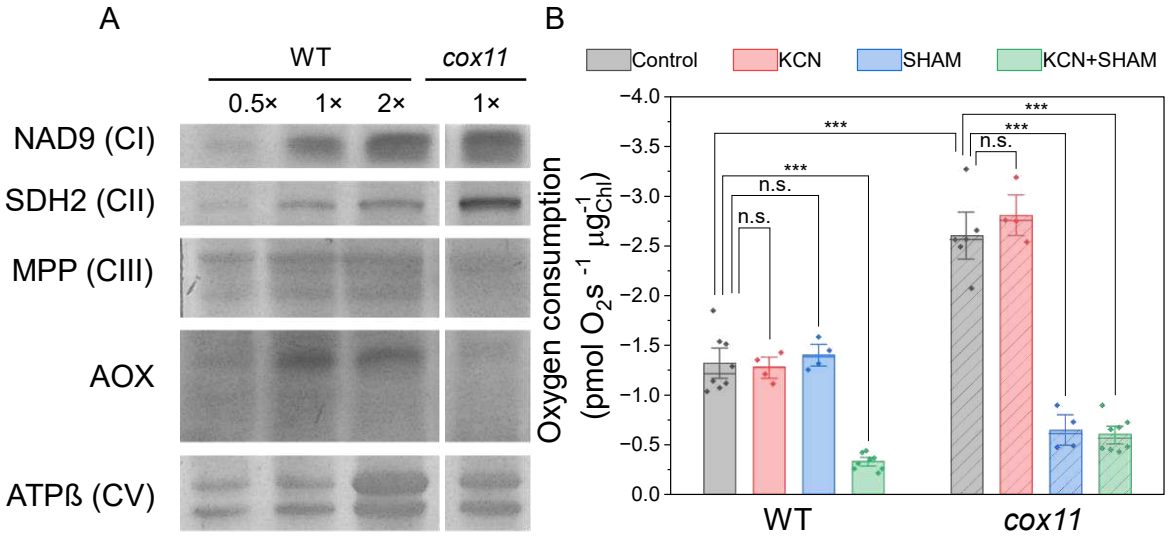

Figure 2.3 | **Alterations in the respiratory machinery of *cox11***. (A) Immunoblot of subunits of the different respiratory complexes. For complexes I, II, III and the AOX, total protein extracts were used. For Complex V, crude mitochondrial extracts were used. Different amounts of proteins were loaded, expressed in multiples of the WT (0.5×, 1×, 2×). 1× corresponds to 2 µg of chlorophylls for NAD9, SDH2 and the AOX, 4 µg of chlorophylls for MPP and 30 µg of proteins for the ß-subunit. (B) Experiments of respirometry on intact protonema. Statistics: two-sample t-test, (***) $p<0.001$; (n.s.) $p>0.05$.

The functionality of respiratory apparatus was assessed by measuring O_2 consumption in dark in intact protonema tissues (Figure 2.3B). Interestingly, dark respiration was enhanced in *cox11* lines, with approximately twice the activity than WT

plants. This was independent of normalization to the amount of protein or chlorophylls, since the protein/chlorophyll ratio was unchanged between WT and *cox11*, with values (average ± StDev) of 90.7±4.0 mg_{prot}/mg_{Chl} (WT) and 90.8 ±0.6 mg_{prot}/mg_{Chl} (*cox11*). To better understand the site of increase in O_2 consumption in *cox11* plants, we repeated the measurements with the addition of chemicals that inhibit either the cyanide-sensitive or the cyanide-insensitive pathways, i.e., potassium cyanide (KCN) or salicylhydroxamic acid (SHAM), respectively.

In WT, the effects of either KCN or SHAM on dark respiration were not significant when applied alone (Figure 2.3B). However, when applied combined they abolished virtually all the dark respiration activity (Figure 2.3B). This suggests that, when the cytochrome pathway is chemically blocked, the excess of electrons can be readily redirected through the AOX, showing a high AOX capacity in WT protonema. To confirm that this effect was not due to chemical specificity, we repeated the experiment using two alternative chemicals, antimycin A and n-propylgallate, reaching to the same conclusions (Supplementary Figure 2.8A). In *cox11*, like in the WT, KCN alone had no effect on O_2 consumption (Figure 2.3B). However, the sole addition of SHAM could completely inhibit O_2 consumption (Figure 2.3B). This strongly suggests that the higher respiration in *cox11* was entirely attributable to an increased activity of the cyanide-insensitive, AOX-mediated pathway. The same effect was observed when the alternative AOX inhibitor n-propylgallate was used instead (Supplementary Figure 2.8B).

These results confirm that *cox11* plants lack a functional Complex IV, and that this loss compromises completely the cyanide-sensitive pathway. Furthermore, the capacity of the cyanide-insensitive pathway is increased in *cox11*, and it is the exclusive responsible of O_2 consumption during dark respiration.

2.3. Photosynthetic performance is altered but not in light-dependent phase.

Once we validated that *cox11* plants had impaired respiration, we evaluated the photosynthetic performance of the mutants. We quantified the abundance of different components of the photosynthetic machinery by immunoblotting and found no major differences (Supplementary Figure 2.9)

We then quantified the photosynthetic activity of protonema pieces by measuring the rate of O_2 evolution under a saturating illumination that induced maximal photosynthesis. We designed an experimental protocol so we could measure the values of dark respiration and net photosynthesis (Supplementary Figure 2.10). The O_2 evolution flux measured under saturating light is the result of the positive contribution of O_2 evolution at photosystem II and the negative contribution of mitochondrial respiration. Therefore, we can refer to this value as net photosynthesis. We hence calculated the rate of gross photosynthesis as the difference between the rates of net photosynthesis and dark respiration. In *cox11*, gross photosynthesis was not different from the WT (Figure 2.4A), suggesting a good performance of the light reactions of photosynthesis.

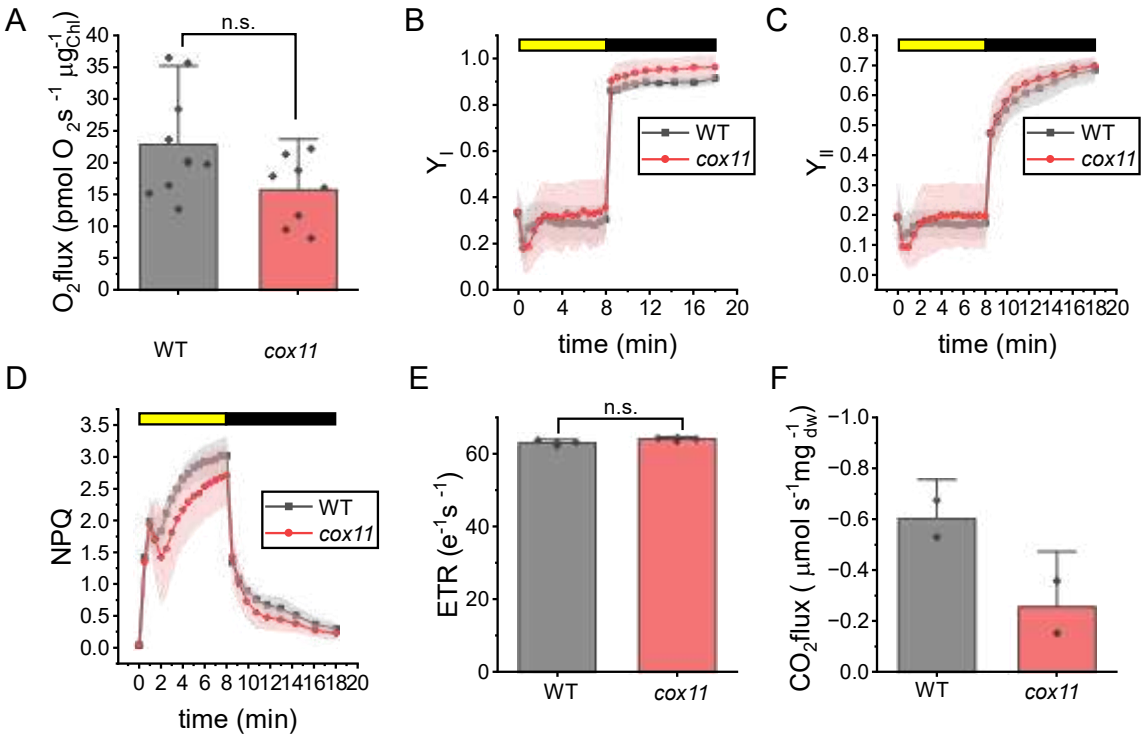

Figure 2.4 | **Evaluation of photosynthetic properties in *cox11***. (A) Gross evolution of O_2 under saturating illumination. (B-D) The yield of PSI (YI, B), PSII (YII, C) and non-photochemical quenching (NPQ, D) were measured with Dual PAM 100 in plants exposed to 330 µmol photons m^{-2} s^{-1} of actinic light intensity. Yellow / black bars indicate when actinic light was on / off respectively. WT and *cox11* are shown respectively with black squares and red circles. Data are shown as average ± SD (n > 4). No statistically significant differences from WT plants were identified. (E) Electron transport rate of dark-acclimated plants grown under dim light, calculated from the ECS (electrochromic shift signal) after exposition to saturating light (300 µmol photons m^{-2} s^{-1}) for 3-5 minutes. Activity was normalized to the total photosystem (PSI+PSII) content. Standard deviation is also reported (n > 6). (F) Net CO_2 fixation rate under a control light of 50 µmol photons m^{-2} s^{-1}. Error bars in A, E and F represent 1.5 times the SD.

Photosynthetic activity was further assessed using chlorophyll fluorometry (Figure 2.4B, D, E, F). The efficiencies of both photosystems I and II, quantified from Y_I and Y_{II} respectively, were indistinguishable between WT and *cox11* (Figure 2.4D, E). The induction of non-photochemical quenching (NPQ), a photoprotection mechanism activated by the decrease of pH in the thylakoid's lumen and the protonation of specific activators PsbS or LHCSR (Alboresi et al., 2010; Li et al., 2002; Liguori et al., 2016) was also unaltered (Figure 2.4F). Finally, also the photosynthetic electron transport rate (ETR), quantified at the steady state after 3 to 5 minutes of illumination was indistinguishable between WT and *cox11* plants (Figure 2.4B). These data demonstrate that the light phase of photosynthesis did not have major alterations in *cox11* mutants, which is different of what we reported on Complex I deficient mutants *ndufa5* (Mellon et al., 2021).

2.4. The cox11 transcriptome shows alterations in stress signalling and metabolism that are associated with the time of the day

2.4.1. There are genes differentially expressed regardless of the time

To globally assess the impact of the *cox11* mutation on metabolism, plant material harvested at different zeitgeber times (ZT) was used for analysis of the transcriptome by RNA-sequencing. We compared samples harvested at the end of the night (ZT0), at the beginning of the day (ZT2) or at the middle of the day (ZT6) and performed pathway enrichment analysis on the detected lists of differentially expressed genes (DEGs) (Figure 2.5).

After comparing the lists of differentially expressed genes (DEGs), we identified 612 genes as significantly upregulated at all conditions (Figure 2.6, left), including a group of 29 genes linked to stress response that included the mitochondrial heat shock protein Hsp70 (Pp3c2_12240) and the chloroplast ascorbate peroxidase (Pp3c2_15430), showing alterations on different cellular compartments. A group of 7 genes annotated as histone methyl transferases was also always upregulated.

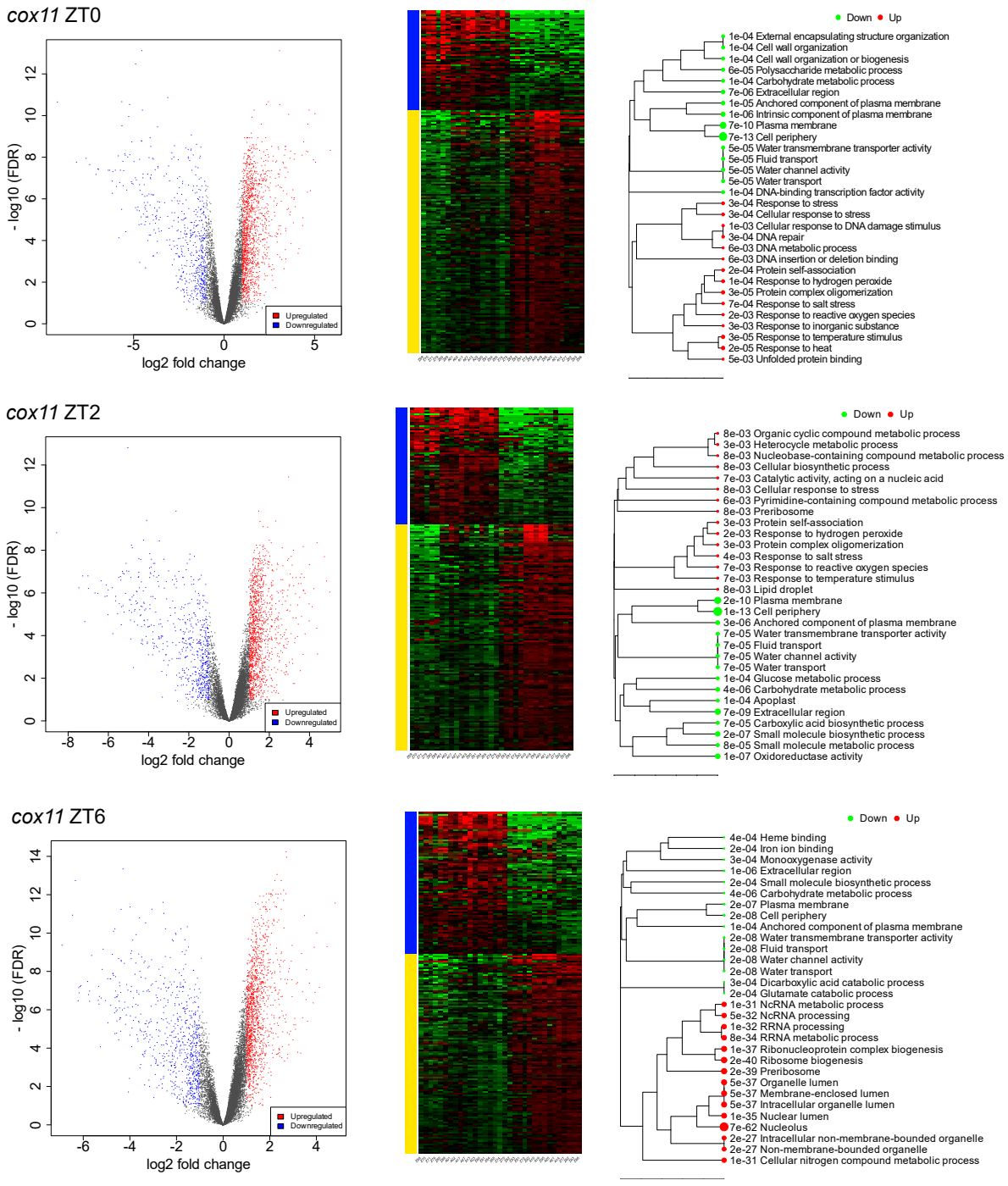

Figure 2.5 | **Data overview and enriched pathways segregated for the three zeitgeber times tested**. For each zeitgeber time the figure- includes the following items: i) a volcano plot showing data distribution and the number of significant DEGs; ii) a heatmap of the significant DEGs where lower and higher expression values are expressed in green and red, respectively; iii) a tree of the most significant enriched pathways, where pathways with many shared genes are clustered together, and bigger dots indicate more significant p-values.

On the other hand, we identified 310 genes whose expression in *cox11* was always repressed (Figure 2.6, right). We identified many of these genes as involved in cell wall biogenesis and remodelling, or metabolism of structural polysaccharides. We

hypothesize that this is due to a general alteration in cell division and proliferation rates, that could respond either to a lack of energy or to stress signalling (Le Gall et al., 2015). The expression of different transporters is also always limited in *cox11*, including several aquaporin isoforms, many transmembrane transporters predicted to transport amino acids, as well as transporters of inositol, ammonium, phosphate, or zinc. This could reflect a reprogramming of the metabolic machinery of the cell to cope with the shortage or excess of some metabolites due to alterations in central metabolism (Boursiac et al., 2008; X. Liu & Bush, 2006; Vandeleur et al., 2014; Yang et al., 2020).

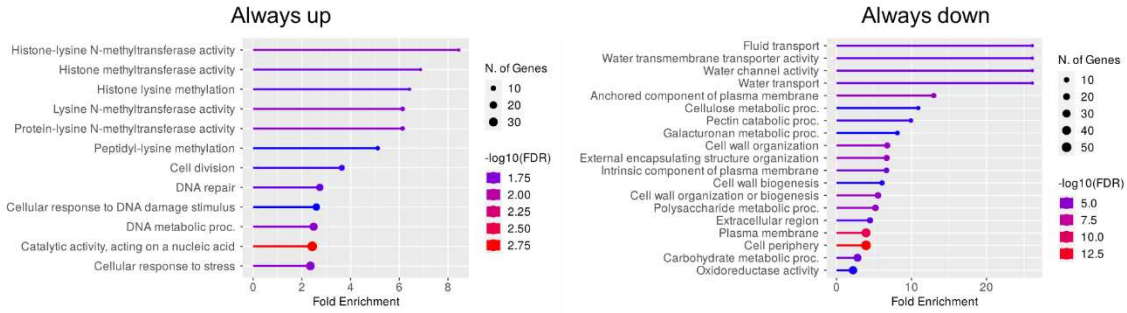

Figure 2.6 | **Bar plots with the most significant pathways enriched in cox11 independently of the time**. Bar length represents fold enrichment, colour represents significance, size of the circle represents number of genes.

2.4.2. During night, *cox11* suffer of developmental reprogramming, altered nitrogen assimilation and stress signalling

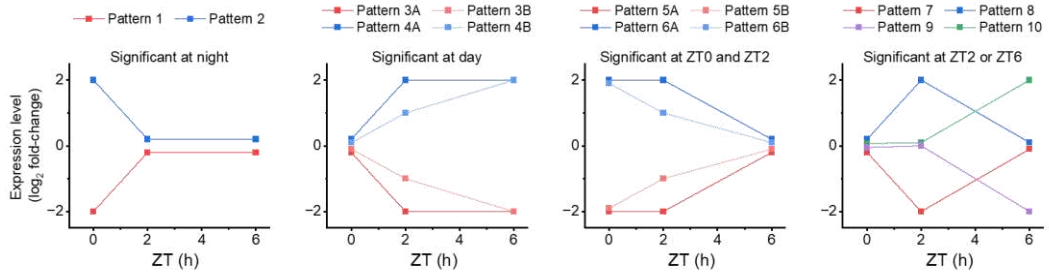

Figure 2.7 | **10 possible patterns of expression of the genes**. A value of expression level of 2 or -2 is used to represent significantly different expression.

Mutant *cox11* plants have altered mitochondrial activity, and we expect this to have a variable effect depending on the time of the day, in function of whether photosynthesis is active or not. Therefore, besides the pathways permanently dysregulated, it might be informative to observe the pathways that are enriched only in specific times of the day. Therefore, we defined 10 different patterns of expression

in function of the circadian behaviour (Figure 2.7) and classified the identified DEGs accordingly.

An important number of genes showed differential expression only during night, but normal levels during the day. Regarding those repressed by night (Pattern 1 of Figure 2.7; Figure 2.8), there was a group of 35 transcription factors (TFs) of different families, including apetala 2 (AP2), MYB, MYC, ABA-inducible and GRAS. Some of these retained their regulation also during the first ours of day (ZT2), but all of them recovered normal values at ZT6 (Pattern 3; Figure 2.8). AP2 is a very large family in *P. patens*, with 149 members (J. Zhang et al., 2020), 70 of which have been experimentally detected previously at significant levels (Khraiwesh et al., 2015). In angiosperms, AP2 TFs have been linked to growth, development, and defence responses to abiotic and biotic stress (Z. S. Xu et al., 2011). In *P. patens*, specific AP2 TFs are required for the formation of gametophore apical cells from protonema cells (Aoyama et al., 2012), and others induce the reprogramming of leaf cells into chloronema apical cells (Ishikawa et al., 2019). In turn, MYB factors have been linked to protonemal growth and chloronema to caulonema transition (Pu et al., 2020), and GRAS factors to the development of gametophores and spores (Beheshti et al., 2021).

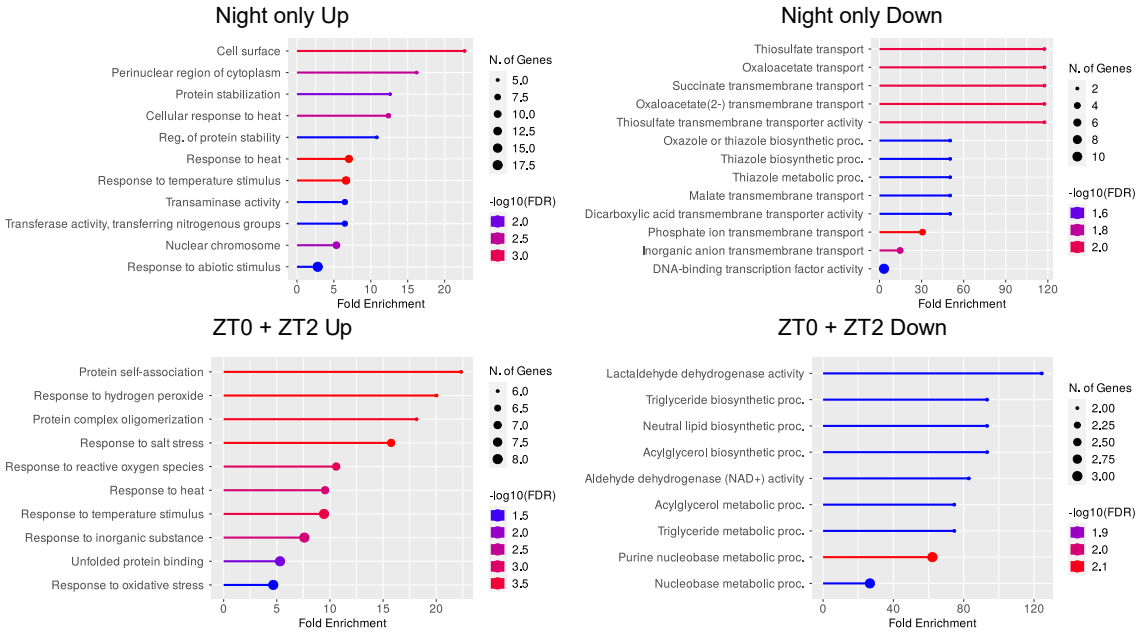

Figure 2.8 | Bar plots showing the most significantly enriched pathways at ZT0, but no longer significant at ZT2 or ZT6, or significant also at ZT2 but not ZT6. Bar length represents fold enrichment, colour represents significance, size of the circle represents number of genes.

Overall, the lower levels of these TFs are most likely correlated with the delay in development program observed in *cox11*.

Furthermore, repressed at night there was a group of metal ion transport that included mostly proteins with a PTHR22814 heavy metal transport domain, and three zinc transporters. Some of these remained repressed also at ZT2. This domain is present in several copper transporters (Bull & Cox, 1994), and could indicate a dysregulation in copper transport in the cell linked to the role of *cox11* as a copper chaperone. We also identified one gene with nitrate reductase activity (Pp3c14_9410), out of a family of three genes (Medina-Andrés & Lira-Ruan, 2012); noteworthy, it is the only of the three genes detected at significant levels in our RNAseq dataset (Supplementary Table 2.6). In *P. patens*, nitrate reductase is a key enzyme for nitrogen assimilation (Chamizo-Ampudia et al., 2017) and for the production of the key signalling molecule nitric oxide (NO) (Medina-Andrés et al., 2015), a small molecule related to development and stress signalling (Cervantes-Pérez et al., 2020; Delledonne et al., 1998; Mata & Lamattina, 2001). Regulation of its activity has been observed upon abiotic stress in *P. patens* (Fu et al., 2018). This suggests that *cox11* could suffer from reduced assimilation of nitrogen, which could have an impact in central nitrogen metabolism NO signalling.

The upregulated pathways at night (Pattern 2) included a group of 7 genes that have transaminase activity, annotated as aspartate aminotransferase (Pp3c10_1870), tyrosine aminotransferases (Pp3c22_9790, Pp3c22_9793), serine-glyoxylate transaminase (Pp3c18_8240) and branched-chain amino acid aminotransferases (Pp3c14_21300, Pp3c17_21600). These enzymes are involved in the metabolism of amino acids, and therefore our data reinforces the hypothesis that nitrogen metabolism might be altered in *cox11*, particularly at night. Following the same trend we detected several genes associated to stress responses that included many different types of heat shock proteins (Hsp), either from the small (Hsp17.4, Hsp17.6, Hsp20) or large (Hsp90) families (Waters & Vierling, 2020), or proteins of the BAG family, which are likely chaperone regulators and could aid heat shock proteins in their chaperone role (Doong et al., 2002; Kabbage & Dickman, 2008). There were also genes involved in pathways regarding response to DNA damage (helicases, polymerases, ribonucleases, and other enzymes involved in DNA repair), which could be a general response downstream to stress signalling (Nisa et al., 2019).

To better understand the alterations in chaperone levels, we observed the expression pattern of all the identified heat shock proteins in *P. patens*. Out of the 20 genes encoding small heat shock proteins (sHsps) that had been identified in *P. patens* previously (Ruibal et al., 2013), 18 are represented in the most recent gene model version. Of these, 7 were not detected at significant levels in our dataset, 1 was expressed but not regulated in *cox11* and 10 were induced in *cox11* at ZT0, ZT2 or both, but not at ZT6 (except for 1) (Supplementary Table 2.7). Regarding proteins of the Hsp90 family, there are 17 genes classified under the family PTHR11528 (Hsp90) in Phytozome, of which 6 are not detected at significant levels in our RNAseq dataset, 5 are significantly induced at ZT0 and 6 are not regulated at ZT0, 2 of which are induced at ZT6 (

Supplementary Table **2.8**). The induction of heat shock proteins could be part of a more general response to the accumulation of unfolded proteins, which would trigger the unfolded protein response in the endoplasmic reticulum (UPR^{ER}). However, the expression levels of some genes defined as markers of UPR^{ER} in *P. patens* (Lloyd et al., 2018) were not significantly higher in *cox11* (Supplementary Table 2.9), therefore not supporting a general induction of UPR^{ER} in *cox11*.

We also checked the expression levels of antioxidant enzymes, which are considered markers of oxidative stress. None of these were significantly upregulated in *cox11* plants (Supplementary Table 2.10), suggesting that plants were not suffering of general oxidative stress. The only exception was a superoxide dismutase, PpFSD2, predicted to be chloroplastic, which was always induced in *cox11* plants.

Therefore, the expression pattern of the different heat shock proteins suggests that a stress response is induced by night, but it is then alleviated during day, likely by exposure to light, which apparently can relieve the stress. The induction of heat shock proteins is likely not due to oxidative stress, because antioxidant did not get induced.

Altered carbon metabolism in the night-to-day interface

We found gene sets whose expression was normal at night but altered during the day. Some of these were repressed only at the beginning of the day (Pattern 7; Figure 2.9, top right), including: a set of proteins with cupredoxin domain, linked to

copper binding (Dennison, 2013); two putative transporters of urea (Pp3c14_7160 and Pp3c1_21890); enzymes required for amino acids metabolism such as alanine, aspartate, glutamate or arginine; and enzymes required for the metabolism of glucose, including many enzymes of glycolysis. Others were repressed both at ZT2 and ZT6 (Pattern 3, Figure 2.9, bottom right), including genes linked to nucleotide metabolism and two genes annotated to be required for ascorbic acid biosynthesis (one gluconolactonase and one inositol oxygenase); however, these enzymes are not involved in synthesis of ascorbic acid in plants (Smirnoff, 2018). This observation further strengthens the previously proposed hypothesis of *cox11* showing altered central metabolism at night, affecting both N and C pathways, and at the night-to-day interface.

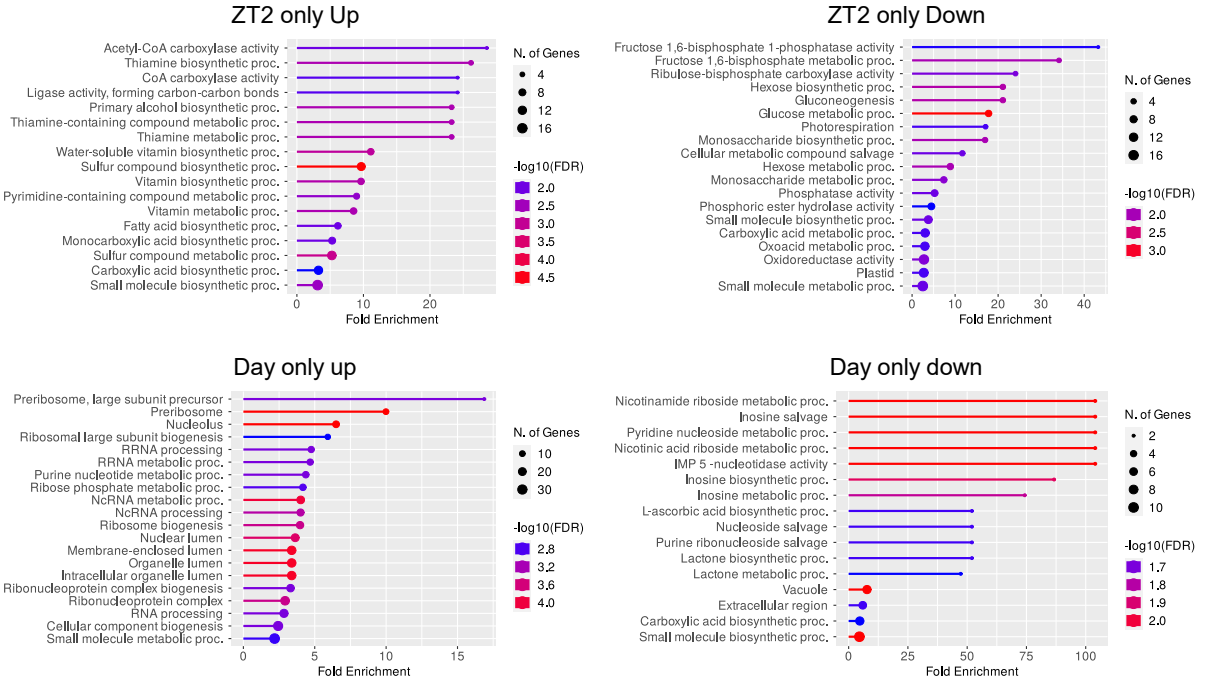

Figure 2.9 | **Bar plots showing the most significantly enriched pathways at ZT2 only but not at ZT0 or ZT6, or during day (ZT2 and ZT6, but not ZT0).** Bar length represents fold enrichment, colour represents significance, size of the circle represents number of genes.

Some genes were instead upregulated during day. Most of those upregulated only at the beginning of the day (Pattern 8; Figure 2.9, top left) encoded chloroplastic proteins, including: starch synthases, required for carbon storage (Pfister & Zeeman, 2016); arogenate hydratases, required for biosynthesis of the amino acid phenylalanine (Bonner & Jensen, 1987; El-Azaz et al., 2022); a thiamine thiazole synthase, required for the biosynthesis of the cofactor thiamine (Jurgenson et al., 2009); subunits of an acetyl-CoA carboxylase, involved in regulation of fatty acid and

polyketide biosynthesis (Cronan & Waldrop, 2002; Nikolau et al., 2003; Tong, 2012); and ATP/ADP transporters, which might be linked to the inter-compartment trafficking of energy equivalents (Spetea et al., 2012).

On the other hand, the genes found at higher level through the day (Pattern 4; Figure 2.9, bottom left) included 6 genes related to starch biosynthesis, including ADP-glucose synthases, which catalyse the compromising step of starch biosynthesis (Pfister & Zeeman, 2016; Stitt & Zeeman, 2012) and several genes involved in ribosome biogenesis, transcription, and translation (Supplementary Figure 2.11). This group also includes genes that form part of the mitochondrial ribosomal machinery but, since many components of mitoribosomes are mitochondrially encoded (Terasawa et al., 2007), and we do not have data on transcription levels of mtDNA-encoded genes, we cannot conclude that there is also increased expression of ribosomal proteins in mitochondria. Among the genes exclusively regulated at ZT6, we could not identify any relevant pathways that were not already included in the previous paragraphs.

This data suggests that the gene expression and protein synthesis rates are increased in *cox11*, particularly during day.

2.5. Metabolomics and joint pathway analysis show altered carbon and nitrogen metabolism in *cox11*

The transcriptomics data showed that *cox11* plants suffered from alterations in central metabolism, affecting both carbon and nitrogen compounds, that were particularly relevant at the night-to-day interface. To gain information in this regard, we performed untargeted metabolomic analysis on samples harvested at the three zeitgeber times already discussed (ZT0, 2, 6). We could uniquely identify a total of 78 compounds, 34 by GC-MS and 44 by IC-MS, which include most of the 20 primary amino acids except for arginine, cysteine, histidine, lysine, proline and tryptophan; different monosaccharides; intermediates of glycolysis and TCA cycle; intermediates of the CBB cycle; and nucleotides, among other compounds (Figure 2.10). Pairwise comparisons of samples at each zeitgeber time identified 37 metabolites significantly up- or down-regulated in one or more conditions.

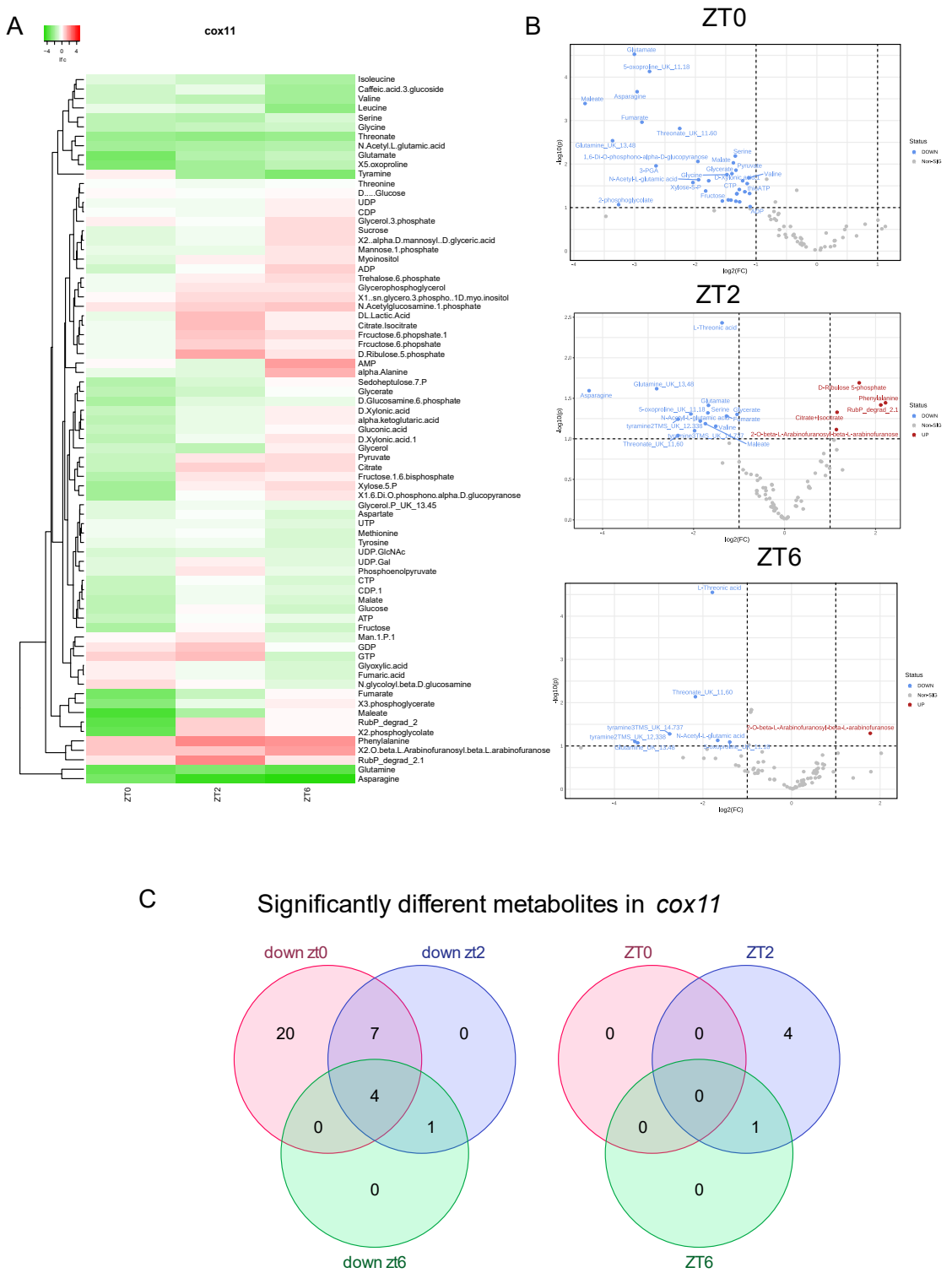

Figure 2.10 | **Overview of metabolomics data**. (A) Heatmap showing hierarchical clustering of compounds. (B) Volcano plots. (C) Venn diagram comparing the metabolites accumulated at higher or lower levels in *cox11* on different zeitgeber times, as shown in the volcano plots.

As we observed from the transcriptome, also the metabolome reflected a stronger impairment of *cox11* cellular homeostasis by the end of the night and early in the morning. We identified 20 metabolites whose levels were reduced at the end of night (ZT0) but not during the day (ZT2, ZT6), and these included mostly intermediates of glycolysis or the TCA cycle. There was another group of 7 metabolites which remained at lower levels both at ZT0 and ZT2, but then recovered the normal values at ZT6, that included four of the primary amino acids (asparagine, glutamate, serine and valine), the TCA cycle intermediate fumarate and its isomer maleate, and a degradation product of ribulose-5-phosphate. The only metabolite detected at lower levels through the day was tyramine. Finally, 4 metabolites were always detected at lower levels in *cox11*: threonate, 5'-oxoproline, glutamine, and N-acetyl-L-glutamic acid.

Few compounds significantly accumulated in *cox11*. At ZT2 we detected higher levels of citrate/isocitrate, which could not be distinguished in our experiments; ribulose 5-phosphate, a degradation product of ribulose-1,5-bisphosphate; and phenylalanine, the only amino acid detected at higher levels in *cox11*. Through the day we found increased levels of the disaccharide 2-O-beta-L-Arabinofuranosyl-beta-L-arabinofuranose.

Both the transcriptome and metabolome showed important alterations in carbon metabolism (Figure 2.11). Six out of the ten intermediates of the glycolytic pathway were identified in our experiments and, except for fructose-6-phosphate, all of them accumulated at lower levels in *cox11* at ZT0. The transcript levels of the enzymes of the pathway were either upregulated, downregulated or not regulated. Similarly, five of the eight intermediates of the TCA cycle were detected through our metabolomics approach (citrate, isocitrate, malate, fumarate and 2-ketoglutarate), and all besides isocitrate were lower. In the past, comparison of transcriptomics and proteomics experiments have shown poor correlation between transcript abundance and protein levels of the chloroplast proteome of *P. patens* (Fesenko et al., 2016), and therefore we must be careful when interpreting RNAseq data. However, these data strongly suggest that carbon catabolism was blocked or slowed down in *cox11* at night. Interestingly, this alteration was no longer observed during day, when intermediates recovered their normal values (Supplementary Figure 2.12). Remarkably, at ZT2 we observed the accumulation of both ribulose-5-phosphate and ribulose-1,5-

bisphosphate, the carbon skeleton required for rubisco to fix CO_2 and its immediate precursor; this is consistent with the lowered rate of carbon fixation that we reported previously.

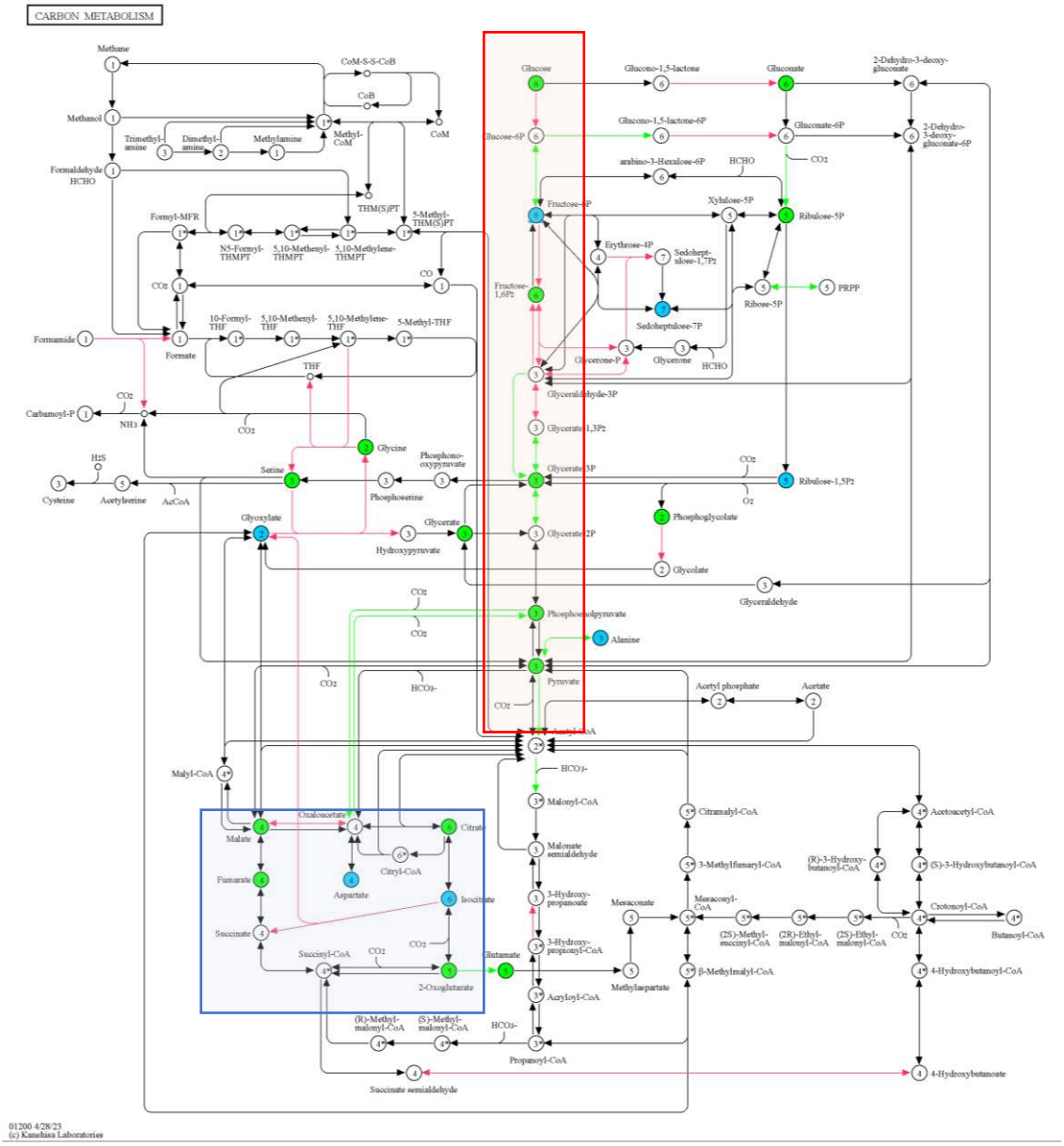

Figure 2.11 | **Joint pathway analysis on the map depicting carbon metabolism at ZT0**. KEGG map showing Carbon metabolism (KEGG ID ppp01200), with manually highlights of glycolysis (red rectangle) and the TCA cycle (blue rectangle). Significantly induced (red) or repressed (green) genes are represented by arrows. Significantly lower (green) or unaltered (blue) levels of metabolites are represented by circles; empty circles represent metabolites not detected by our untargeted metabolomics experiment. Colouring was used using the Mapper Color function of KEGG.

Not only carbon, but also nitrogen metabolism is clearly altered in *cox11* plants. The levels of several proteinogenic amino acids were reduced in *cox11* at ZT0 only (glycine), at ZT0 and ZT2 (asparagine, glutamate, serine, valine) or always (glutamine)

(Figure 2.10A). Moreover, during the day we found a reduction in tyramine, which can be produced by catabolism of the amino acid tyrosine (Araji et al., 2014; Maeda & Dudareva, 2012; P. Zhang et al., 2005), although the levels of tyrosine were not altered. Phenylalanine was the only amino acid identified at higher levels in *cox11* at the beginning of the day, consistent with the upregulation of arogenate hydratases, enzymes involved in phenylalanine biosynthesis.

Glycine and serine are readily interconvertible, they have a role in photorespiration, and in illuminated leaves glycine represents the main source of electrons for mitochondrial Complex I (Schertl & Braun, 2014). Valine is one of the three branched chain amino acids, along with leucine and isoleucine (Binder, 2010), which showed normal levels in *cox11* instead. Glutamate and glutamine are among the main metabolites involved in nitrogen assimilation from inorganic nitrogen sources in plants (Liao et al., 2022). Furthermore, glutamate represents an important bridge between carbon and nitrogen metabolism, as it can be reversibly converted into the TCA intermediate 2-ketoglutarate (Forde & Lea, 2007; Hodges, 2002). A glutamine-sensing mechanism has been described in chloroplasts that controls the activity of the plastid N-acetyl-L-glutamate kinase (NAGK) (Chellamuthu et al., 2014), a key enzyme of the ornithine synthesis pathway that leads to the formation of arginine (Slocum, 2005). The substrate of the NAGK enzyme and intermediate of the arginine biosynthesis, N-acetyl-L-glutamate, was always found at lower levels in *cox11*. Arginine, like asparagine, has a high nitrogen-to-carbon ratio, and therefore is one of the major compounds exploited for nitrogen storage and mobilization in plants (Winter et al., 2015; Yoneyama & Suzuki, 2020). We could not detect arginine in our metabolomics, but we found enzymes involved in arginine metabolism to be downregulated in our RNAseq data. Overall, these data show how nitrogen assimilation and mobilization must be altered in *cox11*, likely reduced by night, and potentially affecting a plethora of metabolic and cellular processes.

In Arabidopsis, one gene encoding for an asparagine synthase is repressed by carbon starvation (Gonzali et al., 2006; Xiao et al., 2020). We identified three orthologs of this gene in *P. patens*, and two of these were always strongly repressed in cox11 (Supplementary Table 2.11). This is consistent with *cox11* cells modulating its metabolism towards a starvation situation, blocking the energetically dispendious process of nitrogen assimilation, during night.

Two of the compounds found to be always reduced in *cox11* were threonate and 5'-oxoproline, likely related to the two antioxidants ascorbate and glutathione. In tomato, the degradation of ascorbate can produce threonate (Truffault et al., 2017). Importantly, the biosynthesis of ascorbic acid in plants requires cytochrome c as an acceptor of electrons (Bartoli et al., 2000). We showed how the respiratory chain in *cox11* was altered, and electrons from ubiquinone were accepted by the alternative oxidase and did not go through the cytochrome pathway. Therefore, we may assume that the cytochrome c pool was more reduced, and therefore the biosynthesis of ascorbic acid is hampered. This could have a negative effect on *cox11*, as it would reduce the antioxidant capacity of the plants. On the other hand, 5'-oxoproline is produced in Arabidopsis during degradation of glutathione (Kumar et al., 2015; Ohkama-Ohtsu et al., 2008; Paulose et al., 2013).

2.6. Energy accumulates in form of starch in *cox11*

By observing moss sample micrographs through transmission electron microscopy (TEM), we found that *cox11* accumulates large starch granules in their chloroplasts. In WT, starch granules were not present or were relatively small, but in *cox11* they were large and occupied most of the chloroplast area (Figure 2.12A). We then quantified the starch content on plants at ZT6 and confirmed that *cox11* had more than double amounts of starch compared to the WT (Figure 2.12B).

An accumulation of starch could be due to a major synthesis, a lower degradation, or both. To gain information about the capacity of starch degradation in *cox11*, we separated total *cox11* extracts in native conditions in gel and then performed in-gel activity staining for amylase activity. We could identify different bands with amylase activity, that had different apparent molecular weight, here named as A-D (Figure 2.12C). We do not know the precise identity of each band, as identification experiments are not available in literature regarding amylases in *P. patens*. In WT, band A had similar activity through the day, while bands B and D showed a peak at ZT6. It was unclear whether band D was very active causing a smear (Figure 2.12C, marked "?"), or whether there was a different activity at ZT6 only. One would expect the peak of hydrolytic activity to be identified at night, but the only timepoint at night in our setup was ZT23 i.e., the end of night, where maybe the activity was already going back to low levels to anticipate the coming day. In *cox11*, intensity of bands A and B

was similar to WT. We could identify another band, C, not seen in WT. This band C has increased activity at ZT0 and ZT23. Band D was more active at ZT23. The data together suggest that hydrolytic activity was increased in *cox11*.

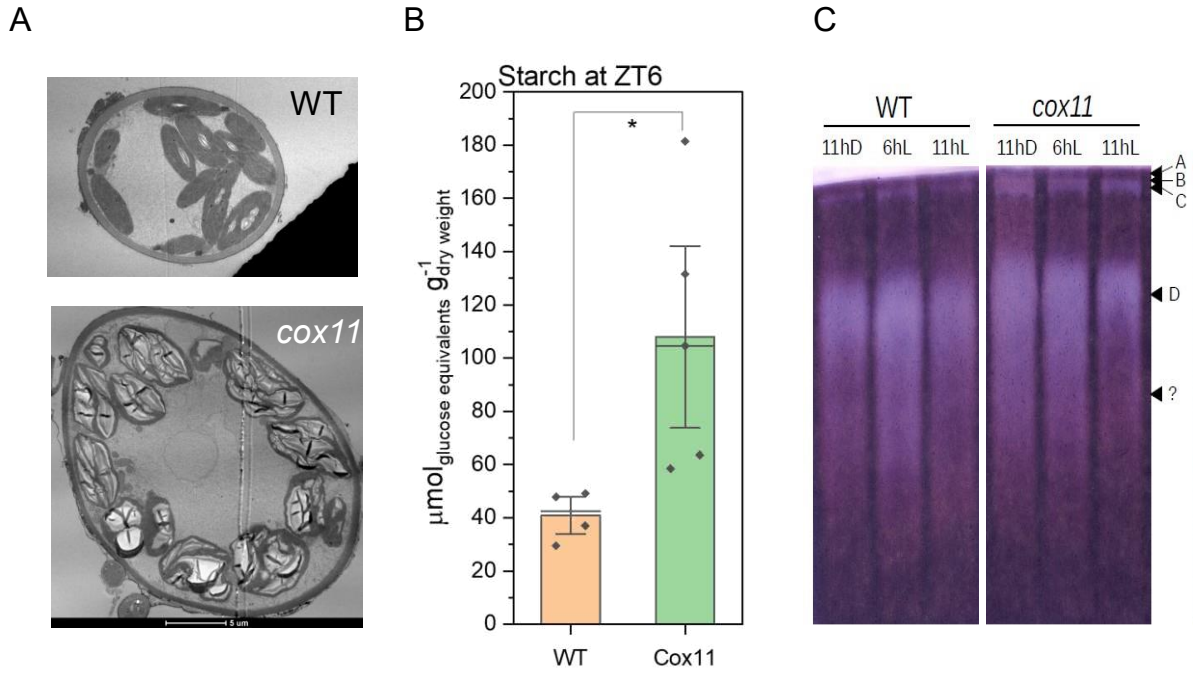

Figure 2.12 | **Starch accumulation in *cox11***. (A) Representative micrographs of WT and *cox11* cells showing differences in the amount and dimension of starch granules inside of chloroplasts. Plant samples were fixed after 16 hours of darkness. Scale is the same for both micrographs. (B) Quantification of starch in total extracts harvested at ZT6. (C) In-gel activity of starch degrading enzymes. Arrows A-D show the identified bands of activity. Symbol "?" marks a possible additional isoform or a smear produced by the increased activity of the isoform D.

Both the previously reported shortage of glycolysis intermediates and the accumulation of starch suggest a deficient mobilization of carbon storage during the night and a deficient use of energy in *cox11*. A way to measure the amount of energy available for the cell is to quantify the adenylate energy charge (AEC) (Atkinson, 1968), based on the levels of adenosine-5'-tri-, -di- and -monophosphates (ATP, ADP, AMP). We therefore calculated this value for both WT and *cox11* plants (Figure 2.13). We found the values of AEC in *P. patens* to be between 0.6 and 0.8, which fall in the range previously described for other plants (Hampp et al., 1982; Lange et al., 2008). In WT, the AEC increased through the day, with the difference becoming significant at ZT6. In *cox11*, the value at ZT0 was not significantly different from that of the WT; then, we observed an increase at ZT2 similar to that of WT, but afterward the AEC dropped down almost to ZT0 values as the day passed by (Figure 2.13). This suggests

that there was plenty of available energy at ZT2, but after some hours this availability was lost.

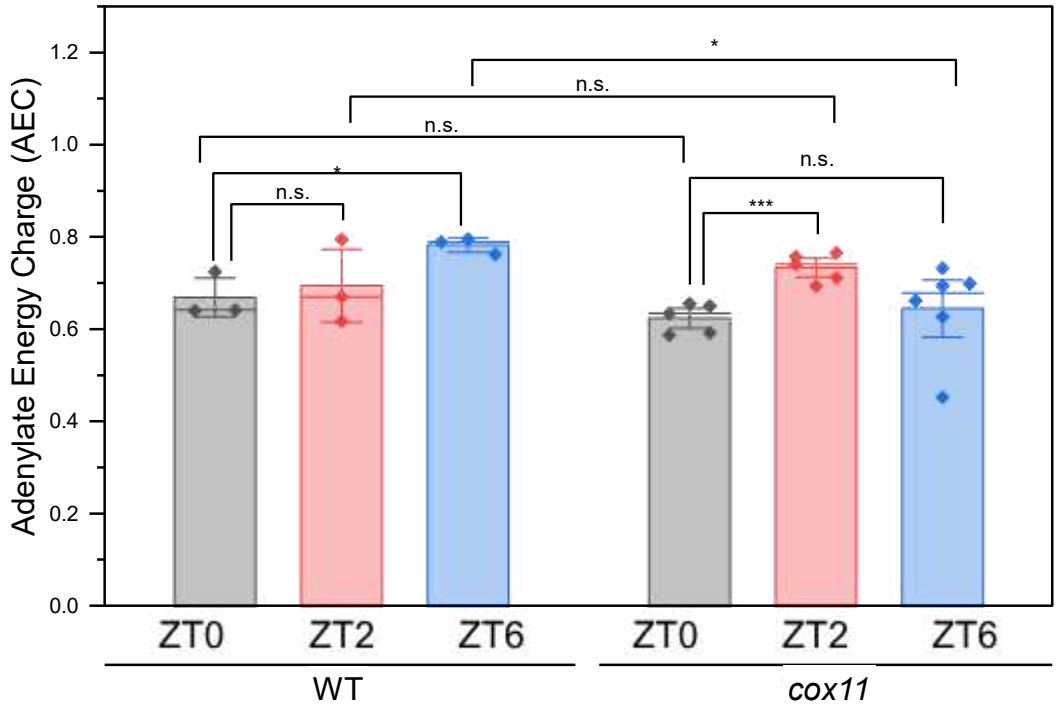

Figure 2.13 | **Adenylate energy chare (AEC) of WT and *cox11***. Statistics: two-sample t test. (***), p<0.001; (*), p<0.05; (n.s.), p>0.05.

2.7. External apport of amino acids could partially rescue the growth phenotype of *cox11* plants

So far, we reported a significant shortage of carbon intermediary metabolites and amino acids in *cox11* that was particularly relevant by night. Moreover, we also detected altered ratios of the related metabolites malate/fumarate, aspartate/asparagine, and glutamate/glutamine (Figure 2.14). Both fumarate and malate were lower at the end of night, but the relative proportion was also altered. The malate/fumarate ratio was higher in *cox11* at the end of the night (Figure 2.14), suggesting a displacement of the redox equilibrium towards malate. Lower malate/fumarate ratios have been associated to advantageous growth in natural variants of Arabidopsis (Le et al., 2019; Riewe et al., 2016), so the reduction in fumarate availability could be one factor impairing growth in *cox11*. The aspartate/asparagine ratio was always higher in *cox11*, showing a displacement in the amination equilibrium; the difference was stronger at night, with values 5× higher than

the WT. This was consistent with the observed transcriptomic repression of asparagine synthases, probably in response to starvation signalling. Also, the glutamate/glutamine ratio was higher in *cox11*. This was particularly notable during the day, when nitrogen assimilation sustains a low Glu/Gln ratio in the WT, pointing to a strongly reduced usage of glutamate as a carbon skeleton for nitrogen assimilation.

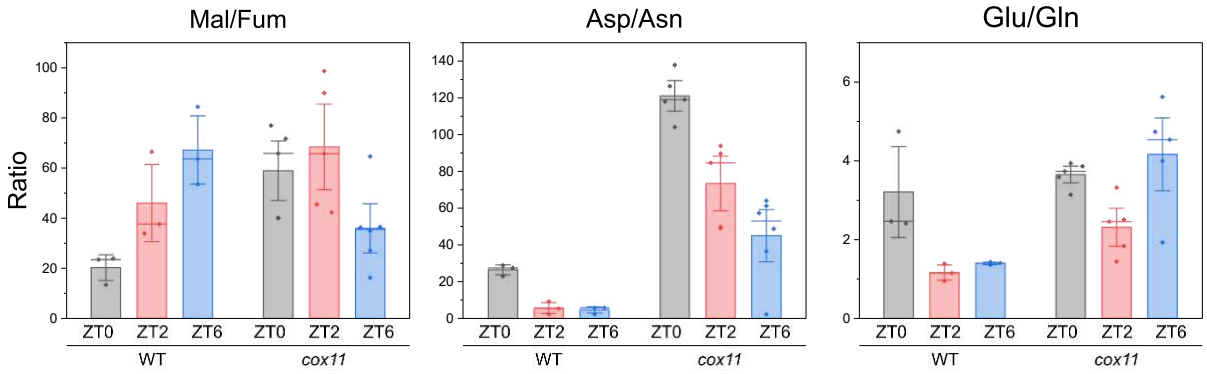

Figure 2.14 | **Ratios comparing relative abundances of malate and fumarate, aspartate and asparagine, and glutamate and glutamine**. Colours represent ZT0 (grey), ZT2 (red) and ZT6 (blue).

Given the general alteration of levels and relative abundance of several amino acids, we hypothesized whether the external apport of amino acids could rescue the growth phenotype of *cox11* by providing metabolic intermediates that could restore one or more essential metabolic pathways that were impaired in *cox11* under control conditions. Therefore, we compared the growth of *cox11* plants grown under control conditions, i.e., where the sole source of nitrogen was inorganic nitrate, or in enriched media where the source of nitrogen was both inorganic nitrate and organic nitrogen in the form of one type of amino acid.

Except for glutamate, all the tested amino acid had either a positive or negative effect on the growth of WT and *cox11* plants (Figure 2.15A). On one hand, there was a group of amino acids that had a negative effect on WT but had no significant effects on *cox11*. On the other hand, another group of amino acids had a positive effect on both WT and *cox11*, which was significant after four or more weeks of growth. Some of these had a very positive effect on *cox11* growth, increasing the spot area to up to 3 times the control (Supplementary Figure 2.13). Among these, the one that caused a stronger improvement of growth was serine, reported here as an example (Figure 2.15B, C). Serine did not only increase the growth area of the plant, but it also induced an earlier formation of phyllids and gametophore-like structures on *cox11* (Figure 2.15C, bottom), suggesting a faster rate of development. This was observed also for

glycine, which is not surprising considering that serine and glycine are easily interconvertible.

A

WT

Amino acid	Days 14	24	35	49	63
Cys	Down	Down	Down	Down	n. s.
His	Down	Down	Down	Down	Down
Ile	Down	Down	Down	Down	Down
Leu	Down	Down	Down	Down	Down
Lys	Down	Down	Down	Down	Down
Met	Down	Down	Down	Down	Down
Pro	Down	Down	Down	Down	Down
Thr	Down	Down	Down	Down	Down
Trp	Down	Down	Down	Down	Down
Val	Down	Down	Down	Down	Down
Phe	Down	Down	Down	n. s.	n. s.
Ala	n. s.	n. s.	Up	Up	Up
Arg	n. s.	Down	n. s.	Up	Up
Asn	Down	n. s.	n. s.	Up	Up
Asp	Down	n. s.	Up	Up	Up
Gln	n. s.	n. s.	Up	Up	Up
Gly	n. s.	n. s.	Up	Up	Up
Ser	n. s.	n. s.	Up	Up	Up
Glu	n. s.	Down	n. s.	n. s.	n. s.

cox11

Amino acid	Days 14	24	35	49	63
Cys	n. s.	n. s.	n. s.	n. s.	n. s.
His	n. s.	n. s.	n. s.	n. s.	n. s.
Ile	n. s.	n. s.	n. s.	n. s.	n. s.
Leu	n. s.	n. s.	n. s.	n. s.	n. s.
Lys	n. s.	n. s.	n. s.	n. s.	n. s.
Met	n. s.	n. s.	n. s.	n. s.	n. s.
Pro	n. s.	n. s.	n. s.	n. s.	n. s.
Thr	n. s.	n. s.	n. s.	n. s.	n. s.
Trp	n. s.	n. s.	n. s.	n. s.	n. s.
Val	n. s.	n. s.	n. s.	n. s.	n. s.
Phe	n. s.	n. s.	n. s.	n. s.	n. s.
Ala	n. s.	n. s.	n. s.	Up	Up
Arg	n. s.	n. s.	n. s.	Up	Up
Asn	n. s.	n. s.	n. s.	n. s.	Up
Asp	n. s.	n. s.	n. s.	Up	Up
Gln	n. s.	n. s.	n. s.	Up	Up
Gly	n. s.	n. s.	Up	Up	Up
Ser	n. s.	n. s.	n. s.	Up	Up
Glu	n. s.	n. s.	n. s.	n. s.	n. s.

B

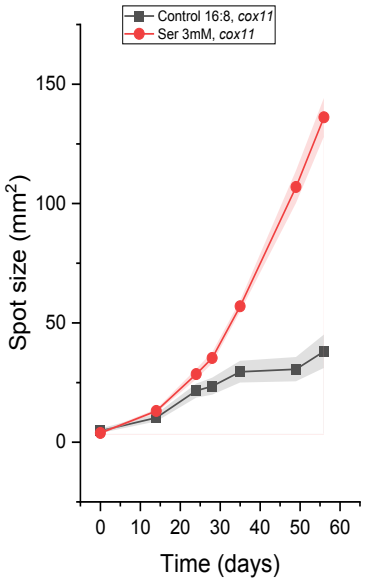

C

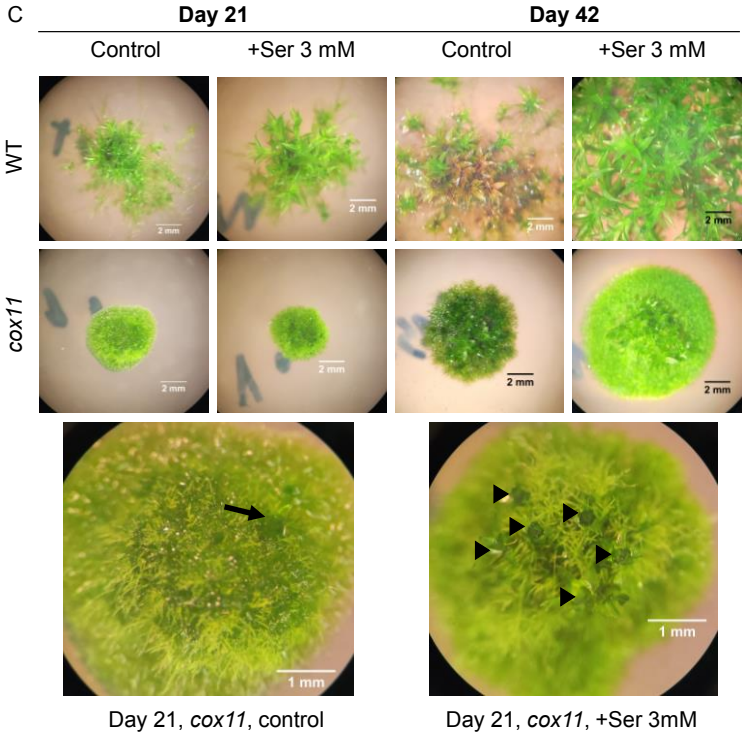

Day 21, *cox11*, control Day 21, *cox11*, +Ser 3mM

Figure 2.15 | Effect of external supply of amino acids on growth. (A) Time-resolved effect on growth of addition of the different amino acids. The size of the spots was quantified at each given timed and compared with the control by multiple one-way ANOVA, Tukey test. For significant comparisons ($p<0.05$), the direction of growth is shown (Up, Down). Not significant comparisons are depicted as "n. s.". (B) Growth curve of *cox11* supplemented with 3 mM serine. (C) Details on the effects of serine, the amino acid that exerted a more positive effect on growth of *cox11*. The comparison of plants at two different times is shown (upper images), and a detail on gametophore buds is included (bottom images). Black arrows mark developing gametophores.

Overall, we demonstrated that the external addition of some amino acids could partially rescue the phenotype of *cox11*, which is consistent with *cox11* having a globally altered metabolism where some metabolites are lowly available, compromising the functioning of anaplerotic reactions required for the correct usage of energy and resources.

3. Discussion

3.1. *cox11* plants lack a functional cytochrome c oxidase

Here we report the isolation and characterization of mutant lines of the moss *Physcomitrium patens* knocked out for the copper chaperone COX11. Previously, only knockdown lines could be isolated in the vascular model *Arabidopsis thaliana*, since the complete knockout would not be viable (Radin et al., 2015). Therefore, this is the first time that a plant completely depleted of COX11 has been produced.

COX11 has a reported role in biogenesis of the mitochondrial Complex IV or cytochrome c oxidase complex, playing a role in the insertion of copper ion into the active site of COX2 (Meyer et al., 2019). Accordingly, the knockdown lines in Arabidopsis showed a strong reduction in Complex IV activity (Radin et al., 2015). Here, we confirm that COX11 is essential for correct functioning of Complex IV also in the moss *P. patens*, as crude membrane extracts of *cox11* plants had undetectable levels of cytochrome c oxidase activity (Figure 2.1). To our knowledge, there is only another reported plant mutant that showed undetectable levels of cytochrome c oxidase, the *cod1* mutant in Arabidopsis (Dahan et al., 2014). However, *cod1* plants suffered of general and severe alterations in development, morphology, and general physiology (Dahan et al., 2014) that questions its role as a model for better understanding the role that respiration and in particular the cyanide-sensitive pathway has in plants during night and day metabolisms.

Therefore, we believe that the novel *cox11* plants that we present here represent the most valuable model currently available for studying the physiological consequences of the constitutive blockade of the cyanide-sensitive respiratory pathway in plants. This consolidates the moss *P. patens* as a suitable model for studying mitochondrial mutants that are not viable in vascular plants, as it was already suggested by the previously described *ndufa5* and *ndufb10* mutants lacking a functional Complex I (Mellon et al., 2021).

3.2. *cox11* have altered mitochondrial respiratory chain composition and activity

By monitoring the rate of oxygen consumption, we demonstrated that the cyanide-sensitive pathway is completely inactivated in *cox11* plants, which completely rely on the AOX-mediated alternative pathway to keep the pool of ubiquinone in the oxidized form. The action of the alternative pathway allows the only available complex for proton translocation in *cox11* mitochondria, the Complex I, to sustain a gradient of protons to fuel oxidative phosphorylation. Interestingly, we verified that the oxygen consumption rate was increased in *cox11*, demonstrating that a higher flux of electrons was induced to compensate, at least partially, for the loss of the two proton-translocating sites that are bypassed in *cox11*. The protein levels of NAD9, a core subunit of Complex I, and SDH1, the catalytic subunit of Complex II, were increased in *cox11* mutants, further suggesting an increased capacity for electrons to enter the modified respiratory chain. Although protein levels of Complex II were increased, we found fumarate, produced from succinate through the Complex II, at lower levels in *cox11*. Fumarate can be easily converted into malate, which is a well-known carrier of electrons between cell compartments; however, malate levels were also lower in *cox11* at night, as were all the other intermediates of the TCA cycle detected. It remains thus elusive whether the Complex II was indeed a major contributor to the flow of electrons in *cox11*, in which case the resulting fumarate was likely consumed faster in *cox11* than the WT; or whether Complex II was less active in *cox11*, maybe due to a low availability of succinate because of a slowed TCA cycle, and therefore fumarate was produced less efficiently in the mutants. In the latter case, the increase in O_2 consumption could be due to electrons that entered the respiratory chain through the Complex I or via one of the alternative NAD(P)H dehydrogenases. We might hypothesize that electrons entered through the external NAD(P)H dehydrogenases, exploiting reducing power available in the cytosol.

While AOX protein levels were not higher in the mutant, as described in CHAPTER I, a higher activity could be explained by different means of post-translational regulation (Ho et al., 2008; Moellering & Benning, 2010; Rhoads et al., 1998). Remarkably, although AOX induction is a common feature of plants with altered Complex I activity, Arabidopsis plants with reduced levels of cytochrome c and

Complex IV also showed unaltered or reduced levels of Aox1a, the homolog of PpAox (Florez-Sarasa et al., 2021).

While the transfer of electrons from Complex I to molecular oxygen through the alternative oxidase is much less efficient than the cytochrome pathway for ATP production, it ensures the consumption of reducing power, which is likely a pivotal function in photosynthetic active cells where chloroplasts generate additional reducing power (Dahal et al., 2017; Krämer & Kunz, 2021; Moreno-García et al., 2022). It is well known that the photosynthetic electron transport produces NADPH in excess with respect to ATP for CO_2 fixation, and multiple mechanisms exist to balance this ratio, such as cyclic and pseudo cyclic electron transport (Alboresi et al., 2010; Storti et al., 2019, 2020). Mitochondrial respiration is probably a major contributor in balancing the extra reducing power in the cell, as it has been suggested from experiments with inhibitors (Yoshida et al., 2006) or modelling analyses (Shameer et al., 2019). Further supporting this idea, the overexpression of a protein that increased the flow of reducing equivalents from chloroplasts to mitochondria had a positive effect in balancing the NADPH/ATP ratio in chloroplasts and increased the efficiency of photosynthesis (Voon et al., 2021).

3.3. Energy is not correctly mobilized in *cox11*

cox11 plants could be propagated vegetatively and were viable, but their growth was strongly impaired. Remarkably, cells that form protonema, the tissue that we used for our experiments, are fully photosynthetically active cells. Respiratory mutants depleted in Complex IV activity in the green alga *Chlamydomonas reinhardtii* showed a growth delay only when grown under mixotrophic conditions but were not different than the WT when photosynthesis was active (Colin et al., 1995).

In the past it was shown that CMSII tobacco plants depleted in Complex I activity could remodulate the *in vivo* partitioning of electrons through the cyanide-sensitive and cyanide-insensitive pathways during stress conditions so the predicted ATP production by oxidative phosphorylation was not lower in the mutants compared to the WT (Vidal et al., 2007). In *cox11*, the increase in electron transport rate could have a similar effect, with *cox11* plants producing the same or only slightly lower levels of ATP via oxidative phosphorylation. This is supported by the observation that the

adenylate energy charge (AEC) is not significantly different in *cox11* at night. Moreover, the AEC showed a peak at ZT2 and then a strong decrease in ZT6, suggesting that during the first hours of the day photosynthesis provided the cell with energy that was not efficiently used and therefore accumulated.

We verified that *cox11* plants converted energy from light to ATP and NADPH, as supported by unaltered light reactions of photosynthesis. Despite suffering of a general metabolic rearrangement that altered the use of carbon, as seen by lower rates of carbon fixation, *cox11* mutants accumulated more starch, which is a product of photosynthesis, and therefore the inability to harvest energy could not be the cause of the growth defects described in *cox11*. Accordingly, the removal of photorespiration by growing plants under an elevated CO_2 concentration did not have a positive effect on growth. The synthesis of starch was upregulated also at the transcript level, by the induction of several starch synthases during the day. This is opposite of what has been observed for the Complex I deficient CMSII tobacco mutants (Dutilleul et al., 2005), although these mutants had a phenotype that depended on the growth environment such as the light conditions (De Paepe et al., 1990; Priault et al., 2006). Interestingly, the starch accumulation was instead reported for Arabidopsis mutants with decreased activity of the cyanide-sensitive pathway, although it was totally degraded during the night (Racca et al., 2018).

Apparently, carbon could be fixed and stored in form of starch but then could not be efficiently mobilized, as seen by the reduced levels of glycolytic intermediates at night when the catabolism of starch should provide the cell with monosaccharides to fuel respiration. Surprisingly, the amylase activity of *cox11* extracts was higher, suggesting a higher capacity of *cox11* for starch degradation despite the striking starch accumulation. One possibility is that the excess of starch itself stimulates the production of amylolytic enzymes. However, another hypothesis is that chloroplast stroma is altered and therefore carbon fixation is increased, maybe even at night, producing more starch than can be degraded and causing a carbon deprivation in the plant.

Attempts to rescue the growth phenotype largely failed. No extra light or extra CO_2 were able to rescue the phenotype, suggesting that photosynthesis, CO_2 fixation nor photorespiration, even if affected, were not responsible of the growth impairment.

The addition of glucose and ammonium tartrate did have a positive effect on the growth, although the treated plants where still largely impaired when compared to the WT. In summary, the growth defects of *cox11* could not be attributed to a simple energy deficit, but rather to an inefficient mobilization of energy equivalents.

3.4. Mitochondrial metabolism has an essential role in amino acid biosynthesis.

The blockade in respiration also had a consequence in the metabolism of amino acids. Glycolysis and the TCA cycle are pivotal for the cell because they provide not only readily available energy in form of nucleotide phosphates such as ATP and GTP, but they also provide metabolic intermediates required for anaplerotic reactions (Sweetlove et al., 2010; Y. Zhang et al., 2018). We can thus hypothesize that the shortage of intermediates of glycolysis and the TCA cycle altered the processes of nitrogen assimilation and mobilization. In leaves of vascular plants, nitrate assimilation can occur by night by using stored carbohydrates (Yoneyama et al., 1987; Yoneyama & Suzuki, 2020).

Ammonium assimilation is done mainly through the glutamine synthetase/glutamate synthase (GS/GOGAT) cycle, although it could also possibly be assimilated via glutamate dehydrogenase (GDH) (Singh, 1998). The GS/GOGAT cycle requires glutamate, glutamine, and 2-ketoglutarate, which were all found at lower levels in *cox11* at night. Asparagine, which is also an important metabolite for nitrogen assimilation (Gaufichon et al., 2010; Yoneyama & Suzuki, 2020), was found at lower levels in *cox11* at ZT0 and ZT2. Nitrogen assimilation proceeds in part by the amination of aspartate and glutamate into asparagine and glutamine, respectively. Notably, the aspartate/asparagine and glutamate/glutamine ratios were much higher in *cox11*, particularly at day, suggesting that nitrogen assimilation was indeed not taking place efficiently.

Although we did not measure the amount of arginine, N-acetyl-L-glutamic acid, an intermediate of its biosynthesis pathway, was always reduced in cox11, suggesting that also arginine levels could be low in *cox11*. Arginine has been demonstrated to have a role in the control of development of *P. patens* (Kawade et al., 2020).

Accordingly, *cox11* plants grown on media supplemented with arginine had a improved growth phenotype (Supplementary Figure 2.13).

We tried different treatments to rescue the growth phenotype of *cox11* plants. While we could not truly rescue the growth, we found treatments capable of significantly improving the growth. The most significant improvement was achieved when plants were grown in the presence of the amino acid serine. The positive effect of serine was likely not linked to photorespiration, as growth under high CO_2 did not have a positive effect on *cox11* plants. Also, other amino acids could improve the growth by more than 4× area size.

3.5. Induction of heat shock proteins is observed at the night-to-day interface

The transcriptomics and metabolomics data showed that the major affectations in metabolism concentrated at night and disappeared after exposure to illumination. This was also true for the stress response, based on the induction of several isoforms of heat shock proteins.

It has long been described and assumed that ROS are the main signal that trigger response to stress upon mitochondrial malfunctioning (Garmash, 2023; Møller & Sweetlove, 2010; Noctor et al., 2007; Zhao et al., 2020) and this could be the case in *cox11* plants. The induction of heat shock proteins, which we reported in *cox11* plants, is considered a response to oxidative stress induced by H_2O_2 signalling (Mehterov et al., 2012; Qureshi et al., 2011; Vaahtera et al., 2014). COX11 has been shown to provide antioxidative protection independently of its role in the assembly of Complex IV in the yeast *Saccharomyces cerevisiae* (Veniamin et al., 2011), in rice (Luo et al., 2013) and in Arabidopsis (Radin et al., 2021). However, Arabidopsis plants with reduced levels of COX11 did not have an increase in ROS (Radin et al., 2021).

Another marker of oxidative stress is the induction of the AOX (Garmier et al., 2008; Millar et al., 2011), although it is not induced in *cox11*. Noteworthy, the AOX is induced in most plants with altered levels of Complex I and this is also the case of Complex I deficient *ndufa5* plants in *P. patens*, as we show in CHAPTER III. Therefore, we may consider other hypotheses for the induction of heat shock proteins beyond ROS signalling. In 2014, (Kuzmin et al., 2004) hypothesized a model by which the

mitochondrial alteration of Complex I deficient maize NCS2 mutants led to a decrease in the mitochondrial membrane potential, which can potentially affect the function of the protein import machinery (Kuhn et al., 2009; Whelan & Glaser, 2011). According to the heir hypothesis, these de-energized mitochondria would import less efficiently the protein precursors, that would accumulate in the cytosol and/or intermembrane space, and this accumulation would induce the expression of heat shock proteins, which are chaperones that aid in protein folding. Very interestingly, small heat shock proteins have been recently described to accumulate not only in the cytosol, but also in the mitochondrial intermembrane space in mammals (Adriaenssens et al., 2023). Therefore, we could hypothesize that, in *cox11*, small heat shock proteins are induced in response to mitochondria dysfunction and help to alleviate the stress caused by the accumulation of protein precursors. Some genes have been identified as markers of the unfolded protein response in *P. patens* (Lloyd et al., 2018), but they were not significantly induced in *cox11*. Therefore, while it is possible that the accumulation of unfolded mitochondrial protein precursors induces the expression of heat shock proteins, we did not observe the activation of a complete unfolded protein response.

Opposite to the stress response represented by heat shock proteins, the transcriptomic profile of *cox11* suggests that during the day, when metabolite levels are virtually back to normal levels, there is an induction of the biogenesis of ribosomes. This could mark the re-activation of anabolic processes that had been inhibited earlier by the SnrK1 system, remarking the role of illumination in furnishing *cox11* with available energy.

3.6. Snrk1 complex, a candidate for modulating the metabolic response in *cox11*

Our data is largely compatible with *cox11* modulating their metabolism towards a starvation situation, inhibiting carbon mobilization and blocking nitrogen assimilation. A good candidate to regulate this behaviour is the evolutionary conserved SNF1-related protein kinase 1 (SnRK1) complex, homolog of the yeast SNF1 and the mammalian AMPK systems (Baena-González & Sheen, 2008; Crozet et al., 2014; Gutierrez-Beltran & Crespo, 2022). The SnRK1 complex is an important regulator that gets activated upon energy deficit for adjusting cell metabolism during starvation,

stress, and development (Gutierrez-Beltran & Crespo, 2022; Wurzinger et al., 2018). In a variety of plants, activation of SnRK1 funnels carbon towards starch biosynthesis by modulating the gene expression of sucrose synthases and ADP-glucose pyrophosphorylases (Jain et al., 2008; Kanegae et al., 2005; McKibbin et al., 2006; Purcell et al., 1998; Tiessen et al., 2003; Y. Zhang et al., 2001). Interestingly, SnRK1 is required also for the expression of some alpha amylases, which catalyse starch degradation (Laurie et al., 2003). SnRK1 can also modulate nitrogen metabolism by two different means, as it can phosphorylate and inactivate the nitrate reductase (Sugden et al., 1999), and it can also modulate gene expression of asparagine synthetase (Baena-González et al., 2007).

All these observations point towards the SnRK1 system being potentially activated in *cox11*, particularly at ZT0. We did not test it and therefore cannot confirm whether the SnRK1 system is the main responsible of the phenotype observed in *cox11*, but it emerges as an interesting hypothesis to be tested in future studies.

4. Conclusions

We presented here the first plant model genetically depleted in COX11, an assembly factor of cytochrome c oxidase. This represents the best model isolated so far of an embryophyte completely depleted on the cytochrome pathway. The plants with depleted Complex IV sustained an increased flow of electrons through a modified respiratory chain based on a transfer of electrons from reducing equivalents towards molecular oxygen by the important action of the AOX. While light reactions of photosynthesis were not hampered, there was a reduction in carbon fixation efficiency. The impact of Complex IV deficiency was more relevant during night, when the cells switch their metabolic system towards an energy-depleted situation, possibly by the activation of the SnrK1 system, that mobilizes carbon towards starch synthesis and blocks nitrogen assimilation and amino acid biosynthesis. Overall, we showed how a correct and efficient functioning of mitochondrial function is required for the correct functioning of both carbon and nitrogen metabolism in plants and is essential not only at night but also when photosynthesis is active.

5. Material and methods

5.1.1. Plant material and growth conditions

The moss *Physcomitrium patens* (Gransden ecotype) was propagated on solid culture medium under sterile conditions. Protonema was collected using a spatula and transferred to a 50-mL tube filled with approximately 10 mL of Milli-Q® purified water. The collected tissue was then homogenised using an Ultra-Turrax® disperser. The homogenised tissue was used immediately or kept at 4 °C until used. For inoculation, approximately 1 mL of the homogenate was poured on a Petri dish containing 23 mL of solid culture medium and covered with a cellophane filter. The filter allowed nutrient exchange between the medium and plant cells and impeded the protonema to grow inside the agar medium, making plant collection easier.

Two types of culture media were used, and their composition is reported in Supplementary Table 2.1. The $PpNO_3$ medium contained nitrate ions as a source of nitrogen and did not contain organic carbon. It was used for amplification of plant tissues destined to physiological analyses. The peak of photosynthetic performance was achieved after approximately 10 days of growth, so physiological measurements were performed at this time. The $PpNH_4$ medium results from supplementation of $PpNO_3$ with ammonium tartrate and glucose as sources of nitrogen and carbon, which allow a faster growth. WT plants grown in $PpNH_4$ medium were collected after 5 or 6 days of growth for WT and most mutants, because after this time they began to senescence. Other mutants, like cox11 or ndufa5, grew very slowly, so I collected them after 10 to 14 days of growth.

Plants were incubated in growth chambers at 24 °C and a defined light intensity and photoperiodicity. In standard conditions, plants were exposed to light at 50 µmol photons m-2 s-1. Depending on the experiments, the light/night regime (hours of light:hours of darkness) was set at either long day (16:8), short day (12:12) or continuous illumination (24:0) conditions.

5.1.2. Generation of cox11 knockout lines

For generation of cox11 knockout (KO) lines, up- and downstream regions of the locus harbouring the PpCox11 gene were cloned into a BHRf plasmid, which carries a hygromycin resistance cassette (Supplementary Figure 2.1A). The construct

was linearized with the restriction enzyme PvuII and used for gene targeting through polyethyleneglycol (PEG)-mediated transformation as described previously (Mellon et al., 2021). To confirm that *cox11* lines lacked the PpCox11 expression, reverse transcription (RT)-PCR was performed on cDNA (RevertAid ReverseTranscriptase; Thermo Scientific) synthesized after RNA extraction. Primers used for construct design and line validation are included as Supplementary Table 2.2.

5.1.3. Genomic DNA extraction

Extraction of genomic DNA was done following a fast extraction protocol with some modifications (Edwards et al., 1991). Protonemata of *P. patens* grown on $PpNH_4$ were collected in 1.5 mL tubes and snap frozen at -80 °C using liquid nitrogen. Each sample was then grinded using a plastic tip with the addition of 500 µL of cold TEN buffer (Tris-HCl 100 mM, pH 8.0; EDTA 50 mM; NaCl 500 mM). After the addition of 35 µL of SDS 20 %, samples were incubated at 65 °C for 5 minutes. Then, 130 µL of potassium acetate 5 M were added, the samples were kept on ice for 5 minutes and centrifuged at 4 °C for 10 minutes at 13,000 g. The supernatant was transferred to a clean 1.5 mL tube containing 500 µL of isopropanol at -20 °C, mixed by inversion and incubated at -20 °C for 10 minutes. Then a series of centrifuges at 4 °C and 13,000 g were performed. After a first centrifuge of 10 minutes, the supernatant was discarded and the pellet resuspended in 500 µL of 70 %ethanol. Then, the resultant pellet of a second centrifuge of 5 minutes was resuspended in 150 µL of 70 %ethanol. A last centrifuge of 2 minutes was performed and the resultant pellet was dried off under the chemical fume hood. The pellet was then resuspended in 50 µL of water. This DNA solution was kept at -20 °C until used.

5.1.1. Public transcriptomic data and phylogenetic tree

We compared the expression levels of PpCox11 using the publicly available data from PeatMOSS (Fernandez-Pozo et al., 2020).

For phylogenesis, we retrieved a set of 46 protein sequences from different organisms that were homologous to those of PpCOX11 (Supplementary Table 2.5). The sequences were aligned using the tool MUSCLE (Madeira et al., 2022) and then envisioned and formatted using the program JalView (Waterhouse et al., 2009). We manually removed the non-conserved segments of the multiple alignment to reduce

the noise. The modified alignments were used to build a Bayesian inference-based phylogenetic tree using the program MrBayes (Ronquist et al., 2012). The consensus tree was visualised and formatted with the software FigTree (https://github.com/rambaut/figtree/).

Sequence alignment of COX11 sequences from *Saccharomyces cerevisiae*, *Bos taurus* and *P. patens* was done using MUSCLE.

5.1.2. Protein extraction and chlorophylls quantification

Protein extraction for denaturing polyacrylamide gel electrophoresis (PAGE) was performed on fresh or frozen protonema grown on $PpNO_3$ for 10 days. The protonema was macerated in a 1.5 mL tube using a plastic tip. Then, 100 to 150 µL of sample buffer (SB 3x) (Tris-HCl 125 mM, pH 6.8; 30 % (w/v) glycerol; 9 % (w/v) sodium dodecyl sulphate ; dithiothreitol 100 mM) were added. After vortexing a few seconds, samples were centrifuged at 13,000 g for 10 min at room temperature. The supernatant was collected in new 1.5 mL tubes and centrifuged again at the same conditions. This supernatant was the extract used to load the acrylamide gel, containing proteins and chlorophylls.

For chlorophyll quantification, 2 mL of protein extract were diluted in 68 µL of acetone 80 % in 0.5 mL tubes. The tubes were vortexed briefly and centrifuged at 13,000 g for 5 min at room temperature. Proteins precipitated forming a pellet and chlorophylls remained in solution. The supernatant was transferred to clean 0.5 mL tubes. The absorption spectrum (from 750 to 600 nm) of the supernatant was measured using a Cary 100 UV-Vis spectrophotometer (Agilent Technologies). The chlorophylls concentration of the protein extract, [*Chl*], was calculated applying the following formula, where OD stands for optical density (Porra et al., 1989):

$$[Chl]\left(\frac{\mu g}{mL}\right)=\{20.20\cdot[OD(645)-OD(750)]+8.02\cdot[OD(663)-OD(750)]\}$$

After quantification, the pure protein extracts were incubated 1 min at 100 °C.

Total protein content was determined by the bicinchoninic acid (BCA) assay (He, 2011).

5.1.3. Crude membrane isolation, blue-native polyacrylamide gel electrophoresis (BN-PAGE) and in-gel activity staining

Crude membrane extracts were prepared on ice and using chilled tubes and reagents to avoid protein denaturation. All the centrifuges were performed at 4 °C. Approximately 300 mg of fresh or frozen (-80 °C) protonema grown on $PpNO_3$ for 10 days were homogenised using a Potter-Elvehjem glass tissue grinder in 2mL of MOPS-KOH 75mM, pH 7.6; sucrose 0.6 M; EDTA 4 mM; polyvinylpyrrolidone-40 0.2 %; cysteine 8 mM and bovine serum albumin 0.2 %. The homogenate was transferred to a 15 mL conical tube lined with a square of miracloth with 20 µm pores to filter unbroken cells and tissue debris. The filtered homogenate was then transferred to a 2 mL tube (for convenience in the next steps) and centrifuged for 4 min at 1,300 g to pull down the cellular debris. The supernatant was collected in a clean 2 mL tube and centrifuged for 20 min at 21,470 g to pellet the thylakoid and mitochondrial membranes. The supernatant was discarded, and the pellet was resuspended in 200 µL of MOPS-KOH, pH 7.2 and sucrose 0.3 M. This solution was the crude membrane extract.

5.1.4. SDS-PAGE and Urea-PAGE for immunoblotting

Sodium dodecyl sulphate (SDS) or urea denaturing polyacrylamide gels were freshly prepared using a *Mini-PROTEAN® Tetra* handcast system (Bio-Rad Laboratories, Hercules, CA). We used discontinuous gels, with a stacking gel at 4 % acrylamide and a running gel at 12 % acrylamide.

Either total protein or crude membrane extracts were used. A suitable volume of each extract was aliquoted into 0.5 mL tubes to reach the desired amount of chlorophylls (or proteins, in crude membrane extracts). Then, the suitable volume of sample buffer (SB) 1x was added to get the same final volume in all the tubes. The full volume of each tube was loaded in the wells.

Gels were run at 30 V for 40 min or until the migration front reached the running gel, followed by 110 V until the migration front exited the gel (approximately 120 min). Immediately after, the gels were transferred to a polyvinylidene fluoride (PVDF) membrane. The transfer was done applying a constant current of 100 V for 1 hour. The gel and the membrane were covered with transfer buffer (20 mM Tris, 152 mM

glycine, 20 % methanol). An ice block was added to the transfer chamber to avoid overheating of the buffer. After the transfer, the success of the process was assessed staining the membrane with Ponceau S solution (Ponceau S 0.1 % (w/v), acetic acid 5 %), which binds proteins in a reversive manner. The staining was then removed with a few washes on deionised water.

Membranes were then used for hybridisation with antibodies. First, we blocked the membrane by incubating it in a solution of non-fat dry milk at 10 % in TBS (Tris-Buffered Saline: Tris-HCl 20 mM, pH 7.4; NaCl 150 mM) for 1 to 16 h. This step prevents antibodies from binding to the membrane non-specifically. After the blocking step, we removed the excess of proteins with six washings of TBS, of 5 minutes each. Successively, we incubated the membrane with the corresponding solution of primary antibody diluted in TTBS (Tween®-20 Tris-Buffered Saline: Tris-HCl 20 mM, pH 7.4; NaCl 150 mM, Tween®-20 0.05 % (v/v)) for 2 h. We removed the solution of primary antibody, performed six washings with TTBS and incubated the membrane with a solution of secondary antibody diluted at 1:10,000 in TTBS for 1 h. The secondary antibody used in all the experiments was a mouse anti-rabbit antibody conjugated with alkaline phosphatase. Six more washings were performed with TTBS, and the membrane was ready for development.

The development solution was freshly prepared mixing 10 mL of alkaline phosphatase buffer (100 mM Tris-HCl, pH 9.5; 100 mM NaCl; 5 mM $MgCl_2$) with 33 µL of BCIP (5-bromo-4-chloro-3-indolyl phosphate, from a stock at 50 mg/mL in 70 % dimethylformamide) and 66 µL of NBT (nitro blue tetrazolium chloride, from a stock at 50 mg/mL in 70 % dimethylformamide). The membrane was treated with the development solution until a coloured band appeared, due to the colorimetric reaction catalysed by the alkaline phosphatase; depending on the antibody this took seconds to minutes. The colorimetric reaction was quenched transferring the membrane to a tray that contained deionised water and few drops of glacial acetic acid.

The list of antibodies used is attached as Supplementary Table 2.3. For all the antibodies except for the ß-subunit of Complex V, total protein extracts were resolved by SDS-PAGE. For the ß-subunit of Complex V, crude mitochondria extracts were separated by Urea-PAGE.

5.1.5. Blue native protein electrophoresis (BN-PAGE)

A 4-12% gradient polyacrylamide gel was prepared using a gradient mixer connected to a peristaltic pump. The 4 % and 12 % running solutions were prepared and transferred to the respective chambers in the gradient mixer. The peristaltic pump was turned on and the gradient solution was poured into the mounted glass. The running gel was covered with deionised water until it solidified. We then prepared and poured the stacking gel and added the comb, let the stacking gel solidify and kept it at 4 °C until used.

Crude membrane extracts were prepared and total proteins were quantified as described earlier in this section. For protein solubilization, 20 µL of digitonin 4 % (w/v) prepared in ACA buffer (1.5 M aminocaproic acid, 0.1 M BisTris pH 7.0, 2 mM EDTA) were added to the tubes containing 20 µL of sample in ACA buffer that corresponded to 50 µg of proteins, reaching 2 % digitonin in ACA buffer. Each tube was incubated on ice for 20 min and centrifuged at 4 ºC, 22,000g for 8 min. The supernatant was transferred to a clean tube, supplemented with 4 µL of 5 % Coomassie Blue solution (20 mM Bis-Tris, 0.5 M aminocaproic acid, Coomassie Blue G-250 5% (w/v)) and loaded to the gel.

Sample loading and gel running were performed in a cold chamber at 4 °C. The electrode assembly with the mounted gel was filled with both cathode buffer (15 mM Bis-Tris-HCl, pH 7.0; 50 mM tricine) containing Coomassie Blue G-250 0.02 % (w/v) and anode buffer (50 mM Bis-Tris-HCl, pH 7.0). The wells were loaded with the solubilised samples using a Hamilton syringe. The gel was run at 75 V for 30 minutes. Then, the cathode buffer was replaced with fresh cathode buffer without Coomassie Blue and the gel was run at 100 V for 30 min, at 125 V for 30 min, at 150 V for 60 min, at 175 V for 30 min and at 200 V for 60 min. The total running time was about 4 hours. After running, the gel was kept at 4 °C until used for in-gel activity staining.

After running, in-gel activity staining was done as described in (Sabar et al., 2005). The gel was incubated for 1 h in Complex IV buffer (50 mM potassium phosphate buffer pH 7.4, 75 mg/mL sucrose). Then, the buffer was replaced with Complex IV staining solution [1 mg/mL DAB (3,3′-Diaminobenzidine tetrahydrochloride hydrate; Sigma-Aldrich D5637), 1 mg/mL cytochrome c (Sigma-Aldrich C7752)] in

Complex IV buffer). The gel was incubated in the staining solution for 24 h at room temperature before image acquisition.

5.1.6. Growth test

2-mm disks of protonema of *P. patens* grown for 10 days in long day conditions were distributed in 92 mm Petri dishes filled with either solid $PpNO_3$, $PpNH_4$ or amino acid-enriched media. The plates were not covered with a cellophane filter as for other experiments. Each plate contained 10 plant disks and at least two technical replicates per genotype were included. The space distribution of the disks on the plate was homogenous and the relative position of each disk was aleatory, but the same loading scheme was followed for the different conditions to be compared. The plates were then sealed with parafilm and incubated under the corresponding conditions. Except for plates containing $PpNH_4$, which were completely sealed with parafilm, a 2 cm section was not sealed with parafilm but with a tape that allowed gas exchange.

Colony size was measured periodically. Photographs of the plates were acquired using a smartphone and analysed using *ImageJ* Fiji (https://imagej.nih.gov/ij/index.html) to quantify the area of each plant. Using the tool Colour Threshold, only the green spots were selected, and area was quantified after setting the scale using the diameter of the Petri dish (92 mm).

The effect of photoperiod was assessed by growing identical plates under either long day (16h:8h day:night) or continuous illumination (24h light). The effect of high CO_2 was done by keeping the Petri dishes in a growth chamber with controlled atmosphere of 1 % CO_2 in continuous illumination and 22 ºC. The effect of amino acid addition was done by performing the growth test on solid $PpNO_3$ medium containing additional 3 mM of each of the twenty primary amino acids except for tyrosine, which could not be dissolved without strongly acidifying the medium. A stock at 50 mM of each amino acid was prepared, that was sterile-filtered using a 0.2 µm filter. We transferred 3 mL of the amino acid stock into a 50 mL tube and then we added melted solid PpNO3 medium at approx. 50 ºC up to 50 mL, to reach a final concentration of 3 mM. The supplemented medium was gently mixed and poured into the plates. Once solidified, the plates were used for growth test as described. The final concentration of 3 mM was chosen according to previous experiments done in Arabidopsis (Forsum et al., 2008).

5.1.7. Measurement of oxygen consumption and evolution

Measurements of oxygen consumption (respirometry) and oxygen evolution were performed on pieces of intact protonema from 10-day old plants grown on $PpNO_3$ and dark adapted for 40 minutes before the experiments. Measurements were performed using a test version of the NextGen-O2k and the PhotoBiology (PB)-Module (Oroboros Instruments, Innsbruck) with the software DatLab 7.4.0.4 (Went et al., 2021). The PB light source contained a blue OSLON® LED (emitting wavelength range 439-457 nm with the peak at 451 nm, manufactured by OSRAM) attached to the window of the NextGen-O2k chamber. The oxygen concentration was assessed in 2-mL measuring chambers at 22 °C with a 2-seconds frequency and samples were magnetically stirred at 750 rpm. Two measurements were done in parallel at each time, taking advantage of the two chambers of the instrument.

To avoid disruption of the moss samples during the measurement, we used a sample holder developed by Oroboros Instruments, Innsbruck (Schmitt & Gnaiger, 2022). At first, we filled the measuring chambers with a volume slightly higher than 2 mL of fresh and sterile PpNO3 medium containing 10 mM NaHCO3 (to avoid carbon limitation during photosynthetic measurements), we inserted the sample holder and closed the chamber removing excess volume to ensure that precise 2 mL were inside. Then, we moved the stopper to the open position and let the system equilibrate for few minutes with the stirring on. This served both to bring the medium to the experimental temperature and to equilibrate the oxygen concentration of the medium to the atmospheric oxygen values. Then, we opened the chamber, added a piece of protonema of approximately 1 cm^2 on top of the sample holder and closed the chamber. This operation was done minimizing the exposure of moss samples to light. The oxygen concentration in the chamber was monitored for 10 minutes at dark to assess the rate of dark respiration, and we proceeded either with the quantification of photosynthesis or with the assessment of the effect of respiratory inhibitors.

For quantifying oxygen evolution, after stabilization of the respiration signal, blue light was turned on at 500 µmol photons m^{-2} s^{-1}, which was well above the saturating levels for *P. patens*. We kept the sample under this illumination for 10 minutes to achieve the stabilization of the oxygen evolution rate. The values of oxygen evolution rate reported in this work correspond to the median of 40-50 points in the

stable region of oxygen flux. We then turned the light off again and measured the post-illumination peak in respiration. The plot of a representative experiment is shown as Supplementary Figure 2.10.

For quantifying the effect of inhibitors on dark respiration, after stabilization of the respiration signal, inhibitors were added sequentially to the chamber. The plot of a representative experiment is shown as Supplementary Figure 2.8.Inhibitors were added through the stopper using Hamilton syringes, therefore not interrupting the measurements. For titrations using KCN or Antimycin A, we added to the chamber 4 uL of a stock 500 mM; for titrations using SHAM or n-propylgallate, we added to the chamber 8 uL of a stock 250 mM. In all cases the final concentration of the inhibitor was 1 mM.

After each experiment, the moss sample was recovered from the chamber, transferred to a screw-cap 1.5 mL tube and snap frozen in liquid nitrogen. Samples were either kept at -80 ºC or used for chlorophyll quantification immediately. Chlorophyll extraction was done by homogenizing the samples in 600 µL of acetone 80 % using 3-mm zirconium glass beads (Sigma-Aldrich) in the tube. Chlorophyll quantification in the extract was done by spectrophotometry as described earlier in this section. The measure of oxygen consumption and evolution was therefore normalized to the amount of chlorophylls in the sample.

5.1.8. Spectroscopic analyses

Spectroscopic analyses were performed as described previously (Mellon et al., 2021).

5.1.9. Transmission electron microscopy (TEM)

10 days old plants grown under long day were kept at dark for circa 20 h before inclusion, to avoid overaccumulation of starch. A portion of protonema was then chemically included using Epon resin, sliced and visualized using a transmission electron microscope.

5.1.10. Sample harvesting for systems analysis

We optimized the following system for growing moss samples for systems level analyses (Supplementary Figure 2.2). Protonema grown for approximately one week

on solid $PpNH_4$ medium under continuous illumination was disrupted using a UltraTurrax and used for the inoculation of 20 mL of liquid culture inside of a 100 mL Erlenmeyer flask. After one week of growth under continuous illumination, the plant was harvested, disrupted and used for the inoculation of 50 mL of liquid culture inside of a 250 mL Erlenmeyer flask. After one week of growth under continuous illumination, the plant was harvested, disrupted and used for the inoculation of 100 mL of liquid culture inside of a 500 mL Erlenmeyer flask. After one week of growth, the plant material was distributed into a layer of miracloth (pore?) arranged on top of a plastic cylinder, inside of a magenta box filled with fresh medium. The plant was in contact with the medium through the filter, allowing growth under this “hydroponics” system. Plants in closed magenta boxes were grown for 15 days under a short day regime (light:dark 12h:12h). The day of harvesting, plants were immediately snap frozen at the corresponding zeitgeber time (ZT0, ZT2, ZT6). For plants harvested at ZT0, magenta boxes were enclosed in aluminium foil at the beginning of the night period (ZT12) and samples were snap frozen at ZT0 in a dark room illuminated with dim, green light. For plants harvested at ZT2 or ZT6, plants were snap frozen directly in the growth chamber, avoiding to shade the plant until it had been frozen. Frozen samples were kept at -80 ºC until used.

Harvested samples were powdered using a cold mortar and pestle, in presence of liquid nitrogen. 50 to 100 mg of powder were used for metabolite extraction. Approximately 150 mg of powder was used for RNA extraction using the kit RNeasy Plant Mini Kit, ref. 74904 (Qiagen).

RNA was used to build cDNA libraries using the kit QuantSeq 3’ mRNA-Seq Library Prep Kit FWD (Lexogen), which exploits oligo-d(T) primers therefore enriching the cDNA library in cDNA representative of mRNA, but not ribosomal RNA or other types of RNA. Libraries were then sequenced with a depth of 5 million of reads using Illumina technology. After extraction of RNA, we built a cDNA library using oligodT primers, therefore including only polyA transcripts, i.e. mostly messenger RNA (mRNA). Therefore, we did not remove ribosomal cDNA (it was not present) and we did not normalize the reads, as coverage during sequencing is not proportional to the transcript length (in all cases, but to transcript abundance only.

After aligning the reads to the *P. patens* genome and performing differential expression analysis, 3,749 genes were found to be differentially expressed in at least one condition in *cox11* compared to WT. We then performed pathway enrichment analysis on the single lists of differentially expressed genes (DEGs) at the different zeitgeber times and looked for pathways that were either up- or downregulated in one or more conditions.

After alignment to the *P. patens* genome, we could identify 22,527 genes. After filtering for expression threshold, 16,101 remained of which 3,749 were differentially expressed in one or more conditions.

The list of genes encoding for ascorbate peroxidase was retrieved from three different sources. Some of them had alternative names in different publications. The summarized information is included as Supplementary Table 2.4. The list of genes encoding for superoxide dismutases and glutathione reductases were retrieved from Higashi et al., 2013 and L. Xu et al., 2013, respectively. For glutathione reductase, the five genes defined as H_2O_2-responsive by Y. J. Liu et al., 2013 were included.

5.1.11. Untargeted metabolomics

To a 1.5 mL tube containing 50-100 mg of powdered, frozen moss samples, we added 350 uL of extraction solution (chloroform:methanol 10:4.28), vortexed and incubated at -20 ºC for 1 h. Then we added 560 uL of stock of internal standard solution, kept on ice for 5 min with frequent vortexing and centrifuged 2 min at 20,000 g. We then collected the supernatant into clean, 2 mL tubes and performed a second extraction of the remaining organic phase by adding 260 uL of H2O2, incubating on ice for 5 min with frequent vortexing and centrifuging 2 min at 20,000 g. The second supernatant was added to the previous one. The extracts were kept at -80 ºC until processing through two different methods: GC-MS and IC-MS. Since we produced 2 or 3 biological replicas for each genotype for each condition, we combined the replicas from the two independent *cox11* lines into a broader group that contained 4 to 6 replicas per each condition. This gives robustness to the statistical analyses. The abundance of metabolites was normalized to the internal standard and to the dry weight.

We thank Professor Andreas Weber and Philipp Westhoff, from CEPLAS (Düsseldorf), for their contribution in analysing samples through GC-MS and IC-MS.

We then used the data as input values for the publicly available tool MetaboAnalyst (Xia & Wishart, 2011), and used the graphic user interface to generate volcano plots and compare metabolite levels between mutant and WT at the different zeitgeber times. As an output we obtained the logfoldchange values and p values of every single comparison. To elaborate lists of metabolites that were significantly accumulated or depleted at a given condition, we established the significance threshold at $p<0.1$.

Adenylate Energy Charge (AEC) was calculated as ([ATP] + 1/2[ADP])/([ATP] + [ADP] + [AMP]) (Tyutereva et al., 2022)

5.1.12. Quantification of starch

Quantification of starch was done on total extracts of 10 days-old *P. patens* samples following the protocol described in A. M. Smith & Zeeman, 2006.

5.1.13. Pathway enrichment analysis after RNAseq

Pathway enrichment analysis was done on DEGs using the publicly available tool iDEP (Ge et al., 2018). We used all the databases available for *P. patens*, which were based in Gene Orthology (GO), or annotated protein domains coming from different databases (UniProt, InterPro, Pfam, SMART). We compared the found enriched pathways between the three timepoints tested.

We integrated and mapped the transcriptomics and metabolomics data on the publicly available pathways from the KEGG database (Kanehisa et al., 2021)

6. References

Adriaenssens, E., Asselbergh, B., Rivera-Mejías, P., Bervoets, S., Vendredy, L., De Winter, V., Spaas, K., de Rycke, R., van Isterdael, G., Impens, F., Langer, T., & Timmerman, V. (2023). Small heat shock proteins operate as molecular chaperones in the mitochondrial intermembrane space. *Nature Cell Biology 2023 25:3*, *25*(3), 467–480. https://doi.org/10.1038/s41556-022-01074-9

Alboresi, A., Gerotto, C., Giacometti, G. M., Bassi, R., & Morosinotto, T. (2010). *Physcomitrella patens* mutants affected on heat dissipation clarify the evolution of photoprotection mechanisms upon land colonization. *Proceedings of the National Academy of Sciences*, *107*(24), 11128–11133. https://doi.org/10.1073/pnas.1002873107

Alric, J., & Johnson, X. (2017). Alternative electron transport pathways in photosynthesis: a confluence of regulation. *Current Opinion in Plant Biology*, *37*, 78–86. https://doi.org/10.1016/J.PBI.2017.03.014

Aoyama, T., Hiwatashi, Y., Shigyo, M., Kofuji, R., Kubo, M., Ito, M., & Hasebe, M. (2012). AP2-type transcription factors determine stem cell identity in the moss Physcomitrella patens. *Development*, *139*(17), 3120–3129. https://doi.org/10.1242/DEV.076091

Araji, S., Grammer, T. A., Gertzen, R., Anderson, S. D., Mikulic-Petkovsek, M., Veberic, R., Phu, M. L., Solar, A., Leslie, C. A., Dandekar, A. M., & Escobar, M. A. (2014). Novel Roles for the Polyphenol Oxidase Enzyme in Secondary Metabolism and the Regulation of Cell Death in Walnut. *Plant Physiology*, *164*(3), 1191–1203. https://doi.org/10.1104/PP.113.228593

Ashton, N. W., Grimsley, N. H., & Cove, D. J. (1979). Analysis of gametophytic development in the moss, Physcomitrella patens, using auxin and cytokinin resistant mutants. *Planta*, *144*(5), 427–435. https://doi.org/10.1007/BF00380118/METRICS

Atkinson, D. E. (1968). The Energy Charge of the Adenylate Pool as a Regulatory Parameter. Interaction with Feedback Modifiers. *Biochemistry*, *7*(11), 4030–4034. https://doi.org/10.1021/BI00851A033/ASSET/BI00851A033.FP.PNG_V03

Baena-González, E., Rolland, F., Thevelein, J. M., & Sheen, J. (2007). A central integrator of transcription networks in plant stress and energy signalling. *Nature 2007 448:7156*, *448*(7156), 938–942. https://doi.org/10.1038/nature06069

Baena-González, E., & Sheen, J. (2008). Convergent energy and stress signaling. *Trends in Plant Science*, *13*(9), 474–482. https://doi.org/10.1016/J.TPLANTS.2008.06.006

Bailleul, B., Berne, N., Murik, O., Petroutsos, D., Prihoda, J., Tanaka, A., Villanova, V., Bligny, R., Flori, S., Falconet, D., Krieger-Liszkay, A., Santabarbara, S., Rappaport, F., Joliot, P., Tirichine, L., Falkowski, P. G., Cardol, P., Bowler, C., & Finazzi, G. (2015). Energetic coupling between plastids and mitochondria drives CO 2 assimilation in diatoms. *Nature*, *524*(7565), 366–369. https://doi.org/10.1038/nature14599

Banting, G. S., & Glerum, D. M. (2006). Mutational Analysis of the *Saccharomyces cerevisiae* Cytochrome *c* Oxidase Assembly Protein Cox11p. *Eukaryotic Cell*, *5*(3), 568–578. https://doi.org/10.1128/EC.5.3.568-578.2006

Bartoli, C. G., Pastori, G. M., & Foyer, C. H. (2000). Ascorbate biosynthesis in mitochondria is linked to the electron transport chain between complexes III and IV. *Plant Physiology*, *123*(1), 335–343. https://doi.org/10.1104/PP.123.1.335

Beheshti, H., Strotbek, C., Arif, M. A., Klingl, A., Top, O., & Frank, W. (2021). PpGRAS12 acts as a positive regulator of meristem formation in Physcomitrium patens. *Plant Molecular Biology*, *107*(4–5), 293–305. https://doi.org/10.1007/S11103-021-01125-Z

Binder, S. (2010). Branched-Chain Amino Acid Metabolism in Arabidopsis thaliana. *The Arabidopsis Book / American Society of Plant Biologists*, *8*, e0137. https://doi.org/10.1199/TAB.0137

Bonner, C., & Jensen, R. (1987). Prephenate aminotransferase. In *Methods in Enzymology* (Vol. 142, Issue C, pp. 479–487). Academic Press. https://doi.org/10.1016/S0076-6879(87)42059-4

Boursiac, Y., Boudet, J., Postaire, O., Luu, D. T., Tournaire-Roux, C., & Maurel, C. (2008). Stimulus-induced downregulation of root water transport involves reactive oxygen species-activated cell signalling and plasma membrane intrinsic protein internalization. *The Plant Journal*, *56*(2), 207–218. https://doi.org/10.1111/J.1365-313X.2008.03594.X

Bull, P. C., & Cox, D. W. (1994). Wilson disease and Menkes disease: new handles on heavy-metal transport. *Trends in Genetics*, *10*(7), 246–252. https://doi.org/10.1016/0168-9525(94)90172-4

Carr, H. S., George, G. N., & Winge, D. R. (2002). Yeast Cox11, a protein essential for cytochrome c oxidase assembly, is a Cu(I)-binding protein. *Journal of Biological Chemistry*, *277*(34), 31237–31242. https://doi.org/10.1074/jbc.M204854200

Cervantes-Pérez, D., Ortega-García, A., Medina-Andrés, R., Batista-García, R. A., & Lira-Ruan, V. (2020). Exogenous Nitric Oxide Delays Plant Regeneration from Protoplast and Protonema Development in Physcomitrella patens. *Plants*, *9*(10), 1–9. https://doi.org/10.3390/PLANTS9101380

Chamizo-Ampudia, A., Sanz-Luque, E., Llamas, A., Galvan, A., & Fernandez, E. (2017). Nitrate Reductase Regulates Plant Nitric Oxide Homeostasis. *Trends in Plant Science*, *22*(2), 163–174. https://doi.org/10.1016/J.TPLANTS.2016.12.001

Chellamuthu, V. R., Ermilova, E., Lapina, T., Lüddecke, J., Minaeva, E., Herrmann, C., Hartmann, M. D., & Forchhammer, K. (2014). A Widespread Glutamine-Sensing Mechanism in the Plant Kingdom. *Cell*, *159*(5), 1188–1199. https://doi.org/10.1016/J.CELL.2014.10.015

Colin, M., Dorthu, M. P., Duby, F., Remacle, C., Dinant, M., Wolwertz, M. R., Duyckaerts, C., Sluse, F., & Matagne, R. F. (1995). Mutations affecting the mitochondrial genes encoding the cytochrome oxidase subunit I and apocytochrome b of Chlamydomonas reinhardtii. *Molecular and General Genetics MGG 1995 249:2*, *249*(2), 179–184. https://doi.org/10.1007/BF00290364

Cronan, J. E., & Waldrop, G. L. (2002). Multi-subunit acetyl-CoA carboxylases. *Progress in Lipid Research*, *41*(5), 407–435. https://doi.org/10.1016/S0163-7827(02)00007-3

Crozet, P., Margalha, L., Confraria, A., Rodrigues, A., Martinho, C., Adamo, M., Elias, C. A., & Baena-González, E. (2014). Mechanisms of regulation of SNF1/AMPK/SnRK1 protein kinases. *Frontiers in Plant Science*, *5*(MAY), 83320. https://doi.org/10.3389/FPLS.2014.00190/BIBTEX

Dahal, K., Martyn, G. D., Alber, N. A., & Vanlerberghe, G. C. (2017). Coordinated regulation of photosynthetic and respiratory components is necessary to maintain chloroplast energy balance in varied growth conditions. *Journal of Experimental Botany*, *68*(3), 657–671. https://doi.org/10.1093/JXB/ERW469

Dahan, J., Tcherkez, G., Macherel, D., Benamar, A., Belcram, K., Quadrado, M., Arnal, N., & Mireau, H. (2014). Disruption of the *CYTOCHROME C OXIDASE DEFICIENT1* Gene Leads to Cytochrome c Oxidase Depletion and Reorchestrated Respiratory Metabolism in Arabidopsis . *Plant Physiology*, *166*(4), 1788–1802. https://doi.org/10.1104/pp.114.248526

De Col, V., Fuchs, P., Nietzel, T., Elsä Sser, M., Pao Voon, C., Candeo, A., Seeliger, I., Fricker, M. D., Grefen, C., Møller, I. M., Bassi, A., Lim, B. L., Zancani, M., Meyer, A. J., Costa, A., Wagner, S., & Schwarzlä Nder, M. (2017). *ATP sensing in living plant cells reveals tissue gradients and stress dynamics of energy physiology*. https://doi.org/10.7554/eLife.26770.001

De Paepe, R., Chétrit, P., Vitart, V., Ambard-Bretteville, F., Prat, D., & Vedel, F. (1990). Several nuclear genes control both male sterility and mitochondrial protein synthesis in Nicotiana sylvestris protoclones. *MGG Molecular & General Genetics*, *222*(2–3), 206–210. https://doi.org/10.1007/BF00633819/METRICS

Delledonne, M., Xia, Y., Dixon, R. A., & Lamb, C. (1998). Nitric oxide functions as a signal in plant disease resistance. *Nature*, *394*(6693), 585–588. https://doi.org/10.1038/29087

Dennison, C. (2013). Cupredoxins. *Encyclopedia of Biophysics*, 404–406. https://doi.org/10.1007/978-3-642-16712-6_37

Doong, H., Vrailas, A., & Kohn, E. C. (2002). What's in the "BAG"? - A functional domain analysis of the BAG-family proteins. *Cancer Letters*, *188*(1–2), 25–32. https://doi.org/10.1016/S0304-3835(02)00456-1

Dutilleul, C., Lelarge, C., Prioul, J. L., De Paepe, R., Foyer, C. H., & Noctor, G. (2005). Mitochondria-Driven Changes in Leaf NAD Status Exert a Crucial Influence on the Control of Nitrate Assimilation and the Integration of Carbon and Nitrogen Metabolism. *Plant Physiology*, *139*(1), 64–78. https://doi.org/10.1104/PP.105.066399

Edwards, K., Johnstone, C., & Thompson, C. (1991). A simple and rapid method for the preparation of plant genomic DNA for PCR analysis. *Nucleic Acids Research*, *19*(6), 1349. https://doi.org/10.1093/NAR/19.6.1349

El-Azaz, J., Cánovas, F. M., Barcelona, B., Ávila, C., & de la Torre, F. (2022). Deregulation of phenylalanine biosynthesis evolved with the emergence of vascular plants. *Plant Physiology*, *188*(1), 134–150. https://doi.org/10.1093/PLPHYS/KIAB454

Esposti, M. D. (2020). On the evolution of cytochrome oxidases consuming oxygen. *Biochimica et Biophysica Acta (BBA) - Bioenergetics*, *1861*(12), 148304. https://doi.org/10.1016/j.bbabio.2020.148304

Fernandez-Pozo, N., Haas, F. B., Meyberg, R., Ullrich, K. K., Hiss, M., Perroud, P., Hanke, S., Kratz, V., Powell, A. F., Vesty, E. F., Daum, C. G., Zane, M., Lipzen, A., Sreedasyam, A., Grimwood, J., Coates, J. C., Barry, K., Schmutz, J., Mueller, L. A., & Rensing, S. A. (2020). PEATmoss (*Physcomitrella* Expression Atlas Tool): a unified gene expression atlas for the model plant *Physcomitrella patens*. *The Plant Journal*, *102*(1), 165–177. https://doi.org/10.1111/tpj.14607

Fesenko, I., Seredina, A., Arapidi, G., Ptushenko, V., Urban, A., Butenko, I., Kovalchuk, S., Babalyan, K., Knyazev, A., Khazigaleeva, R., Pushkova, E., Anikanov, N., Ivanov, V., & Govorun, V. M. (2016). The Physcomitrella patens chloroplast proteome changes in response to protoplastation. *Frontiers in Plant Science*, *7*(NOVEMBER2016), 222359. https://doi.org/10.3389/FPLS.2016.01661/BIBTEX

Florez-Sarasa, I., Welchen, E., Racca, S., Gonzalez, D. H., Vallarino, J. G., Fernie, A. R., Ribas-Carbo, M., & Del-Saz, N. F. (2021). Cytochrome c Deficiency Differentially Affects the In Vivo Mitochondrial Electron Partitioning and Primary Metabolism Depending on the Photoperiod. *Plants 2021, Vol. 10, Page 444*, *10*(3), 444. https://doi.org/10.3390/PLANTS10030444

Forde, B. G., & Lea, P. J. (2007). Glutamate in plants: metabolism, regulation, and signalling. *Journal of Experimental Botany*, *58*(9), 2339–2358. https://doi.org/10.1093/JXB/ERM121

Forsum, O., Svennerstam, H., Ganeteg, U., & Näsholm, T. (2008). Capacities and constraints of amino acid utilization in Arabidopsis. *New Phytologist*, *179*(4), 1058–1069. https://doi.org/10.1111/J.1469-8137.2008.02546.X

Fu, Y. F., Zhang, Z. W., & Yuan, S. (2018). Putative Connections Between Nitrate Reductase S-Nitrosylation and NO Synthesis Under Pathogen Attacks and Abiotic Stresses. *Frontiers in Plant Science*, *9*. https://doi.org/10.3389/FPLS.2018.00474

Fukasawa, Y., Tsuji, J., Fu, S. C., Tomii, K., Horton, P., & Imai, K. (2015). MitoFates: Improved prediction of mitochondrial targeting sequences and their cleavage sites. *Molecular and Cellular Proteomics*, *14*(4), 1113–1126. https://doi.org/10.1074/mcp.M114.043083

Garmash, E. V. (2023). Suppression of mitochondrial alternative oxidase can result in upregulation of the ROS scavenging network: some possible mechanisms underlying the compensation effect. *Plant Biology*, *25*(1), 43–53. https://doi.org/10.1111/PLB.13477

Garmier, M., Carroll, A. J., Delannoy, E., Vallet, C., Day, D. A., Small, I. D., & Millar, A. H. (2008). Complex I Dysfunction Redirects Cellular and Mitochondrial Metabolism in Arabidopsis. *Plant Physiology*, *148*(3), 1324–1341. https://doi.org/10.1104/PP.108.125880

Gaufichon, L., Reisdorf-Cren, M., Rothstein, S. J., Chardon, F., & Suzuki, A. (2010). Biological functions of asparagine synthetase in plants. *Plant Science*, *179*(3), 141–153. https://doi.org/10.1016/J.PLANTSCI.2010.04.010

Ge, S. X., Son, E. W., & Yao, R. (2018). iDEP: an integrated web application for differential expression and pathway analysis of RNA-Seq data. *BMC Bioinformatics 2018 19:1*, *19*(1), 1–24. https://doi.org/10.1186/S12859-018-2486-6

Gonzali, S., Loreti, E., Solfanelli, C., Novi, G., Alpi, A., & Perata, P. (2006). Identification of sugar-modulated genes and evidence for in vivo sugar sensing in Arabidopsis. *Journal of Plant Research*, *119*(2), 115–123. https://doi.org/10.1007/S10265-005-0251-1

Gutierrez-Beltran, E., & Crespo, J. L. (2022). Compartmentalization, a key mechanism controlling the multitasking role of the SnRK1 complex. *Journal of Experimental Botany*, *73*(20), 7055–7067. https://doi.org/10.1093/JXB/ERAC315

Hampp, R., Goller, M., & Ziegler, H. (1982). Adenylate Levels, Energy Charge, and Phosphorylation Potential during Dark-Light and Light-Dark Transition in Chloroplasts, Mitochondria, and Cytosol of Mesophyll Protoplasts from Avena sativa L. *Plant Physiology*, *69*(2), 448–455. https://doi.org/10.1104/PP.69.2.448

He, F. (2011). BCA (Bicinchoninic Acid) Protein Assay. *BIO-PROTOCOL*, *1*(5). https://doi.org/10.21769/BioProtoc.44

Higashi, Y., Takechi, K., Takano, H., & Takio, S. (2013). Involvement of MicroRNA in Copper Deficiency-Induced Repression of Chloroplastic CuZn-Superoxide Dismutase Genes in the Moss Physcomitrella patens. *Plant and Cell Physiology*, *54*(8), 1345–1355. https://doi.org/10.1093/PCP/PCT084

Ho, L. H. M., Giraud, E., Uggalla, V., Lister, R., Clifton, R., Glen, A., Thirkettle-Watts, D., Van Aken, O., & Whelan, J. (2008). Identification of Regulatory Pathways Controlling Gene Expression of Stress-Responsive Mitochondrial Proteins in Arabidopsis. *Plant Physiology*, *147*(4), 1858–1873. https://doi.org/10.1104/PP.108.121384

Hodges, M. (2002). Enzyme redundancy and the importance of 2-oxoglutarate in plant ammonium assimilation. *Journal of Experimental Botany*, *53*(370), 905–916. https://doi.org/10.1093/JEXBOT/53.370.905

Igamberdiev, A. U. (2020). Citrate valve integrates mitochondria into photosynthetic metabolism. *Mitochondrion*, *52*, 218–230. https://doi.org/10.1016/j.mito.2020.04.003

Igamberdiev, A. U., & Bykova, N. V. (2022). Mitochondria in photosynthetic cells: Coordinating redox control and energy balance. *Plant Physiology*. https://doi.org/10.1093/PLPHYS/KIAC541

Ishikawa, M., Morishita, M., Higuchi, Y., Ichikawa, S., Ishikawa, T., Nishiyama, T., Kabeya, Y., Hiwatashi, Y., Kurata, T., Kubo, M., Shigenobu, S., Tamada, Y., Sato, Y., & Hasebe, M. (2019). Physcomitrella STEMIN transcription factor induces stem cell formation with epigenetic reprogramming. *Nature Plants 2019 5:7*, *5*(7), 681–690. https://doi.org/10.1038/s41477-019-0464-2

Jain, M., Li, Q. B., & Chourey, P. S. (2008). Cloning and expression analyses of sucrose non-fermenting-1-related kinase 1 (SnRK1b) gene during development of sorghum and maize endosperm and its implicated role in sugar-to-starch metabolic transition. *Physiologia Plantarum*, *134*(1), 161–173. https://doi.org/10.1111/J.1399-3054.2008.01106.X

Jurgenson, C. T., Begley, T. P., & Ealick, S. E. (2009). The Structural and Biochemical Foundations of Thiamin Biosynthesis. *Https://Doi.Org/10.1146/Annurev.Biochem.78.072407.102340*, *78*, 569–603. https://doi.org/10.1146/ANNUREV.BIOCHEM.78.072407.102340

Kabbage, M., & Dickman, M. B. (2008). The BAG proteins: A ubiquitous family of chaperone regulators. *Cellular and Molecular Life Sciences*, *65*(9), 1390–1402. https://doi.org/10.1007/S00018-008-7535-2/METRICS

Kanegae, H., Miyoshi, K., Hirose, T., Tsuchimoto, S., Mori, M., Nagato, Y., & Takano, M. (2005). Expressions of rice sucrose non-fermenting-1 related protein kinase 1 genes are differently regulated during the caryopsis development. *Plant Physiology and Biochemistry*, *43*(7), 669–679. https://doi.org/10.1016/J.PLAPHY.2005.06.004

Kanehisa, M., Furumichi, M., Sato, Y., Ishiguro-Watanabe, M., & Tanabe, M. (2021). KEGG: integrating viruses and cellular organisms. *Nucleic Acids Research*, *49*(D1), D545–D551. https://doi.org/10.1093/NAR/GKAA970

Kawade, K., Horiguchi, G., Hirose, Y., Oikawa, A., Hirai, M. Y., Saito, K., Fujita, T., & Tsukaya, H. (2020). Metabolic Control of Gametophore Shoot Formation through Arginine in the Moss Physcomitrium patens. *Cell Reports*, *32*(10), 108127. https://doi.org/10.1016/J.CELREP.2020.108127

Khraiwesh, B., Qudeimat, E., Thimma, M., Chaiboonchoe, A., Jijakli, K., Alzahmi, A., Arnoux, M., & Salehi-Ashtiani, K. (2015). Genome-wide expression analysis offers new insights into the origin and evolution of Physcomitrella patens stress response. *Sci Rep*, *5*, 1–15. https://doi.org/10.1038/srep17434

Krämer, M., & Kunz, H. H. (2021). Indirect Export of Reducing Equivalents From the Chloroplast to Resupply NADP for C3 Photosynthesis—Growing Importance for Stromal NAD(H)? *Frontiers in Plant Science*, *12*, 719003. https://doi.org/10.3389/FPLS.2021.719003/BIBTEX

Kuhn, S., Bussemer, J., Chigri, F., & Vothknecht, U. C. (2009). Calcium depletion and calmodulin inhibition affect the import of nuclear-encoded proteins into plant mitochondria. *The Plant Journal*, *58*(4), 694–705. https://doi.org/10.1111/J.1365-313X.2009.03810.X

Kumar, S., Kaur, A., Chattopadhyay, B., & Bachhawat, A. K. (2015). Defining the cytosolic pathway of glutathione degradation in Arabidopsis thaliana: role of the ChaC/GCG family of γ-glutamyl cyclotransferases as glutathione-degrading enzymes and AtLAP1 as the Cys-Gly peptidase. *The Biochemical Journal*, *468*(1), 73–85. https://doi.org/10.1042/BJ20141154

Kuzmin, E. A., Karpova, O., Elthon, T. E., & Newton, K. (2004). Mitochondrial Respiratory Deficiencies Signal Up-Regulation of Genes for Heat Shock Proteins. *Journal of Biological Chemistry*. https://doi.org/10.1074/jbc.m400640200

Lange, P. R., Geserick, C., Tischendorf, G., & Zrenner, R. (2008). Functions of Chloroplastic Adenylate Kinases in Arabidopsis. *Plant Physiology*, *146*(2), 492. https://doi.org/10.1104/PP.107.114702

Larosa, V., Meneghesso, A., Rocca, N. La, Steinbeck, J., Hippler, M., Szabò, I., & Morosinotto, T. (2018). Mitochondria affect photosynthetic electron transport and photosensitivity in a green alga. *Plant Physiology*, *176*(3), 2305–2314. https://doi.org/10.1104/pp.17.01249

Laurie, S., McKibbin, R. S., & Halford, N. G. (2003). Antisense SNF1-related (SnRK1) protein kinase gene represses transient activity of an α-amylase (α-Amy2) gene promoter in cultured wheat embryos. *Journal of Experimental Botany*, *54*(383), 739–747. https://doi.org/10.1093/JXB/ERG085

Le Gall, H., Philippe, F., Domon, J. M., Gillet, F., Pelloux, J., & Rayon, C. (2015). Cell Wall Metabolism in Response to Abiotic Stress. *Plants*, *4*(1), 112. https://doi.org/10.3390/PLANTS4010112

Le, Q. T. N., Sugi, N., Furukawa, J., Kobayashi, M., Saito, K., Kusano, M., & Shiba, H. (2019). Association analysis of phenotypic and metabolomic changes in Arabidopsis accessions and their F1 hybrids affected by different photoperiod and sucrose supply. *Plant Biotechnology*, *36*(3), 155–165. https://doi.org/10.5511/PLANTBIOTECHNOLOGY.19.0604A

Li, X. P., Müller-Moulé, P., Gilmore, A. M., & Niyogi, K. K. (2002). PsbS-dependent enhancement of feedback de-excitation protects photosystem II from photoinhibition. *Proceedings of the National Academy of Sciences of the United States of America*, *99*(23), 15222–15227. https://doi.org/10.1073/PNAS.232447699/SUPPL_FILE/4476FIG7.PDF

Liao, H. S., Chung, Y. H., & Hsieh, M. H. (2022). Glutamate: A multifunctional amino acid in plants. *Plant Science*, *318*, 111238. https://doi.org/10.1016/J.PLANTSCI.2022.111238

Liguori, N., Novoderezhkin, V., Roy, L. M., Van Grondelle, R., & Croce, R. (2016). Excitation dynamics and structural implication of the stress-related complex LHCSR3 from the green alga Chlamydomonas reinhardtii. *Biochimica et Biophysica Acta*, *1857*(9), 1514–1523. https://doi.org/10.1016/J.BBABIO.2016.04.285

Liu, X., & Bush, D. R. (2006). Expression and transcriptional regulation of amino acid transporters in plants. *Amino Acids*, *30*(2), 113–120. https://doi.org/10.1007/s00726-005-0248-z

Liu, Y. J., Han, X. M., Ren, L. L., Yang, H. L., & Zeng, Q. Y. (2013). Functional Divergence of the Glutathione S-Transferase Supergene Family in Physcomitrella patens Reveals Complex Patterns of Large Gene Family Evolution in Land Plants. *Plant Physiology*, *161*(2), 773–786. https://doi.org/10.1104/PP.112.205815

Lloyd, J. P. B., Lang, D., Zimmer, A. D., Causier, B., Reski, R., & Davies, B. (2018). The loss of SMG1 causes defects in quality control pathways in Physcomitrella patens. *Nucleic Acids Research*, *46*(11), 5822. https://doi.org/10.1093/NAR/GKY225

Luo, D., Xu, H., Liu, Z., Guo, J., Li, H., Chen, L., Fang, C., Zhang, Q., Bai, M., Yao, N., Wu, H., Wu, H., Ji, C., Zheng, H., Chen, Y., Ye, S., Li, X., Zhao, X., Li, R., & Liu, Y. G. (2013). A detrimental mitochondrial-nuclear interaction causes cytoplasmic male sterility in rice. *Nature Genetics 2013 45:5*, *45*(5), 573–577. https://doi.org/10.1038/ng.2570

Madeira, F., Pearce, M., Tivey, A. R. N., Basutkar, P., Lee, J., Edbali, O., Madhusoodanan, N., Kolesnikov, A., & Lopez, R. (2022). Search and sequence analysis tools services from EMBL-EBI in 2022. *Nucleic Acids Research*, *50*(W1), W276–W279. https://doi.org/10.1093/nar/gkac240

Maeda, H., & Dudareva, N. (2012). The Shikimate Pathway and Aromatic Amino Acid Biosynthesis in Plants. *Https://Doi.Org/10.1146/Annurev-Arplant-042811-105439*, *63*, 73–105. https://doi.org/10.1146/ANNUREV-ARPLANT-042811-105439

Maldonado, M., Guo, F., & Letts, J. A. (2021). Atomic structures of respiratory complex III2, complex IV, and supercomplex III2-IV from vascular plants. *ELife*, *10*. https://doi.org/10.7554/eLife.62047

Maruta, T., Sawa, Y., Shigeoka, S., & Ishikawa, T. (2016). Diversity and Evolution of Ascorbate Peroxidase Functions in Chloroplasts: More Than Just a Classical Antioxidant Enzyme? *Plant and Cell Physiology*, *57*(7), 1377–1386. https://doi.org/10.1093/PCP/PCV203

Mata, C. G., & Lamattina, L. (2001). Nitric oxide induces stomatal closure and enhances the adaptive plant responses against drought stress. *Plant Physiology*, *126*(3), 1196–1204. https://doi.org/10.1104/PP.126.3.1196

McKibbin, R. S., Muttucumaru, N., Paul, M. J., Powers, S. J., Burrell, M. M., Coates, S., Purcell, P. C., Tiessen, A., Geigenberger, P., & Halford, N. G. (2006). Production of high-starch, low-glucose potatoes through over-expression of the metabolic regulator SnRK1. *Plant Biotechnology Journal*, *4*(4), 409–418. https://doi.org/10.1111/J.1467-7652.2006.00190.X

Medina-Andrés, R., & Lira-Ruan, V. (2012). In silico characterization of a nitrate reductase gene family and analysis of the predicted proteins from the moss Physcomitrella patens. *Http://Www.Tandfonline.Com/Action/AuthorSubmission?JournalCode=kcib20&page=instructions* , *5*(1), 19–25. https://doi.org/10.4161/CIB.18534

Medina-Andrés, R., Solano-Peralta, A., Saucedo-Vázquez, J. P., Napsucialy-Mendivil, S., Pimentel-Cabrera, J. A., Sosa-Torres, M. E., Dubrovsky, J. G., & Lira-Ruan, V. (2015). The Nitric Oxide Production in the Moss Physcomitrella patens Is Mediated by Nitrate Reductase. *PLoS ONE*, *10*(3). https://doi.org/10.1371/JOURNAL.PONE.0119400

Mehterov, N., Balazadeh, S., Hille, J., Toneva, V., Mueller-Roeber, B., & Gechev, T. (2012). Oxidative stress provokes distinct transcriptional responses in the stress-tolerant atr7 and stress-sensitive loh2 Arabidopsis thaliana mutants as revealed by multi-parallel quantitative real-time PCR analysis of ROS marker and antioxidant genes. *Plant Physiology and Biochemistry : PPB*, *59*, 20–29. https://doi.org/10.1016/J.PLAPHY.2012.05.024

Mellon, M., Storti, M., Vera-Vives, A. M., Kramer, D. M., Alboresi, A., & Morosinotto, T. (2021). Inactivation of mitochondrial Complex I stimulates chloroplast ATPase in Physcomitrium patens . *Plant Physiology*. https://doi.org/10.1093/plphys/kiab276

Meyer, E. H., Welchen, E., & Carrie, C. (2019). Assembly of the Complexes of the Oxidative Phosphorylation System in Land Plant Mitochondria. *Annual Review of Plant Biology*, *70*(1), 23–50. https://doi.org/10.1146/annurev-arplant-050718-100412

Millar, A. H., Whelan, J., Soole, K. L., & Day, D. A. (2011). Organization and Regulation of Mitochondrial Respiration in Plants. *Annual Review of Plant Biology*, *62*(1), 79–104. https://doi.org/10.1146/annurev-arplant-042110-103857

Moellering, E. R., & Benning, C. (2010). Phosphate Regulation of Lipid Biosynthesis in Arabidopsis Is Independent of the Mitochondrial Outer Membrane DGS1 Complex. *Plant Physiology*, *152*(4), 1951–1959. https://doi.org/10.1104/PP.110.153262

Møller, I. M., & Sweetlove, L. J. (2010). ROS signalling – specificity is required. *Trends in Plant Science*, *15*(7), 370–374. https://doi.org/10.1016/J.TPLANTS.2010.04.008

Moreno-García, B., López-Calcagno, P. E., Raines, C. A., & Sweetlove, L. J. (2022). Suppression of metabolite shuttles for export of chloroplast and mitochondrial ATP and NADPH increases the cytosolic NADH:NAD+ ratio in tobacco leaves in the dark. *Journal of Plant Physiology*, *268*, 153578. https://doi.org/10.1016/J.JPLPH.2021.153578

Nikolau, B. J., Ohlrogge, J. B., & Wurtele, E. S. (2003). Plant biotin-containing carboxylases. *Archives of Biochemistry and Biophysics*, *414*(2), 211–222. https://doi.org/10.1016/S0003-9861(03)00156-5

Nisa, M. U., Huang, Y., Benhamed, M., & Raynaud, C. (2019). The plant DNA damage response: Signaling pathways leading to growth inhibition and putative role in response to stress conditions. *Frontiers in Plant Science*, *10*, 463467. https://doi.org/10.3389/FPLS.2019.00653/BIBTEX

Noctor, G., De Paepe, R., & Foyer, C. H. (2007). Mitochondrial redox biology and homeostasis in plants. *Trends in Plant Science*, *12*(3), 125–134. https://doi.org/10.1016/j.tplants.2007.01.005

Ohkama-Ohtsu, N., Oikawa, A., Zhao, P., Xiang, C., Saito, K., & Oliver, D. J. (2008). A γ-Glutamyl Transpeptidase-Independent Pathway of Glutathione Catabolism to Glutamate via 5-Oxoproline in Arabidopsis. *Plant Physiology*, *148*(3), 1603–1613. https://doi.org/10.1104/PP.108.125716

Ozyigit, I. I., Filiz, E., Vatansever, R., Kurtoglu, K. Y., Koc, I., Öztürk, M. X., & Anjum, N. A. (2016). Identification and comparative analysis of H2O2-scavenging enzymes (ascorbate peroxidase and glutathione peroxidase) in selected plants employing bioinformatics approaches. *Frontiers in Plant Science*, *7*(MAR2016), 178931. https://doi.org/10.3389/FPLS.2016.00301/BIBTEX

Paulose, B., Chhikara, S., Coomey, J., Jung, H. II, Vatamaniuk, O., & Dhankher, O. P. (2013). A γ-Glutamyl Cyclotransferase Protects Arabidopsis Plants from Heavy Metal Toxicity by Recycling Glutamate to Maintain Glutathione Homeostasis. *The Plant Cell*, *25*(11), 4580–4595. https://doi.org/10.1105/TPC.113.111815

Pfister, B., & Zeeman, S. C. (2016). Formation of starch in plant cells. *Cellular and Molecular Life Sciences 2016 73:14*, *73*(14), 2781–2807. https://doi.org/10.1007/S00018-016-2250-X

Porra, R. J., Thompson, W. A., & Kriedemann, P. E. (1989). Determination of accurate extinction coefficients and simultaneous equations for assaying chlorophylls a and b extracted with four different solvents: verification of the concentration of chlorophyll standards by atomic absorption spectroscopy. *BBA - Bioenergetics*, *975*(3), 384–394. https://doi.org/10.1016/S0005-2728(89)80347-0

Priault, P., Fresneau, C., Noctor, G., De Paepe, R., Cornic, G., & Streb, P. (2006). The mitochondrial CMSII mutation of Nicotiana sylvestris impairs adjustment of photosynthetic carbon assimilation to higher growth irradiance. *Journal of Experimental Botany*, *57*(9), 2075–2085. https://doi.org/10.1093/jxb/erj161

Pu, X., Yang, L., Liu, L., Dong, X., Chen, S., Chen, Z., Liu, G., Jia, Y., Yuan, W., & Liu, L. (2020). Genome-Wide Analysis of the MYB Transcription Factor Superfamily in Physcomitrella patens. *Mdpi.ComX Pu, L Yang, L Liu, X Dong, S Chen, Z Chen, G Liu, Y Jia, W Yuan, L LiuInternational Journal of Molecular Sciences, 2020•mdpi.Com*, *21*(3). https://doi.org/10.3390/ijms21030975

Purcell, P. C., Smith, A. M., & Halford, N. G. (1998). Antisense expression of a sucrose non-fermenting-1-related protein kinase sequence in potato results in decreased expression of sucrose synthase in tubers and loss of sucrose-inducibility of sucrose synthase transcripts in leaves. *The Plant Journal*, *14*(2), 195–202. https://doi.org/10.1046/J.1365-313X.1998.00108.X

Qureshi, M. K., Radeva, V., Genkov, T., Minkov, I., Hille, J., & Gechev, T. S. (2011). Isolation and characterization of Arabidopsis mutants with enhanced tolerance to oxidative stress. *Acta Physiologiae Plantarum*, *33*(2), 375–382. https://doi.org/10.1007/S11738-010-0556-0/TABLES/3

Racca, S., Welchen, E., Gras, D. E., Tarkowská, D., Turečková, V., Maurino, V. G., & Gonzalez, D. H. (2018). Interplay between cytochrome c and gibberellins during Arabidopsis vegetative development. *The Plant Journal*, *94*(1), 105–121. https://doi.org/10.1111/TPJ.13845

Radin, I., Kost, L., Gey, U., Steinebrunner, I., & Rödel, G. (2021). The mitochondrial copper chaperone COX11 has an additional role in cellular redox homeostasis. *PLOS ONE*, *16*(12), e0261465. https://doi.org/10.1371/JOURNAL.PONE.0261465

Radin, I., Mansilla, N., Rödel, G., & Steinebrunner, I. (2015). The Arabidopsis COX11 Homolog is Essential for Cytochrome c Oxidase Activity. *Frontiers in Plant Science*, *6*(DEC), 1–17. https://doi.org/10.3389/fpls.2015.01091

Rhoads, D. M., Umbach, A. L., Sweet, C. R., Lennon, A. M., Rauch, G. S., & Siedow, J. N. (1998). Regulation of the Cyanide-resistant Alternative Oxidase of Plant Mitochondria. *Journal of Biological Chemistry*, *273*(46), 30750–30756. https://doi.org/10.1074/jbc.273.46.30750

Riewe, D., Jeon, H. J., Lisec, J., Heuermann, M. C., Schmeichel, J., Seyfarth, M., Meyer, R. C., Willmitzer, L., & Altmann, T. (2016). A naturally occurring promoter polymorphism of the Arabidopsis FUM2 gene causes expression variation, and is associated with metabolic and growth traits. *The Plant Journal : For Cell and Molecular Biology*, *88*(5), 826–838. https://doi.org/10.1111/TPJ.13303

Ronquist, F., Teslenko, M., Van Der Mark, P., Ayres, D. L., Darling, A., Höhna, S., Larget, B., Liu, L., Suchard, M. A., & Huelsenbeck, J. P. (2012). Mrbayes 3.2: Efficient bayesian phylogenetic inference and model choice across a large model space. *Systematic Biology*, *61*(3), 539–542. https://doi.org/10.1093/sysbio/sys029

Ruibal, C., Castro, A., Carballo, V., Szabados, L., & Vidal, S. (2013). Recovery from heat, salt and osmotic stress in Physcomitrella patens requires a functional small heat shock protein PpHsp16.4. *BMC Plant Biology*, *13*(1), 1–18. https://doi.org/10.1186/1471-2229-13-174/FIGURES/6

Sabar, M., Balk, J., & Leaver, C. J. (2005). Histochemical staining and quantification of plant mitochondrial respiratory chain complexes using blue-native polyacrylamide gel electrophoresis. *Plant Journal*, *44*(5), 893–901. https://doi.org/10.1111/j.1365-313X.2005.02577.x

Sakakibara, K., Nishiyama, T., Sumikawa, N., Kofuji, R., Murata, T., & Hasebe, M. (2003). Involvement of auxin and a homeodomain-leucine zipper I gene in rhizoid development of the moss Physcomitrella patens. *Development*, *130*(20), 4835–4846. https://doi.org/10.1242/DEV.00644

Schertl, P., & Braun, H.-P. (2014). Respiratory electron transfer pathways in plant mitochondria. *Frontiers in Plant Science*, *5*(APR), 1–11. https://doi.org/10.3389/fpls.2014.00163

Schmitt, S., & Gnaiger, E. (2022). O2k-Manual: Sample Holder. *Mitochondrial Physiology Network*, *27*(01), 1–4. https://wiki.oroboros.at/index.php/MiPNet27.07_Sample_Holder

Shameer, S., Ratcliffe, R. G., & Sweetlove, L. J. (2019). Leaf energy balance requires mitochondrial respiration and export of chloroplast NADPH in the light. *Plant Physiology*, *180*(4), 1947–1961. https://doi.org/10.1104/pp.19.00624

Singh, B. K. (1998). The Enzymes of Glutamine. Glutamate, Asparagine, and Aspartate Metabolism. *Plant Amino Acids*, 63–124. https://doi.org/10.1201/9781482270068-3

Slocum, R. D. (2005). Genes, enzymes and regulation of arginine biosynthesis in plants. *Plant Physiology and Biochemistry*, *43*(8), 729–745. https://doi.org/10.1016/J.PLAPHY.2005.06.007

Smirnoff, N. (2018). Ascorbic acid metabolism and functions: A comparison of plants and mammals. *Free Radical Biology and Medicine*, *122*, 116–129. https://doi.org/10.1016/J.FREERADBIOMED.2018.03.033

Smith, A. M., & Zeeman, S. C. (2006). Quantification of starch in plant tissues. *Nature Protocols*, *1*(3), 1342–1345. https://doi.org/10.1038/nprot.2006.232

Smith, S. R., Abbriano, R. M., & Hildebrand, M. (2012). Comparative analysis of diatom genomes reveals substantial differences in the organization of carbon partitioning pathways. *Algal Research*, *1*(1), 2–16. https://doi.org/10.1016/J.ALGAL.2012.04.003

Spetea, C., Pfeil, B. E., & Schoefs, B. (2012). Phylogenetic analysis of the thylakoid ATP/ADP carrier reveals new insights into its function restricted to green plants. *Frontiers in Plant Science*, *2*(JAN). https://doi.org/10.3389/FPLS.2011.00110/ABSTRACT

Stitt, M., & Zeeman, S. C. (2012). Starch turnover: pathways, regulation and role in growth. *Current Opinion in Plant Biology*, *15*(3), 282–292. https://doi.org/10.1016/J.PBI.2012.03.016

Storti, M., Alboresi, A., Gerotto, C., Aro, E. M., Finazzi, G., & Morosinotto, T. (2019). Role of cyclic and pseudo-cyclic electron transport in response to dynamic light changes in Physcomitrella patens. *Plant, Cell & Environment*, *42*(5), 1590–1602. https://doi.org/10.1111/PCE.13493

Storti, M., Segalla, A., Mellon, M., Alboresi, A., & Morosinotto, T. (2020). Regulation of electron transport is essential for photosystem I stability and plant growth. *New Phytologist*, *228*(4), 1316–1326. https://doi.org/10.1111/NPH.16643

Sugden, C., Donaghy, P. G., Halford, N. G., & Hardie, D. G. (1999). Two SNF1-Related Protein Kinases from Spinach Leaf Phosphorylate and Inactivate 3-Hydroxy-3-Methylglutaryl-Coenzyme A Reductase, Nitrate Reductase, and Sucrose Phosphate Synthase in Vitro. *Plant Physiology*, *120*(1), 257–274. https://doi.org/10.1104/PP.120.1.257

Sweetlove, L. J., Beard, K. F. M., Nunes-Nesi, A., Fernie, A. R., & Ratcliffe, R. G. (2010). Not just a circle: Flux modes in the plant TCA cycle. *Trends in Plant Science*, *15*(8), 462–470. https://doi.org/10.1016/j.tplants.2010.05.006

Terasawa, K., Odahara, M., Kabeya, Y., Kikugawa, T., Sekine, Y., Fujiwara, M., & Sato, N. (2007). The Mitochondrial Genome of the Moss Physcomitrella patens Sheds New Light on Mitochondrial Evolution in Land Plants. *Molecular Biology and Evolution*, *24*(3), 699–709. https://doi.org/10.1093/MOLBEV/MSL198

Tiessen, A., Prescha, K., Branscheid, A., Palacios, N., McKibbin, R., Halford, N. G., & Geigenberger, P. (2003). Evidence that SNF1-related kinase and hexokinase are involved in separate sugar-signalling pathways modulating post-translational redox activation of ADP-glucose pyrophosphorylase in potato tubers. *The Plant Journal*, *35*(4), 490–500. https://doi.org/10.1046/J.1365-313X.2003.01823.X

Timón-Gómez, A., Nývltová, E., Abriata, L. A., Vila, A. J., Hosler, J., & Barrientos, A. (2018). Mitochondrial cytochrome c oxidase biogenesis: Recent developments. *Seminars in Cell & Developmental Biology*, *76*, 163–178. https://doi.org/10.1016/j.semcdb.2017.08.055

Tong, L. (2012). Structure and function of biotin-dependent carboxylases. *Cellular and Molecular Life Sciences 2012 70:5*, *70*(5), 863–891. https://doi.org/10.1007/S00018-012-1096-0

Truffault, V., Fry, S. C., Stevens, R. G., & Gautier, H. (2017). Ascorbate degradation in tomato leads to accumulation of oxalate, threonate and oxalyl threonate. *The Plant Journal*, *89*(5), 996–1008. https://doi.org/10.1111/TPJ.13439

Tyutereva, E. v., Murtuzova, A. v., & Voitsekhovskaja, O. v. (2022). Autophagy and the Energy Status of Plant Cells. *Russian Journal of Plant Physiology 2022 69:2*, *69*(2), 1–15. https://doi.org/10.1134/S1021443722020212

Vaahtera, L., Brosché, M., Wrzaczek, M., & Kangasjärvi, J. (2014). Specificity in ROS Signaling and Transcript Signatures. *Antioxidants & Redox Signaling*, *21*(9), 1422. https://doi.org/10.1089/ARS.2013.5662

Vandeleur, R. K., Sullivan, W., Athman, A., Jordans, C., Gilliham, M., Kaiser, B. N., & Tyerman, S. D. (2014). Rapid shoot-to-root signalling regulates root hydraulic conductance via aquaporins. *Plant, Cell and Environment*, *37*(2), 520–538. https://doi.org/10.1111/PCE.12175/SUPPINFO

Veniamin, S., Sawatzky, L. G., Banting, G. S., & Glerum, D. M. (2011). Characterization of the peroxide sensitivity of COX-deficient yeast strains reveals unexpected relationships between COX

assembly proteins. *Free Radical Biology & Medicine*, *51*(8), 1589–1600. https://doi.org/10.1016/J.FREERADBIOMED.2011.06.024

Vidal, G., Ribas-Carbo, M., Garmier, M., Dubertret, G., Rasmusson, A. G., Mathieu, C., Foyer, C. H., & De Paepe, R. (2007). Lack of Respiratory Chain Complex I Impairs Alternative Oxidase Engagement and Modulates Redox Signaling during Elicitor-Induced Cell Death in Tobacco. *The Plant Cell*, *19*(2), 640–655. https://doi.org/10.1105/tpc.106.044461

Voon, C. P., Law, Y.-S., Guan, X., Lim, S.-L., Xu, Z., Chu, W.-T., Zhang, R., Sun, F., Labs, M., Leister, D., Pribil, M., Hronková, M., Kubásek, J., Cui, Y., Jiang, L., Tsuyama, M., Gardeström, P., Tikkanen, M., & Lim, B. L. (2021). Modulating the activities of chloroplasts and mitochondria promotes adenosine triphosphate production and plant growth. *Quantitative Plant Biology*, *2*. https://doi.org/10.1017/qpb.2021.7

Waterhouse, A. M., Procter, J. B., Martin, D. M. A., Clamp, M., & Barton, G. J. (2009). Jalview Version 2—a multiple sequence alignment editor and analysis workbench. *Bioinformatics*, *25*(9), 1189–1191. https://doi.org/10.1093/bioinformatics/btp033

Waters, E. R., & Vierling, E. (2020). Plant small heat shock proteins – evolutionary and functional diversity. *New Phytologist*, *227*(1), 24–37. https://doi.org/10.1111/nph.16536

Went, N., Di Marcello, M., & Gnaiger, E. (2021). Oxygen dependence of photosynthesis and light-enhanced dark respiration studied by High-Resolution PhotoRespirometry. *MitoFit Preprints*, *05*.

Whelan, J., & Glaser, E. (2011). Protein Import into Plant Mitochondria. *Plant Mitochondria*, 261–287. https://doi.org/10.1007/978-0-387-89781-3_11

Winter, G., Todd, C. D., Trovato, M., Forlani, G., & Funck, D. (2015). Physiological implications of arginine metabolism in plants. *Frontiers in Plant Science*, *6*(JULY). https://doi.org/10.3389/FPLS.2015.00534

Wu, B., & Wang, B. (2019). Comparative analysis of ascorbate peroxidases (APXs) from selected plants with a special focus on Oryza sativa employing public databases. *PLoS ONE*, *14*(12). https://doi.org/10.1371/JOURNAL.PONE.0226543

Wurzinger, B., Nukarinen, E., Nägele, T., Weckwerth, W., & Teige, M. (2018). The SnRK1 Kinase as Central Mediator of Energy Signaling between Different Organelles. *Plant Physiology*, *176*(2), 1085. https://doi.org/10.1104/PP.17.01404

Xia, J., & Wishart, D. S. (2011). Web-based inference of biological patterns, functions and pathways from metabolomic data using MetaboAnalyst. *Nature Protocols*, *6*(6), 743–760. https://doi.org/10.1038/nprot.2011.319

Xiao, L., Jiang, S., Huang, P., Chen, F., Wang, X., Cheng, Z., Miao, Y., Liu, L., Searle, I., Liu, C., Wu, X. X., Fu, Y. F., Chen, Q., & Zhang, X. M. (2020). Two Nucleoporin98 homologous genes jointly participate in the regulation of starch degradation to repress senescence in Arabidopsis. *BMC Plant Biology*, *20*(1), 292. https://doi.org/10.1186/S12870-020-02494-1/FIGURES/7

Xu, L., Carrie, C., Law, S. R., Murcha, M. W., & Whelan, J. (2013). Acquisition, Conservation, and Loss of Dual-Targeted Proteins in Land Plants. *Plant Physiology*, *161*(2), 644–662. https://doi.org/10.1104/PP.112.210997

Xu, Z. S., Chen, M., Li, L. C., & Ma, Y. Z. (2011). Functions and Application of the AP2/ERF Transcription Factor Family in Crop ImprovementF. *Journal of Integrative Plant Biology*, *53*(7), 570–585. https://doi.org/10.1111/J.1744-7909.2011.01062.X

Yang, G., Wei, Q., Huang, H., & Xia, J. (2020). Amino Acid Transporters in Plant Cells: A Brief Review. *Plants*, *9*(8), 967. https://doi.org/10.3390/plants9080967

Yoneyama, T., & Suzuki, A. (2020). Light-Independent Nitrogen Assimilation in Plant Leaves: Nitrate Incorporation into Glutamine, Glutamate, Aspartate, and Asparagine Traced by 15N. *Plants*, *9*(10), 1–12. https://doi.org/10.3390/PLANTS9101303

Yoneyama, T., Yamada, H., … M. Y.-P. and cell, & 1987, undefined. (1987). Nitrate Reduction and Partitioning of Nitrogen in Komatsuna (Brassica campestris L. var. rapa) Plants: Compartmental

Analysis in Combination with 15N Tracer. *Academic.Oup.ComT Yoneyama, H Yamada, M Yamagata, H KouchiPlant and Cell Physiology, 1987•academic.Oup.Com*, *28*(4), 679–696. https://academic.oup.com/pcp/article-abstract/28/4/679/1805445

Yoshida, K., Terashima, I., & Noguchi, K. (2006). Distinct Roles of the Cytochrome Pathway and Alternative Oxidase in Leaf Photosynthesis. *Plant and Cell Physiology*, *47*(1), 22–31. https://doi.org/10.1093/pcp/pci219

Zhang, J., Fu, X. X., Li, R. Q., Zhao, X., Liu, Y., Li, M. H., Zwaenepoel, A., Ma, H., Goffinet, B., Guan, Y. L., Xue, J. Y., Liao, Y. Y., Wang, Q. F., Wang, Q. H., Wang, J. Y., Zhang, G. Q., Wang, Z. W., Jia, Y., Wang, M. Z., … Chen, Z. D. (2020). The hornwort genome and early land plant evolution. *Nature Plants 2020 6:2*, *6*(2), 107–118. https://doi.org/10.1038/s41477-019-0588-4

Zhang, P., Foerster, H., Tissier, C. P., Mueller, L., Paley, S., Karp, P. D., & Rhee, S. Y. (2005). MetaCyc and AraCyc. Metabolic pathway databases for plant research. *Plant Physiology*, *138*(1), 27–37. https://doi.org/10.1104/PP.105.060376

Zhang, Y., Shewry, P. R., Jones, H., Barcelo, P., Lazzeri, P. A., & Halford, N. G. (2001). Expression of antisense SnRK1 protein kinase sequence causes abnormal pollen development and male sterility in transgenic barley. *The Plant Journal*, *28*(4), 431–441. https://doi.org/10.1046/J.1365-313X.2001.01167.X

Zhang, Y., Swart, C., Alseekh, S., Scossa, F., Jiang, L., Obata, T., Graf, A., & Fernie, A. R. (2018). The extra-pathway interactome of the TCA cycle: Expected and unexpected metabolic interactions. *Plant Physiology*, *177*(3), 966–979. https://doi.org/10.1104/pp.17.01687

Zhao, Y., Yu, H., Zhou, J. M., Smith, S. M., & Li, J. (2020). Malate circulation: Linking chloroplast metabolism to mitochondrial ROS. *Trends in Plant Science*, *25*(5), 446–454. https://doi.org/10.1016/j.tplants.2020.01.010

7. Supplementary material

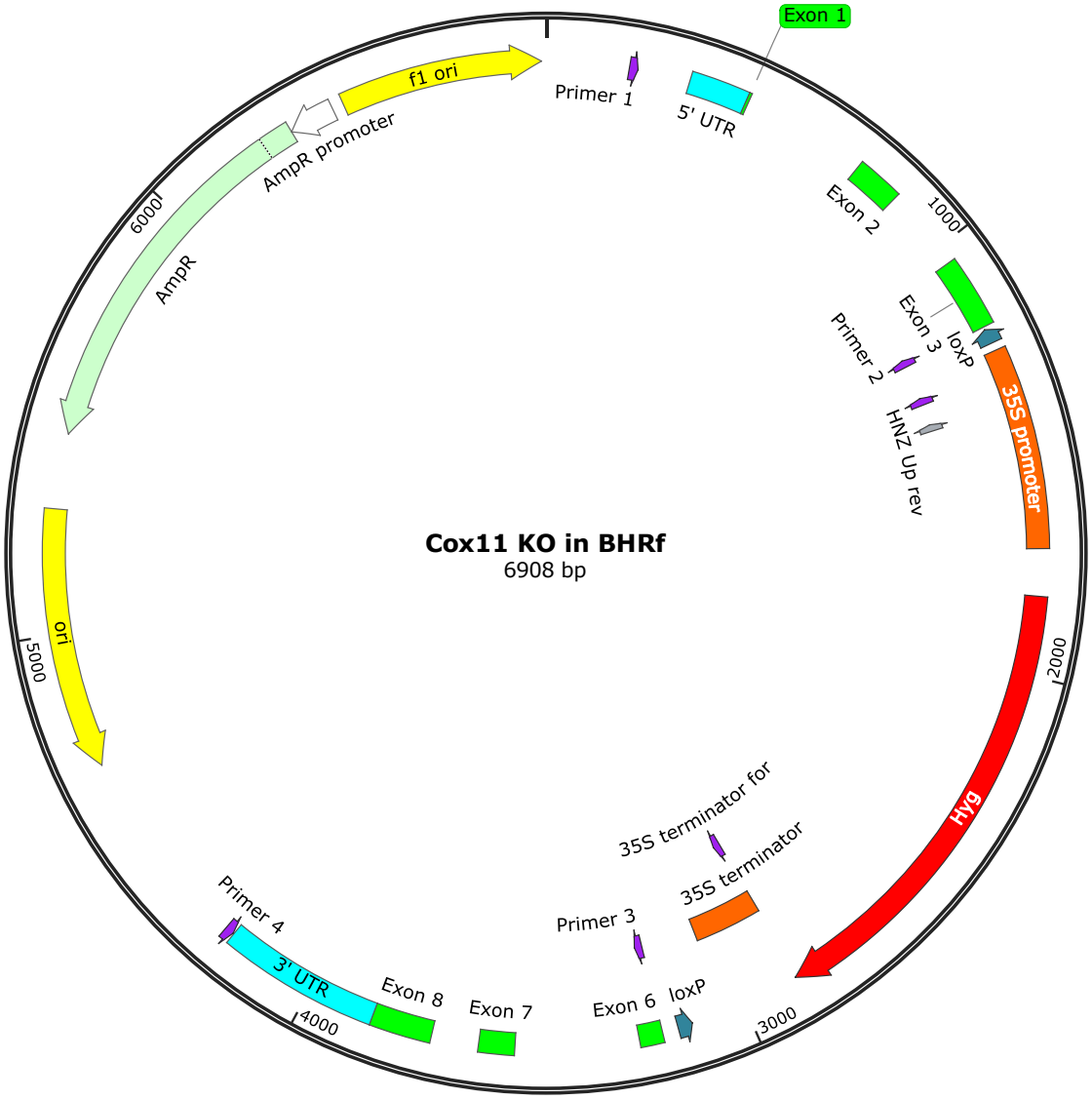

Supplementary Figure 2.1 | **Map of the construct used for knocking out PpCox11**.

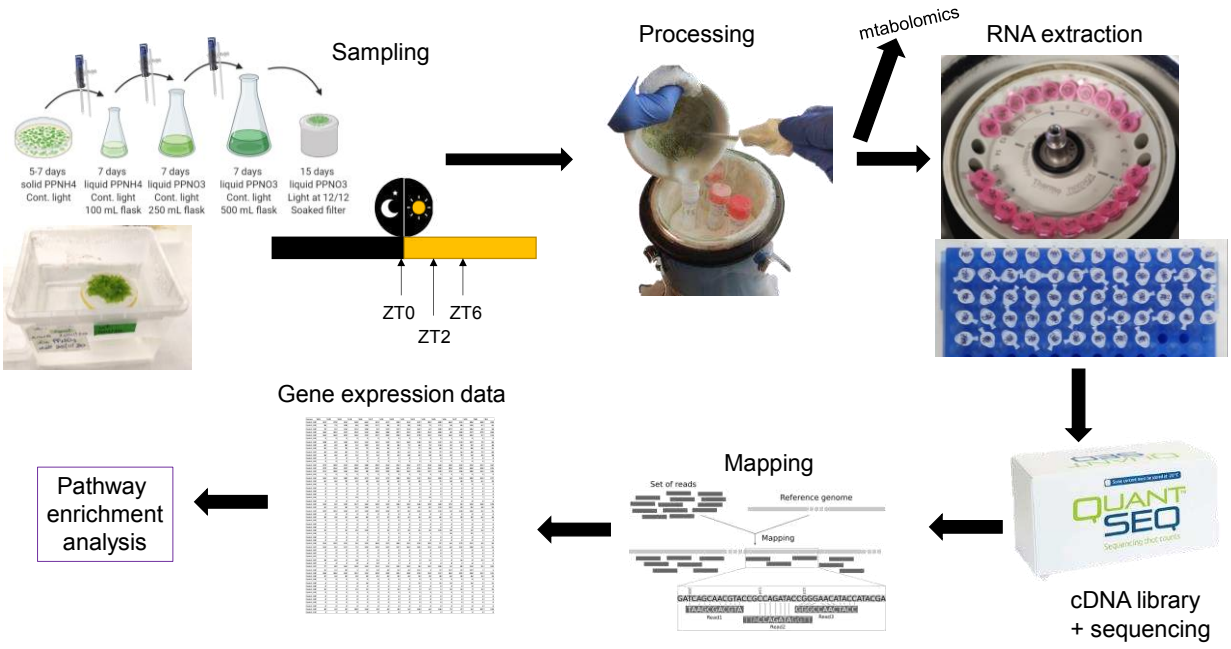

Supplementary Figure 2.2 | **Workflow for transcriptomics and metabolomics**.

```
Yeast       MIRICPIVRS----------------------------------------------KVPLLGTFL
Cattle      MGGLWRPAWR----------------------------------------------RVVFCGWS-
P. patens   MMNRWRCVKSLSEALHRHGLAAAASNSFTADLTLAKPLPNIYAKEASTSHSEKLVLPSVAV

Yeast       RSDS------WLAPHALALRR---AICKNVALRSYSVNSEQPKHTFDISKL-TRNEIQQLR
Cattle      ----------WSHLGRPTRAAERAEPCLRPG-RSGPAGTEQGLRRLGTWRRPSPAEQPARR
P. patens   RTDVHSLCFLWSTLSRLSLNREYSTLLANHRFCSIPSRGGAEIYGFRTRGFSSQAEIAAKA

Yeast       ELKRAR-------ERKFKDRTVAFYFSSVAVLFLGLAYAAVPLYRAICARTGFGGIPITDR
Cattle      PKSTNPYTRSQEEDWRRRNKTVLTYMAAAAVGMLGASYAAVPLYRLYCQTTGLGGSAVAGH
P. patens   GARRAKLTWESQTAGKKKSEAMLMYLVAMVTAMVGITYAAVPLYRKFCQATGYGGTV---Q

Yeast       RKFTDDKLIP------VDTEKRIRISFTSEVSQILPWKFVPQQREVYVLPGETALAFYKAK
Cattle      ASDQIENMVP------VK-DRIIKITFNADVHASLQWNFRPQQTEIYVVPGETALAFYKAK
P. patens   RKETVEEKIARHKGEEAESSRELVVQFNADVADGMPWKFTPCQREIRVRPGQSTLAFYTAE

Yeast       NYSDKDIIGMATYSIAPGEAAQYFNKIQCFCFEEQKLAAGEEIDMPVFFFIDPDFASDPAM
Cattle      NPTDKPVIGISTYNVVPFEAGQYFNKIQCFCFEEQRLNPQEEVDMPVFFYIDPEFAEDPRM
P. patens   NTSSVPITGVSTYNVTPMKAGLYFNKIQCFCFEEQRLLPGEKIDMPVFFFIDPEFATDPKM

Yeast       RNIDDIILHYTFFRAHYGDGTAVSDSKKEPEMNADEKAASLANAAILSPEVIDTRKDNSN
Cattle      VNVDLITLSYTFFEAKEGHTLPV------PGYNSNQQLSPASNL----------------
P. patens   KGINSLILSYTFFKVEEA----------PQKETVASPQPA--------------------
```

Supplementary Figure 2.3 | **Multiple sequence alignment of protein Cox11 of *P. patens* and their homologs in yeast (*Saccharomyces cerevisiae*) and cattle (*Bos taurus*)**. The multiple sequence alignment was performed using the tool *MUSCLE*. Bold letters with cyan background indicate the cleavage

sites predicted by the tool *MitoFates*. Letters with yellow background are the conserved Cys residues involved in copper binding as identified by Carr et al., 2002.

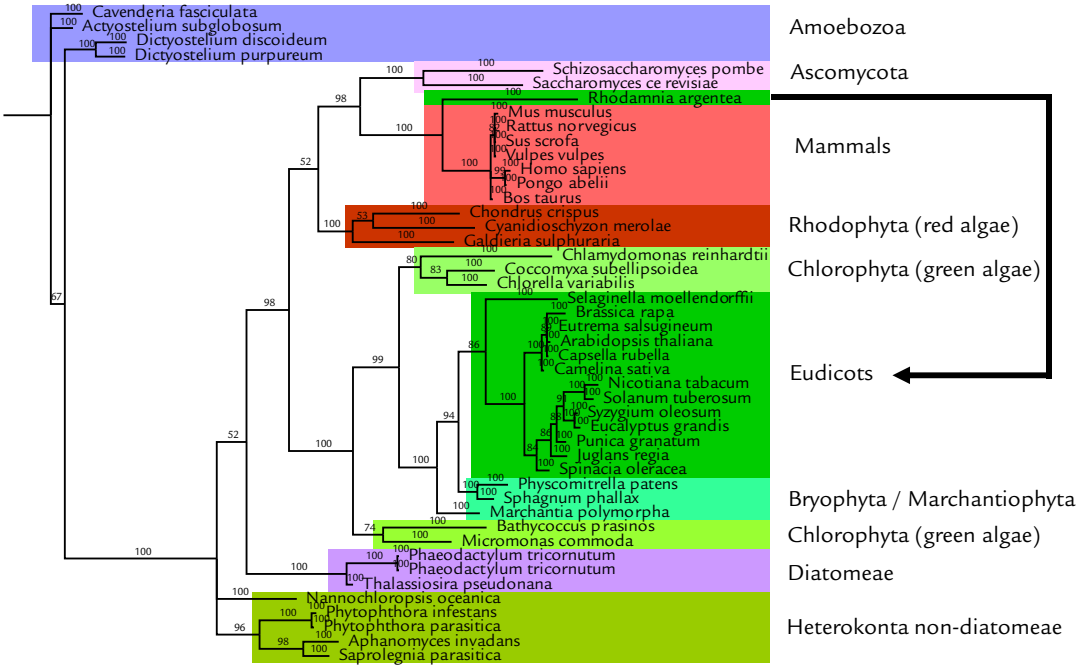

Supplementary Figure 2.4 | **Phylogenetic tree of Cox11 proteins and their homologs in different organisms**. The branches are labelled with the posterior probability of each split expressed in percentage. Different clusters are manually colourised to highlight defined taxa. The trees were built based on Bayesian inference.

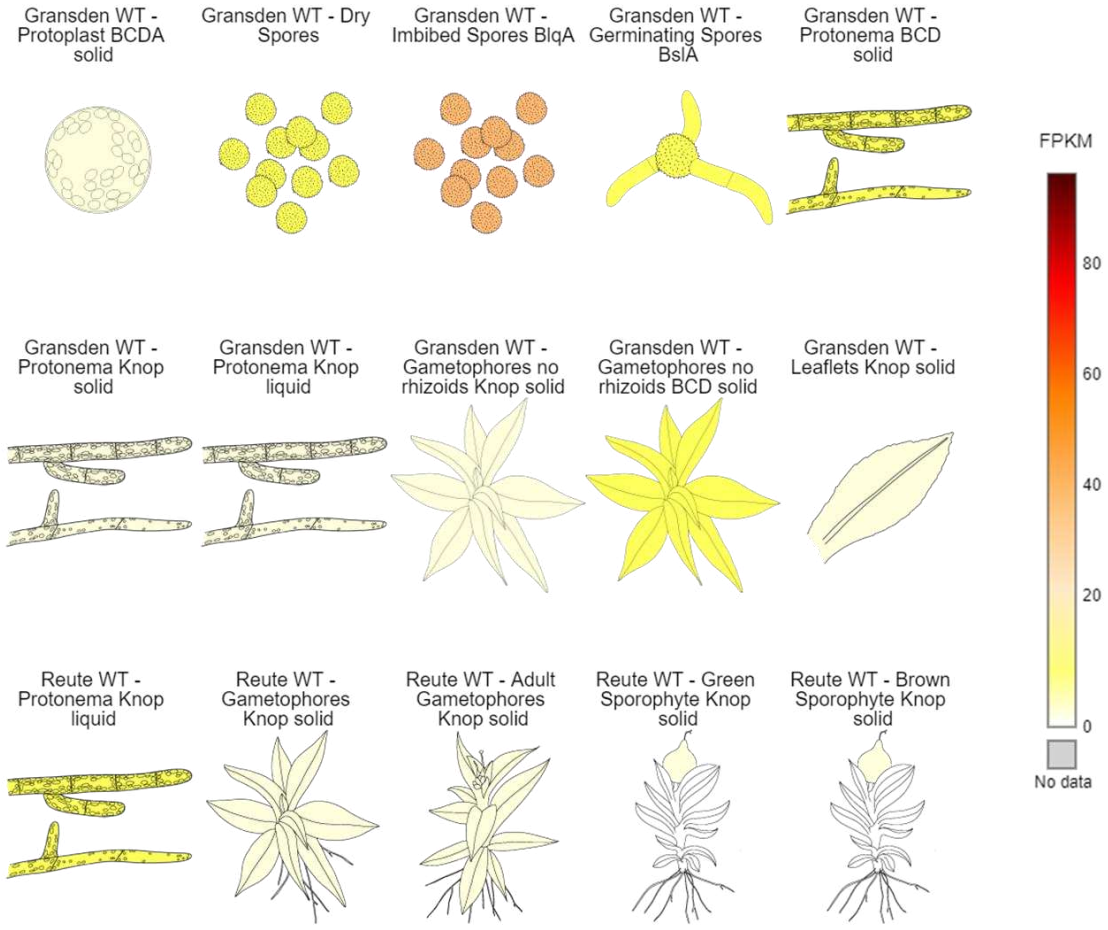

Supplementary Figure 2.5 | **Expression levels of PpCox11 in different developmental stages**. Note that the FPKM are relatively low for all stages, with imbibed spores presenting the higher expression of PpCox11. Data and figure- retrieved from the PeatMOSS Gene Atlas Database.

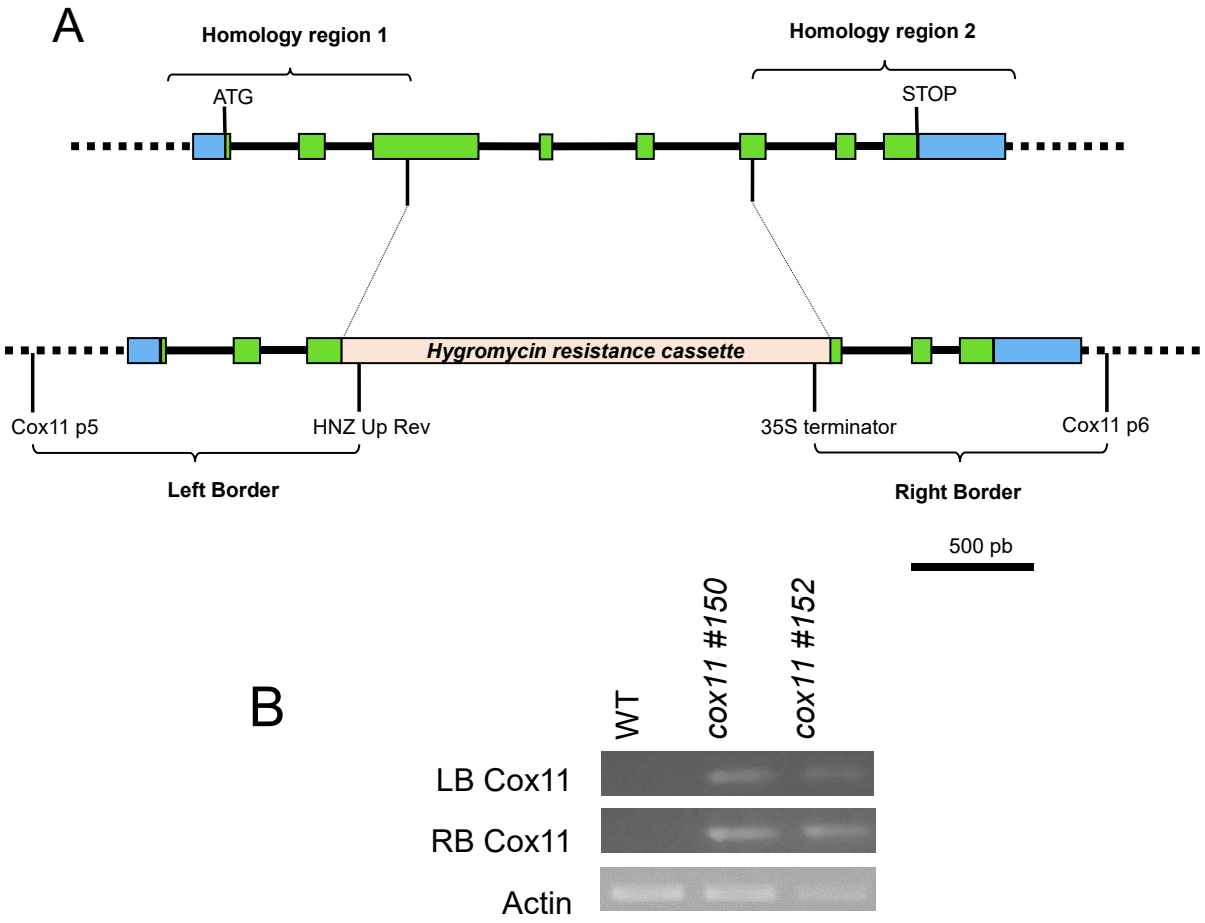

Supplementary Figure 2.6 | Visual summary of the disruption of the PpCox11-encoding locus used for producing the knockout mutant lines. The gene map (A, top) and the corresponding region after construct insertion through homologous recombination (A, bottom) are shown. Green portions represent the exons, blue portions represent the 5' and 3' untranslated regions (UTR). The positions of the first and last codon of each coding region are marked with ATG and STOP, respectively. Integration of the antibiotic resistance cassette occurs through recombination of the respective homology regions. The two regions used for validation of their identity through PCR analysis using the annotated primers are marked as Left Border (LB) and Right Border (RB), and the corresponding bands are shown in B.

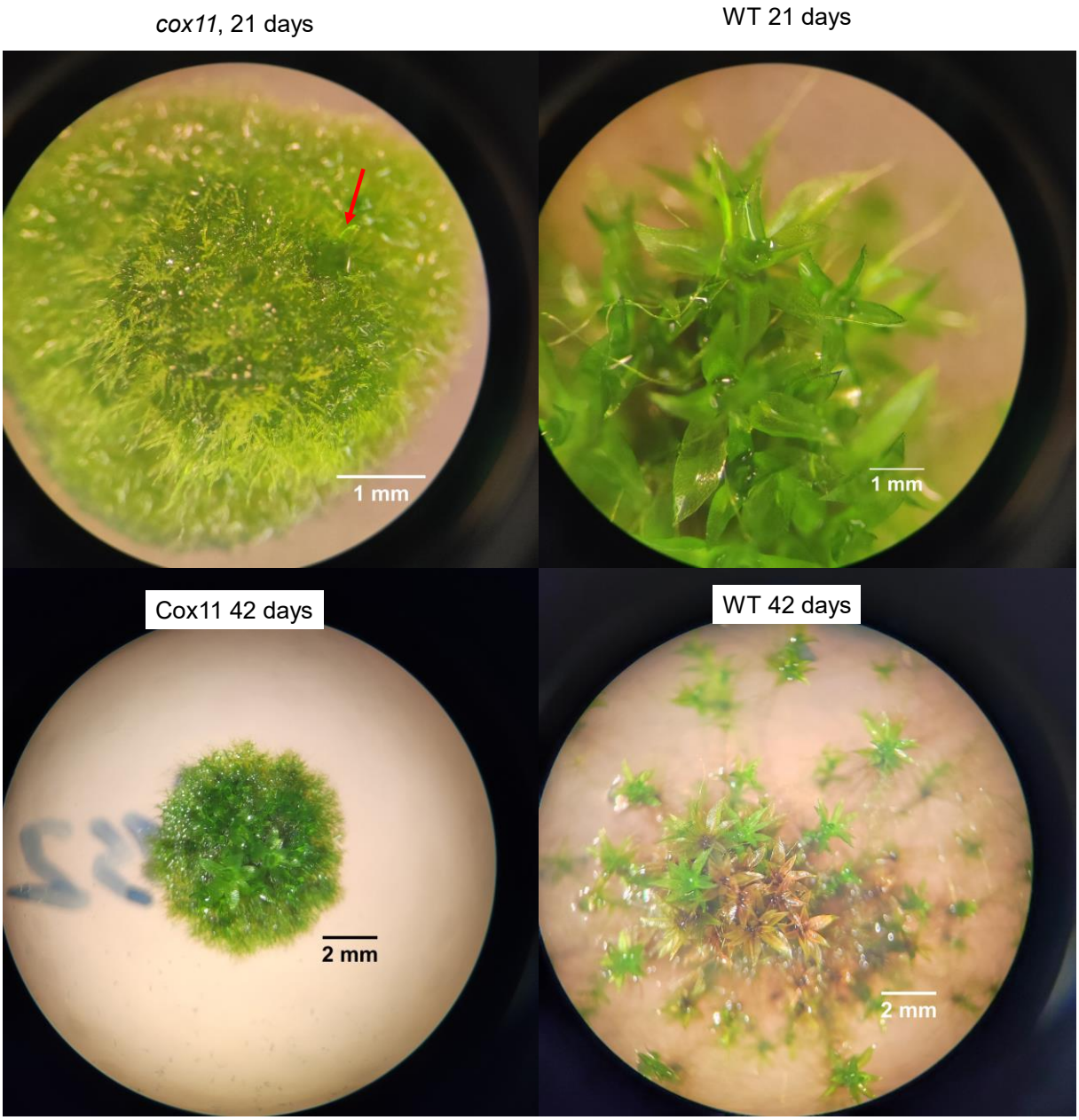

Supplementary Figure 2.7 | **Differential development of gametophores in *cox11***. Images of plant colonies after 21 or 42 days of growth. A developing gametophore is marked with a red arrow in *cox11* at 21 days.

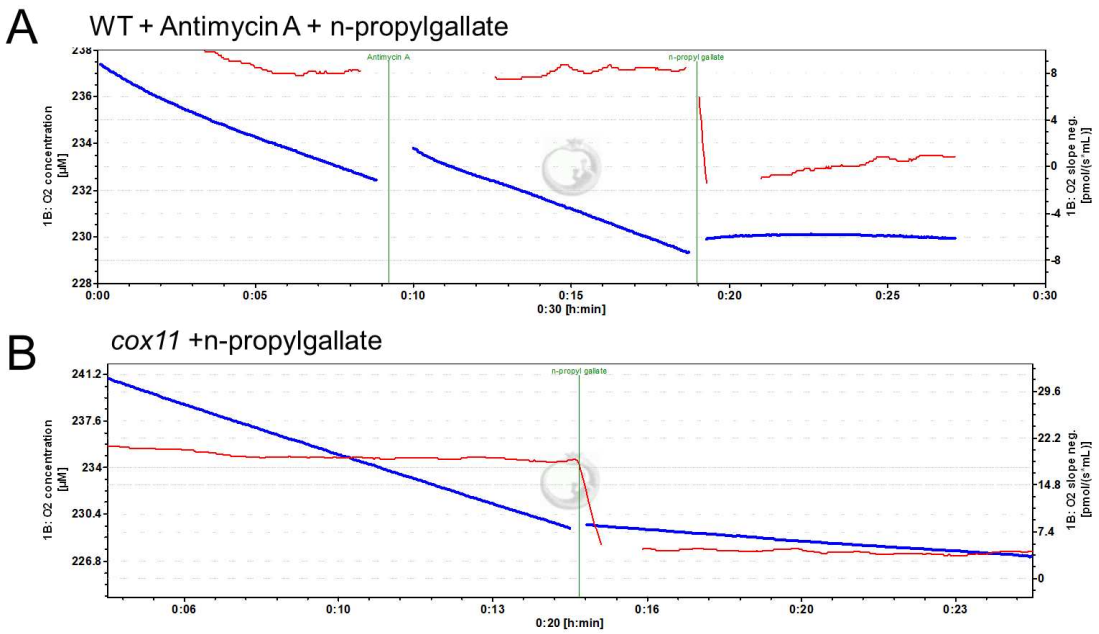

Supplementary Figure 2.8 | **Effect of antimycin and n-propylgallate on dark respiration of intact protonema**. Two representative traces of experiments of respirometry performed on WT (A) or *cox11* (B) are shown. The blue plot (left axis) shows O_2 concentration, while the red plot (right axis) shows O_2 flux. On WT, the addition of Antimycin A did not have an effect in O_2 consumption rate, but n-propylgallate abolished it (A). On *cox11*, n-propylgallate alone was sufficient to block all O_2 consumption (B).

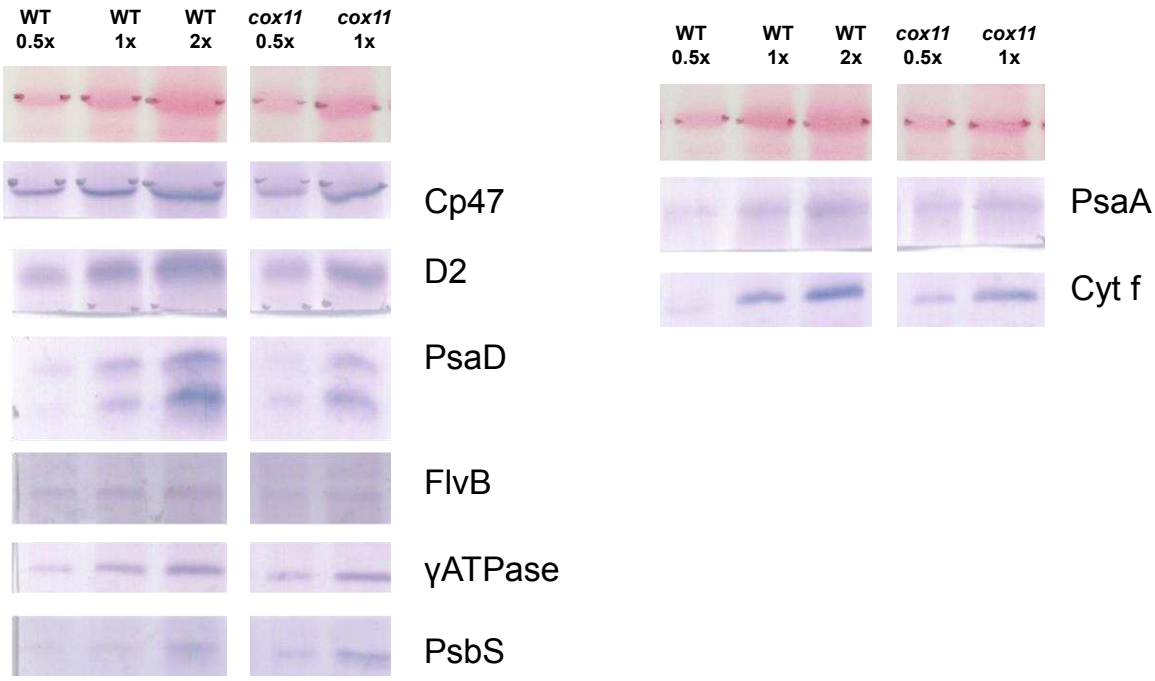

Supplementary Figure 2.9 | **Immunoblotting against subunits of the photosynthetic machinery**. No major alterations in photosynthetic components were detected. The only exceptions were the two components of Photosystem II PsaD and PsbS, that showed slightly higher levels in cox11; however, this increase could be due to a different time harvesting of the samples.

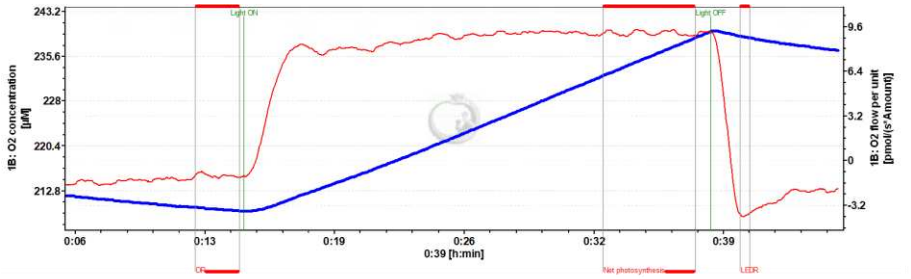

Supplementary Figure 2.10 | **Scheme for measuring photosynthesis and net photosynthesis on intact protonema**. The representative traces of one experiment of respirometry performed on is shown. After the quantification of dark respiration (DR), saturating light was turned on. When the O2 flux was stable (red plot), the net photosynthesis was measured. Then, light was turned off and the post-illumination peak was measured (LEDR).

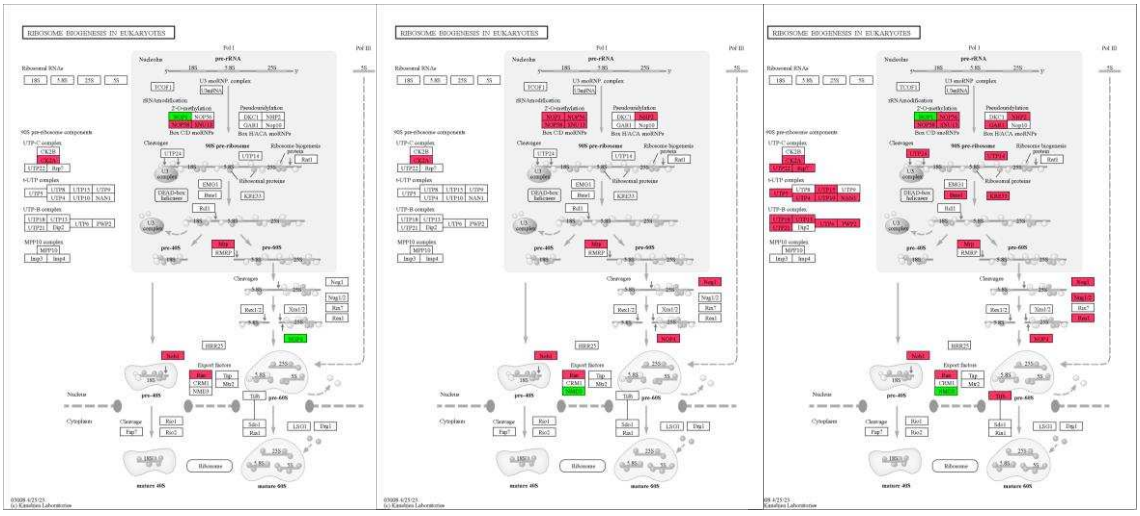

Supplementary Figure 2.11 | **Map of the ribosome biogenesis machinery, showing an induction of most components through the day**. Significantly induced (red) or repressed (green) genes were represented on top of the KEGG map showing Ribosome biogenesis (KEGG ID ppp03008).

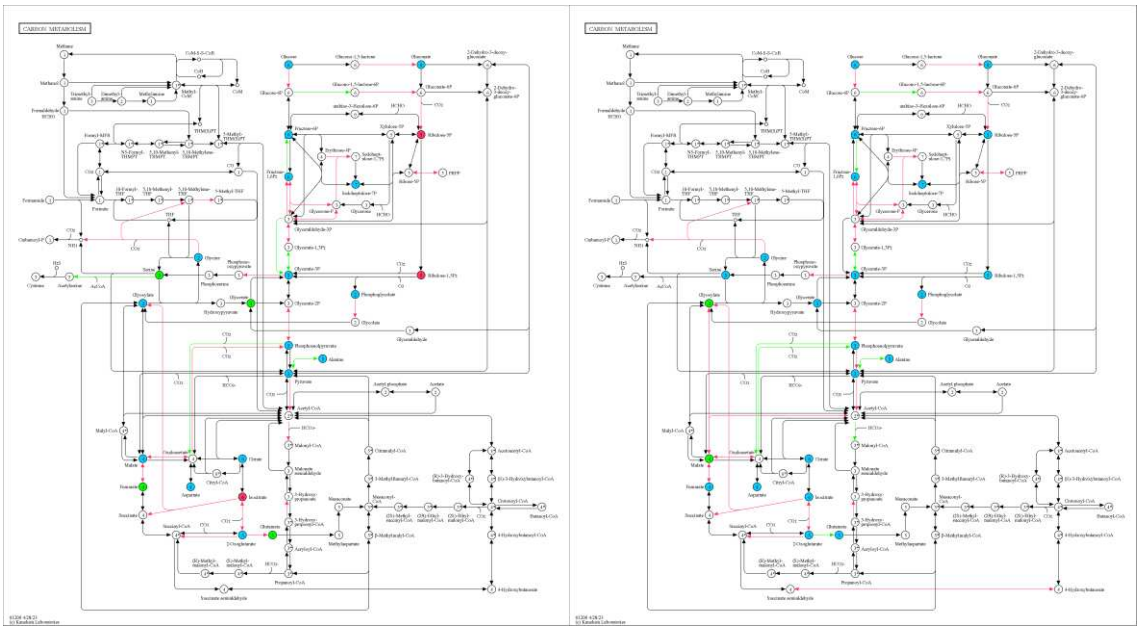

Supplementary Figure 2.12 | **Carbon metabolism at ZT2 and ZT6 in *cox11***. EGG map showing Carbon metabolism (KEGG ID ppp01200), with manually highlights of glycolysis (red rectangle) and the TCA cycle (blue rectangle). Significantly induced (red) or repressed (green) genes are represented by arrows. Significantly higher (red), lower (green) or unaltered (blue) levels of metabolites are represented by circles; empty circles represent metabolites not detected by our untargeted metabolomics experiment. Colouring was used using the Color Mapper function of KEGG.

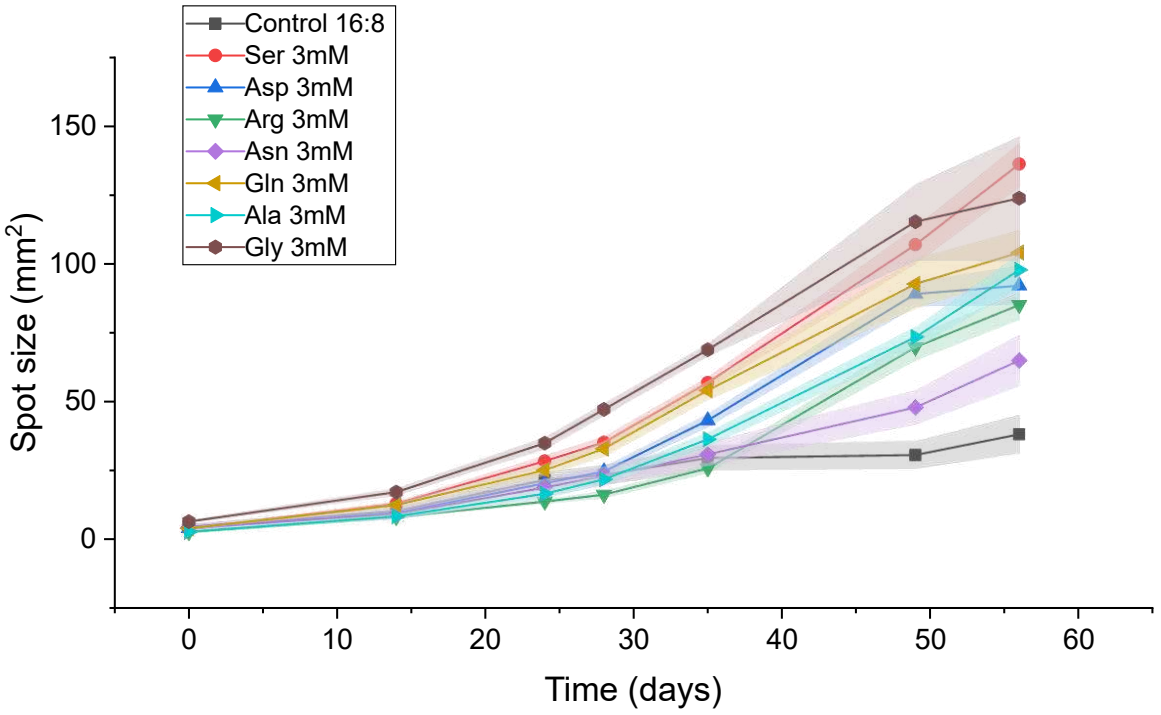

Supplementary Figure 2.13 | Effect of different amino acids on *cox11* growth. The area of the spots of *cox11* plants grown on $PpNO_3$ + ammino acids are reported. Only the amino acids that caused an improvement of growth in *cox11* are included.

Supplementary Table 2.1 | **Composition of the culture media used for plant propagation.** The solid compounds were weighted and dissolved in Milli-Q® purified water. The phosphate buffer and microelements were aliquoted from a master mix solution. The composition of the master mix solution of microelements at 1,000x concentration is shown at the bottom of the table. Culture media were autoclaved and kept at room temperature until used. Original reference: Ashton et al., 1979.

Compound	**Concentration**	
	$PpNO_3$	**$PpNH_4$**
$MgSO_4 \cdot 7\ H_2O$	0.25 g/L	0.25 g/L
$Ca(NO_3)_2 \cdot 4\ H_2O$	0.80 g/L	0.80 g/L
$FeSO_4 \cdot 7\ H_2O$	0.0125 g/L	0.0125 g/L
Microelements (1,000 x)	1 mL/L	1 mL/L
KH_2PO_4-KOH 250 g/L, pH 7.0	1 mL/L	1 mL/L
Ammonium tartrate	-	0.5 g/L
Glucose	-	5 g/L
Agar	8 g/L	7.2 g/L
Microelements 1,000 x		
Compound	**Concentration**	
$CuSO_4 \cdot 5\ H_2O$	5.5 mg/L	
$ZnSO_4 \cdot 7\ H_2O$	5.5 mg/L	
H_3BO_3	61.4 mg/L	
$MnCl_2 \cdot 4\ H_2O$	38.9 mg/L	
$CoCl_2 \cdot 6\ H_2O$	5.5 mg/L	
KI	2.8 mg/L	
$Na_2MoO_4 \cdot 4\ H_2O$	2.5 mg/L	

Supplementary Table 2.2 | **Primers used in this chapter.**

Name	5' → 3' sequence
Actin2 for	GCGAAGAGCGAGTATGACGAG
Actin2 rev	AGCCACGAATCTAACTTGTGAT
Cox11 p5	TGTTGTTCAAATGTCGTCAT
Cox11 p6	TGGACAAATTATTCCATGCT
Cox11-p1	CCTAGGTCGATGATTTGTGTTTTTGA
Cox11-p2	CTCGAGCCTATGGTTTGCAAGTAAGG
Cox11-p3	GTTAACACAAGCTCAGTACCCATCAC
Cox11-p4	TTAATTAAAAAAAGACGCAAACACAGAT
Cox11-p5	TGTTGTTCAAATGTCGTCAT
Cox11-p6	TGGACAAATTATTCCATGCT
Cox11-RTf	CATCCAGGGAATTGGTAGTA
Cox11-RTr	ATCTTCAAATCACGAAGGTG
HNZ Up Rev	TGCGCAACTGTTGGGAAG
35S terminator	CGCTGAAATCACCAGTCTCTCT

Supplementary Table 2.3 | **Antibodies used in this chapter**.

Complex target	Subunit	Ref
Complex I	Nad9	Lamattina et al., 1993
Complex II	SDH 1-1	Peters et al., 2012
Complex III	MPP alpha	Peters et al., 2012
Complex V	Beta subunit	Peters et al., 2012
AOX	AOX	Agrisera AS04 054
	Cp47	
	D2	
	PsaD	
	FlvB	
	y ATPase	
	PsbS	
	PsaA	
	Cyt f	

Supplementary Table 2.4 | **Available information on ascorbate peroxidase encoding genes in *P. patens***, retrieved from three different publications, regarding gene name and predicted localization.

Ref:	(Ozyigit et al., 2016)		(Maruta et al., 2016)		(Wu & Wang, 2019)	
ID (v3)	Name	Localiz	Name	Local	Name	Local
Pp3c1_26270	Phpat.001G104200	Chlo/Cyt	APX3	Perox	PpAPX3	Perox
Pp3c1_40650	Phpat.001G162800	Chlo	APX4	Chloro	PpAPX-S	Mito/Chloro
Pp3c17_7560	Phpat.017G025400	Chloro	-	-	PpAPX6-related	Chloro
Pp3c20_2050	Phpat.020G011100	Cyto	APX1	Cyto	PpAPX2.1	Cyto
Pp3c20_2100	-	-	APX2	Cyto	PpAPX2.2	Cyto

Supplementary Table 2.5 | **Accession codes of the protein sequences used for building the tree**. For each organism, the accession codes of proteins otrthologous to Cox11 is shown. Source database: N, NCBI; U, UniProt; P, Phytozome.

Organism	Source	Accession ID
Acytostelium subglobosum	N	XP_012752147.1
Aphanomyces invadans	N	XP_008867627.1
Arabidopsis thaliana	U	Q8GWR0
Bathycoccus prasinos	N	XP_007513386.1
Bos taurus	U	A3KMZ6
Brassica rapa	N	XP_009119634.1
Camelina sativa	N	XP_010480959.1
Capsella rubella	N	XP_006305482.1
Cavenderia fasciculata	N	XP_004350816.1
Chlamydomonas reinhardtii	N	XP_001700235.1
Chlorella variabilis	N	XP_005846291.1
Chondrus crispus	N	XP_005715775.1
Coccomyxa subellipsoidea	N	XP_005646193.1
Cyanidioschyzon merolae	N	XP_005535875.1
Dictyostelium purpureum	N	XP_003294442.1
Dictyostellium discoideum	U	Q54HM6
Eucalyptus grandis	N	XP_010032744.1
Eutrema salsugineum	N	XP_006418345.1
Galdieria sulphuraria	N	XP_005706970.1
Homo sapiens	U	Q9Y6N1
Juglans regia	N	XP_018847089.1
Marchantia polymorpha	N	PTQ35596.1
Micromonas commoda	N	XP_002499665.1
Mus musculus	U	Q6P8I6
Nannochloropsis oceanica	N	CP038114.1
Nicotiana tabacum	N	XP_016501024.1
Phaeodactylum tricornutum	N	XP_002184365.1
Phaeodactylum tricornutum	N	AC151921.1
Physcomitrella patens	P	Pp3c16_1230V3.2
Phytophthora infestans	N	XP_002901677.1
Phytophthora parasitica	N	XP_008913468.1
Pongo abelii	U	Q5R7U6
Punica granatum	N	XP_031389890.1
Rattus norvegicus	U	M0RE03
Rhodamnia argentea	N	XP_030536428.1
Saccharomyces cerevisiae	U	P19516
Saprolegnia parasitica	N	XP_012194574.1
Schizosaccharomyces pombe	U	Q9UTM2
Selaginella moellendorffii	N	XP_002977639.2
Solanum tuberosum	N	XP_006348705.1
Sphagnum phallax	P	Sphfalx0067s0102.1
Spinacia oleracea	N	XP_021847907.1
Sus scrofa	U	F1RSF6
Syzygium oleosum	N	XP_030452046.1
Thalassiosira pseudonana	N	XP_002293512.1
Vulpes vulpes	U	A0A3Q7T9N9

Supplementary Table 2.6 | **Relative expression of nitrate reductase encoding genes in *cox11***. Genes retrieved from Medina-Andrés & Lira-Ruan, 2012. Missing data (-) means that the gene was not detected as significantly expressed in any condition. (***) p<0.001; (**) p<0.01; (*) p<0.1; (n.s.) p>0.1 Source: Ruibal et al., 2013.

		cox11 ZT0		cox11 ZT2		cox11 ZT6	
Gene ID (original ref)	Gene ID (v3.3)	lfc	padj	lfc	padj	lfc	padj
Pp1s79_76v6.1	Pp3c14_9410	-1.35	**	-0.57	n.s.	-0.42	n.s.
Pp1s58_252v6.1	Pp3c10_9670	-	-	-	-	-	-
Pp1s58_249v6.1	Pp3c10_9540	-	-	-	-	-	-

Supplementary Table 2.7 | **Relative expression of small heat shock proteins in *cox11***. Missing data (-) means that the gene was not detected as significantly expressed in any condition. (***) p<0.001; (**) p<0.01; (*) p<0.1; (n.s.) p>0.1 Source: Ruibal et al., 2013. Localizations are predicted.

	cox11 ZT0		*cox11* ZT2		*cox11* ZT6				
Gene ID	lfc	Sig	lfc	Sig	lfc	Sig	From original ref		
Pp3c25_14630	5.88	***	3.26	***	0.50	n.s.	PpHsp21.5	Pp1s129_85V6.1	nuc/cyto
Pp3c19_14230	0.50	n.s.	2.72	***	-0.15	n.s.	PpHsp20.1	Pp1s20_253V6.1	cyto
Pp3c5_13280	1.09	n.s.	1.98	n.s.	0.83	n.s.	PpHsp19.4	Pp1s350_28V6.1	cyto
Pp3c25_8880	-	-	-	-	-	-	PpHsp19.2	Pp1s50_96V6.1	cyto
Pp3c16_7110	1.47	*	3.68	***	1.69	*	PpHsp22.0	Pp1s194_15V6.1	cyto
Pp3c6_3710	3.66	***	4.13	***	3.86	***	PpHsp22.5	Pp1s77_290V6.1	chlo
Pp3c16_1550	2.84	*	3.25	*	1.09	n.s.	PpHsp18.4b	Pp1s144_148V6.1	cyto
Pp3c11_14810	2.93	***	0.68	n.s.	-0.57	n.s.	PpHsp18.4a	Pp1s11_289V6.1	cyto
Pp3c13_6160	-	-	-	-	-	-	PpHsp13.4	Pp1s182_60V6.1	cyto
Pp3c18_16670	-	-	-	-	-	-	PpHsp12.5	Pp1s3_114V6.1	nucl
Pp3c21_6480	-	-	-	-	-	-	PpHsp16.4b	Pp1s27_332V6.1	cyto
Pp3c21_6480	-	-	-	-	-	-	PpHsp16.4a	Pp1s27_331V6.1	cyto
Pp3c21_19080	1.62	***	0.70	n.s.	-1.06	**	PpHsp17.2c	Pp1s85_11V6.1	cyto
Pp3c12_24560	3.39	***	1.99	**	-0.32	n.s.	PpHsp17.3b	Pp1s372_62V6.1	cyto
Pp3c19_22640	1.83	***	0.67	n.s.	-0.30	n.s.	PpHsp17.8	Pp1s380_17V6.1	cyto
Pp3c17_10780	-	-	-	-	-	-	PpHsp17.6	Pp1s105_133V6.1	cyto
Pp3c8_6770	2.02	***	2.10	***	-0.03	n.s.	PpHsp17.3a	Pp1s8_86V6.1	chlo
Pp3c8_9380	-	-	-	-	-	-	PpHsp17.2b	Pp1s8_249V6.1	chlo
Pp3c8_9380	-	-	-	-	-	-	PpHsp17.2d	Pp1s8_209V6.1	chlo
Pp3c8_9230	-	-	-	-	-	-	PpHsp17.2a	Pp1s8_244V6.1	chlo
Pp3c7_25570	4.14	***	3.54	**	2.04	*	PpHsp27.5	Pp1s97_106V6.1	chlo
Pp3c1_7030	1.31	**	0.74	n.s.	-1.40	**	PpHsp27.3	Pp1s38_338V6.1	mito

Supplementary Table 2.8 | **Relative expression of large heat shock proteins in *cox11***. Missing data (-) means that the gene was not detected as significantly expressed in any condition. (***) p<0.001; (**) p<0.01; (*) p<0.1; (n.s.) p>0.1 Source: Phytozome.

		ZT0		ZT2		ZT6	
Gene ID	Annotation Phytozome	lfc	sig	lfc	sig	lfc	sig
Pp3c15_4270	PTHR11528 - HEAT SHOCK PROTEIN 90	0.57	*	0.37	n.s.	0.21	n.s.
Pp3c15_12515	PTHR11528 - HEAT SHOCK PROTEIN 90	1.96	***	0.53	n.s.	-0.62	*
Pp3c12_22440	PTHR11528:SF41 - HEAT SHOCK PROTEIN 89.1	-0.54	*	-0.10	n.s.	1.36	***
Pp3c4_810	PTHR11528:SF41 - HEAT SHOCK PROTEIN 89.1	0.44	n.s.	-0.03	n.s.	0.75	**
Pp3s58_270	PTHR11528:SF44 - HEAT SHOCK PROTEIN 75 KDA, MITOCHONDRIAL	-	-	-	-	-	-
Pp3c15_12510	PTHR11528 - HEAT SHOCK PROTEIN 90	1.96	***	0.53	n.s.	-0.62	*
Pp3c15_6620	PTHR11528 - HEAT SHOCK PROTEIN 90	2.28	***	0.60	n.s.	0.41	n.s.
Pp3c9_6690	PTHR11528 - HEAT SHOCK PROTEIN 90	0.83	***	0.72	**	0.90	***
Pp3c8_6510	PTHR11528:SF45 - ENDOPLASMIN HOMOLOG	-	-	-	-	-	-
Pp3c14_3360	PTHR11528:SF45 - ENDOPLASMIN HOMOLOG	0.48	*	0.33	n.s.	0.48	*
Pp3c9_6640	PTHR11528 - HEAT SHOCK PROTEIN 90	1.66	***	0.36	n.s.	-0.14	n.s.
Pp3c1_39580	PTHR11528//PTHR11528:SF49 - HEAT SHOCK PROTEIN 90	-	-	-	-	-	-
Pp3c9_20160	PTHR11528:SF53 - HEAT SHOCK PROTEIN 90-1	-	-	-	-	-	-
Pp3s58_301	KOG0019 - Molecular chaperone (HSP90 family)	-	-	-	-	-	-
Pp3c15_6622	PTHR11528 - HEAT SHOCK PROTEIN 90	2.28	***	0.60	n.s.	0.41	n.s.
Pp3c19_15000	PTHR11528:SF41 - HEAT SHOCK PROTEIN 89.1	0.04	n.s.	0.81	**	1.27	***
Pp3c2_6890	PTHR11528:SF45 - ENDOPLASMIN HOMOLOG	-	-	-	-	-	-

Supplementary Table 2.9 | **Relative expression of genes induced during UPR^{ER} in *P. patens***. Missing data (-) means that the gene was not detected as significantly expressed in any condition. (***) p<0.001; (**) p<0.01; (*) p<0.1; (n.s.) p>0.1 Source: Lloyd et al., 2018.

		ZT0	ZT0	ZT2	ZT2	ZT6	ZT6
ID in original ref	Gene ID	lfc	Significance	lfc	Significance	lfc	Significance
Pp1s181_3V6	Pp3c10_17310	0.775151	**	0.747739	*	0.692297	**
Pp1s566_63V6	Pp3c15_22880	0.661125	*	0.392066	n.s.	0.011001	n.s.
Pp1s368_19V6	Pp3c20_14730	0.75546	**	0.321133	n.s.	-0.18138	n.s.
Pp1s298_70V6	Pp3c4_21130	0.474109	n.s.	0.512159	n.s.	0.339215	n.s.
Pp1s91_238V6	Pp3c12_8210	0.135946	n.s.	0.247674	n.s.	0.227956	n.s.
Pp1s64_46V6	Pp3c5_8550	-0.49928	n.s.	0.194747	n.s.	0.235977	n.s.
Pp1s213_66V6	Pp3c9_3330	0.13643	n.s.	0.191789	n.s.	0.256384	n.s.
Pp1s34_189V6	Pp3c14_20430	0.135925	n.s.	-0.14901	n.s.	-0.03236	n.s.
Pp1s241_31V6	Pp3c20_22800	-0.41355	*	0.248586	n.s.	0.461581	*
Pp1s15_112V	Pp3c16_14150	-0.47964	n.s.	0.313201	n.s.	0.301257	n.s.
Pp1s288_23V6	Pp3c3_25750	-	-	-	-	-	-
Pp1s34_31V6	Pp3c14_18900	-	-	-	-	-	-

Supplementary Table 2.10 | **Relative expression of antioxidant enzymes in *cox11***. Missing data (-) means that the gene was not detected as significantly expressed in any condition. (***) p<0.001; (**) p<0.01; (*) p<0.1; (n.s.) p>0.1. References: (a) Wu & Wang, 2019; (b) Higashi et al., 2013; (c) Y. J. Liu et al., 2013; (d) L. Xu et al., 2013.

				cox11 ZT0		cox11 ZT2		cox11 ZT6	
Symbol	Name	Ref	Gene ID	lfc	sig	lfc	sig	lfc	sig
PpAPX2 (PpAPX2.1)	Ascorbate peroxidase	a	Pp3c20_2050	0.51	*	0.27	n.s.	0.19	n.s.
PpAPX6-related	Ascorbate peroxidase	a	Pp3c17_7560	0.88	**	0.61	n.s.	0.73	*
PpAPX-S	Ascorbate peroxidase	a	Pp3c1_40650	0.13	n.s.	-0.60	*	-0.10	n.s.
PpAPX3	Ascorbate peroxidase	a	Pp3c1_26270	0.05	n.s.	-0.30	n.s.	0.11	n.s.
PpAPX2 (PpAPX2.2)	Ascorbate peroxidase	a	Pp3c20_2100	0.01	n.s.	0.28	n.s.	0.60	*
PpCSD2	CuZn-SOD - chloroplast (predicted)	b	Pp3c9_25690	0.35	n.s.	0.35	n.s.	0.51	n.s.
PpCSD1	CuZn-SOD - chloroplast (predicted)	b	Pp3c9_24840	0.02	n.s.	0.17	n.s.	0.90	*
PpCSD4	CuZn-SOD - cytosol (predicted)	b	Pp3c24_4100	0.60	*	0.39	n.s.	0.01	n.s.
PpCSD3	CuZn-SOD - cytosol (predicted)	b	Pp3c20_17920	0.37	n.s.	0.11	n.s.	-0.03	n.s.
PpFSD1	Fe-SOD - apoplast (predicted)	b	Pp3c7_19790	-0.26	n.s.	0.31	n.s.	1.37	***
PpFSD2	Fe-SOD - chloroplast (predicted)	b	Pp3c2_27440	1.16	***	1.07	***	1.43	***
PpFSD3	Fe-SOD - pseudogene	b	Pp3c17_14510	-2.06	n.s.	-2.03	n.s.	-2.97	*
PpGSTF7	Glutathione S-transferase	c	Pp3c7_13080	-0.34	n.s.	-0.83	n.s.	0.22	n.s.
PpGSTF2	Glutathione S-transferase	c	Pp3c3_31590	0.86	*	-0.05	n.s.	-0.25	n.s.
PpGSTF2	Glutathione S-transferase	c	Pp3c23_20550	-	-	-	-	-	-
PpGSTF5	Glutathione S-transferase	c	Pp3c17_6080	-	-	-	-	-	-
PpGSTF6	Glutathione S-transferase	c	Pp3c23_20550	-	-	-	-	-	-
PpGSTT3	Glutathione S-transferase	c	Pp3c7_26710	-	-	-	-	-	-
PpMSD	Mn-SOD - mitochondrion (predicted)	b	Pp3c19_10240	-0.02	n.s.	-0.06	n.s.	-0.12	n.s.
	Glutathione reductase	d	Pp3c4_17890	0.19	n.s.	0.27	n.s.	-0.05	n.s.
	Glutathione reductase	d	Pp3c5_16850	0.09	n.s.	-0.24	n.s.	0.13	n.s.

Supplementary Table 2.11 | **Relative expression of genes orthologs of Arabidopsis Asn1/Din6 (AT3G47340)**. Orthologs were identified by similarity at Phytozome. (***) p<0.001; (**) p<0.01; (*) p<0.1; (n.s.) p>0.1.

	cox11 ZT0		cox11 ZT2		cox11 ZT6	
	lfc	sig	lfc	sig	lfc	sig
Gene ID	lfc	Significance	lfc	Significance	lfc	Significance
Pp3c20_17620	-3.65	***	-3.49	***	-3.96	***
Pp3c24_13160	-2.45	***	-1.91	**	-3.73	***
Pp3c5_13310	0.48	*	0.66	*	0.65	**

CHAPTER III

Genetic inactivation of Complex I in *Physcomitrium patens* induces mitochondrial retrograde signalling particularly during night

Antoni M. Vera-Vives[1], Marco Mellon[1], Anna Segalla[1], Libero Gurrieri[2], Edoardo Bizzotto[1], Stefano Campanaro[1], Francesca Sparla[2], Alessandro Alboresi[1] and Tomas Morosinotto[1]

1. Department of Biology, University of Padova, Italy
2. Department of Pharmacy and Biotechnology (FABIT), University of Bologna, Italy

Authorship statement:

The idea of the main research question was mine, with significant input from my supervisor. I delineated the experimental design, with critical input from my supervisor and collaborators. I designed and conducted the experiments, with the collaboration of: Dr. Anna Segalla, who aided in sample harvesting for omics experiments; Prof. Francesca Sparla and Dr. Libero Gurrieri, who aided designing and performed experiments of starch quantification and amylolytic activity. I conducted all the data analysis, except for the alignment of RNAseq reads onto the reference genome, which was done with the aid of PhD student Edoardo Bizzotto and Prof. Stefano Campanaro; all other downstream omics analyses were designed and performed by myself. I wrote the manuscript, designed the graphs and revised the text after the comments of my supervisor.

Abstract

We previously isolated and characterized the mutant *ndufa5*, completely depleted in Complex I activity, which represented the first respiratory mutant in a non-vascular land plant. Here, we applied time-resolved transcriptomics and metabolomics to describe the metabolic consequences of the Complex I depletion in *ndufa5* and compared our data with the described phenotypes of other available Complex I-deficient embryophyte models. *ndufa5* plants showed alterations in carbon and nitrogen metabolism that are consistent with those reported in other Complex I mutants in vascular plants. One of the general features of Complex I-deficient plants, that was observed also in *ndufa5*, is the induction of the alternative oxidase (AOX). We found the metabolic alterations and the AOX induction in *ndufa5* to be more severe by the end of the night than during day. The transcriptome of *ndufa5* plants suggests that mitochondria-to-nucleus retrograde signalling pathways are strongly induced by the end of the night, which are probably mediated by a homolog of the transcription factor ANAC017, described in vascular plants. This represents the most solid evidence of a mitochondrial retrograde signalling pathway being active in a bryophyte, and we hypothesize that this activation is at the root of the phenotypic differences between *ndufa5* and the Complex IV mutant *cox11*.

1. Introduction

Cells compartmentalization is important for isolating bioenergetic processes in specialized organelles. Plants have specialized organelles such as mitochondria, chloroplasts, and peroxisomes where most bioenergetic processes occur. The different compartments of the cell must be efficiently coordinated and respond synergically to environmental clues in other to ensure optimal performance (Lunn, 2007). Mitochondria and chloroplasts have their own genomes, derived originally from the ancestor during endosymbiosis. During evolution, most of the organellar proteins have become encoded by nuclear genes (Martin & Herrmann, 1998). It is therefore pivotal that there is communication between the nucleus and organelles, so gene transcription can be regulated and respond to stimuli to ensure optimal performance. The molecular pathways that connect the organelles with the nucleus are called anterograde signalling, when signals are emitted from the nucleus and sensed by organelles, or retrograde signalling, when the signals are sent in the opposite direction (Mielecki et al., 2020). Retrograde signalling (Figure 3.1) allows the nucleus to have information about the functional state of the organelles and respond accordingly to adapt to changes and maintain cellular homeostasis (Schwarzländer et al., 2011; Schwarzländer & Finkemeier, 2013). So far, different retrograde signalling pathways have been identified, that are proposed to work either for chloroplasts, mitochondria, or both (Meng et al., 2019; Y. Wang et al., 2020; Zhu et al., 2022).

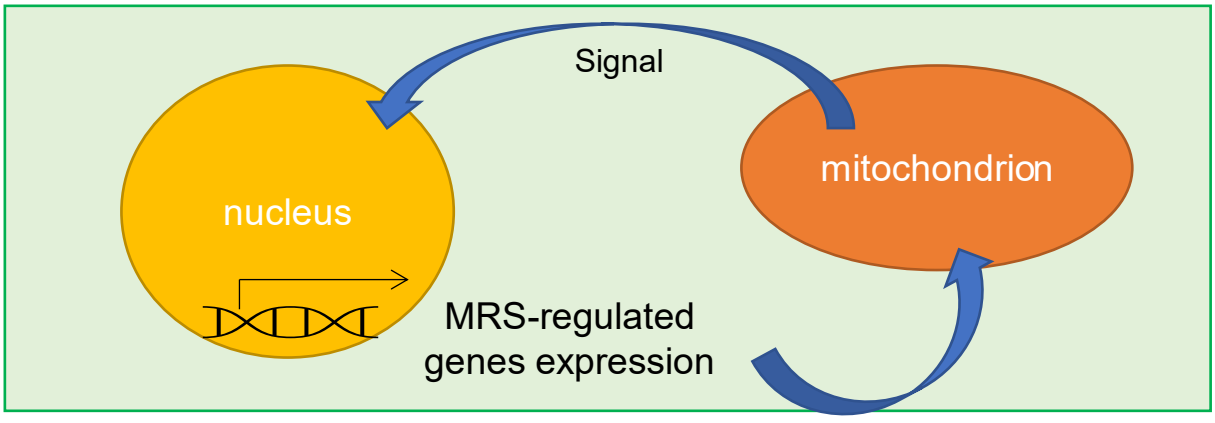

Figure 3.1 | **Basic scheme of mitochondrial retrograde signalling**. The diagram represents a plant cell. Alterations in mitochondrial function are sensed at the nucleus, where there is the regulation of the expression of genes that help cope with the situation sensed by mitochondria.

The concept of retrograde signalling has been studied for decades in plants focusing mostly on chloroplasts (Richter et al., 2023). While mitochondrial retrograde signalling (MRS) has been well studied in other eukaryotes (da Cunha et al., 2015; Z. Liu & Butow, 2006), the most significant advances in plant MRS have been produced more recently (Leister, 2012; Rhoads & Subbaiah, 2007) even though the notion that mitochondria had a role as a hub for processing stress responses also in plants is not new (Gray et al., 2004; Maxwell et al., 2002). Among the early observations, there was the notion that the alternative oxidase (AOX), which is localized in mitochondria but encoded in the nucleus, was induced during biotic and abiotic stresses in plants (Simons et al., 1999; Vanlerberghe & McIntosh, 1997; Vanlerberghe & McIntosh, 1994). This has been reported several times in multiple species and in response to different stressors there since. For instance, this induction has been reported in response to stressors that acted on mitochondria, such as drugs that blocked one or more respiratory complexes like antimycin A in Arabidopsis (Clifton et al., 2006; De Clercq et al., 2013; Kacprzak et al., 2020; Ng, Giraud, et al., 2013; Ng, Ivanova, et al., 2013) and tobacco (Gray et al., 2004), or rotenone in Arabidopsis (Clifton et al., 2005). Indeed, the induction of the AOX is considered a hallmark of mitochondrial retrograde signalling in plants (Giraud et al., 2009; Millar et al., 2011).

For the signalling pathways to get activated and induce the MRS response, an upstream signal is required. Different pathways and metabolites have been related to the induction of MRS in plants. One type of MRS is redox signalling, based on redox signals that might derive from the redox status of the quinone pools in either the photosynthetic and the mitochondrial electron transport chains; from redox-active compounds that contain thiols, such as thioredoxins; or from reactive oxygen species (ROS) (Schwarzländer et al., 2011; Schwarzländer & Finkemeier, 2013). These redox signals can activate downstream signalling pathways and eventually modulate gene expression and cellular responses to maintain mitochondrial and cellular homeostasis (Ježek et al., 2020; van Aken, 2021). On another hand, calcium signalling, which is known to be an important second messenger in plant cells (Kudla et al., 2018; Pirayesh et al., 2021), has also been proposed as involved in the transduction of mitochondrial retrograde signals (Vanderauwera et al., 2012). Another kind of signal that can induce a transcriptomic

response is the accumulation of misfolded or unfolded mitochondrial protein precursors, which induces the activation of the mitochondria-specific unfolded protein response (UPR^{mt}). UPR^{mt} is a variant of the more general unfolded protein response of the endoplasmic reticulum (UPR^{ER}) (Y. Liu et al., 2022; Manghwar & Li, 2022). The UPR^{mt} has been largely studied in different eukaryotes (Baker & Haynes, 2011; Jovaisaite et al., 2014; Quirós et al., 2016), and it has also been described in plants (Kacprzak et al., 2020; X. Wang & Auwerx, 2017).

Regardless of their nature, the primary signalling molecules require downstream effectors for changes in mitochondria to remodel nuclear gene expression. The induction of AOX during MRS has been exploited for the discovery of components of the MRS machinery: a successful experimental approach based on forward genetics, consisting in characterizing mutant lines that failed to induce AOX upon exposure to a mitochondrial stressor, has permitted the identification of several RAO (Regulator Of Aox) proteins including: RAO1/CDKE;1 (Ng, Giraud, et al., 2013); RAO2/ANAC017; RAO3/BIG; RAO4/PIN1; RAO5/MYB91; RAO6/AL1 (Ivanova et al., 2014); and RAO7/MYB29 (Zhang et al., 2017). The subsequent characterization of these RAOs has led to the identification of diverse pathways that mediate MRS in plants.

In the last decade, the increasing availability of bulk transcriptomic data provided invaluable insights into the global gene expression changes associated with MRS in plants (Aken et al., 2016; De Clercq et al., 2013; Kacprzak et al., 2020; Ng, Giraud, et al., 2013; Ng, Ivanova, et al., 2013; Schwarzländer et al., 2011). However, as most of the experimental data comes from the model Arabidopsis, it is impossible to distinguish the general features of the response and the evolutionary or phylogenetic differences of MRS in plants. Through *in silico* analyses, it has been recently shown that, while all the essential components of MRS identified in Arabidopsis can be traced back to green algae, the distinctive attributes enabling these components to orchestrate responses to mitochondrial stress appear to have evolved during the colonization of land (Khan & Van Aken, 2022). Accordingly, some of the key players of MRS pathways defined in Arabidopsis were identified also in bryophytes such as the moss *Physcomitrium patens*, whilst others were defined as exclusive of vascular plants (Khan & Van Aken, 2022).

In this Chapter, we present the analysis of the transcriptome and metabolome of the *P. patens* mutant line *ndufa5*, a previously published mutant plant deficient in mitochondrial Complex I (Mellon et al., 2021). We compare the omics profile of *ndufa5* and *cox11*, a Complex IV deficient plant described in CHAPTER II, and show how impairing Complex I or Complex IV has different consequences in the metabolism of *P. patens*. Moreover, we present the first evidence of a mitochondrial retrograde signalling pathway being active in the moss *P. patens*. We verified the presence in the *P. patens* genome and transcriptome of candidate homologs of master regulators of MRS previously defined in Arabidopsis, and we provide evidence supporting MRS being active in *ndufa5* but not in *cox11* plants. We propose that the substantial differences described between *ndufa5* and *cox11* plants are due to a differential activation of MRS pathways among these two lines.

2. Results

2.1. Time-resolved transcriptomics and metabolomics on *ndufa5* show significant differences with *cox11*

We analysed the transcriptome and metabolome of Complex I deficient *ndufa5* plants at different zeitgeber times, following the same setup described for *cox11* plants in CHAPTER II: the end of the night (ZT0), the beginning of the day (ZT2) and the middle of the day (ZT6). After analysing the distribution of differentially expressed genes (DEGs) in the different conditions, we found that, different to what we described for *cox11*, where the number of DEGs was similar between the three time conditions, most of the regulated genes in *ndufa5* concentrated at ZT0 (Figure 3.2A). Interestingly, there is a low degree of overlap of DEGs between *ndufa5* and *cox11*, this is particularly the case for ZT0 (Figure 3.2B).

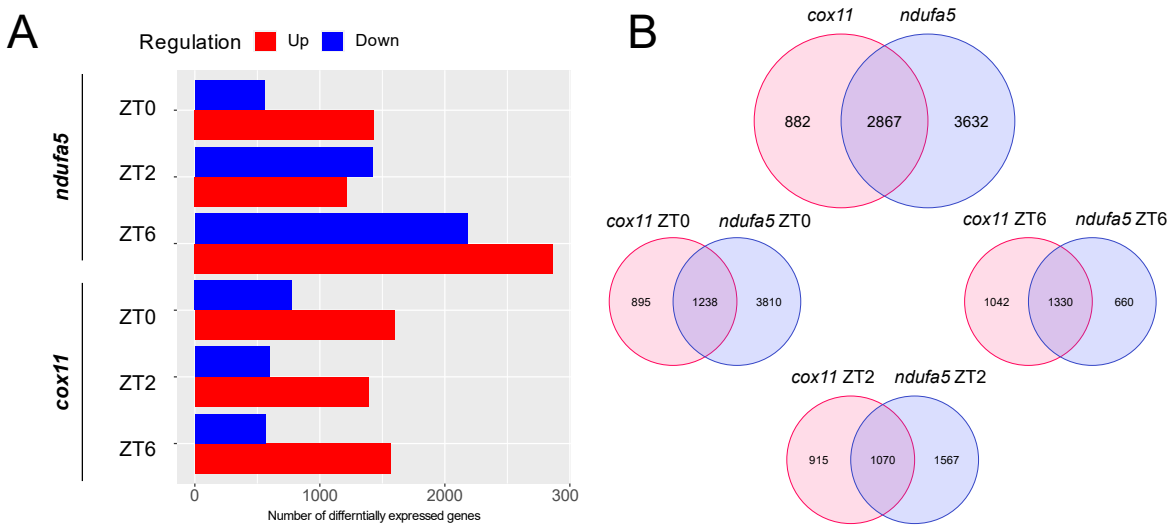

Figure 3.2 | **Comparison of differentially expressed genes (DEGs) between *cox11* and *ndufa5***. A) Bar plot showing the amount of significantly up- and downregulated genes at each condition. B) Venn diagrams showing the overlap of DEGs between genotypes at each condition.

We compared with further detail the profile of the DEGs at each condition between genotypes by performing pathway enrichment on the sets of DEGs and comparing the resulting lists, confirming the existence of relevant differences between *ndufa5* and *cox11* (Figure 3.3). In *ndufa5*, we observed a general repression of the photosynthetic

machinery by the end of night and the beginning of the day, which was no longer observed at ZT6. This affected both the components of the photosynthetic electron transport chain (Figure 3.3B, C; Supplementary Figure 3.1) and the multiple enzymes of the Calvin-Benson cycle (Supplementary Figure 3.2). There was also a general induction of the ribosomal machinery, in particular at ZT0 and ZT6 (Figure 3.3B, C; Supplementary Figure 3.1), which is essentially the opposite of what we described for *cox11* in CHAPTER II. We also identified an enrichment in ROS-responsive pathways, which included a set of small heat shock proteins that were induced only during day (Figure 3.3C). Not only photosynthetic carbon anabolism, but also glycolysis, and therefore carbohydrates catabolism, was repressed in *ndufa5* at ZT0 and ZT2 (Figure 3.3B; Supplementary Figure 3.2).

The transcriptomics data suggested a general repression of energetic metabolism during night and the beginning of the day. We gained more detail on this by looking also at the metabolome of *ndufa5* (Figure 3.4). At the end of the night (ZT0), *ndufa5* plants showed increased levels of four amino acids (glutamate, tyrosine, methionine, phenylalanine), N-Glycolyl-D-glucosamine and phosphoenol-pyruvate (PEP), the latter remaining at significantly higher levels also at ZT2. At ZT2 only, we found increased levels of the rubisco substrate ribulose-1,5-bisphosphate, as well as the secondary metabolite caffeic acid 3-glucoside. There was a large group of metabolites that were found at normal levels at the end of the night but accumulated specifically during the day, including: key intermediate metabolites of carbon metabolism such as pyruvate, 3-phosphoglycerate, citrate/isocitrate, sucrose, α-ketoglutarate and sedoheptulose-7-phosphate; xylonic acid, a likely derivative of the cell wall component xylose (X. Zhao et al., 2018); the amino acids aspartate and alanine; glucose-1,6-bisphosphate; myoinositol and gluconic acid. Remarkably, the levels of the glycolytic intermediate fructose-6-phosphate were always high in *ndufa5*. Some compounds accumulated at ZT0 and ZT6 but were not significantly different at ZT2, including glycerol-3-phosphate, trehalose-6-phosphate and N-acetylglucosamine 1-phosphate. At night, we found lower levels of fructose, malate, maleate, N-acetylglutamate, glutamine and fumarate. Fumarate remained significantly lower also at ZT2. During day there were lower levels of tyramine, and the sole metabolite to be always downregulated was threonate.

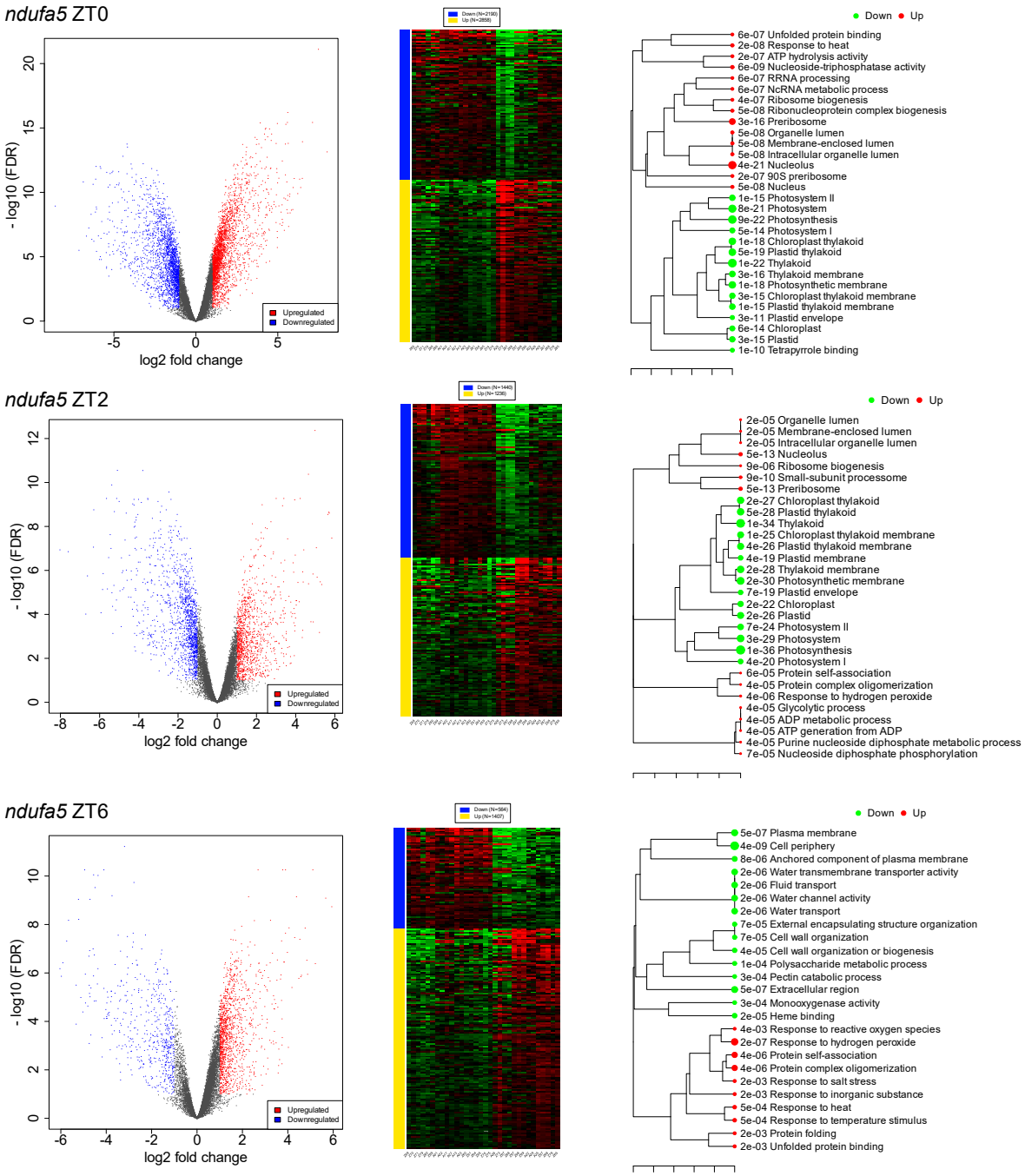

Figure 3.3 | **Overview of the DEGs in *ndufa5* segregated by zeitgeber times, and clustering of the enriched pathways**. For each zeitgeber time the figure includes the following items: i) a volcano plot showing data distribution and the number of significant DEGs; ii) a heatmap of the significant DEGs where lower and higher expression values are expressed in green and red, respectively; iii) a tree of the most significant enriched pathways, where pathways with many shared genes are clustered together, and bigger dots indicate more significant p-values.

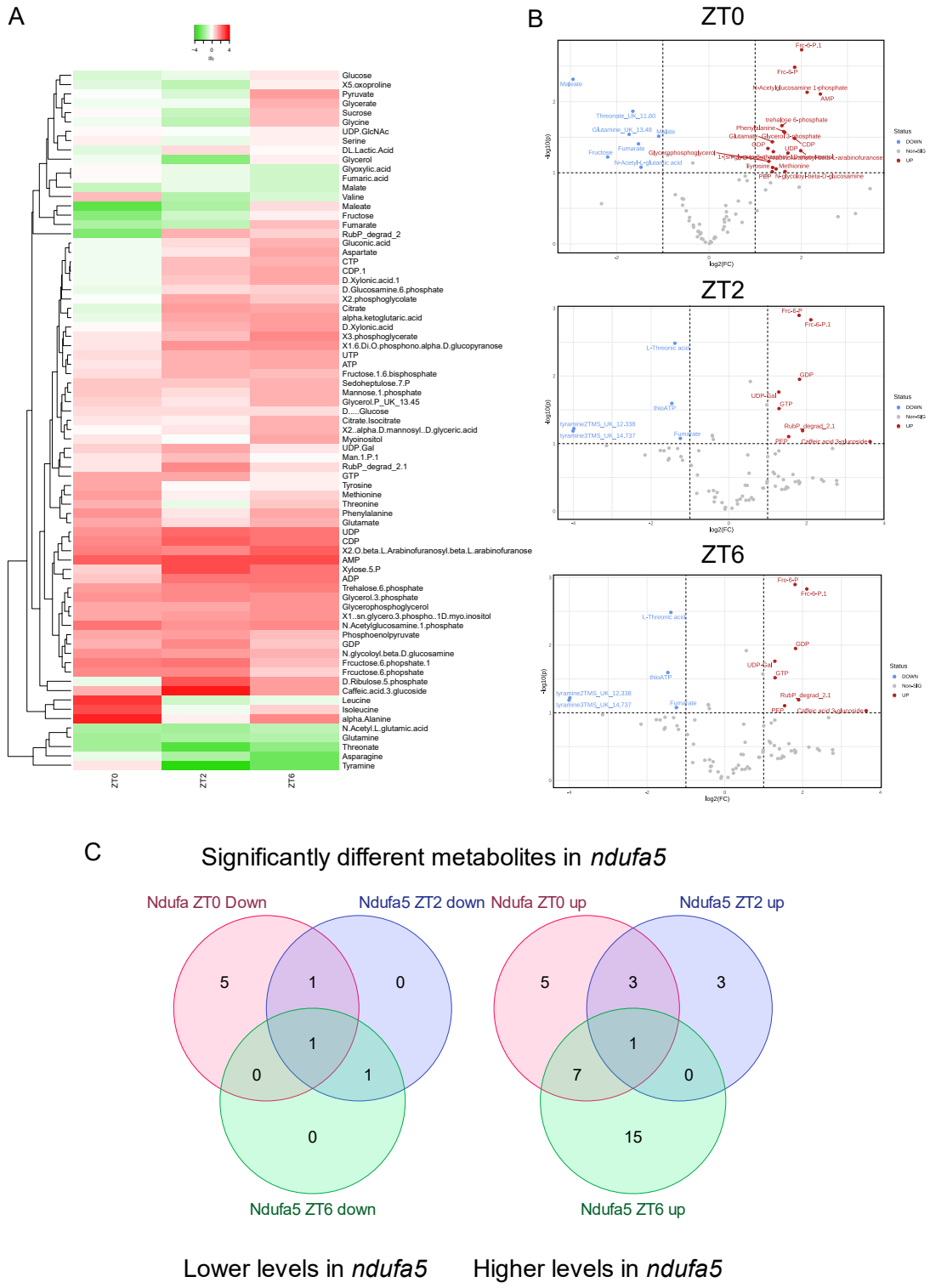

Figure 3.4 | **Overview of the time-resolved metabolome of *ndufa5* plants**. (A) Heatmap showing hierarchical clustering of compounds. (B) Volcano plots. (C) Venn diagram comparing the metabolites accumulated at higher or lower levels in *cox11* on different zeitgeber times, as shown in the volcano plots.

The pool of nucleotide phosphates of adenosine, guanine, cytidine and uracil was increased in *ndufa5* (Figure 3.4A). Regarding the pool of adenosine-5'-tri-, -di- and -monophosphates (ATP, ADP, AMP), all three species were significantly higher than WT at night (AMP) or day (ADP, ATP). As we discussed in CHAPTER II, the adenylate energy charge (AEC) is a more accurate parameter than absolute ATP levels for assessing the energy availability. Despite the increased adenylate pool, the AEC levels in *ndufa5* were always lower than WT, with the difference being significant at night and ZT6 (Figure 3.5A). This shows general depletion of available energy in *ndufa5*. Remarkably, *ndufa5* accumulated large starch granules in their chloroplasts and total cell extracts showed a large increase in starch compared to the WT (Figure 3.5B, C), showing that energy from light was stored but then was not mobilized for supply the cellular processes with ATP.

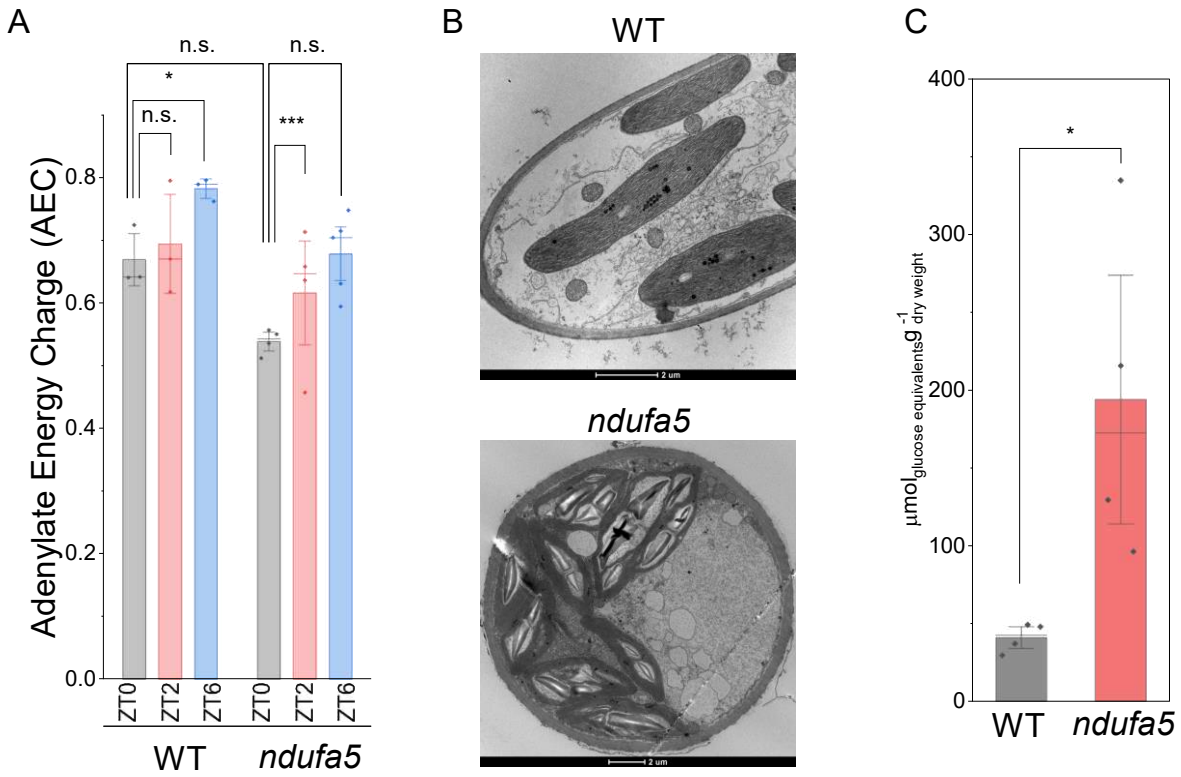

Figure 3.5 | **Adenylate energy charge (AEC) and starch accumulation in WT and *ndufa5***. A) AEC; B) Micrographs showing the transversal section of WT or *ndufa5* cells; C) Starch quantification on total extracts.

Consistent with the transcriptomic profile, the metabolic profile was also remarkably different in *ndufa5* compared to that of *cox11* described in CHAPTER II. The

general increase in amino acid content in *ndufa5* at night or day contrasts with the general shortage described in *cox11*. The levels of available energy at night were lower in *ndufa5* than in *cox11*, although the accumulation of starch was seen for both mutants (Supplementary Figure 3.3).

In summary, *ndufa5* at night showed a transcriptional repression of glycolysis and carbon fixation pathways, which however did not have a major impact in the content of the involved metabolites. The same pathways and the TCA cycle were instead transcriptionally induced at the middle of the day, causing the accumulation of some of their intermediary metabolites (Supplementary Figure 3.2).

2.2. Mitochondrial retrograde signalling (MRS) is activated in *ndufa5* but only at night

We previously quantified the protein levels of core subunits of all main five respiratory complexes and detected an accumulation of the core subunits of complexes II (SDH1) and III (MPP) (Mellon et al., 2021). Here, we monitored the expression levels of all the identified subunits of the respiratory complexes (Supplementary Figure 3.4). We could confirm a general and strong accumulation of Complex II subunit transcripts, as well as a moderate but significant accumulation of Complex III subunits transcripts. We also noticed a mild but significant accumulation of transcripts encoding for most of the nuclear encoded subunits of Complex I, especially at ZT0. There was a single exception to this, involving the gene Pp3c12_14210, which was always reduced to almost undetectable levels in *ndufa5* (Supplementary Figure 3.5). In *ndufa5* we also observed the induction of most genes that encode Complex IV subunits, which was always significant but stronger by night. Also, nuclear-encoded subunits of the Complex V were identified as upregulated, except for the ortholog of ATP5 (At4g09650/At5g13450), which was downregulated instead.

We also monitored the transcript levels of the alternative oxidase, AOX, which in *P. patens* is encoded by a single gene, Pp3c2_12680 (Neimanis et al., 2013). We previously found AOX protein to be highly overaccumulated in *ndufa5* (Mellon et al., 2021), which is consistent with published data from other Complex I deficient plants

(Brangeon et al., 2000; De Longevialle et al., 2007; Dutilleul et al., 2003; Fromm et al., 2016; Juszczuk et al., 2007; Meyer et al., 2009). We here monitored the time-resolved expression of the PpAox gene (Figure 3.6). PpAox transcript levels were always detected in *ndufa5* at higher levels than WT, but its accumulation was extreme at ZT0 (more than 20 times the WT value), and much less pronounced during the day (ZT2 or ZT6). We also observed the transcript levels of PpAox in the Complex IV mutant *cox11*, where it was significantly induced at the middle of the day (ZT6), but to a degree much smaller than the one observed for *ndufa5* at night (Figure 3.6).

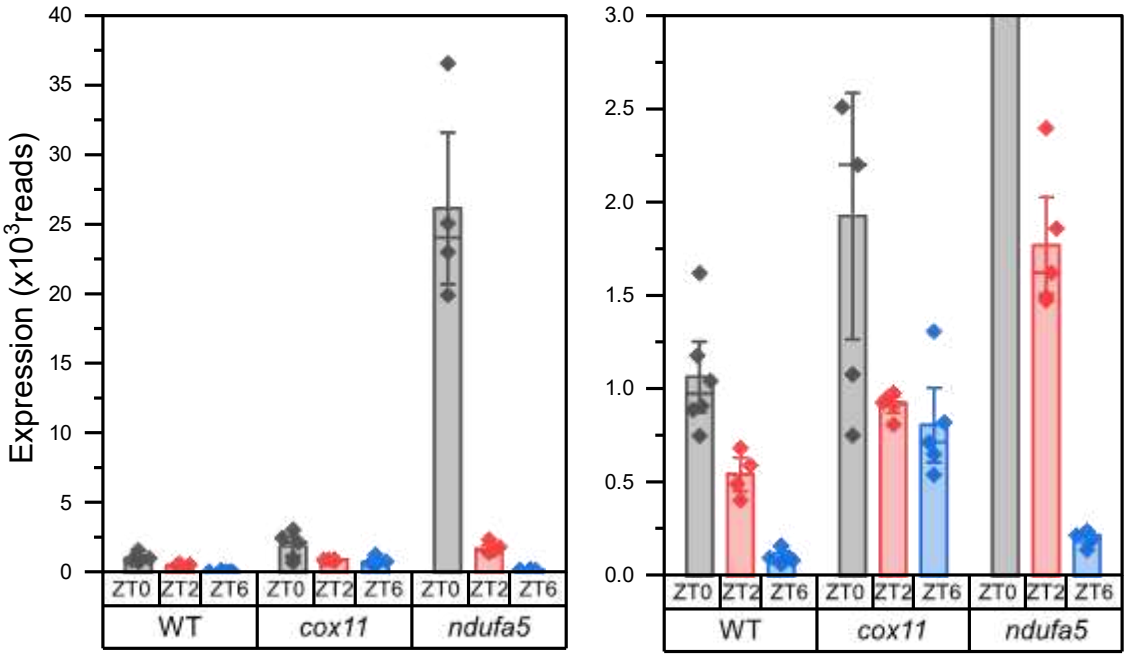

Figure 3.6 | **PpAox expression levels in WT, *cox11* and *ndufa5***. Graph on right shows zoomed version of the graph on left.

2.3. An ortholog of AtANAC017 is likely inducing MRS in *ndufa5* at ZT0

2.3.1. Description of the approach for identifying MRS

As we discussed in the Introduction, the transcriptional induction of the alternative oxidase is one of the early events observed after activation of mitochondrial retrograde

signalling pathway. Data described so far suggest the possibility that mitochondrial retrograde signalling pathways could be activated in *ndufa5* at night, but not during day.

To investigate this hypothesis, we aimed to identify one or more molecular candidates acting upstream of the Aox induction that could be linked to a mitochondrial retrograde signalling (MRS) pathway. We are not aware of any experimental studies regarding MRS pathways in *P. patens*, and most of the information that has been produced regarding MRS in plants used *Arabidopsis thaliana* as the experimental model. Therefore, we analysed the transcriptome of *ndufa5* at ZT0 aiming to identify signatures that could be linked to the activation of one or more retrograde signalling pathways in *ndufa5*, using the available experimental knowledge obtained in other plant models.

2.3.2. Myb29, Myb91 and Abi4 do not have orthologs in *P. patens*

MYB is a big family of transcription factors in eukaryotes and present in plants, including *P. patens*, which has 116 Myb genes (Pu et al., 2020). Two members of the MYB family have been experimentally proved to be essential for the induction of Aox1a in Arabidopsis during MRS: MYB29/RAO7 (Zhang et al., 2017) and MYB91/RAO5 (Ivanova et al., 2014). We could not identify any orthologs of the AtMyb91 gene in *P. patens* by BLAST search in Phytozome. On the other hand, the Arabidopsis Information Resource (TAIR) includes five orthologs of AtMyb29 in *P. patens* (Pp3c7_23490, Pp3c6_9970, Pp3c7_23490, Pp3c6_9970, Pp3c7_23490), but none of them was expressed at significant levels in our RNAseq dataset (i.e. >50 reads in at least one condition), and indeed they were not identified by ortholog search in Phytozome. Therefore, MYB transcription factors are likely not responsible of MRS in *ndufa5*.

ABI4 (ABA Insensitive 4) is another transcription factor that has been shown to regulate the retrograde expression of AtAox1a gene (Giraud et al., 2009). ABI4 binds to the promoter region of AtAox1a and acts as a repressor; in response to mitochondrial dysfunction or stress signals, ABI4 becomes activated and leads to the activation of AtAox1a (Giraud et al., 2009). ABI4 is a member of the large family of Apetala2/Ethylene-responsive element binding protein (AP2/EREBP). In Arabidopsis, ABI4 is the only member of a AP2/EREBP subfamily characterized by containing the conserved ABI4

motif, defined by the residue sequence LRPLLPRP (Gregorio et al., 2014; Wind et al., 2013). Sequence analyses have shown that *P. patens* does not contain any orthologs of ABI4 (Khan & Van Aken, 2022; Wind et al., 2013). Therefore, it is not a good candidate for mediating MRS in *ndufa5*.

In summary, the genome of *P. patens* does not contain any clear orthologs of the transcription factors MYB91 or ABI4, and none of the five orthologs of MYB29 is significantly expressed in *ndufa5*. Consequently, these proteins are likely not involved in the activation of MRS in *ndufa5*.

2.3.3. AtWRKY15 has orthologs in *P. patens*, but a WRKY15-mediated response is not detected in *ndufa5*

Another family of transcription factors that has been related to MRS is that of WRKY proteins (Shang et al., 2010; Van Aken et al., 2013). The WRKY family of transcription factors includes both repressors and activators of genes involved in the MRS response (Dojcinovic et al., 2005; Van Aken et al., 2013). This family can be found through all the viridiplantae clade (Chen et al., 2019), and their components are classified in different groups (I, IIa, IIb, III) according to the characteristics of the protein domains that they include (Bakshi & Oelmüller, 2014). The main WRKY factors related to MRS in Arabidopsis are WRKY18, WRKY40 and WRKY60, all of them included in the IIa group, which has no orthologs in *P. patens* (Khan & Van Aken, 2022).

The only member of the WRKY family in Arabidopsis that has homologs in *P. patens* is WRKY15, part of the group IIb (Khan & Van Aken, 2022). Previous studies showed that expression of AtWrky15 can be induced by reactive oxygen species (ROS) (Eulgem et al., 2000; Vanderauwera et al., 2005), exposure to low CO_2 or salt stress (Vanderauwera et al., 2012) or treatment with the inhibitors of mitochondrial Complex III myxothiazol or antimycin A (Zhu et al., 2022). The transcriptome of Arabidopsis lines constitutive overexpressing AtWrky15 included a group of genes that were constitutively upregulated, which are likely targets of the transcription factor activity of WRKY15. These genes in part overlap with genes upregulated during the unfolded protein response in the endoplasmic reticulum (UPR^{ER}) and include some of the so-called mitochondrial

dysfunction regulon genes (Vanderauwera et al., 2012), considered components of the MRS pathway (Rhoads & Subbaiah, 2007; Van Aken et al., 2007). Therefore, AtWRKY15 has also been linked to the activation of MRS (Vanderauwera et al., 2012).

In *P. patens*, four genes encode WRKY proteins evolutionary close to AtWRKY15 (Supplementary Table 3.1; Khan & Van Aken, 2022; Mohanta et al., 2016). One of these genes, PpWrky74, is not expressed at significant levels in our dataset, and therefore either it is a pseudogene or it gets induced upon stimuli not tested by us. The other three genes, PpWrky15, PpWrky21-1 and PpWrky21-3, are expressed at significant levels, and therefore they are candidates of mediating a stress response also in *P. patens*.

In case the PpWRKY15 proteins were active in *ndufa5*, we would expect the transcriptome of *ndufa5* to overlap at some degree with the transcriptome of Arabidopsis transgenic lines overexpressing AtWrky15. To test this hypothesis, we retrieved a list with the genes in *P. patens* orthologs of the 598 genes identified as constitutively upregulated in Arabidopsis lines that overexpressed AtWrky15 (Vanderauwera et al., 2012). Only a 12 % of the corresponding orthologs in *P. patens* were significantly upregulated in *ndufa5* at ZT0 (Figure 3.7). The percentage of overlap between the transcriptome of *ndufa5* and AtWrky15 overexpressors was thus low, and the overlapping genes could be convergence points of different signalling pathways.

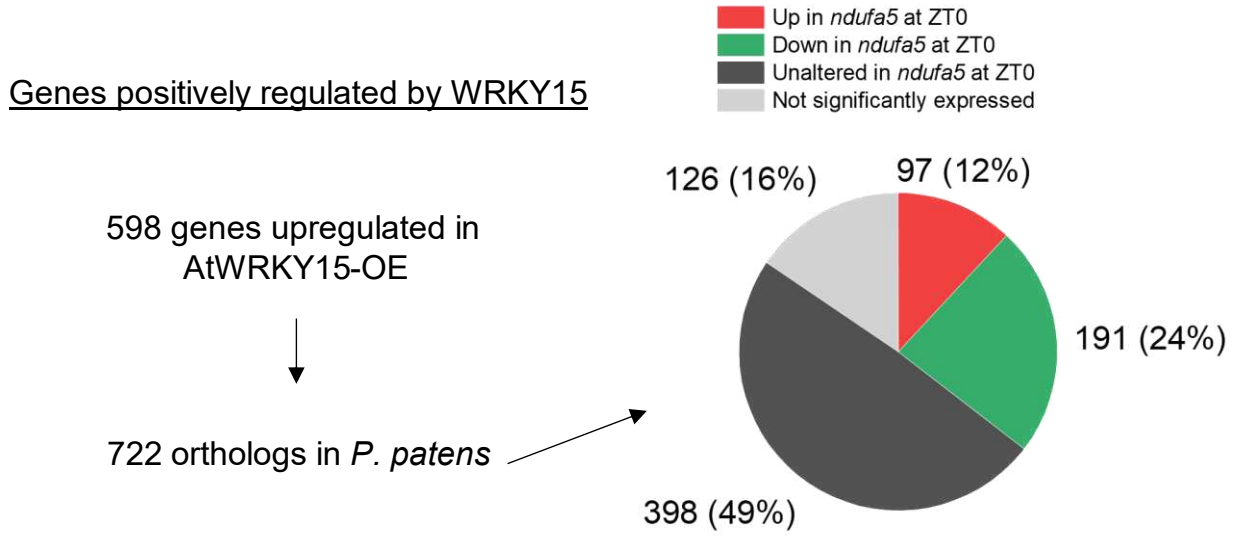

Figure 3.7 | Comparison of *ndufa5* transcriptome at ZT0 and orthologs of genes positively regulated by WRKY15. Genes upregulated in Arabidopsis overexpressors of WRKY15 were retrieved from Vanderauwera et al., 2012. Orthologs in *P. patens* were retrieved from Phytozome.

In conclusion, two orthologs of AtWRKY15 are expressed in *P. patens*, but the transcriptome of *ndufa5* plants does not support the hypothesis of WRKY15 being the main responsible of the hypothesized activation of MRS.

2.3.4. CDKE;1 has orthologs in *P. patens* and is a candidate for inducing MRS in *ndufa5*

Another candidate that we considered as a possible regulator of MRS in *ndufa5* plants was the cyclin dependent kinase CDKE;1, which was identified as the first essential component upstream of AtAox1a induction upon mitochondrial stress in Arabidopsis (Ng, Giraud, et al., 2013). In plants, CDKE;1 has been proposed to locate at the interface between mitochondrial and chloroplast retrograde signalling (Blanco et al., 2014).

In contrast with all the other regulators that we considered so far, CDKE;1 is not a transcription factor, but an interactor of the metabolic regulator SnRK1 complex, which is functional also in *P. patens* (Peixoto & Baena-González, 2022; Thelander et al., 2004, 2007). 2 orthologs of AtCdke;1 have been identified in *P. patens*, Pp3c19_12350 and Pp3c22_16110 (Khan & Van Aken, 2022), and therefore are candidates for exerting the role of CDKE;1 in relaying the MRS signal in *P. patens*. Following the same approach described for WRKY15, we compared the transcriptome of *ndufa5* plants with a list of genes reported to be positively regulated by CDKE;1 in response mitochondrial stress (Ng, Giraud, et al., 2013). The 337 genes of Arabidopsis retrieved 208 orthologs in *P. patens*, of which a 33 % was significantly upregulated in *ndufa5* at ZT0 (Figure 3.8). In contrast with what we observed for WRKY15, the percentage of overlap in this case was relatively high, with almost half of the significantly expressed orthologs defined as CDKE;1-induced in Arabidopsis being also induced in *ndufa5* at ZT0. It is true that approximately half of the orthologs were not regulated or even downregulated in *ndufa5* at ZT0, but we must consider that we are comparing relatively large lists of orthologs retrieved by sequence similarity and not filtered or verified through experimental approaches.

Overall, our observations are compatible with CDKE;1-mediated signalling being involved in the induction of a MRS response in *ndufa5* at ZT0.

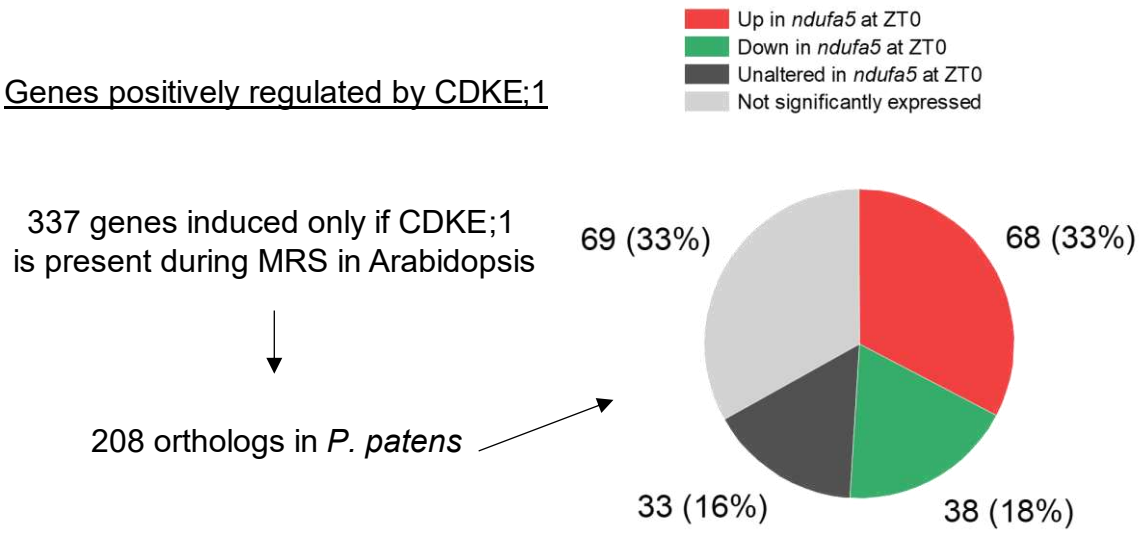

Figure 3.8 | Comparison of *ndufa5* transcriptome at ZT0 and orthologs of genes positively regulated by CDKE;1 during mitochondrial retrograde signalling. Gene list was retrieved from Ng, Giraud, et al., 2013. Orthologs in *P. patens* were retrieved from Phytozome.

2.3.5. Members of the ANAC family and RCD1 are present in *P. patens*, and they are good candidates for inducing MRS in *ndufa5*

Another couple of transcription factors that must be considered in our analyses is that of ANAC013 and ANAC017. The transcription factor ANAC017 was identified as mediator of MRS induction in Arabidopsis (Ng, Ivanova, et al., 2013), and is currently considered to be the most important pathway in MRS induction (Kacprzak et al., 2020; Khan & Van Aken, 2022). It has been recently related to the reorganization of the respiratory chain in response to hypoxia and reoxygenation (Jethva et al., 2023).

ANAC017 is a protein that has a transmembrane domain that anchors it to the membrane of the endoplasmic reticulum (Ng, Ivanova, et al., 2013). The activity of upstream signalling molecules induces, through a mechanism that is not yet clearly defined, the proteolysis of ANAC017 by a rhomboid protease (Ng, Ivanova, et al., 2013). The cleaved version of ANAC017 is now soluble and capable of reaching the nucleus, where it physically interacts with DNA and serves as a transcription factor, inducing the expression of several genes (Ng, Ivanova, et al., 2013). A specific motif has been identified in the promoter of some of the genes that are induced by ANAC017 that works as a cis-regulatory element (De Clercq et al., 2013). Among the genes induced by ANAC017, there is the related transcription factor Anac013, which shares most of the

target genes with ANAC017 and serves as a positive feedback regulator (De Clercq et al., 2013).

Both ANAC013 and ANAC017 are members of the large family of NAC transcription factors ([no apical meristem (NAM), Arabidopsis transcription activation factor (ATAF1/2), and cup-shaped cotyledon (CUC)]). In *P. patens*, 35 genes of the NAC family have been identified (Pereira-Santana et al., 2015), and some of them have been defined as essential for *P. patens* development (Xu et al., 2014). 23 out of the 35 NAC genes were detected at significant levels in our dataset and, interestingly, 10 were significantly upregulated in *ndufa5* at ZT0 (Supplementary Table 3.2). These 10 genes include the 4 genes previously identified as orthologs of AtAnac017 in *P. patens* (Khan & Van Aken, 2022), of which 3 (Pp3c20_18130, Pp3c23_9520, Pp3c24_8270) are predicted to contain the transmembrane domain which is required for attachment of ANAC017 to the membrane of the ER (Khan & Van Aken, 2022) and are therefore good candidates for encoding functional ANAC017 homologs.

The mechanism of action of ANAC017 imposes that the protein must be present in the cell in control conditions (i.e. when retrograde signalling is not activated), serving as a latent and readily-activable signalling agent that is kept inactive by the attachment to the ER membrane (Ng, Ivanova, et al., 2013). Therefore, we expect the transcript levels of Anac017 candidates to be detectable even under non-stress conditions. This was indeed the case of the orthologs identified in *P. patens* (Figure 3.9A). In Arabidopsis, the Anac017 transcript levels were slightly higher at night than during day (Zhu et al., 2022), and we verified this also in three of the orthologs of *P. patens* (Supplementary Figure 3.6). The only exception was Pp3c23_9520, that was the isoform expressed at lower levels. Interestingly, the transcription of all ANAC017 orthologs was also induced in *ndufa5* at ZT0 (Figure 3.9A). Although this induction has not been shown in Arabidopsis for ANAC017 itself (Meng et al., 2019; Ng, Ivanova, et al., 2013), it has been reported for other related ANAC proteins that act as additional positive feedback regulators, such as ANAC013, ANAC053 or ANAC016 (Broda et al., 2021; van Aken et al., 2016).

Therefore, from this *in silico* analysis, we conclude that there are three good candidates of having ANAC017 function in *P. patens*. The fourth candidate, Pp3c8_6080,

which is also transcribed at high levels and strongly induced in *ndufa5* at ZT0 but lacks the transmembrane domain, could have a role as a positive regulator of the response, like it has been shown for AtANAC053, which also lacks the transmembrane domain (Khan & Van Aken, 2022; van Aken et al., 2016).

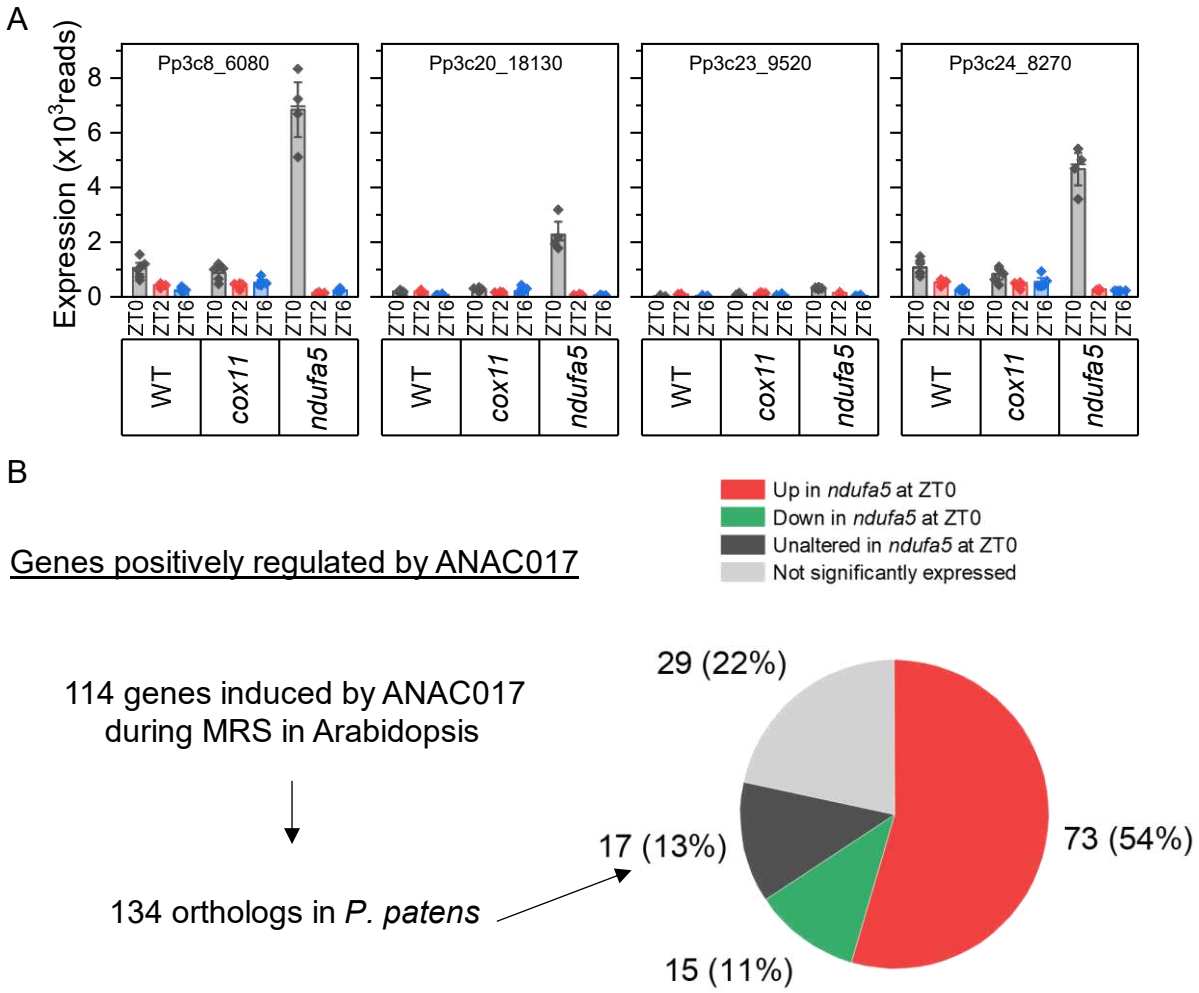

Figure 3.9 | Expression levels of ANAC homologs in P. patens and comparison of *ndufa5* transcriptome at ZT0 and orthologs of genes positively regulated by ANAC017 during mitochondrial retrograde signalling. A) Expression levels for the four genes identified as homologs of ANAC017. A detailed version of the graph is available as **Supplementary Figure 3.6**. B) Comparison of genes positively regulated in *ndufa5* and ANAC017-regulated genes retrieved from Ng, Ivanova, et al., 2013. Orthologs in *P. patens* were retrieved from Phytozome.

To verify whether the ANAC017 pathway could be active in *ndufa5* at ZT0, we compared the list of induced transcripts in *ndufa5* at ZT0 with a list of 114 Arabidopsis genes induced during retrograde signalling in an ANAC017-dependent manner (Kacprzak et al., 2020). 54 % of the orthologs in *P. patens* were upregulated in *ndufa5* at ZT0, and

the percentage becomes 70 % if we omit the orthologs that were not detected at significant levels in our RNAseq (Figure 3.9B). We retain this percentage of overlap between the gene lists relevantly high, which strongly supports the idea that ANAC017 could be involved in the response of *ndufa5* observed at night but not during day.

We could identify more evidence that supports our hypothesis. Arabidopsis lines overexpressing a truncated version of ANAC017 that lacks the transmembrane domain and is therefore constitutively active have a strong growth retardation had smaller cells and an overall reduction of mass of over 50 % the WT (Meng et al., 2019), which is relatively similar to the phenotype described for *ndufa5* plants (Mellon et al., 2021). The transcriptome of these Arabidopsis ANAC017-overexpressing plants showed an induction of ribosome biogenesis and a repression of photosynthesis, carbon fixation and carbohydrate catabolism (Meng et al., 2019), which is very similar to what we observed in *ndufa5* at ZT0.

Although the mechanism by which ANAC factors are activated and released in response to a stress is not well understood, rhomboid-like proteases have been proposed as required for the cleavage and release of the factor from the membrane of the endoplasmic reticulum (Ng, Ivanova, et al., 2013). Recently, ANAC013 in Arabidopsis was shown to be cleaved and activated in response to hypoxia through the protease Rhomboid-like 2 (RL2) (Eysholdt-Derzsó et al., 2023). In Arabidopsis, 16 rhomboid-like genes have been identified (Adam, 2013; Knopf & Adam, 2012), and we could identify 11 orthologs of these in *P. patens* (Supplementary Table 3.3).

Another component related to the ANAC017-mediated MRS is the nuclear protein RCD1, which in Arabidopsis it represses ANAC017 (Tao et al., 2023) and plays a role in turning off the positive feedback loop of ANAC013, ANAC017 and other related transcription factors (Shapiguzov et al., 2019). AtRcd1 is included in the list of genes that are induced through an ANAC017-dependent manner during MRS (Kacprzak et al., 2020; Ng, Ivanova, et al., 2013). We could identify three orthologs of AtRcd1 in *P. patens* and all of them are expressed at significant levels in our RNAseq dataset. Moreover, all three are significantly induced in *ndufa5* at ZT0 (Supplementary Table 3.4).

Therefore, we showed evidence of *P. patens* having a complete and functional machinery for ANAC017-mediated retrograde signalling, including three ANAC017 homologs, several orthologs of the rhomboid proteases linked to ANAC017 activation and at least one negative regulator (RCD1). These data suggest that the ANAC017-based MRS system exists in *P. patens*, is likely active and is likely involved in the induction of MRS pathways in *ndufa5* specifically by the end of the night, but not during day.

2.4. Stress signalling markers not MRS-specific

We have found evidence of a possible induction of MRS through ANAC017. However, it is possible that, besides the ANAC017-mediated pathway, other signalling pathways are active in *ndufa5* plants. Therefore, we further analysed our RNAseq data looking for transcriptomic signatures that could be related to the activation of one or more general stress signalling pathways.

2.4.1. Is H_2O_2 the signal inducing mitochondrial retrograde signalling?

We showed that CDKE;1 and/or, most likely, ANAC017 are the master regulators that induce the expression of several genes in response to a stress signal emitted by *ndufa5* mitochondria at the end of the night. However, we do not have information regarding the identity of this signal. There is little evidence about the metabolites that could act as signals for inducing MRS in plants, but both 3′-phosphoadenosine 5′-phosphate (PAP) (De Souza et al., 2017) and ROS, in particular H_2O_2 (Møller & Sweetlove, 2010), have been proposed.

In plants, PAP has been suggested to be involved in chloroplast-to-nucleus retrograde signalling, and this has been experimentally proven true also for *P. patens* (Estavillo et al., 2011; C. Zhao et al., 2019), but so far there is no evidence of its role in mitochondrial retrograde signalling. On the other hand, there is a good amount of literature that supports ROS as relevant players during induction of retrograde pathways. For instance, the induction of Aox after treatment with Antimycin A in tobacco cell cultures was abolished by scavenging superoxide $O_2^{\cdot-}$, although scavenging H_2O_2 and $OH\cdot$ did not have the same effect (Vanlerberghe et al., 2002). The same system provided insights in

protein dephosphorylation being involved at some level in the transduction pathway (Vanlerberghe et al., 2002). However, the induction of Aox occurred faster in response to Antimycin A than in response to H_2O_2, and the accumulation of ROS was slower than the induction of Aox upon Antimycin A treatment (Maxwell et al., 2002), questioning whether H_2O_2 or other ROS were indeed the first messengers involved in Aox induction. In the maize mitochondrial mutants NCS2, which also accumulate Aox, an increase in H_2O_2-responsive transcripts was observed; however, it could not be demonstrated that H_2O_2 or other ROS induced Aox directly (Karpova et al., 2002). In Arabidopsis, the ANAC017 response could be induced by treatment with H_2O_2, but the details on the precise mechanism are still missing (Ng, Ivanova, et al., 2013).

With this information, we checked for ROS-specific signatures in the transcriptome of *ndufa5*. We retrieved a list of 11 genes described as H_2O_2-induced in Arabidopsis (Vaahtera et al., 2014), that we converted into 22 unique orthologs in *P. patens* (Supplementary Table 3.5). Of these, 15 were detected at significant levels in our dataset and 11 (73 %) were significantly upregulated in *ndufa5* at ZT0 (Supplementary Table 3.5). However, for most of them the upregulation was maintained through the day, which would mean that either i) H_2O_2 is produced always but is capable of triggering MRS only at ZT0, due to the interplay of different cellular processes such as the circadian clock, which can modulate the ANAC017-mediated response (Zhu et al., 2022); ii) H_2O_2 is produced always and therefore the induction of MRS in *ndufa5* at ZT0 relies on another player; or iii) these marker genes are not a good proxy for inferring H_2O_2 levels in *P. patens*.

Therefore, with the data we have, we cannot confidently propose or discard reactive oxygen species to be at the source of the mitochondrial retrograde signalling pathway induced in *ndufa5* at ZT0.

2.4.2. An Unfolded Protein Response (UPR^{ER}) is not detected in *ndufa5*

The effectors and regulators of the UPR^{mt} in plants have been poorly studied, in contrast with other biological systems such as mammals or yeast, and the UPR^{mt} has been shown to largely overlap with the general mitochondrial retrograde response mediated by ANAC017 (Kacprzak et al., 2020).

On the other hand, some genes that are transcriptionally upregulated during UPR^{ER} in *P. patens* have been identified (Lloyd et al., 2018). Only 2 of the 12 genes were significantly induced in *ndufa5* at ZT0 (Supplementary Table 3.6). Therefore, we conclude that our transcriptomics data does not support the hypothesis of UPR^{ER} being significantly activated in *ndufa5* at ZT0 (nor ZT2 or ZT6).

2.4.3. Chloroplast retrograde signalling (CRS) pathways are likely not induced in *ndufa5*

As we described earlier, genes involved in photosynthesis (both light reactions and carbon fixation reactions) are strongly repressed at ZT0 and ZT2 in *ndufa5* mutants. We hypothesized that at ZT0 there is the activation of ANAC017-mediated retrograde signalling. There is increasing evidence that ANAC017 could act at the interface between mitochondria and chloroplasts, integrate signals emitted from both organelles and elaborating a coordinate response (Kleine & Leister, 2016; Shapiguzov et al., 2019; Zhu et al., 2022), and therefore ANAC017 could be the responsible of the photosynthetic repression that we reported. However, we cannot ignore that the repression of photosynthesis-associated nuclear genes (PhANGs) is a typical marker of chloroplast retrograde signalling (Mielecki et al., 2020; Nott et al., 2006). Therefore, we considered the hypothesis of canonical pathways of chloroplast retrograde signalling being activated in parallel with ANAC017.

Chloroplast retrograde signalling (CRS) can be mediated by different metabolites, upon biotic or abiotic stresses (Kleine & Leister, 2016), and induces a transcriptomic response regulated by different master regulators. A well-studied system for CRS is the SAL1-PAP pathway (Kleine & Leister, 2016; Litthauer et al., 2018). In this system, upstream signals can impair the activity of the enzyme SAL1, causing to the accumulation of its substrate PAP, which inhibits XRN 5′→3′ exoribonucleases in the nucleus and therefore modulates gene expression (Chan et al., 2016; Estavillo et al., 2011; Litthauer et al., 2018; Pornsiriwong et al., 2017). The key component of the system, the enzyme SAL1, is present also in *P. patens*, and PAP-treated *P. patens* plants show markers of stress response induction, confirming that the SAL1-PAP pathway is active also in *P. patens* (C. Zhao et al., 2019).

The SAL1-PAP-XRN system is convergent with abscisic acid (ABA) signalling (Phua et al., 2018; Pornsiriwong et al., 2017). The ABA signalling system is present in *P. patens* and ABA has a confirmed role as a hormone in this organism (Arif et al., 2019; Stevenson et al., 2016; Timmerhaus et al., 2011). We monitored the expression pattern of genes previously shown to be induced by exposure to ABA in *P. patens* but we could not observe a general upregulation of these genes in *ndufa5* (Supplementary Table 3.7). The protein COR413, localized in chloroplast of *P. patens*, has been shown to regulate changes in growth changes during stress through ABA signalling, and might be involved in chloroplast retrograde signalling (Ruibal et al., 2020). It is encoded by the gene Pp3c7_22090, whose expression is induced during its activity (Ruibal et al., 2020). This gene was not induced in *ndufa5* (Supplementary Table 3.7), further supporting the idea of ABA signalling not being active in *ndufa5* and making it unlikely that the SAL1-PAP is active either.

We therefore looked for evidence supporting the activation of one or more of the most well-known regulators of CRS in plants: GUN1, PRL1/EX1 and MPK6 (Baruah et al., 2009; Colombo et al., 2016; Kleine & Leister, 2016; Vogel et al., 2014).

AtGun1 has a single ortholog in *P. patens*, encoded by the gene Pp3c5_16950 (Honkanen & Small, 2022). In the liverwort *Marcanthia polymorpha*, evolutionary close to *P. patens* (Naramoto et al., 2022), GUN1 does not play a relevant role in CRS (Honkanen & Small, 2022) and therefore, it is likely that this is the case also for *P. patens*. Accordingly, GUN1 is thought to have acquired the role of integrator of signals and mediator of CRS later in evolution (Honkanen & Small, 2022).

Another known inductor of CRS is singlet oxygen (Li et al., 2022), a type of ROS generated during photosynthesis mainly at the antenna complex of photosystem II (Triantaphylidès & Havaux, 2009). Among the first mediators of the cascade triggered by singlet oxygen, there are the proteins EX1 and PRL1, the latter being activated downstream of the first (Baruah et al., 2009; Dogra et al., 2017; Keun et al., 2007). Both proteins have orthologs in *P. patens* (Supplementary Table 3.8), and therefore are considered for further analysis. The effect of the EX1/PRL1 cascade is the induction of expression of the so-called singlet oxygen responsive genes (SORGs) (Danon et al.,

2006). We retrieved a list of 160 SORGs from experimental assays in Arabidopsis (Dogra et al., 2017) that we could convert into 151 orthologs in *P. patens*, of which a 16 % was significantly induced in *ndufa5* at ZT0 (Figure 3.10). These include 5 small heat shock proteins, which are likely induced by other signalling mechanisms, and 6 are overlapping with the ANAC017-responsive genes. Overall, these results do not support a singlet oxygen dependent response in our plants, nor a PRL1/EXECUTER1-mediated induction of CRS.

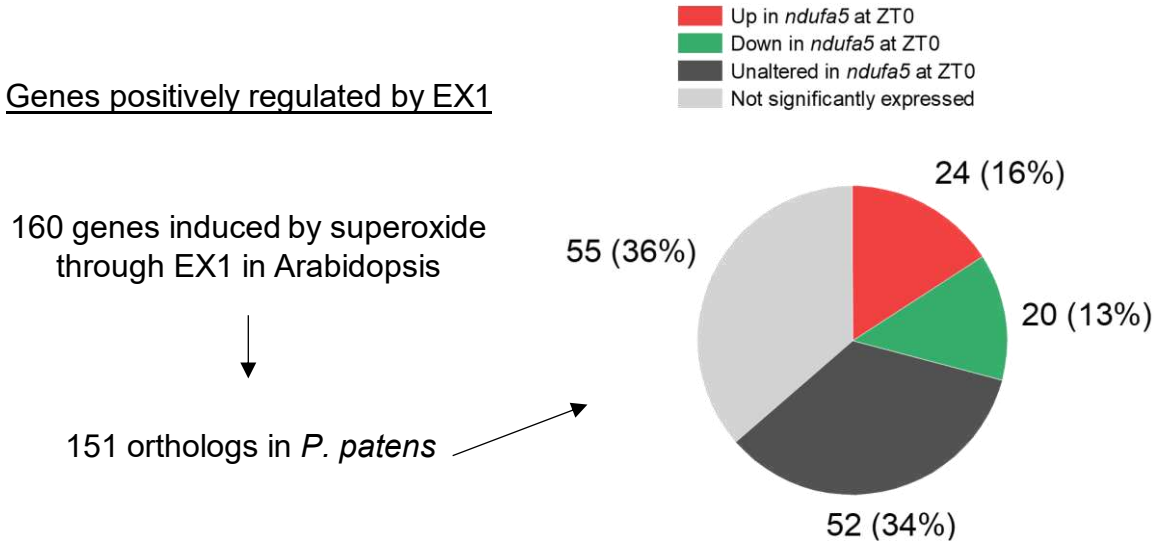

Figure 3.10 | Comparison of *ndufa5* transcriptome at ZT0 and orthologs of superoxide-responding genes positively regulated by EX1. Gene list was retrieved from Dogra et al., 2017. Orthologs in *P. patens* were retrieved from Phytozome.

A further known effector of CRS is MPK6, a member of the AP2 family (Kleine & Leister, 2016; Vogel et al., 2014). In response to high light, MPK6 gets activated and induces the transcription of some factors such as ERF6 (Vogel et al., 2014). ERF6 has 9 orthologs in P. patens, but none of them are induced in *ndufa5* at ZT0 (Supplementary Table 3.9). Apparently, MPK6 is a downstream effector of the GUN1-regulated pathway, which also requires ABI4 (Guo et al., 2016; Koussevitzky et al., 2007; Sun et al., 2011). As we discussed, *P. patens* does not have ABI4 homologs, so this pathway must be discarded.

In conclusion, even if the observe a general repression of photosynthesis-associated nuclear genes (PhANGs) in *ndufa5*, which is a typical marker of chloroplast retrograde signalling, we could not identify any good candidates to be considered as

effectors in *P. patens*. Therefore, we could not confidently detect the activation of any CRS pathway in *ndufa5* plants.

3. Discussion

3.1. Metabolic alterations of *ndufa5* are different of those described for *cox11*

We previously presented a set of mutants in *P. patens* depleted in the respiratory Complex I, *ndufa5* and *ndufb10* (Mellon et al., 2021). Both mutants had a severe growth impairment even in fully autotrophic conditions, demonstrating that respiration is essential for photosynthesis to work efficiently. At the protein level, we described alterations in the stoichiometry of the respiratory chain, but not in the photosynthetic apparatus (Mellon et al., 2021). Complex I mutants had likely an increased activity of the chloroplast ATPase, which translated in a higher activity of both photosystems PSI and PSII (Mellon et al., 2021).

In Chapter II of this thesis, we presented and characterized a newly isolated line of *P. patens* with a completely inactivated Complex IV, *cox11*. Despite showing a strong growth impairment, the phenotype of *cox11* plants was largely divergent with that previously described for *ndufa5* plants. Although growth was reduced in both plants, the phenotype of *ndufa5* was in general more severe. Given sufficient time *cox11* plants outperformed *ndufa5* and were able to grow more biomass. Also, the growth defects in *cox11* could be partially rescued by growing the plants on medium enriched with glucose as an external source of reduced carbon, which was not the case for *ndufa5* (Mellon et al., 2021).

The aim of this work was to further characterize the consequences of the depletion of Complex I in *P. patens* using information obtained from transcriptomic and metabolomic approaches. Since the phenotype of the two independent lines were indistinguishable, confirming that the phenotype of both *ndufa5* and *ndufb10* was linked to the loss of Complex I and not to a gene-specific feature (Mellon et al., 2021), we here focused on only one of the lines, *ndufa5*. In this Chapter we also aimed to focus on the differences between the two related mutants *ndufa5* and *cox11*. The difference that was observed at the macroscopic level between *ndufa5* and *cox11* mutants could be observed also at the molecular level, by comparing their transcriptomic and metabolic profiles.

The photosynthetic machinery and the components of the Calvin-Benson cycle were significantly repressed in *ndufa5* during night and, more strikingly, they remained repressed also after two hours of exposure to the light, when they are expected to be induced. By the middle of the day, transcript levels returned to normal values. Despite the transcriptomic alteration, in the past we did not find significant differences in pigment levels or protein composition of the photosynthetic machinery, except for an accumulation of the chloroplast ATPase (Mellon et al., 2021). Accordingly, the photosynthetic performance of *ndufa5* was not significantly impaired but for an altered regulation of chloroplast ATPase (Mellon et al., 2021). In *cox11*, the transcriptomic repression of the photosynthetic machinery was not observed, and consistently photosynthetic properties were maintained with WT (CHAPTER II).

On the other hand, we also detected in *ndufa5* a general transcriptomic repression of central carbon catabolism, with many genes encoding for enzymes of glycolysis detected at lower levels at night and at the beginning of the day. In *cox11*, the downregulation of glycolytic enzymes was less evident (CHAPTER II). Despite the transcriptomic repression, in *ndufa5* we did not find lower levels of intermediates of carbon metabolism, which was instead observed in *cox11* plants (CHAPTER II). Intermediary metabolites of glycolysis were actually over-accumulated in *ndufa5* during the day. Alterations in nitrogen metabolism could also be observed in *ndufa5*, although pointing towards an opposite direction when compared to *cox11*. *ndufa5* showed increased levels of amino acids, whilst in *cox11* we described a general shortage of amino acids and during the night that was shown to have a major impact on the mutant phenotype (CHAPTER II).

The only amino acid that was upregulated in both mutants is phenylalanine, higher at ZT2 in *cox11*. Tyramine levels during day were lower in *ndufa5* and higher in *cox11*. Furthermore, while in *cox11* we identified a general shortage of intermediates of the carbon metabolism at night, this is not the case in *ndufa5*, where carbon metabolites compounds are unaltered at night and tend to accumulate during day. In *ndufa5* levels of fructose-6-phosphate are always high.

We must also consider that some metabolites followed similar trends in *ndufa5* and *cox11*. Fumarate and maleate were lower in *ndufa5* at night, with fumarate remaining low also at ZT2. In *cox11*, fumarate and maleate followed the same trend, remaining low at ZT0 and ZT2. The disaccharide 2-O-beta-L-Arabinofuranosyl-beta-L-arabinofuranose was high at ZT6 both in *cox11* and *ndufa5*. In *cox11*, threonate and N-acetylglutamate were always at lower levels. Threonate was always lower also in *ndufa5*, and N-acetylglutamate was lower during night.

Fumarate is produced from succinate by the enzymatic activity of the Complex II, which is a component of both the TCA cycle and the respiratory chain. Complex II protein levels accumulated at higher levels in both mutants. The activity of Complex II is expected to be particularly important for *ndufa5*, as it can partially substitute the role of Complex I in supplying electrons to ubiquinone. Fumarate is converted to malate by the enzyme fumarase. While in WT the fumarate:malate ratio increased through the day, this increase was not observed in *ndufa5*, where the ratio remained always more or less constant. Assuming an increased total succinate dehydrogenase activity in *ndufa5*, then the lower levels of fumarate might indicate an increased consumption of fumarate by other metabolic pathways, which would be supported by the lower fumarate:malate ratio that shows a shift towards the production of malate.

3.2. The transcriptome of *ndufa5* suggests that mitochondrial retrograde signalling is strongly activated at night

By comparing the transcriptomes of *ndufa5* and *cox11*, we detected a severe induction of Aox transcription only in *ndufa5* at night, but not in *cox11* or in *ndufa5* during the day (Figure 3.6). In the tobacco Complex I-deficient CMSII plants, AOX induction was also more significant at night (Dutilleul et al., 2003). Since AOX induction is an early marker of mitochondrial retrograde signalling, we hypothesized that that mitochondrial retrograde signalling (MRS) was active in *ndufa5* at ZT0, causing a reprogramming of the cell metabolism.

Since there is no experimental evidence of mitochondrial retrograde signalling in *P. patens*, we looked for the presence in *P. patens* of orthologs of genes experimentally

linked to MRS regulation in other organisms. The most well studied regulators of MRS in Arabidopsis are MYB29, MYB91, ABI4, different members of the WRKY family, CDKE;1, ANAC017 and other members of the NAC family. We could not identify orthologs of MYB91 or ABI4, and the five identified orthologs of MYB29 were very lowly expressed in *P. patens* WT and *ndufa5*, concluding that homologs of MYB29, MYB91 or ABI4 could not be involved in the induction of MRS in *ndufa5*. We could instead identify one or more homolog candidates for WRKY15, CDKE;1 and ANAC017, making it compatible that one or more of these homologs were responsible of the activation of MRS in *ndufa5* plants. To test this, we used lists of Arabidopsis genes experimentally shown to be positively regulated by these proteins during MRS, retrieved the corresponding list of orthologs in *P. patens* and analysed their behaviour in the transcriptome of *ndufa5* plants at ZT0.

The comparison of the transcriptome of Arabidopsis plants with a constitutively active WRKY15-mediated signalling pathway with that of *ndufa5* plants at ZT0 showed a low degree of overlap, suggesting that WKRY15 in *P. patens* was likely not the master regulator involved in MRS in *ndufa5*. Results were instead more promising when focusing on CDKE;1, as half of the orthologs of the CDKE;1-induced genes in Arabidopsis were also induced in *ndufa5* at ZT0. The highest degree of overlap was obtained when comparing the transcriptomic profile of *ndufa5* with a list of gene orthologs positively regulated by ANAC017. From these results we concluded that CDKE;1 and ANAC017 are good candidates for mediating MRS in *P. patens*, and particularly in *ndufa5* plants during the night.

We found further evidence that supports the activation of ANAC017-mediated MRS in *ndufa5* plants. On one hand, Arabidopsis plants with constitutive activation of ANAC017-mediated MRS suffered of transcriptomic repression of photosynthesis, carbon fixation and carbon catabolism, as well as the induction of ribosome biogenesis (Meng et al., 2019). We reported all these transcriptomic signatures also in *ndufa5* at ZT0. Moreover, another component of the ANAC017 pathway, the negative regulator RCD1, could also be identified in *P. patens* and was induced in *ndufa5* at ZT0, consistent with its role of induced negative regulator of the ANAC017 pathway (Shapiguzov et al., 2019; Tao et al., 2023). We also could identify in the genome of *P. patens* orthologs of different

rhomboid-like (RL) proteases, which are the proposed activators of ANAC017 (Ng, Ivanova, et al., 2013), including orthologs of AtRL2, experimentally linked to the activation of ANAC013 (Eysholdt-Derzsó et al., 2023).

Interestingly, all three candidate homologs of ANAC017 in *P. patens* were also induced during night. In Arabidopsis, ANAC017 transcriptomic induction after its activation has not been shown (Meng et al., 2019; Ng, Ivanova, et al., 2013), but it has been instead reported for other ANAC proteins involved in MRS including ANAC016 (Broda et al., 2021; De Clercq et al., 2013; van Aken et al., 2016). ANAC016 is one of the closest homologs of ANAC017, and the two proteins are very similar through all their sequence (Khan & Van Aken, 2022). It is possible that the roles of ANAC017 and ANAC016 in MRS in Arabidopsis (i.e. initial inductor and positive feedback regulator, respectively) are done by a single operator in *P. patens*. This would justify why all the ANAC17 orthologs in *P. patens* are also induced during MRS in *ndufa5* at ZT0. Interestingly, the ANAC017-mediated retrograde pathway has suggested to be activated also in Arabidopsis lines with reduced levels of Complex V (Yang et al., 2022). Furthermore, the ANAC017-pathway can be modulated by the circadian clock, having a different capacity of action through the day (Zhu et al., 2022). One could hypothesize that the different activation of MRS in *ndufa5* during night and day is in part regulated by the circadian clock. Also, since ANAC017 is proposed to respond also to chloroplast signals (Shapiguzov et al., 2019), it is possible that the energetic status of chloroplasts could also influence the ANAC017 response, inhibiting it during the day.

In the recent years, increasing evidence has underlined the process of land colonization as a pressure event towards the development of MRS (Khan & Van Aken, 2022; C. Zhao et al., 2019). Overall, we present a set of evidence showing that key components of two MRS pathways, mediated by CDKE;1 and ANAC017, exist in *P. patens*, suggesting that this mitochondrial retrograde signalling is evolutionary conserved. Moreover, the transcriptome of *ndufa5* plants is consistent with the ANAC017-mediated pathway being active during the night and triggering the molecular reprogramming that we described through RNA-sequencing and untargeted metabolomics.

3.3. The ANAC017-mediated reprogramming exacerbates the negative effects of Complex I depletion

As we reviewed in CHAPTER I, plants with a depleted Complex I have a strong impairment in their metabolism. Complex I is one of the main sites for electrons to enter the respiratory chain, and therefore its depletion reduces the capacity of producing ATP by oxidative phosphorylation. This is supported by the observation that moss lines without a functional Complex I have a reduced capacity for synthesizing ATP during dark-to-light transitions (CHAPTER IV). We showed here how the Complex I depletion impacts both the transcriptome and the metabolome of mutant plants.

In *ndufa5*, there was a general shortage of energy that was particularly relevant by night. The levels of AEC were lower in *ndufa5*, suggesting a shortage of energy, although carbon could be fixed and stored in form of starch, which accumulated in chloroplasts as granules.

On the other hand, we proposed here that Complex I depletion induced the activation of the ANAC017-mediated retrograde signalling in *ndufa5* plants. Apparently, the activation of this pathway has deep consequences on the transcriptome of the plants, which causes a general reprogramming of metabolism. Therefore, it seems that it is the activation of this signalling programme, rather than a simple deficiency of metabolism, that has the biggest impact on the phenotype of *ndufa5* plants. We presented here different observations that agree with this view. For instance, we could not rescue the growth by supplying the plants with additional light (i.e. removing the photoperiod) or adding additional reduced organic molecules to the growth media such as glucose or amino acids.

If the phenotype of *ndufa5* was only due to a reduced capacity in oxidative phosphorylation, we would expect these treatments to have a positive effect on growth. Indeed, this has been verified in the Complex IV deficient lines *cox11*, which did not undergo the ANAC017-mediated reprogramming.

4. Conclusions

We previously isolated *ndufa5*, a Complex I deficient line of the moss *P. patens*, which showed a very strong growth impairment that could not be explained by a simple shortage of energy or reduction in photosynthetic efficiency. Here, we characterized the transcriptome and metabolome of these plants. We found severe alterations of metabolism which were dependent on the time of the day, and that are consistent with data produced using similar vascular plant models. Furthermore, our data support the idea that mitochondrial retrograde signalling (MRS) could be activated in *ndufa5*, and that this activation could be much stronger during the night. We identified in the transcriptome *P. patens* several of the key components required for the ANAC017-mediated retrograde signalling pathway to work, strongly supporting that this pathway is functional in *P. patens*. We hypothesize that ANAC017 could be the main regulator in the induction of MRS in *ndufa5*, being therefore a major contributor to the macroscopic phenotype of *ndufa5* plants. By taking advantage of the differential activation during day and night, further experiments on this model could help to identify upstream regulators of MRS, which is one of the key pieces of knowledge currently missing in the field.

5. Material and methods

5.1. Plant material, transcriptomics and metabolomics

Plant growth, harvesting and subsequent transcriptomics and metabolomics analysis have been performed as already described for *cox11* in CHAPTER II. Analyses have been performed exploiting the publicly available tools MetaboAnalyst 5.0 (Xia & Wishart, 2011), iDEP 0.96 (Ge et al., 2018), HeatMapper (Babicki et al., 2016) and MolBioTools (https://molbiotools.com/listcompare.php).

5.2. Orthology

Where not stated otherwise, orthologs were retrieved from the JGI-based Phytozome website, exploiting the tool BioMART, using the databases *Arabidopsis thaliana Araport11* and *Physcomitrium patens v3.3* (https://phytozome-next.jgi.doe.gov/biomart) (Nordberg et al., 2014).

Genes were considered not to be significantly expressed when they were not identified as more than 50 reads in any of all the samples analysed in our RNAseq.

6. References

Adam, Z. (2013). Emerging roles for diverse intramembrane proteases in plant biology. *Biochimica et Biophysica Acta (BBA) - Biomembranes*, *1828*(12), 2933–2936. https://doi.org/10.1016/J.BBAMEM.2013.05.013

Aken, O. Van, Ford, E., Lister, R., Huang, S., & Millar, A. H. (2016). Retrograde Signalling Caused by Heritable Mitochondrial Dysfunction Is Partially Mediated by ANAC017 and Improves Plant Performance. *The Plant Journal*. https://doi.org/10.1111/tpj.13276

Arif, M. A., Hiss, M., Tomek, M., Busch, H., Meyberg, R., Tintelnot, S., Reski, R., Rensing, S. A., & Frank, W. (2019). ABA-Induced Vegetative Diaspore Formation in Physcomitrella patens. *Frontiers in Plant Science*, *10*, 440044. https://doi.org/10.3389/fpls.2019.00315

Babicki, S., Arndt, D., Marcu, A., Liang, Y., Grant, J. R., Maciejewski, A., & Wishart, D. S. (2016). Heatmapper: web-enabled heat mapping for all. *Nucleic Acids Research*, *44*(W1), W147–W153. https://doi.org/10.1093/nar/gkw419

Baker, B. M., & Haynes, C. M. (2011). Mitochondrial protein quality control during biogenesis and aging. *Trends in Biochemical Sciences*, *36*(5), 254–261. https://doi.org/10.1016/J.TIBS.2011.01.004

Bakshi, M., & Oelmüller, R. (2014). WRKY transcription factors: Jack of many trades in plants. *Plant Signaling & Behavior*, *9*(FEB). https://doi.org/10.4161/PSB.27700

Baruah, A., Šimková, K., Hincha, D. K., Apel, K., & Laloi, C. (2009). Modulation of 1O2-mediated retrograde signaling by the PLEIOTROPIC RESPONSE LOCUS 1 (PRL1) protein, a central integrator of stress and energy signaling. *The Plant Journal*, *60*(1), 22–32. https://doi.org/10.1111/J.1365-313X.2009.03935.X

Blanco, N. E., Guinea-Díaz, M., Whelan, J., & Strand, Å. (2014). Interaction between plastid and mitochondrial retrograde signalling pathways during changes to plastid redox status. *Philosophical Transactions of the Royal Society B: Biological Sciences*, *369*(1640). https://doi.org/10.1098/RSTB.2013.0231

Brangeon, J., Sabar, M., Gutierres, S., Combettes, B., Bove, J., Gendy, C., Chétrit, P., Colas Des Francs-Small, C., Pla, M., Vedel, F., & De Paepe, R. (2000). Defective splicing of the first nad4 intron is associated with lack of several complex I subunits in the Nicotiana sylvestris NMS1 nuclear mutant. *The Plant Journal : For Cell and Molecular Biology*, *21*(3), 269–280. https://doi.org/10.1046/J.1365-313X.2000.00679.X

Broda, M., Khan, K., O'Leary, B., Pruzinska, A., Pong Lee, C., Harvey Millar, A., & Van Aken, O. (2021). Increased expression of ANAC017 primes for accelerated senescence. *Plant Physiology*, *186*(4), 2205–2221. https://doi.org/10.1093/PLPHYS/KIAB195

Chan, K. X., Mabbitt, P. D., Phua, S. Y., Mueller, J. W., Nisar, N., Gigolashvili, T., Stroeher, E., Grassl, J., Arlt, W., Estavillo, G. M., Jackson, C. J., & Pogson, B. J. (2016). Sensing and signaling of oxidative stress in chloroplasts by inactivation of the SAL1 phosphoadenosine phosphatase. *Proceedings of the National Academy of Sciences of the United States of America*, *113*(31), E4567–E4576. https://doi.org/10.1073/PNAS.1604936113/SUPPL_FILE/PNAS.201604936SI.PDF

Chen, X., Li, C., Wang, H., & Guo, Z. (2019). WRKY transcription factors: evolution, binding, and action. *Phytopathology Research 2019 1:1*, *1*(1), 1–15. https://doi.org/10.1186/S42483-019-0022-X

Clifton, R., Lister, R., Parker, K. L., Sappl, P. G., Elhafez, D., Millar, A. H., Day, D. A., & Whelan, J. (2005). Stress-induced co-expression of alternative respiratory chain components in Arabidopsis

thaliana. *Plant Molecular Biology*, *58*(2), 193–212. https://doi.org/10.1007/S11103-005-5514-7/METRICS

Clifton, R., Millar, A. H., & Whelan, J. (2006). Alternative oxidases in Arabidopsis: A comparative analysis of differential expression in the gene family provides new insights into function of non-phosphorylating bypasses. *Biochimica et Biophysica Acta (BBA) - Bioenergetics*, *1757*(7), 730–741. https://doi.org/10.1016/J.BBABIO.2006.03.009

Colombo, M., Tadini, L., Peracchio, C., Ferrari, R., & Pesaresi, P. (2016). GUN1, a jack-of-all-trades in chloroplast protein homeostasis and signaling. *Frontiers in Plant Science*, *7*(September), 221110. https://doi.org/10.3389/FPLS.2016.01427/BIBTEX

da Cunha, F. M., Torelli, N. Q., & Kowaltowski, A. J. (2015). Mitochondrial Retrograde Signaling: Triggers, Pathways, and Outcomes. *Oxidative Medicine and Cellular Longevity*, *2015*, 1–10. https://doi.org/10.1155/2015/482582

Danon, A., Coll, N. S., & Apel, K. (2006). Cryptochrome-1-dependent execution of programmed cell death induced by singlet oxygen in Arabidopsis thaliana. *Proceedings of the National Academy of Sciences of the United States of America*, *103*(45), 17036. https://doi.org/10.1073/PNAS.0608139103

De Clercq, I., Vermeirssen, V., Van Aken, O., Vandepoele, K., Murcha, M. W., Law, S. R., Inzé, A., Ng, S., Ivanova, A., Rombaut, D., van de Cotte, B., Jaspers, P., Van de Peer, Y., Kangasjärvi, J., Whelan, J., & Van Breusegem, F. (2013). The Membrane-Bound NAC Transcription Factor ANAC013 Functions in Mitochondrial Retrograde Regulation of the Oxidative Stress Response in Arabidopsis. *The Plant Cell*, *25*(9), 3472–3490. https://doi.org/10.1105/TPC.113.117168

De Longevialle, A. F., Meyer, E. H., Andrés, C., Taylor, N. L., Lurin, C., Millar, A. H., & Smalla, I. D. (2007). The Pentatricopeptide Repeat Gene OTP43 Is Required for trans-Splicing of the Mitochondrial nad1 Intron 1 in Arabidopsis thaliana. *The Plant Cell*, *19*(10), 3256. https://doi.org/10.1105/TPC.107.054841

De Souza, A., Wang, J. Z., & Dehesh, K. (2017). Retrograde Signals: Integrators of Interorganellar Communication and Orchestrators of Plant Development. *Https://Doi.Org/10.1146/Annurev-Arplant-042916-041007*, *68*, 85–108. https://doi.org/10.1146/ANNUREV-ARPLANT-042916-041007

Dogra, V., Duan, J., Lee, K. P., Lv, S., Liu, R., & Kim, C. (2017). FtsH2-dependent proteolysis of EXECUTER1 is essential in mediating singlet oxygen-triggered retrograde signaling in Arabidopsis thaliana. *Frontiers in Plant Science*, *8*, 1145. https://doi.org/10.3389/FPLS.2017.01145/BIBTEX

Dojcinovic, D., Krosting, J., Harris, A. J., Wagner, D. J., & Rhoads, D. M. (2005). Identification of a region of the Arabidopsis AtAOX1a promoter necessary for mitochondrial retrograde regulation of expression. *Plant Molecular Biology 2005 58:2*, *58*(2), 159–175. https://doi.org/10.1007/S11103-005-5390-1

Dutilleul, C., Garmier, M., Noctor, G., Mathieu, C., Chétrit, P., Foyer, C. H., & De Paepe, R. (2003). Leaf Mitochondria Modulate Whole Cell Redox Homeostasis, Set Antioxidant Capacity, and Determine Stress Resistance through Altered Signaling and Diurnal Regulation. *The Plant Cell*, *15*(5), 1212–1226. https://doi.org/10.1105/TPC.009464

Estavillo, G. M., Crisp, P. A., Pornsiriwong, W., Wirtz, M., Collinge, D., Carrie, C., Giraud, E., Whelan, J., David, P., Javot, H., Brearley, C., Hell, R., Marin, E., & Pogson, B. J. (2011). Evidence for a SAL1-PAP Chloroplast Retrograde Pathway That Functions in Drought and High Light Signaling in Arabidopsis. *The Plant Cell*, *23*(11), 3992–4012. https://doi.org/10.1105/TPC.111.091033

Eulgem, T., Rushton, P. J., Robatzek, S., & Somssich, I. E. (2000). The WRKY superfamily of plant transcription factors. *Trends in Plant Science*, *5*(5), 199–206. https://doi.org/10.1016/S1360-1385(00)01600-9

Eysholdt-Derzsó, E., Renziehausen, T., Frings, S., Frohn, S., von Bongartz, K., Igisch, C. P., Mann, J., Häger, L., Macholl, J., Leisse, D., Hoffmann, N., Winkels, K., Wanner, P., De Backer, J., Luo, X., Sauter, M., De Clercq, I., van Dongen, J. T., Schippers, J. H. M., & Schmidt-Schippers, R. R. (2023). Endoplasmic reticulum–bound ANAC013 factor is cleaved by RHOMBOID-LIKE 2 during the initial response to hypoxia in Arabidopsis thaliana. *Proceedings of the National Academy of Sciences of the United States of America*, *120*(11), e2221308120. https://doi.org/10.1073/PNAS.2221308120/SUPPL_FILE/PNAS.2221308120.SD05.XLSX

Fromm, S., Senkler, J., Eubel, H., Peterhänsel, C., & Braun, H. P. (2016). Life without complex I: Proteome analyses of an Arabidopsis mutant lacking the mitochondrial NADH dehydrogenase complex. *Journal of Experimental Botany*, *67*(10), 3079–3093. https://doi.org/10.1093/jxb/erw165

Ge, S. X., Son, E. W., & Yao, R. (2018). iDEP: an integrated web application for differential expression and pathway analysis of RNA-Seq data. *BMC Bioinformatics 2018 19:1*, *19*(1), 1–24. https://doi.org/10.1186/S12859-018-2486-6

Giraud, E., van Aken, O., Ho, L. H. M., & Whelan, J. (2009). The Transcription Factor ABI4 Is a Regulator of Mitochondrial Retrograde Expression of ALTERNATIVE OXIDASE1a. *Plant Physiology*, *150*(3), 1286–1296. https://doi.org/10.1104/PP.109.139782

Gray, G. R., Maxwell, D. P., Villarimo, A. R., & McIntosh, L. (2004). Mitochondria/nuclear signaling of alternative oxidase gene expression occurs through distinct pathways involving organic acids and reactive oxygen species. *Plant Cell Reports*, *23*(7), 497–503. https://doi.org/10.1007/S00299-004-0848-1/FIGURES/4

Gregorio, J., Hernández-Bernal, A. F., Cordoba, E., & León, P. (2014). Characterization of Evolutionarily Conserved Motifs Involved in Activity and Regulation of the ABA-INSENSITIVE (ABI) 4 Transcription Factor. *Molecular Plant*, *7*(2), 422–436. https://doi.org/10.1093/MP/SST132

Guo, H., Feng, P., Chi, W., Sun, X., Xu, X., Li, Y., Ren, D., Lu, C., David Rochaix, J., Leister, D., & Zhang, L. (2016). Plastid-nucleus communication involves calcium-modulated MAPK signalling. *Nature Communications*, *7*. https://doi.org/10.1038/NCOMMS12173

Honkanen, S., & Small, I. (2022). The GENOMES UNCOUPLED1 protein has an ancient, highly conserved role but not in retrograde signalling. *The New Phytologist*, *236*(1), 99–113. https://doi.org/10.1111/NPH.18318

Ivanova, A., Law, S. R., Narsai, R., Duncan, O., Lee, J. H., Zhang, B., Van Aken, O., Radomiljac, J. D., van der Merwe, M., Yi, K. K., & Whelan, J. (2014). A Functional Antagonistic Relationship between Auxin and Mitochondrial Retrograde Signaling Regulates Alternative Oxidase1a Expression in Arabidopsis. *Plant Physiology*, *165*(3), 1233–1254. https://doi.org/10.1104/PP.114.237495

Jethva, J., Lichtenauer, S., Schmidt-Schippers, R., Steffen-Heins, A., Poschet, G., Wirtz, M., van Dongen, J. T., Eirich, J., Finkemeier, I., Bilger, W., Schwarzländer, M., & Sauter, M. (2023). Mitochondrial alternative NADH dehydrogenases NDA1 and NDA2 promote survival of reoxygenation stress in Arabidopsis by safeguarding photosynthesis and limiting ROS generation. *The New Phytologist*, *238*(1), 96–112. https://doi.org/10.1111/nph.18657

Ježek, P., Holendová, B., & Plecitá-hlavatá, L. (2020). Redox Signaling from Mitochondria: Signal Propagation and Its Targets. *Biomolecules 2020, Vol. 10, Page 93*, *10*(1), 93. https://doi.org/10.3390/BIOM10010093

Jovaisaite, V., Mouchiroud, L., Auwerx, J., Davies, S. A., Dow, J. A. T., & Lukowiak, K. (2014). The mitochondrial unfolded protein response, a conserved stress response pathway with implications in health and disease. *Journal of Experimental Biology*, *217*(1), 137–143. https://doi.org/10.1242/JEB.090738

Juszczuk, I. M., Flexas, J., Szal, B., Dąbrowska, Z., Ribas-Carbo, M., & Rychter, A. M. (2007). Effect of mitochondrial genome rearrangement on respiratory activity, photosynthesis, photorespiration and energy status of MSC16 cucumber (Cucumis sativus) mutant. *Physiologia Plantarum*, *131*(4), 527–541. https://doi.org/10.1111/j.1399-3054.2007.00984.x

Kacprzak, S. M., Dahlqvist, A., & Van Aken, O. (2020). The transcription factor ANAC017 is a key regulator of mitochondrial proteotoxic stress responses in plants. *Philosophical Transactions of the Royal Society B*, *375*(1801). https://doi.org/10.1098/RSTB.2019.0411

Karpova, O. V., Kuzmin, E. V., Elthon, T. E., & Newton, K. J. (2002). Differential Expression of Alternative Oxidase Genes in Maize Mitochondrial Mutants. *The Plant Cell*, *14*(12), 3271–3284. https://doi.org/10.1105/tpc.005603

Keun, P. L., Kim, C., Landgraf, F., & Apel, K. (2007). EXECUTER1- and EXECUTER2-dependent transfer of stress-related signals from the plastid to the nucleus of Arabidopsis thaliana. *Proceedings of the National Academy of Sciences of the United States of America*, *104*(24), 10270–10275. https://doi.org/10.1073/PNAS.0702061104/SUPPL_FILE/02061DATASET.XLS

Khan, K., & Van Aken, O. (2022). The colonization of land was a likely driving force for the evolution of mitochondrial retrograde signalling in plants. *Journal of Experimental Botany*. https://doi.org/10.1093/JXB/ERAC351

Kleine, T., & Leister, D. (2016). Retrograde signaling: Organelles go networking. *Biochimica et Biophysica Acta (BBA) - Bioenergetics*, *1857*(8), 1313–1325. https://doi.org/10.1016/J.BBABIO.2016.03.017

Knopf, R. R., & Adam, Z. (2012). Rhomboid proteases in plants – still in square one? *Physiologia Plantarum*, *145*(1), 41–51. https://doi.org/10.1111/J.1399-3054.2011.01532.X

Koussevitzky, S., Nott, A., Mockler, T. C., Hong, F., Sachetto-Martins, G., Surpin, M., Lim, J., Mittler, R., & Chory, J. (2007). Signals from Chloroplasts Converge to Regulate Nuclear Gene Expression. *Science*, *316*(5825), 715–719. https://doi.org/10.1126/SCIENCE.1140516/SUPPL_FILE/PAPV2.PDF

Kudla, J., Becker, D., Grill, E., Hedrich, R., Hippler, M., Kummer, U., Parniske, M., Romeis, T., & Schumacher, K. (2018). Advances and current challenges in calcium signaling. *New Phytologist*, *218*(2), 414–431. https://doi.org/10.1111/NPH.14966

Leister, D. (2012). Retrograde signaling in plants: from simple to complex scenarios. *Frontiers in Plant Science*, *3*. https://doi.org/10.3389/fpls.2012.00135

Li, Y., Liu, H., Ma, T., Li, J., Yuan, J., Xu, Y.-C., Sun, R., Zhang, X., Jing, Y., Guo, Y.-L., & Lin, R. (2022). *Arabidopsis EXECUTER1 interacts with WRKY transcription factors 2 to mediate plastid-to-nucleus singlet oxygen signaling Short title: EX1 mediates plastid-to-nucleus signaling*. https://doi.org/10.1093/plcell/koac330/6845761

Litthauer, S., Chan, K. X., & Jones, M. A. (2018). 3′-Phosphoadenosine 5′-Phosphate Accumulation Delays the Circadian System. *Plant Physiology*, *176*(4), 3120–3135. https://doi.org/10.1104/PP.17.01611

Liu, Y., Lv, Y., Wei, A., Guo, M., Li, Y., Wang, J., Wang, X., & Bao, Y. (2022). Unfolded protein response in balancing plant growth and stress tolerance. *Frontiers in Plant Science*, *13*, 1019414. https://doi.org/10.3389/FPLS.2022.1019414/BIBTEX

Liu, Z., & Butow, R. A. (2006). Mitochondrial Retrograde Signaling. *Annual Review of Genetics*, *40*(1), 159–185. https://doi.org/10.1146/annurev.genet.40.110405.090613

Lloyd, J. P. B., Lang, D., Zimmer, A. D., Causier, B., Reski, R., & Davies, B. (2018). The loss of SMG1 causes defects in quality control pathways in Physcomitrella patens. *Nucleic Acids Research*, *46*(11), 5822. https://doi.org/10.1093/NAR/GKY225

Lunn, J. E. (2007). Compartmentation in plant metabolism. *Journal of Experimental Botany*, *58*(1), 35–47. https://doi.org/10.1093/JXB/ERL134

Manghwar, H., & Li, J. (2022). Endoplasmic Reticulum Stress and Unfolded Protein Response Signaling in Plants. *International Journal of Molecular Sciences*, *23*(2). https://doi.org/10.3390/IJMS23020828

Martin, W., & Herrmann, R. G. (1998). Gene Transfer from Organelles to the Nucleus: How Much, What Happens, and Why? *Plant Physiology*, *118*(1), 9–17. https://doi.org/10.1104/PP.118.1.9

Maxwell, D. P., Nickels, R., & McIntos, L. (2002). Evidence of mitochondrial involvement in the transduction of signals required for the induction of genes associated with pathogen attack and senescence. *The Plant Journal*, *29*(3), 269–279. https://doi.org/10.1046/J.1365-313X.2002.01216.X

Mellon, M., Storti, M., Vera-Vives, A. M., Kramer, D. M., Alboresi, A., & Morosinotto, T. (2021). Inactivation of mitochondrial Complex I stimulates chloroplast ATPase in Physcomitrium patens . *Plant Physiology*. https://doi.org/10.1093/plphys/kiab276

Meng, X., Li, L., Clercq, I. De, Narsai, R., Xu, Y., Hartmann, A., Claros, D. L., Custovic, E., Lewsey, M. G., Whelan, J., & Berkowitz, O. (2019). ANAC017 Coordinates Organellar Functions and Stress Responses by Reprogramming Retrograde Signaling. *Plant Physiology*, *180*(1), 634–653. https://doi.org/10.1104/PP.18.01603

Meyer, E. H., Tomaz, T., Carroll, A. J., Estavillo, G., Delannoy, E., Tanz, S. K., Small, I. D., Pogson, B. J., & Millar, A. H. (2009). Remodeled Respiration in ndufs4 with Low Phosphorylation Efficiency Suppresses Arabidopsis Germination and Growth and Alters Control of Metabolism at Night. *Plant Physiology*, *151*(2), 603–619. https://doi.org/10.1104/PP.109.141770

Mielecki, J., Gawroński, P., & Karpiński, S. (2020). Retrograde Signaling: Understanding the Communication between Organelles. *International Journal of Molecular Sciences 2020, Vol. 21, Page 6173*, *21*(17), 6173. https://doi.org/10.3390/IJMS21176173

Millar, A. H., Whelan, J., Soole, K. L., & Day, D. A. (2011). Organization and Regulation of Mitochondrial Respiration in Plants. *Annual Review of Plant Biology*, *62*(1), 79–104. https://doi.org/10.1146/annurev-arplant-042110-103857

Mohanta, T. K., Park, Y. H., & Bae, H. (2016). Novel Genomic and Evolutionary Insight of WRKY Transcription Factors in Plant Lineage. *Scientific Reports 2016 6:1*, *6*(1), 1–22. https://doi.org/10.1038/srep37309

Møller, I. M., & Sweetlove, L. J. (2010). ROS signalling – specificity is required. *Trends in Plant Science*, *15*(7), 370–374. https://doi.org/10.1016/J.TPLANTS.2010.04.008

Naramoto, S., Hata, Y., Fujita, T., & Kyozuka, J. (2022). The bryophytes Physcomitrium patens and Marchantia polymorpha as model systems for studying evolutionary cell and developmental biology in plants. *The Plant Cell*, *34*(1), 228–246. https://doi.org/10.1093/PLCELL/KOAB218

Neimanis, K., Staples, J. F., Hüner, N. P. A., & McDonald, A. E. (2013). Identification, expression, and taxonomic distribution of alternative oxidases in non-angiosperm plants. *Gene*, *526*(2), 275–286. https://doi.org/10.1016/J.GENE.2013.04.072

Ng, S., Giraud, E., Duncan, O., Law, S. R., Wang, Y., Xu, L., Narsai, R., Carrie, C., Walker, H., Day, D. A., Blanco, N. E., Strand, Å., Whelan, J., & Ivanova, A. (2013). Cyclin-dependent kinase E1 (CDKE1) provides a cellular switch in plants between growth and stress responses. *The Journal of Biological Chemistry*, *288*(5), 3449–3459. https://doi.org/10.1074/JBC.M112.416727

Ng, S., Ivanova, A., Duncan, O., Law, S. R., Van Aken, O., De Clercq, I., Wang, Y., Carrie, C., Xu, L., Kmiec, B., Walker, H., Van Breusegem, F., Whelan, J., & Giraud, E. (2013). A Membrane-Bound

NAC Transcription Factor, ANAC017, Mediates Mitochondrial Retrograde Signaling in Arabidopsis. *The Plant Cell*, *25*(9), 3450–3471. https://doi.org/10.1105/TPC.113.113985

Nordberg, H., Cantor, M., Dusheyko, S., Hua, S., Poliakov, A., Shabalov, I., Smirnova, T., Grigoriev, I. V., & Dubchak, I. (2014). The genome portal of the Department of Energy Joint Genome Institute: 2014 updates. *Nucleic Acids Research*, *42*(D1), D26–D31. https://doi.org/10.1093/nar/gkt1069

Nott, A., Jung, H. S., Koussevitzky, S., & Chory, J. (2006). Plastid-to-nucleus retrograde signaling. *Annual Review of Plant Biology*, *57*, 739–759. https://doi.org/10.1146/ANNUREV.ARPLANT.57.032905.105310

Peixoto, B., & Baena-González, E. (2022). Management of plant central metabolism by SnRK1 protein kinases. *Journal of Experimental Botany*. https://doi.org/10.1093/JXB/ERAC261

Pereira-Santana, A., Alcaraz, L. D., Castaño, E., Sanchez-Calderon, L., Sanchez-Teyer, F., & Rodriguez-Zapata, L. (2015). Comparative Genomics of NAC Transcriptional Factors in Angiosperms: Implications for the Adaptation and Diversification of Flowering Plants. *PLOS ONE*, *10*(11), e0141866. https://doi.org/10.1371/JOURNAL.PONE.0141866

Phua, S. Y., Yan, D., Chan, K. X., Estavillo, G. M., Nambara, E., & Pogson, B. J. (2018). The arabidopsis SAL1-PAP pathway: A case study for integrating chloroplast retrograde, light and hormonal signaling in modulating plant growth and development? *Frontiers in Plant Science*, *9*. https://doi.org/10.3389/FPLS.2018.01171/FULL

Pirayesh, N., Giridhar, M., Ben Khedher, A., Vothknecht, U. C., & Chigri, F. (2021). Organellar calcium signaling in plants: An update. *Biochimica et Biophysica Acta (BBA) - Molecular Cell Research*, *1868*(4), 118948. https://doi.org/10.1016/J.BBAMCR.2021.118948

Pornsiriwong, W., Estavillo, G. M., Chan, K. X., Tee, E. E., Ganguly, D., Crisp, P. A., Phua, S. Y., Zhao, C., Qiu, J., Park, J., Yong, M. T., Nisar, N., Yadav, A. K., Schwessinger, B., Rathjen, J., Cazzonelli, C. I., Wilson, P. B., Gilliham, M., Chen, Z. H., & Pogson, B. J. (2017). A chloroplast retrograde signal, 3'phosphoadenosine 5'-phosphate, acts as a secondary messenger in abscisic acid signaling in stomatal closure and germination. *ELife*, *6*. https://doi.org/10.7554/ELIFE.23361

Pu, X., Yang, L., Liu, L., Dong, X., Chen, S., Chen, Z., Liu, G., Jia, Y., Yuan, W., & Liu, L. (2020). Genome-Wide Analysis of the MYB Transcription Factor Superfamily in Physcomitrella patens. *International Journal of Molecular Sciences*, *21*(3). https://doi.org/10.3390/IJMS21030975

Quirós, P. M., Mottis, A., & Auwerx, J. (2016). Mitonuclear communication in homeostasis and stress. *Nature Reviews Molecular Cell Biology 2016 17:4*, *17*(4), 213–226. https://doi.org/10.1038/nrm.2016.23

Rhoads, D. M., & Subbaiah, C. C. (2007). Mitochondrial retrograde regulation in plants. *Mitochondrion*, *7*(3), 177–194. https://doi.org/10.1016/J.MITO.2007.01.002

Richter, A. S., Nägele, T., Grimm, B., Kaufmann, K., Schroda, M., Leister, D., & Kleine, T. (2023). Retrograde signaling in plants: A critical review focusing on the GUN pathway and beyond. *Plant Communications*, *4*(1), 100511. https://doi.org/10.1016/J.XPLC.2022.100511

Ruibal, C., Castro, A., Fleitas, A. L., Quezada, J., Quero, G., & Vidal, S. (2020). A Chloroplast COR413 Protein From Physcomitrella patens Is Required for Growth Regulation Under High Light and ABA Responses. *Frontiers in Plant Science*, *11*, 845. https://doi.org/10.3389/FPLS.2020.00845/BIBTEX

Schwarzländer, M., & Finkemeier, I. (2013). Mitochondrial energy and redox signaling in plants. *Antioxidants and Redox Signaling*, *18*(16), 2122–2144. https://doi.org/10.1089/ARS.2012.5104/ASSET/IMAGES/LARGE/FIGURE8.JPEG

Schwarzländer, M., König, A.-C., Fernie, A. R., & Finkemeier, I. (2011). The Impact of Impaired Mitochondrial Function on Retrograde Signalling: A Meta-Analysis of Transcriptomic Responses. *Journal of Experimental Botany*. https://doi.org/10.1093/jxb/err374

Shang, Y., Yan, L., Liu, Z. Q., Cao, Z., Mei, C., Xin, Q., Wu, F. Q., Wang, X. F., Du, S. Y., Jiang, T., Zhang, X. F., Zhao, R., Sun, H. L., Liu, R., Yu, Y. T., & Zhang, D. P. (2010). The Mg-Chelatase H Subunit of Arabidopsis Antagonizes a Group of WRKY Transcription Repressors to Relieve ABA-Responsive Genes of Inhibition. *The Plant Cell*, *22*(6), 1909–1935. https://doi.org/10.1105/TPC.110.073874

Shapiguzov, A., Vainonen, J. P., Hunter, K., Tossavainen, H., Tiwari, A., Järvi, S., Hellman, M., Aarabi, F., Alseekh, S., Wybouw, B., Van Der Kelen, K., Nikkanen, L., Krasensky-Wrzaczek, J., Sipari, N., Keinänen, M., Tyystjärvi, E., Rintamäki, E., De Rybel, B., Salojärvi, J., … Kangasjärvi, J. (2019). Arabidopsis RCD1 coordinates chloroplast and mitochondrial functions through interaction with ANAC transcription factors. *ELife*, *8*. https://doi.org/10.7554/eLife.43284

Simons, B. H., Millenaar, F. F., Mulder, L., Van Loon, L. C., & Lambers, H. (1999). Enhanced expression and activation of the alternative oxidase during infection of Arabidopsis with Pseudomonas syringae pv tomato. *Plant Physiology*, *120*(2), 529–538. https://doi.org/10.1104/PP.120.2.529

Stevenson, S. R., Kamisugi, Y., Trinh, C. H., Schmutz, J., Jenkins, J. W., Grimwood, J., Muchero, W., Tuskan, G. A., Rensing, S. A., Lang, D., Reski, R., Melkonian, M., Rothfels, C. J., Li, F. W., Larsson, A., Wong, G. K. S., Edwards, T. A., & Cuming, A. C. (2016). Genetic Analysis of Physcomitrella patens Identifies ABSCISIC ACID NON-RESPONSIVE, a Regulator of ABA Responses Unique to Basal Land Plants and Required for Desiccation Tolerance. *The Plant Cell*, *28*(6), 1310–1327. https://doi.org/10.1105/TPC.16.00091

Sun, X., Feng, P., Xu, X., Guo, H., Ma, J., Chi, W., Lin, R., Lu, C., & Zhang, L. (2011). A chloroplast envelope-bound PHD transcription factor mediates chloroplast signals to the nucleus. *Nature Communications*, *2*(1). https://doi.org/10.1038/NCOMMS1486

Tao, J., Wu, F., Wen, H., Liu, X., Luo, W., Gao, L., Jiang, Z., Mo, B., Chen, X., Kong, W., & Yu, Y. (2023). RCD1 Promotes Salt Stress Tolerance in Arabidopsis by Repressing ANAC017 Activity. *International Journal of Molecular Sciences*, *24*(12), 9793. https://doi.org/10.3390/IJMS24129793/S1

Thelander, M., Nilsson, A., Olsson, T., Johansson, M., Girod, P.-A., Schaefer, D. G., Zrÿd, J.-P., & Ronne, H. (2007). The moss genes PpSKI1 and PpSKI2 encode nuclear SnRK1 interacting proteins with homologues in vascular plants. *Plant Molecular Biology*, *64*(5), 559–573. https://doi.org/10.1007/s11103-007-9176-5

Thelander, M., Olsson, T., & Ronne, H. (2004). Snf1-related protein kinase 1 is needed for growth in a normal day–night light cycle. *The EMBO Journal*, *23*(8), 1900–1910. https://doi.org/10.1038/sj.emboj.7600182

Timmerhaus, G., Hanke, S. T., Buchta, K., & Rensing, S. A. (2011). Prediction and Validation of Promoters Involved in the Abscisic Acid Response in Physcomitrella patens. *Molecular Plant*, *4*(4), 713–729. https://doi.org/10.1093/MP/SSR009

Triantaphylidès, C., & Havaux, M. (2009). Singlet oxygen in plants: production, detoxification and signaling. *Trends in Plant Science*, *14*(4), 219–228. https://doi.org/10.1016/J.TPLANTS.2009.01.008

Vaahtera, L., Brosché, M., Wrzaczek, M., & Kangasjärvi, J. (2014). Specificity in ROS Signaling and Transcript Signatures. *Antioxidants & Redox Signaling*, *21*(9), 1422. https://doi.org/10.1089/ARS.2013.5662

van Aken, O. (2021). Mitochondrial redox systems as central hubs in plant metabolism and signaling. *Plant Physiology*, *186*(1), 36. https://doi.org/10.1093/PLPHYS/KIAB101

van Aken, O., de Clercq, I., Ivanova, A., Law, S. R., van Breusegem, F., Millar, A. H., & Whelan, J. (2016). Mitochondrial and Chloroplast Stress Responses Are Modulated in Distinct Touch and Chemical Inhibition Phases. *Plant Physiology*, *171*(3), 2150–2165. https://doi.org/10.1104/PP.16.00273

Van Aken, O., Pečenková, T., Van De Cotte, B., De Rycke, R., Eeckhout, D., Fromm, H., De Jaeger, G., Witters, E., Beemster, G. T. S., Inzé, D., & Van Breusegem, F. (2007). Mitochondrial type-I prohibitins of Arabidopsis thaliana are required for supporting proficient meristem development. *The Plant Journal : For Cell and Molecular Biology*, *52*(5), 850–864. https://doi.org/10.1111/J.1365-313X.2007.03276.X

Van Aken, O., Zhang, B., Law, S., Narsai, R., & Whelan, J. (2013). AtWRKY40 and AtWRKY63 modulate the expression of stress-responsive nuclear genes encoding mitochondrial and chloroplast proteins. *Plant Physiology*, *162*(1), 254–271. https://doi.org/10.1104/PP.113.215996

Vanderauwera, S., Vandenbroucke, K., Inzé, A., Van De Cotte, B., Mühlenbock, P., De Rycke, R., Naouar, N., Van Gaever, T., Van Montagu, M. C. E., & Van Breusegem, F. (2012). AtWRKY15 perturbation abolishes the mitochondrial stress response that steers osmotic stress tolerance in Arabidopsis. *Proceedings of the National Academy of Sciences of the United States of America*, *109*(49), 20113–20118. https://doi.org/10.1073/PNAS.1217516109/SUPPL_FILE/ST04.DOC

Vanderauwera, S., Zimmermann, P., Rombauts, S., Vandenabeele, S., Langebartels, C., Gruissem, W., Inzé, D., & Van Breusegem, F. (2005). Genome-Wide Analysis of Hydrogen Peroxide-Regulated Gene Expression in Arabidopsis Reveals a High Light-Induced Transcriptional Cluster Involved in Anthocyanin Biosynthesis. *Plant Physiology*, *139*(2), 806–821. https://doi.org/10.1104/PP.105.065896

Vanlerberghe, G. C., & McIntosh, L. (1997). ALTERNATIVE OXIDASE: From Gene to Function. *Annual Review of Plant Physiology and Plant Molecular Biology*. https://doi.org/10.1146/annurev.arplant.48.1.703

Vanlerberghe, G. C., & McIntosh, L. (1994). Mitochondrial electron transport regulation of nuclear gene expression. Studies with the alternative oxidase gene of tobacco. *Plant Physiology*, *105*(3), 867–874. https://doi.org/10.1104/PP.105.3.867

Vanlerberghe, G. C., Robson, C. A., & Yip, J. Y. H. (2002). Induction of Mitochondrial Alternative Oxidase in Response to a Cell Signal Pathway Down-Regulating the Cytochrome Pathway Prevents Programmed Cell Death. *Plant Physiology*, *129*(4), 1829–1842. https://doi.org/10.1104/PP.002691

Vogel, M. O., Moore, M., König, K., Pecher, P., Alsharafa, K., Lee, J., & Dietz, K. J. (2014). Fast Retrograde Signaling in Response to High Light Involves Metabolite Export, MITOGEN-ACTIVATED PROTEIN KINASE6, and AP2/ERF Transcription Factors in Arabidopsis. *The Plant Cell*, *26*(3), 1151–1165. https://doi.org/10.1105/TPC.113.121061

Wang, X., & Auwerx, J. (2017). Systems Phytohormone Responses to Mitochondrial Proteotoxic Stress. *Molecular Cell*, *68*(3), 540-551.e5. https://doi.org/10.1016/J.MOLCEL.2017.10.006

Wang, Y., Selinski, J., Mao, C., Zhu, Y., Berkowitz, O., & Whelan, J. (2020). Linking mitochondrial and chloroplast retrograde signalling in plants. *Philosophical Transactions of the Royal Society B*, *375*(1801). https://doi.org/10.1098/RSTB.2019.0410

Wind, J. J., Peviani, A., Snel, B., Hanson, J., & Smeekens, S. C. (2013). ABI4: versatile activator and repressor. *Trends in Plant Science*, *18*(3), 125–132. https://doi.org/10.1016/J.TPLANTS.2012.10.004

Xia, J., & Wishart, D. S. (2011). Web-based inference of biological patterns, functions and pathways from metabolomic data using MetaboAnalyst. *Nature Protocols*, *6*(6), 743–760. https://doi.org/10.1038/nprot.2011.319

Xu, B., Ohtani, M., Yamaguchi, M., Toyooka, K., Wakazaki, M., Sato, M., Kubo, M., Nakano, Y., Sano, R., Hiwatashi, Y., Murata, T., Kurata, T., Yoneda, A., Kato, K., Hasebe, M., & Demura, T. (2014). Contribution of NAC transcription factors to plant adaptation to land. *Science*, *343*(6178), 1505–1508. https://doi.org/10.1126/SCIENCE.1248417/SUPPL_FILE/XU.B.SM.PDF

Yang, H., Xue, Y., Li, B., Lin, Y., Li, H., Guo, Z., Li, W., Fu, Z., Ding, D., & Tang, J. (2022). The chimeric gene atp6c confers cytoplasmic male sterility in maize by impairing the assembly of the mitochondrial ATP synthase complex. *Molecular Plant*, *15*(5), 872–886. https://doi.org/10.1016/J.MOLP.2022.03.002

Zhang, X., Ivanova, A., Vandepoele, K., Radomiljac, J., Van De Velde, J., Berkowitz, O., Willems, P., Xu, Y., Ng, S., Van Aken, O., Duncan, O., Zhang, B., Storme, V., Chan, K. X., Vaneechoutte, D., Pogson, B. J., Van Breusegem, F., Whelan, J., & De Clercq, I. (2017). The Transcription Factor MYB29 Is a Regulator of ALTERNATIVE OXIDASE1a. *Plant Physiology*, *173*(3), 1824–1843. https://doi.org/10.1104/PP.16.01494

Zhao, C., Wang, Y., Chan, K. X., Marchant, D. B., Franks, P. J., Randall, D., Tee, E. E., Chen, G., Ramesh, S., Phua, S. Y., Zhang, B., Hills, A., Dai, F., Xue, D., Gilliham, M., Tyerman, S., Nevo, E., Wu, F., Zhang, G., … Chen, Z. H. (2019). Evolution of chloroplast retrograde signaling facilitates green plant adaptation to land. *Proceedings of the National Academy of Sciences of the United States of America*, *116*(11), 5015–5020. https://doi.org/10.1073/PNAS.1812092116/SUPPL_FILE/PNAS.1812092116.SAPP.PDF

Zhao, X., Liu, N., Shang, N., Zeng, W., Ebert, B., Rautengarten, C., Zeng, Q.-Y., Li, H., Chen, X., Beahan, C., Bacic, A., Heazlewood, J. L., & Wu, A.-M. (2018). Three UDP-xylose transporters participate in xylan biosynthesis by conveying cytosolic UDP-xylose into the Golgi lumen in Arabidopsis. *Journal of Experimental Botany*, *69*(5), 1125–1134. https://doi.org/10.1093/jxb/erx448

Zhu, Y., Narsai, R., He, C., Wang, Y., Berkowitz, O., Whelan, J., & Liew, L. C. (2022). Coordinated regulation of the mitochondrial retrograde response by circadian clock regulators and ANAC017. *Plant Communications*, 100501. https://doi.org/10.1016/J.XPLC.2022.100501

7. Supplementary information

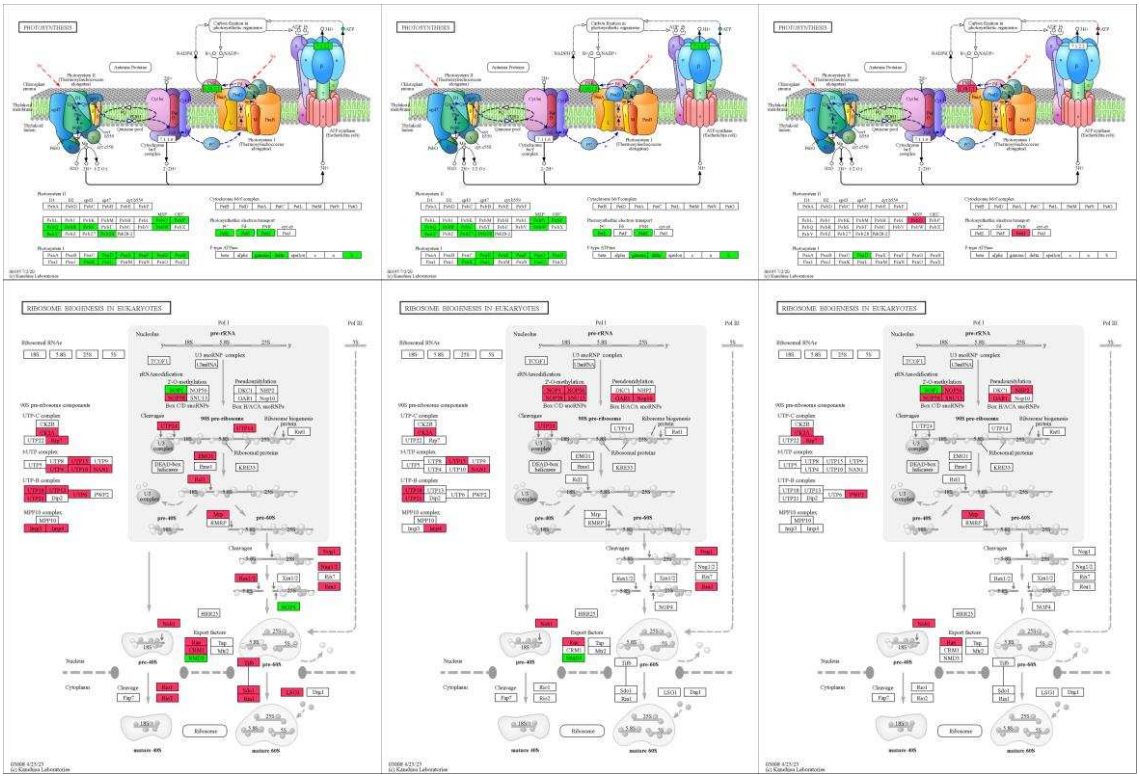

Supplementary Figure 3.1 | **Mapping of DEGs in *ndufa5* on KEGG maps**. Red: upregaulted; green: downregulated. Maps show, from left to right, ZT0, ZT2 and ZT6 data. Photosynthesis is transcriptionally repressed, and ribosome biogenesis is induced in *ndufa5* at ZT0 and ZT2.

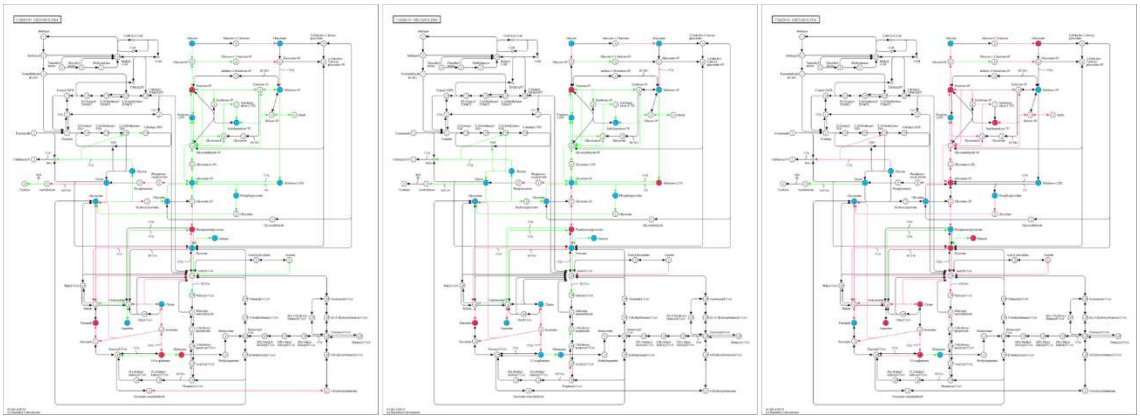

Supplementary Figure 3.2 | **Mapping of DEGs in *ndufa5* on KEGG map showing carbon metabolism**. Red: upregulated; green: downregulated. Maps show, from left to right, ZT0, ZT2 and ZT6 data. Note the general repression of Calvin cycle and carbon catabolism at ZT0 and ZT2, and general induction at ZT6.

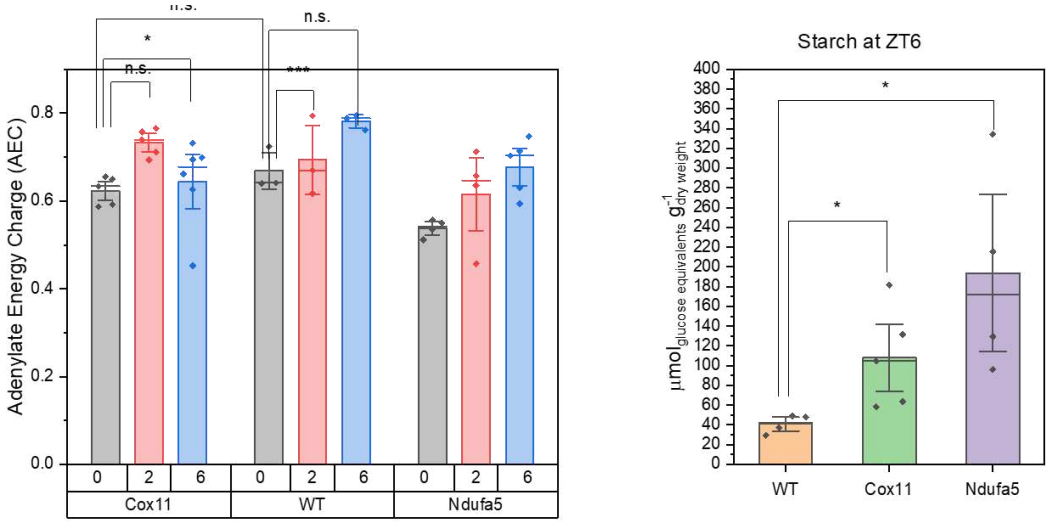

Supplementary Figure 3.3 | AEC and starch quantification, including *cox11* for comparison.

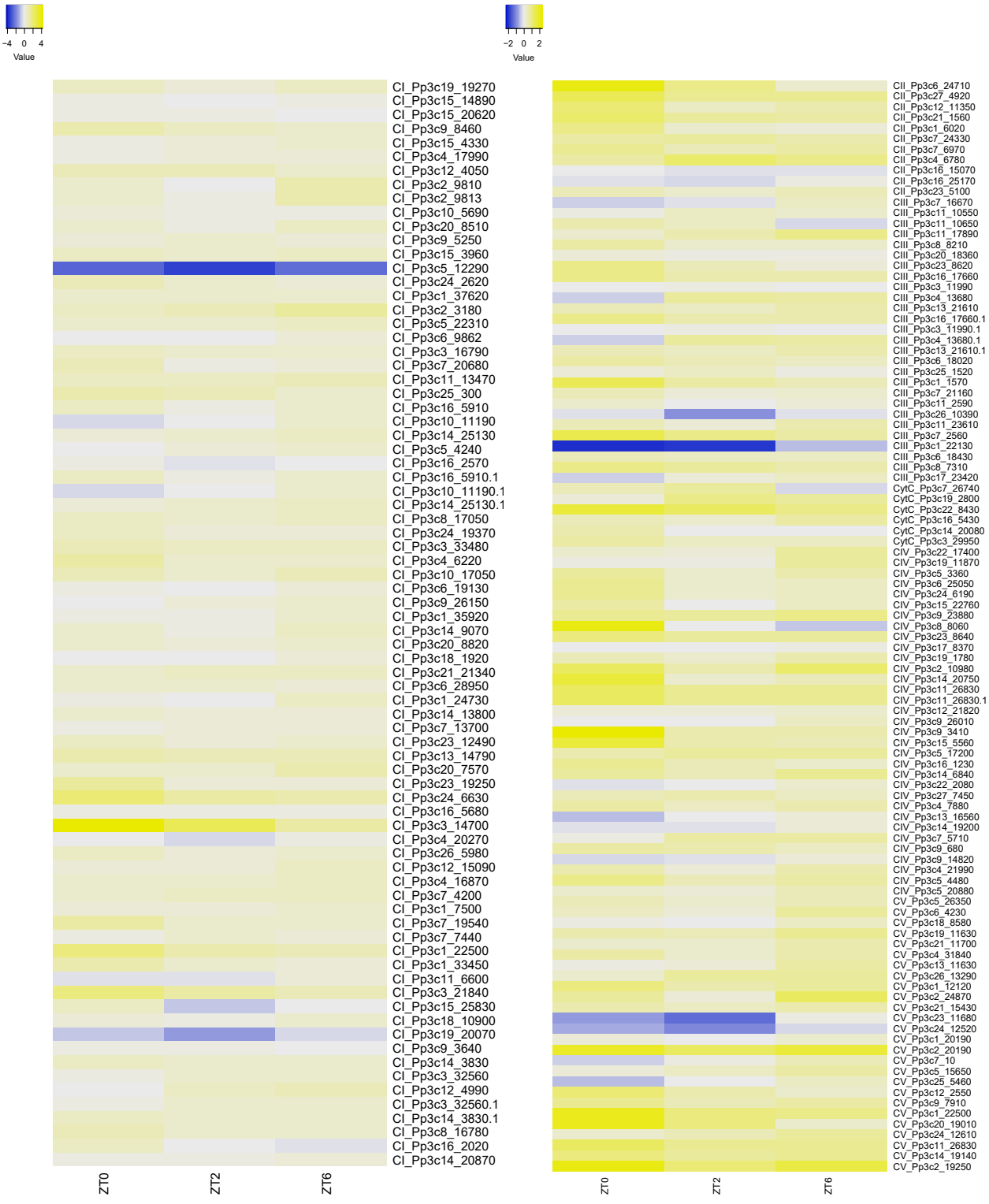

Supplementary Figure 3.4 | Relative expression levels of subunits of the respiratory complexes at ZT0, 2, 6. Color represents log fold change (*ndufa5* vs WT).

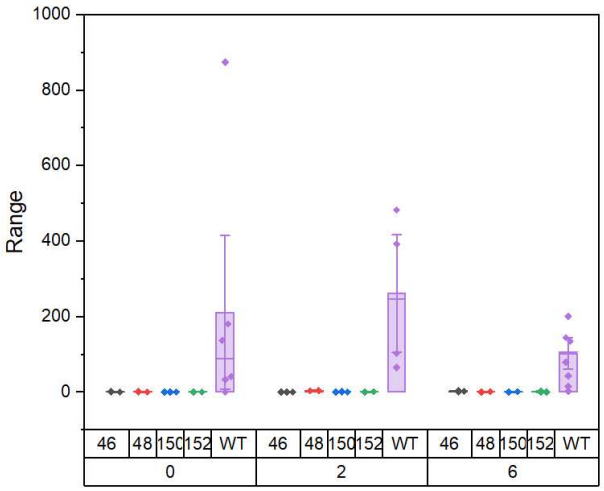

Supplementary Figure 3.5 | **Expression levels of Complex I subunit Pp3c12_14210**

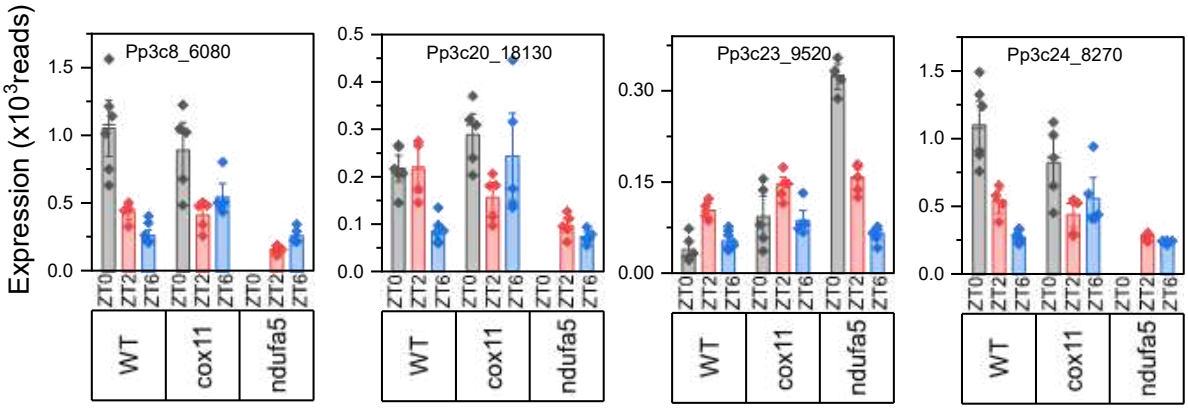

Supplementary Figure 3.6 | **Detailed expression levels of ANAC017 orthologs in *P. patens***. These graphs represent a zoomed version of those included in **Figure 3.9**. In some cases, data corresponding to *ndufa5* at ZT0 have been omitted because they were out of the scale.

Supplementary Table 3.1 | Relative expression in *ndufa5* of the four genes encoding WRKY transcription factors evolutionary close to AtWKRY15 according to Mohanta et al., 2016 and Khan & Van Aken, 2022. Missing data (-) means that the gene was not detected as significantly expressed in any condition. (***) p<0.001; (**) p<0.01; (*) p<0.1; (n.s.) p>0.1

			ZT0	ZT0	ZT2	ZT2	ZT6	ZT6
Gene name	ID in Mohanta et al., 2016	Gene ID	lfc	Sig	lfc	Sig	lfc	Sig
PpWRKY15	Pp1s48_141V6	Pp3c14_17020	0.42	n.s.	0.10	n.s.	0.19	n.s.
PpWRKY21-1	Pp1s163_112V	Pp3c1_40230	0.03	n.s.	-0.26	n.s.	-0.25	n.s.
PpWRKY21-3	Pp1s7_13V6	Pp3c2_2510	1.00	***	-0.84	**	0.17	n.s.
PpWRKY74	Pp1s65_236V6	Pp3c17_19970	-	-	-	-	-	-

Supplementary Table 3.2 | Relative expression in *ndufa5* of all the NAC transcription factors identified in *P. patens*. Source: . Asterisks next to the Gene ID mark the four homolog candidates of ANAC017. Missing data (-) means that the gene was not detected as significantly expressed in any condition. (***) p<0.001; (**) p<0.01; (*) p<0.1; (n.s.) p>0.1

	ndufa5	ndufa5	ndufa5	ndufa5	ndufa5	ndufa5
	ZT0	ZT0	ZT2	ZT2	ZT6	ZT6
Gene ID	lfc	Significance	lfc	Significance	lfc	Significance
Pp3c20_18130 (*)	3.377017	***	-1.1208	**	-0.16643	n.s.
Pp3c26_4660	3.253954	***	0.798364	n.s.	-0.39666	n.s.
Pp3c23_9520 (*)	3.150513	***	0.572226	n.s.	0.258824	n.s.
Pp3c8_6080 (*)	2.741445	***	-1.42182	***	-0.0088	n.s.
Pp3c3_8880	2.324385	***	0.658957	n.s.	-0.40422	n.s.
Pp3c24_8270 (*)	2.106882	***	-0.90111	**	-0.1671	n.s.
Pp3c3_12890	1.308745	*	0.518375	n.s.	-1.07423	n.s.
Pp3c13_6470	1.295894	*	-0.6259	n.s.	-0.44516	n.s.
Pp3c4_11490	1.125555	*	-0.14255	n.s.	0.124067	n.s.
Pp3c6_27690	0.869699	**	-1.43698	***	-1.70398	***
Pp3c5_570	0.412999	n.s.	0.107893	n.s.	-0.65096	*
Pp3c27_7560	0.355337	n.s.	0.547975	n.s.	-0.27344	n.s.
Pp3c13_20650	0.318284	n.s.	0.4302	n.s.	-1.35777	***
Pp3c6_28230	0.285344	n.s.	-0.75593	**	-0.45439	*
Pp3c22_130	0.27549	n.s.	0.191644	n.s.	0.298937	*
Pp3c12_18020	0.068888	n.s.	-3.25755	***	-1.37899	***
Pp3c16_19830	-0.34218	n.s.	-1.45656	**	0.148326	n.s.
Pp3c27_7430	-0.59368	*	-0.09101	n.s.	-0.62336	*
Pp3c19_1580	-0.76125	***	-0.70485	***	-0.49854	**
Pp3c16_13150	-0.83326	*	0.627357	n.s.	-1.08226	**
Pp3c3_25610	-1.02292	***	-0.77932	*	-0.08017	n.s.
Pp3c12_15190	-1.28375	*	-1.37157	*	-0.9804	*
Pp3c5_740	-3.43052	***	-1.92441	***	-1.34967	***
Pp3c13_10800	-	-	-	-	-	-
Pp3c16_23260	-	-	-	-	-	-
Pp3c2_32530	-	-	-	-	-	-
Pp3c26_10130	-	-	-	-	-	-
Pp3c26_13950	-	-	-	-	-	-
Pp3c27_7510	-	-	-	-	-	-
Pp3c3_2470	-	-	-	-	-	-
Pp3c4_20430	-	-	-	-	-	-
Pp3c4_29470	-	-	-	-	-	-
Pp3c5_630	-	-	-	-	-	-
Pp3c6_1310	-	-	-	-	-	-
Pp3c7_6590	-	-	-	-	-	-

Supplementary Table 3.3 | Relative expression in *ndufa5* of all the rhomboid proteases identified in *P. patens*. Genes were retrieved by orthology to the 16 genes annotated as rhomboid proteases in Arabidopsis, defined in Knopf & Adam, 2012. Missing data (-) means that the gene was not detected as significantly expressed in any condition. (***) p<0.001; (**) p<0.01; (*) p<0.1; (n.s.) p>0.1

	ZT0	ZT0	ZT2	ZT2	ZT6	ZT6
Gene ID	lfc	Significance	lfc	Significance	lfc	Significance
Pp3c2_10440	0.648521	*	0.678819	*	1.145382	***
Pp3c14_10400	-0.48536	*	0.007783	n.s.	-0.10832	n.s.
Pp3c17_14100	-1.60896	***	-0.88512	**	0.04388	n.s.
Pp3c22_7870	0.785495	***	0.911422	***	0.462598	*
Pp3c1_43050	0.211117	n.s.	0.059438	n.s.	0.455185	*
Pp3c9_8740	-	-	-	-	-	-
Pp3c15_4650	0.952136	***	0.178298	n.s.	0.302358	n.s.
Pp3c8_11670	-0.10901	n.s.	-0.39039	n.s.	0.101015	n.s.
Pp3c18_5250	0.745404	*	-0.22061	n.s.	0.028203	n.s.
Pp3c19_20960	-0.37718	*	-0.78898	***	-0.40705	*
Pp3c22_8560	0.238752	n.s.	0.027458	n.s.	-0.06116	n.s.

Supplementary Table 3.4 | Relative expression in *ndufa5* of the three identified orthologs of AtRcd1 identified in *P. patens*. Source: Phytozome. (***) p<0.001; (**) p<0.01; (*) p<0.1; (n.s.) p>0.1

	ZT0	ZT0	ZT2	ZT2	ZT6	ZT6
Gene ID	lfc	Significance	lfc	Significance	lfc	Significance
Pp3c2_13820	1.779544	***	-0.79753	***	0.359713	*
Pp3c16_6270	3.722389	***	0.206	n.s.	0.210387	n.s.
Pp3c25_950	2.475913	***	1.450172	***	0.204583	n.s.

Supplementary Table 3.5 | Relative expression in *ndufa5* of H2O2 responsive genes. Genes are orthologs of genes defined as H2O2 responsive in Arabidopsis, ref: (Vaahtera et al., 2014). Missing data (-) means that the gene was not detected as significantly expressed in any condition. (***) p<0.001; (**) p<0.01; (*) p<0.1; (n.s.) p>0.1

	ZT0	ZT0	ZT2	ZT2	ZT6	ZT6
Gene ID	lfc	Significance	lfc	Significance	lfc	Significance
Pp3c8_6770	3.156311	***	2.029732	***	1.470114	***
Pp3c12_24560	3.829957	***	1.420374	*	3.079261	***
Pp3c21_19080	2.0599	***	1.23978	**	1.180442	***
Pp3c8_8490	4.040954	***	1.878141	**	3.520538	***
Pp3c19_4790	0.36644	n.s.	0.348888	n.s.	0.897656	***
Pp3c14_4780	1.165974	***	0.000943	n.s.	-0.14108	n.s.
Pp3c8_8860	4.013145	***	1.768575	*	3.561018	***
Pp3c1_22120	-0.02178	n.s.	-0.24838	n.s.	0.202642	n.s.
Pp3c1_20930	-2.74257	***	-0.79645	*	-0.70284	*
Pp3c10_3790	0.02774	n.s.	-0.47756	n.s.	-0.63905	*
Pp3c17_10780	-	-	-	-	-	-
Pp3c8_9380	-	-	-	-	-	-
Pp3c8_9230	-	-	-	-	-	-
Pp3c14_1520	-	-	-	-	-	-

Supplementary Table 3.6 | **Relative expression of genes induced during UPR^{ER} in *P. patens***. Source: Lloyd et al., 2018. Missing data (-) means that the gene was not detected as significantly expressed in any condition. (***) p<0.001; (**) p<0.01; (*) p<0.1; (n.s.) p>0.1.

		ZT0	ZT0	ZT2	ZT2	ZT6	ZT6
ID in original ref	Gene ID	lfc	Significance	lfc	Significance	lfc	Significance
Pp1s181_3V6	Pp3c10_17310	2.638031	***	0.891821	**	0.742927	**
Pp1s566_63V6	Pp3c15_22880	0.669932	**	0.220841	n.s.	0.330718	n.s.
Pp1s368_19V6	Pp3c20_14730	1.56207	***	0.7003	*	0.366334	n.s.
Pp1s298_70V6	Pp3c4_21130	0.700672	*	0.715471	*	0.594678	*
Pp1s91_238V6	Pp3c12_8210	0.816523	***	0.419108	n.s.	0.26351	n.s.
Pp1s64_46V6	Pp3c5_8550	-0.53373	n.s.	0.268331	n.s.	0.284544	n.s.
Pp1s213_66V6	Pp3c9_3330	0.673949	**	0.384103	n.s.	0.724916	**
Pp1s34_189V6	Pp3c14_20430	0.408345	*	-0.66286	**	-0.31054	n.s.
Pp1s241_31V6	Pp3c20_22800	0.402884	*	0.465957	*	0.374772	*
Pp1s15_112V	Pp3c16_14150	0.406192	n.s.	0.894176	*	-0.01042	n.s.
Pp1s288_23V6	Pp3c3_25750	-	-	-	-	-	-
Pp1s34_31V6	Pp3c14_18900	-	-	-	-	-	-

Supplementary Table 3.7 | **Relative expression of ABA-induced genes in *P. patens***. References are (a) Timmerhaus et al., 2011; (b) Stevenson et al., 2016; (c) Ruibal et al., 2020. Missing data (-) means that the gene was not detected as significantly expressed in any condition. (***) p<0.001; (**) p<0.01; (*) p<0.1; (n.s.) p>0.1

	ZT0	ZT0	ZT2	ZT2	ZT6	ZT6	
Gene ID	lfc	Significance	lfc	Significance	lfc	Significance	Ref
Pp3c9_20090	-	-	-	-	-	-	a
Pp3c23_8630	-	-	-	-	-	-	a
Pp3c5_17150	2.05	***	1.25	**	0.23	n.s.	b
Pp3c15_23450	1.62	***	0.55	n.s.	0.00	n.s.	a
Pp3c16_2800	1.45	**	-0.51	n.s.	-0.90	*	a
Pp3c5_15770	1.40	*	3.91	***	2.30	**	a
Pp3c2_3370	1.07	***	0.52	*	0.43	*	b
Pp3c21_10290	0.77	**	-1.41	***	-0.79	**	a
Pp3c20_16340	0.44	*	0.13	n.s.	0.00	n.s.	b
Pp3c16_17210	0.43	n.s.	-0.13	n.s.	-0.15	n.s.	b
Pp3c18_19240	0.33	n.s.	-0.26	n.s.	-0.24	n.s.	a
Pp3c13_13320	0.26	n.s.	-0.12	n.s.	0.08	n.s.	b
Pp3c5_7630	0.16	n.s.	0.27	n.s.	0.38	n.s.	a
Pp3c7_5390	0.03	n.s.	0.74	*	-0.28	n.s.	b
Pp3c9_19760	-0.51	*	0.46	n.s.	-0.03	n.s.	b
Pp3c3_8540	-0.56	n.s.	0.99	*	0.29	n.s.	b
Pp3c11_18330	-0.57	*	0.79	*	-0.13	n.s.	b
Pp3c13_7110	-0.62	**	-0.34	n.s.	-0.33	*	b
Pp3c10_11910	-0.62	n.s.	2.22	**	0.47	n.s.	a
Pp3c10_11910	-0.62	n.s.	2.22	**	0.47	n.s.	b
Pp3c5_21160	-0.62	*	0.81	*	-0.07	n.s.	b
Pp3c8_13720	-0.84	*	1.92	***	0.63	*	a
Pp3c17_16470	-1.14	**	0.40	n.s.	-0.52	n.s.	b
Pp3c17_11030	-1.29	***	1.16	**	-0.03	n.s.	b
Pp3c9_5650	-1.35	***	0.47	n.s.	0.06	n.s.	b
Pp3c6_11090	-1.38	***	-0.50	n.s.	-0.58	*	b
Pp3c5_20390	-1.57	**	0.69	n.s.	0.23	n.s.	b
Pp3c15_4030	-2.23	***	-0.17	n.s.	1.05	*	b
Pp3c8_7340	-3.01	***	1.99	**	-0.56	n.s.	b
Pp3c7_22090	-1.66	***	0.48	n.s.	0.09	n.s.	c

Supplementary Table 3.8 | **Relative expression of Ex1 and Prl1 ortholog genes in *P. patens***. Orthologs were retrieved from Phytozome. (***) p<0.001; (**) p<0.01; (*) p<0.1; (n.s.) p>0.1

		ZT0	ZT0	ZT2	ZT2	ZT6	ZT6
	Gene ID	lfc	Significance	lfc	Significance	lfc	Significance
Ex1	Pp3c14_18650	0.739747	***	0.129085	n.s.	-0.12339	n.s.
Ex1	Pp3c16_980	0.353796	n.s.	-0.66318	*	0.045808	n.s.
Ex1	Pp3c17_21130	-0.80534	***	-0.97261	***	-0.27757	n.s.
Ex1	Pp3c27_3300	0.73879	**	0.430932	n.s.	0.099175	n.s.
Prl1	Pp3c5_15520	0.270544	n.s.	0.300565	n.s.	0.132158	n.s.
Prl1	Pp3c16_8560	0.223331	n.s.	0.270228	n.s.	0.203775	n.s.

Supplementary Table 3.9 | **Relative expression of Erf6 ortholog genes in *P. patens***. Orthologs were retrieved from Phytozome. (***) p<0.001; (**) p<0.01; (*) p<0.1; (n.s.) p>0.1

	ZT0	ZT0	ZT2	ZT2	ZT6	ZT6
Gene ID	lfc	Significance	lfc	Significance	lfc	Significance
Pp3c15_1990	-2.00948	***	-1.17827	**	-0.84977	**
Pp3c16_3770	-0.71103	n.s.	-1.95991	**	-0.61247	n.s.
Pp3c17_10170	0.297486	n.s.	-0.37568	n.s.	0.317546	n.s.
Pp3c19_20650	-0.76072	**	-1.33993	***	-0.80717	**
Pp3c26_1890	-0.0142	n.s.	-0.4057	n.s.	0.984716	***
Pp3c27_1350	0.610116	n.s.	-1.26221	*	-0.98089	n.s.
Pp3c27_5180	-1.3549	**	-0.82756	n.s.	-0.50818	n.s.
Pp3c9_2020	0.38453	n.s.	-0.67212	*	0.647016	*

CHAPTER IV

Mitochondrial respiration is essential for light-dependent ATP biosynthesis in *Physcomitrium patens*.

Antoni M. Vera-Vives[1], Piero Novel[1], Ke Zheng[2], Shun-ling Tan[1], Marco Mellon[1], Markus Schwarzländer[2], Alessandro Alboresi[1] and Tomas Morosinotto[1]

1. Department of Biology, University of Padova, Italy
2. Institute of Plant Biology and Biotechnology (IBBP), University of Münster, Germany

Authorship statement

The general research question was proposed by my supervisor Prof. Tomas Morosinotto and Prof. Alessandro Alboresi. ATeam reporter lines were produced by Piero Novel and me. FAd construct and mutant lines were produced by PhD student Marco Mellon, and line verification and characterization were done by me. The experimental approach was defined through the critical apport of all contributors. Experiments of *in vivo* monitoring of ATP were done by Piero Novel and me. Experiments of chlorophyll fluorescence were done by PhD student Shun-ling Tan. I performed data analysis with valuable input from PhD student Ke Zheng. I designed the graphs, wrote the manuscript, and revised it after the comments of PhD student Ke Zheng, Prof. Markus Schwarzländer and my supervisor.

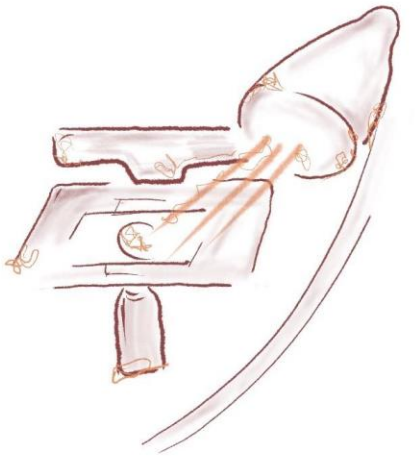

Abstract

Plants depend on sunlight energy for ATP and NADPH synthesis that ultimately fuel all cellular metabolism, including CO2 fixation. The dynamics of ATP synthesis in response to light thus have major importance for photosynthetic organisms. Yet, our current understanding of subcellular ATP dynamics in living plant tissue is surprisingly sketchy. In this chapter, we investigated how cytosolic $MgATP^{2-}$ concentrations responded to illumination in vivo making use of the fluorescence protein biosensor ATeam1.03-nD/nA in the moss *Physcomitrium patens* as a fully photoautotrophic organism without heterotrophic developmental stages. We observed a light-dependent increase in ATP concentration in the cytosol upon light exposition, which was dependent on the activity of photosynthetic electron transport. The same $MgATP^{2-}$ probe expressed in moss backgrounds depleted of respiratory Complex I caused a pronounced decrease in the rate of ATP synthesis in the cytosol, indicating that mitochondrial respiration provides an essential contribution to the light-dependent accumulation of ATP in the cytosol. This conclusion is supported by the generation of mutants depleted in mitochondrial ATPase (complex V) by homologous recombination mediated gene targeting that caused a drastic growth reduction even though photosynthetic electron transport was not impaired. These results demonstrate that even in full photoautotrophic organisms like *P. patens* that do not encounter any heterotrophic phase throughout their life cycle photosynthesis is the ultimate source of energy, but it is mitochondrial respiration that converts the energy and reducing power exported from the chloroplast to supply ATP the cytosol.

1. Introduction

Photosynthetic organisms are the main primary producers on our planet, fixing approximately 110 Gt Carbon per year and providing the chemical energy supporting most lifeforms (Ringsmuth et al., 2016). In photosynthetic organisms, sunlight powers the photosynthetic electron flow catalysed by photosystem (PS) I and II, cytochrome b_6f and ATPase that drives the synthesis of NADPH and ATP sustaining cellular metabolism. In photosynthetic organisms also have an active mitochondrial respiration, with its specific electron transport pathway, transferring electrons from NADH and succinate to oxygen through the activity of enzymatic complexes localized in the inner mitochondrial membrane, Complex I, II, III, IV. This electron transfer is coupled to the generation of an electrochemical transmembrane gradient that drives the synthesis of ATP through ATP-synthase, also called complex V. The NADH dehydrogenase complex (Complex I, CI) is the main site for electron insertion into the mitochondrial electron transport chain (mETC) and it can provide up to 40% of the protons for mitochondrial ATP formation (Braun et al., 2014; Watt et al., 2010).

Respiration in plants is essential to support the energy demand during the night, in non-photosynthetic tissues such as roots or in developmental stages like seed germination where photosynthesis is not active. An increasing set of evidence from various photosynthetic organisms, however, underlines the importance of respiration also for sustaining optimal photosynthetic activity (Bailleul et al., 2015; Joliot & Joliot, 2008; Noguchi & Yoshida, 2008) with a strong functional link between chloroplasts and mitochondria bioenergetic metabolism (Cardol et al., 2003; Dutilleul et al., 2003; Mellon et al., 2021; Schönfeld et al., 2004). In the diatom *Phaeodactylum tricornutum* it was demonstrated that metabolites exchange between chloroplast and mitochondria is essential for carbon fixation (Bailleul et al., 2015). Moreover, excess reducing power produced via photosynthesis can be routed to mitochondrial respiration, preventing over-reduction of electron transporters and generation of reactive oxygen species (ROS) in the plastid (Noguchi & Yoshida, 2008; Zhang et al., 2012).

Consistently with the essential role of mitochondrial respiration in plant metabolism, as reviewed in Chapter I, Knock-Out (KO) mutants completely depleted in complex II, complex III and complex IV are not viable and, so far, only knock-down plants have been isolated and studied. Mutants completely lacking mitochondrial

Complex I activity have instead been described in *Arabidopsis thaliana* as well as in *Nicotiana tabacum* and the moss *Physcomitrium patens* where they showed a severe growth phenotype and alterations in germination, fertilization, and pollen development (Fromm et al., 2016b). Interestingly, European mistletoe *Viscum album* was shown to be able to live without a functional CI, but this organism is an obligate semi-parasite living on branches of trees, and thus its energetic metabolism is likely remodelled (Maclean et al., 2018; Senkler et al., 2018).

Differently from plants, many respiratory mutants depleted in all respiratory complexes have been isolated in the green alga *Chlamydomonas reinhardtii* where they generally show strong phenotypes under heterotrophic conditions but grow similarly to WT under photoautotrophic conditions (Larosa et al., 2018; Salinas et al., 2014). This difference suggests that the role of respiration in cell metabolism adapted during plant evolution and, in obligatory autotrophs like most plants, adapted to work synergically with photosynthesis (Mellon et al., 2021).

In photosynthetic active cells both chloroplasts and mitochondria are functioning in ATP production and support energy demand of their respective organelle. ATP is however also essential in other cellular compartments, as in the cytosol where it is used for many seminal metabolic pathways such as lipid and protein anabolism, sucrose biosynthesis or active transport of various molecules and ions. It was proposed that when chloroplasts are actively reducing CO_2, cytosolic ATP originates mostly from mitochondria with ATP export from chloroplast being enhanced only under stress conditions, when CO_2 fixation is reduced (Gardeström & Igamberdiev, 2016). These conclusions derive from observations made from experiments with biochemical fractionations and use of inhibitors and were supported by modelling studies (Shameer et al., 2019). On the other hand, information from intact systems, also exploring dynamic transitions and responses to variable environmental conditions are instead still missing.

This limitation can be addressed using genetically encoded indicators that allow the monitoring of fast-occurring biological processes *in vivo*, enabling the observation of highly dynamic processes that would not be assessable otherwise. This is the case of the Förster resonance energy transfer (FRET)-based sensor ATeam1.03-nD/nA,

which has been successfully used for monitoring ATP in Arabidopsis (De Col et al., 2017; Lim et al., 2022; Voon et al., 2018).

Non-vascular plants like the moss *P. patens* diverged from vascular plant ancestors early after land colonization and they are thus valuable models to investigate the role of respiration in photosynthetic metabolism and its adaptation during evolution, highlighting the adaptation response to the new environmental conditions (Knight et al., 2009; Rensing et al., 2020). This model organism was chosen here also because *P. patens* plants depleted of active respiratory Complex I were recently isolated and they showed a strong growth reduction in autotrophic conditions demonstrating a role of respiration in cell metabolism like vascular plants (Mellon et al., 2021).

In this work the cytosolic ATP dynamics *in vivo* were investigated in *P. patens* using the ATeam probe, to investigate the impact of photosynthetic activity on the energy status of the cytosol. While photosynthesis is the ultimate source of energy, ATP supply to the cytosol was shown to be dependent on mitochondrial respiration. This was confirmed by the strong phenotype of mutants depleted of Complex V and thus impaired in mitochondrial ATP biosynthesis. The work thus demonstrates that mitochondrial respiration is essential for ATP supply to the cytosol and supporting metabolism in the light when photosynthesis is active.

2. Results

2.1. Generation of *P. patens* plants accumulating ATP probe ATeam in the cytosol.

Stable *P. patens* wild-type (WT) lines constitutively accumulating ATeam1.03-nD/nA in the cytosol, referred to as WT-ATeam, were generated by protoplast transformation. After transformation, lines stably resistant to zeocin were screened through the fluorescence of the mVenus channel to select the ones with detectable accumulation of the probe. In each transformation, at least three independent lines were selected among the ones showing mVenus fluorescence signal (Supplementary Figure 4.1).The ATeam-expressing lines did not show any visible growth defect and showed normal development with the ability to grow leaflets, rhizoids and sporophytes and produce viable spores as well as the parental line (Supplementary Figure 4.1), suggesting that the probe accumulation did not cause major alterations in metabolism and development.

The localization of the mVenus fluorescent signal in the lines was verified by confocal microscopy, with chlorophyll fluorescence marking chloroplast localization. The mVenus signal showed no overlap with chlorophyll fluorescence and was localized in large areas inside the cell, consistent with a cytosolic expression, confirming the expected localization (Figure 4.1A).

In the long term (> 1 year) we observed a decrease in the fluorescence signal, most likely due to silencing effects, as similarly observed for different biosensor proteins in Arabidopsis (De Col et al., 2017; Schwarzländer et al., 2016) and for overexpressed proteins in more general sense in *P. patens* (Kubo et al., 2017). All imaging experiments were performed on protonema, a young tissue regenerated vegetatively, and we did not observe any mosaic silencing of the probe, meaning that the silencing, if present, was homogenous in all the cells. Because the probe is ratiometric, a moderate silencing would not cause any drift in FRET, as the value is self-normalized. In any case, WT-ATeam plants were newly re-isolated every 18 months to ensure maintenance of a good signal-to-noise ratio.

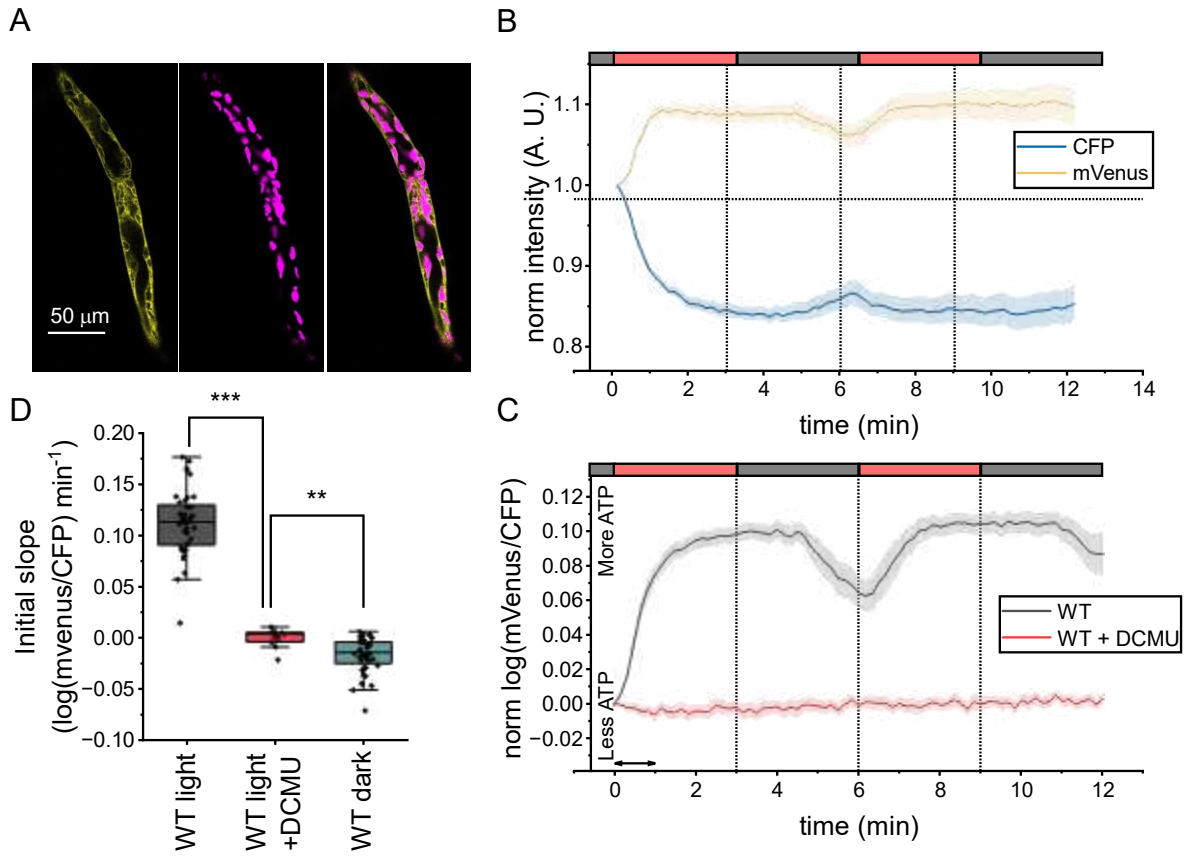

Figure 4.1 | Light induced $MgATP^{2-}$ accumulation in the cytosol of *Physcomitrium patens*. (A) Confocal images of two cells of protonema of one of the WT-ATeam lines showing mVenus channel (yellow), chlorophyll autofluorescence (magenta) and the merged image. (B) Normalized intensities of the single channels showing their changes upon dark-to-light transitions. All measurements started in the dark for 10 seconds before switching light on. Light periods are marked with a red bar and correspond to 50 µmol photons m^{-2} s^{-1} of red light. (C) Normalized FRET ratio during dark-to-light transitions. Light periods are marked with a red bar and correspond to 50 µmol photons m^{-2} s^{-1} of red light. The bidirectional arrow marks the timelapse used for the calculation of slopes shown in (D). The error band represents the SE of mean (n>10). (D) Quantification of slope of the normalized FRET ratio during the first minute of illumination in WT without / with DCMU, and after 2 minutes in the dark. Statistics: two-sample t-test, (***) p<0.001; (**) p<0.01.

2.2. Photosynthesis drives the increase of ATP concentration during dark-to-light transitions.

In each round of transformation, three independent lines generated were used to observe the cytosolic $MgATP^{2-}$ dynamics in the cytosol during dark-to-light transitions and assess changes in $MgATP^{2-}$ levels associated with the activation of photosynthesis. To this end, photosynthesis activity was induced using 50 µmol photons m^{-2} s^{-1} of red (λ > 630 nm) actinic light that does not interfere with the acquisition parameters of mVenus or CFP channels (465-561 nm). This choice of wavelengths enabled to keep the actinic light on during the acquisition without adding

signal to the detector (Supplementary Figure 4.2). Taking advantage of the ratiometric nature of the probe and the natural distribution of protonema in single-cell layers, we quantified the CFP and mVenus signals and calculated the corresponding FRET ratio (mVenus/CFP) in whole focal planes that contained dozens of different cells (Figure 4.1A, Supplementary Figure 4.2).

To follow the dynamic response of ATP, plants were first incubated in the dark for 40 minutes to relax all photosynthesis-related processes and enable all samples to start from a homogeneous, dark-adapted state. When actinic illumination was switched on the mVenus signal increased immediately with a corresponding decrease in the CFP channel (Figure 4.1B). This behaviour indicates a *bona fide* increase in FRET efficiency. mVenus/CFP ratio increased within seconds of illumination, reaching a plateau after 1.5 minutes (Figure 4.1C). After light was turned off FRET signal remained steady for approx. 1.5 minutes and then started to decrease, with a kinetic less steep than the light-driven increase ((Figure 4.1C). When the light was switched on a second time, the signal increased again, confirming that $MgATP^{2-}$ concentration depended on the light presence. In the second exposure to dark we observed a slightly longer period of stability (about 2 minutes), before it started to decrease again.

The same measurements were repeated in the presence of the PSII inhibitor 3-(3,4-dichlorophenyl)-1,1-dimethylurea (DCMU) that blocks all photosynthetic electron transport, that completely abolished all the above-mentioned dynamics (Figure 4.1C, D; Supplementary Figure 4.3), demonstrating that light alone did not affect the FRET signal and that the observed dynamics were fully dependent on photosynthetic electron transport fuelled by actinic light.

Since the quality of light could influence the cytosolic $MgATP^{2-}$ dynamics, the same experiment was repeated using a different setup already used for similar experiments in Arabidopsis, where the white light supporting photosynthesis is switched off during the confocal measurement, creating a pseudo-continuous light effect (Elsässer et al., 2020). These experiments confirmed the dynamics induced by light and induction of $MgATP^{2-}$ accumulation in cytosol induced by light, independently from the setup and light wavelength (Supplementary Figure 4.4). The comparison further validates both on-stage live illumination approaches as usable.

2.3. Synthesis of cytosolic ATP depends on light intensity.

To test the effect of light intensity on the increase of $MgATP^{2-}$ during dark-to-light transitions, we compared the kinetics of FRET upon illumination with different intensities, namely 5, 50 or 200 µmol photons m^{-2} s^{-1} of red light (Figure 4.2).

An intensity of 5 µmol photons m^{-2} s^{-1} of red light, which is low and limiting for *P. patens* growth but high enough to initiate photosynthetic activity, was sufficient to trigger an increase in cytosolic $MgATP^{2-}$ (Figure 4.2A), that was, however, slower than in 50 µmol photons m^{-2} s^{-1} (Figure 4.2B). This is in line with our finding that the increase in cytosolic ATP is fully dependent on the activation of electron transport in the thylakoids by light. On the other hand, using a higher light intensity (200 µmol photons m^{-2} s^{-1}) did not alter the shape or magnitude of the increase of cytosolic ATP, even before reaching the plateau (Figure 4.2A, B), meaning that 50 µmol photons m^{-2} s^{-1} are sufficient to saturate ATP biosynthesis capacity in these conditions. This was also the case using the white light setup (Supplementary Figure 4.4).

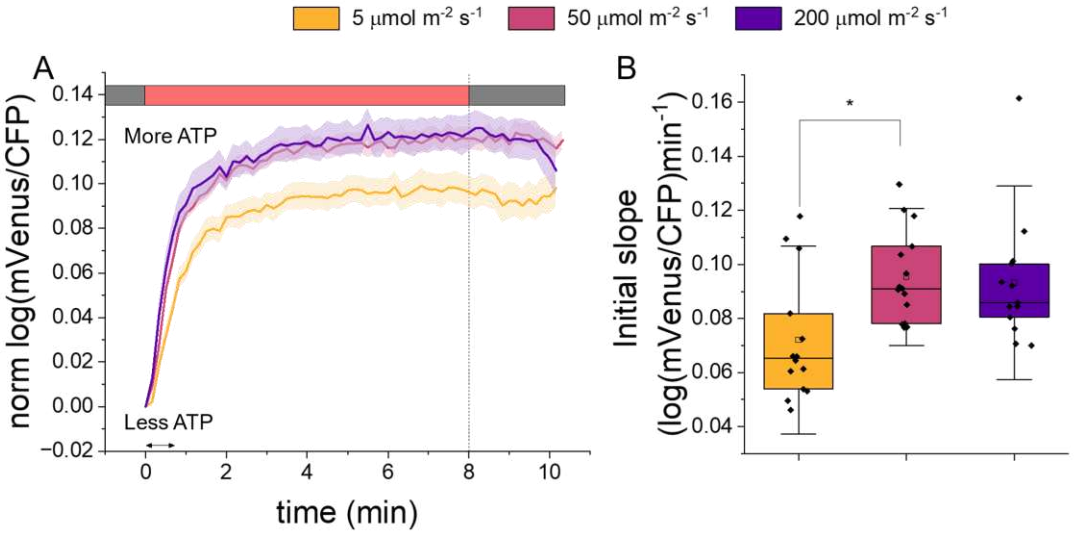

Figure 4.2 | Effect of light intensity on the cytosolic increase of ATP during dark-to-light transitions. (A) Dark-adapted WT-ATeam plants were illuminated for 8 minutes with red light of either 5, 50 or 200 µmol photons m−2 s−1, followed by 2 minutes of darkness. The bidirectional arrow marks the timelapse used for the calculation of slopes shown in (B). Error bands represent the SE of mean (n = 13-15). (B) Slope during the first minute of illumination. Statistics: two-sample t-test, (*) $p<0.05$. Error bars represent 1.5 times the SD.

2.4. Mitochondrial respiration is essential for ATP supply in the cytosol

Mitochondrial activity has been suggested to contribute to cytosolic ATP biosynthesis in photosynthetic organisms and inhibitors of the mitochondrial respiratory chain, such as the uncoupler carbonyl cyanide m-chlorophenyl hydrazone (CCCP) or the Complex III inhibitor Antimycin A, have been shown to alter cytosolic ATP in Arabidopsis seedlings (de Col et al., 2017). Any intervention using inhibitors has the potential caveat of unknown pharmacokinetics, possible undesired secondary effects. In the light, inhibitors affecting respiration can have indirect impact on photosynthesis (Bendall & Manasse, 1995; Forti & Gerola, 1977). To assess impact of mitochondrial respiration on ATP biosynthesis using an orthogonal genetic approach, the ATeam1.03-nD/nA probe was introduced in *P. patens* lines lacking the Complex I structural subunit NDUFA5 (*ndufa5* KO) previously shown to completely lack mitochondrial NADH dehydrogenase activity (Mellon et al., 2021). Three independent lines stably expressing the cytosolic probe in *ndufa5* background, that we will refer to as *ndufa5*-ATeam, were isolated.

Complex I mutants showed impaired cell and tissue morphology: cells are smaller and protonema filaments more condensed than in WT (Mellon et al., 2021) (Supplementary Figure 4.5). The probe expression showed no additional impact on growth beyond the defects associated with *ndufa5* depletion (Supplementary Figure 4.5). The fluorescence intensity of the single channels was in all cases in a range close to the WT-ATeam lines and thus the same confocal settings were used for both lines to enable a reliable comparison of FRET signals between WT and *ndufa5* KO.

ndufa5-ATeam plants were exposed to the same light treatment shown in Figure 4.1, observing an increase in ATP during dark-to-light transitions also in these mutants (Figure 4.3). However, the kinetics of FRET signal in *ndufa5*-ATeam plants was clearly affected and the slope 2.7 times slower than the one from WT-ATeam lines (Figure 4.3B). Differently to WT-ATeam, the signal also rapidly decreased when the light was turned off after the first 3 minutes of light. A second light treatment caused a further increase in cytosolic ATP, as in WT-ATeam, without reaching a plateau as observed in WT plants. These results suggest that mitochondrial respiration is an

important contributor to the synthesis of cytosolic ATP and, remarkably, that Complex I is strictly required for efficient cytosolic ATP kinetics during dark-to-light transitions.

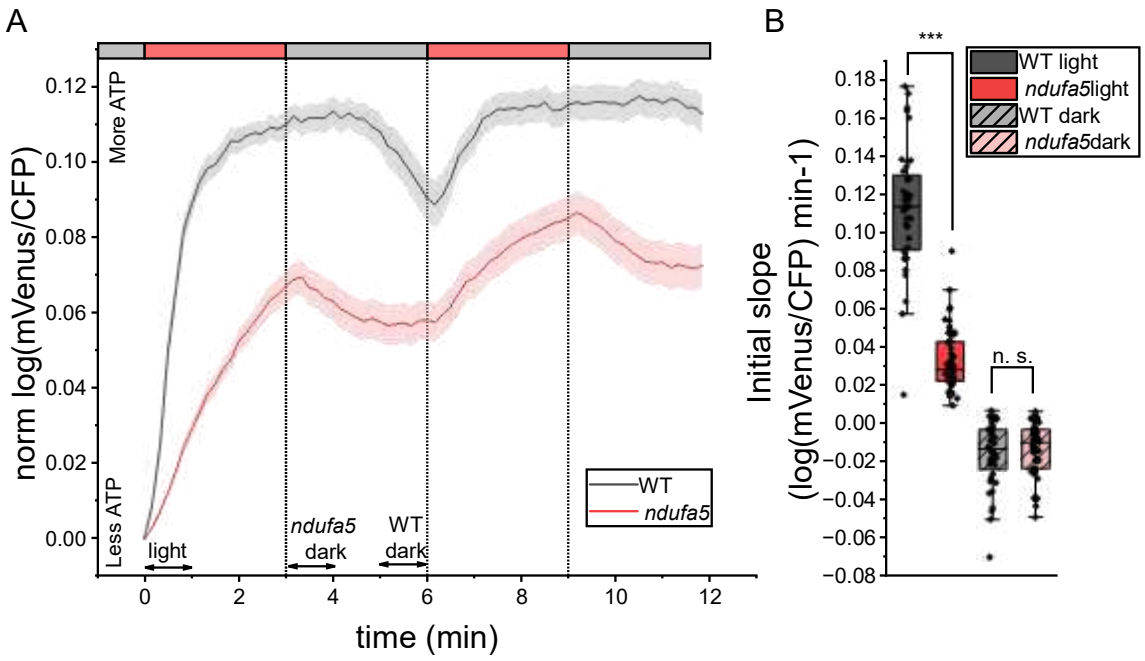

Figure 4.3 | **Cytosolic ATP dynamics in the Complex I deficient plant *ndufa5*-ATeam.** (A) Normalized FRET ratio during dark-to-light transitions in WT and *ndufa5* KO. Light periods are marked with a red bar and correspond to 50 µmol photons m^{-2} s^{-1} of red light. Bidirectional arrows mark the timelapse used for the calculation of slopes shown in (B). The error band represents the SE of mean (n > 10). (B) Slope of the normalized FRET ratio during the first minute of illumination and the first (*ndufa5*) or last (WT) minute of darkness. Error bars represent 1.5 times the SD. Statistics: two-sample t-test, (***) p<0.001, (n.s.) p>0.05.

To further investigate the ATP dynamics, WT-ATeam and *ndufa5*-ATeam plants were exposed to light treatments of different duration. The extension of the illumination phase up to 8 minutes (Figure 4.4A) showed that even though the rate of ATP biosynthesis was slower in the mutant, it eventually reached the same normalized value of FRET as WT.

On the other hand, when the illumination phase was reduced to 1 minute (Figure 4.4B), this time was sufficient for WT-ATeam to show a sustained increase in cytosolic ATP. One minute of darkness was instead not enough to observe a signal decrease. A following longer darkness period indeed showed that at least one and a half minutes of darkness were needed to observe the signal decrease. In *ndufa5*-ATeam, instead, FRET signal increase was slower during illumination, and it decreased immediately in the dark, confirming that ATP biosynthesis capacity was reduced in the mutant.

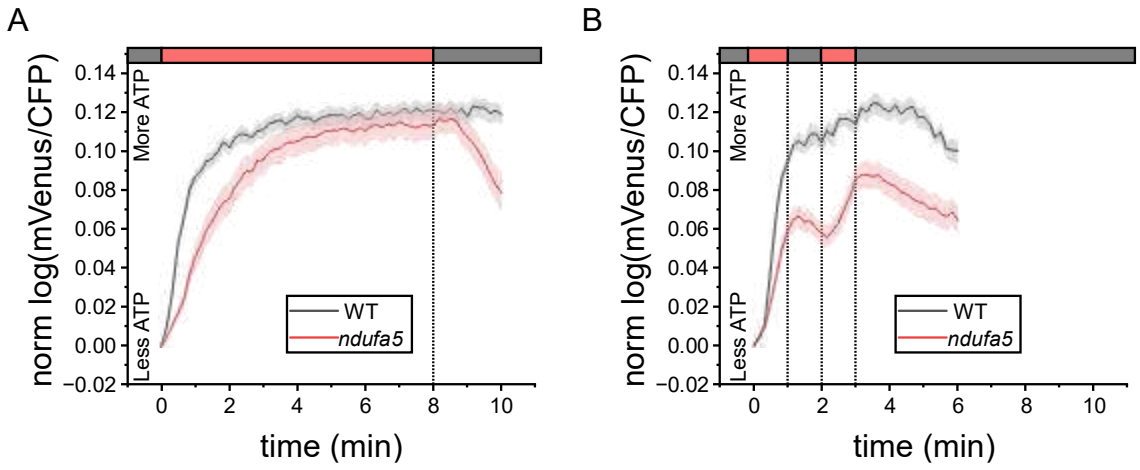

Figure 4.4 | **Cytosolic ATP dynamics in the Complex I deficient plant *ndufa5* under alternative light-dark cycles**. Dark-adapted plants were exposed (A) to 8 min of light followed by 2 min of darkness or (B) to a light fluctuation that consisted in 1 min of light, 1 min of darkness, 1 min of light and 4 min of darkness. In both cases light used was 50 µmol photons m^{-2} s^{-1} of red light. Light and dark periods are marked with red and grey bars, respectively. Error bands represent the SE of mean. Sample sizes are n=15 (A, WT), n=14 (A, *ndufa5*), n=4 (B, WT) and n=25 (B, *ndufa5*).

2.5. Impairment of mitochondrial ATP biosynthesis drastically decrease growth without impacting photosynthesis.

To further verify the biological relevance of mitochondrial ATP synthesis for plant metabolism we aimed to generate knock-out mutants of the mitochondrial F_1F_O-ATP synthase (Complex V), the complex responsible of exploiting the electrochemical gradient generated by the mETC to synthesize ATP. As described in detail in CHAPTER I, the holoenzyme is composed by two sub-complexes: the F_1 hydrophilic head where ATP is formed and the F_O hydrophobic moiety, which is embedded in the membrane and acts as a rotor fuelled by the movements of protons. These two subcomplexes are linked through the central and the peripheral stalks that are required for the stability of the complex and for the energy transfer between F_O and F_1 domains.

Most of the F_1F_O-ATP synthase complexes are conserved among eukaryotes with homologs of yeast and mammals subunits found conserved in green algae and plants. Hence those can be identified in *P. patens* genome as well (Supplementary Table 4.2). Proteomics approaches further identified two additional subunits in plants associated with the F_O domain, referred as F_Ad and 6 kDa, that present no counterparts in mammals or yeast (Senkler et al., 2017). Both subunits are also conserved in *P. patens* genome (Supplementary Table 4.2). In particular, the subunit F_Ad has been linked with development and fertility in wheat where its repression leads

to sterile plants (Li et al., 2010). In Arabidopsis, the gene is highly expressed in pollen during late developmental stages and the homozygous mutants are not viable. The hemizygous mutant shows altered mitochondrial morphology during the dehydration phase of pollen, causing their degeneration (Li et al., 2010).

Considering its functional impact and the fact that a single nuclear gene encodes for F_Ad, this subunit was chosen as target for the inactivation of Complex V in *P. patens*. Two independent *f_Ad* lines, depleted of the gene Pp3c9_7910, were isolated and verified to have an insertion of the resistance cassette in the locus of interest (Supplementary Figure 4.6). This was possible because *P. patens* tissues are mostly haploid and the transformation procedure proceeds by vegetative propagation and it is thus possible to generate full knockout plants without passing through heterotrophic developmental stages, like spore formation and germination.

f_Ad plants showed a pronounced growth defect, much stronger than the one observed in the Complex I deficient *ndufa5*. Indeed, plants took 4 months to reach a size similar to 21 days-old *ndufa5* plants that already have a growth reduction with respect to WT plants (Figure 4.5). Growth could not be rescued by exposure to continuous illumination or external feeding of glucose. The growth defect strongly limited the experimental analyses possible for these plants but after approximately 6 months it was possible to obtain enough tissue to perform photosynthetic measurements using chlorophyll fluorescence. Upon exposition to mild illumination (50 µmol photons m^{-2} s^{-1}), efficiency of photosystem PSI (Y_I) was indistinguishable between WT and *f_Ad* plants. The efficiency of PS (Y_{II}) instead in the same conditions showed larger saturation and correspondingly the mutant showed a stronger reduction of plastoquinone, as estimated from 1-qL (Figure 4.5), suggesting that electron transport capacity for PSII was reduced in the mutant with respect to the WT. The same measurements repeated with a stronger, saturating light intensity (300 µmol photons m^{-2} s^{-1}), however, showed instead no differences between WT and the Complex V mutant, suggesting the photosynthetic light conversion is functional in the mutant. It only showed mild alterations that could be due with the different age and growth rate of plants. In any case, the observed alterations in photosynthetic activity cannot explain the major growth phenotype (Supplementary Figure 4.7).

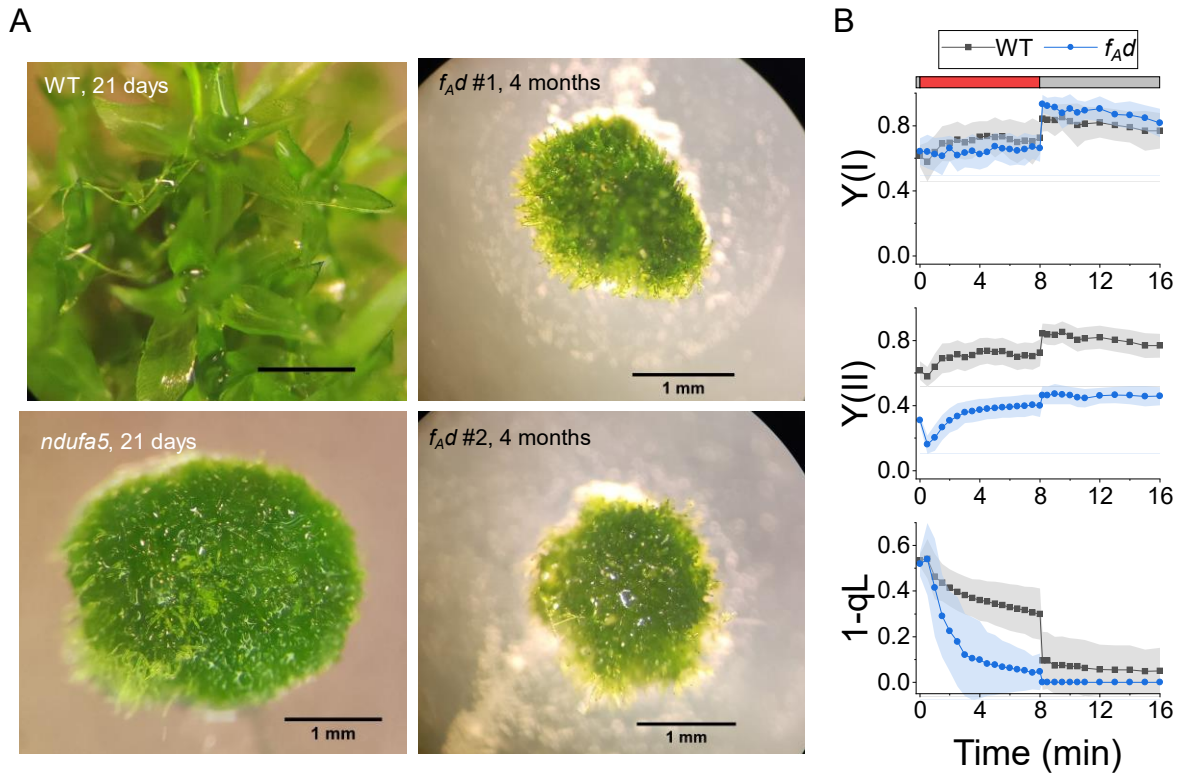

Figure 4.5 | **Growth phenotype and photosynthetic properties of *f_Ad* plants**. (A) Comparison of 4 months-old *f_Ad* colonies with 21 days old WT and *ndufa5* colonies. (B, C) Quantum yield of Photosystem I (Y_I) (B) and Photosystem II (Y_{II},) (C) monitored with PAM during exposition to 8 minutes of actinic light at 50 µmol photons m^{-2} s^{-1} followed by 8 minutes of dark. (D) Redox state of plastoquinone assessed by the fluorescence parameter 1- qL. All kinetics were measured after 40 minutes of dark adaptation of WT, *f_Ad* KO plants grown photoautotrophically for respectively 10 days and 4 months. Data are expressed as the means ±SD, n = 4.

3. Discussion

3.1. Light induces ATP accumulation in the cytosol of *P. patens*.

A set of *Physcomitrium patens* lines expressing constitutively the FRET based sensor ATeam1.03-nD/nA in the cytosol enabled the *in vivo* monitoring of the cytosolic ATP dynamics during dark-to-light transitions. These experiments show that plant illumination activates photosynthesis and triggers an increase of cytosolic ATP that can be abolished by DCMU, demonstrating the ATP accumulation is fully dependent on photosynthetic activity. The use of different light intensities showed that 50 µmol photons m^{-2} s^{-1} of red light, that is efficiently absorbed by chlorophylls, are already saturating ATP biosynthesis.

We should consider that the biologically most relevant form of ATP, i.e., the magnesium complex $MgATP^{2-}$, is stabilized in alkaline pH, due to a pKa of ATP close to 7.0. In Arabidopsis, illumination has been shown to induce the alkalinization of different compartments, including cytosol, chloroplast and mitochondria (Elsässer et al., 2020). Therefore, we must consider that the increment in cytosolic ATP in WT and *ndufa5* moss plants could in part be due to the alkalization of the cytosol. However, the alkalization of the cytosol of Arabidopsis seedlings did not cause an increase in ATP in Arabidopsis (Elsässer et al., 2020), as we report here for *P. patens*. Consequently, although we do not have experimental proof that the alkalization occurs also in cytosol of *P. patens*, if it occurred it would not necessarily cause an increase in the signal. Therefore, we believe that the increase in ATP reported by the ATeam sensor is likely due to an effective increase in ATP concentration, and not only an artifact caused by the alkalization of the cytosol.

Earlier work studied cytosolic ATP dynamics *in vivo* during dark-to-light transitions in cotyledons of Arabidopsis seedlings also showed an illumination driven increase of ATP (Elsässer et al., 2020; Voon et al., 2018). This however required a pre-treatment with the Complex I inhibitor rotenone to decrease of cytosolic ATP levels prior to observations to stay within the dynamic range of the probe (Voon et al., 2018). This was explained suggesting that steady state levels of cytosolic ATP of cotyledons of Arabidopsis seedlings were high and saturating for the probe, and thus light induced differences were observable only if ATP levels were decreased before the illumination.

Results with *P. patens* were confirmed using the setup described by Elsässer et al., 2020 (Supplementary Figure 4.4) and thus the differences cannot be attributed to the system of illumination employed, i.e., red light against pseudo-continuous white illumination.

The most likely explanation is thus that ATP levels in the dark are different between Arabidopsis cotyledons and *P. patens* protonema cells and this ultimately enabled to easily observe the light induced increase in the latter. Cells in the two tissues are indeed in a different physiological state, since protonema is fully dependent on photosynthetic activity for growth and actively fixing CO_2, and this can easily drive to lower $MgATP^{2-}$ levels when plants are moved in the dark.

In *P. patens* WT plants, the light-driven increase of FRET signal reaches a plateau after approx. 1 minute of illumination. When the light is switched off, it takes instead approx. 1.5 minutes in the dark for the FRET signal to decrease (Figure 4.1). These dynamics could be due to a possible saturation of the probe that is not able to detect ATP concentration changes beyond its dynamic range, as already observed in Arabidopsis (Voon et al., 2018). Following this hypothesis, ATP would overcome probe dynamic range after 1 minute of illumination and it would take 1.5 minutes in the dark to consume enough ATP to re-enter. If this is the case, however, in the case of a shorter illumination (1 minute, Figure 4.5B), where the FRET signal just approached the saturation level, ATP concentration should start decreasing immediately after the light is switched off, while instead it still takes 1.5 minutes, as with longer illumination. Indeed, the FRET signal is stable for approximately 1.5 minutes in the dark irrespectively if the light treatment is 1, 3 or 8 minutes long. This observation is not consistent with the idea that the ATP levels are still increasing but the probe is saturated.

While the possibility that probe saturation is occurring in some points cannot be completely ruled out, the most likely explanation for all the dynamics observed is that the ATP concentration reaches a steady concentration after 1 minutes of illumination. If this is the case, final ATP levels would indeed be similar in all experiments with 1, 3 or 8 minutes of illumination, thus explaining why they all have similar decrease dynamics in the dark. The signal stability when the light is switched off for approx. 1.5 minutes can instead be explained because mitochondrial respiration is still active and

it can work in the dark converting into ATP reducing equivalents produced earlier by photosynthesis and transferred into mitochondria either through redox shuttles such as the malate valve (Igamberdiev & Bykova, 2022) or via photorespiratory metabolism, thus maintaining its supply in the cytosol. After 1.5 minutes in the dark the impairment of redox power export from chloroplast would be finally perceived by the ATP levels. We must consider that a second exposure to a light-dark cycle results in a signal that is stable for longer time, about 2 minutes. This could be explained by the fact that the three minutes of darkness are not sufficient for the cytosolic concentration to return to the original value.

The observation of these kinetics is particularly interesting because they show that, while the photosynthetic activity responds very fast to the light availability, the ATP dynamics in the cells are slower, suggesting the presence of metabolic mechanisms to convert an unstable form of energy such as light to forms compatible with metabolic reactions.

3.2. Mitochondrial respiration is essential for cytosolic ATP accumulation.

As discussed earlier, in WT-ATeam one minute of illumination is sufficient to rise the levels of $MgATP^{2-}$ to a steady level that is maintained for 1.5 minutes after the light is switched off (Figure 4.4B). Same experiments in *ndufa5* plants that lack a functional mitochondrial NADH-CoQ oxidoreductase (Complex I) showed different dynamics and in *ndufa5*-ATeam the rate of ATP accumulation in the cytosol is approx. 3 times slower. Because of this slower synthesis, in *ndufa5*-ATeam the mVenus/CFP signal reach a stable value only if light exposure was prolonged up to 8 minutes, finally reaching the same values as in WT-ATeam lines.

The role of respiration in ATP supply is confirmed by the dynamics immediately after the light is switched off. In *ndufa5*-ATeam the FRET signal decreased relatively faster than WT in the dark, where it remained steady for approx. 1.5 minutes. This is consistent with the hypothesis that mitochondrial respiration is responsible of ATP biosynthesis in the dark and that this is affected in *ndufa5*-ATeam.

The different dynamics of cytosolic ATP in WT-ATeam and *ndufa5*-ATeam plants strongly support the idea of the respiratory chain contributing to cytosolic ATP

during dark-to-light transitions. *ndufa5* plants are depleted in Complex I, which is estimated to contribute to 40% of proton translocation for mitochondrial ATP biosynthesis (Braun et al., 2014).We previously reported *ndufa5* plants to have increased respiration through the alternative respiratory pathway (Mellon et al., 2021), which could partially compensate for the loss of the proton-translocating complex in terms of ATP synthesis capacity by oxidative phosphorylation. However, we here showed that *ndufa5* plants still suffer from a strong impact on ATP dynamics. This suggests that mitochondrial respiration is quantitatively the major contributor to ATP biosynthesis in plants. This is fully consistent with the phenotype of plants where mitochondrial ATP biosynthesis is impaired (F_Ad). These mutants, in fact, showed a huge growth reduction even if exposed to continuous illumination and their photosynthetic activity is only mildly altered, confirming that mitochondrial ATP biosynthesis is essential in metabolism of photosynthetically active cells.

Besides this essential involvement of mitochondria, all dynamics observed are dependent on the photosynthetic activity, as DCMU abolishes this phenomenon. This observation can be explained with the idea of chloroplasts exporting mainly reducing equivalents that are readily imported and used by mitochondria to synthetize ATP that is rapidly exported to the cytosol.

These observations provide a much-needed *in vivo* confirmation of biochemical studies on ATP compartmentalization in plants conducted in the last decades. These showed that chloroplasts capacity to export ATP was limited in mature leaves, since chloroplasts also have an adenylate translocator but with a much lower capacity, that was suggested to be mainly involved in ATP uptake in darkness (Flügge, 1998). On the contrary, mitochondria are capable of an efficient ATP/ADP exchange over the inner mitochondrial membrane (Gout et al., 2014) and thus were identified as suitable candidates for converting reducing equivalents exported from chloroplast in ATP (Gardeström & Igamberdiev, 2016; Gout et al., 2014; Shameer et al., 2019).

These earlier data could be consistent with the alternative possibility that chloroplasts export ATP to the cytosol using metabolite shuttles instead of transporters. Data presented here, however, enable to discard this idea and fully confirm that mitochondria have a quantitatively major role in ATP supply. If ATP biosynthesis is affected by the Complex I depletion, this drastically decreases ATP

supply in the cytosol. *F_Ad* mutants, where ATP biosynthesis is drastically impaired, plants can barely grow even if photosynthesis show only minor alterations. This clearly suggests that even if other pathways for ATP supply are present, they are not able to quantitatively compensate for the inactivation of the main pathway.

3.3. Evolutionary advantage of localizing ATP biosynthesis in the mitochondria.

In the past few years several studies showed the role of respiration in different photosynthetic organisms such as diatoms, green algae and plants. While these studies all share a common biological relevance of respiration, they also showed mechanistic differences. Respiratory mutants have been studied longer in the green alga *Chlamydomonas reinhardtii*. In this organism, while respiration has a major metabolic role, photosynthesis and growth can proceed in the absence of inactive complexes III and IV in photoautotrophic conditions, while this is not the case for plants (Salinas et al., 2014). This difference can be explained considering that Chlamydomonas can grow both autotrophically and heterotrophically and in its natural environment it can be even exposed to anoxia. On the contrary, plants mostly are obligatory autotrophs, that are adapted to constant presence of oxygen so that they are even sensitive to hypoxia (Loreti & Perata, 2020). If in plants cells respiration can always be active this can explain why evolutionarily they adapted to photosynthesis working with respiration. Interestingly, this is also consistent with the observation that *Viscum album*, an obligate semi-parasite with a different metabolic mode, also reduced the metabolic influence of respiration and was shown to have lost a functional Complex I (Maclean et al., 2018; Senkler et al., 2018).

Following the hypothesis that mitochondrial respiration assumed an essential role in ATP supply in plants cells, there should be some evolutionary advantage in delegating ATP supply to the cytosol to mitochondrial respiration. In fact, having a significant respiration active under illumination generates a futile cycle where O_2 and reducing power generated by photosynthesis are consumed by mitochondrial respiration, with a consequent decrease in light use efficiency. Such a distribution of roles between mitochondria and chloroplasts has an efficiency cost that must be compensated by some other advantage.

One possible explanation can be found analysing the kinetics of the ATP dynamics during light-dark transitions. Light changes are in fact very common in a natural, dynamic, environment and have a major impact on plants photosynthetic productivity and the ability to respond to these dynamics is expected to be a major evolutionary driving force (Long et al., 2022). Data presented in figures 1-5 shows that when light is switched on ATP starts accumulating in the cytosol very fast, within seconds, enabling a fast reaction to light availability. When the light is switched off, instead, mitochondrial activity is maintained for several seconds. In the case of light fluctuations, this mitochondrial activity thus enables maintaining a steady ATP supply to the cytosol, buffering the changes in photosynthetic activity induced by fast light changes. This could be a major advantage over having ATP supply to rely more directly on the photosynthetic apparatus. In the absence of such a “metabolic buffer” provided by mitochondria, ATP availability would closer react to light dynamics thus generating fast and large changes in ATP levels following light availability.

Another possible advantage could be identified considering that the gradient of protons (ΔpH) across the thylakoid's membrane is the energy source for ATP biosynthesis in the chloroplast but also a major signal for regulation of photosynthesis, controlling several major mechanisms such as nonphotochemical quenching (NPQ), xanthophyll cycle and photosynthetic control (Eberhard et al., 2008). Indeed, regulation of the chloroplast ATPase has a major impact on modulation of photosynthesis (Kanazawa et al., 2017; Kramer et al., 1990). If mitochondria are the major responsible of ATP supply for the cell this enable to disentangle the metabolic demand for ATP supply from regulation of photosynthesis. In the opposite alternative, instead, limiting ATPase activity for increasing ΔpH and thus induce photosynthesis regulation would also limit ATP supply to the cell. In case of stress, thus the regulation of photosynthesis by chloroplast ATPase would also cut the ATP supply to the cell, impairing other essential metabolic pathways that in case of stress likely instead have higher energy demand.

4. Material and Methods

4.1. Plant growth

Plant growth and propagation was done as described in CHAPTER II. Monitoring of ATP levels by confocal microscopy was done on 10 days old tissue cultivated on solid PpNO3 medium.

Growth of *f_Ad* KO lines was also tested under continuous illumination. In this case, temperature and light conditions were unchanged, with removal of photoperiod (24 h of illumination).

4.2. Generation of lines

For generation of ATP reporter lines, a construct with a constitutively active elongation factor 1 alpha (EF1α) promoter-driven ATeam1.03-nD/nA was designed (Supplementary Figure 4.8) and introduced into the neutral site *P. patens targeting site 1* (PTA1) (Aoyama et al., 2012). The plasmid was linearized with PmeI and used for gene targeting through a PEG-mediated transformation as described previously (Mellon et al., 2021). Transformation was done using either protoplasts of WT (Gransden ecotype) or *ndufa5* (published previously, Mellon et al., 2021), to generate reporter lines in both WT and *ndufa5* backgrounds. Screening of stably resistant lines was done through quantification of mVenus fluorescence, as described in the main results section.

For generation of plants missing a functional mitochondrial ATP synthase, we targeted the subunit F_Ad, using the f_Ad KO construct (Supplementary Figure 4.8). Resulting transformants were homogenized using 3-mm zirconium glass beads (Sigma-Aldrich), and genomic DNA (gDNA) was isolated according to a rapid extraction protocol (Edwards et al., 1991) with minor modifications. PCR amplifications of the recombination cassette were performed on extracted gDNA. Primers used for construct design and line validation are included as Supplementary Table 4.1.

4.3. Confocal imaging

Plants were grown for 10 days on solid $PPNO_3$ medium and dark adapted for 40 min. A piece of protonema was extended on a slide with a drop of liquid $PPNO_3$ medium and covered with a coverslip. The coverslip was then fixed with duct tape to avoid desiccation of the sample during the measurement (Supplementary Figure 4.9).

Samples were illuminated with 50 µmol photons m^{-2} s^{-1} using a red-filtered (580-630 nm) light (halogen lamp connected to an optic fibre, Supplementary Figure 4.10). Light intensity was set to 50 µmol photons m^{-2} s^{-1} using a light meter (LI-COR LI-250A). The spectrum of the filtered light is included in the Supplementary Figure 4.2B.

Imaging was performed using a 40× oil immersion lens using a Leica SP5 confocal microscope (Leica Microsystems). An Argon laser (488 nm) was used to excite both CFP and chlorophylls, with laser power set at 12.5 %. A scan was performed every 10 seconds. Three emission channels were set up: CFP (465-500 nm), mVenus (525-561 nm) and autofluorescence of chlorophylls (670-690 nm) (see Supplementary Figure 4.2).

4.4. Image processing

The acquired datasets were analysed using the MatLab-based Redox Ratio Analysis software (RRA) (Fricker, 2016). For each dataset, five square regions of interest (ROIs) were analysed (see Supplementary Figure 4.11). Each ROI was analysed as a single replicate, and at least three biological replicates were analysed per genotype. First, background signal was removed using the integrated functionality of the RRA software. The intensities of the single mVenus and CFP channels were then exported and used for further analysis and plotting with OriginPro 2023b (v. 10.0.5.153) (http://www.originlab.com/). We calculated the mVenus/CFP intensity ratio, which was then log-transformed to approach the normal distribution. The log-normalized values were then normalized to the value at time 0, i.e., to the steady state in the dark.

4.5. Chlorophyll fluorescence experiments

Photosynthetic parameters were retrieved from chlorophyll fluorescence as described in CHAPTER II. In case of f_Ad plants, samples were grown for approximately four months under continuous illumination.

5. References

Aoyama, T., Hiwatashi, Y., Shigyo, M., Kofuji, R., Kubo, M., Ito, M., & Hasebe, M. (2012). AP2-type transcription factors determine stem cell identity in the moss Physcomitrella patens. *Development (Cambridge, England)*, *139*(17), 3120–3129. https://doi.org/10.1242/DEV.076091

Bailleul, B., Berne, N., Murik, O., Petroutsos, D., Prihoda, J., Tanaka, A., Villanova, V., Bligny, R., Flori, S., Falconet, D., Krieger-Liszkay, A., Santabarbara, S., Rappaport, F., Joliot, P., Tirichine, L., Falkowski, P. G., Cardol, P., Bowler, C., & Finazzi, G. (2015). Energetic coupling between plastids and mitochondria drives CO2 assimilation in diatoms. *Nature*, *524*(7565), 366–369. https://doi.org/10.1038/nature14599

Bendall, D. S., & Manasse, R. S. (1995). Cyclic photophosphorylation and electron transport. *Biochimica et Biophysica Acta (BBA) - Bioenergetics*, *1229*(1), 23–38. https://doi.org/10.1016/0005-2728(94)00195-B

Braun, H. P., Binder, S., Brennicke, A., Eubel, H., Fernie, A. R., Finkemeier, I., Klodmann, J., König, A. C., Kühn, K., Meyer, E., Obata, T., Schwarzländer, M., Takenaka, M., & Zehrmann, A. (2014). The life of plant mitochondrial complex I. *Mitochondrion*, *19*(PB), 295–313. https://doi.org/10.1016/j.mito.2014.02.006

Cardol, P., Gloire, G., Havaux, M., Remacle, C., Matagne, R., & Franck, F. (2003). Photosynthesis and state transitions in mitochondrial mutants of Chlamydomonas reinhardtii affected in respiration. *Plant Physiology*, *133*(4), 2010–2020. https://doi.org/10.1104/pp.103.028076

Cardol, P., González-Halphen, D., Reyes-Prieto, A., Baurain, D., Matagne, R. F., & Remacle, C. (2005). The Mitochondrial Oxidative Phosphorylation Proteome of Chlamydomonas reinhardtii Deduced from the Genome Sequencing Project. *Plant Physiology*, *137*(2), 447–459. https://doi.org/10.1104/PP.104.054148

De Col, V., Fuchs, P., Nietzel, T., Elsä Sser, M., Pao Voon, C., Candeo, A., Seeliger, I., Fricker, M. D., Grefen, C., Møller, I. M., Bassi, A., Lim, B. L., Zancani, M., Meyer, A. J., Costa, A., Wagner, S., & Schwarzlä Nder, M. (2017). *ATP sensing in living plant cells reveals tissue gradients and stress dynamics of energy physiology*. https://doi.org/10.7554/eLife.26770.001

Dutilleul, C., Driscoll, S., Cornic, G., De Paepe, R., Foyer, C. H., & Noctor, G. (2003). Functional mitochondrial complex I is required by tobacco leaves for optimal photosynthetic performance in photorespiratory conditions and during transients. *Plant Physiology*, *131*(1), 264–275. https://doi.org/10.1104/pp.011155

Eberhard, S., Finazzi, G., & Wollman, F. A. (2008). The Dynamics of Photosynthesis. *Https://Doi.Org/10.1146/Annurev.Genet.42.110807.091452*, *42*, 463–515. https://doi.org/10.1146/ANNUREV.GENET.42.110807.091452

Edwards, K., Johnstone, C., & Thompson, C. (1991). A simple and rapid method for the preparation of plant genomic DNA for PCR analysis. *Nucleic Acids Research*, *19*(6), 1349. https://doi.org/10.1093/NAR/19.6.1349

Elsässer, M., Feitosa-Araujo, E., Lichtenauer, S., Wagner, S., Fuchs, P., Giese, J., Kotnik, F., Hippler, M., Meyer, A. J., Maurino, V. G., Finkemeier, I., Schallenberg-Rüdinger, M., & Schwarzländer, M. (2020). Photosynthetic activity triggers pH and NAD redox signatures across different plant cell compartments. *BioRxiv*, 2020.10.31.363051. https://doi.org/10.1101/2020.10.31.363051

Flügge, U. I. (1998). Metabolite transporters in plastids. *Current Opinion in Plant Biology*, *1*(3), 201–206. https://doi.org/10.1016/S1369-5266(98)80105-2

Forti, G., & Gerola, P. (1977). Inhibition of photosynthesis by azide and cyanide and the role of oxygen in photosynthesis. *Plant Physiology*, *59*(5), 859–862. https://doi.org/10.1104/PP.59.5.859

Fricker, M. D. (2016). Quantitative Redox Imaging Software. *Https://Home.Liebertpub.Com/Ars*, *24*(13), 752–762. https://doi.org/10.1089/ARS.2015.6390

Fromm, S., Braun, H.-P., & Peterhansel, C. (2016). Mitochondrial gamma carbonic anhydrases are required for complex I assembly and plant reproductive development. *The New Phytologist*, *211*(1), 194–207. https://doi.org/10.1111/nph.13886

Gardeström, P., & Igamberdiev, A. U. (2016). The origin of cytosolic ATP in photosynthetic cells. *Physiologia Plantarum*, *157*(3), 367–379. https://doi.org/10.1111/ppl.12455

Gout, E., Rébeillé, F., Douce, R., & Bligny, R. (2014). Interplay of Mg2+, ADP, and ATP in the cytosol and mitochondria: Unravelling the role of Mg2+ in cell respiration. *Proceedings of the National Academy of Sciences of the United States of America*, *111*(43), E4560–E4567. https://doi.org/10.1073/PNAS.1406251111/SUPPL_FILE/PNAS.201406251SI.PDF

Igamberdiev, A. U., & Bykova, N. V. (2022). Mitochondria in photosynthetic cells: Coordinating redox control and energy balance. *Plant Physiology*. https://doi.org/10.1093/PLPHYS/KIAC541

Joliot, P., & Joliot, A. (2008). Quantification of the electrochemical proton gradient and activation of ATP synthase in leaves. *Biochimica et Biophysica Acta (BBA) - Bioenergetics*, *1777*(7–8), 676–683. https://doi.org/10.1016/j.bbabio.2008.04.010

Kanazawa, A., Ostendorf, E., Kohzuma, K., Hoh, D., Strand, D. D., Sato-Cruz, M., Savage, L., Cruz, J. A., Fisher, N., Froehlich, J. E., & Kramer, D. M. (2017). Chloroplast ATP synthase modulation of the thylakoid proton motive force: implications for photosystem I and photosystem II photoprotection. *Frontiers in Plant Science*, *8*, 264832. https://doi.org/10.3389/FPLS.2017.00719/BIBTEX

Knight, C. D., Perroud, P.-F., & Cove, D. J. (2009). *Annual Plant Reviews - The moss Physcomitrella patens* (C. D. Knight, Ed.; Vol. 36). Wiley-Blackwell.

Kramer, D. M., Wise, R. R., Frederick, J. R., Alm, D. M., Hesketh, J. D., Ort, D. R., & Crofts, A. R. (1990). Regulation of coupling factor in field-grown sunflower: A Redox model relating coupling factor activity to the activities of other thioredoxin-dependent chloroplast enzymes. *Photosynthesis Research*, *26*(3), 213–222. https://doi.org/10.1007/BF00033134

Kubo, M., Fujita, T., & Hasebe, M. (2017). *PHYSCOmanual, version 2.0*. Chapter 11.6, Overexpression. https://www.nibb.ac.jp/evodevo/PHYSCOmanual/11.6_revised_170727.htm

Larosa, V., Meneghesso, A., La Rocca, N., Steinbeck, J., Hippler, M., Szabò, I., & Morosinotto, T. (2018). Mitochondria Affect Photosynthetic Electron Transport and Photosensitivity in a Green Alga. *Plant Physiology*, *176*(3), 2305–2314. https://doi.org/10.1104/pp.17.01249

Li, W. Q., Zhang, X. Q., Xia, C., Deng, Y., & Ye, D. (2010). MALE GAMETOPHYTE DEFECTIVE 1, Encoding the FAd Subunit of Mitochondrial F1F0-ATP Synthase, is Essential for Pollen Formation in Arabidopsis thaliana. *Plant and Cell Physiology*, *51*(6), 923–935. https://doi.org/10.1093/PCP/PCQ066

Lim, S. L., Flütsch, S., Liu, J., Distefano, L., Santelia, D., & Lim, B. L. (2022). Arabidopsis guard cell chloroplasts import cytosolic ATP for starch turnover and stomatal opening. *Nature Communications*, *13*(1). https://doi.org/10.1038/s41467-022-28263-2

Long, S. P., Taylor, S. H., Burgess, S. J., Carmo-Silva, E., Lawson, T., De Souza, A. P., Leonelli, L., & Wang, Y. (2022). Into the Shadows and Back into Sunlight: Photosynthesis in Fluctuating Light. *Https://Doi.Org/10.1146/Annurev-Arplant-070221-024745*, *73*, 617–648. https://doi.org/10.1146/ANNUREV-ARPLANT-070221-024745

Loreti, E., & Perata, P. (2020). The Many Facets of Hypoxia in Plants. *Plants 2020, Vol. 9, Page 745*, *9*(6), 745. https://doi.org/10.3390/PLANTS9060745

Maclean, A. E., Hertle, A. P., Ligas, J., Bock, R., Balk, J., & Meyer, E. H. (2018). Absence of Complex I Is Associated with Diminished Respiratory Chain Function in European Mistletoe. *Current Biology : CB*, *28*(10), 1614-1619.e3. https://doi.org/10.1016/j.cub.2018.03.036

Mellon, M., Storti, M., Vera-Vives, A. M., Kramer, D. M., Alboresi, A., & Morosinotto, T. (2021). Inactivation of mitochondrial Complex I stimulates chloroplast ATPase in Physcomitrium patens . *Plant Physiology*. https://doi.org/10.1093/plphys/kiab276

Noguchi, K., & Yoshida, K. (2008). Interaction between photosynthesis and respiration in illuminated leaves. *Mitochondrion*, *8*(1), 87–99. https://doi.org/10.1016/j.mito.2007.09.003

Rensing, S. A., Goffinet, B., Meyberg, R., Wu, S.-Z., & Bezanilla, M. (2020). The Moss Physcomitrium (Physcomitrella) patens: A Model Organism for Non-Seed Plants. *The Plant Cell*, *32*(5), 1361–1376. https://doi.org/10.1105/tpc.19.00828

Ringsmuth, A. K., Landsberg, M. J., & Hankamer, B. (2016). Can photosynthesis enable a global transition from fossil fuels to solar fuels, to mitigate climate change and fuel-supply limitations? *Renewable and Sustainable Energy Reviews*, *62*, 134–163. https://doi.org/10.1016/J.RSER.2016.04.016

Salinas, T., Larosa, V., Cardol, P., Maréchal-Drouard, L., & Remacle, C. (2014). Respiratory-deficient mutants of the unicellular green alga Chlamydomonas: a review. *Biochimie*, *100*(1), 207–218. https://doi.org/10.1016/j.biochi.2013.10.006

Schönfeld, C., Wobbe, L., Borgstädt, R., Kienast, A., Nixon, P. J., & Kruse, O. (2004). The nucleus-encoded protein MOC1 is essential for mitochondrial light acclimation in Chlamydomonas reinhardtii. *The Journal of Biological Chemistry*, *279*(48), 50366–50374. https://doi.org/10.1074/jbc.M408477200

Schwarzländer, M., Dick, T. P., Meyer, A. J., & Morgan, B. (2016). Dissecting Redox Biology Using Fluorescent Protein Sensors. *Antioxidants & Redox Signaling*, *24*(13), 680–712. https://doi.org/10.1089/ars.2015.6266

Senkler, J., Rugen, N., Eubel, H., Hegermann, J., & Braun, H.-P. (2018). Absence of Complex I Implicates Rearrangement of the Respiratory Chain in European Mistletoe. *Current Biology*, *28*(10), 1606-1613.e4. https://doi.org/10.1016/j.cub.2018.03.050

Senkler, J., Senkler, M., Eubel, H., Hildebrandt, T., Lengwenus, C., Schertl, P., Schwarzländer, M., Wagner, S., Wittig, I., & Braun, H. P. (2017). The mitochondrial complexome of Arabidopsis thaliana. *The Plant Journal*, *89*(6), 1079–1092. https://doi.org/10.1111/TPJ.13448

Shameer, S., Ratcliffe, R. G., & Sweetlove, L. J. (2019). Leaf energy balance requires mitochondrial respiration and export of chloroplast NADPH in the light. *Plant Physiology*, *180*(4), 1947–1961. https://doi.org/10.1104/pp.19.00624

Terasawa, K., Odahara, M., Kabeya, Y., Kikugawa, T., Sekine, Y., Fujiwara, M., & Sato, N. (2007). The Mitochondrial Genome of the Moss Physcomitrella patens Sheds New Light on Mitochondrial Evolution in Land Plants. *Molecular Biology and Evolution*, *24*(3), 699–709. https://doi.org/10.1093/MOLBEV/MSL198

Voon, C. P., Guan, X., Sun, Y., Sahu, A., Chan, M. N., Gardeström, P., Wagner, S., Fuchs, P., Nietzel, T., Versaw, W. K., Schwarzländer, M., & Lim, B. L. (2018). ATP compartmentation in plastids and cytosol of Arabidopsis thaliana revealed by fluorescent protein sensing. *Proceedings of the National Academy of Sciences of the United States of America*, *115*(45), E10778–E10787. https://doi.org/10.1073/pnas.1711497115

Watt, I. N., Montgomery, M. G., Runswick, M. J., Leslie, A. G. W., & Walker, J. E. (2010). Bioenergetic cost of making an adenosine triphosphate molecule in animal mitochondria. *Proceedings of the National Academy of Sciences of the United States of America*, *107*(39), 16823–16827. https://doi.org/10.1073/pnas.1011099107

Zancani, M., Braidot, E., Filippi, A., & Lippe, G. (2020). Structural and functional properties of plant mitochondrial F-ATP synthase. *Mitochondrion*, *53*, 178–193. https://doi.org/10.1016/j.mito.2020.06.001

Zhang, L.-T., Zhang, Z.-S., Gao, H.-Y., Meng, X.-L., Yang, C., Liu, J.-G., & Meng, Q.-W. (2012). The mitochondrial alternative oxidase pathway protects the photosynthetic apparatus against photodamage in Rumex K-1 leaves. *BMC Plant Biology*, *12*(1), 40. https://doi.org/10.1186/1471-2229-12-40

6. Supplementary material

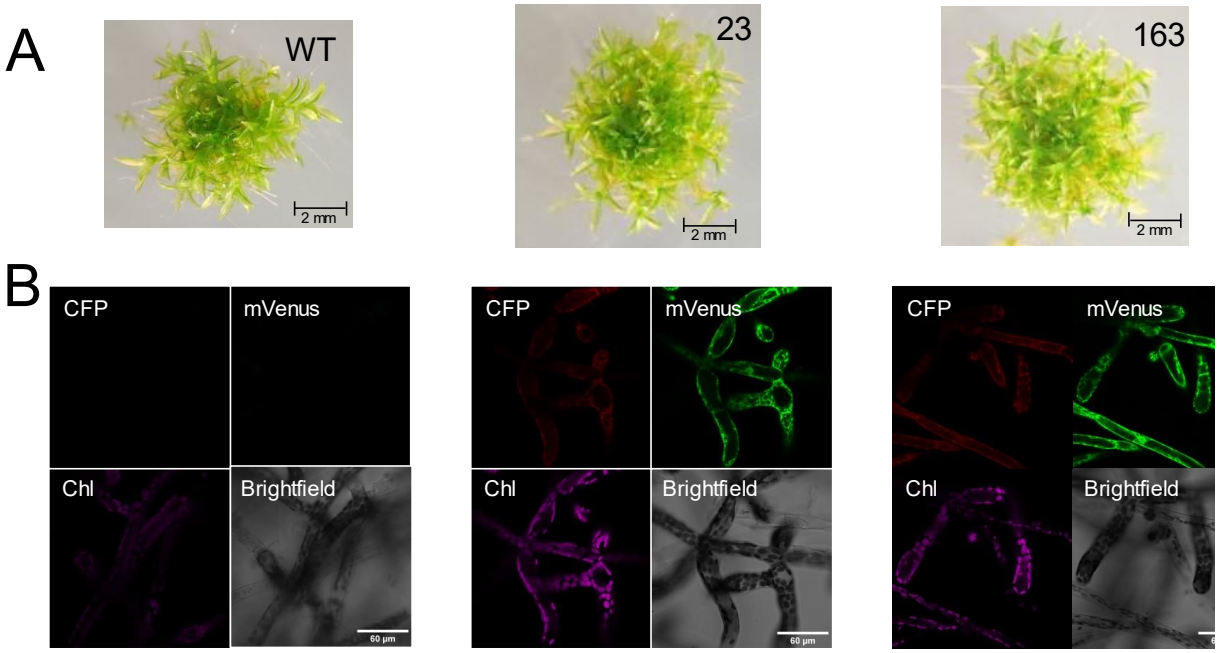

Supplementary Figure 4.1 | **Isolation of WT-ATeam *P. patens* plants.** As examples, two representative WT-Ateam lines, #23 and #163, are shown. (A) Plants after 28 days of growth in solid PPNO3 medium. (B) Fluorescence signal and brightfield images of 10 days old protonema.

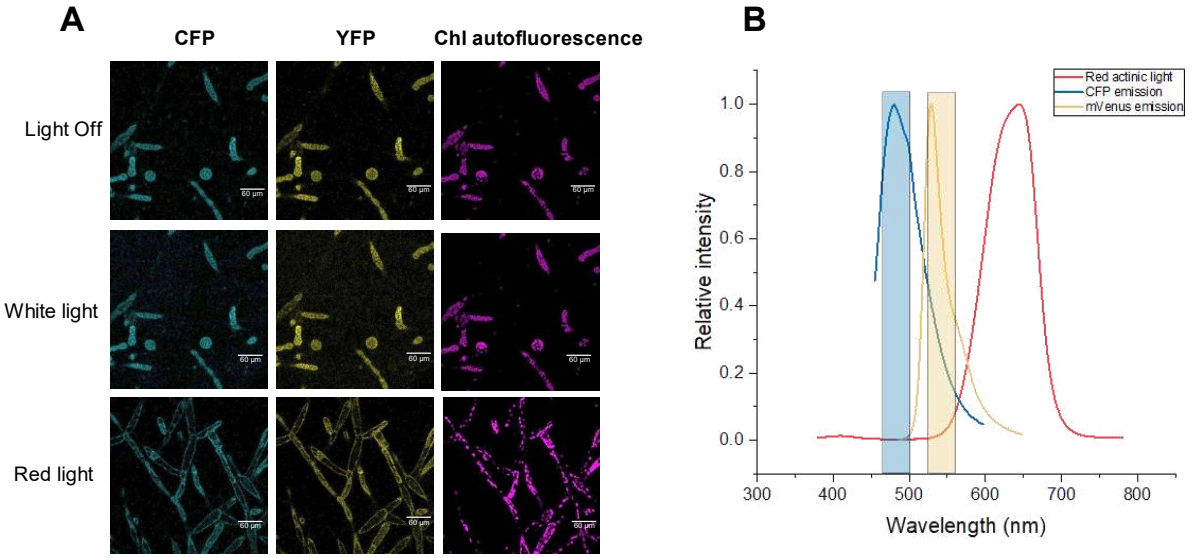

Supplementary Figure 4.2 | **Verification of impact of actinic light on fluorescence determination.** (A) White light does interfere with CFP and mVenus channels, as shown by the noisy background under white illumination, that is not present when light is red or absent. (B) Emission spectra of CFP and mVenus and the corresponding acquisition ranges of the microscope (rectangles). There is no significant overlap with red actinic light employed.

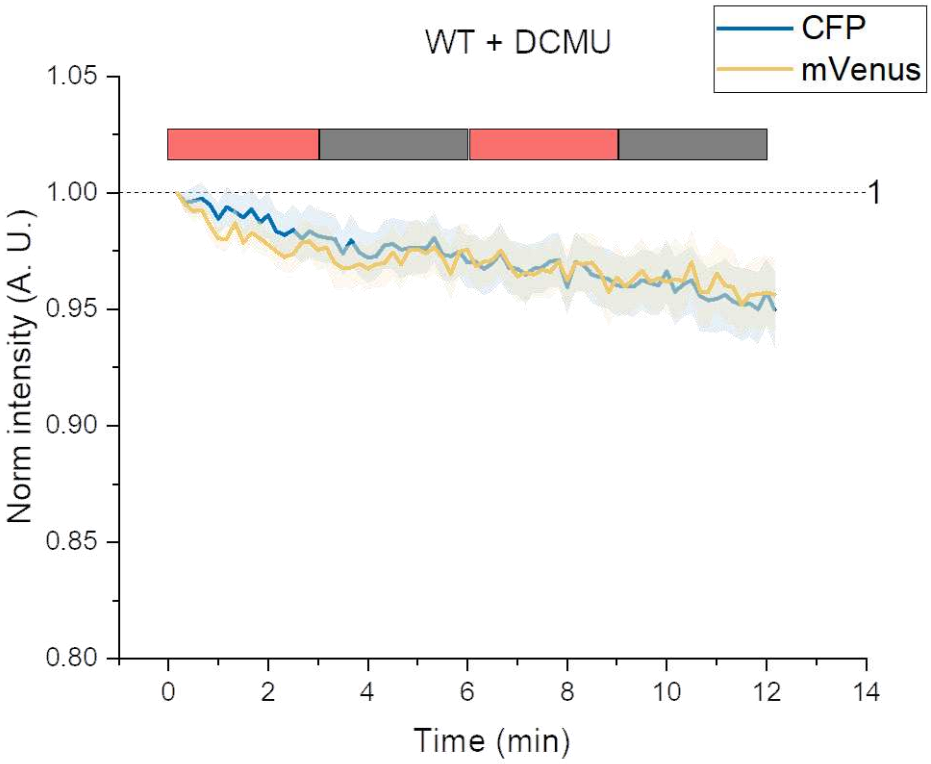

Supplementary Figure 4.3 | **Signals of the single CFP and mVenus channels during dark-to-light transitions.** (A) When dark-adapted plants are exposed to light, the intensity of the CFP channel decreases in parallel with at increase in the mVenus channel, clear indication of an increase FRET between the two fluorophores, shown in Figure 4.1. (B) This antiparallel behaviour is not observed when samples are treated with DCMU is present.

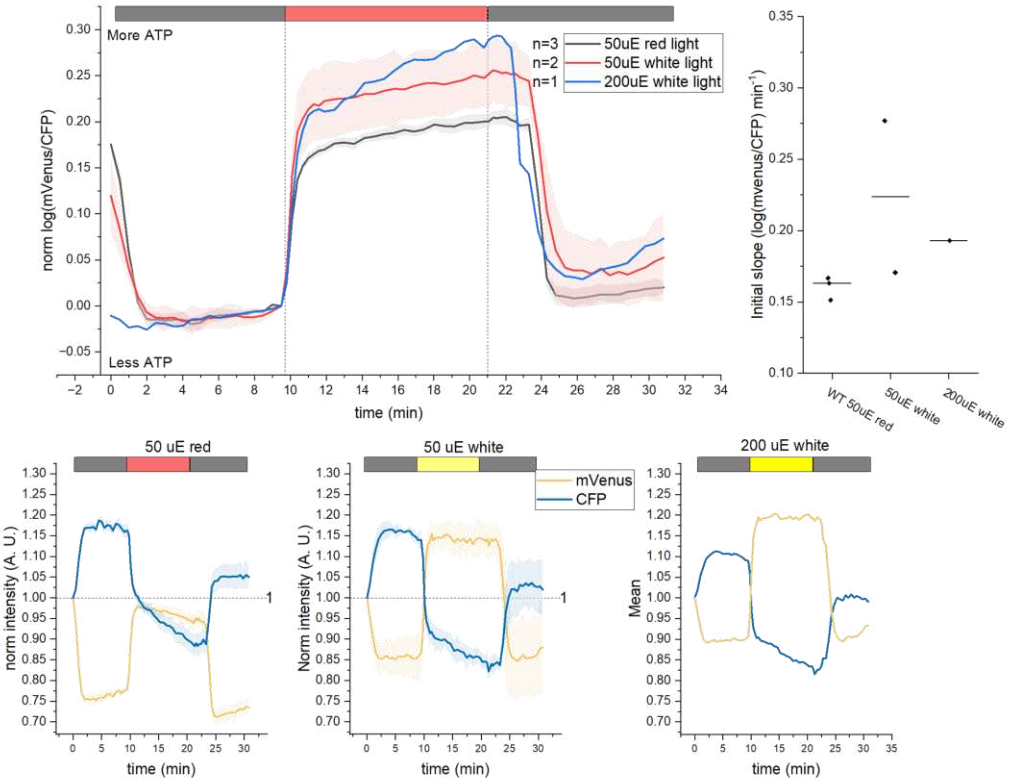

Supplementary Figure 4.4 | **Increase in cytosolic ATP during dark-to-light transitions using a pseudo-continuous light system**, as described by Elsässer et al., 2020. The CFP/mVenus ratio (A) was calculated for 10 minutes at darkness, followed by 12 minutes of illumination and further 10 minutes of darkness. We compared the effect of different light qualities (red/white) and intensities (50/200 mol photons s^{-1} m^{-2}). (B) Slope during the first minute of illumination. (C-E) Single channel intensity.

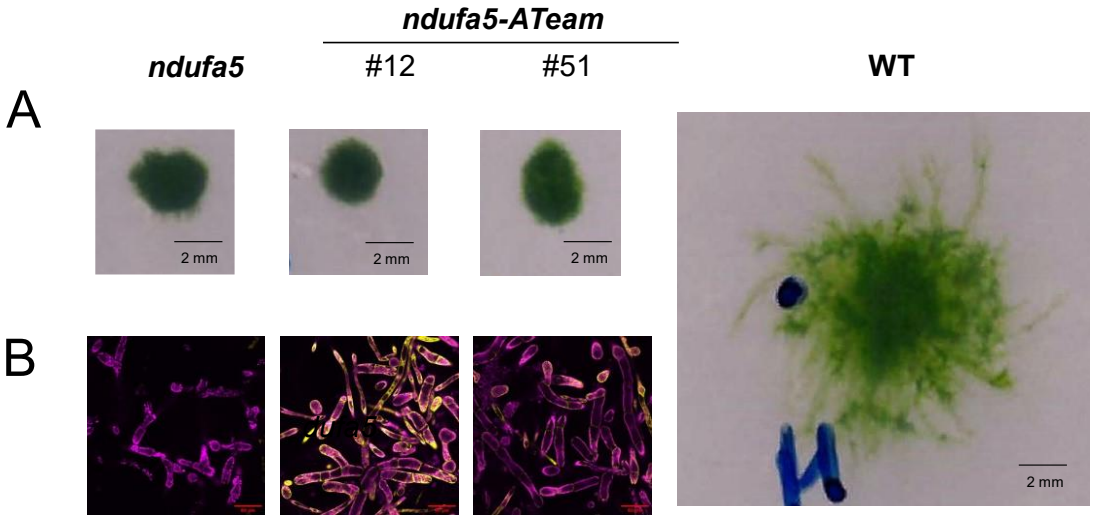

Supplementary Figure 4.5 | **Isolation of *ndufa5*-Ateam plants.** A negative control, two ndufa5-ATeam lines and a WT for comparison. (A) Aspect of colonies after 21 days of growth. (B) Merged image of chlorophyll autofluorescence (magenta) and mVenus channel (yellow).

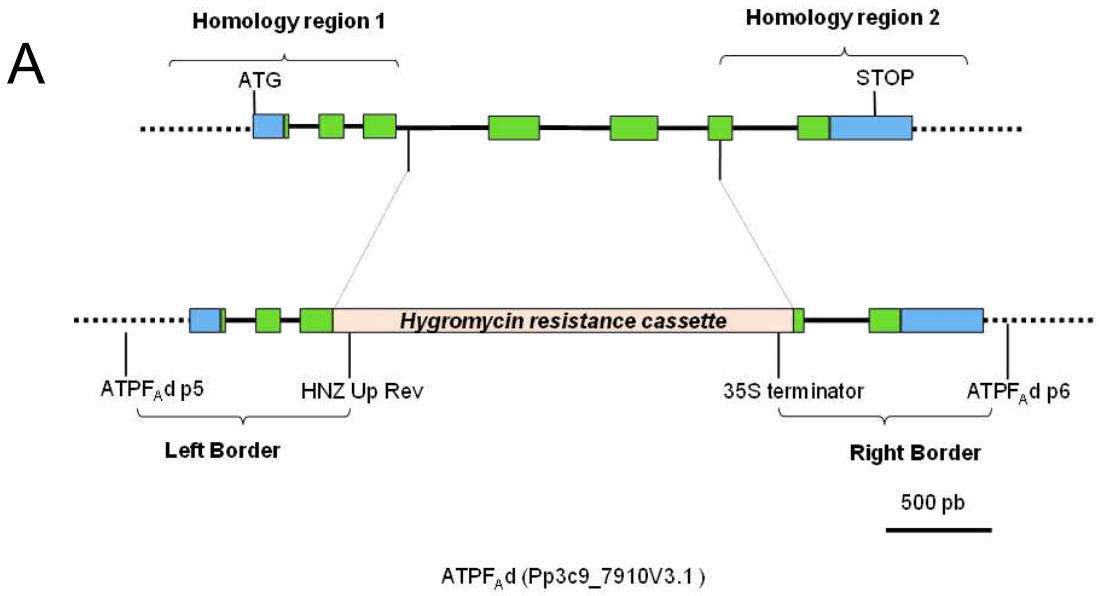

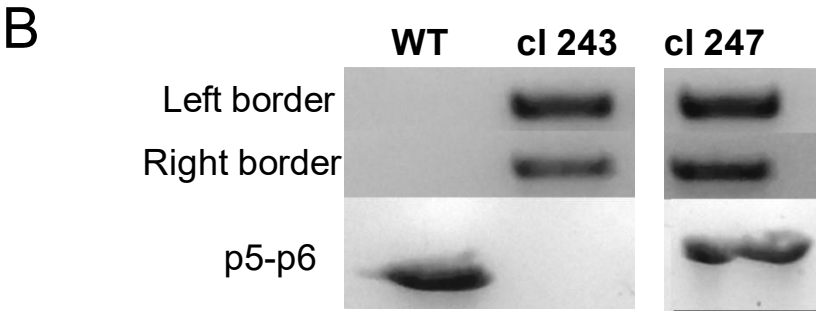

Supplementary Figure 4.6 | Generation of *P. patens* mutant lines lacking ATP synthase subunit F_Ad. (A) Scheme showing the CDS, the regions of homology chosen to drive homologous recombination and insertion of the resistance cassette. (B) Example of PCR for verification of the homologous recombination event. PCR products called Left and Right Border are generated only if the resistance cassette is inserted in the expected genomic region. PCR product called p5-p6 is generated only if the cassette is not inserted (small fragment, WT) or inserted only once (larger fragment, cl 147). Lines 143 and 146 lack the p5-p6 product, meaning that the WT gene is missing, maybe through insertion in tandem of multiple repeats of the resistance cassette.

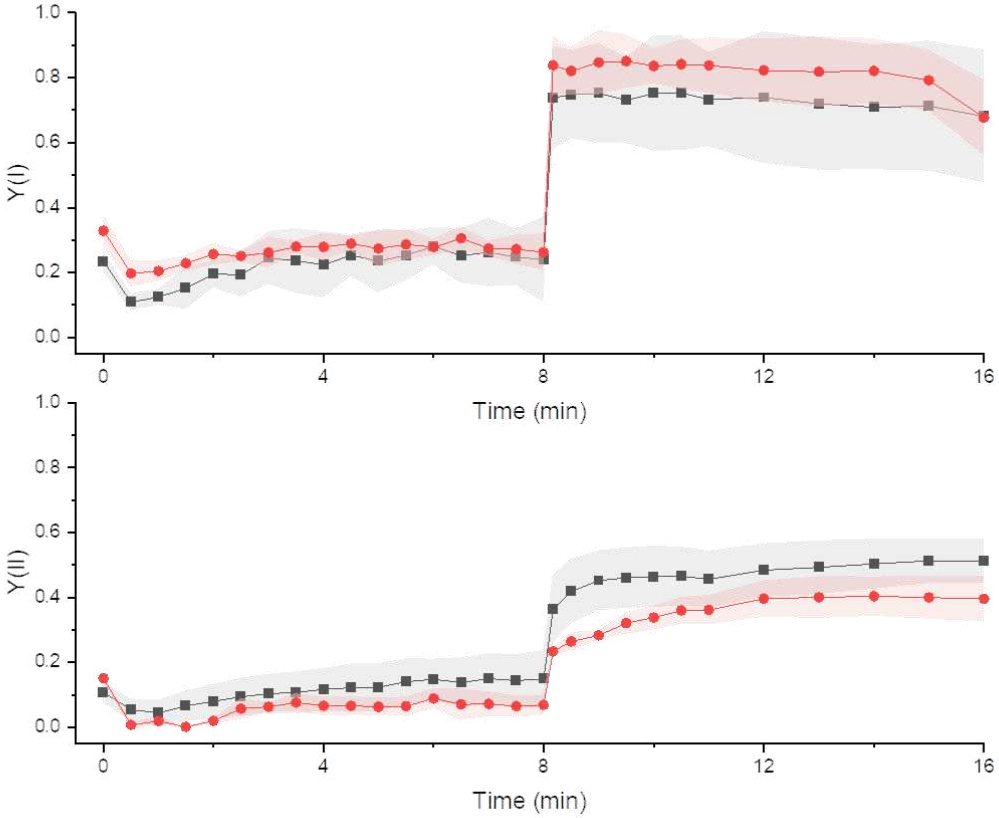

Supplementary Figure 4.7 | Yield of PSI and PSII exposed to 330 µmol photons m^{-2} s^{-1}.

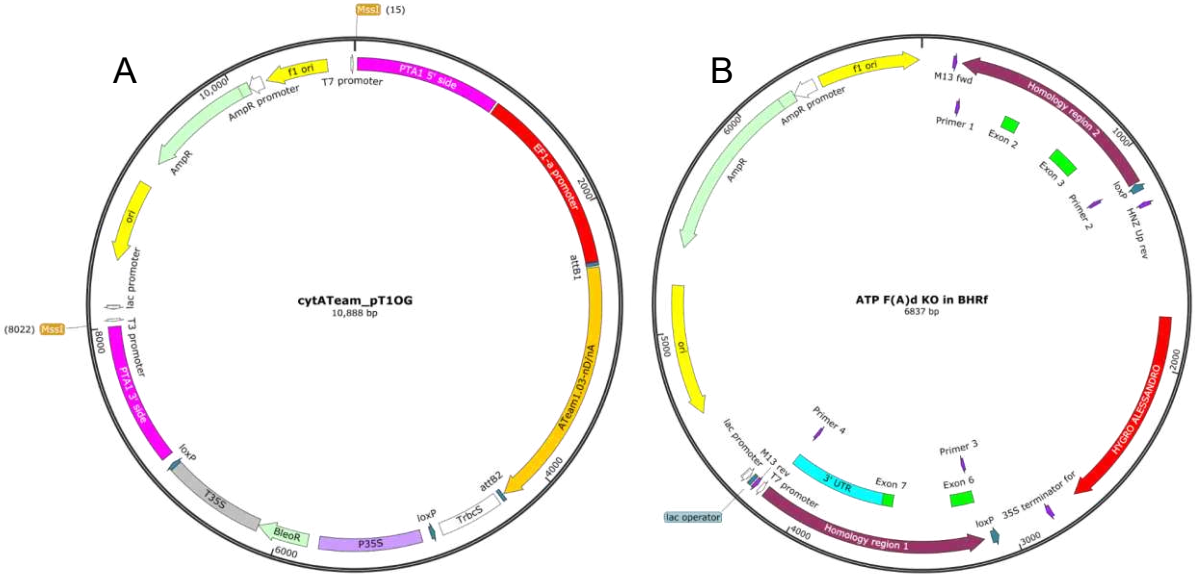

Supplementary Figure 4.8 | **Map of the vectors used for transformation**. (A) The cytATeam_pT1OG construct. The MssI (isoschizomer of PmeI) cutting site is shown. (B) The F_Ad KO construct.

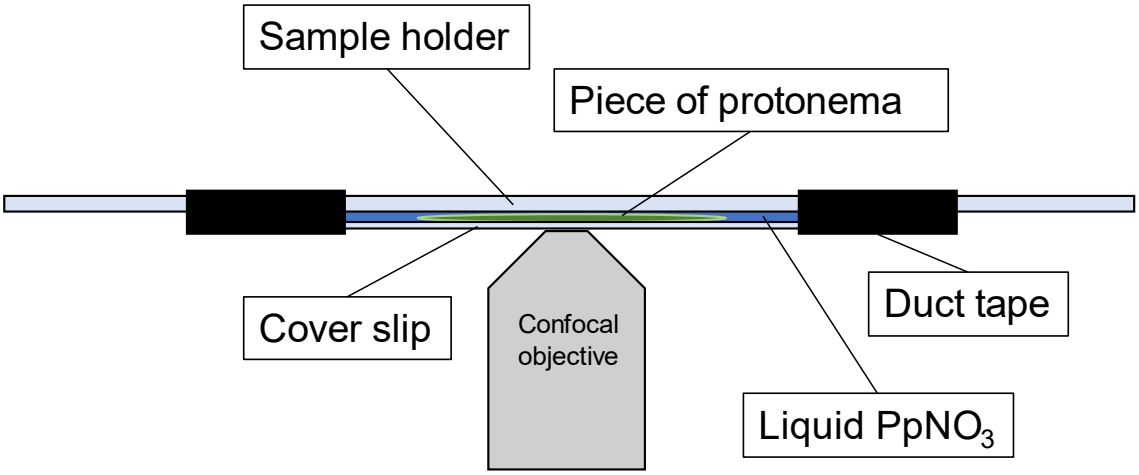

Supplementary Figure 4.9 | **The setup used for sample mounting**.

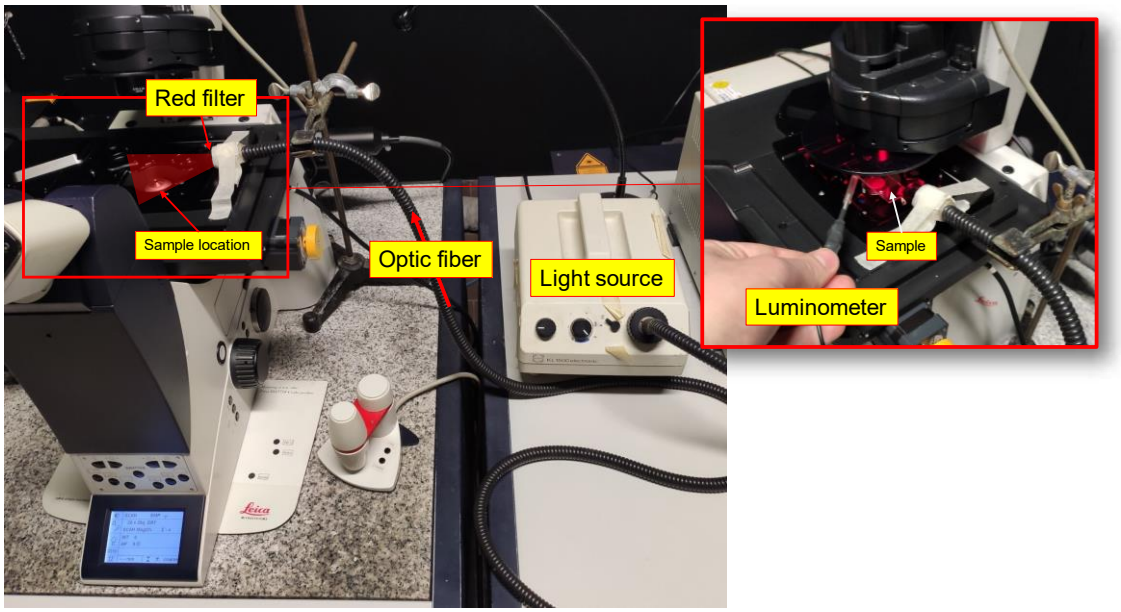

Supplementary Figure 4.10 | **The setup used for monitoring of cytosolic ATP levels during dark-to-light transitions**. The image at right shows a detail of a illuminated sample, with light intensity being monitored with the probe of a luminometer.

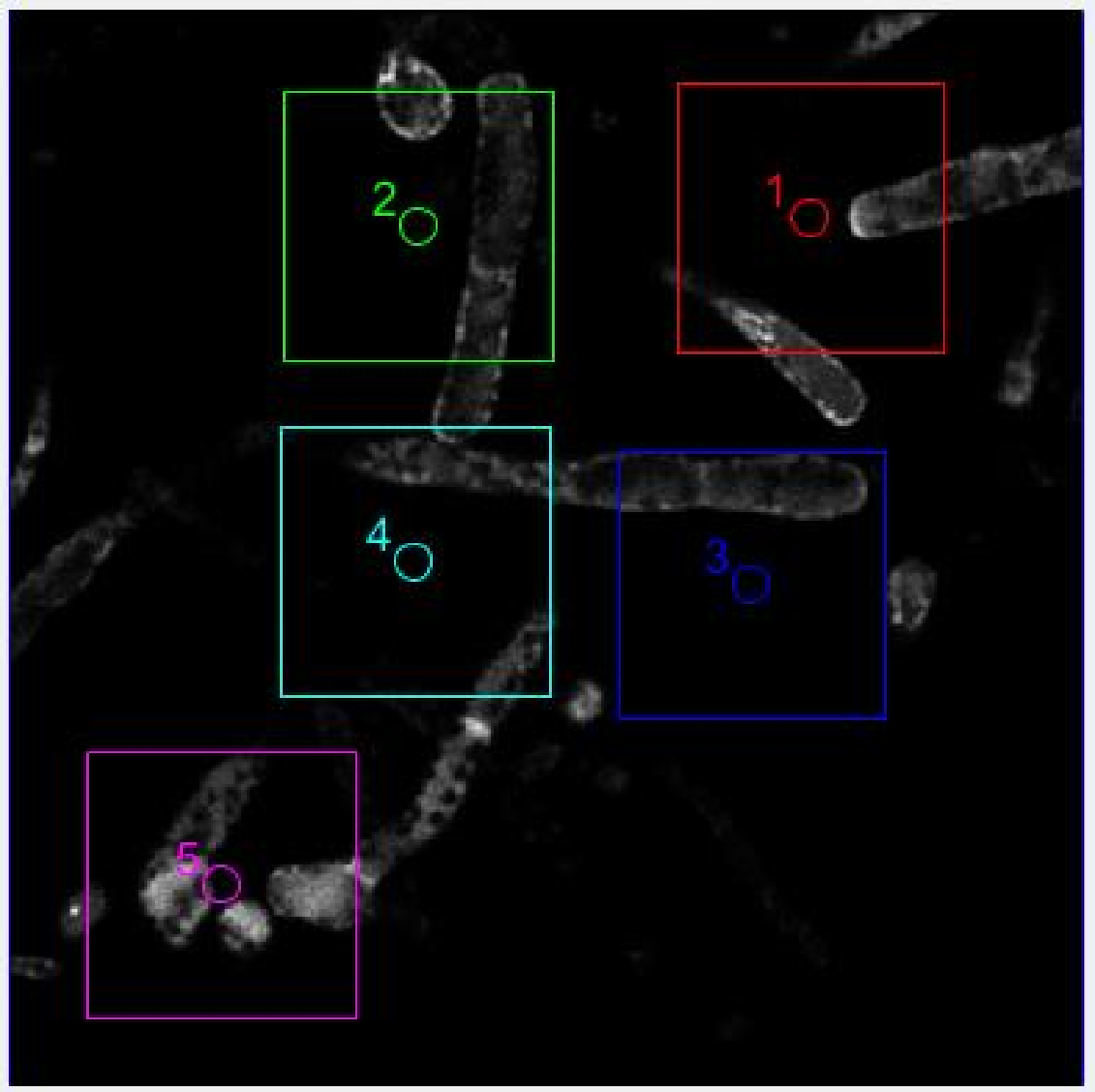

Supplementary Figure 4.11 | Screenshot of a frame out of a dark-to-light transition experiment during image analysis. The five regions of interest (ROIs) used for downstream analyses are shown.

Supplementary Table 4.1 | **Primers used in this chapter**.

Primer name	Sequence (5’ → 3’)
FAd-p1	GTGGAATGGCATGATTTTAT
FAd-p2	ACTAAACAACCAGACCAGGA
FAd-p3	CTTGGGATTGATGATGCTAT
FAd-p4	TGGGTATTATCGGAGTCAAC
FAd-p5	CATCTACCATTTTGGGTTTC
FAd-p6	ACTTCGAACCAGTTCCAGTA
HNZ Up Rev	TGCGCAACTGTTGGGAAG
35S terminator	CGCTGAAATCACCAGTCTCTCT

Supplementary Table 4.2 | **Identification of homologous sequences responsible for the formation and assembly of respiratory Complex V in eukaryotic organisms.** Protein and gene sequences from *Bos taurus*, *Saccharomyces cerevisiae* and *Chlamydomonas reinhardtii*, were obtained from ENTREZ at the National Center for Biotechnology Information (NCBI) server (http://www.ncbi.nlm.nih.gov/) while in *Arabidopsis thaliana* were obtained from the Arabidopsis Information Resource (http://arabidopsis.org/info/agi.jsp) or were identified using the PSI-BLAST tool available at the NCBI server. Names of proteins are based on published papers and reviews (see references). *P. patens* nuclear homologous sequences were identified using BLAST facilities with fungal, mammal, and plant protein and genic sequences against the *P. patens* genome (v3.3) (Lang et al., 2018; https://phytozome.jgi.doe.gov/pz/portal.html). Subunits encoded in the mitochondrial genome were identified from Terasawa et al., 2007 and GenBank accession numbers are given. Name for the subunits in plants are reported only when they differ from cattle or yeast. a) Cardol et al., 2005; b) Terasawa et al., 2007; c) Zancani et al., 2020; d) Li et al., 2010.

B. taurus	*S. cerevisiae*	*A. thaliana*	*C. reinhardtii*	*P. patens*	Ref.
F_1 head					
ATP5A1/α	*α (ATP1)*	AtMg01190, At2g07698	XP_001699641	YP_539029	a, b, c
ATP5B/β	*β (ATP2)*	At5g08670, At5g08680, At5g08690	XP_001691632	Pp3c5_26340, Pp3c5_26350, Pp3c6_4230	a, c
Central stalk					
ATP5C1/γ	*γ (ATP3)*	At2g33040	XP_001700627	Pp3c18_8580, Pp3c19_11630, Pp3c19_5760, Pp3c21_11700	a, c
ATP5D/δ	*δ (ATP16)*	At5g47030	XP_001698736	Pp3c4_31840, Pp3c13_11630, Pp3c26_13290	a, c
ATP5E/ε	*ε (ATP15)*	At1g51650	XP_001702609	Pp3c1_10140, Pp3c1_12120, Pp3c2_24870	a, c
Peripheral stalk					
ATP5F1/B	ATPB (ATP4)	AtMg00640	–	YP_539002	a, b, c
ATP5O/OSCP	ATP5	At4g09650, At5g13450	XP_001695985	Pp3c11_16260, Pp3c21_15430, Pp3c23_11680, Pp3c24_12520	a, c
ATP5H/D	ATPD (ATP7)	At3g52300	–	Pp3c20_2830, Pp3c20_2850, Pp3c24_13710	a, c
ATP5PF	ATPH (ATP14)	–	–	–	c
F_O motor					
ATP6/A	ATPA (ATP6)	AtMg00410, AtMg01170	XP_001689492	YP_539022	a, b, c
ATP5G3/C	ATPC (ATP9)	AtMg01080	XP_001701531, XP_001701500	YP_539041	a, b, c
ATP5I/E	ATPE (ATP21)	At5g15320	–	Pp3c1_20190, Pp3c2_20190	a, c
ATP5L/G	ATPG (ATP20)	At2g19680, At4g26210, At4g29480	–	Pp3c7_10, Pp3c17_14360	a, c
ATP5J2/F	ATPF (ATP17)	At4g30010	–	Pp3c5_15280, Pp3c5_15650, Pp3c25_5460, Pp3c25_5490	a, c
–	APTI (ATP18)	–	–	–	c
–	ATPK (ATP19)	–	–	–	c
ATP8/A6L	ATP8	AtMg00480	–	YP_539003	a, b, c
Plant specific					
–	**–**	At3g46430, At5g59613 (6Kda)	**–**	Pp3c12_2550	c
–	**–**	At2g21870 (ATP7, F_Ad)	–	Pp3c9_7910	a, c, d
Inhibitory Factors					
ATPI/IF1	INH1, STF1	At5g04750 (IFI-1), At2g27730 (IFI-2)	–	Pp3c1_22500	a, c
Assembly factors					
F_O subcomplex					
–	ATP10	At1g08220	–	–	a
ATP23	ATP23	At3g03420.1	XP_001691633	Pp3c20_19010, Pp3c24_12610	a
–	ATP25	–	–		a
OXA1L	OXA1	At5g62050	XP_001693158	Pp3c11_26830	a
F_1 subcomplex					
ATPAF1	ATP11	At2g34050	XP_001690396	Pp3c14_19140	a
ATPAF2	ATP12	At5g40660	XP_001697254	Pp3c2_19250	a
–	FMC1	–	–		a

APPENDIX I

Light dose activation of alternative electron transport mechanisms in the moss *Physcomitrium patens*

Shun-ling Tan[1], Antoni M. Vera-Vives[1], Alessandro Alboresi[1] and Tomas Morosinotto[1]

1. Department of Biology, University of Padova, Italy

Authorship statement:

The research question was proposed by Prof. Alessandro Alboresi and Prof. Tomas Morosinotto. The experimental design was defined by Prof. Tomas Morosinotto, PhD student Shun-ling Tan and me. Shun-ling Tan collected and analysed the data under my supervision. Shun-ling Tan wrote the first draft of the manuscript, which I revised.

Abstract

Photosynthetic organisms exploit sunlight to drive an electron transport chain and obtain the chemical energy supporting their metabolism. In highly dynamic environmental conditions, excitation energy and electron transport in the photosynthetic apparatus need to be continuously modulated to prevent the over-reduction of the electron carriers and the consequent damage. An essential role in the regulation of electron transport and protection from over-reduction is played by alternative electron transport mechanisms such as cyclic electron transport (CET) mediated by PGRL1/PGR5 and NDH complex and pseudo-cyclic electron transport (PCET) mediated by the flavodiiron proteins (FLV) and the Mehler reaction.

Here mutant lines of the moss *Physcomitrium patens* depleted in PCET (*flva* KO) or CET (*pgrl1/ndhm* KO) were compared to wild-type plants for their ability to regulate photosynthetic electron transport in response to light fluctuations of different intensities. Results showed that FLV enables a very fast increase in electron transport capacity that is however transient with an undetectable impact after 3 minutes from the light change. The FLV electron transport capacity is saturated at 100 µmol photons m^{-2} s^{-1} and does not increase even if exposed to stronger illumination. On the other hand, CET activation after an increase in illumination is slower and has a smaller electron transport capacity but its activity is maintained with time and provides a steady contribution for several minutes after a change in illumination intensity.

These results demonstrate that CET and PCET are effective in adjusting temporary unbalances in electron transport and enable plants to fully respond to 2-4 times increases in illumination. In case of larger increases, the electron transport capacity of alternative electron transport mechanisms is saturated but they still contribute to protection from light damage.

1. Introduction

Photosynthetic organisms convert light energy into chemical energy by the activity of two photosystems (PS) to generate the NADPH and ATP providing the reducing power and chemical energy to support CO_2 fixation and all cellular metabolism. PSI and PSII catalyze a light-driven transfer of electrons from water to $NADP^+$ coupled with the formation of a proton motive force across the thylakoid membrane, which enables ATP synthesis.

Plants grown in natural conditions face a highly dynamic environment that affects metabolism, ATP and NADPH consumption, the flow of excitation energy and electrons (Allahverdiyeva et al., 2015; Peltier et al., 2010). The light intensity in particular can abruptly change because of weather changes, cloud movement or shading by overlying leaves within a canopy (Slattery et al., 2018; Tanaka et al., 2019; Wang et al., 2020). The CO_2 assimilation rate is modulated in response to changes in environmental conditions and in particular according to light intensity. The speed of this process depends on several reactions such as ribulose-1, 5-bisphosphate (RuBP) regeneration, RuBP carboxylase/oxygenase (Rubisco) activity (Kimura et al., 2020; Long et al., 2022), which in general have slower kinetics than environmental dynamics (Eberhard et al., 2008). Sudden changes in illumination are thus particularly challenging because they do not allow for efficient metabolism modulation with the same timing and they can drive the absorption of an excess of light energy, over-reduction of electron transporters leading to the photoinhibition of both photosystems (Hahn et al., 2018; Melis, 1999; Sonoike, 2011).

Plants evolved several regulatory pathways to modulate light harvesting efficiency and electron transport in response to light fluctuations to avoid excess excitation energy and over-reduction. Among them, cyclic electron transport (CET) around PSI redirects electrons from PSI to PQ contributing to proton translocation and ATP synthesis without NADPH formation (Munekage et al., 2002). Two distinct mechanisms involved in CET have been identified, one dependent on PGR5/ PGRL1 complex (DalCorso et al., 2008; Munekage et al., 2002) and another from the NADH dehydrogenase-like (NDH) complex (Chadee et al., 2021; Peltier et al., 2016). CET contributes to photoprotection by avoiding PSI acceptor side limitation and its over-reduction (Munekage et al., 2002; Yamamoto & Shikanai, 2019). CET further

contributes to photoprotection by enhancing luminal acidification (Shikanai, 2014, 2016; Shikanai & Yamamoto, 2017), inducing further regulatory mechanisms, namely the inhibition of electron flow through Cyt*b*$_6$*f* called photosynthetic control, and the induction of heat dissipation in PSII, called non-photochemical quenching (NPQ) (Joliot & Finazzi, 2010; ShunichiT akahashi, 2009). In Arabidopsis PGR5/ PGRL1 complex dependent-CET activity is particularly important to protect PSI under fluctuating light (ARNON & Chain, 1975). In the moss *Physcomitrium patens,* PGRL1 absence was shown to be impactful in particular under strong continuous illumination (Kukuczka et al., 2014; Storti et al., 2019) while the impact of NDH knockout lines was detectable during dark-to-light transitions and particularly evident as light conditions continued to fluctuate (Kato et al., 2018; Storti, Puggioni, et al., 2020).

Another major mechanism for electron transport regulation is pseudo-cyclic electron transport (PCET), where electrons from PSI are donated to oxygen, producing water. PCET is also called water-water cycle since electrons extracted from water at the level of PSII by the oxygen-evolving complex are regenerating water at the level of PSI. PCET as well contributes to the generation of ΔpH across the thylakoids' membrane but without any net NADPH production.

Two known mechanisms contribute to PCET. The first is the Mehler reaction, where the O_2^- generated from PSI is converted to water by the concerted activity of super-oxide dismutase (SOD) and ascorbate peroxidase (APX) (Badger et al., 2000). While important for ROS detoxification, the quantitative contribution of Mehler reaction to electron transport was found to be minor and variable depending on the species and conditions (Kozi Asada, 1999; K. Asada, 2000; Yang et al., 2020).

A second PCET mechanism depends on Flavodiiron proteins (FLV), that were first described in cyanobacteria as enzymes that catalyze O_2 photo-reduction to modulate photosynthetic electron transport under dynamic light conditions (Allahverdiyeva et al., 2013; Gerotto et al., 2016; Storti et al., 2019). FLVs are also present in green algae, mosses, liverworts, ferns and gymnosperms, where they have been shown to have a conserved activity in protecting PSI under fluctuating light conditions, avoiding over-reduction by ensuring the availability of electron acceptors even after abrupt increases in illumination (Gerotto et al., 2016; Setif et al., 2020). The FLV-dependent pathway was lost during the evolution of Angiosperms where the role

of relieving the accumulation of electrons in PSI upon light changes is at least partially compensated by CET (Kono et al., 2014; Suorsa et al., 2012; Yamamoto & Shikanai, 2019).

Consistently with this hypothesis, in the moss *Physcomitrium patens* CET and FLV were both shown to protect PSI from photoinhibition ensuring the availability of electron acceptors and protecting it from over-reduction. Mutants depleted of both CET and FLV-dependent PCET are severely delayed in growth and drastically impaired in electron transport capacity, while mutants missing only one mechanism have a much smaller phenotype, demonstrating a strong complementary and functional overlap (Storti, Segalla, et al., 2020).

While there is an increasing set of information on these mechanisms in different organisms and an understanding of their biological role, the light dependence of these two pathways in the modulation of electron transport activity is poorly investigated. In other words, what light intensity each alternative pathway can handle remains to be clarified. To address this question, we assessed the response to light dynamics of *P. patens* plants affected in either CET or FLV-dependent PCET, investigating the light dose responses of the mechanisms for regulation of electron transport. The moss *P. patens* was chosen as a model organism for the possibility of testing both CET and PCET mediated by FLV in the same organism (Alboresi, Storti, & Morosinotto, 2019; Storti et al., 2019). A further advantage is that in Angiosperms the photosynthesis induction after a sudden change in illumination could be also limited by stomatal conductance and mesophyll conductance (Brodribb et al., 2007; De Souza et al., 2020; Faralli et al., 2019; Yamori et al., 2020). On the contrary, the main photosynthetic tissues in *P. patens* consist of protonema and phyllids that are single-cell-layer structures without stomata and therefore take CO_2 up directly from the environment (Prigge & Bezanilla, 2010; Strotbek et al., 2013). The absence of a possible further layer of regulation on CO_2 diffusion limitation in *P. patens* thus enables a more direct elucidation of the impact of light dynamics on electron transport regulation.

Results obtained show that in *P. patens* thanks to the combined FLV and CET activities enable plants to respond to different time and light intensity dynamics, fully adjusting ETR capacity to 2-4 times increases in light intensity while also providing photoprotection if the illumination is stronger.

2. Results

2.1. Photosynthetic response to light dynamics

Light fluctuations are particularly challenging for photosynthetic organisms because they drive sudden changes in the absorbed excitation energy that cause over-reduction of electron transporters without allowing the time for modulation of CO_2 assimilation. The impact of light fluctuations and the role of different mechanisms in electron transport regulation were here assessed by exposing *P. patens* plants to light fluctuations. To this aim, the mosses were first exposed for 9 minutes to a low, limiting light (20 µmol photons m^{-2} s^{-1}). During this first phase, the illumination was low but capable of driving significant photosynthetic activity, thus enabling the activation of responses associated with the dark-to-light transition. The low light was followed by 3 minutes of illumination of different intensities, ranging from 20 to 553 µmol photons m^{-2} s^{-1} corresponding to a more than 25 times increase. This protocol was designed to highlight the effect of light changes at different intensities while maintaining the same time dynamics.

During the treatments, multiple photosynthetic parameters describing PSI and PSII activity were monitored, as shown in Figure 1 and Supplementary Figure 1. When the low light was first switched on, dark-adapted plants showed a small decrease in PSI and PSII yields (YI and YII, Figure 1A, B) as a result of the dark-to-light transition. However, all parameters recovered in 2-3 minutes and showed stable values after 9 minutes of low light exposure, demonstrating that plants had reached steady-state photosynthesis (Figure 1, Supplementary Figure 1). These plants were then treated with a stronger light intensity for another 3 minutes. After 10 seconds from the light change a reduction of YI and YII was visible that was partially recovered within three minutes of high light treatment (**Figure 1**A, B).

YI and YII can be exploited to estimate the electron transport rate (ETR) of the two photosystems. In both ETRI and ETRII, there was a sudden increase upon light changes that was followed by a further, slower increase, which was particularly evident with the light > 200 µmol photons m^{-2} s^{-1} (**Figure 1**C, D). Both ETRI and ETRII were indistinguishable for light intensities > 200 µmol photons m^{-2} s^{-1} suggesting that saturation of transport capacity had been reached (**Figure 1**C, D).

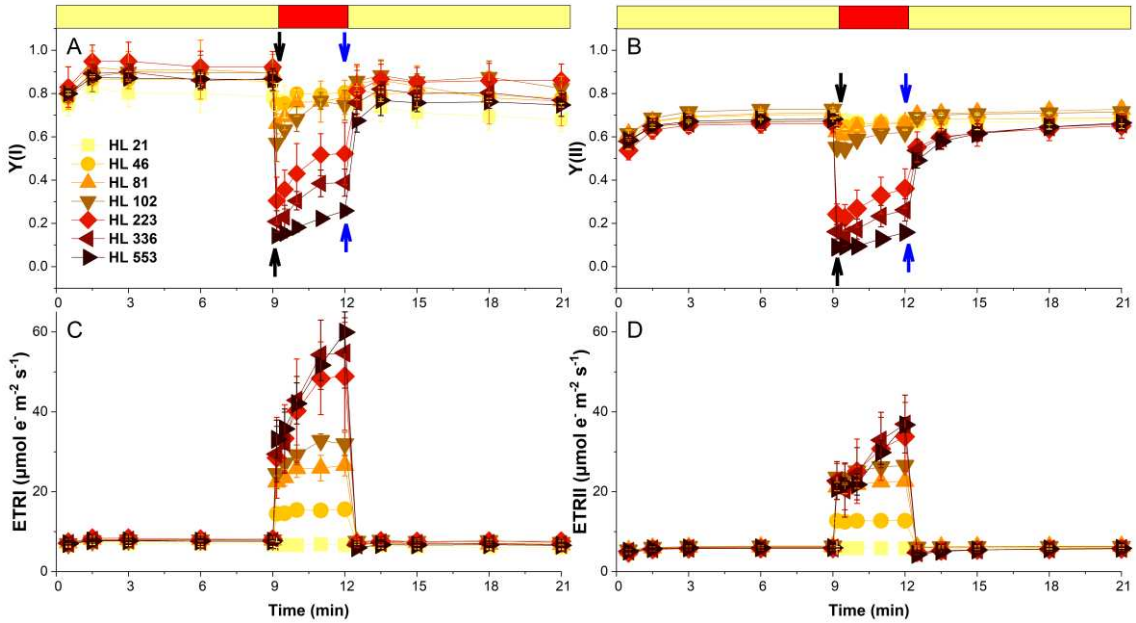

Figure 1 | **Effect of photosystem efficiency of different intensities on WT plants.** Dark-acclimated 10-day-old fresh protonemal tissues of WT were exposed to low light (21 µmol photons m^{-2} s^{-1}, 9 min) and high light (21, 46, 81, 102, 223, 336 or 553 µmol photons m^{-2} s^{-1}, 3 min). YI, the quantum yield of PSI photochemistry; YII, the effective quantum yield of PSII photochemistry; ETRI or ETRII, the electron transport rate of ETRI or ETRII; ETRI and ETRII were calculated using YI and YII, respectively. Values are means ± SD (n = 4). Different samples were used for each measurement replicate to avoid any possible interference from previous treatments.

The reduction in YI upon an increase in illumination was mostly attributable to an increase in PSI donor side limitation (Supplementary Figure 1). In fact, while donor side limitation [Y(ND)] showed progressively higher values following the increase of the illumination, acceptor side limitation [(Y(NA)] remained similarly low in all treatments (Supplementary Figure 1). This observation is consistent with the reduction of the PQ redox state, as estimated from the 1- qL (Supplementary Figure 1), progressively higher with the more intense light. The increase in illumination also drove the induction of NPQ. Its induction was stronger for illumination beyond 200 µmol photons m^{-2} s^{-1}, thus when ETR capacity was saturated (Supplementary Figure 1).

After high light treatments, plants were re-exposed to another 9 minutes of low light, reaching a new steady state, as shown in Figure 1, Supplementary Figure 1. After 9 minutes of the second low light treatment, all the PSI and PSII parameters were similar to the values before the treatment (Supplementary Figure 1), with the only exception of NPQ, which was not completely relaxed (Supplementary Figure 1D). A second high light treatment caused a highly similar impact on photosynthetic parameters, with no clear difference between the first and the second high light

treatment (Supplementary Figure 2). The only exception was a faster NPQ induction, an acceleration likely due to the residual accumulation of zeaxanthin (Supplementary Figure 2) (Suorsa et al., 2012). Because of this similarity, all following analyses concentrated on the first low light to high light transition only.

To better quantify how changes in light intensity affected photosynthesis, the data collected 10 seconds (marked with black arrows in **Figure 1**) and 3 minutes (marked with blue arrows in **Figure 1**) after the high light had been switched on were extracted. The increase in illumination caused a clear, fast reduction in both the YI and YII values, that progressively decreased with increasing light intensity (**Figure 2**A, B). For example, YI went from 0.77 at 20 µmol photons m^{-2} s^{-1} to 0.14 after exposure to 550 µmol photons m^{-2} s^{-1}, while similarly YII decreased from 0.67 to 0.10 with the same light intensities, clearly showing that PSI and PSII were becoming progressively saturated with the increase of the light intensity.

The same parameters extrapolated at the end of the high illumination treatments (3 minutes) showed a partial recovery of both YI and YII, whose values increased for all light intensities, suggesting an increase in photochemical and photo-regulation activity capable of reducing saturation levels of both photosystems (**Figure 2**A, B). It is interesting to observe that with light intensities up to 100 µmol photons m^{-2} s^{-1}, the recovery was sufficient to reach YI and YII levels equivalent to low light (0.75 and 0.62 respectively, Figure 2A, B). This suggests that plants were able to withstand an approximately 5-fold increase in light intensity (from 20 to 100 µmol photons m^{-2} s^{-1}), and within 3 minutes restore photosystems activity and oxidation state. If the light intensities were stronger, instead, both YI and YII still showed a clear recovery during the 3 minutes of high light but PSI and PSII remained partially saturated (Figure 2A, B).

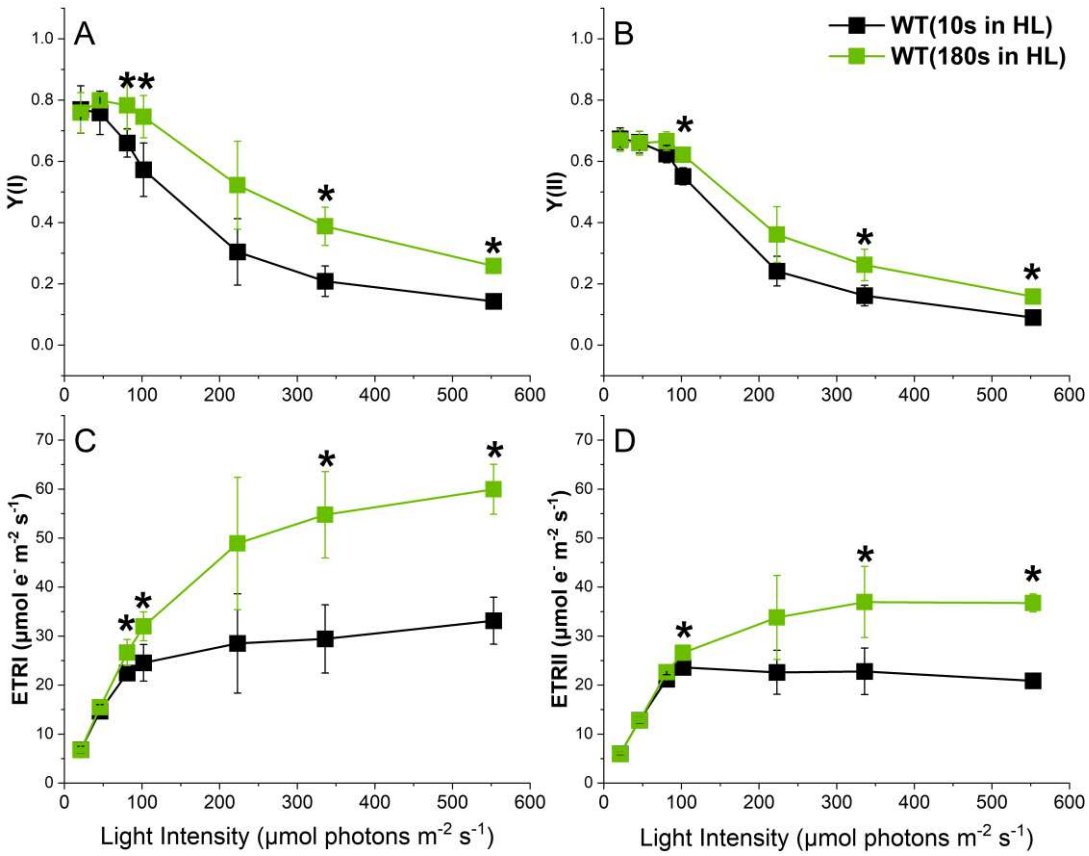

Figure 2 | **Light intensity dependence of photosynthetic parameters in WT.** The light intensity dependence of YI and YII (A, B); The light intensity dependence of ETRI and ETRII (C, D); Black squares represent the data of the first 10 s in high-light period (marked with black arrows in Figure 1), green squares represent the data after 3 min in high-light period (marked with blue arrows in Figure 1). Asterisks indicate statistically significant differences ($p<0.05$). Values are means ± SD (n=4).

Similar analysis of photosynthetic values at different times enabled to obtain more details on the response of the plants to light transition. ETRI and ETRII showed a dependence on the light intensity, as expected (Figure 2C, D). It is interesting to observe that after 10 seconds from the light increase, there was already a strong increase in photosynthetic electron transport, suggesting that plants possess excess electron transport capacity that is not fully exploited at low light. The ETR values increased proportionally to the light intensity in the range up to 80 µmol photons m^{-2} s^{-1} (Supplementary Figure 3) but beyond this intensity, the capacity for ETR was saturated, and stronger light intensities did not stimulate more electron transport within 10 seconds, independently from the light intensity used.

The same data after 3 minutes of high light show that within this timeframe ETR can further increase with a trend that reaches saturation at approximately 500 µmol

photons m^{-2} s^{-1}. Up to 100 µmol photons m^{-2} s^{-1} (5 times higher than the low light), the ETR after 3 minutes was still responding linearly to the light intensity, while with stronger illumination ETR was not able to keep the pace of light increases (Supplementary Figure 3).

After the increase in illumination, Y(ND) increased dramatically with the increasing high light, in particular when the intensity was above 100 µmol photons m^{-2} s^{-1} (Supplementary Figure 4A). On the contrary, Y(NA) showed no significant differences in any of the fluctuating light treatments (Supplementary Figure 4B). The correlation analysis with data after 10 seconds of high light showed that YI had a negative correlation with Y(ND) while there was no relationship with Y(NA) (Supplementary Figure 5). These results suggest that PSI donor side limitation is the major factor of decreased PSI photochemical efficiency under sharply increased light. This hypothesis was supported by the PQ reduction state aggravated as the high light intensity increased (Supplementary Figure 4C). These results indicate that in WT, the limitation of electron transport from PSII to PSI is a major factor for electron transport limitation under rapidly excess excitation energy conditions.

NPQ was not fully activated after 10 seconds and required longer illumination to reach its maximal values. Its intensity showed a clear light dependence with no significant activation up to 100 µmol photons m^{-2} s^{-1} (Supplementary Figure 4D), that instead was observable starting from 200 and reaching maximal values over 500 µmol photons m^{-2} s^{-1}. This suggests that the differences observed in YII and ETRII at lower light intensities are mostly attributable to photochemical activity and not to photo-regulation, especially at the 10-second timescale.

2.2. Light intensity dependence of pseudo-cyclic electron transport.

To assess the impact of alternative electron transport mechanisms and analyze the light dependence of the FLV-dependent PCET, *flva* KO mutant lines were exposed to the same light fluctuations employed for WT plants (Supplementary Figure 6). No significant differences were observed with WT during the first 9 minutes of low light, while differences were observable after the light increased.

The photosynthetic parameters extrapolated 10 seconds after the light increase (**Figure 3**) showed a more severe decrease in both YI and YII in the *flva* KO mutant than in WT. Remarkably, the *flva* KO mutant showed a sharp decrease in YI reaching the lowest values already at approximately 100 µmol photons m^{-2} s^{-1} (**Figure 3**A). Interestingly, the difference in YI and YII between the WT and *flva* KO mutant was particularly large in the 100-200 µmol photons m^{-2} s^{-1} range, where *flva* KO showed a major reduction in yield while WT still showed values close to the low light. With higher light intensities, instead, the difference between the WT and *flva* KO mutant decreased, and the value of YI in the mutant differed negligibly from WT with the higher light intensities.

The immediate increase in ETRI and ETRII observed in WT plants is not present in the *flva* KO mutant, where the electron transport rate is substantially unaffected 10 seconds after a light change (Figure 3C, D). This indicates that the FLV-dependent pathway plays a major role in providing an extra electron transport capacity that, upon 5-fold increases in illumination (from 20 to 100 µmol photons m^{-2} s^{-1}), enables a fast adjustment of electron transport following light intensity changes.

As a consequence of this reduced electron transport capacity, even with the lowest light intensities the *flva* KO mutant showed a rapid increase in Y(NA) within the first 10 seconds after light transition, indicating over-reduction of PSI electron acceptors (Figure 3E). This effect is completely saturated at 100 µmol photons m^{-2} s^{-1}, synchronized with YI. The opposite trend was observed for Y(ND) (Figure 3F); within the first 10 s transition from low light to high light, the donor limitation progressively increased with light intensity in WT plants, while it maintained very low values for the *flva* KO mutant (Figure 3F). The *flva* mutant showed low NPQ in the first 10 s even when the high light intensity was over 100 µmol photons m^{-2} s^{-1} (Figure 3G), indicating that the absence of the FLV-dependent pathway influenced the NPQ trigger immediately after the light was suddenly increased. All observed differences between the WT and *flva* KO mutant were much smaller with the continuation of the light treatment and after 3 minutes of illumination all parameters become indistinguishable between the WT and mutant (Figure 4), consistent with earlier results showing a transient effect on FLV activity (Gerotto et al., 2016).

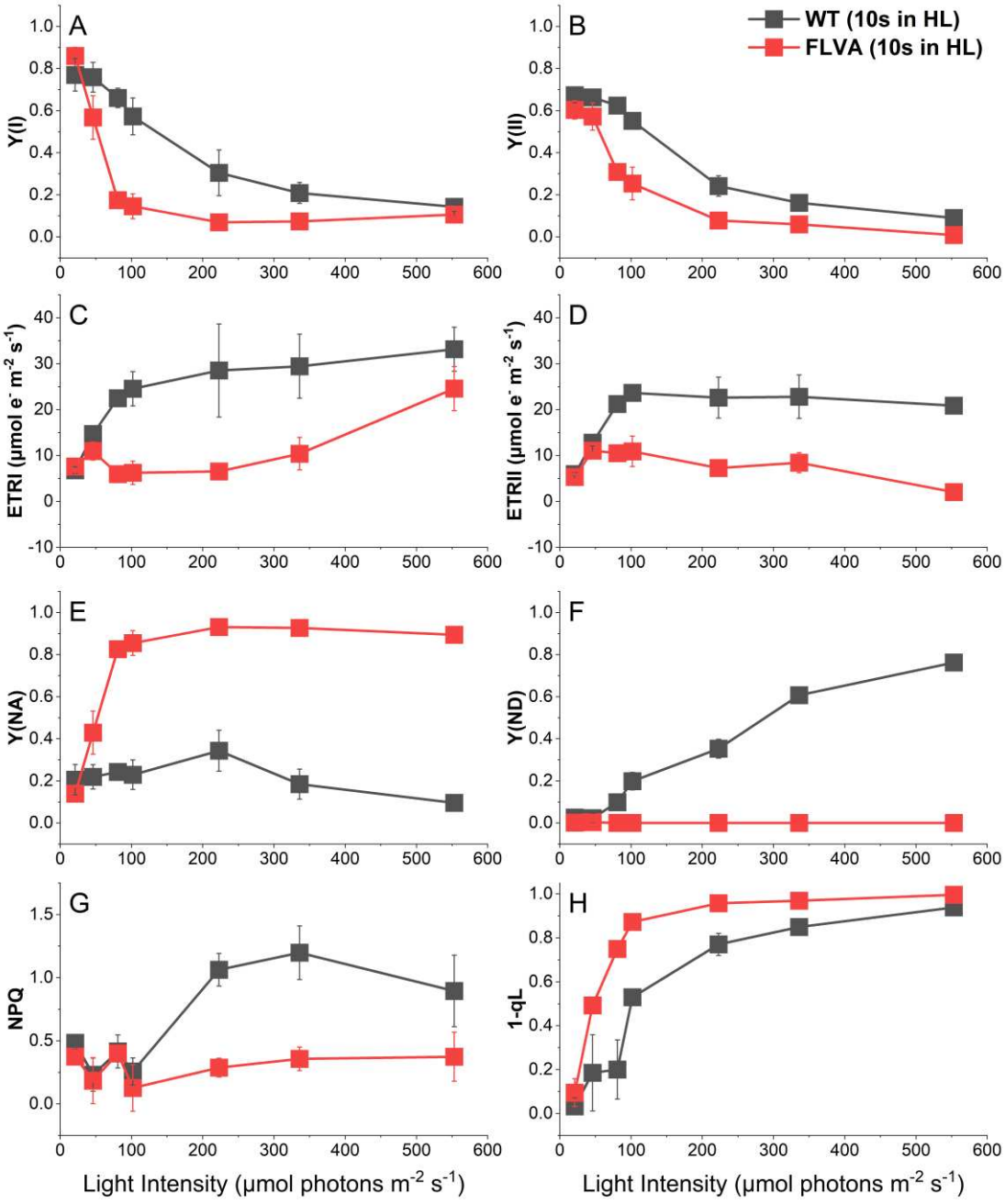

Figure 3 | Impact of light changes on photochemistry efficiency and photoinhibition in WT and *flva* KO mutants within 10 s after light transition. Y(NA), the quantum yield of PSI non-photochemical energy dissipation due to acceptor side limitation; Y(ND), the quantum yield of PSI non-photochemical energy dissipation due to donor side limitation; NPQ, non-photochemical quenching in PSII; 1-qL, Q_A relative reduction; Black and red squares represent the data of first 10 s under high-light period in WT and *flva* mutant, respectively. Values are means ± SD (n = 4).

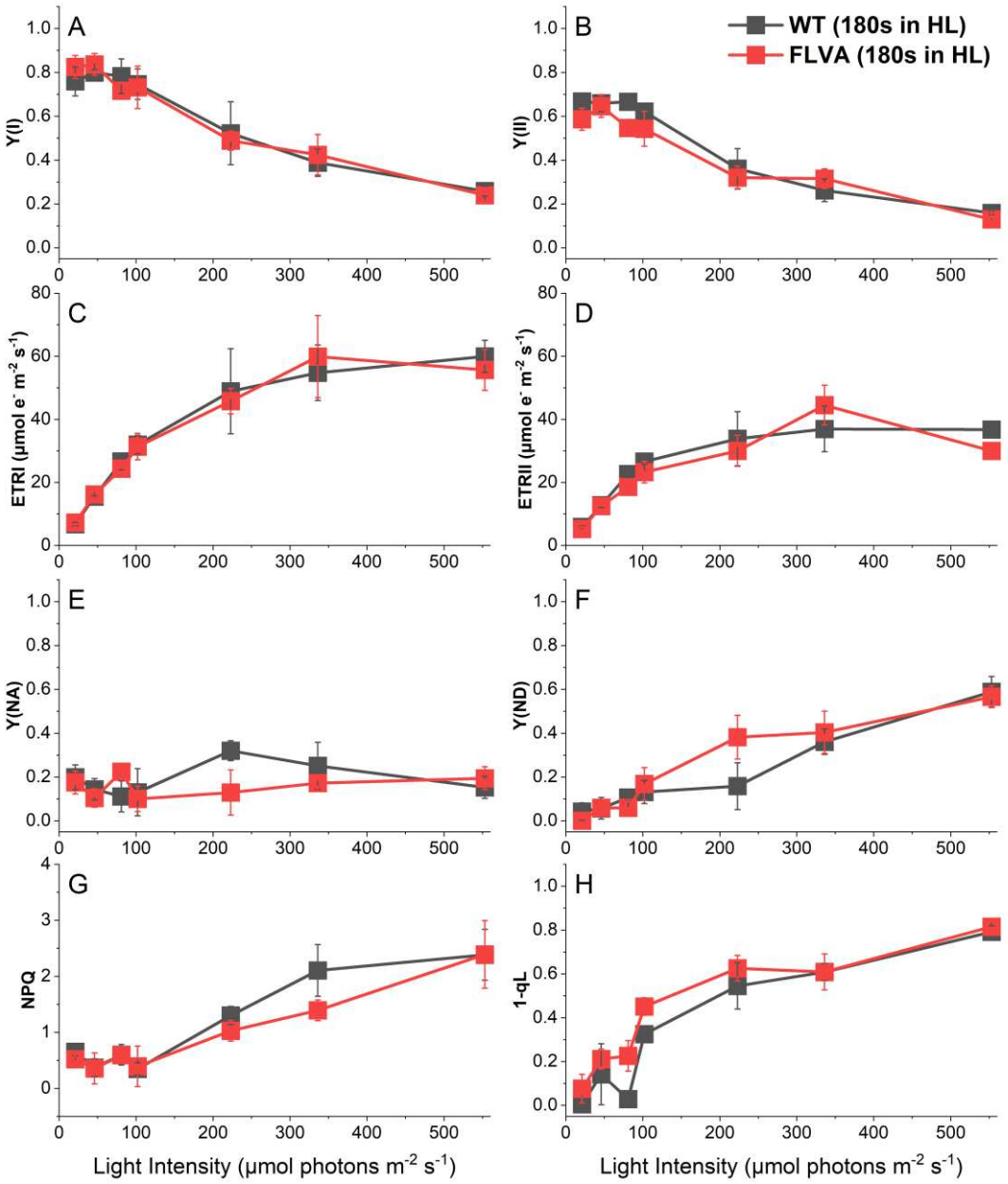

Figure 4 | Impact of light changes on photochemistry efficiency and photoinhibition in WT and *flva* KO mutants within 3 min after light transition. Black squares and red circles represent the data of 3 min under a high-light period in WT and *flva* mutant, respectively. Values are means ± SD (n = 4).

2.3. Light intensity dependence of cyclic electron transport.

The *pgrl1/ndhm* KO mutant was similarly analyzed to assess the impact of CET (Supplementary Figure 7). Plants showed an impact on both YI and YII after a sudden increase in illumination, which was immediately visible 10 seconds after a light change (Figure 5A, B). The difference between WT and mutant is visible for lower light intensities while from 200 µmol photons m^{-2} s^{-1} and above there was no difference in

YI/YII and ETRI/II from the WT, indicating that the cyclic electron transport capacity was completely saturated at this light intensity and its inactivation had no impact on photosystems saturation.

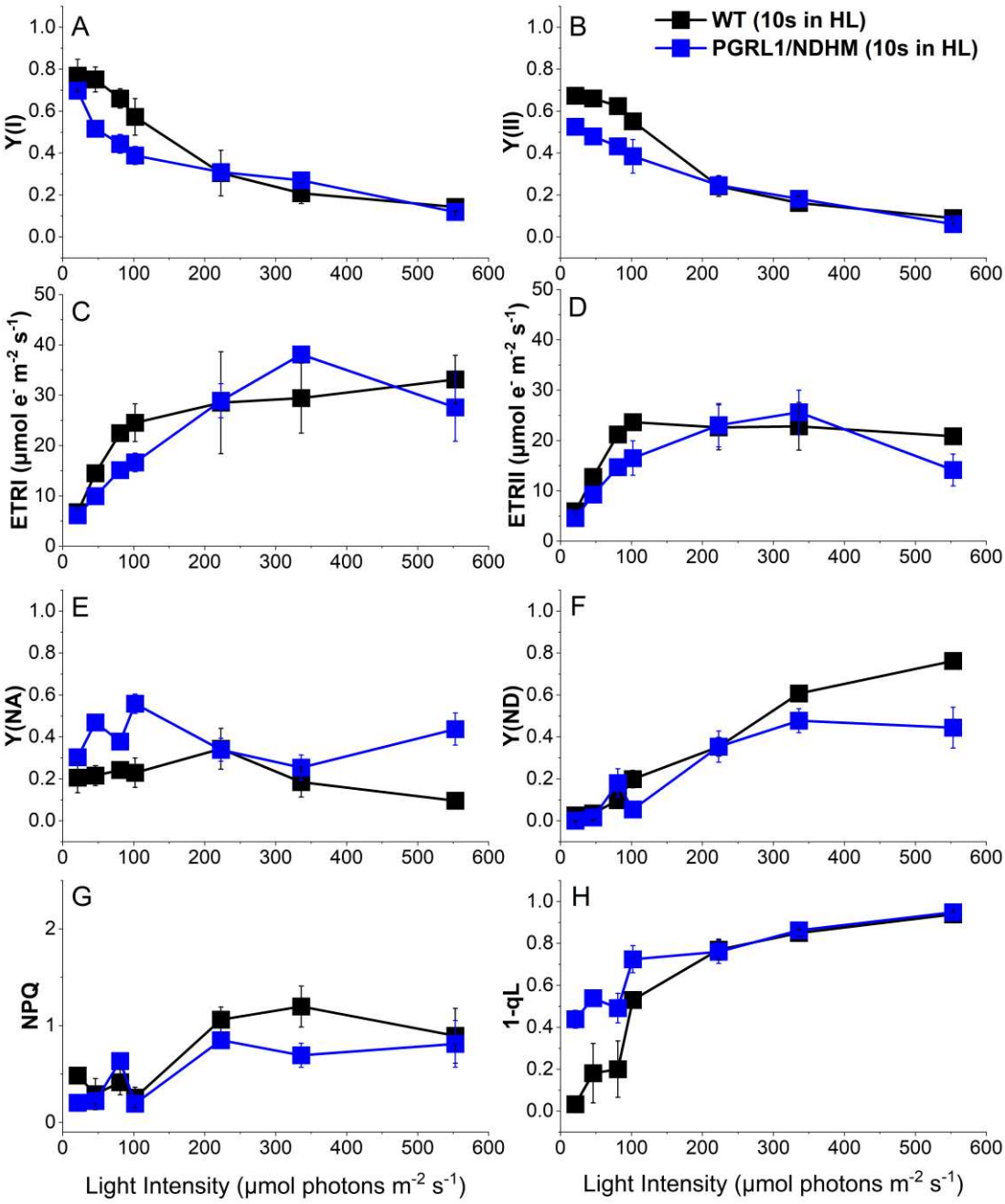

Figure 5 | Impact of light changes on photochemistry efficiency and photoinhibition for first 10s after light transition in WT and *pgrl1/ndhm* double mutants. Black and red circles represent the data of the first 10 s under the high-light period in WT and *pgrl1/ndhm* mutant, respectively. Values are means ± SD (n = 4). Values are means ± SD (n = 4).

In contrast to what was previously observed in the *flva* KO mutant, which showed recovery after exposure to high light for three minutes, the difference between

the WT and *pgrl1/ndhm* KO mutant was stable and maintained after 3 minutes of high light, showing that the CET contribution was constant in time and the effect of its absence was still perceived (Figure 6A, B).

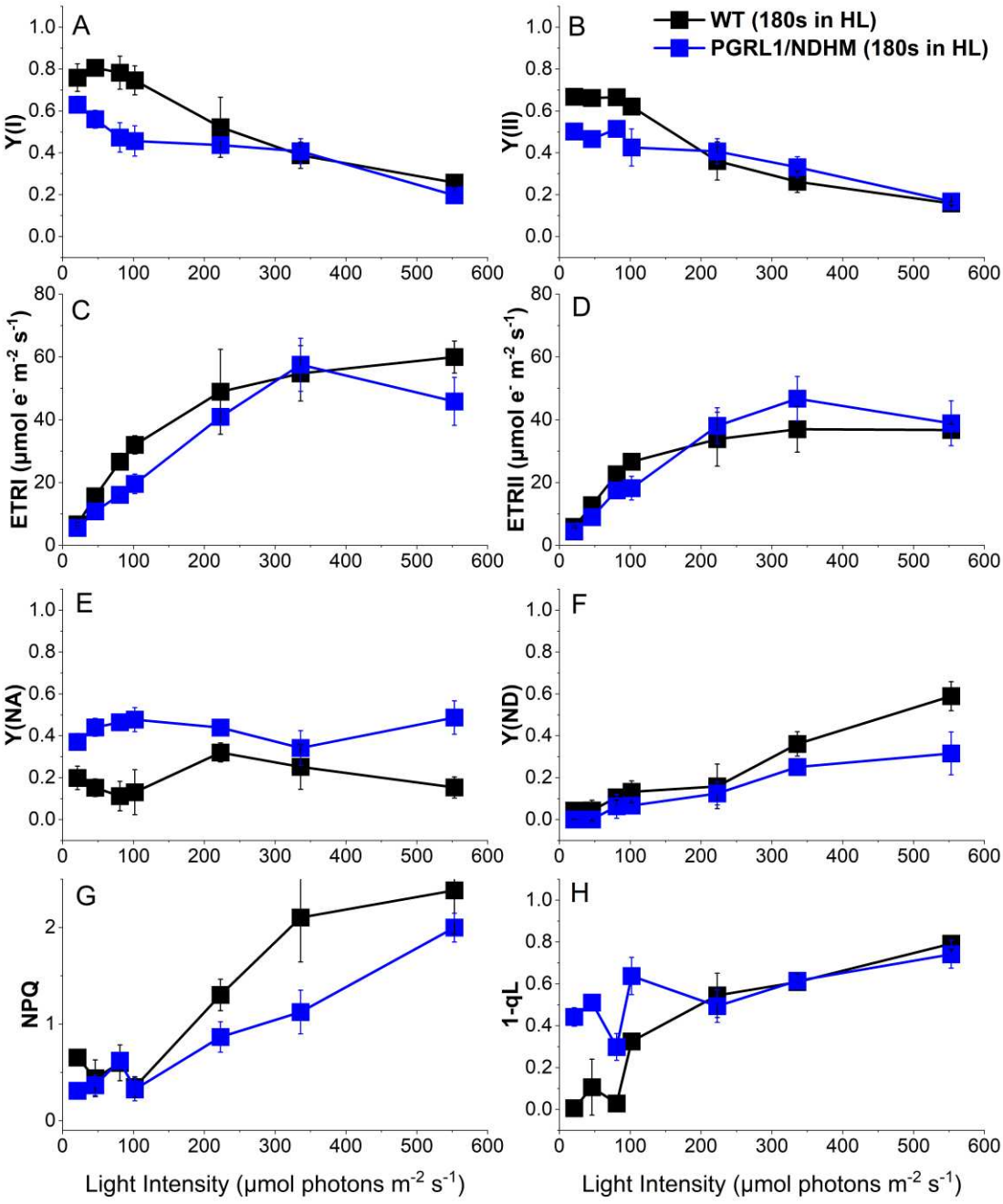

Figure 6 | Impact of light changes on photochemistry efficiency and photoinhibition for 3 min after light transition in WT and *pgrl1/ndhm* double mutants. Black squares and red circles represent the data of 3 min under a high-light period in WT and *pgrl1/ndhm* mutant, respectively. Values are means ± SD (n = 4). Values are means ± SD (n = 4).

Contrary to WT, analysis of PSI parameters showed that the *pgrl1/ndhm* KO mutant had higher Y(NA) after a light transition, suggesting that CET is active in stimulating electron transport from the PSI acceptor side providing extra electron acceptors (Figure 5E). The difference with WT is not as large as with *flva* KO, but it is still maintained at the same levels after 3 minutes of strong illumination (Figure 6E). It is also interesting to note that this higher acceptor side limitation in comparison with WT is present for all light intensities, even the strongest ones (Figure 6E). WT and *pgrl1/ndhm* KO mutant have similar YI at all light intensities over 200 μmol photons m^{-2} s^{-1}, but in the former, this is due to higher donor side limitation, while in the *pgrl1/ndhm* KO mutant, it is caused by the higher acceptor side limitation. Thus at higher light intensities even if CET contribution to ETRI becomes neglectable it still affects the donor/acceptor balance.

This picture is consistent with the effect of knockout of *pgrl1/ndhm* on the PQ redox state at a light intensity below 200 μmol photons m^{-2} s^{-1} as the result of cyclic electron transport deficiency (Figure 5H). The impact of CET on NPQ is instead not detectable, as CET shows effects with light below 200 μmol photons m^{-2} s^{-1} and NPQ is not activated at these light intensities (Figure 5G).

3. Discussion

3.1. *P. patens* plants have excess ETR capacity, not fully exploited at low light.

Plants in natural environments are exposed to light fluctuations of different duration and kinetics and it is now well established that these changes have a major impact on photosynthesis, eventually driving to damage and requiring the evolution of complex regulatory mechanisms (Chaux et al., 2015; Shubin et al., 2008; Sonoike, 2011), with a strong impact also on crops productivity in the field (Kaiser et al., 2018; Long et al., 2022; Slattery et al., 2018).

The rate of photosynthesis under any condition is the integrated result of the light absorption, the photochemical capacity of photosystems and of the use of that energy to drive carbon assimilation and other metabolic processes (Kaiser et al., 2016). Sudden increases in illumination have a different impact on these different processes since light absorption changes instantaneously, while metabolic regulation is slower and takes minutes to adjust (Pearcy, 1990; Watanabe et al., 2016). These different kinetics are sources of unbalances between light absorption and its utilization from the metabolism that can drive undesired reactions and eventually damage.

The study of the impact of light fluctuations experienced a strong increase in the recent literature, as a consequence of the realization that these are fundamental for plant life in the natural environment (Kono & Terashima, 2014; Long et al., 2022). Most studies investigated how different alternations of dark/light affect photosynthesis. However, some photosynthetic pathways, starting with CO_2 fixation, are inhibited in the dark and thus when the light is switched on the impact of illumination intensity is combined with the time needed for the induction of carbon fixation.

Plants in nature are instead more likely to experience transitions from low light to high light and for this reason in this work *P. patens* plants were treated with a light protocol designed to highlight the effect of light transitions when plants were already performing photosynthesis, thus avoiding the impact of all the regulations associated with dark to light transitions and highlighting the impact of the increase in light flux. The protocol also aimed at investigating the effect of the difference in intensity during the light change, while maintaining the same temporal dynamics. The first observation

is that *P. patens* plants have an extra capacity for ETR that can increase by approximately three times within 10 seconds (estimated ETR were 7.7 / 6.3 µmol e^- m^{-2} s^{-1} at 21 µmol photons m^{-2} s^{-1} to 22.5 / 21.2 µmol e^- m^{-2} s^{-1} at 81 µmol photons m^{-2} s^{-1} for PSI / PSII respectively, see Figure 2). Plants thus have a higher ETR capacity available that enables them to cover and exploit light increases for photochemistry. Up to 80 µmol photons m^{-2} s^{-1}, the increased photochemical capacity in the high-light period is capable of compensating for the light increase and indeed YI and YII recover to the low light levels (Figure 3).

It is interesting to observe that a four times increase in illumination drove an approximately 3 times increase in estimated ETR, suggesting this increase in photochemical activity occurred while also maintaining a similar conversion efficiency. This capacity should be particularly beneficial in case of sun flecks, suggesting that in case of fast changes in illumination there is the ability to use light energy efficiently for photosynthesis (CHAZDON, 1988; Pearcy, 1990). In this way, *P. patens* increase the ETR immediately within 10 s after a light change to efficiently utilize available light in a short time. This extra ETR capacity with fast activation was completely saturated at 80 µmol photons m^{-2} s^{-1} and stronger increases in illumination showed no significant effects within a 10 seconds timeframe (Figure 2).

A further increase in ETR is indeed possible, but its activation takes longer and is detectable after 3 minutes of high light (Figure 2). This slower increase shows a light dependence (with saturation at around 600 µmol photons m^{-2} s^{-1}), suggesting that the rate of metabolism (e.g. consumption of NADPH) is likely involved. The most likely explanation is that in this timeframe there is metabolic modulation, starting with the induction of a stronger CO_2 fixation that, by enhancing the consumption of electron acceptors, increases the maximal ETR further. For light intensities over 100 µmol photons m^{-2} s^{-1} (Eberhard et al., 2008), however, this increased ETR capacity is still not sufficient to exploit all absorbed energy and both PSI and PSII get progressively saturated, and this is accompanied by full activation of NPQ (Supplementary Figure 4).

3.2. Light dose dependency of FLV mediated electron transport.

Treatment of FLV-dependent PCET and CET mutants with light fluctuations of different intensities enabled to highlight the role of these mechanisms in the response to light fluctuations and assess their dependence on light intensity. *flva* KO shows a much reduced ability to fast activate ETR, suggesting that FLV is the largest contributor to this sudden increase in ETR activated upon abrupt changes in illumination (Alboresi, Storti, Cendron, et al., 2019). This is fully consistent with the experimental evidence clarifying that the FLV- dependent pathway acts as a safety electron sink during rapid light fluctuations in all organisms from cyanobacteria to gymnosperms (Ilik et al., 2017; Yamamoto et al., 2016; Zhang et al., 2009). Here, the *flva* ko mutant showed a more severe decrease in YI and YII and a much-reduced ability of ETR fast activation compared with WT 10 seconds after exposure to high light (Fig. 3). Meanwhile, the reduced ETR in the *flva* KO mutant caused over-reduction of PSI (Fig. 3E) owing to its role as a safety electron sink. These results suggest that the FLV-dependent pathway is the largest contributor to this sudden increase in ETR activated upon illumination transition, preventing the production of ROS triggered by the over-reduction of PSI electron carriers (Armbruster et al., 2017; Suorsa et al., 2012).

The impact of FLV absence was particularly noticeable at the lower light intensities up to approximately 100 µmol photons m^{-2} s^{-1}, where the WT plants were able to sustain a fast increase in ETR in response to light intensity increases. FLV provide an extra electron transport capacity enabling fast adjustment of electron transport following light intensity changes, that could provide an advantage in case of low-intensity fluctuations to exploit the energy for driving photochemical reactions.

With stronger illuminations, on the other hand, FLV capacity is saturated and ETR cannot increased further, driving to photosystems saturation (Figure 3). While FLVs are not able to provide sufficient extra electron transport capacity upon exposure to strong increases in illumination, they still have a crucial impact on PSI redox state (Chaux et al., 2017; Shimakawa et al., 2017). In fact, in the absence of FLV light transitions drive strong acceptor side limitation in PSI, a state where PSI is prone to damage from over-reduction (Tiwari et al., 2016). In the presence of FLV even if PSI is saturated by the light excess it remains limited from the donor side, a condition

where it is much more stable to photooxidation (Alboresi, Storti, & Morosinotto, 2019; Yamamoto et al., 2016).

3.3. Role of cyclic electron transport in response to light fluctuations of different intensities.

The mutants affected in CET showed similar phenotypes to *flva* KO, supporting the idea of a partial overlap of activity between the two mechanisms (Storti, Segalla, et al., 2020). The time kinetics and electron transport capacities are however different in comparison with FLV-dependent PCET. CET contribution is smaller but stable, and it affects YI, YII and all other photosynthetic parameters after 3 minutes of increase of light intensity (Fig.5). On the contrary, within this timeframe the PSI redox status in *flva* ko mutant is completely identical to WT in almost all fluctuations (Fig. 4E, F). FLV-dependent pathway has a clear impact after light sudden transitions and a negligible difference compared with WT after three minutes under high light, implying its crucial role in regulating electron transport at the moment when the light increases (Storti et al., 2019) . CET partially compensates for the FLV-dependent pathway but activation kinetics are different, modulated electron transport in all light intensities and situations not only a moment when the light intensity changes (Yamori et al., 2016).

On the other hand, CET has a smaller electron transport capacity and it shows no effect on YI/YII and ETR with light intensities > 200 µmol photons m^{-2} s^{-1}. It is interesting to note, however, that while the WT and *pgrl1/ndhm* KO mutants had similar YI in all experiments when high light was over 200 µmol photons m^{-2} s^{-1}, in the former this was due to higher donor side limitation of PSI, while in *pgrl1/ndhm* KO mutants this was caused by the higher acceptor side limitation (Fig. 4). These results thus suggest that cyclic electron transport works as an important electron sink around PSI at any light intensity in steady or unsteady light conditions and, even if the contribution on ETRI is small (Figure 5C), it still affects the balance between acceptor and donor side limitation (Yamamoto & Shikanai, 2019). This is biologically highly relevant since PSI is sensitive to oxidation in case of acceptor side limitation while it is very stable in case of donor limitation (Tiwari et al., 2016). This effect could be due to CET promoting the NPQ induction and photosynthetic control by regulating proton motive force across the chloroplast thylakoid membrane (Joliot & Finazzi, 2010; ShunichiT akahashi,

2009). Thus even if CET electron transport capacity is not strong enough to provide a significant impact on ETR at high light intensities, the absence of CET causes the over-reduction of P700 under high illumination seen from the higher Y(NA) (Figure 5), indicating the CET alleviates PSI photoinhibition from both donor and acceptor side limitations (Yamamoto & Shikanai, 2019), even without a strong capacity for electron transport.

The *P. patens* response to increases in illumination and the contribution of different regulatory mechanisms is summarized in the scheme in Figure 7. In limiting light (20 μmol photons m^{-2} s^{-1}) photosynthetic apparatus in *P. patens* drives electron transport from water to NADPH by the activity of PSII and PSI. An increase in illumination (80 μmol photons m^{-2} s^{-1}) drives a very fast increase in ETR by the activation of CET and FLV-dependent activity. This extra electron transport capacity, largely associated with FLV, enables to maintain the saturation levels of PSI and PSII even if illumination is stronger. After 3 minutes from light increase, CET is still active, while FLV activity is down regulated. The increase in ETR is maintained thanks to the activation of metabolic pathways, such as CO_2 fixation, that increase NADPH consumption and thus enables a faster biosynthesis rate.

If the light increase is much stronger, > 200 μmol photons m^{-2} s^{-1}, FLV and CET are not able to accept all extra electrons and their transport capacity is saturated. After 10 seconds from the increase in illumination, ETR is equivalent than the one estimated with 80 μmol photons m^{-2} s^{-1} and, as a consequence, PSI and PSII are saturated. After 3 minutes of strong illumination, as in the earlier case CET is present while FLV activity is inhibited. Metabolic NADPH consumption is also induced, strongly than with lower light intensities, enabling an approx. 6 times increase of total ETR as compared with low light. NPQ is also induced, reducing the excitation pressure on PSII. Despite all the mechanisms activated, ETR capacity is still not capable to fully respond to the increase in harvested light and thus PSII and PSI are saturated. While FLV and CET are not able to accept all electrons it is important to highlight that even in these conditions their presence still enables PSI to be donor side limited, a condition in which PSI is less prone to photooxidation. FLV and CET activities thus depending on the light intensities have a slightly different role. In fact, upon small increases in light intensities they enable to transiently increase electron transport capacity

sustaining ETR while in case of stronger changes in illumination they also contribute to photoprotection.

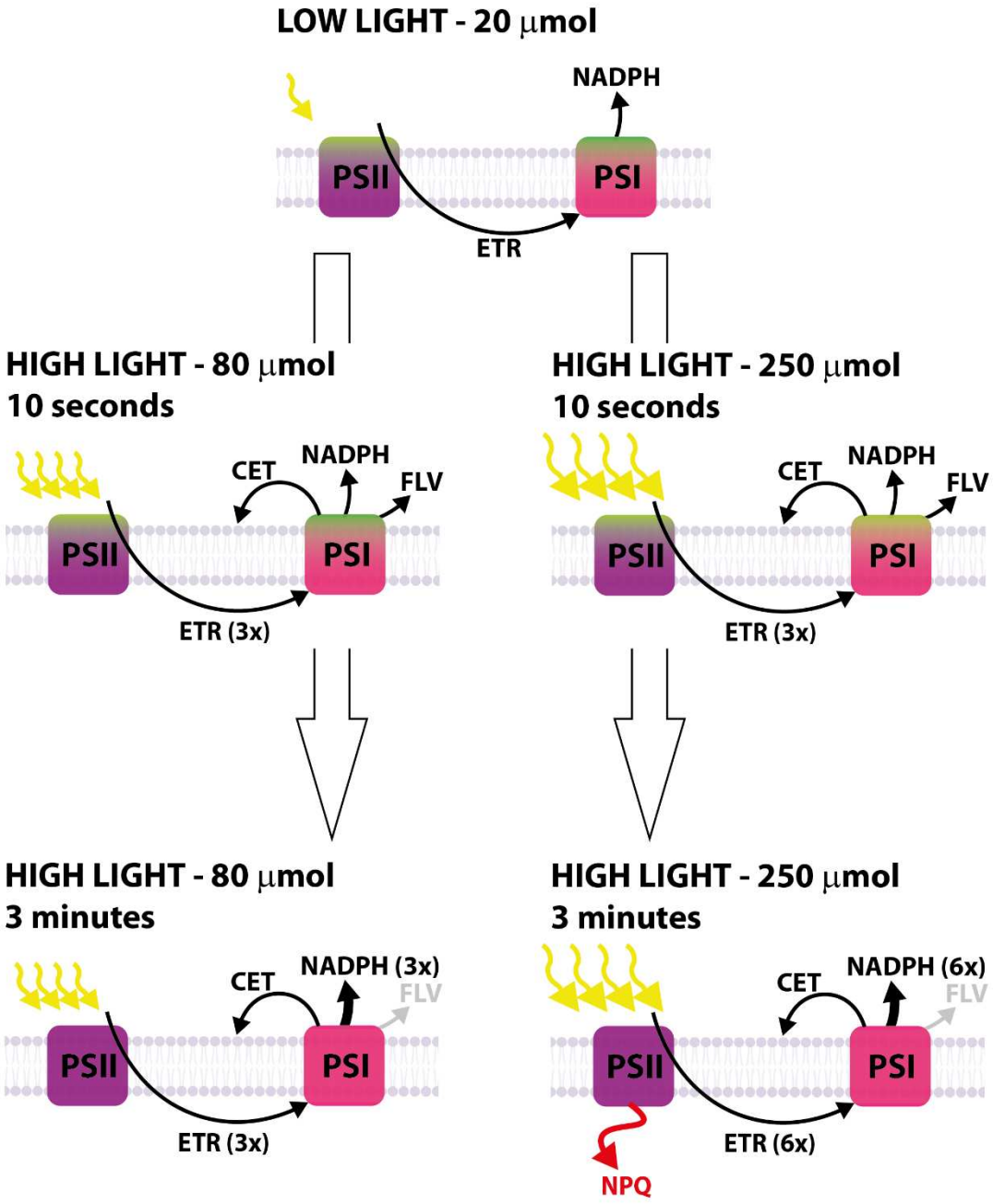

Figure 7 | **Model of impact of light fluctuations of different intensity on *P. patens*.** In low, limiting, light (20 µmol photons m^{-2} s^{-1}) photosynthetic apparatus in *P. patens* drives electron transport from water to NADPH by the activity of PSII and PSI. A small increase in illumination (80 µmol photons m^{-2} s^{-1}).

4. Materials and methods

4.1. Plant material and growth

P. patens (Gransden ecotype) wild-type (WT), *flva* KO lines *pgrl1/ndhm* doubled KO lines (Gerotto et al., 2016; Kono et al., 2014; Kukuczka et al., 2014) were maintained in the protonemal stage by vegetative propagation on $PpNH_4$ medium (N.W. Ashton et al., 1979) and grown under controlled conditions: 22°C, 16 h light/ 8 h dark photoperiod with 50 µmol photons m^{-2} s^{-1}. Experiments were all performed on 10-day-old plants grown on solid $PpNO_3$ medium (N.W. Ashton et al., 1979).

4.2. Spectroscopic analyses

In vivo chlorophyll fluorescence and $P700^+$ absorption were monitored simultaneously at room temperature with a Dual-PAM 100 system (Walz) on protonemal tissue grown for 10 days on $PpNO_3$. Before the measurements, the plants were dark-acclimated for 40 min and illuminated with far-red light for 20 s, then the F_v/F_m parameter was calculated as $(F_m-F_0)/F_m$; the maximum $P700^+$ signal (Pm), was determined by applying a saturation pulse (300 ms and 20, 000 µmol photons m^{-2} s^{-1}) after pre illumination with far-red light for 10 s. Afterward, leaves were illuminated at fluctuating light alternative between low light (21 µmol photons m^{-2} s^{-1}, 9 min) and high light (21, 46, 81, 102, 223, 336 or 553 µmol photons m^{-2} s^{-1}, 3 min) for 24 min. During this fluctuating light treatment, PSI and PSII parameters were recorded simultaneously. The photosynthetic parameters were calculated as follows: YII as $(Fm'-F_0)/Fm'$; qL as $(Fm'-F)/(Fm'-F_0') * F_0'/F$; NPQ as $(Fm-Fm')/Fm'$; YI as 1-Y(ND)-Y(NA); Y(NA) as (Pm-Pm')/Pm; Y(ND) as $(P-P_0/Pm)$ (Christof Klughammer & Schreiber, 1994; Klughammer & Schreiber, 2008; Kramer et al., 2004). The electron transport rate through PSI (ETRI) was calculated as PPFD × YI × 0.84 × 0.5, the electron transport rate through PSII (ETRII) was calculated as PPFD × YII × 0.84 × 0.5. Each replica was performed on independent samples to avoid any possible interference.

5. References

Alboresi, A., Storti, M., Cendron, L., & Morosinotto, T. (2019). Role and regulation of class-C flavodiiron proteins in photosynthetic organisms. *Biochem J,* 476(17), 2487-2498.

Alboresi, A., Storti, M., & Morosinotto, T. (2019). Balancing protection and efficiency in the regulation of photosynthetic electron transport across plant evolution. *New Phytologist,* 221(1), 105-109.

Allahverdiyeva, Y., Mustila, H., Ermakova, M., Bersanini, L., Richaud, P., Ajlani, G., . . . Aro, E. M. (2013). Flavodiiron proteins Flv1 and Flv3 enable cyanobacterial growth and photosynthesis under fluctuating light. *Proceedings of the National Academy of Sciences,* 110(10), 4111-4116.

Allahverdiyeva, Y., Suorsa, M., Tikkanen, M., & Aro, E. M. (2015). Photoprotection of photosystems in fluctuating light intensities. *Journal of Experimental Botany.,* 66(9), 2427-2436.

Armbruster, U., Correa Galvis, V., Kunz, H. H., & Strand, D. D. (2017). The regulation of the chloroplast proton motive force plays a key role for photosynthesis in fluctuating light. *Current Opinion in Plant Biology,* 37, 56-62.

ARNON, D. I., & Chain, R. K. (1975). Regulation of ferredoxin-catalyzed photosynthetic pkosphorylations. *Proceedings of the National Academy of Sciences,* 72(12), 4961-4965.

Asada, K. (1999). THE WATER-WATER CYCLE IN CHLOROPLASTS: Scavenging of Active Oxygens and Dissipation of Excess Photons. *Annual Review of Plant Physiology and Plant Molecular Biology,* 50, 601-639.

Asada, K. (2000). The water-water cycle as alternative photon and electron sinks. *Philosphical Transactions of the Royal Society Biological science,* 355(1402), 1419-1431.

Badger, M. R., von Caemmerer, S., Ruuska, S., & Nakano, H. (2000). Electron flow to oxygen in higher plants and algae: rates and control of direct photoreduction (Mehler reaction) and rubisco oxygenase. *Philosphical Transactions of the Royal Society Biological science,* 355(1402), 1433-1446.

Brodribb, T. J., Feild, T. S., & Jordan, G. J. (2007). Leaf maximum photosynthetic rate and venation are linked by hydraulics. *Plant Physiology,* 144(4), 1890-1898.

Chadee, A., Alber, N. A., Dahal, K., & Vanlerberghe, G. C. (2021). The Complementary Roles of Chloroplast Cyclic Electron Transport and Mitochondrial Alternative Oxidase to Ensure Photosynthetic Performance. *Frontiers in Plant Science,* 12.

Chaux, F., Burlacot, A., Mekhalfi, M., Auroy, P., Blangy, S., Richaud, P., & Peltier, G. (2017). Flavodiiron Proteins Promote Fast and Transient O2 Photoreduction in Chlamydomonas. *Plant Physiology,* 174(3), 1825-1836.

Chaux, F., Peltier, G., & Johnson, X. (2015). A security network in PSI photoprotection: regulation of photosynthetic control, NPQ and O2 photoreduction by cyclic electron flow. *Frontiers in Plant Science,* 6, 875.

CHAZDON, R. L. (1988). Sunfleks and their importance to foest understorey plants. *Advances in Ecological Research,* 18, 1-63.

Christof Klughammer, & Schreiber, U. (1994). An improved method, using saturating light pulses, for the determination of photosystem I quantum yield via P700+absorbance changes at 830 nm. *Planta,* 192, 261-268.

DalCorso, G., Pesaresi, P., Masiero, S., Aseeva, E., Schunemann, D., Finazzi, G., . . . Leister, D. (2008). A complex containing PGRL1 and PGR5 is involved in the switch between linear and cyclic electron flow in Arabidopsis. *cell,* 132(2), 273-285.

De Souza, A. P., Wang, Y., Orr, D. J., Carmo-Silva, E., & Long, S. P. (2020). Photosynthesis across African cassava germplasm is limited by Rubisco and mesophyll conductance at steady state, but by stomatal conductance in fluctuating light. *New Phytologist,* 225(6), 2498-2512.

Eberhard, S., Finazzi, G., & Wollman, F. A. (2008). The dynamics of photosynthesis. *The Annual Review of Genetics,* 42, 463-515.

Faralli, M., Cockram, J., Ober, E., Wall, S., Galle, A., Van Rie, J., . . . Lawson, T. (2019). Genotypic, Developmental and Environmental Effects on the Rapidity of g(s) in Wheat: Impacts on Carbon Gain and Water-Use Efficiency. *Frontiers in Plant Science,* 10, 492.

Gerotto, C., Alboresi, A., Meneghesso, A., Jokel, M., Suorsa, M., Aro, E. M., & Morosinotto, T. (2016). Flavodiiron proteins act as safety valve for electrons in Physcomitrella patens. *Proceedings of the National Academy of Sciences,* 113(43), 12322-12327.

Hahn, A., Vonck, J., Mills, D. J., Meier, T., & Kuhlbrandt, W. (2018). Structure, mechanism, and regulation of the chloroplast ATP synthase. *science,* 360(6389).

Ilik, P., Pavlovic, A., Kouril, R., Alboresi, A., Morosinotto, T., Allahverdiyeva, Y., . . . Shikanai, T. (2017). Alternative electron transport mediated by flavodiiron proteins is operational in organisms from cyanobacteria up to gymnosperms. *New Phytologist,* 214(3), 967-972.

Joliot, P. A., & Finazzi, G. (2010). Proton equilibration in the chloroplast modulates multiphasic kinetics of nonphotochemical quenching of fluorescence in plants. *Proceedings of the National Academy of Sciences,* 107(28), 12728-12733.

Kaiser, E., Morales, A., & Harbinson, J. (2018). Fluctuating Light Takes Crop Photosynthesis on a Rollercoaster Ride. *Plant Physiology,* 176(2), 977-989.

Kaiser, E., Morales, A., Harbinson, J., Heuvelink, E., Prinzenberg, A. E., & Marcelis, L. F. (2016). Metabolic and diffusional limitations of photosynthesis in fluctuating irradiance in Arabidopsis thaliana. *Scientific Reports,* 6, 31252.

Kato, Y., Odahara, M., Fukao, Y., & Shikanai, T. (2018). Stepwise evolution of supercomplex formation with photosystem I is required for stabilization of chloroplast NADH dehydrogenase-like complex: Lhca5-dependent supercomplex formation in Physcomitrella patens. *The Plant Journal,* 96(5), 937-948.

Kimura, H., Hashimoto-Sugimoto, M., Iba, K., Terashima, I., & Yamori, W. (2020). Improved stomatal opening enhances photosynthetic rate and biomass production in fluctuating light. *Journal of Experimental Botany,* 71(7), 2339-2350.

Klughammer, C., & Schreiber, U. (2008). Saturation Pulse method for assessment of energy conversion in PS I. *PAM Application Notes,* 1, 11-14.

Kono, M., Noguchi, K., & Terashima, I. (2014). Roles of the cyclic electron flow around PSI (CEF-PSI) and O(2)-dependent alternative pathways in regulation of the photosynthetic electron flow in short-term fluctuating light in Arabidopsis thaliana. *Plant Cell Physiology,* 55(5), 990-1004.

Kono, M., & Terashima, I. (2014). Long-term and short-term responses of the photosynthetic electron transport to fluctuating light. *Journal of Photochemistry and Photobiology B: Biology,* 137, 89-99.

Kramer, D. M., Johnson, G., Kiirats, O., & Edwards, G. E. (2004). New Fluorescence Parameters for the Determination of QA Redox State and Excitation Energy Fluxes. *Photosynthesis Research,* 79, 209-218.

Kukuczka, B., Magneschi, L., Petroutsos, D., Steinbeck, J., Bald, T., Powikrowska, M., . . . Hippler, M. (2014). Proton Gradient Regulation5-Like1-Mediated Cyclic Electron Flow Is Crucial for Acclimation to Anoxia and Complementary to Nonphotochemical Quenching in Stress Adaptation. *Plant Physiology,* 165(4), 1604-1617.

Long, S. P., Taylor, S. H., Burgess, S. J., Carmo-Silva, E., Lawson, T., De Souza, A. P., . . . Wang, Y. (2022). Into the Shadows and Back into Sunlight: Photosynthesis in Fluctuating Light. *Annual Review of Plant Biology,* 73, 617-648.

Melis, A. (1999). Photosystem-II damage and repair cycle in chloroplasts: what modulates the rate of photodamage in vivo? . *Trends in Plant Science,* 4(4), 130-135.

Munekage, Y., Hojo, M., Meurer, J., Endo, T., Tasaka, M., & Shikanai, T. (2002). PGR5 is involved in cyclic electron flow around photosystem I and is essential for photoprotection in Arabidopsis. *cell,* 110(3), 361-371.

N.W. Ashton, N.H. Grimsley, & Cove., D. J. (1979). Analysis of gametophytic development in the moss, Physcomitrella patens, using auxin and cytokinin resistant mutants. *Planta,* 144, 427-435.

Pearcy, R. W. (1990). Sunflecks and Photosynthesis in Plant Canopies. *Annual Review of Plant Biology,* 41, 421-453.

Peltier, G., Aro, E. M., & Shikanai, T. (2016). NDH-1 and NDH-2 Plastoquinone Reductases in Oxygenic Photosynthesis. *Annual Review of Plant Biology,* 67, 55-80.

Peltier, G., Tolleter, D., Billon, E., & Cournac, L. (2010). Auxiliary electron transport pathways in chloroplasts of microalgae. *Photosynthsis Research,* 106(1-2), 19-31.

Prigge, M. J., & Bezanilla, M. (2010). Evolutionary crossroads in developmental biology: Physcomitrella patens. *Development,* 137(21), 3535-3543.

Setif, P., Shimakawa, G., Krieger-Liszkay, A., & Miyake, C. (2020). Identification of the electron donor to flavodiiron proteins in Synechocystis sp. PCC 6803 by in vivo spectroscopy. *Biochimica et Biophysica Acta Bioenergetics,* 1861(10), 148256.

Shikanai, T. (2014). Central role of cyclic electron transport around photosystem I in the regulation of photosynthesis. *Current Opinion in Biotechnology,* 26, 25-30.

Shikanai, T. (2016). Regulatory network of proton motive force: contribution of cyclic electron transport around photosystem I. *Photosynthsis Research,* 129(3), 253-260.

Shikanai, T., & Yamamoto, H. (2017). Contribution of Cyclic and Pseudo-cyclic Electron Transport to the Formation of Proton Motive Force in Chloroplasts. *Molecular Plant,* 10(1), 20-29.

Shimakawa, G., Ishizaki, K., Tsukamoto, S., Tanaka, M., Sejima, T., & Miyake, C. (2017). The Liverwort, Marchantia, Drives Alternative Electron Flow Using a Flavodiiron Protein to Protect PSI. *Plant Physiol,* 173(3), 1636-1647.

Shubin, V. V., Terekhova, I. N., Kirillov, B. A., & Karapetyan, N. V. (2008). Quantum yield of P700+ photodestruction in isolated photosystem I complexes of the cyanobacterium Arthrospira platensis. *Photochemical and Photobiological Sciences,* 7(8), 956-962.

ShunichiT akahashi, S. a. E. M., D a-YongF an, Wah Soon Chow,a nd MurrayR . Badger. (2009). How Does Cyclic ElectronF low Alleviate Photoinhibition? *Plant Physiology,* 149, 1560-1567.

Slattery, R. A., Walker, B. J., Weber, A. P. M., & Ort, D. R. (2018). The Impacts of Fluctuating Light on Crop Performance. *Plant Physiology,* 176(2), 990-1003.

Sonoike, K. (2011). Photoinhibition of photosystem I. *Physiologia Plantarum, 142*(1), 56-64.

Storti, M., Alboresi, A., Gerotto, C., Aro, E. M., Finazzi, G., & Morosinotto, T. (2019). Role of cyclic and pseudo-cyclic electron transport in response to dynamic light changes in Physcomitrella patens. *Plant Cell and Environment,* 42(5), 1590-1602.

Storti, M., Puggioni, M. P., Segalla, A., Morosinotto, T., & Alboresi, A. (2020). The chloroplast NADH dehydrogenase-like complex influences the photosynthetic activity of the moss Physcomitrella patens. *J Exp Bot,* 71(18), 5538-5548.

Storti, M., Segalla, A., Mellon, M., Alboresi, A., & Morosinotto, T. (2020). Regulation of electron transport is essential for photosystem I stability and plant growth. *New Phytologist,* 228(4), 1316-1326.

Strotbek, C., Krinninger, S., & Frank, W. (2013). The moss Physcomitrella patens: methods and tools from cultivation to targeted analysis of gene function. *Int J Dev Biol,* 57(6-8), 553-564.

Suorsa, M., Jarvi, S., Grieco, M., Nurmi, M., Pietrzykowska, M., Rantala, M. & Aro, E. M. (2012). PROTON GRADIENT REGULATION5 is essential for proper acclimation of Arabidopsis photosystem I to naturally and artificially fluctuating light conditions. *Plant Cell,* 24(7), 2934-2948.

Tanaka, Y., Adachi, S., & Yamori, W. (2019). Natural genetic variation of the photosynthetic induction response to fluctuating light environment. *Current Opinion in Plant Biology,* 49, 52-59.

Tiwari, A., Mamedov, F., Grieco, M., Suorsa, M., Jajoo, A., Styring, S., & Aro, E. M. (2016). Photodamage of iron-sulphur clusters in photosystem I induces non-photochemical energy dissipation. *Nature Plants,* 2, 16035.

Wang, Y., Burgess, S. J., de Becker, E. M., & Long, S. P. (2020). Photosynthesis in the fleeting shadows: an overlooked opportunity for increasing crop productivity? *The Plant Journal,* 101(4), 874-884.

Watanabe, C. K., Yamori, W., Takahashi, S., Terashima, I., & Noguchi, K. (2016). Mitochondrial Alternative Pathway-Associated Photoprotection of Photosystem II is Related to the Photorespiratory Pathway. *Plant Cell Physiology,* 57(7), 1426-1431.

Yamamoto, H., & Shikanai, T. (2019). PGR5-Dependent Cyclic Electron Flow Protects Photosystem I under Fluctuating Light at Donor and Acceptor Sides. *Plant Physiology,* 179(2), 588-600.

Yamamoto, H., Takahashi, S., Badger, M. R., & Shikanai, T. (2016). Artificial remodelling of alternative electron flow by flavodiiron proteins in Arabidopsis. *Nature Plants,* 2, 16012.

Yamori, W., Kusumi, K., Iba, K., & Terashima, I. (2020). Increased stomatal conductance induces rapid changes to photosynthetic rate in response to naturally fluctuating light conditions in rice. *Plant Cell Environment,* 43(5), 1230-1240.

Yamori, W., Makino, A., & Shikanai, T. (2016). A physiological role of cyclic electron transport around photosystem I in sustaining photosynthesis under fluctuating light in rice. *Sci Rep,* 6, 20147.

Yang, Y.-J., Tan, S.-L., Huang, J.-L., Zhang, S.-B., & Huang, W. (2020). The water-water cycle facilitates photosynthetic regulation under fluctuating light in the epiphytic orchid Dendrobium officinale. *Environmental and Experimental Botany,* 180.

Zhang, P., Allahverdiyeva, Y., Eisenhut, M., & Aro, E. M. (2009). Flavodiiron proteins in oxygenic photosynthetic organisms: photoprotection of photosystem II by Flv2 and Flv4 in Synechocystis sp. PCC 6803. *PLoS One,* 4(4), e5331.

6. Supplementary material

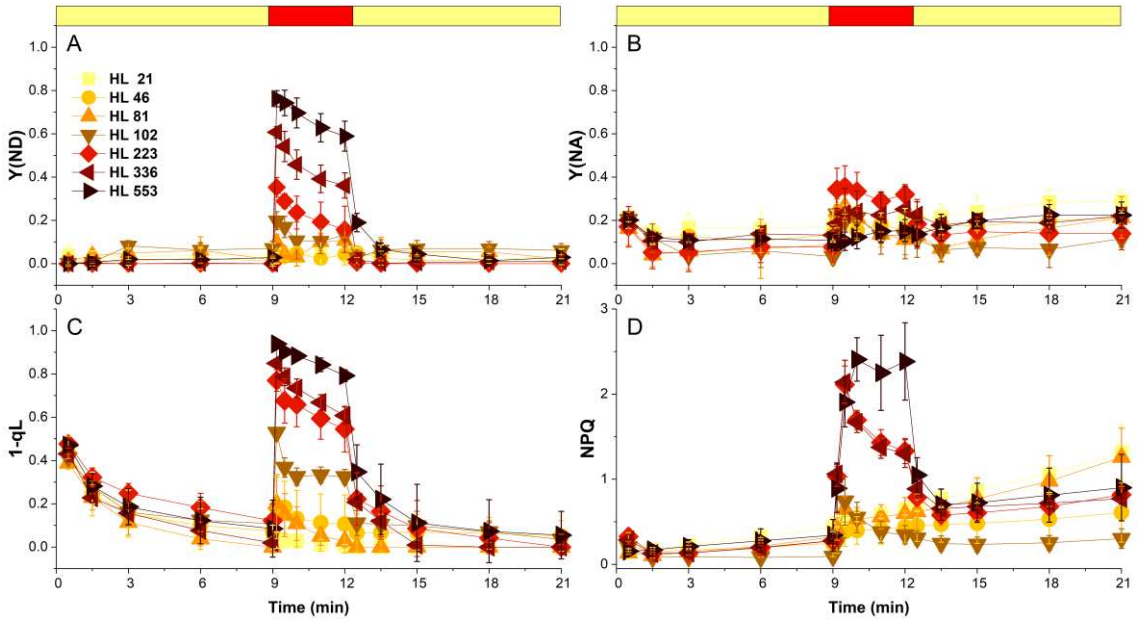

Supplementary Figure 1 | **Effect of light fluctuations of different intensities on WT plants.** Dark-acclimated 10-day-old fresh protonemal issues of WT were exposed to low light (21 µmol photons m^{-2} s^{-1}, 9 min) and high light (21, 46, 81, 102, 223, 336, 553 µmol photons m^{-2} s^{-1}, 3 min). Y(NA), quantum yield of PSI non-photochemical energy dissipation due to acceptor side limitation; Y(ND), quantum yield of PSI non-photochemical energy dissipation due to donor side limitation; NPQ, non-photochemical quenching in PSII; 1-qL, Q_A relative reduction; Values are means ± SD (n = 4).

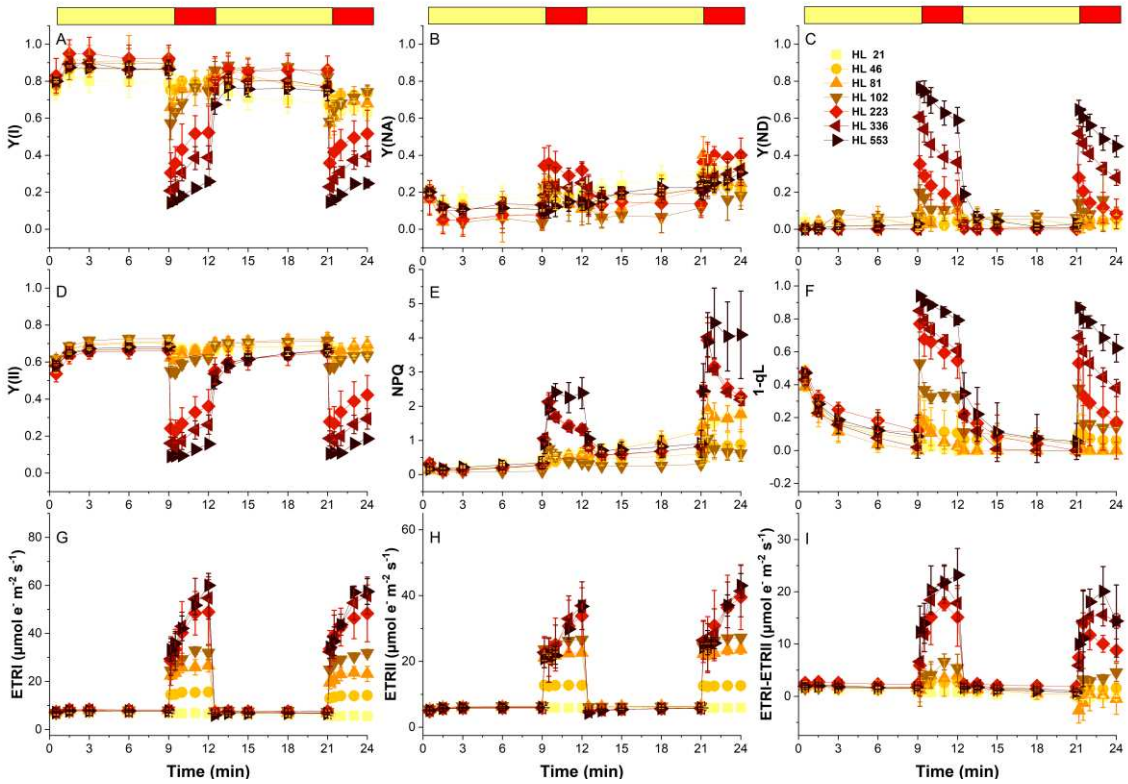

Supplementary Figure 2 | Effect of two light fluctuation cycles of different intensities on WT plants. Dark-acclimated 10-day-old fresh protonemal issues of WT were exposed to two cycles of low light (21 μmol photons m^{-2} s^{-1}, 9 min) and high light (21, 46, 81, 102, 223, 336, 553 μmol photons m^{-2} s^{-1}, 3 min). Y(I), quantum yield of PSI photochemistry; Y(II), the effective quantum yield of PSII photochemistry; Y(NA), quantum yield of PSI non-photochemical energy dissipation due to acceptor side limitation; Y(ND), quantum yield of PSI non-photochemical energy dissipation due to donor side limitation; NPQ, non-photochemical quenching in PSII;1-qL,Q_A relative reduction; ETRI or ETRII, the electron transport rate of ETRI or ETRII;ETRI and ETRII were calculated using Y(I) and Y(II), respectively. ETRI-ETRII represents cyclic electron flow estimated by subtracting ETRII from PSI. Values are means ± SD (n = 4).

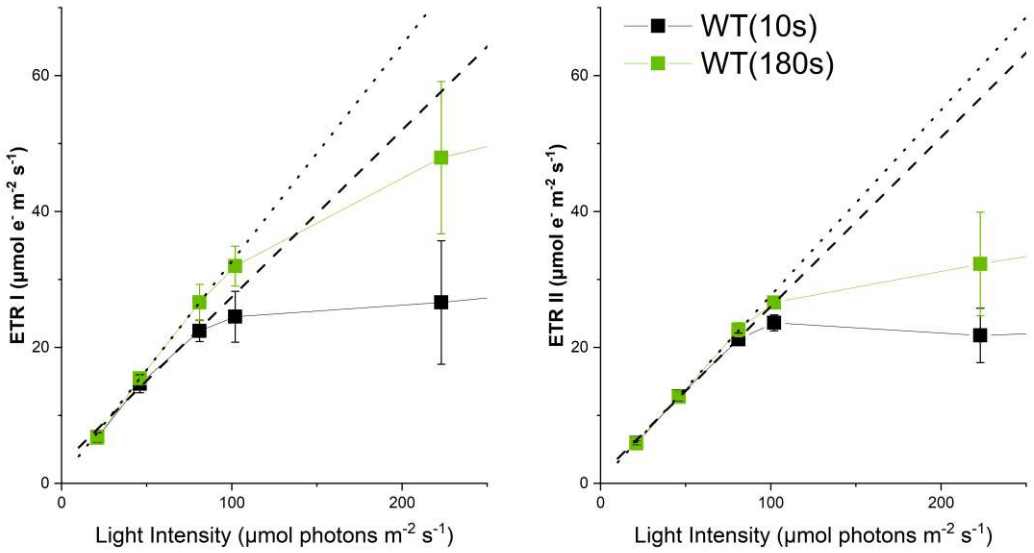

Supplementary Figure 3 | The light response of ETRI and ETRII in WT after transition from high light 10s and 180s with linear trend lines. ETRI or ETRII, the electron transport rate of ETRI or ETRII;ETRI and ETRII were calculated using Y(I) and Y(II), respectively. Values are means ± SD (n = 4).

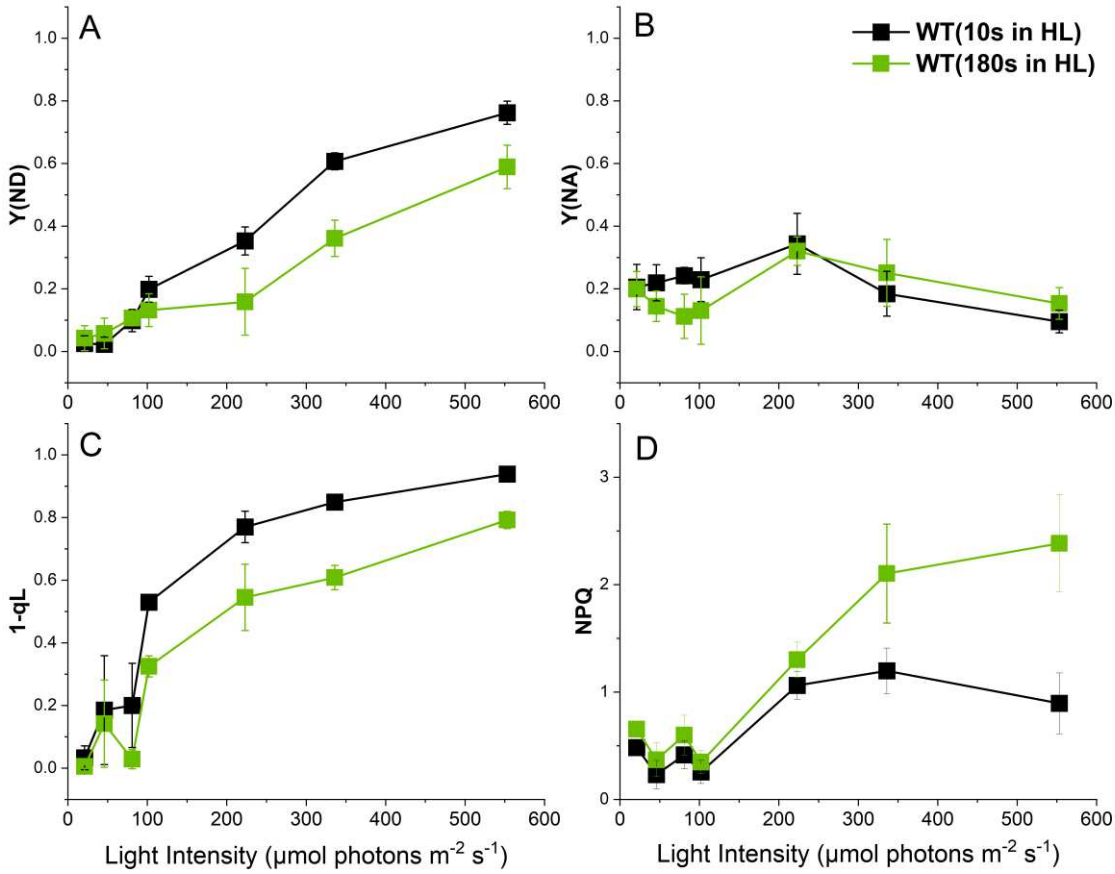

Supplementary Figure 4 | Light intensity dependence of photosynthetic parameters in WT. A, B: The light intensity dependence of Y(NA) and Y(ND); C, D: The light intensity dependence of NPQ and 1-qL; The black square represents the data of first 10 s in high-light period, the green square represents the data of 3 min in high-light period. Values are means ± SD (n=4).

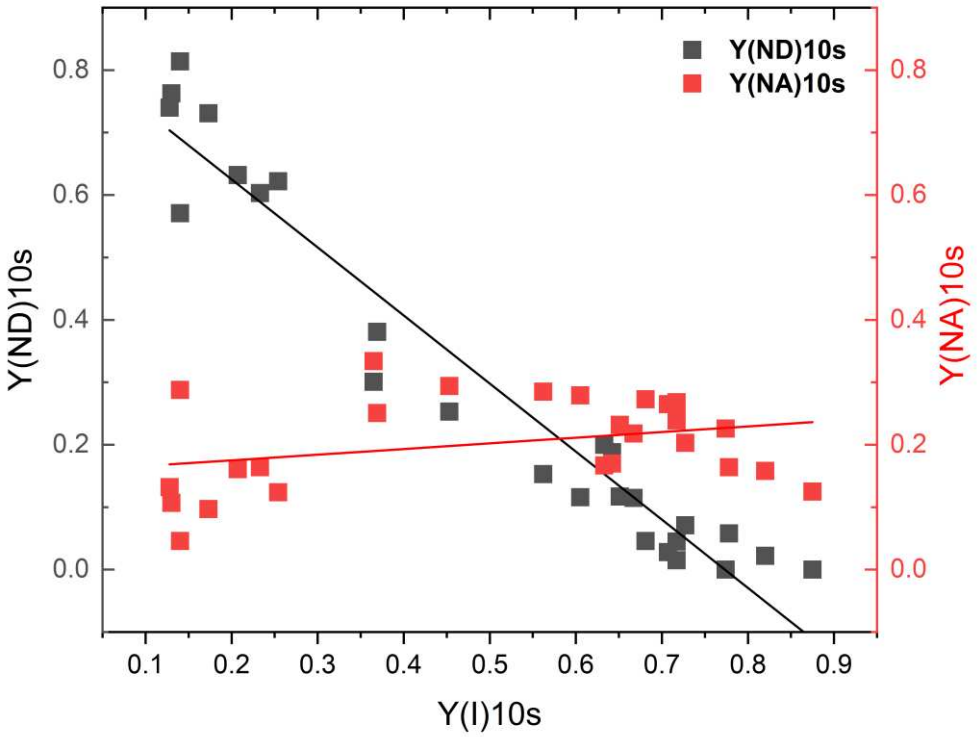

Supplementary Figure 5 | The high value of Y(ND) is responsible for the decrease of Y(I) under high light. The black line represents the relationship between the value of Y(I) and Y(ND) after transition to high light for 10 s. The regression line is shown: y = 0.84306-1.09025*x,R^2=0.94025; The red line represents the relationship between the value of Y(I) and Y(NA) after transition to high light for 10 s. The regression line is shown: y = 0.15695+0.09045*x, R^2=0.09793.

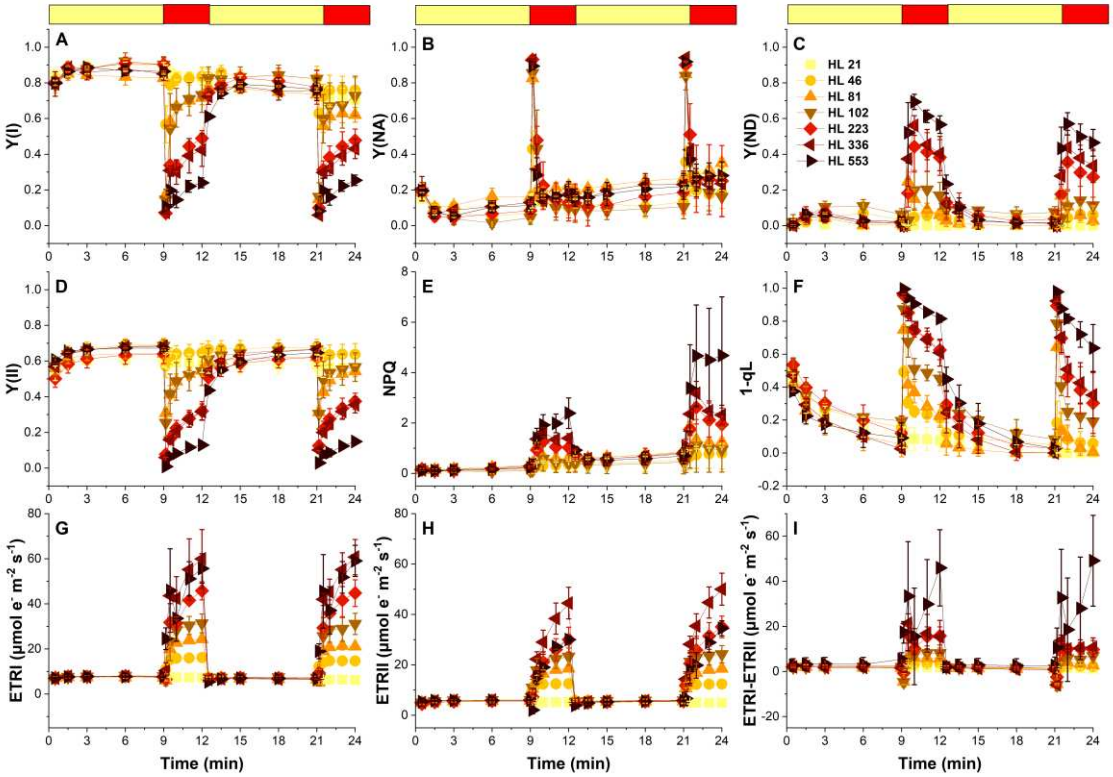

Supplementary Figure 6 | **Impact of two light fluctuations cycles on *flva* KO mutants** Dark-acclimated 10-day-old fresh protonemal issues of *flva* KO mutants were exposed to two cycles of low light (21 µmol photons m^{-2} s^{-1}, 9 min) and high light (21,46,81,102,223,336,553 µmol photons m^{-2} s^{-1}, 3 min). Y(I), quantum yield of PSI photochemistry; Y(II), the effective quantum yield of PSII photochemistry; Y(NA), quantum yield of PSI non-photochemical energy dissipation due to acceptor side limitation; Y(ND), quantum yield of PSI non-photochemical energy dissipation due to donor side limitation; NPQ, non-photochemical quenching in PSII; 1-qL, Q_A relative reduction; ETRI or ETRII, the electron transport rate of ETRI or ETRII;ETRI and ETRII were calculated using Y(I) and Y(II), respectively. Values are means ± SD (n = 4).

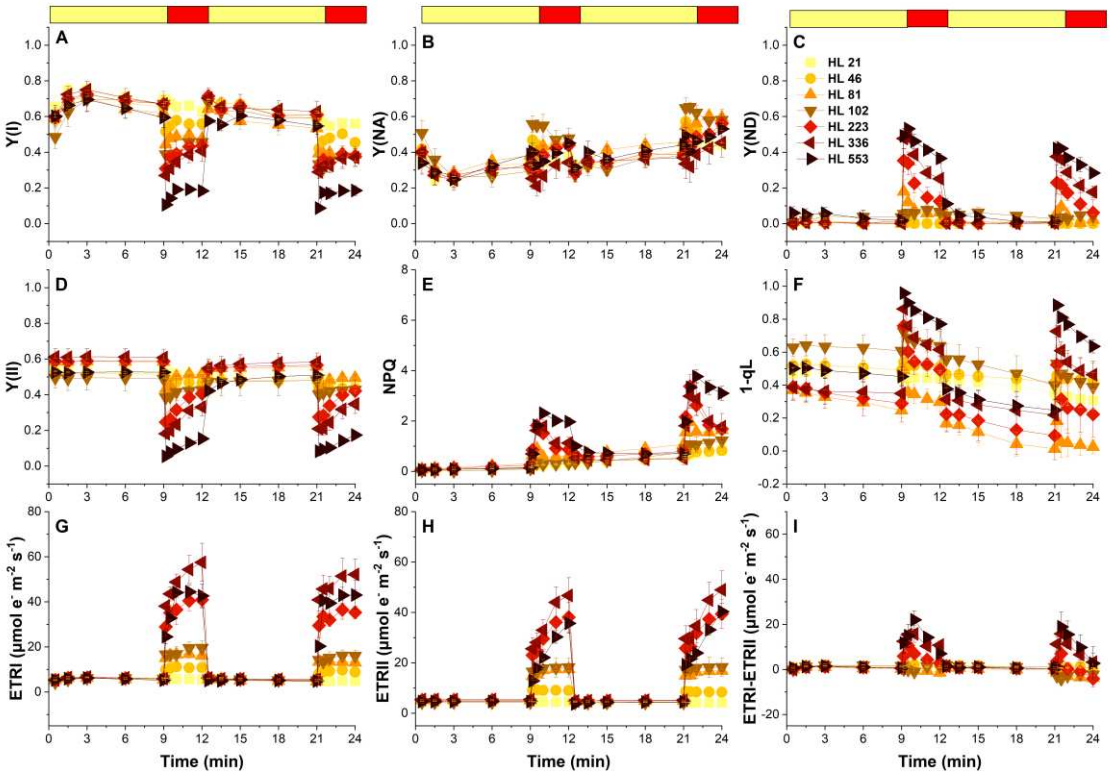

Supplementary Figure 7 | **Impact of light fluctuations on *pgrl1/ndhm* double KO mutants** Dark-acclimated 10-day-old fresh protonemal issues of *pgrl1/ndhm* KO mutants were exposed to two cycles of low light (21 µmol photons m^{-2} s^{-1}, 9 min) and high light (21, 46, 81, 102, 223, 336, 553 µmol photons m^{-2} s^{-1}, 3 min). Y(I), quantum yield of PSI photochemistry; Y(II), the effective quantum yield of PSII photochemistry; Y(NA), quantum yield of PSI non-photochemical energy dissipation due to acceptor side limitation; Y(ND), quantum yield of PSI non-photochemical energy dissipation due to donor side limitation; NPQ, non-photochemical quenching in PSII; 1-qL, Q_A relative reduction; ETRI or ETRII, the electron transport rate of ETRI or ETRII;ETRI and ETRII were calculated using Y(I) and Y(II), respectively. Values are means ± SD (n = 4).

APPENDIX II

Inactivation of mitochondrial Complex I stimulates chloroplast ATPase in *Physcomitrium patens*

Marco Mellon[1], Mattia Storti[1], Antoni M Vera-Vives[1], David M. Kramer[2], Alessandro Alboresi[1] and Tomas Morosinotto[1]

1. Department of Biology, University of Padova, Italy

2. MSU-DOE Plant Research Laboratory, Michigan State University, East Lansing, MI 48824,United States of America; Biochemistry and Molecular Biology, Michigan State University,East Lansing, MI 48824, United States of America.

This appendix was published in “Plant Physiology” (2021)

Authorship statement:

My main contribution to this work was to perform and analyze the experiments regarding separation of protein complexes through BN-PAGE and in-gel activity staining, and comment the draft during the revision process.

doi:10.1093/plphys/kiab276 PLANT PHYSIOLOGY 2021: 187: 931–946

Plant Physiology®

Research Article

Inactivation of mitochondrial complex I stimulates chloroplast ATPase in *Physcomitrium patens*

Marco Mellon [1], Mattia Storti [1], Antoni M. Vera-Vives [1], David M. Kramer,[2,3] Alessandro Alboresi [1] and Tomas Morosinotto [1,*,†]

1 Department of Biology, University of Padova, 35121 Padova, Italy
2 MSU-DOE Plant Research Laboratory, Michigan State University, East Lansing, Michigan 48824, USA
3 Department of Biochemistry and Molecular Biology, Michigan State University, East Lansing, Michigan 48824, USA

*Author for communication: tomas.morosinotto@unipd.it
†Senior author.

T.M. and A.A. designed the research; M.M., M.S., and A.M.V.V. performed research; M.M., M.S., D.M.K., A.A., and T.M. analyzed data; T.M. and M.M. wrote the article. All authors critically revised the manuscript.
The author responsible for distribution of materials integral to the findings presented in this article in accordance with the policy described in the Instructions for Authors (https://academic.oup.com/plphys/pages/general-instructions) is: Tomas Morosinotto (tomas.morosinotto@unipd.it).

Abstract

Light is the ultimate source of energy for photosynthetic organisms, but respiration is fundamental for supporting metabolism during the night or in heterotrophic tissues. In this work, we isolated Physcomitrella (*Physcomitrium patens*) plants with altered respiration by inactivating Complex I (CI) of the mitochondrial electron transport chain by independently targeting on two essential subunits. Inactivation of CI caused a strong growth impairment even in fully autotrophic conditions in tissues where all cells are photosynthetically active, demonstrating that respiration is essential for photosynthesis. CI mutants showed alterations in the stoichiometry of respiratory complexes while the composition of photosynthetic apparatus was substantially unaffected. CI mutants showed altered photosynthesis with high activity of both Photosystems I and II, likely the result of high chloroplast ATPase activity that led to smaller ΔpH formation across thylakoid membranes, decreasing photosynthetic control on cytochrome *b6f* in CI mutants. These results demonstrate that alteration of respiratory activity directly impacts photosynthesis in *P. patens* and that metabolic interaction between organelles is essential in their ability to use light energy for growth.

Introduction

In photosynthetic organisms, sunlight powers the linear electron flow from water to $NADP^+$ catalyzed by two photosystems (PS), PSII and PSI, cytochrome b_6f and ATPase, ultimately generating NADPH and ATP to sustain cellular metabolism. In photosynthetic organisms, mitochondrial respiration is also active with its specific electron transport pathway, or oxidative phosphorylation (OXPHOS). OXPHOS transfers electrons from the substrates NADH and succinate to molecular oxygen (O_2) through the activity of enzymatic complexes localized in the inner mitochondrial membrane, Complex I (CI), CII, CIII, and CIV. This electron transfer is coupled to the generation of electrochemical transmembrane gradient that drives the synthesis of ATP through ATP-synthase, also called complex V. The NADH dehydrogenase complex (CI) is the main site for electron insertion into the mitochondrial electron transport chain (ETC) and it can provide up to 40% of the protons for mitochondrial ATP formation (Watt et al., 2010; Braun et al., 2014). In plants, ETC electrons can also follow alternative routes bypassing CI

Received December 7, 2020. Accepted May 18, 2021. Advance access publication June 15, 2021

via alternative NADH dehydrogenases (Lecler et al., 2012) and CIII/IV via the alternative terminal oxidase (AOX; Dinant et al., 2001). These alternative routes partly uncouple the electron transport and the electrochemical transmembrane gradient, thus reducing the energy yield of respiration with beneficial effects especially in stress conditions (Zalutskaya et al., 2015), reducing reactive oxygen species (ROS) production from mETC (Møller, 2001; Vanlerberghe et al., 2020).

Respiration in photosynthetic organisms is essential to support energy demand during the night in nonphotosynthetic tissues such as roots or in developmental stages where photosynthesis is not active (e.g. seed germination). An increasing set of evidence, however, underlines the importance of respiration also for sustaining optimal photosynthetic activity (Joliot and Joliot, 2008; Noguchi and Yoshida, 2008; Bailleul et al., 2015) with a strong functional link between chloroplasts and mitochondria bioenergetic metabolism (Cardol et al., 2003; Dutilleul et al., 2003; Schönfeld et al., 2004). In the diatom, *Phaeodactylum tricornutum* metabolite exchange between chloroplast and mitochondria is essential for carbon fixation (Bailleul et al., 2015). In another example of such a functional link, excess reducing power produced via photosynthesis can be routed to mitochondrial respiration, preventing over-reduction and eventual ROS production in the plastid (Noguchi and Yoshida, 2008; Zhang et al., 2012). AOX activity has also been shown to influence photosynthetic metabolism response to stresses when it consumes excess reductant while decreasing mitochondrial ATP synthesis (Cheung et al., 2015) and maintaining redox balance of plastoquinone pool (Yoshida and Noguchi, 2011; Vanlerberghe et al., 2020). Consistently, AOX protein level was shown to be linked to differences in chloroplast energetic balance, being induced under strong irradiance, suggesting the presence of regulation signals originated from photosynthetic electron transport (Dahal et al., 2016).

Imbalances between the relative rates of production and consumption of ATP/NADPH utilization can lead to the build-up of reactive intermediates of electron transfer processes, driving the formation of harmful ROS (Eberhard et al., 2008; Li et al., 2009). Photosynthetic organisms evolved multiple regulatory mechanisms to balance light-dependent processes and metabolic exploitation of photosynthesis products. Examples of such mechanisms are the dissipation of excess excitation energy as heat (nonphotochemical quenching [NPQ]) or the photosynthetic control to reduce electron transport capacity at the level of cytochrome b_6f and prevent over-reduction. Both mechanisms are activated by a decrease of lumenal pH that represents a major signal for regulation of photosynthesis (Eberhard et al., 2008; Li et al., 2009).

Consistent with the essential role of mitochondrial respiration in plant metabolism, knockout (KO) mutants completely depleted in CII (Leon et al., 2007), CIII (Colas Des Francs-Small and Small, 2014), and CIV (Radin et al., 2015) are not viable and so far only knockdown (KD) plants have been isolated and studied. Mutants completely lacking mitochondrial CI activity have instead been described in Arabidopsis (*Arabidopsis thaliana*; Kühn et al., 2015; Fromm et al., 2016a), as well as in tobacco (*Nicotiana tabacum*; Vidal et al., 2007) where they showed a severe growth phenotype and alterations in germination, fertilization, and pollen development (Fromm et al., 2016a). European mistletoe *Viscum album* can live without CI, but it is an obligate semiparasite living on branches of trees, and thus its energy metabolism is likely remodeled (Maclean et al., 2018; Senkler et al., 2018).

Differently from plants, a large number of respiratory mutants have instead been isolated in the green alga *Chlamydomonas reinhardtii* where they generally show strong phenotypes under heterotrophic conditions but grow similarly to wild-type (WT) under photoautotrophic conditions (Salinas et al., 2014; Larosa et al., 2018).

These differences suggest that the role of respiration on cell metabolism adapted during plant evolution, motivating the investigation of species that diverged at different times during evolution. Nonvascular plants like the moss *Physcomitrium patens* diverged from vascular plant ancestors early after land colonization and thus their study allows highlighting the first adaptation to the new environmental conditions. To assess how the biological role of respiration adapted during the evolution of photosynthetic organisms in this work, we generated *P. patens* plants depleted of active respiratory CI and investigated effects on photosynthetic activity. Results show that the absence of CI stimulates photosynthetic transport caused by more active chloroplast ATPase with alteration of pmf and ΔpH across the thylakoid membranes and impairment of photosynthetic control.

Results

CI in eukaryotes is composed of over 40 subunits and, among them, 14 are highly conserved across kingdoms (Ligas et al., 2019). Plant CI includes nine additional subunits that form a carbonic anhydrase domain (Braun et al., 2014; Fromm et al., 2016a; Subrahmanian et al., 2016). For all CI subunits identified in Arabidopsis, it is possible to identify a putative homolog in *P. patens* genome, suggesting a general conservation of CI subunits between the two organisms (Supplemental Table S1), consistent with similarities observed between plants and green algae (Klusch et al., 2020). Based on this analysis, *NDUFA5* and *NDUFB10* (NADH: Ubiquinone Oxidoreductase Subunit A5 and B10) genes were selected to generate *P. patens* mutants depleted in CI based on two criteria: (1) they encoded for conserved proteins known to be essential for CI activity in *C. reinhardtii*, *A. thaliana*, or *Homo sapiens* (Barbieri et al., 2011; Rak and Rustin, 2014); (2) they were present in a single copy in *P. patens* nuclear genome, facilitating the generation of mutants and ensuring that any eventual phenotype would be readily assessable. NDUFA5 is localized in the hydrophilic region of the complex binding the substrate NADH (Figure

1A), and it is required for assembly and stability of the matrix arm of CI in human mitochondria (Rak and Rustin, 2014). NDUFB10 deletion in *C. reinhardtii* impairs the assembly of the distal part of CI membrane module (Figure 1A), responsible for the proton pumping activity coupled with the electron transfer (Barbieri et al., 2011).

KO lines for both genes were generated by homologous recombination-mediated gene targeting (Supplemental Figure S1, A and B). Multiple independent KO lines for each gene were isolated, and the insertion of DNA in the expected position of the genome was verified by PCR (Supplemental Figure S1C). The loss of expression of the target gene was also confirmed by reverse transcriptase PCR (RT-PCR; two lines shown in Figure 1B). In the following sections, results from one line per gene are reported, but at least four independent confirmed lines per gene were isolated per each genotype.

All confirmed KO plants showed strongly impaired growth (Figure 2) that was visible upon cultivation on a glucose-enriched medium but also on a mineral media in fully autotrophic conditions. Remarkably, the growth defect was also observed if plants were grown autotrophically under 24 h of continuous illumination, thus avoiding any dark time when respiration is expected to be essential (Figure 2). Glucose presence in the media and continuous illumination stimulated a faster growth in WT plants while the mutants remained unaffected (Supplemental Figure S2).

Impact of mutations on respiratory apparatus composition was assessed using specific antibodies (Figure 3A). NAD9, a CI core subunit localized in the Q module of the matrix arm, was missing in *ndufa5* mutant, consistently with recently reported evidence that NDUFA5 directly interacts with NAD9 during CI biogenesis (Ligas et al., 2019). NAD9 was instead present in *ndufb10* mosses, suggesting that at least part of CI was still present, as observed for other analogous mutants (Ligas et al., 2019). Both *ndufa5* and *ndufb10* KO plants showed changes in other complexes of the respiratory apparatus and in particular CII and CIII subunits were more abundant in the mutants as compared with WT plants by, respectively, ~3 and 1.5 times. The most striking difference, however, was that AOX accumulated to ~10 times higher levels in *ndufa5* and *ndufb10* than in WT. All differences in protein accumulation were consistent between the two independent mutant lines.

The impact of mutations on CI was also assessed by blue native-polyacrylamide gel electrophoresis (BN-PAGE) on crude membrane extracts, containing both mitochondria and chloroplasts (Supplemental Figure S3). The detection of CI enzymatic activity after electrophoresis showed that in both mutant lines the correct assembly of CI was compromised (Figure 3B). No CI activity was detectable in the case of *ndufa5*. In the *ndufb10* mutant, instead, the complete holoenzyme was absent but a partially assembled CI retaining the NADH dehydrogenase activity was detectable (CI*, Figure 3B) consistent with earlier results in other species (Barbieri et al., 2011).

The impact of mutations on respiratory activity was assessed measuring O_2 consumption rate. In both *ndufa5* and *ndufb10* plants, O_2 consumption in the dark was higher than that in WT (Figure 4). While this seems counterintuitive for mutants affected in a respiratory complex, this observation can be explained by the compensatory over-accumulation of CII, CIII, and AOX. A similar increase in O_2 consumption was indeed also observed in Arabidopsis CI mutants (Kühn et al., 2015). This hypothesis is confirmed by the observation that O_2 consumption activity in *ndufa5* and *ndufb10* was insensitive to the addition of rotenone, a specific CI inhibitor that in WT plants instead reduced O_2 consumption by ~ 40% (Figure 4A).

O_2 consumption activity was similarly reduced by the addition of KCN, a CIV inhibitor, in both WT and mutants (Figure 4B). The significant residual activity still present was mostly attributable to the presence of alternative oxidases like AOX, as confirmed by the further decrease in O_2 evolution induced when its specific inhibitor SHAM was added together with KCN (Figure 4C). While 2 mM SHAM was a saturating dose for WT, a four-fold higher dose was necessary to obtain a full inhibition in the mutants, consistent

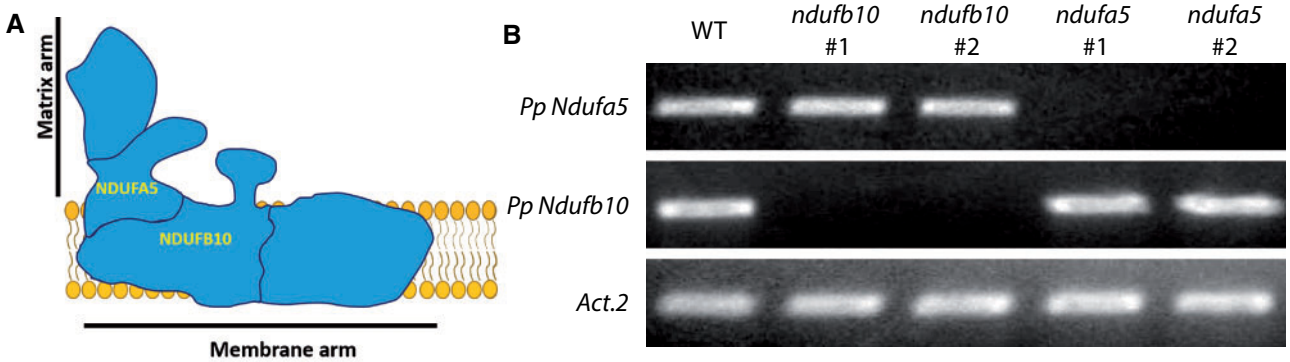

Figure 1 Generation of *P. patens* plants depleted in CI. A, Schematic representation of CI structure with NDUFA5 and NDUFB10 localization. B, RT-PCR to assess the accumulation of the mRNA encoding for *NDUFA5* and *NDUFB10* in two independent KO lines.

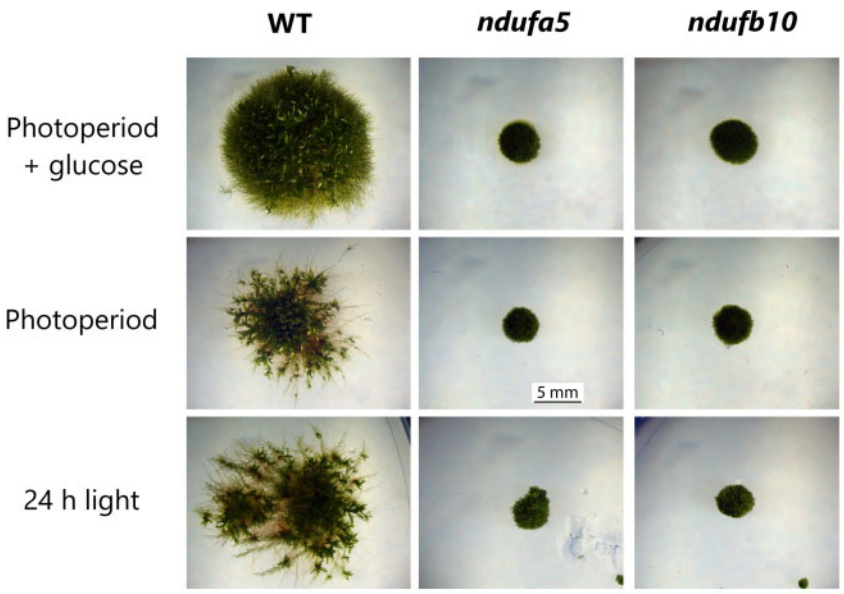

Figure 2 Impact of CI inactivation on *P. patens* growth. WT, *ndufa5*, and *ndufb10* KO lines growth after 28 d under 16 d/8-h light/dark photoperiod either with (top) or without (middle) the addition of 0.5% (w/v) glucose in the media or under 24-h continuous illumination without glucose (bottom).

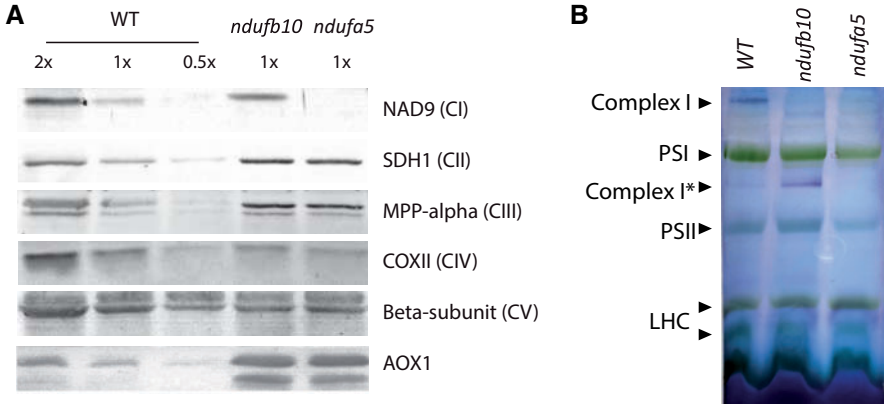

Figure 3 Impact of CI mutation on the respiratory apparatus composition and CI assembly. A, Immunoblot analysis using antibodies against various subunits of respiratory complexes. Total protein extracts were loaded, and 1× samples correspond to 2 µg of total Chl. B, BN-PAGE separation of crude organelles extracts. Following separation (see Supplemental Figure S3), CI activity was detected with in-gel NADH/NBT staining. Membrane proteins from WT, *ndufb10*, and *ndufa5* were solubilized with 1% (w/v) of β-DM. Main complexes of thylakoid and mitochondrial CI are indicated on the profiles. CI is expected to be ∼1,000 kDa as in Arabidopsis (Klodmann et al., 2010; Oldenkott et al., 2020). SDH, succinate dehydrogenase; MPP, mitochondrial-processing peptidase; COX, cytochrome c oxidase; CI* indicates an assembly intermediate of CI of ∼850 kDa lacking the distal part of the membrane arm (Schimmeyer et al., 2016); LHC, light-harvesting Chl complexes.

with their increased AOX content. Calculations as in (Vanlerberghe et al., 2002) show that the mutations did not affect the capacity of the cytochrome pathway, but increased that of the AOX pathway (Supplemental Table S2), supporting its role in the stronger rates of O_2 uptake.

Maximal photosynthetic O_2 evolution activity was measured in the same samples upon exposure to saturating light. *ndufa5* and *ndufb10* KO mutants showed a reduction in net photosynthesis of ∼50% compared with the WT (Figure 4D). A large portion of this difference can be explained by the higher O_2 consumption rate in *ndufa5* and *ndufb10* plants, where the difference from WT could be even larger in illuminated plants (Gauthier et al., 2018).

Impact of CI depletion on photosynthesis

Plants depleted of CI showed reduced photoautotrophic growth and alterations in O_2 evolution activity, motivating a deeper investigation of the impact of the mutation on photosynthetic activity. Chlorophyll (Chl) content, Chl a/b, and Chl/carotenoid (Car) ratio were unchanged in mutant and WT plants (Table 1). Consistently, the accumulation of

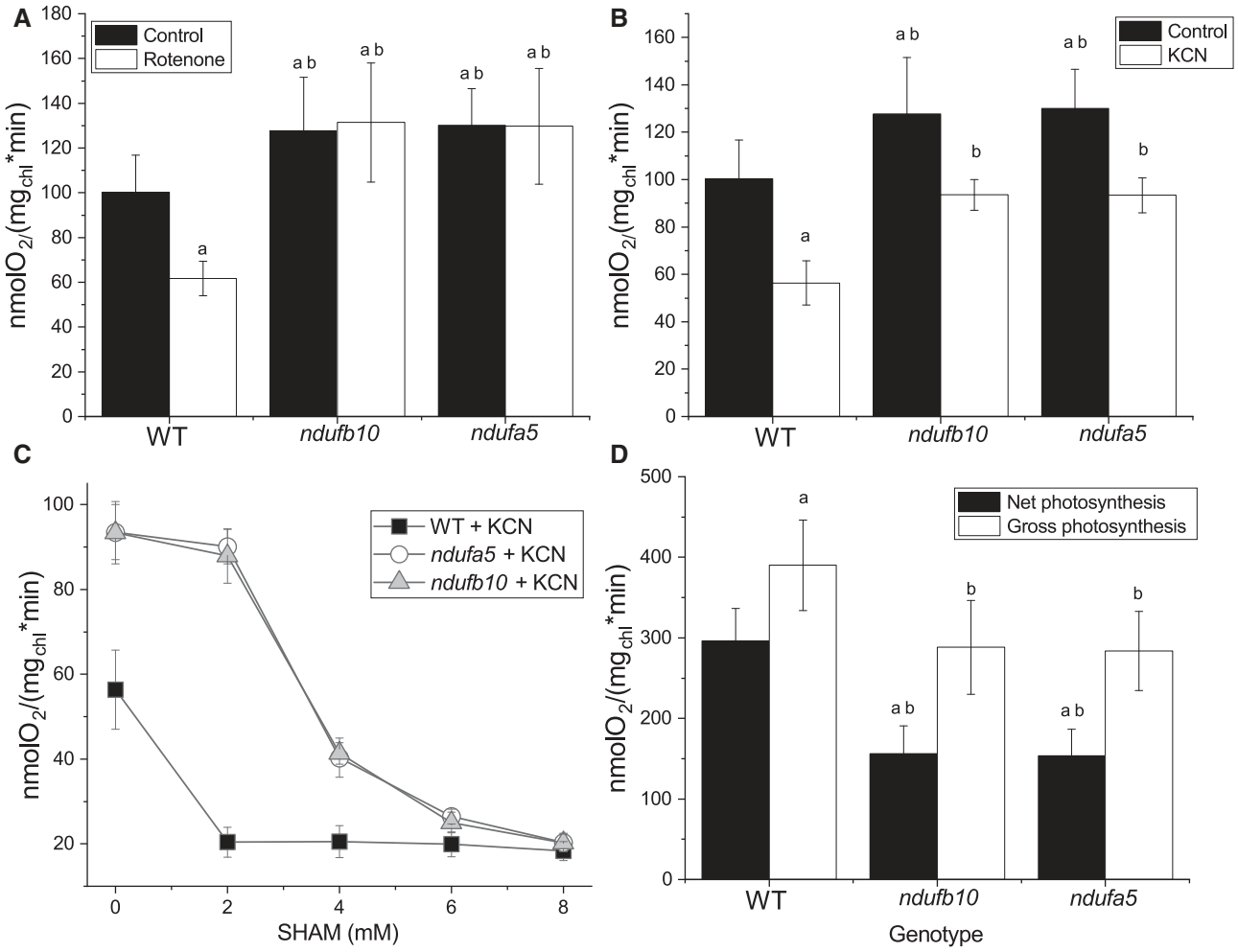

Figure 4 O_2 consumption and evolution capacity in *ndufb10* and *ndufa5*. A, O_2 consumption was monitored with a Clark-type O_2 electrode on WT and *ndufb10* and *ndufa5* plants grown for 10 d in minimal medium. Mosses were maintained in the dark in the absence (black) or presence of 50-µM rotenone (white columns). B, Effect of cyanide (KCN) on O_2 consumption. Controls without the inhibitor are in black, samples with addition 1 mM KCN in white. In both A and B, "a" indicates a statistically significant difference compared to untreated WT, "b" indicates significant difference compared to WT treated with the same inhibitor (one-way ANOVA, $n > 5$, $P < 0.01$). C, Effect of different concentration of SHAM on O_2 consumption in the presence of 1 mM KCN. WT is showed as black square, *ndufb10* as gray triangles, *ndufa5* as white circles. Average ± SD ($n \geqslant 5$) are reported. D, O_2 production of protonema illuminated with a light at 850 µmol photons m^{-2} s^{-1} measured with a Clark-type O_2 electrode. Net photosynthesis (black) is calculated directly from the O_2 evolution rate during illumination. Gross photosynthesis (white) is calculated by adding net photosynthesis with O_2 consumption in the dark. Statistically significant differences are indicated by "a" for comparison with WT net O_2 evolution, and "b" for comparisons with WT gross O_2 evolution (one-way ANOVA, $n > 5$, $P < 0.01$). In all panels, average ± SD are reported.

Table 1 Pigment composition and PSII quantum efficiency of *P. patens* WT and *ndufb10* and *ndufa5* mutant lines

Genotype	Chl a/Chl b	Chl/Car	Chl content (µg mg^{-1} DW)	F_v/F_m
WT	2.62 ± 0.14	3.73 ± 0.37	18.5 ± 2.7	0.79 ± 0.01
ndufb10	2.59 ± 0.20	3.65 ± 0.40	18.9 ± 3.0	0.78 ± 0.02
ndufa5	2.64 ± 0.21	3.60 ± 0.42	18.7 ± 2.7	0.79 ± 0.01

Chl a/b ratio, Chl/car ratio, total Chl content and PSII quantum yield (estimated by F_v/F_m) were evaluated in plants cultivated for 10 d in a minimal medium at 50 µmol photons m^{-2} s^{-1}. For each measurement, average ± SD ($n \geqslant 5$) is reported.

all main components of the photosynthetic apparatus (PSI, PSII, cyt *b6f*, ATPase) showed no major alterations in the mutants except for a slight increase in chloroplast ATPase content (Supplemental Figure S4). Subunits involved in regulatory mechanisms of photosynthesis such as PsbS and LHCSR (Alboresi et al., 2010) were also similarly accumulated in the mutants as in WT plants (Supplemental Figure S4).

Photosynthetic functionality was analyzed in more detail by fluorescence and Near InfraRed (NIR) spectroscopy analyses. PSII maximum quantum yield (F_v/F_m) in dark-adapted plants was not altered by the mutations (Table 1). However, when plants were exposed to sub-saturating light conditions (330 µmol photons m^{-2} s^{-1}) both *ndufa5* and *ndufb10* showed a higher yield for both PSI (Figure 5A) and PSII (Figure 5B), indicative of a higher electron transport rate (ETR). At the level of PSI, the higher yield was attributable to a lower donor side limitation (Y(ND)) while acceptor side limitation (Y(NA)) was negligible in WT and mutant plants (Figure 5, C and D). The lower PSI donor side limitation is consistent with higher rates of electron transport to PSI and with a less reduced quinone A (Q_A) in the mutants than in the WT, as estimated by 1-q_L (Figure 5E). After actinic light was switched off, the estimated maximal quantum yield of PSI recovered to the same level in WT and mutants, whereas the recovery of PSII maximal yield and oxidation of Q_A was faster in the mutants. NPQ in *ndufa5* and *ndufb10* was activated as in WT plants but after a few minutes of illumination, it showed a partial relaxation in mutants (Figure 5F).

The same analyses showed similar results upon exposure to dim light (50 µmol photons m^{-2} s^{-1}), corresponding to the illumination in the growth chamber (Supplemental Figure S5). If plants were exposed to 2,000 µmol photons m^{-2} s^{-1}, a light intensity completely saturating photosynthetic capacity of the plants, WT, and mutants showed instead no significant differences (Supplemental Figure S6).

The impact of CI mutations on photosynthetic electron transport was further investigated by measuring electrochromic shift (ECS) caused by the generation of transmembrane potential at the level of the thylakoid membranes (Witt, 1979; Bailleul et al., 2010). The total ECS signal (ECS_t), a proxy of the total proton motive force (pmf) generated, was found to be similar in WT and *ndufa5* and *ndufb10* mutants over different times of illumination with the same actinic light intensity (330 µmol photons m^{-2} s^{-1}; Figure 6A).

ECS relaxation kinetics measured after the light was switched off after 300 s of illumination, however, indicated an altered partition between the electric and pH component of the transmembrane potential (Figure 6B; Cruz et al., 2001). These differences were dependent on illumination and became detectable only if plants were exposed to light for >120 s (Figure 6B; Supplemental Figure S7). This suggests that the alterations in pmf partitioning emerged as a result of modifications in the photosynthetic activity (Avenson et al., 2005; Wang and Shikanai, 2019). This difference between genotypes was again light intensity-dependent, and when using a stronger, fully saturating, illumination (1,000 µmol photons m^{-2} s^{-1}) mutants were indistinguishable from WT (Supplemental Figure S8).

The differences in ΔpH could not be attributed to differential activation of cyclic electron transport, the activity of which appeared to be low in both mutants and WT *P. patens* (Supplemental Figure S9, see also Kukuczka et al., 2014). To assess the impact of mutations on proton translocation, conductivity (g_H^+) through the ATPase complex was estimated from the decay lifetime of ECS signal after the light was switched off. In both *ndufa5* and *ndufb10*, the ECS decay kinetics was faster than WT, indicating that proton conductivity due to ATPase was higher (Supplemental Figure S10). Monitoring of g_H+ using actinic illumination of different duration (between 30 and 480 s) showed that g_H+ in WT plants increased with the duration of the illumination reaching a steady state after ~5 min, consistently with a progressive activation of ATPase (Figure 6C), following a modulation of chloroplast ATPase activity by the sensing of stromal metabolic status and redox state during steady-state photosynthesis (Kramer et al., 1990; Takizawa et al., 2008; Kohzuma et al., 2013; Sekiguchi et al., 2020). Interestingly, in *ndufa5* and *ndufb10* mutants, the g_H+ was higher but also more rapidly activated and it reached the maximal activity after about 120 s of illumination instead of the 300 s required by WT plants (Figure 6C).

Lumenal pH is a major factor for regulation of photosynthesis and its decrease under strong illumination is known to activate protective mechanisms such as heat dissipation of excess energy (NPQ) and the xanthophyll cycle (Li et al., 2009). Low lumenal pH is also known to inhibit cytochrome b_6f activity to avoid over-reduction of PSI, a mechanism known as photosynthetic control (Nishio and Whitmarsh, 1993). When photosynthetic control is active, the ETR from plastoquinol (PQH_2) is slower, to reduce possibilities of PSI over-reduction. The impact of CI mutations on Cyt b_6f activity was assessed by monitoring Cytochrome *f* (Cyt *f*) oxidation state from an absorption signal at 554 nm (Figure 7A; Supplemental Figure S11, see "Materials and methods" for details). The oxidation state in illuminated samples can be estimated by comparing the signal with plants treated with PSII and Cyt b_6f inhibitors 3-(3,4-dichlorophenyl)-1,1-dimethylurea (DCMU) and 2,5-Dibromo-6-isopropyl-3-methyl-1,4-benzoquinone (DBIMB) where electron transport from PQ is blocked and thus Cyt *f* is fully oxidized. In *ndufb10* and *ndufa5* illuminated with sub-saturating light (300 µmol photons m^{-2} s^{-1}) Cyt *f* is less oxidized than in WT plants (Figure 7B). When the light was switched off, Cyt *f* reduction in mutant plants was also faster than in WT (Figure 7C), thus suggesting that in these plants electron transport from PQH_2 is faster (Stiehl and Witt, 1969).

In the same measuring conditions, the impact on PSI was monitored from P700 oxidation state using a similar spectrophotometric approach, monitoring a differential absorption signal at 705 nm (ΔOD_{705}, Figure 7D). CI mutants showed similar P700 oxidation level compared to WT plants at steady-state illumination (Figure 7E). However, when the light was switched off, the rate of P700 reduction was faster in the mutants, suggesting that electrons flux toward P700

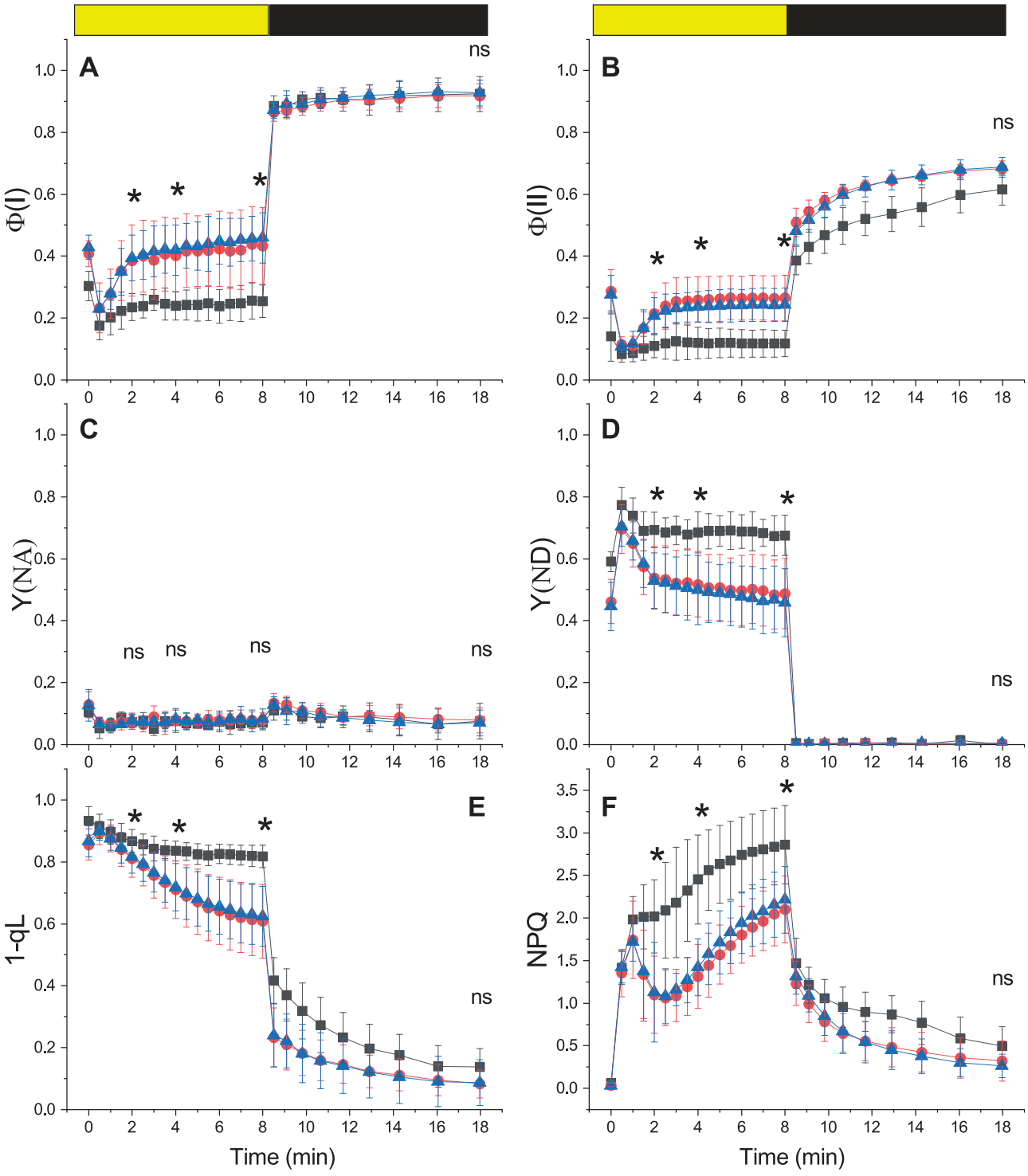

Figure 5 Alterations in PS functionality in CI mutants. The yield of PSI (Φ(I), A), PSII (Φ(II), B). PSI acceptor side limitation (Y(NA), C), PSI donor side limitation (Y(ND), D). PQ redox state (1-q_L, E) and NPQ (F) were measured with Dual PAM 100 in plants exposed to 330 µmol photons m^{-2} s^{-1} of actinic light intensity. Yellow/black bar indicates when actinic light was on/off, respectively. WT, *ndufb10*, and *ndufa5* KO are shown, respectively, with black squares, red circles, and blue triangles. Data are shown as average ± SD ($n > 4$). Asterisks indicate statistically significant differences of both mutants from WT plants (one-way ANOVA, $n > 5$, $P < 0.01$) after 2, 4, and 8 min of illumination and after 10 min in the dark; ns indicates nonstatistically significant differences.

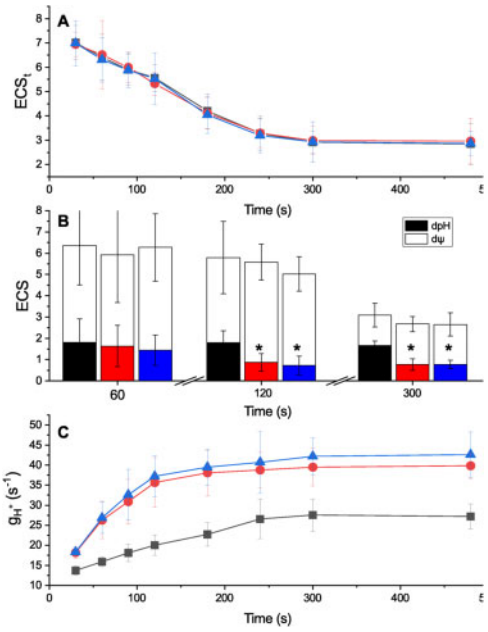

Figure 6 Impact of CI inactivation on pmf composition and proton conductivity (g_H^+). A, ECS_t generated by illumination with sub-saturating light (300 µmol photons m^{-2} s^{-1}) at different time points. ECS_t was quantified as (ECS_{520} − ECS_{546})/PSI Charge Separation and indicative of the pmf generated. WT, *ndufb10*, and *ndufa5* KO are shown, respectively, in black, red, and blue. Average ± SD ($n \geqslant 5$) are reported. B, quantification of total pmf as well as its partition in different components. ΔpH is shown in black, red and blue for WT, *ndufb10*, and *ndufa5* KO, respectively. The electric component (ΔΨ) in shown in white. Averages ± SD ($n \geqslant 5$) are reported and asterisks indicate statistically significant differences (one-way ANOVA, $n > 5$, $P < 0.01$). C, g_H^+ measures the proton conductivity of protons across the thylakoid membrane and it reflects the activity of ATPase. This was measured after exposing plants to light with different duration. WT, *ndufb10*, and *ndufa5* KO are shown, respectively, as black squares, red circles, and blue triangles. Averages ± SD ($n \geqslant 5$) are reported.

was more rapid (Figure 7F) consistent with a higher PQH_2 oxidation rate.

Discussion

Inactivation of CI by targeting two different subunits produced similar photosynthetic phenotypes

In this work, independent KO lines targeting two subunits of CI were generated and verified to have the insertion of the resistance cassette in the expected genome position and to lose the mRNA expression (Figure 1; Supplemental Figure S1). *ndufa5* KO showed complete depletion of CI activity in BN-PAGE (Figure 3B) and it did not accumulate NAD9 (Figure 3A), a core subunit of the Q module that is directly involved in the transfer of electrons to the ubiquinone which is required for the complex functionality (Massoz et al., 2013). This is consistent with the previous results showing that NDUFA5 interacts with NAD7 and NAD9 to form an 80 kDa sub-complex that successively is integrated into the CI (Ligas et al., 2019). The second targeted subunit, NDUFB10, is instead integrated later during CI assembly and, in its absence, there is the formation of an incomplete CI of 800 kDa including both the N and Q modules but missing the proton pumping module and thus the biological activity (Barbieri et al., 2011). Despite this partial retention of some subunits (Figure 3), both mutants showed inactive CI as shown by the insensitivity of O_2 consumption to the specific inhibitor rotenone (Figure 4A).

In both CI mutant lines, O_2 consumption in the dark was enhanced compared to WT plants. This observation can be explained by the increased CII and CIII content but is more likely related to strong over-accumulation of AOX, as evident from the larger fraction of O_2 consumption through AOX in the mutants (Figures 3 and 4; Supplemental Table S3). Increased flux through AOX may compensate for the absence of CI activity, which normally accounts for ∼40% of O_2 consumption rate in WT (Figure 4A). However, flux through AOX is not expected to translate in a full recovery of the capacity of ATP biosynthesis in the mutants since CII and alternative pathways like AOX do not contribute to the generation of transmembrane potential, whereas flux through CI does (Vanlerberghe et al., 2020).

Similar alterations in respiratory complexes were also observed in CI mutants from Arabidopsis (Fromm et al., 2016b) and *Nicotiana* (Vidal et al., 2007) that also showed increased AOX accumulation and higher O_2 consumption in the dark. In Arabidopsis, it was demonstrated that such increased O_2 consumption in the dark is a distinctive feature of complete CI KOs, while this is not observed in CI partial mutants or KD lines (Kühn et al., 2015). Based on this observation, the increase in O_2 consumption observed in *P. patens ndufa5* and *ndufb10* KO is a further confirmation that both lines have fully inactivated CI.

It is remarkable to observe that *ndufa5* and *ndufb10* KO regardless of the specific mutation showed the same decreases in photosynthetic control, increases in PSI and PSII activities and enhanced proton conductivity (Figures 2–7), even if the targeted genes were different. This similarity strongly suggests that plant responses observed are attributable to the lack of CI activity, while the impact of the absence of specific subunits is minor, at least on the phenotypes analyzed.

CI deficiency alters chloroplast ATP synthase activity and photosynthetic control of electron transport

All *P. patens* cells in various developmental stages contain chloroplasts and are photosynthetically active even if at different levels (Sakakibara et al., 2003). Here, plants were analyzed 10 d after inoculum on a mineral medium containing no reduced carbon and were mainly composed by chloronema, a developmental stage containing phototrophic cells particularly rich in chloroplasts (Furt et al., 2012). The combined choice of the model organism and developmental stage, thus, enable to assess the impact of respiration on

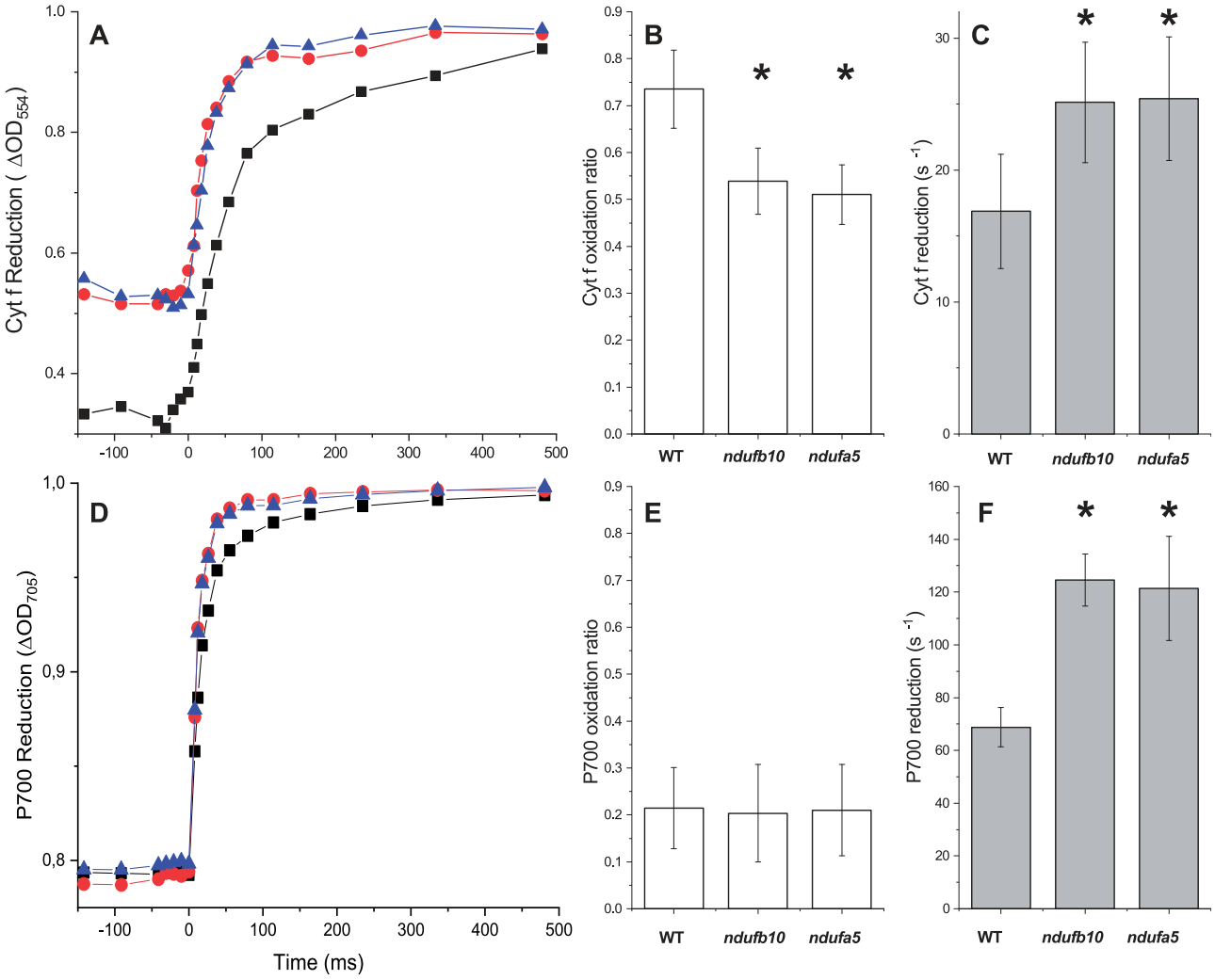

Figure 7 Cytochrome *f* and PSI oxidation. A, Cytochrome *f* reduction monitored from ΔOD_{554} in dark-adapted plants subjected to constant illumination (300 µmol photons m^{-2} s^{-1}) for 480 s before the light was switched off. WT, *ndufb10*, and *ndufa5* KO are shown, respectively, as black squares, red circles, and blue triangles. B, Oxidation state is expressed as the ratio between Cyt *f* signals at the end of illumination and the maximal oxidation levels obtained by addition of DCMU/DBMIB to obtain complete oxidation. Reported values are average ± SD ($n \geqslant 4$). C, Cyt *f* reduction rate in the different genotypes after 480 s actinic light exposure, quantified from half-time reduction. For B and C asterisks, indicate statistically significant differences (one-way ANOVA, $n > 4$, $P < 0.01$). D, PSI reduction monitored from ΔOD_{705} in dark-adapted plants exposed to constant illumination (300 µmol photons m^{-2} s^{-1}) for 480 s. WT, *ndufb10*, and *ndufa5* KO are shown, respectively, as black squares, red circles, and blue triangles. E, P700 oxidized fraction is expressed as the ratio between $P700^+$ signals at the end of illumination and the maximal oxidation levels obtained by addition of DCMU and DBMIB to block the PSI re-reduction. Reported values are average ± SD ($n \geqslant 4$). F, $P700^+$ reduction rate estimated from half-time reduction after 480 s actinic light exposure in the different genotypes. Average values ± SD are shown. For F, asterisks indicate statistically significant differences (one-way ANOVA, $n > 5$, $P < 0.01$).

photosynthesis disentangling it from the influence of heterotrophic tissues like roots that are expected to be largely impacted by the lack of respiration, something that is not possible working with vascular plants.

Despite the lack of heterotrophic cells, *P. patens* plants depleted in CI present a strong phenotype with a drastically impaired growth (Figure 2), demonstrating that respiration plays a major role in photosynthetically active cells in plants. Plants exposed to continuous light regime did not show any growth recovery, suggesting that the impact of respiration is also not limited to sustaining metabolism during the night (Figure 2; Supplemental Figure S2). Even more strikingly, while WT plants exposed to continuous illumination showed faster growth than the ones under 16-h/8-h d/night cycles (Supplemental Figure S2), this is not the case for CI mutants that are not able to exploit the extra light energy available. These observations demonstrate that inactivation of respiration directly impacts photosynthetic metabolism in *P. patens* plants and their ability to use light energy for growth.

This phenotype is not attributable to drastic changes in photosynthetic apparatus composition since plants depleted in CI did not show any major alteration in pigments (Table 1) nor in the content of protein complexes, PSI, PSII, Cyt *b6f*

with only a slight increase in Chloroplast ATPase (Supplemental Figure S4). Photosynthetic functionality is nevertheless altered, and plants exposed to sub-saturating illumination (300 μmol photons m^{-2} s^{-1} and below) show several differences. Both PSI and PSII show a higher yield upon illumination in mutant plants, suggesting a lower saturation level in illuminated plants and thus higher transport rate (Supplemental Figure S9). CI mutants also show increased proton conductivity across the thylakoids membrane (Figure 6C) that, combined with an equivalent pmf, is again consistent with a higher ETR (Supplemental Figure S9).

The higher g_H+ observed in the mutants cannot be completely attributed to the observed slight increase accumulation in chloroplast ATPase in the mutants but is more likely caused by a higher activation state or substrate availability, as suggested by the larger changes in g_H+ during the dark to light transitions (Figure 6C; Supplemental Figure S10). The turnover rate of the ATPase is known to be limited by the depletion of inorganic phosphate (Pi) or ADP pool through metabolic feedback (Takizawa et al., 2008) and an eventual smaller impact of this metabolic control in CI mutants could also contribute to the higher activity. Consistent with this hypothesis, blocking respiration with various inhibitors strongly affected ATPase activity (Supplemental Figure S12). On the other hand, the presence of inhibitors did not abolish completely the difference between WT and mutants (Supplemental Figure S12), suggesting other mechanisms influencing proton conductivity beyond metabolic feedback must be altered by CI inactivation. A likely candidate is the modulation of the ATPase γ-subunit thiol redox state by thioredoxin (Trx; Kramer et al., 1990; Sekiguchi et al., 2020). The hypothesis of an alteration of Trx control system due to CI inactivation would in fact explain the faster activation observed in *ndufa5* and *ndufb10* KO (Figure 6C).

The higher ATPase activity in the CI mutants causes a faster translocation of protons in the stroma and an increase in the lumenal pH (Figure 6B), in turn, affecting photosynthesis regulatory mechanisms modulated by lumen acidification. NPQ is induced by a decrease of lumenal pH and the protonation of specific activators PsbS or LHCSR (Li et al., 2002; Alboresi et al., 2010; Liguori et al., 2016). WT and CI mutants accumulated similarly PsbS and LHCSR (Supplemental Figure S4) and, consistently, the maximal NPQ capacity is equivalent in all genotypes (Supplemental Figure S6F). However, mutants exposed to sub-saturating illumination show a larger relaxation of NPQ than WT after a few minutes (Figure 5F) that can be explained by a reduction of ΔpH across thylakoid membrane (Joliot and Finazzi, 2010; Figure 6B). This difference in NPQ does not occur immediately after light is switched on but it only emerges after 2 min of exposition, a time needed for the difference in proton conductivity between WT and mutants to generate a significant separation in ΔpH and consequently NPQ (Figures 5F and 6B).

An altered lumen acidification is also expected to affect photosynthetic control, the modulation of PQH_2 oxidation at the Cyt *b6f*. Mutants exposed to sub-saturating illumination indeed showed a faster rate of Cyt *f* reduction (Figure 7C), suggesting a higher electron transport activity and a lower photosynthetic control. This hypothesis is consistent with several other differences observed such as the higher efficiency in both PSs (Figure 5, A and B; Supplemental Figure S5, A and B), a less pronounced PSII acceptor limitation (1-q_L; Figure 5E; Supplemental Figure S5E) and PSI donor limitation (Y(ND); Figure 5D and Supplemental Figure S5D) compared to WT. PSI also shows faster reduction kinetics (Figure 7F). All the differences observed between the WT and mutants, summarized in Supplemental Figure S13, can be explained with a decreased photosynthetic control and thus a higher Cyt b_6f activity, thus increasing the rate of transport of electrons from PQ to PSI as the result of higher ATPase activity and higher lumenal pH (Takizawa et al., 2007, 2008).

It is interesting to observe that when light is in strong excess (1,000–2,000 μmol m^{-2} s^{-1}; Supplemental Figures S6 and S8), thus 25–50 times higher than the illumination used for plants growth, the mutants become indistinguishable from WT. Under such high light intensities, metabolic processes become equally saturated in WT and mutants, leading to similar ATPase activity and extents of photosynthetic control. The lack of differences at very strong illumination, on the other hand, supports the conclusion that photosynthetic apparatus is not altered in CI mutants. The effects on photosynthesis observed at lower light can thus be attributed to downstream processes, due to respiration alterations.

All these results globally suggest that CI inactivation not only alters respiratory activity in mitochondria but also impacts ATP biosynthesis in the chloroplast. This demonstrates the key role of the metabolic connection between photosynthesis and respiration through the transport of reduced molecules (e.g. malate, citrate, triose-Pi, and glycolate; Shameer et al., 2019) for plants metabolism.

Impact of respiration on photosynthesis adapted during evolution

All CI subunits identified in Arabidopsis are well conserved in *P. patens* genome (Supplemental Table S1), consistent with the recent observation that CI structure and composition show several similarities between the plant Arabidopsis and the green alga *Polytomella sp* (Klusch et al., 2020). CI inactivation also have similar effects in both Arabidopsis and *P. patens* with a strong impact on growth and an increased O_2 consumption activity, as the result of changes in composition of respiratory apparatus and an higher AOX content, which ultimately lead to an increase of the electron flow through alternative respiratory pathways (Figures 3A and 4A; Kühn et al., 2015; Fromm et al., 2016a).

Because the *P. patens* tissues studied here contain only photosynthetically active cells, the observed effects can be

attributed to intracellular interactions between chloroplasts and extraplastid within autotrophic cells, excluding any indirect effect from heterotrophic tissues that are instead always a possibility in vascular plants. On the other hand, the similarity of the alterations of respiratory apparatus composition and activity with the ones seen in Arabidopsis (Kühn et al., 2015) and tobacco (Vidal et al., 2007) suggests CI should have a similar influence in metabolism of these vascular plants leaves as well, though there may also be longer-range interactions, including changes in metabolic sinks at in heterotrophic cells like roots.

In contrast with the major impact in *P. patens* and vascular plants, the role of CI in the green alga *C. reinhardtii* appears to be more restricted to heterotrophy, since CI KO mutants show similar growth rates under photoautotrophic conditions, but markedly slower growth under heterotrophic conditions (Salinas et al., 2014; Larosa et al., 2018). CI mutants in *Chlamydomonas* also do not show any reorganization of respiratory apparatus, and showed reduced O_2 consumption activity compared to WT (Barbieri et al., 2011; Massoz et al., 2013; Larosa et al., 2018).

While it is not possible to make general conclusions based on comparisons of a few selected species among the highly diverse phototrophic Eukaryotes, these examples suggest the interaction between photosynthesis and respiration changed during evolution. Plants rely on photo-autotrophy and normally cannot complete their developmental cycle in the dark even if reduced carbon is supplied (Neff et al., 2000). The fact that obligate photo-autotrophic organisms rely more on respiration seems counterintuitive, but it can be explained considering that in these organisms mitochondrial respiration activity gradually adapted to work in synergy with photosynthesis, optimizing the metabolite fluxes between organelles (Gardeström and Igamberdiev, 2016; Shameer et al., 2019). Respiration thus could gradually assume a specialized role in essential processes for photosynthesis such as redox balance and photorespiration, becoming itself indispensable for the cells.

On the other hand, *Chlamydomonas* have a highly flexible metabolism and in their natural environment can growth in autotrophic, heterotrophic, or mixotrophic conditions depending on the presence of light and carbon sources (Harris, 2001; Yang et al., 2015). *Chlamydomonas* cells can even be exposed to anaerobic conditions when it can activate fermentative metabolism and hydrogen production (Ghirardi et al., 2007; Grossman et al., 2011; Grechanik et al., 2020). In those anaerobic conditions, O_2 is absent and respiration is inactivated but still cells can perform photosynthesis (Godaux et al., 2015) that must thus be fully independent of respiratory activity. In organisms with such large metabolic flexibility, and particularly if they are exposed to anaerobic conditions, respiration cannot assume an essential role in the photosynthesis, explaining why they are less impacted by an inactivation. The recent observation that the European mistletoe *Viscum album*, an obligate semi-parasite living on branches of trees, can live without CI (Maclean et al., 2018; Senkler et al., 2018) is consistent with this idea, suggesting that when the species lost their energy dependence from photosynthesis also its role of respiration for cells could change and become less essential.

Materials and methods

Plant material and growth *P. patens*

Physcomitrium patens (Gransden) WT, *ndufb10* and *ndufa5* KO lines were cultivated in the protonemal phase by vegetative propagation on $PpNH_4$ medium (Ashton et al., 1979) and grown under standard conditions: 24°C, long photoperiod (16:8 light: dark) with 50 µmol photons m^{-2} s^{-1}. Physiological and biochemical characterizations were performed on 10-d-old tissue cultivated in $PpNO_3$ medium (Ashton et al., 1979). The growth rate in all the media and light conditions was evaluated starting from protonema colonies of 2 mm in diameter followed for 21 d. Colony size was measured as in Storti et al. (2019). In brief, high-quality images (600 ppi) were acquired using a Konica Minolta Bizhub C280 scanner. Images were analyzed with FIJI (https://fiji.sc/) using the "threshold color" plugin to subtract the plate background. Colony size was calculated from the integrated density (area × mean density). This strategy was chosen to take into account the development from 2D (chloronema and caulonema) to 3D structures (gametophore and rhizoids) of moss colonies, which are lost when considering only the area.

Moss transformation and mutant selection

The *ndufb10* and *ndufa5* KO constructs were employed to mutate the *Ndufb10* gene and *Ndufa5* gene, respectively (Supplemental Figure S1). The transformation was performed through protoplast DNA uptake as described in Alboresi et al. (2010). Six-day-old protonema tissues grown in $PPNH_4$ medium were treated with fungal driselase (Sigma-Aldrich) to break the cell wall. Resulting protoplasts were filtered with 100-µm micro cloth. Protoplasts were washed and resuspended in PEG-4000-containing solution, mixed with digested linear DNA from KO constructs (20 µg) and exposed to heat shock (5 min at 45°C) to open cell membrane. After 1 d of recovery, protoplasts were first immersed in a top layer solution and plated on agarified medium added with mannitol to prevent their lysis. After 7 d, recovered cells were moved to a new plate with antibiotics for transformants selection. The selection was repeated twice. Resulting transformants were homogenized using 3-mm zirconium glass beads (Sigma-Aldrich), and genomic DNA (gDNA) was isolated according to a rapid extraction protocol (Edwards et al., 1991) with minor modification. PCR amplifications of recombination cassette were performed on extracted gDNA (Supplemental Table S3; Figure 1 and Supplemental Figure S1). To confirm that *ndufb10* and *ndufa5* KO lines were lacking target gene expression RT-PCR was performed on cDNA (RevertAid Reverse Transcriptase; Thermo Scientific) synthesized after RNA extraction.

Western blot analysis

Total protein extracts were obtained by pestled protonema tissue in sample buffer (50 mM TRIS pH 6.8, 100 mM DTT, 2% (w/v) SDS, and 10% (w/v) glycerol). Samples of total Chl were quantified, and every well was loaded accordingly to the quantification. After SDS–PAGE, proteins were transferred to a nitrocellulose membrane (Pall Corporation). Membranes were hybridized with specific primary antibodies: anti-PsaA, Agrisera, catalogue number AS06172; anti-Cyt *f*, Agrisera, catalogue number AS06119; anti-γ ATPase, Agrisera, catalogue number AS08312, anti-AOX1/2, Agrisera, catalogue number AS04054; custom made anti-NAD9 (Lamattina et al., 1993); custom made anti-SDH1-1 (CII), anti-α-MPP (CIII), anti-COX2 (CIV), anti-β subunit (CV; Peters et al., 2012), and custom made anti-D2, anti-PsbS, and anti-LHCSR (Storti et al., 2019). After hybridization, signals were detected with alkaline phosphatase-conjugated antibody (Sigma Aldrich).

Crude membrane extracts preparation

Crude membrane extracts were prepared as in Pineau et al., (2008) with minor modifications. Approximately 300 mg of fresh or frozen (−80°C) protonema grown in $PpNO_3$ for 10 d were homogenized in 2 mL of 75 mM MOPS-KOH, pH 7.6, 0.6 M sucrose, 4 mM EDTA, 0.2% (w/v) polyvinylpyrrolidone 40, 8 mM cysteine, 0.2% (w/v) bovine serum albumin using a plant Potter glass tissue grinder pound at 0°C. The homogenate was filtrated across one layer of micro cloth with 20-μm pores and centrifuged at 4°C at 1,300 g for 4 min. The supernatant was collected and centrifuged again at 22,000*g* for 20 min. The resultant pellet, which contained most of the thylakoid and mitochondria membranes, was resuspended in 200 μL of 10 mM MOPS-KOH, pH 7.2, 0.3 M sucrose. The protein concentration on crude membrane extracts was quantified using the BCA protein assay.

Blue native polyacrylamide gel electrophoresis

Gels were cast in 8 × 10 cm plates using the buffer described by Kügler et al., (1997) with an acrylamide gradient of 4%–12% (w/v) in the running gel and 4% (w/v) acrylamide in the stacking gel. A volume of crude membrane extracts corresponding to 100 mg of proteins was washed with three volumes of H_2O Milli-Q® and centrifuged at 4°C, 21,470*g* for 20 min. The pellet was resuspended in 20 μL of ACA buffer 1× (50 mM Bis–Tris, pH 7.0; 750 mM aminocaproic acid; 1 mM EDTA) Järvi et al., (2011). For protein solubilization 20 μL of β-dodecyl maltoside (β-DM) 2% (w/v) prepared in ACA buffer were added to the tube, to reach a final volume of 40 μL, reaching β-DM 1% in ACA buffer. Each tube was vortexed for 30 s, kept on ice for 5 min, and centrifuged at 4°C, 22,000*g* for 8 min. The supernatant was supplemented with 4 μL of Coomassie Blue 5% solution (20 mM Bis–Tris, 500 mM aminocaproic acid, Coomassie Blue G-250 5% (w/v)). Anode and cathode buffers were the same used by Järvi et al. (2011) for BN gel; the cathode buffer was supplemented with Coomassie Blue G-250 0.02% (w/v). The gel was run at 75 V for 30 min. Then, the cathode buffer was replaced with fresh cathode buffer without Coomassie Blue and the gel was run at 100 V for 30 min, at 125 V for 30 min, at 150 V for 60 min, at 175 V for 30 min, and at 200 V for 60 min. The total running time was about 4 h.

Determination of NAH dehydrogenase in-gel activity

After BN-PAGE, the NADH dehydrogenase activity of CI was revealed by incubation of the gel in the presence of 1 mM nitro blue tetrazolium (NBT) and 0.2 mM NADH in 50-mM potassium Pi buffer (pH 7.0; Barbieri et al., 2011).

Oxygen consumption and oxygen evolution

O_2 consumption and evolution were evaluated as in Storti et al. (2020) with a Clark-type O_2 electrode (Hansatech, King's Lynn, UK). In brief, two protonema disks of about 1 cm of diameter coming from 10-d-old plates were introduced in the measurement chamber filled with 2 mL of a solution containing $NaCO_3$ 0.1 mM maintained at 23°C. After 10 min in the dark (respiratory rate), the light was turned on and the O_2 variation was recorded for other 10 min (photosynthetic rate). O_2 consumption and evolution rates were normalized to the total Chl content of each sample. Chl content was evaluated after extraction with 80% (v/v) acetone (Porra et al., 1989). Inhibitors employed for respiratory analysis were 50-μM rotenone (CI), 1-mM KCN (CIV), and from 2 to 8 mM SHAM (AOX). For inhibitor treatments, protonema tissue was incubated 30 min in the dark in medium supplemented with the inhibitors, for the double inhibition with KCN and SHAM the inhibitors were added simultaneously. Inhibitors were also added at the measuring chamber during O_2 consumption evaluation. The capacity of cytochrome pathway was measured as O_2 consumption that was sensitive to 1 mM KCN in the presence of 8 mM SHAM. The capacity of AOX pathway was measured as O_2 consumption that was sensitive to 8 mM of SHAM in the presence of 1 mM KCN (Vanlerberghe et al., 2002).

Pigment analysis

Ten-day-old protonemal tissues were broken with a plastic grinder and pigments were extracted with 80% acetone. Whole-plant extracts in acetone were fitted with those of individual purified pigments to calculate Chl*a*/*b* and Chl/Car ratios (Croce et al., 2002).

Spectroscopic analyses

In vivo, Chl fluorescence and NIR absorption analyses were performed at room temperature with a Dual-PAM 100 system (Walz) on protonema grown for 10 d in $PpNO_3$ in WT and mutant lines. Before the analysis, the plants were adapted in the dark for 40 min, and the F_v/F_m parameter was calculated as $(F_m - F_o)/F_m$. Induction curves were obtained setting actinic red light at (approx.) 50, 330, or 2,000 μmol photons $m^{-2}s^{-1}$, and photosynthetic parameters were recorded every 30 s. At each step, the photosynthetic parameters were calculated as follows: Φ(II) as $(F_m' - F_o)/$

F_m', qL as $(F_m' - F)/(F_m' - F_o') \times F_o'/F$, and NPQ as $(F_m - F_m')/F_m'$, Φ(I) as 1-Y(ND)-Y(NA); Y(NA) as $(P_m - P_m')/P_m$; Y(ND) as $(P - P_o/P_m$; Klughammer and Schreiber, 1994). ECS spectra were recorded with a JTS-10 system (Biologic) in plants that were dark acclimated for 40 min and imbibed with 20 mM HEPES, pH 7.5 and 10 mM KCl. For each measure, the background signal at 546 nm was subtracted from the 520 nm signal, in this way eliminating the contribution of scattering and cytochromes. Functional total PSs quantification was performed by a single flash turnover using a xenon lamp. The light produced by xenon gas can induce PSI double charge separation, and thus PSI content could be overestimated by ∼40% but it does not affect the comparison of different samples (Gerotto et al., 2016). Moreover, samples were incubated with 20 μM DCMU and 4 mM HA (hydroxylamine) to calculate the contribution of PSI alone (Joliot et al., 2004). Total ETR was measured with dark-induced relaxation kinetic; Sacksteder and Kramer, 2000) analysis as in Gerotto et al. (2016). In samples exposed to continuous illumination at 350 μmol photons m^{-2} s^{-1}, (630 nm LED) light was switched off after 4–5′ to follow relaxation kinetics and evaluate the pmf generated during light treatment as in Storti et al. (2020). The pmf was determined as the difference of the maximum signal at the light steady state and minimum level of ECS in the dark and normalized to total charge separation PSI. The pmf portioning in $\Delta\Psi$ and ΔpH was performed as in Baker et al. (2007). The ECS relaxation was followed for 30 s after light to dark transition and the ECS signal in this relaxed state was recorded. Difference between the relaxed ECS signal and the maximal signal at light steady state is defined as ECS_{ss}, which is proportional to $\Delta\Psi$. ΔpH was calculated from the difference between the relaxed ECS signal and a minimum level of ECS in the dark. Proton conductance (g_H^+) was estimated by fitting the first 300 ms of the ECS decay curve with a first-order exponential decay kinetic and indicated as the inverse of the decay time constant as described earlier (Avenson et al., 2005). g_H^+ was calculated after exposure to 30 s, 60 s, 90 s, 120 s, 180 s, 240 s, 300 s, and 480 s of illumination (350 μmol photons m^{-2} s^{-1}). $P700^+$ absorption kinetics were calculated from the absorption at 705 nm (ΔOD_{705}) and following the re-reduction after plants were illuminated for 5 min at 350 μmol photons m^{-2} s^{-1}. Oxidized P700 was calculated by comparing the maximum signal from $P700^+$ obtained before and after incubating plants with20 μM DCMU and 150 μM DBIMB. $P700^+$ reduction after the actinic light was switched off was fit to first-order exponential decay to obtain $t_{1/2}$ values. Cyt *f* absorption was calculated as for $P700^+$, except for the interference filter at 554 nm. In this case, 546 nm and 573 nm were used as background and removed to 554 nm signal (Kirchhoff et al., 2011). Oxidation status and Cyt *f* kinetic rate measurements were performed as for P700 measurements.

Accession numbers

Accession numbers of genes analyses in this work are reported in Supplemental Table S1.

Supplemental data

The following materials are available in the online version of this article.

Supplemental Figure S1. Generation of *P. patens* mutant lines lacking respiratory CI.

Supplemental Figure S2. Growth kinetics of *P. patens* plants under different conditions.

Supplemental Figure S3. BN-PAGE separation of crude extracts.

Supplemental Figure S4. Impact of CI mutations on the photosynthetic apparatus composition.

Supplemental Figure S5. Photosynthetic efficiency under dim illumination.

Supplemental Figure S6. Photosynthetic efficiency under saturating illumination.

Supplemental Figure S7. Proton motive force composition before the steady state.

Supplemental Figure S8. Photosynthetic proton motive force at saturating illumination.

Supplemental Figure S9. Photosynthetic electron transfer in *P. patens* plants.

Supplemental Figure S10. ATPase activity assessed from ECS relaxation.

Supplemental Figure S11. Cyt b_6f reduction state estimation.

Supplemental Figure S12. Influence of respiration inhibition on proton conductivity in WT and CI mutants.

Supplemental Figure S13. Summary of photosynthetic electron transport alterations in CI depleted plants.

Supplemental Table S1. Identification of conserved CI subunits in *P. patens*.

Supplemental Table S2. Cytochrome and AOX Capacity in WT and *ndufb10* and *ndufa5* plants.

Supplemental Table S3. Primers employed in this work.

Acknowledgments

We thank Dr Etienne Meyer (Institute of Plant Physiology; the Martin-Luther-University, Halle-Wittemberg) for providing the NAD9 antibody and Prof. Hans-Peter Braun (Institute of Plant Genetics; Leibniz University, Hannover) for the SDH1-1, α-MPP, COX2, and ATPase β-subunit antibodies.

Funding

M.M. was funded by the University of Padova. D.M.K. was supported by Division of Chemical Sciences, Geosciences, and Biosciences, Office of Basic Energy Sciences of the US Department of Energy (DE-FG02-91ER20021).

Conflict of interest statement. The authors declare that the research was conducted in the absence of any commercial orfinancial relationships that could be construed as a potential conflict of interest.

References

Alboresi A, Gerotto C, Giacometti GM, Bassi R, Morosinotto T (2010) Physcomitrella patens mutants affected on heat dissipation

clarify the evolution of photoprotection mechanisms upon land colonization. Proc Natl Acad Sci U S A **107**: 11128–11133

Ashton NW, Grimsley NH, Cove DJ (1979) Analysis of gametophytic development in the moss, Physcomitrella patens, using auxin and cytokinin resistant mutants. Planta **144**: 427–435

Avenson TJ, Cruz JA, Kanazawa A, Kramer DM (2005) Regulating the proton budget of higher plant photosynthesis. Proc Natl Acad Sci U S A **102**: 9709–9713

Bailleul B, Berne N, Murik O, Petroutsos D, Prihoda J, Tanaka A, Villanova V, Bligny R, Flori S, Falconet D, et al. (2015) Energetic coupling between plastids and mitochondria drives CO2 assimilation in diatoms. Nature **524**: 366–369

Bailleul B, Cardol P, Breyton C, Finazzi G (2010) Electrochromism: A useful probe to study algal photosynthesis. Photosynth Res **106**: 179–189

Baker NR, Harbinson J, Kramer DM (2007) Determining the limitations and regulation of photosynthetic energy transduction in leaves. Plant Cell Environ **30**: 1107–1125

Barbieri MR, Larosa V, Nouet C, Subrahmanian N, Remacle C, Hamel PP (2011) A forward genetic screen identifies mutants deficient for mitochondrial complex I assembly in Chlamydomonas reinhardtii. Genetics **188**: 349–358

Braun H-P, Binder S, Brennicke A, Eubel H, Fernie AR, Finkemeier I, Klodmann J, König A-C, Kühn K, Meyer E, et al. (2014) The life of plant mitochondrial complex I. Mitochondrion **19 (**Pt B): 295–313

Cardol P, Gloire G, Havaux M, Remacle C, Matagne R, Franck F (2003) Photosynthesis and state transitions in mitochondrial mutants of Chlamydomonas reinhardtii affected in respiration. Plant Physiol **133**: 2010–2020

Cheung MCY, Ratcliffe GR, Sweetlove LJ (2015) A method of accounting for enzyme costs in flux balance analysis reveals alternative pathways and metabolite stores in an illuminated Arabidopsis leaf. Plant Physiol **169**: 1671–1682

Colas Des Francs-Small C, Small I (2014) Surrogate mutants for studying mitochondrially encoded functions. Biochimie **100**: 234–242

Croce R, Canino G, Ros F, Bassi R (2002) Chromophore organization in the higher-plant photosystem II antenna protein CP26. Biochemistry **41**: 7334–7343

Cruz JA, Sacksteder CA, Kanazawa A, Kramer DM (2001) Contribution of electric field ($\Delta\psi$) to steady-state transthylakoid proton motive force (pmf) in vitro and in vivo. Control of pmf parsing into $\Delta\psi$ and ΔpH by ionic strength. Biochemistry **40**: 1226–1237

Dahal K, Martyn GD, Alber NA, Vanlerberghe GC (2016) Coordinated regulation of photosynthetic and respiratory components is necessary to maintain chloroplast energy balance in varied growth conditions. J Exp Bot **68**: erw469

Dinant M, Baurain D, Coosemans N, Joris B, Matagne RF (2001) Characterization of two genes encoding the mitochondrial alternative oxidase in Chlamydomonas reinhardtii. Curr Genet **39**: 101–108

Dutilleul C, Driscoll S, Cornic G, De Paepe R, Foyer CH, Noctor G (2003) Functional mitochondrial complex I is required by tobacco leaves for optimal photosynthetic performance in photorespiratory conditions and during transients. Plant Physiol **131**: 264–275

Eberhard S, Finazzi G, Wollman F-A (2008) The dynamics of photosynthesis. Annu Rev Genet **42**: 463–515

Edwards K, Johnstone C, Thompson C (1991) A simple and rapid method for the preparation of plant genomic DNA for PCR analysis. Nucleic Acids Res **19**: 1349

Fromm S, Braun H-P, Peterhansel C (2016a) Mitochondrial gamma carbonic anhydrases are required for complex I assembly and plant reproductive development. New Phytol **211**: 194–207

Fromm S, Senkler J, Eubel H, Peterhänsel C, Braun H-P (2016b) Life without complex I: proteome analyses of an Arabidopsis mutant lacking the mitochondrial NADH dehydrogenase complex. J Exp Bot **67**: 3079–3093

Furt F, Lemoi K, Tüzel E, Vidali L (2012) Quantitative analysis of organelle distribution and dynamics in Physcomitrella patens protonemal cells. BMC Plant Biol **12**: 70

Gardeström P, Igamberdiev AU (2016) The origin of cytosolic ATP in photosynthetic cells. Physiol Plant **157**: 367–379

Gauthier PPG, Battle MO, Griffin KL, Bender ML (2018) Measurement of gross photosynthesis, respiration in the light, and mesophyll conductance using H218O labeling. Plant Physiol **177**: 62–74

Gerotto C, Alboresi A, Meneghesso A, Jokel M, Suorsa M, Aro E-MEM, Morosinotto T (2016) Flavodiiron proteins act as safety valve for electrons in Physcomitrella patens. Proc Natl Acad Sci U S A **113**: 12322–12327

Ghirardi ML, Posewitz MC, Maness P-C, Dubini A, Yu J, Seibert M (2007) Hydrogenases and hydrogen photoproduction in oxygenic photosynthetic organisms. Annu Rev Plant Biol **58**: 71–91

Godaux D, Bailleul B, Berne N, Cardol P (2015) Induction of photosynthetic carbon fixation in anoxia relies on hydrogenase activity and proton-gradient regulation-like1-mediated cyclic electron flow in Chlamydomonas reinhardtii. Plant Physiol **168**: 648–58

Grechanik V, Romanova A, Naydov I, Tsygankov A (2020) Photoautotrophic cultures of Chlamydomonas reinhardtii: Sulfur deficiency, anoxia, and hydrogen production. Photosynth Res **143**: 275–286

Grossman AR, Catalanotti C, Yang W, Dubini A, Magneschi L, Subramanian V, Posewitz MC, Seibert M (2011) Multiple facets of anoxic metabolism and hydrogen production in the unicellular green alga Chlamydomonas reinhardtii. New Phytol **190**: 279–288

Harris EH (2001) As a odel rganism. Mol Biol **52**: 363–406

Järvi S, Suorsa M, Paakkarinen V, Aro E-M (2011) Optimized native gel systems for separation of thylakoid protein complexes: novel super- and mega-complexes. Biochem J **439**: 207–214

Joliot P, Béal D, Joliot A (2004) Cyclic electron flow under saturating excitation of dark-adapted Arabidopsis leaves. Biochim Biophys Acta **1656**: 166–176

Joliot P, Joliot A (2008) Quantification of the electrochemical proton gradient and activation of ATP synthase in leaves. Biochim Biophys Acta-Bioenerg **1777**: 676–683

Joliot PA, Finazzi G (2010) Proton equilibration in the chloroplast modulates multiphasic kinetics of nonphotochemical quenching of fluorescence in plants. Proc Natl Acad Sci U S A **107**: 12728–12733

Kirchhoff H, Hall C, Wood M, Herbstová M, Tsabari O, Nevo R, Charuvi D, Shimoni E, Reich Z (2011) Dynamic control of protein diffusion within the granal thylakoid lumen. Proc Natl Acad Sci U S A **108**: 20248–20253

Klodmann J, Sunderhaus S, Nimtz M, Jänsch L, Braun H-P (2010) Internal architecture of mitochondrial complex I from Arabidopsis thaliana. Plant Cell **22**: 797–810

Klughammer C, Schreiber U (1994) An improved method, using saturating light pulses, for the determination of photosystem I quantum yield via P700 + -absorbance changes at 830 nm. Planta **192**: 261–268

Klusch N, Senkler J, Yildiz Ö, Kühlbrandt W, Braun H-P (2020) A ferredoxin bridge connects the two arms of plant mitochondrial complex I. bioRxiv 2020.11.23.393975

Kohzuma K, Bosco CD, Meurer J, Kramer DM (2013) Light- and metabolism-related regulation of the chloroplast ATP synthase has distinct mechanisms and functions. J Biol Chem **288**: 13156

Kramer DM, Wise RR, Frederick JR, Alm DM, Hesketh JD, Ort DR, Crofts AR (1990) Regulation of coupling factor in field-grown sunflower: A Redox model relating coupling factor activity to the activities of other thioredoxin-dependent chloroplast enzymes. Photosynth Res **26**: 213–222

Kügler M, Jänsch L, Kruft V, Schmitz UK, Braun HP (1997) Analysis of the chloroplast protein complexes by blue-native polyacrylamide gel electrophoresis (BN-PAGE). Photosynth Res **53**: 35–44

Kühn K, Obata T, Feher K, Bock R, Fernie AR, Meyer EH (2015) Complete mitochondrial complex I deficiency induces an up-regulation of respiratory fluxes that is abolished by traces of functional complex I. Plant Physiol **168**: 1537–1549

Kukuczka B, Magneschi L, Petroutsos D, Steinbeck J, Bald T, Powikrowska M, Fufezan C, Finazzi G, Hippler M (2014) Proton gradient regulation5-like1-mediated cyclic electron flow is crucial for acclimation to anoxia and complementary to nonphotochemical quenching in stress adaptation. Plant Physiol **165**: 1604–1617

Lamattina L, Gonzalez D, Gualberto J, Grienenberger J (1993) Higher plant mitochondria encode an homologue of the nuclear-encoded 30-kDa subunit of bovine mitochondrial complex I. Eur J Biochem **217**: 831–838

Larosa V, Meneghesso A, La Rocca N, Steinbeck J, Hippler M, Szabò I, Morosinotto T (2018) Mitochondria affect photosynthetic electron transport and photosensitivity in a green alga. Plant Physiol **176**: 2305–2314

Lecler R, Vigeolas H, Emonds-Alt B, Cardol P, Remacle C (2012) Characterization of an internal type-II NADH dehydrogenase from Chlamydomonas reinhardtii mitochondria. Curr Genet **58**: 205–216

Leon G, Holuigue L, Jordana X (2007) Mitochondrial complex II is essential for gametophyte development in Arabidopsis. Plant Physiol **143**: 1534–1546

Li X-P, Muller-Moule P, Gilmore AM, Niyogi KK (2002) PsbS-dependent enhancement of feedback de-excitation protects photosystem II from photoinhibition. Proc Natl Acad Sci U S A **99**: 15222–15227

Li Z, Wakao S, Fischer BB, Niyogi KK (2009) Sensing and responding to excess light. Annu Rev Plant Biol **60**: 239–260

Ligas J, Pineau E, Bock R, Huynen MA, Meyer EH (2019) The assembly pathway of complex I in Arabidopsis thaliana. Plant J **97**: 447–459

Liguori N, Novoderezhkin V, Roy LM, Van Grondelle R, Croce R (2016) Excitation dynamics and structural implication of the stress-related complex LHCSR3 from the green alga Chlamydomonas reinhardtii. Biochim Biophys Acta-Bioenerg **1857**: 1514–1523

Maclean AE, Hertle AP, Ligas J, Bock R, Balk J, Meyer EH (2018) Absence of Complex I is associated with diminished respiratory chain function in European Mistletoe. Curr Biol **28**: 1614–1619. e3

Massoz S, Larosa V, Plancke C, Lapaille M, Bailleul B, Pirotte D, Radoux M, Leprince P, Coosemans N, Matagne RF, et al. (2013) Inactivation of genes coding for mitochondrial Nd7 and Nd9 complex I subunits in Chlamydomonas reinhardtii. Impact of complex I loss on respiration and energetic metabolism. Mitochondrion **19**: 365–374

Møller IM (2001) Plant mitochondria and oxidative stress: electron transport, NADPH turnover, and metabolism of reactive oxygen species. Annu Rev Plant Physiol Plant Mol Biol **52**: 561–591

Neff MM, Fankhauser C, Chory J (2000) Light: an indicator of time and place. Genes Dev **14**: 257–271

Nishio JN, Whitmarsh J (1993) Dissipation of the proton electrochemical potential in intact chloroplasts II. The pH gradient monitored by cytochrome f reduction kinetics. Plant Physiol **101**: 89–96

Noguchi K, Yoshida K (2008) Interaction between photosynthesis and respiration in illuminated leaves. Mitochondrion **8**: 87–99

Oldenkott B, Burger M, Hein AC, Jörg A, Senkler J, Braun HP, Knoop V, Takenaka M, Schallenberg-Rüdinger M (2020) One C-to-U RNA editing site and two independently evolved editing factors: Testing reciprocal complementation with DYW-Type PPR proteins from the moss physcomitrium (physcomitrella) patens and the flowering plants macadamia integrifolia and Arabidopsis. Plant Cell **32**: 2997–3018

Peters K, Nießen M, Peterhänsel C, Späth B, Hölzle A, Binder S, Marchfelder A, Braun H-P (2012) Complex I–complex II ratio strongly differs in various organs of Arabidopsis thaliana. Plant Mol Biol **79**: 273–284

Pineau B, Layoune O, Danon A, De Paepe R (2008) L-galactono-1, 4-lactone dehydrogenase is required for the accumulation of plant respiratory complex I. J Biol Chem **283**: 32500–32505

Porra RJ, Thompson WA, Kriedemann PE (1989) Determination of accurate extinction coefficients and simultaneous equations for assaying chlorophylls a and b extracted with four different solvents: verification of the concentration of chlorophyll standards by atomic absorption spectroscopy. Biochim Biophys Acta-Bioenerg **975**: 384–394

Radin I, Mansilla N, Rödel G, Steinebrunner I (2015) The Arabidopsis COX11 homolog is essential for cytochrome c oxidase activity. Front Plant Sci **6**: 1–17

Rak M, Rustin P (2014) Supernumerary subunits NDUFA3, NDUFA5 and NDUFA12 are required for the formation of the extramembrane arm of human mitochondrial complex I. FEBS Lett **588**: 1832–1838

Sacksteder CA, Kramer DM (2000) Dark-interval relaxation kinetics (DIRK) of absorbance changes as a quantitative probe of steady-state electron transfer. Photosynth Res **66**: 145–158

Sakakibara K, Nishiyama T, Sumikawa N, Kofuji R, Murata T, Hasebe M (2003) Involvement of auxin and a homeodomain-leucine zipper I gene in rhizoid development of the moss Physcomitrella patens. Development **130**: 4835–4846

Salinas T, Larosa V, Cardol P, Maréchal-Drouard L, Remacle C (2014) Respiratory-deficient mutants of the unicellular green alga Chlamydomonas: A review. Biochimie **100**: 207–218

Schimmeyer J, Bock R, Meyer EH (2016) L-Galactono-1,4-lactone dehydrogenase is an assembly factor of the membrane arm of mitochondrial complex I in Arabidopsis. Plant Mol Biol **90**: 117–126

Schönfeld C, Wobbe L, Borgstädt R, Kienast A, Nixon PJ, Kruse O (2004) The nucleus-encoded protein MOC1 is essential for mitochondrial light acclimation in Chlamydomonas reinhardtii. J Biol Chem **279**: 50366–50374

Sekiguchi T, Yoshida K, Okegawa Y, Motohashi K, Wakabayashi K, Hisabori T (2020) Chloroplast ATP synthase is reduced by both f-type and m-type thioredoxins. Biochim Biophys Acta-Bioenerg **1861**: 148261

Senkler J, Rugen N, Eubel H, Hegermann J, Braun H-P (2018) Absence of Complex I implicates rearrangement of the respiratory chain in European Mistletoe. Curr Biol **28**: 1606–1613.e4

Shameer S, Ratcliffe RG, Sweetlove LJ (2019) Leaf energy balance requires mitochondrial respiration and export of chloroplast NADPH in the light. Plant Physiol **180**: 1947–1961

Stiehl HH, Witt HT (1969) Quantitative treatment of the function of plastoquinone in photosynthesis. Zeitschrift für Naturforsch B **24**: 1588–1598

Storti M, Alboresi A, Gerotto C, Aro E-M, Finazzi G, Morosinotto T (2019) Role of cyclic and pseudo-cyclic electron transport in response to dynamic light changes in Physcomitrella patens. Plant Cell Environ **42**: 1590–1602

Storti M, Segalla A, Mellon M, Alboresi A, Morosinotto T (2020) Regulation of electron transport is essential for photosystem I stability and plant growth. New Phytol **228**: 1316–1326

Subrahmanian N, Remacle C, Hamel PP (2016) Plant mitochondrial Complex I composition and assembly: A review. Biochim Biophys Acta-Bioenerg **1857**: 1001–1014

Takizawa K, Cruz JA, Kanazawa A, Kramer DM (2007) The thylakoid proton motive force in vivo. Quantitative, non-invasive probes, energetics, and regulatory consequences of light-induced pmf. Biochim Biophys Acta **1767**: 1233–1244

Takizawa K, Kanazawa A, Kramer DM (2008) Depletion of stromal Pi induces high "energy-dependent" antenna exciton quenching (qE) by decreasing proton conductivity at CF O-CF1 ATP synthase. Plant, Cell Environ **31**: 235–243

Vanlerberghe GC, Dahal K, Alber NA, Chadee A (2020) Photosynthesis, respiration and growth: A carbon and energy balancing act for alternative oxidase. Mitochondrion **52**: 197–211

Vanlerberghe GC, Robson CA, Yip JYH (2002) Induction of mitochondrial alternative oxidase in response to a cell signal pathway down-regulating the cytochrome pathway prevents programmed cell death. Plant Physiol **129**: 1829–1842

Vidal G, Ribas-Carbo M, Garmier M, Dubertret G, Rasmusson AG, Mathieu C, Foyer CH, De Paepe R (2007) Lack of respiratory chain complex I impairs alternative oxidase engagement and modulates redox signaling during elicitor-induced cell death in tobacco. Plant Cell **19**: 640–655

Wang C, Shikanai T (2019) Modification of activity of the thylakoid H(+)/K(+) antiporter KEA3 disturbs ΔpH-dependent regulation of photosynthesis. Plant Physiol **181**: 762–773

Watt IN, Montgomery MG, Runswick MJ, Leslie AGW, Walker JE (2010) Bioenergetic cost of making an adenosine triphosphate molecule in animal mitochondria. Proc Natl Acad Sci USA **107**: 16823–16827

Witt HT (1979) Energy conversion in the functional membrane of photosynthesis. Analysis by light pulse and electric pulse methods. The central role of the electric field. BBA Rev Bioenerg **505**: 355–427

Yang W, Catalanotti C, Wittkopp TM, Posewitz MC, Grossman AR (2015) Algae after dark: Mechanisms to cope with anoxic/hypoxic conditions. Plant J **82**: 481–503

Yoshida K, Noguchi K (2011) Interaction between chloroplasts and mitochondria: Activity, function, and regulation of the mitochondrial respiratory system during photosynthesis. *In* F Kempken, ed, Plant Mitochondria. Springer, New York, pp 383–409

Zalutskaya Z, Lapina T, Ermilova E (2015) The Chlamydomonas reinhardtii alternative oxidase 1 is regulated by heat stress. Plant Physiol Biochem **97**: 229–234

Zhang L-T, Zhang Z-S, Gao H-Y, Meng X-L, Yang C, Liu J-G, Meng Q-W (2012) The mitochondrial alternative oxidase pathway protects the photosynthetic apparatus against photodamage in Rumex K-1 leaves. BMC Plant Biol **12**: 40

Supplementary material.
Supplemental Figure S1.

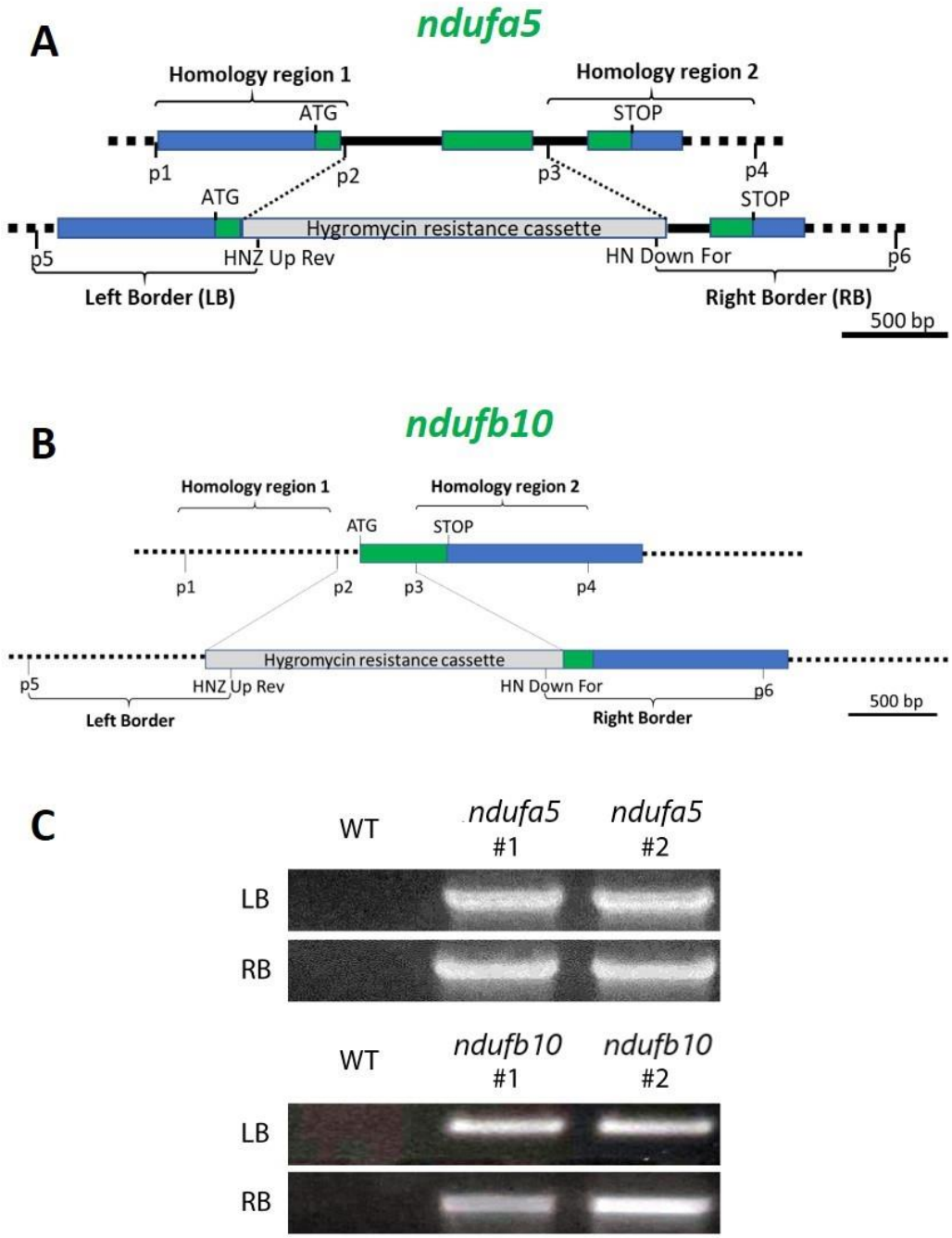

Supplemental Figure S1. Generation of *P. patens* mutant lines lacking respiratory complex I A-B) KO scheme for *Ndufa5* and *Ndufb10* respectively, showing the CDS, the regions of homology chosen to drive homologous recombination and insertion of the resistance cassette. In A and B are indicated the position of the primers employed for recombination cassette construction (p1, p2, p3 and p4) and primers employed in mutant screening (p5, p6, HNZ Up Rev and HN Down for). C) Example of PCR for verification of the homologous recombination event. PCR products (called Left and Right Border, LB and RB; all PCR products have an expected size of ca 1200 bp. LB was performed with primer p5 and HNZ Up rev while RB was performed with HN Down for and p6) are generated only if the resistance cassette is inserted in the expected genomic region.

Supplemental Figure S2.

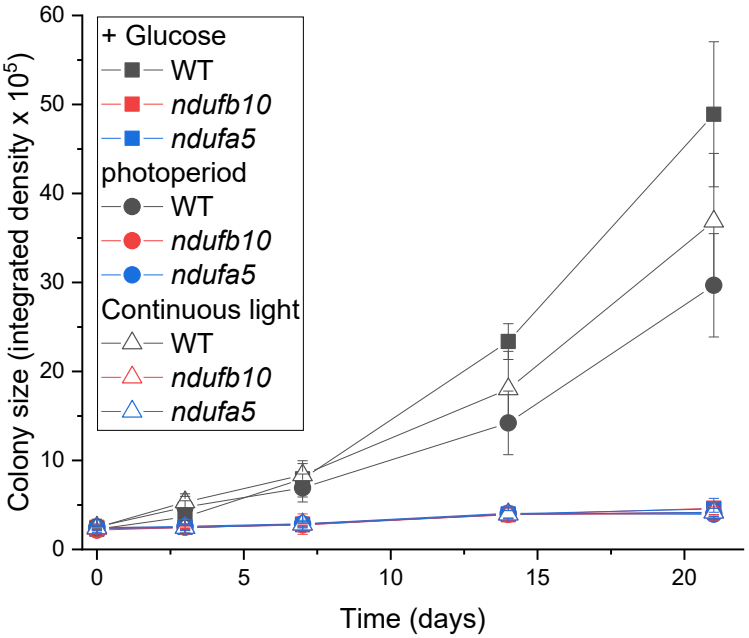

Supplemental Figure S2. Growth kinetics of *P. patens* plants under different conditions. Plants were grown under different light regimes and different medium composition as shown in Figure 2 and their size was evaluated after 0, 3, 7, 14 and 21 days of growth. All plants were exposed to 50 µmol photons m^{-2} s^{-1}. Squares show growth in medium supplemented with 0.5% of glucose, circles growth at 16h light/8h light/dark photoperiod in minimal medium, triangles growth under continuous light regime in minimal medium. WT, *ndufb10* and *ndufa5* KO are shown respectively in black, red and blue. Average ± SD (n ≥ 5) is reported.

Supplemental Figure S3.

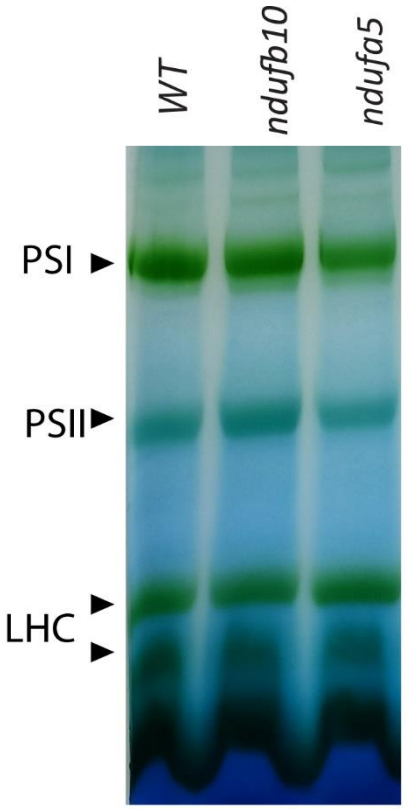

Supplemental Figure S3. BN-PAGE separation of crude extracts. Crude membrane protein extracts from WT, *ndufb10* and *ndufa5* were solubilized with 1% of β-dodecyl maltoside (β-DM). Complexes of thylakoid membranes identifiable as green bands are indicated; PSI, Photosystem I; PSII, photosystem II; LHC, light-harvesting chlorophyll complexes.

Supplemental Figure S4.

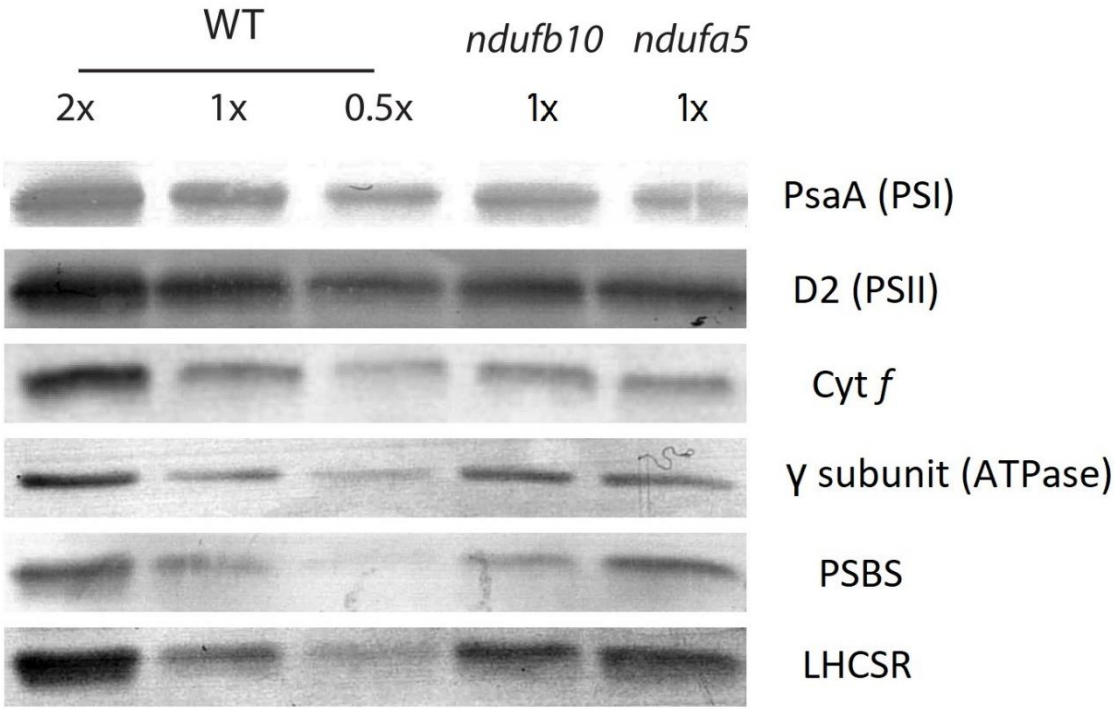

Supplemental Figure S4. Impact of Complex I mutations on the photosynthetic apparatus composition. Immunoblot analysis of various proteins of the photosynthetic apparatus. For WT 1X, *ndufb10* and *ndufa5* a total protein extract amount equivalent to 2 µg of total chlorophyll was loaded. 2X and 0.5X correspond to an equivalent of 4 µg and 1 µg of total chlorophyll. PSI and PSII, Photosystem I and II; Cyt, Cytochrome.

Supplemental Figure S5.

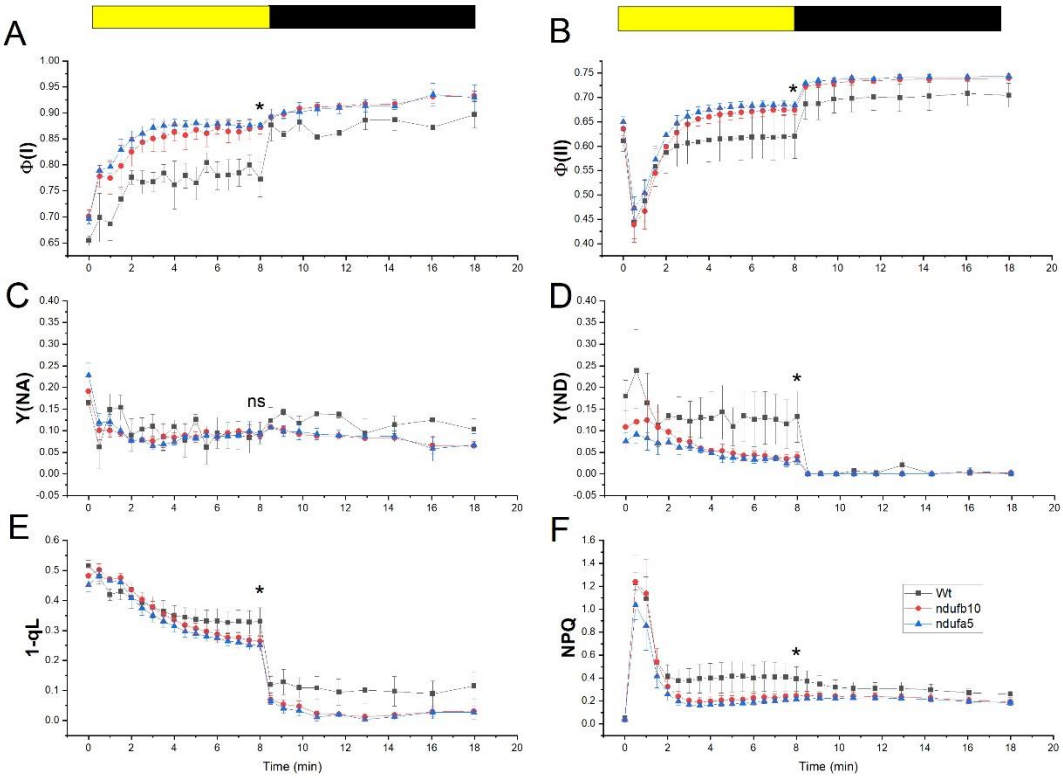

Supplemental Figure S5. Photosynthetic efficiency under dim illumination. The yield of PSI (Φ(I), A), PSII (Φ(II), B). PSI acceptor side limitation (Y(NA), C), PSI donor side limitation (Y(ND), D). PQ redox state (1-qL; E) and non-photochemical quenching (NPQ; F) were monitored under illumination of 50 µmol photons $m^{-2}s^{-1,}$ corresponding to light intensity during growth. WT, *ndufb10* and *ndufa5* KO are shown respectively as black squares, red circles and blue triangles. Yellow/black bar indicates light on/off. Data are shown as average ± SD (n > 4). Asterisks indicate statistically significant differences (one-way ANOVA, n > 5, p < 0.01) between WT and both mutants while ns indicates when eventual differences are not statically significant. Statistical analyses were performed for the last point before light was switched off.

Supplemental Figure S6.

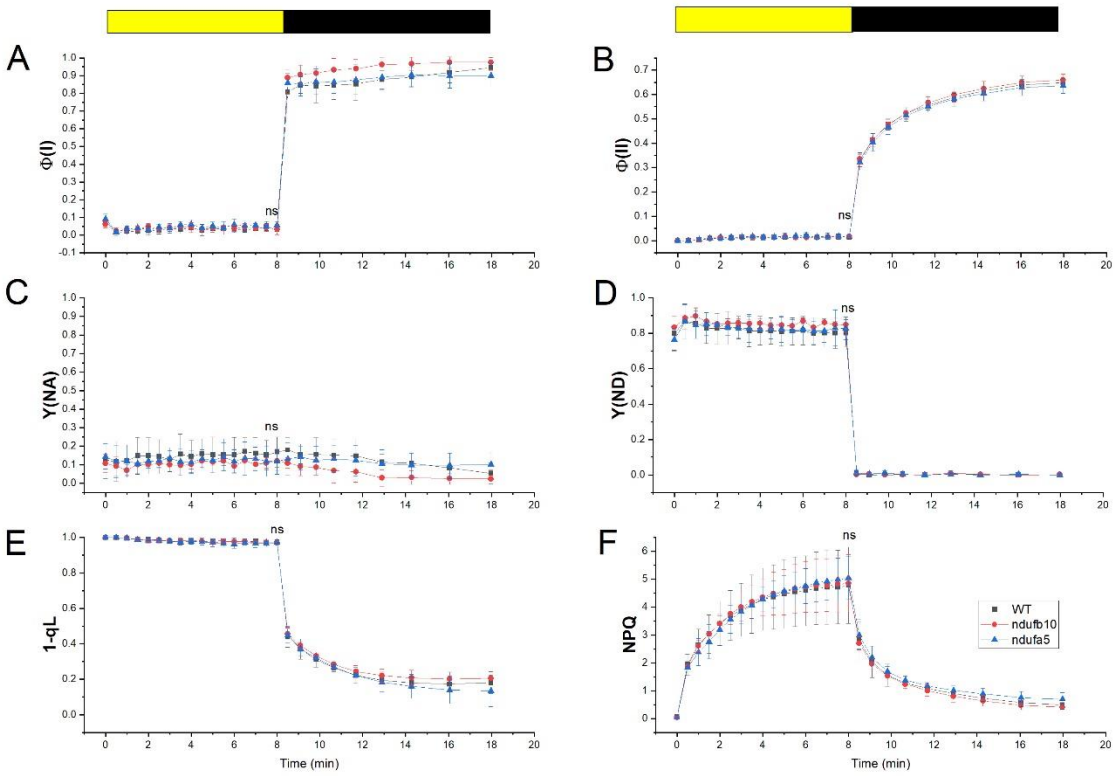

Supplemental Figure S6. Photosynthetic efficiency under saturating illumination. The yield of PSI (Φ(I), A), PSII (Φ(II), B). PSI acceptor side limitation (Y(NA), C), PSI donor side limitation (Y(ND), D). PQ redox state (1-qL; E) and non-photochemical quenching (NPQ; F) under 2000 µmol photons $m^{-2}s^{-1}$ of light intensity. WT, *ndufb10* and *ndufa5* KO are shown respectively with black square, red circle and cyan triangle. Yellow boxes above the panels represent actinic light on, instead black boxes represent actinic light off. Data are shown as average ± SD (n > 4). Statistical analysis was performed for the last point of illumination before light was switched off (one-way ANOVA, n > 4, $p < 0.01$; ns = not significant).

Supplemental Figure S7.

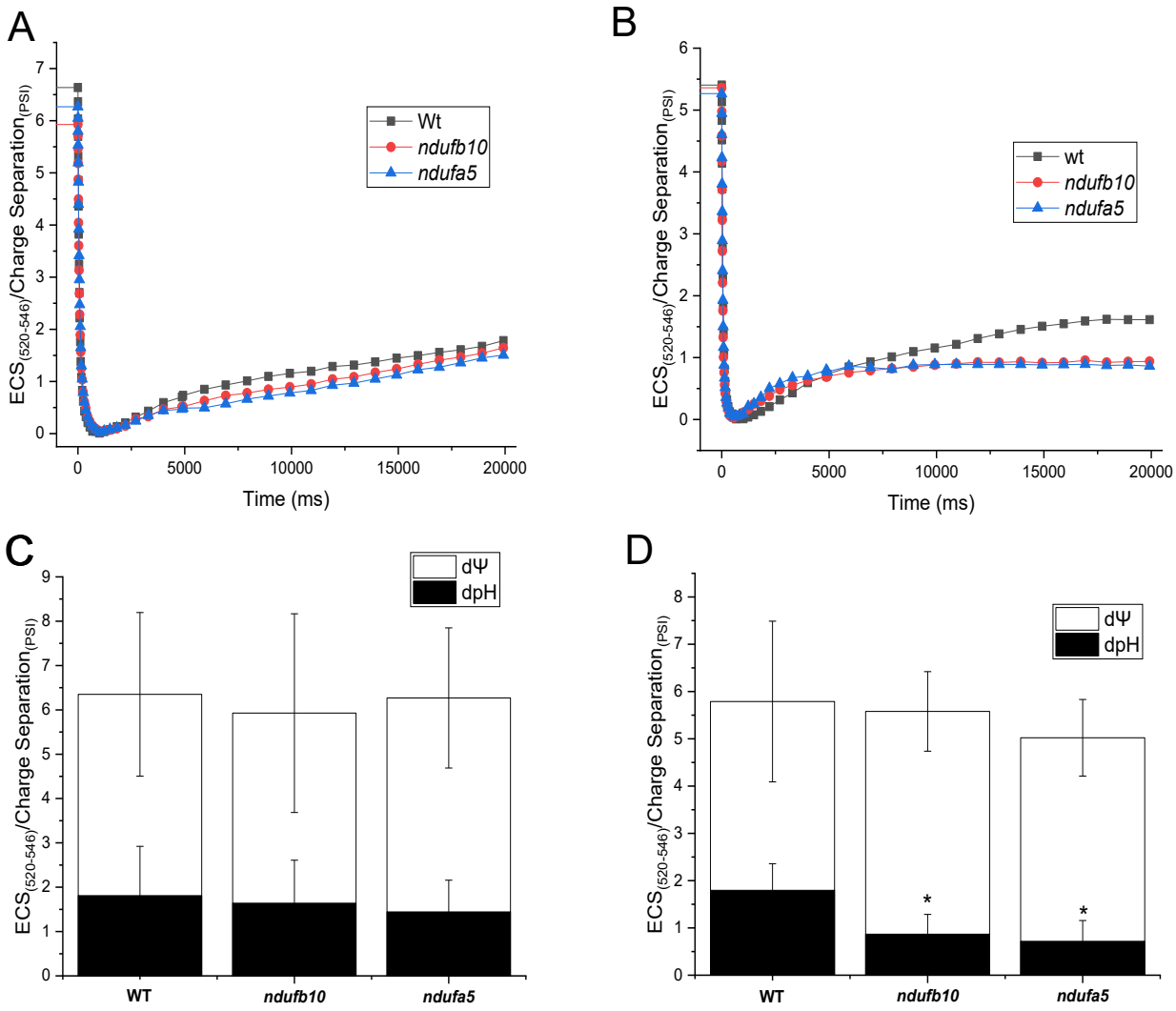

Supplemental Figure S7: Proton motive force composition before the steady state. A-B) Representative traces of the ECS (Electro-Chromic Shift) signal after the light is switch off after 60 s (A) and 120 s (B) of illumination (300 µmol photons m^{-2} s^{-1}). WT, *ndufb10* and *ndufa5* KO are shown respectively as black squares, red circles and blue triangles. C-D) pmf partitioning after 60 s (C) and 120 s (D) is represented with black columns for ΔpH component and white columns for the electrical potential (ΔΨ) Data are shown as average ± SD. For D asterisks indicate statistically significant differences (one-way ANOVA, $n > 5$, $p < 0.01$).

Supplemental Figure S8.

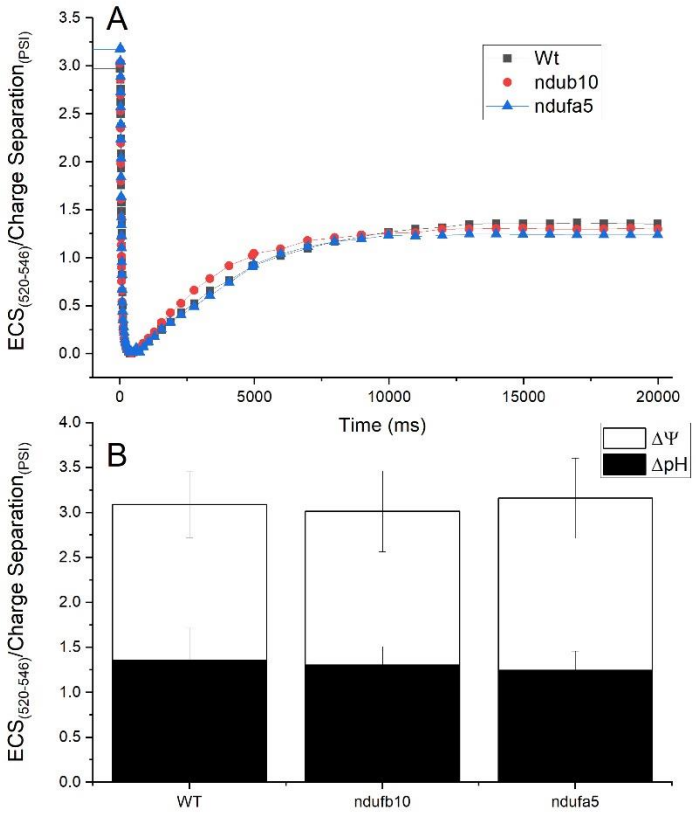

Supplemental Figure S8: Photosynthetic proton motive force at saturating illumination. Proton motive force (pmf) generated in thylakoids membranes assessed by ECS (Electro-Chromic Shift) signal in plants exposed for 300 seconds of illumination with saturating light (900 µmol m^{-2} s^{-1}). A) Representative tracks of the ECS signal after light is switch off. WT, *ndufb10* and *ndufa5* KO are shown respectively with black square, red circle and cyan triangle. B) Black columns are representative for the osmotic components (ΔpH) of pmf while white columns show the electrical potential (ΔΨ). Data are shown as average ± SD (n > 5).

Supplemental Figure S9.

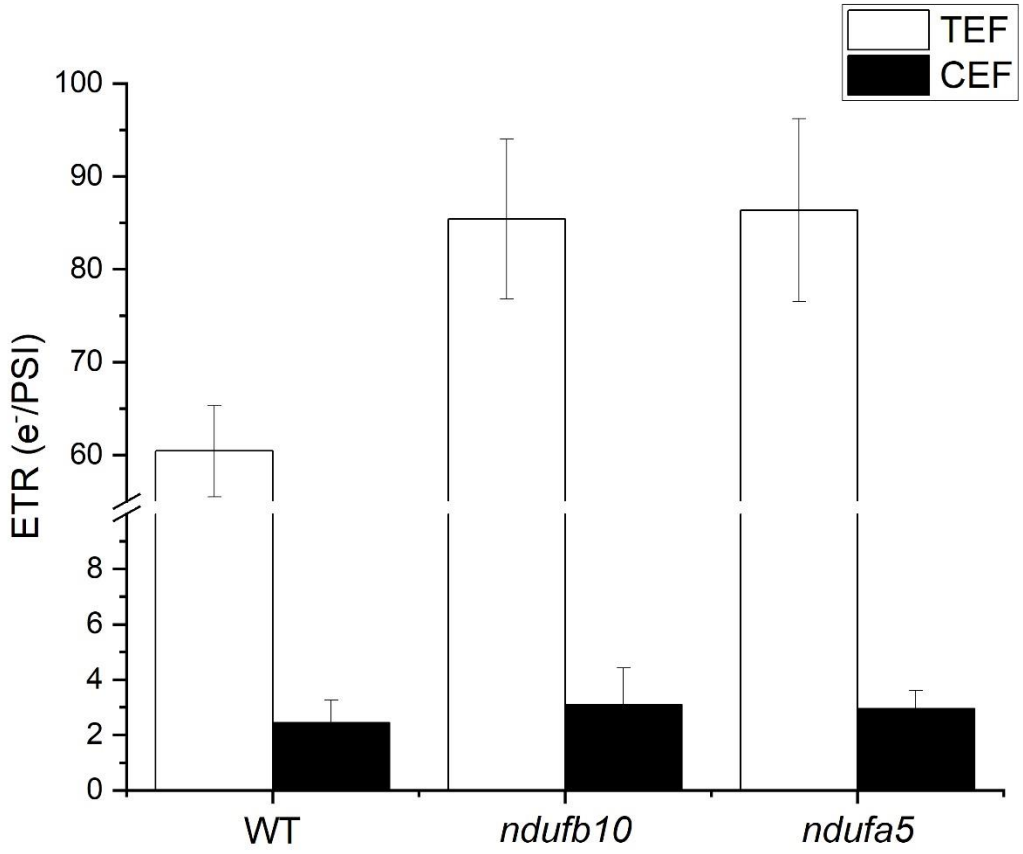

Supplemental Figure S9: Photosynthetic electron transfer (ETR) in *P. patens* plants. A) Total photosynthetic electron flow (TEF) and B) cyclic electron flow (CEF) measured in vivo in WT in *ndufb10* and *ndufa5* KO at 300 µmol photons $m^{-2}s^{-1}$ actinic light, calculated from electrochromic shift signal. Electron transport rate values are normalized to xenon-induced PSI turnovers. Data are shown as average ± SD (n > 4).

Supplemental Figure S10.

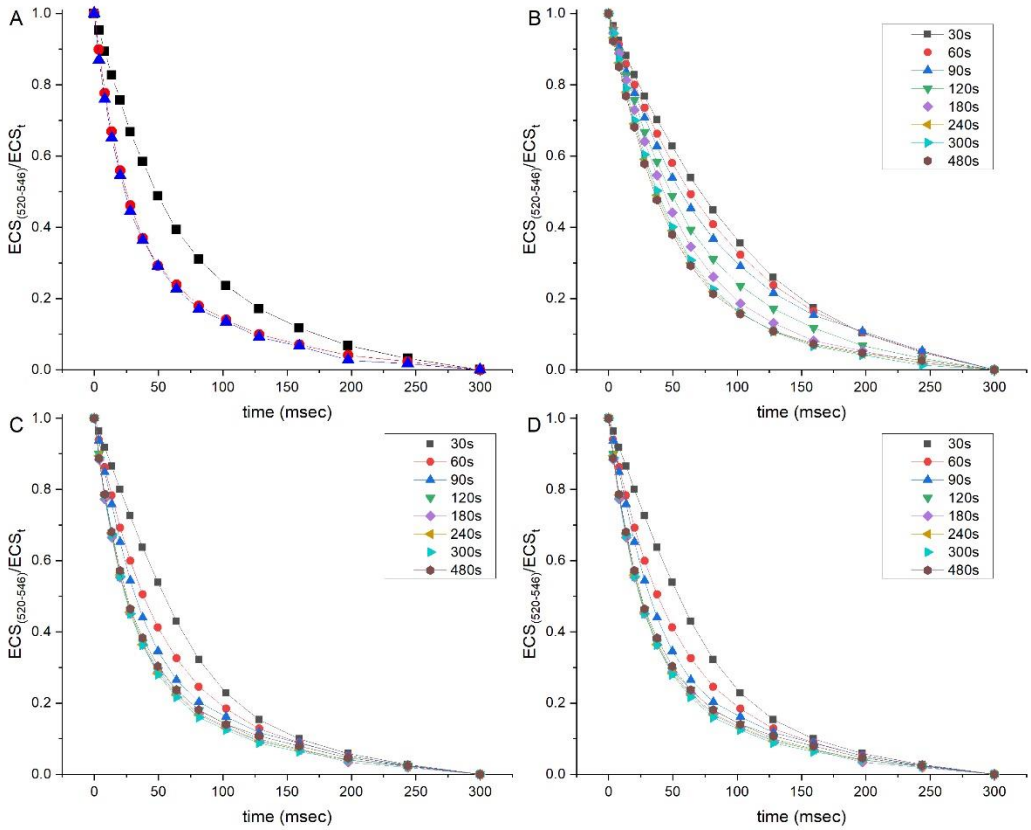

Supplemental Figure S10. ATPase activity assessed from ECS relaxation. A) Examples of ECS (Electro-Chromic Shift) relaxation kinetics after 120 seconds of illumination with sub-saturating light (300 µmol m^{-2} s^{-1}). WT, *ndufb10* and *ndufa5* KO are shown respectively as black squares, red circles and blue triangles. B-D) Examples of ECS relaxation traces for WT (B), *ndufb10* (C) and *ndufa5* (D) measured after illumination of different length. In every panel traces after 30, 60, 90, 120, 180, 240, 300 and 480 seconds are shown respectively as black squares, red circles, blue triangles, green triangles, magenta squares, ochre triangles, cyan triangles and carmine hexagons.

Supplemental Figure S11.

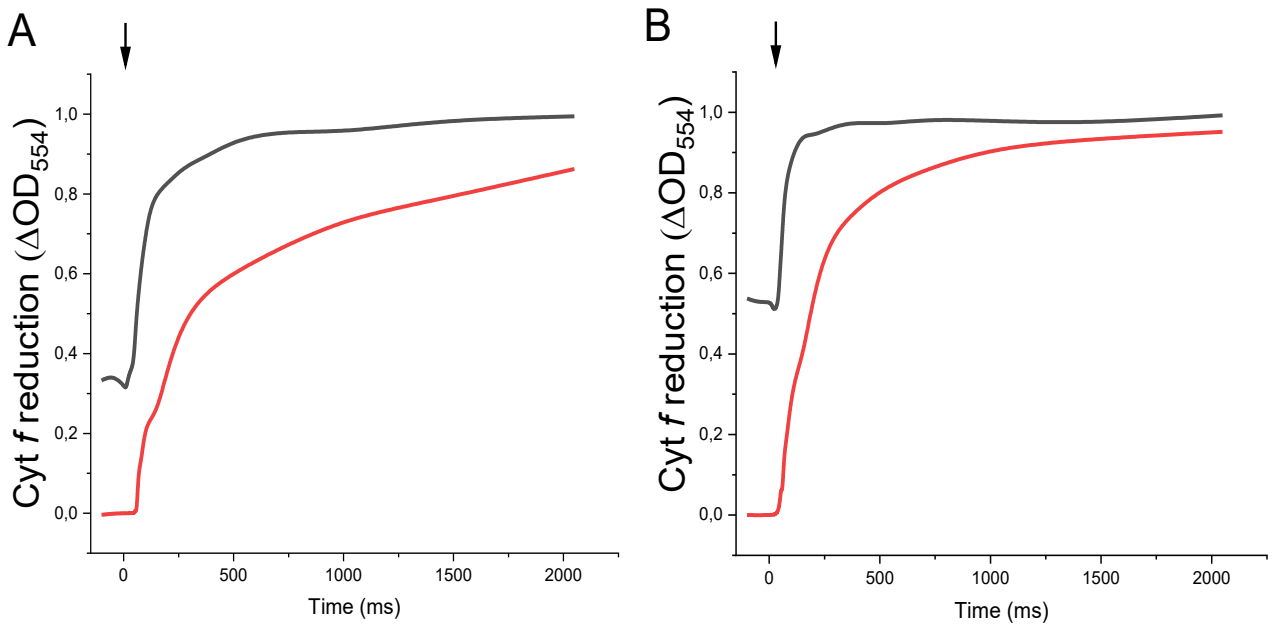

Supplemental Figure S11: Cyt *b6f* reduction state estimation. WT (A) and *ndufa5* (B) are here reported. Cyt *f* (cytochrome *f*) reduction showed in Figure 7 was measured by comparing the maximal signal obtained after 480 seconds under a saturating illumination (black line) with the signal obtained after treating the same sample by DCMU and DBMIB (red line). The traces here reported show the first 2000ms after light is switched off. The cyt *f* reduction rate was measured with a multiple exponential fitting of the complete cyt *f* reduction curve. All samples are normalized to the maximal signal. Arrows (t = 0): light off.

Supplemental Figure S12.

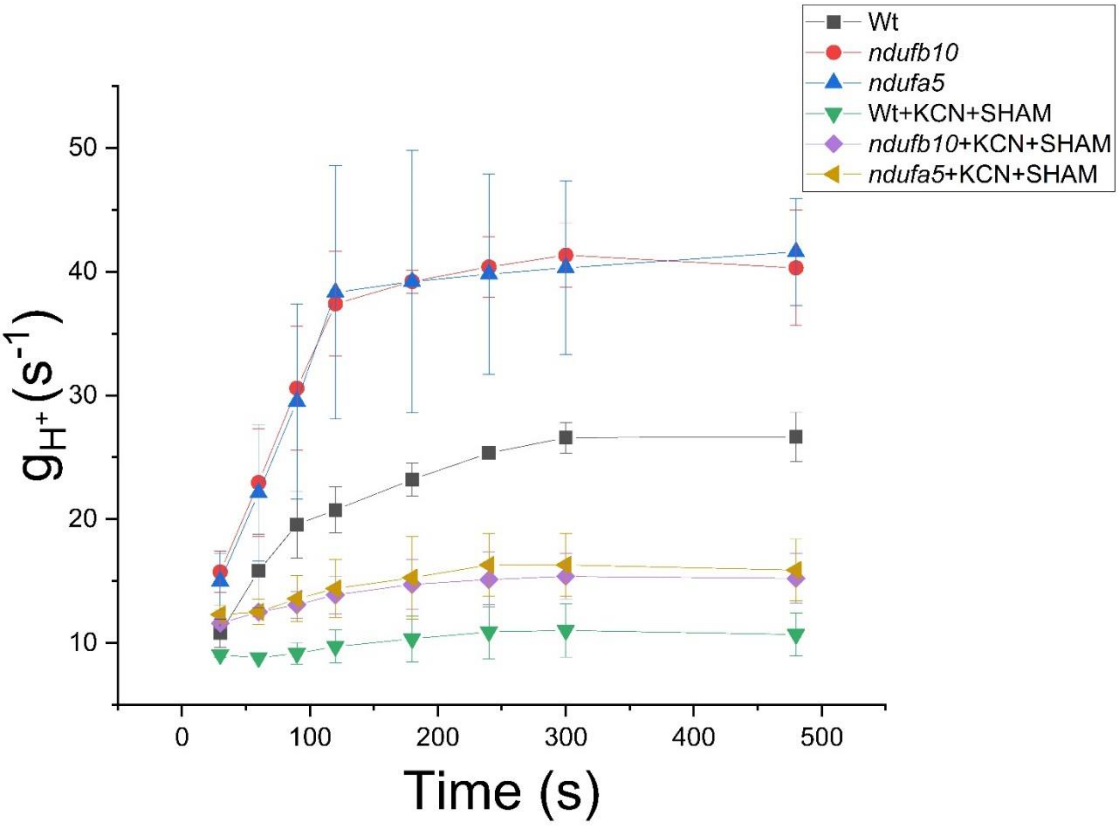

Supplemental Figure S12. Influence of respiration inhibition (KCN+SHAM) on proton conductivity (g_H^+) in WT and CI mutants. Proton conductivity (g_H^+) measured in control conditions and when respiration is fully inhibited in both WT and CI mutants with KCN 1mM and SHAM 8mM (as in Figure 4C). For control conditions WT, *ndufb10* and *ndufa5* KO are shown respectively with black squares, red circles and blue triangles. For the treatment with inhibitors WT, *ndufb10* and *ndufa5* KO are shown respectively with green triangles, magenta squares, ochre triangles. g_H^+ was calculated after exposure to 30s, 60s, 90s, 120s, 180s, 240s, 300s and 480s of illumination (approx. 350 µmol photons $m^{-2}s^{-1}$) by fitting the first 300 ms of the ECS (Electro-Chromic Shift) decay curve with a first-order exponential decay kinetic and indicated as the inverse of the decay time constant (Avenson et al., 2005). Data are shown as average ± SD (n > 3).

Supplemental Figure S13.

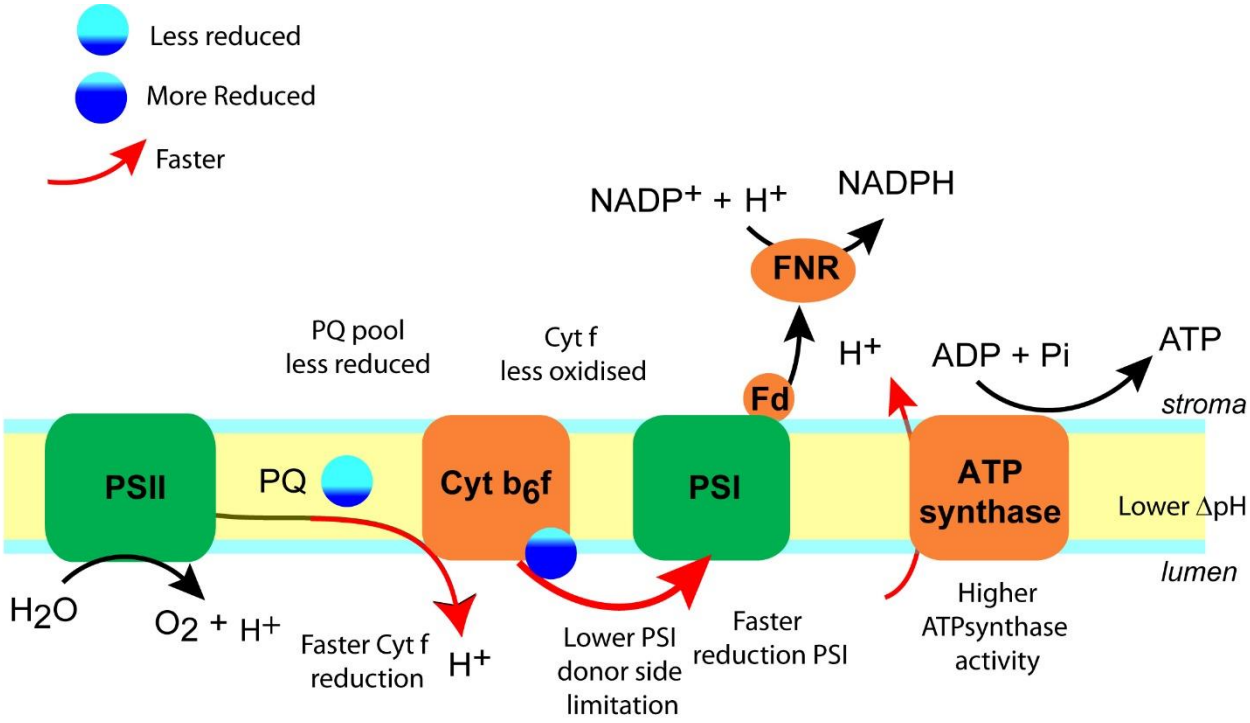

Supplemental Figure S13. Summary of photosynthetic electron transport alterations in CI depleted plants. Scheme of the main components of photosynthetic electron transport from water to NADP+ summarizing all differences observed in the mutants with respect to WT. PSI (II), Photosystem I (II); PQ, plastoquinone; Cyt, cytochrome; Fd, Ferredoxin; FNR, Ferredoxin NADP reductase.

Supplemental Table S1. Identification of conserved CI subunits in *P. patens*. Complex I subunits from *B. taurus*, *Y. lipolytica*, *C. reinhardtii* and *A. thaliana* were obtained from Salinas et al., 2014, Subrahmanian et al., 2016 and Klusch et al., 2020. Names of proteins are based on published papers and reviews (see references). *P. patens* nuclear homologous sequences were identified using BLAST facilities (https://blast.ncbi.nlm.nih.gov/Blast.cgi) with fungal, mammal, and plant protein and genic sequences against the *P. patens* genome (v3.3) (Lang et al., 2018; https://phytozome.jgi.doe.gov/pz/portal.html). Subunits encoded in the mitochondrial genome were identified from Terasawa et al., 2007. Name for the subunits in plants are reported only when they differ from animals or yeast. In red are indicated subunits that were confirmed by proteomic analyses (Mueller et al., 2014) In bold are indicated the subunits choose for inactivation of the complexes. a) Salinas et al., 2014; b) Subrahmanian et al., 2016; c) Terasawa et al., 2007; d)Klusch et al., 2020 e) Rak and Rustin, 2014; f) Barbieri et al., 2011; g) Klodmann et al., 2011, h) Mueller et al., 2014.

B. taurus	*Y. lipolytica*	*A. thaliana*	*C. reinhardtii*	*P. patens*	Ref.
Bacterial core					
ND1	ND1/ NU1M	AtMg00516, AtMg01120, AtMg01275	AAB93446, nd1	YP_539026	a, b, c, d
ND2	ND2/ NU2M	AtMg00285, AtMg01320	AAB93444, nd2	YP_539019	a, b, c, d
ND3	ND3/ NU3M	AtMg00990	AAQ55461, ND3	YP_539030	a, b, c, d
ND4	ND4/ NU4M	AtMg00580	AAB93441, nd4	YP_539018	a, b, c, d
ND4L	ND4L/ NULM	AtMg00650	AAO61142, nd4L	YP_539012	a, b, c, d
ND5	ND5/ NU5M	AtMg00060, AtMg00513, AtMg00665	AAB93442, nd5	YP_539016	a, b, c, d
ND6	ND6/ NU6M	AtMg00270	AAB93445, nd6	YP_539023	a, b, c, d
NDUFS1/ 75 kD	NUO78/ NUAM	At5g37510	XP_001692885, NUOS1	Pp3c1_34110, Pp3c1_34100, Pp3c1_34140, Pp3c19_19270	a, b, d, h
NDUFS2	NUO49/ NUCM	AtMg00510	XP_001697607, ND7	YP_539031	a, b, d, h
NDUFS3	NUO30.4	AtMg00070	XP_001690652, ND9	YP_539028	a, b, d, h
NDUFS7/ PSST	NUO19.3/ NUKM	At5g11770	XP_001700585, NUO10	Pp3c15_14890, Pp3c15_20620	a, b, d
NDUFS8/ TYKY	NUO21.3c/ NUIM	At1g16700, At1g79010	XP_001702368, NUO8	Pp3c9_8460, Pp3c15_4330	a, b, d
NDUFV1	51/ NUBM	At5g08530	XP_001702590, NUO6	Pp3c4_17990, Pp3c12_4050	a, b, d
NDUFV2	NUO24/ NUHM	At4g02580	XP_001698508, NUO5	Pp3c2_9810, Pp3c2_9813	a, b, d
Conserved supernumerary					
NDUFA1/ MWFE	NUO9.8/ NIMM	At3g08610	XP_001698399, NUOA1	Pp3c10_5690, Pp3c10_5720	a, b, d

NDUFA2/ B8	NUO10.5/ NI8M	At5g47890	XP_001695875, NUOB8	Pp3c20_8510	a, b, d
NDUFB3/ B12	NUO10.6/ NB2M	At2g02510, At1g14450	XP_001700920, NUOB12	Pp3c9_5250, Pp3c15_3960	a, b, d
NDUFA5/ B13	**NUO29.9/ NUFM**	**At5g52840**	**XP_001693453, NUOB13**	**Pp3c5_12290**	a, b, d, e
NDUFS6/ 13 kD	NUO18.4/ NUMM	At3g03070	XP_001703419, NUOS6	Pp3c24_2620	a, b, d
NDUFA6/ B14	NUO14.8/ NB4M	At3g12260	XP_001694042, NUOB14	Pp3c1_37620, Pp3c2_3180	a, b, d
NDUFA11/ B14.7	NUO21.3b/ NUJM	At2g42210	XP_001689829, TIM17	Pp3c5_22310, Pp3c6_9862	a, b, d
NDUFB11 /ESSS	NUO11.7/ NUWM	At3g57785, At2g42310	XP_001697702, NUO17	Pp3c3_16790	a, b, d
NDUFS5/ PFFD	NUO11.5/ NIPM	At3g62790, At2g47690	XP_001691060, NUOS5	Pp3c7_20680, Pp3c11_13470	a, b, d
NDUFB4/B15	NUO6.6/ NUVM	At2g31490	XP_001693191, NUOB4	Pp3c16_220, Pp3c25_300	a, b, d
DAP13/ B17.2	NUO13.4	At3g03100	XP_001699522	Pp3c16_5910	a, b, d
NDUFB7/ B18	NB8M	At2g02050	XP_001698082, NUOB18	Pp3c10_11190, Pp3c14_25130	a, b
NDUFA12/ B16.6	NUO14/ NB6M	At1g04630, At2g33220	XP_001701450, NUOB16	Pp3c5_4240, Pp3c16_2570	a, b, d
DAP13/ B17.2	NUO13.4/ N7BM	At3g03100	XP_001699522, NUO13	Pp3c16_5910	a, b
NDUFB7/ B18	NB8M	At2g02050	XP_001698082, NUOB18	Pp3c10_11190, Pp3c14_25130	a, b, d
NDUFS4/ AQDQ	NUO21/ NUYM	At5g67590	XP_001695601, NUOS4	Pp3c8_17050, Pp3c12_14210, Pp3c24_19370	a, b, d
NDUFA8/ PGIV	NUO20.8/ NUPM	At5g18800, At3g06310	XP_001700114, NUOA8	Pp3c3_33480, Pp3c4_6220, Pp3c10_17050	a, b, d
NDUFB9/ B22	NI2M	At4g34700	XP_001698797, NUOB22	Pp3c6_19130	a, b, d
NDUFB10/ PDSW	**NUO12.3/ NIDM**	**At1g49140, At3g18410**	**XP_001694041, NUOB10**	**Pp3c9_26150**	a, b, d, f
NDUFA9/ 39 kD	NUO40/ NUEM	At2g20360	XP_001702653, NUOA9	Pp3c1_35920, Pp3c14_9070	a, b, d
NDUFB8/ ASHI	NUO20.1/ NIAM	At5g47570	XP_001700273, TEF29	Pp3c20_8820	a, b, d
NDUFB2/AGGG	NCU01436	At1g76200	–	Pp3c18_1920, Pp3c21_21340	a, b, d
NDUFB1/ MNLL	NUO20.9/ NUXM	At4g16450	XP_001696533, NUO21	Pp3c6_28950	a, b, d, h
NDUFC2/ B14.5B	NUO10.4	At4g20150 (NDU9)	XP_001693474, NUOP1	Pp3c1_24730, Pp3c14_13800	a, b, d
NDUFC1/ KFYI	NCU08300	At4g00585	XP_001697243	Pp3c7_13700	a, b, d
NDUFA3/ B9	NUO9.5/ NI9M	At2g46540	XP_001692978	Pp3c23_12490	a, b, d

NDUFAB1/ ACPM	SDAP	At1g65290, At2g44620	XP_001699275, ACP1	Pp3c13_14790, Pp3c20_7570, Pp3c23_19250, Pp3c24_6630	a, b, d
NDUFA7	NCU08930	At5g08060	XP_001703194	Pp3c16_5680	a, b, d
NDUFA4/ MLRQ	NCU02016	At3g29970	–	Pp3c3_14700, Pp3c4_20270, Pp3c26_5980	a, b
NDUFA10	–	At1g72040	–	Pp3c12_15090	a, b
Plant specific					
–	–	At5g63510 (CAL1), At1g19580 (CA1), At3g48680 (CAL2), At1g47260 (CA2), At5g66510 (CA3)	XP_001703237, XP_001701594, XP_001696746 (γ-carbonic anhydrase)	Pp3c4_16870, Pp3c7_19540, Pp3c7_4200, Pp3c11_22520, Pp3c1_7500,	a, b, d, g, h
–	–	At2g28430	–	Pp3c7_7440	a, b, g
–	–	At5g14105 (P3), At1g67350 (P1), At1g68680, At2g27730 (P2) (membrane arm subunits)	–	Pp3c1_22500, Pp3c1_33450, Pp3c3_5450, Pp3c11_6600, Pp3c14_2790,	a, b, g, h
–	–	At3g07480 (Ferredoxin)	XP_001699817, NUOP3,	Pp3c2_31000, Pp3c9_680	a, b, d

Supplemental Table S2. Capacities of the cytochrome and the AOX pathways in WT and *ndufb10* and *ndufa5* plants. The cyt pathway capacity is defined as O_2 uptake in the presence of SHAM that was sensitive to KCN. The AOX pathway capacity is defined as the O_2 uptake in the presence of KCN that was sensitive to SHAM. Calculations were made from data in figure 4 and respiration activity in plants treated with SHAM only, also reported here. Data are shown as average ± SD (n > 4).

$nmolO_2/(mg_{Chl}*min)$	WT	*ndufb10*	*ndufa5*
Cyt capacity	52.9 ± 8.1	52.2 ± 8.4	54.4 ± 7.4
AOX capacity	36.0 ± 9.7	73.4 ± 6.6	72.4 ± 7.4
+ 8 mM SHAM	74.3 ± 7.6	73.1 ± 8.0	75.2 ± 7.0

Supplemental Table S3: Primers employed in this work

Gene	Primer Name	Sequence	Use
Ndufb10	Ndufb10-p1	GTTTAAACGGCCCTAATGACATAAGTCCC	KO isolation
	Ndufb10-p2	CTCGAGGTGGATGAATGATGCTGGTG	KO isolation
	Ndufb10-p3	ATCGATCAAGTCGAGAAGGCGAAGATC	KO isolation
	Ndufb10-p4	TTAATTAAGATGGCGTCGAGTTCCTTCATC	KO isolation
	Ndufb10-p5	GGATCCACAATCAGGAATTA	KO screening
	Ndufb10-p6	ACCAAAGCAGTCCTGAAC	KO screening
	Ndufb10-RTf	GTTCAACAGCGACTACCCTA	RT-PCR
	Ndufb10-RTr	GAAACCCTTGTTCTGAAATG	RT-PCR
Ndufa5	Ndufa5-p1	CCTAGGCAATTCAGTATCCCTTACGC	KO isolation
	Ndufa5-p2	CTCGAGGGTCTGGTTTCCAACAATAA	KO isolation
	Ndufa5-p3	GTTAACGATGTTGACATGCACAGAAG	KO isolation
	Ndufa5-p4	TTAATTAAGACAACTAGGAACCATCCAA	KO isolation
	Ndufa5-p5	ATCAAACCCTGTACACCAAC	KO screening
	Ndufa5-p6	TGCAACTCATCTGTCCAATA	KO screening
	Ndufa5-RTf	TGCTTCATCATGTTTTTGAG	RT-PCR
	Ndufa5-RTr	AGAGCCAGATCAACAAGAAA	RT-PCR
Hygromycin resistance cassette	HNZ Up rev	TGCGCAACTGTTGGGAAG	KO screening
	HN Down for	CCGCTGAAATCACCAGTCTC	KO screening
Actin	Actin2f	GCGAAGAGCGAGTATGACGAG	KO screening, RT-PCR
	Actin2r	AGCCACGAATCTAACTTGTGATG	KO screening, RT-PCR

Bibliography

Avenson, T.J., Cruz, J.A., Kanazawa, A., Kramer, D.M., 2005. Regulating the proton budget of higher plant photosynthesis. Proc. Natl. Acad. Sci. U. S. A. 102, 9709–13. https://doi.org/10.1073/pnas.0503952102

Barbieri, M.R., Larosa, V., Nouet, C., Subrahmanian, N., Remacle, C., Hamel, P.P., 2011. A forward genetic screen identifies mutants deficient for mitochondrial complex I assembly in Chlamydomonas reinhardtii. Genetics 188, 349–58. https://doi.org/10.1534/genetics.111.128827

Klodmann, J., Senkler, M., Rode, C., Braun, H.-P., 2011. Defining the protein complex proteome of plant mitochondria. Plant Physiol. 157, 587–598.

Klusch, N., Senkler, J., Yildiz, Ö., Kühlbrandt, W., Braun, H.-P., 2020. A ferredoxin bridge connects the two arms of plant mitochondrial complex I. bioRxiv 2020.11.23.393975. https://doi.org/10.1101/2020.11.23.393975

Lang, D., Ullrich, K.K., Murat, F., Fuchs, J., Jenkins, J., Haas, F.B., Piednoel, M., Gundlach, H., Van Bel, M., Meyberg, R., Vives, C., Morata, J., Symeonidi, A., Hiss, M., Muchero, W., Kamisugi, Y., Saleh, O., Blanc, G., Decker, E.L., van Gessel, N., Grimwood, J., Hayes, R.D., Graham, S.W., Gunter, L.E., McDaniel, S.F., Hoernstein, S.N.W., Larsson, A., Li, F.-W., Perroud, P.-F., Phillips, J., Ranjan, P., Rokshar, D.S., Rothfels, C.J., Schneider, L., Shu, S., Stevenson, D.W., Thümmler, F., Tillich, M., Villarreal Aguilar, J.C., Widiez, T., Wong, G.K.-S., Wymore, A., Zhang, Y., Zimmer, A.D., Quatrano, R.S., Mayer, K.F.X., Goodstein, D., Casacuberta, J.M., Vandepoele, K., Reski, R., Cuming, A.C., Tuskan, G.A., Maumus, F., Salse, J., Schmutz, J., Rensing, S.A., 2018. The Physcomitrella patens chromosome-scale assembly reveals moss genome structure and evolution. Plant J. 93, 515–533. https://doi.org/10.1111/tpj.13801

Mueller, S.J., Lang, D., Hoernstein, S.N.W., Lang, E.G.E., Schuessele, C., Schmidt, A., Fluck, M., Leisibach, D., Niegl, C., Zimmer, A.D., Schlosser, A., Reski, R., 2014. Quantitative Analysis of the Mitochondrial and Plastid Proteomes of the Moss Physcomitrella patens Reveals Protein Macrocompartmentation and Microcompartmentation. Plant Physiol. 164, 2081–2095. https://doi.org/10.1104/pp.114.235754

Rak, M., Rustin, P., 2014. Supernumerary subunits NDUFA3, NDUFA5 and NDUFA12 are required for the formation of the extramembrane arm of human mitochondrial complex I. FEBS Lett. 588, 1832–1838. https://doi.org/10.1016/j.febslet.2014.03.046

Salinas, T., Larosa, V., Cardol, P., Maréchal-Drouard, L., Remacle, C., 2014. Respiratory-deficient mutants of the unicellular green alga Chlamydomonas: a review. Biochimie 100, 207–18. https://doi.org/10.1016/j.biochi.2013.10.006

Subrahmanian, N., Remacle, C., Hamel, P.P., 2016. Plant mitochondrial Complex I composition and assembly: A review. Biochim. Biophys. Acta - Bioenerg. 1857, 1001–1014. https://doi.org/10.1016/j.bbabio.2016.01.009

Terasawa, K., Odahara, M., Kabeya, Y., Kikugawa, T., Sekine, Y., Fujiwara, M., Sato, N., 2007. The mitochondrial genome of the moss Physcomitrella patens sheds new light on mitochondrial evolution in land plants. Mol. Biol. Evol. 24, 699–709. https://doi.org/10.1093/molbev/msl198

APPENDIX III

Assessment of microalgae photosynthetic activity in dense microalgae cultures using oxygen production

Antoni Mateu Vera-Vives[1], Tim Michelberger[1], Tomas Morosinotto[1] and Giorgio Perin[1]

[1] Department of Biology, University of Padova, Padova, Italy

Authorship statement

The general research question and experimental design were proposed by Prof. Tomas Morosinotto and Prof. Giorgio Perin. I collected the data along with PhD student Tim Michelberger. I analyzed the data, wrote the first draft and revised it after the comments of Prof. Giorgio Perin and Prof. Tomas Morosinotto. All authors revised and approved the final manuscript.

Abstract

Microalgae are photosynthetic microorganisms that play a pivotal role in primary production in aquatic ecosystems, sustaining the entry of carbon in the biosphere. Microalgae biomass has also been long recognized as alternative to the current fossil-fuels-based economy to increase the long-term sustainability of our society. In biological systems, the homeostasis of the central metabolism depends on the energetic and redox status of the cell, which in strictly photoautotrophic microalgae is directly controlled by the photosynthetic activity of the chloroplast, that in turn generates molecular oxygen. The concentration of this by-product can therefore be used as proxy of photosynthetic activity. Photosynthesis depends on light availability, that is not constant over time. In nature, sunlight fluctuates over diurnal cycles and weather conditions, affecting photosynthetic functionality with implications on microalgae fitness in natural ecological niches. In microalgae dense cultures in photobioreactors, light availability is complicated even further, and because of self-shading and mixing kinetics, cells here experience artificial fluctuations of irradiance, heavily impacting photosynthetic activity, and biomass productivity. How photosynthesis responds to the artificial light conditions of photobioreactors is still under-investigated and in this work, we validated one state-of-the-art technology to assess microalgae photosynthetic functionality in such a complex light environment, using *Nannochloropsis gaditana* as validation model. The technology was also used to demonstrate at the lab-scale that the reduction of the pigment content is a valuable strategy to increase photosynthetic activity of dense microalgae cultures, typical of photobioreactors at scale.

1. Introduction

Photosynthetic organisms are responsible for primary production, sustaining life on our planet. Among them, eukaryotic microalgae are unicellular aquatic species that play a pivotal role in the biosphere, being responsible for approximately 50 % of global primary production. Thousands of different microalgae species exist, as the result of evolution in a plethora of ecological niches, where they are often placed at the basis of the existing food web, representing the main entry point of atmospheric carbon in the biosphere. Beside their fundamental ecological role, microalgae are also gaining increasing interest as bio-factories to convert the current fossil-fuels-based economy to a bio-based solar-driven alternative, for a more sustainable future. The greater photosynthetic activity than plants leads to higher rates of CO_2 and nutrients sequestration, enabling their cultivation in strict connection to industrial and civil sites to mitigate greenhouse gases emissions and water pollution. Moreover, their huge metabolic plasticity, developed in thousands of years of evolution in different ecological niches shaped the ability to accumulate a plethora of metabolites finding many applications in the current economy, e.g., from biofuels to food additives.

In microalgae, as in many other photosynthetic eukaryotes, the homeostasis of the central metabolism depends on the energetic and redox status of the cell, which is balanced by the activity of two organelles, i.e., chloroplasts and mitochondria. In strictly photoautotrophic microalgae species, mitochondrial respiration shows a minimal activity and only sustains cell maintenance, making the photosynthetic activity of the chloroplast the major regulator of the homeostasis of the central metabolism.

Chloroplasts contain membrane-bound enzymatic complexes that, via photosynthesis, drive both i) the transfer of electrons from a reduced substrate (i.e., water) to an oxidized product (i.e., $NADP^+$) and ii) the translocation of protons across a biological membrane to generate a proton motive force that fuels the synthesis of chemical energy in form of ATP, by the action of ATP synthase. Overall, chloroplasts generate reducing power and chemical energy, and therefore play a key role in the maintenance of the homeostasis of the redox and energetic status of the cell. Photosynthetic activity in the chloroplast depends on the availability of light energy, which in nature changes over diurnal cycles and weather conditions, affecting photosynthetic functionality and consequently microalgae fitness. The ability to

respond to environmental changes in light availability is one of the phenomena at the base of the success of some microalgae species over others in different ecological niches, with implications for the functionality of the very ecosystem.

On the other hand, when microalgae biomass is to be exploited for industrial applications, these organisms are cultivated in open or closed systems outdoors, i.e., ponds or photobioreactors, respectively, in which cells reach high cell density to maximize biomass productivity. In these conditions, beside natural variations of light intensity, microalgae are exposed to faster fluctuations of irradiance because of cells' self-shading and mixing, which are known to affect photosynthesis and biomass productivity in photobioreactors. The impact of this complex light environment on microalgae physiology is still under-investigated and this is one of the most relevant causes for the scarce success of the optimization efforts of microalgae cultivation at scale so far.

A more systematic investigation of how photosynthesis responds to changes in light availability is an unavoidable task to understand how microalgae deal with the complex environmental light conditions of photobioreactors. One of the reasons why this important piece of information is still missing is that most of the phenomena impacting microalgae photosynthesis in photobioreactors can be measured only at large scale, calling for a very time- and resource-consuming approach. However, a good approximation might be achieved also with lab-scale investigations, if the available technology to measure the photosynthesis-irradiance relationship in microalgae is improved to achieve information representative of environmental conditions typical of industrial microalgae cultures.

In this work, we investigated the potentiality of a high-resolution, next-generation technology for lab-scale investigation of photosynthesis-irradiance relationship, comparing very-low concentration with high-density microalgae cultures, using *Nannochloropsis gaditana* as validation model. The reliability and versatility of this technology has been validated also using photosynthetic pale mutants, previously isolated for an improved light penetration in dense cultures, demonstrating the larger the reduction in pigment content, the greater the increase in photosynthetic activity in lab conditions simulating photobioreactors.

2. Results

2.1. Estimation of photosynthetic functionality from oxygen evolution.

Nannochloropsis cells grown in lab-scale cultures, as described in the materials and methods section, were used to investigate the photosynthesis-irradiance relationship of samples with increasing cell concentration. 5×10^6 cells mL^{-1}, corresponding to a chlorophyll concentration of 4 µg Chl mL^{-1} were enough to collect traces of sufficient quality for a reliable extrapolation of the parameters describing the photosynthetic activity of *Nannochloropsis* cells (Figure 1). Lower concentrations have a higher noise but still were able to generate traces of sufficient quality (Supplementary Figure 1).

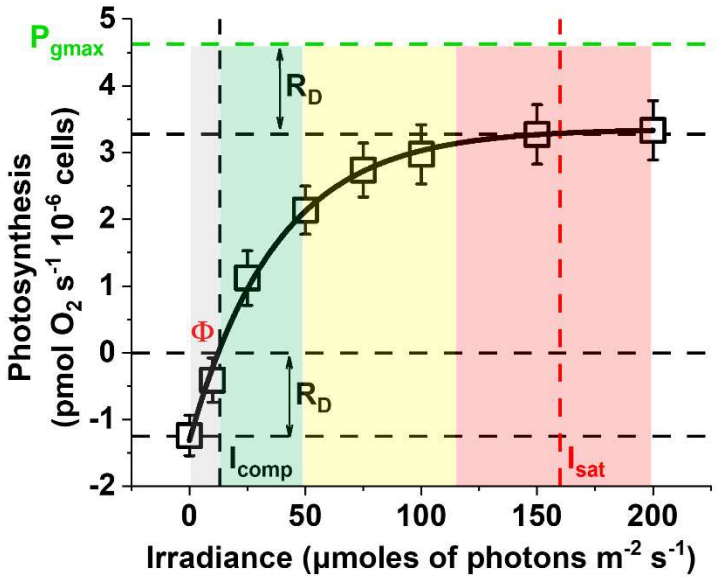

Figure 1 | **Dependence of Photosynthesis on light intensity.** Data here shown belong to a *Nannochloropsis* culture with 5×10^6 cells mL^{-1} cells concentration. Photosynthesis is expressed as O_2 flux and it is normalized to the number of cells. Light intensity is expressed as irradiance. I_{comp} and I_{sat} indicate the light compensation and light saturation points, respectively, both expressed as [µmol photons$\cdot s^{-1}\cdot m^{-2}$]. R_D is the dark O2 respiration rate, expressed as [pmol$\cdot s^{-1}\cdot 10^{-6}$ cells], P_{gmax} is the maximal gross O2 photosynthetic rate, expressed as [pmol$\cdot s^{-1}\cdot 10^{-6}$ cells]. $\Phi_{(I_0\_I_{comp})}$ is the quantum yield in the range between I_0 and I_{comp} [pmol O2$\cdot m^2\cdot$µmol photons$^{-1}\cdot 10^{-6}$cells]. In this scheme, four irradiance regions have been highlighted with different colours: grey, the respiration rate is higher than the photosynthetic rate; green, the photosynthetic rate linearly increases with irradiance; yellow, the photosynthetic rate increases with irradiance up to a saturation limit; red, the photosynthetic rate does not increase with irradiance.

Nannochloropsis samples at a concentration of 5×10^6 cells mL^{-1} showed a dark respiration rate (R_D) of 1.31 ± 0.12 pmol O_2 $s^{-1}\cdot10^{-6}$ cells. Light intensity was then progressively increased from 0 to 200 µmol photons s^{-1} m^{-2}. The light compensation point (i.e., I_{comp}, namely the irradiance value where the dark respiration is fully compensated by the photosynthetic activity rate) was 12.2 ± 1.1 µmol photons s^{-1} m^{-2}, while the saturation threshold (i.e. I_{sat}, namely the irradiance value at which the photosynthetic rate does not linearly increase with irradiance any longer) was 163 ± 27 µmol photons$\cdot s^{-1}\cdot m^{-2}$. The maximal gross photosynthetic rate was instead 4.6 ± 0.2 pmol O_2 $s^{-1}\cdot10^{-6}$ cells.

In this work we present a novel method for quantifying photosynthesis that allows higher resolution compared to the classical methods commonly used in the past. The main difference is the instrument used, which has increased sensitivity compared with a classical Clark-type sensor. The NextGen-O2k has a resolution of 2 nM and a limit of detection of the oxygen flux of 0.001 µM s^{-1} (Doerrier et al., 2018; Gnaiger, 2008), and can therefore reliably detect even small differences in O_2 concentration. It is in fact worth noting that we could decrease the cell concentration by a 30× factor compared to similar experiments done in the past with a classical Clark-type sensor (Perin et al., 2015). Consequently, we could determine the photosynthetic parameters above detailed with relatively low-concentration microalgae samples, without sacrificing the reproducibility. The minimization of the volume of the microalgae culture exploited for these has a twofold important implication: i) self-shading effects during the measurements are minimized for an unbiased determination of photosynthetic parameters and ii) the changes in oxygen flow per volume are small, allowing the system to run for longer times without reaching values of oxygen concentration inside of the chamber that are so high that can have an effect on the sample.

2.2. Dependance of photosynthetic functionality from cell concentration.

Thanks to this sensitivity it is even possible to assess the impact of self-shading by measuring samples of *Nannochloropsis* with increasing cell concentrations, from 2.5 to 100×10^6 cells mL^{-1} (Figure 2). All cells were exposed to the same light conditions

during cultivation ensuring an identical acclimation state (average Chl content of 0.08 µg Chl · 10^{-6} cells).

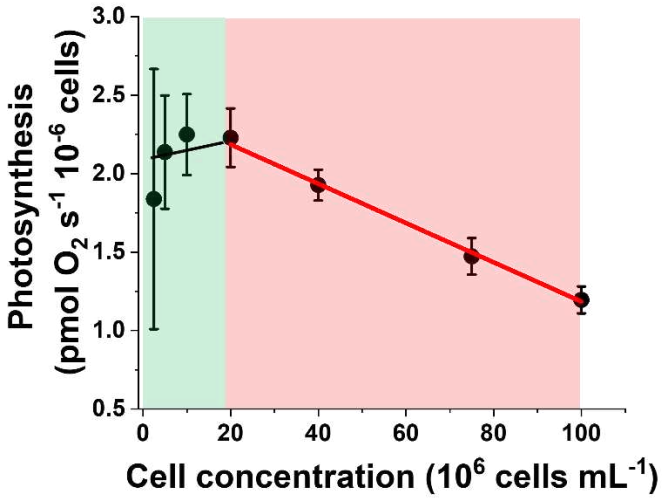

Figure 2 | **Photosynthetic activity as a function of cell concentration.** Photosynthesis is expressed as O_2 flux and it is normalized to the number of cells. The O_2 flux was measured in the linear phase of correlation between photosynthesis and irradiance (i.e. at 50 µmol photons m^{-2} s^{-1}) for *Nannochloropsis* samples with increasing cell concentration: 2.5, 5, 10, 20, 40, 75 and 100 · 10^6 cells mL^{-1} (original traces in Supplementary Figure S1). The O_2 flux is constant in the range 2.5 – 20 · 10^6 cells mL^{-1} (green area), whilst it decreases as the cell concentration increases between 20 – 100 · 10^6 cells mL^{-1} (red area). The slope of the linear correlation equation in the green area is not significantly different from 0 [y = (2.12 ± 0.11) + (0.006 ± 0.007) x, Pearson's R: 0.5, R-Square: 0.25], whilst in the red area it is [y = (2.43 ± 0.03) – (0.01 ± 0.0004) x, Pearson's R: -0.99, R-Square: 0.99 (Test-t, p-value < 0.05). Data refer to the average ± SD of four independent biological replicates.

From 2.5 to 20 · 10^6 cells mL^{-1} samples showed a constant O_2 flux, whilst the latter decreased as the cell concentration increased up to the highest concentration tested in this work (100 · 10^6 cells mL^{-1}, Figure 2). Overall, cell concentrations could be divided into two groups according to the behavior observed in Figure 2: i) for samples between 2.5 and 20 ×10^6 cells mL^{-1} there were no major differences between the measured photosynthetic activity of the different samples, suggesting that in this range the data were not influenced by the cell concentration and thus the impact of self-shading was neglectable. In the former case, noise of the measurements was higher because of the low cell concentration, as observed for data at 2.5 cells mL^{-1}. ii) for samples in the range between 40 and 100 ×10^6 cells mL^{-1}, photosynthetic activity instead dropped as the cell concentration increased. This is likely to depend on the inhomogeneous light distribution in the samples because of their high optical density.

2.3. Measuring photosynthetic functionality in microalgae dense cultures of photobioreactors.

To better assess how self-shading affected photosynthetic activity of *Nannochloropsis* cells, the photosynthesis-irradiance relationship of diluted and dense samples (5 and 100 ×10^6 cells mL^{-1}, respectively) were compared (Figure 3). It is worth noting that for diluted samples we chose the concentration of 5×10^6 cells mL^{-1} to minimize the noise of the measurements.

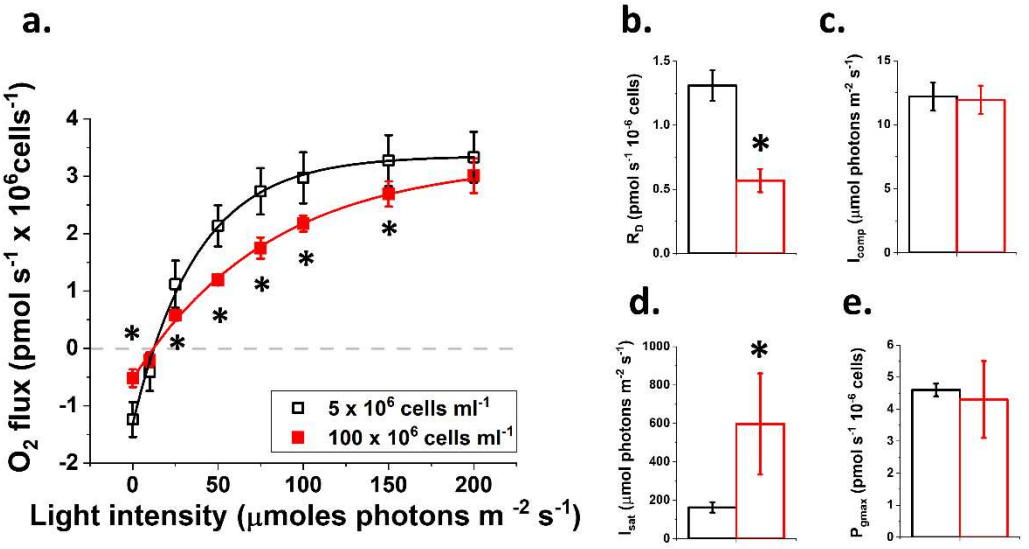

Figure 3 | Photosynthesis-Irradiance dependance as a function of culture density. The Photosynthesis-Irradiance relationship was measured for diluted and dense *Nannochloropsis* cultures (i.e. 5 and 100 ×10^6 cells mL^{-1}, respectively) and fitted with the equation defined in Ye (2007) using a minimum mean square error-based approach. The fitting returned the mathematical parameters indicated in panel from b) to e), that describe the differences in the shapes of the curves represented in panel a). For each mathematical parameter, the asterisk indicates a statistically significant difference between the two culture densities (Test-t, p-value < 0.05). Data refer to the average ± SD of four independent biological replicates. Black, 5 ×10^6 cells mL^{-1} and red, 100 ×10^6 cells mL^{-1} cell concentration. The same parameters for all the other cell concentrations tested in this work are reported in Supplementary Table 1.

We observed that the concentration of cells had a substantial effect on the shape of the photosynthesis-irradiance relationship, especially during the linear phase (Figure 3a). The dark respiration rate (R_D) of the densest sample (100 ×10^6 cells mL^{-1}) was <30% of the value measured for the diluted sample (5 ×10^6 cells mL^{-1}, Figure 3b), whilst no differences were observed for the light compensation point (I_{comp}) (Figure 3c). The light saturation point (I_{sat}) was instead higher in the densest sample (Figure 3d), indeed suggesting that the higher optical density triggered an inhomogeneous light distribution, leading to a shading effect between cells. This hypothesis was

confirmed by the observation that the maximal gross O_2 photosynthetic rate (P_{gmax}) was the same for both cell concentrations (Figure 3e). The value of maximal gross photosynthesis is therefore reliably estimated even in dense microalgae samples, because when light is in excess the effect of self-shading becomes negligible since all cells are exposed to saturating illumination.

Consequently, the photosynthetic parameters extrapolated via this methodology are reliably determined even for samples with high-cell-density. This opens the possibility to estimate at the lab-scale the photosynthetic performances of high-density microalgae cultures, like those found in industrially relevant cultivation plants.

2.4. How does cell's light absorption capacity impact the Photosynthesis-Irradiance relationship in microalgae dense cultures?

The methodology described in this work offers the opportunity to investigate the photosynthetic activity of microalgae in complex light environments, like those of dense cultures of industrial PBRs, to better predict how operational and biological improvements can be tailored to achieve the theoretical growth potential of microalgae mass cultures, long hypothesized in the past, but yet to validate in pilot cultivation plants outdoors.

Microalgae photosynthesis indeed acclimates to the greatest scale of cultivation, as a consequence of the highest cell density, but also of the different operational processes and fluctuations of major metabolic inputs (e.g. light and C O_2 supply). The investigation of this phenomenon is still limited to few examples and a systematic approach to deeply understand it is yet to be developed. As an example, the reduction of the pigment (chlorophyll, Chl) content has been postulated as a promising strategy to improve the light distribution profile in microalgae mass cultures and increase the rate of the photochemical reactions in those layers of cells most distal from the light source, and consequently heavily light-limited, to ultimately improve growth and biomass productivity of the whole culture volume.

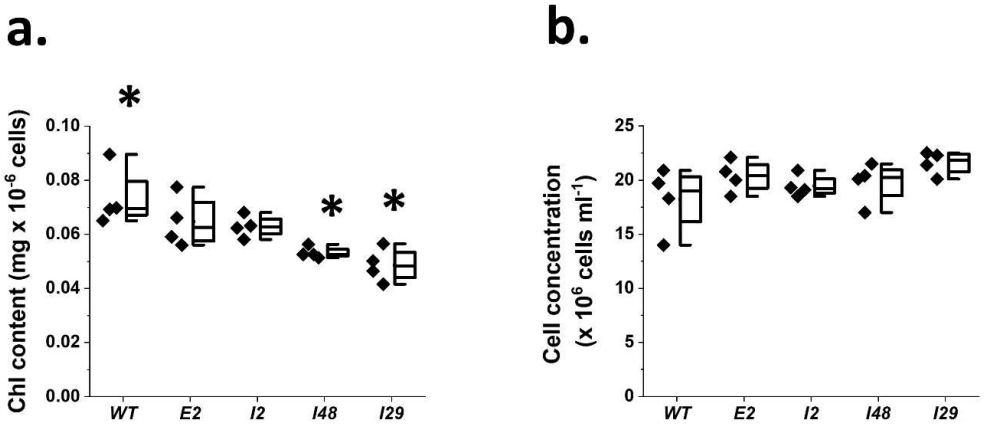

Figure 4 | **Isolation of *Nannochloropsis* mutants with a reduced pigment content and unaffected phototrophic growth.** *Nannochloropsis* mutants showing different degrees of reduction of chlorophyll (Chl) content (a), but an affected phototrophic growth (b) with respect to the parental strain (WT) were isolated. Data refer to the average ± SD of four independent biological replicates, grown in Erlenmeyer flasks for four days, according to the protocol detailed in the materials and methods section. Asterisks indicate statistically significant differences between one mutant and the parental strain (Test-t, p-value < 0.05).

In the past few years, we successfully isolated *Nannochloropsis* mutants with different degrees of reduction in the Chl content (Figure 4a), which did not result in any affected phototrophic growth phenotype at the lab-scale (Figure 4b). When these strains were cultivated in dense cultures simulating industrial cultivation conditions (Perin et al., 2015), we observed an improved growth rate and biomass productivity with respect to the parental strain, with the greatest advantage observed for the strains showing the strongest reduction in the Chl content, up to an optimal threshold (Perin, Bernardi, et al., 2017).

In this work, we measured the photosynthesis-irradiance relationship of these microalgae strains and compared diluted and dense cultures (Figure 5a and b), to i) describe how photosynthetic activity is influenced by cultivation conditions typical of industrial plants and ii) validate that the improved biomass productivity we measured in dense cultures of lab-scale PBR depends on an improved photosynthetic activity indeed. We observed that the effect of cell concentration on the shape of the photosynthesis-irradiance relationship, that we previously measured for the WT (Figure 3a), is maintained also in photosynthetic pale mutants. Also in this case, the dark respiration rate (RD) of dense cultures was lower than in diluted samples, with implications also on the light compensation point, that in the former was significantly lower than in the latter.

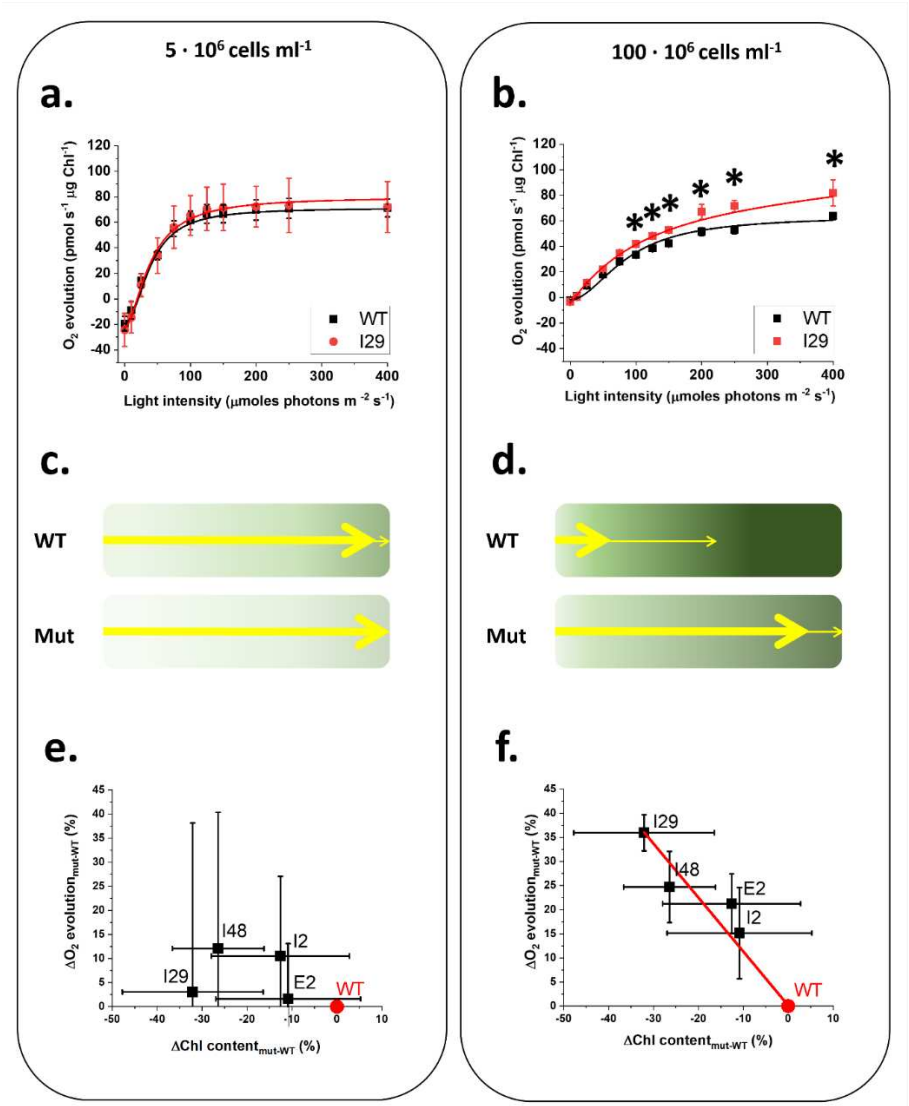

Figure 5 | **Improvement of photosynthetic activity as a function of the reduction of the pigment content, in *Nannochloropsis* cultures with different densities**. Examples of Photosynthesis-Irradiance relationship measured for *Nannochloropsis* WT and I29 strain, showing 30% reduction of Chl content with respect to the former (Figure 4), in diluted (a) (i.e. 5 ×10^6 cells mL^{-1}) and dense (b) (i.e. 100 ×10^6 cells mL^{-1}) cultures. Data were fitted with the equation of Ye (2007) using a minimum mean square error-based approach. Schematic representations of the light distribution profile (yellow arrows) in WT and pale green mutants (Mut) *Nannochloropsis* cultures, in diluted (c) and dense cultures (d). Improvement in O_2 flux at 400 µmol photons·s^{-1}·m^{-2}, expressed as percentage with respect to the parental strain (WT) for the four mutants showing different degrees of reduction in the chlorophyll (Chl) content, expressed as percentage of reduction with respect to the WT, for diluted (e) and dense (f) *Nannochloropsis* cultures. Data in both panels correspond to the photosynthetic activity measured at 400 µmol photons·s^{-1}·m^{-2}, that is the light intensity to which dense cultures in lab-scale PBRs demonstrated an improved biomass productivity (Perin et al., 2017) ref. There is no linear correlation between datapoints in panel c [y = (1.65 ± 7.1) – (0.25 ± 0.46) x, Pearson's R: -0.35, R-Square: 0.12, with the slope not significantly different from 0 (Test-t, p-value < 0.05)], whilst there is linear correlation in panel b (red continuous line), according to the following equation y = (0.12 ± 0.78) – (1.1 ± 0.05) x, Pearson's R: -0.99, R-Square: 0.98, with the slope significantly different from 0 (Test-t, p-value < 0.05). Data refer to the average ± SD of four independent biological replicates. Asterisks indicate statistically significant differences between one mutant and the parental strain (Test-t, p-value < 0.05). The original data used in this figure are reported in Supplementary Figure 2.

Strain I29, that, out of the four strains tested in this work, had the greatest reduction in pigment content with respect to the WT, did not show any difference of photosynthetic functionality than the WT in diluted cultures (Figure 5a). In dense cultures, I29 instead showed a higher photosynthetic activity with respect to the WT at most of the tested irradiances, with the difference increasing with light intensity. In dense cultures, I29 also saturates photosynthesis at higher irradiances than the parental strain (Figure 5b). These data highlight that the improvement of photosynthetic functionality of pale mutants is likely to be dependent on the density of the culture, where self-shading effects become relevant for photosynthesis.

To validate this hypothesis, we measured the Photosynthesis-Irradiance relationship of the other three pale mutants presented in Figure 4. We observed that also for these three other strains, the advantage of photosynthetic functionality with respect to the WT is observable only in dense cultures (Supplementary Figure 2).

This behavior is explainable by the fact that microalgae with a reduced pigment content are expected to trigger a more homogeneous light distribution, with cells most distal from the light source becoming thus exposed to more irradiance than in WT cultures (Figure 5d). This phenomenon is expected to trigger a higher photochemical rate in these regions of the culture volume, with beneficial consequences on the growth of the whole mass culture. This improvement is observable only in dense microalgae cultures, because in diluted conditions light is homogeneously distributed even for WT cells (Figure 5c).

If this phenomenon happened according to this latter explanation, the lower the cell's light absorption capacity, the greater the improvement of photosynthetic activity in microalgae dense cultures. To validate this conclusion, we plotted the improvement of photosynthetic activity measured at 400 µmol photons$\cdot s^{-1} \cdot m^{-2}$ in dense cultures (i.e. expressed as percentage with respect to the WT photosynthetic activity), for the four pale mutants investigated this work, versus the reduction of pigment content, as percentage of the WT (Figure 5e and f). It is worth noting that the strains investigated in this work showed an improved biomass productivity in dense lab-scale PBR cultures exposed at 400 µmol photons$\cdot s^{-1} \cdot m^{-2}$ (Perin, Bernardi, et al., 2017). Moreover, the four pale *Nannochloropsis* mutants of this work showed a progressively greater reduction of pigment content than the WT (Figure 4a), making them the ideal choice to assess

the impact of a wide range of changes in the cells' light absorption capacity. There is a significant linear correlation between improvement in photosynthetic functionality and reduction in pigment content, with the greatest reduction of the latter leading to the greatest improvement of photosynthetic activity in dense cultures (Figure 5e and f), indeed demonstrating that the improvements of photosynthetic functionality in dense microalgae cultures depends on the lower light absorption capacity of pale mutants.

3. Discussion

3.1. Oxygen photoproduction is a good proxy of photosynthetic activity.

Photosynthesis is generally divided into two major phases, namely light and dark reactions. The former harvests light and uses its energy to excite chlorophyll molecules that in turn lose electrons, handing them over to a series of molecular acceptors and starting the so-called photosynthetic electron transport. Electrons lost from chlorophylls are gained back from water, that is split into protons and molecular oxygen. Overall, light reactions of photosynthesis generate molecular oxygen as by-product of water splitting and reducing power and chemical energy in the form of NADPH and ATP, respectively because of electron transport and of the dissipation of the proton motive force generated during the former across the thylakoid membrane.

Dark reactions of photosynthesis instead exploit reducing power and chemical energy from the former set of enzymatic steps to fix atmospheric carbon (i.e., CO_2) in the form of triose phosphates (e.g., G3P), via the so-called Calvin-Beson cycle.

The rate of NADPH and ATP photoproduction is not an ideal proxy of photosynthetic functionality. In fact, beside the Calvin-Benson cycle, other metabolic pathways compete for the chemical energy and reducing power generated by light reactions of photosynthesis, making their concentration highly variable over time and thus not directly proportional to the photosynthetic activity of the sample.

Historically, the functionality of the photosynthetic metabolism has been investigated using the rate of carbon fixation in ^{14}C-treated samples (Jassby & Platt, 1976; Perry et al., 1981). This methodology is complicated by the need of marked carbon which is expensive and requires a complex experimental set-up for the homogenous treatment of the sample under investigation. The development of CO_2 detectors opened the possibility to measure the rate of carbon fixation avoiding the use of marked carbon. Nevertheless, this technology is still limited by operational constraints like i) the sensitivity of the detectors that is currently too low to obtain reliable information in carbon limiting conditions and ii) the need of complex experimental set-ups (e.g., closed chambers) that can affect data reliability and versatility of the methodology.

Molecular oxygen is the other product of photosynthesis, and its concentration is directly proportional to the number of electrons that are vehiculated through the photosynthetic electron transport chain, making the rate of O_2 evolution a good choice for the investigation of photosynthetic functionality. On the other hand, molecular oxygen is also consumed by mitochondrial respiration and measuring its concentration can thus also provide an estimation of the rate of this other metabolic activity in relationship with photosynthesis.

3.2. Photosynthesis-Irradiance relationship: measuring photosynthetic activity in a dynamic light environment.

The metabolic activity of the chloroplasts depends on energy and carbon inputs (i.e., sunlight and atmospheric CO_2) whose availability is not always constant, consequently affecting photosynthetic functionality. As an example, when carbon availability is not limiting, photosynthetic activity strictly depends on light supply. Changes in light intensity affect the photosynthetic rate and consequently the energetic and redox state of any photosynthetic organism, ultimately controlling their growth. When sunlight is not abundant, photosynthesis is limited by the energetic input, that is not enough to drive the water splitting at sufficient rate to provide enough electrons to generate enough NADPH to maintain photochemistry. On the other hand, when light is in excess, the electrons scavenged from water instead exceed the amount needed to reduce the available pool of $NADP^+$ and photochemistry reaches the maximum rate. In these light conditions, the availability of $NADP^+$ controls the rate of photochemistry and strictly depends on the carbon fixation activity by the Calvin-Benson cycle. As photosynthetic activity saturates, excess excitation directly reacts with molecular oxygen and generates reactive oxygen species (ROS) causing photodamage.

In nature, photosynthesis is often limited by light availability, but seasonal and weather conditions are responsible for fluctuations in irradiance with intensity often suddenly increasing. This phenomenon is intensified in aquatic environments, where water movements can cause lens effects with sudden fluctuations in sunlight, peaking up to 100 times the light intensity experienced on average in those natural conditions, affecting photosynthetic functionality and consequently growth of aquatic

photosynthetic organisms, like microalgae. The investigation of the dependance of photosynthetic activity on light intensity (e.g., Photosynthesis-Irradiance relationship, i.e. the so-called PI curve) is an valuable approach to assess how photosynthesis responds to a dynamic light environment, e.g. to enable the elucidation of the biological dynamics behind the success of some microalgae species over others in different ecological niches.

The investigation of the PI relationship is a valuable tool also to assess how microalgae photosynthesis responds to environmental conditions of cultivation plants for industrial applications.

For microalgae biomass-derived commodities (e.g., food supplements, cosmetics, biofuels and biofertilizers) to become competitive in the current global economy, microalgae must be cultivated in photobioreactors at scale where they reach high cell densities to maximize biomass productivity. Such a mass culture leads to an inhomogeneous light distribution, with the volume most exposed to incident light experiencing light excess, whilst cells distal from the light source instead experiencing light limitation (Formighieri et al., 2012; Perin et al., 2019). As described above, both cell populations are in suboptimal light conditions, on one hand experiencing saturation of photosynthesis and on the other limitation by light availability. In both cases microalgae underperform, limiting the values of biomass productivity currently achievable in photobioreactors and curbing both economic feasibility and long-term sustainability of state-of-the-art microalgae cultivation plants.

The investigation of the PI relationship of dense cultures can thus enable to predict the behavior of microalgae in such a complex light environment of photobioreactors, with the potentiality to gain valuable information to i) optimize the design and operational procedures of photobioreactors to improve microalgae productivity and ii) drive an effective biotechnological optimization of photosynthesis for an improved light-use efficiency in the complex light environment of photobioreactors.

3.3. Reliable estimation of PI relationship in both diluted and dense microalgae cultures.

The quantification of the concentration of molecular oxygen has been originally achieved with the so-called clear and dark bottle method (Strickland, 1960). Afterwards, devices based on Clark-type sensors have been developed, yet the information achievable have been limited by the i) low resolution and sensitivity and ii) difficulty in the precise control of light supply to the sample.

In this work we validated one state-of-the-art technology, designed to improve both these constraints. In this work we used *Nannochloropsis* as validation model and demonstrated that the NextGen-O2k technology is very sensitive and enables the detection of the concentration of molecular oxygen in very-low-concentration samples (e.g., 1 and 2.5 $\times 10^6$ cells mL^{-1}, Supplementary Figure 1). These concentration values are on average 30 times lower than those used with classical Clark sensors (Perin et al., 2015), minimizing the volume of culture to sacrifice for the evaluation of photosynthetic activity of microalgae samples. On the other hand, the investigation of photosynthetic functionality at low cell concentration opens the possibility to simulate the light regime of natural environments, enabling the collection of information of relevance for natural ecological niches.

We also demonstrated that the NextGen-O2k technology is capable to reliably assess the impact of different cell densities on microalgae photosynthetic functionality. When we compared the Photosynthesis-Irradiance (PI) relationship of *Nannochloropsis* cultures at different concentrations, from diluted (i.e., 5 $\times 10^6$ cells mL^{-1}) to dense (100 $\times 10^6$ cells mL^{-1}), we observed that there is an effect of cell density on the shape of the PI curve (Figure 2, Figure 3a). At non-saturating irradiances (<150 µmol photons$\cdot s^{-1} \cdot m^{-2}$ for *Nannochloropsis* (Sforza et al., 2012), the photosynthetic activity is lower in dense cultures, indeed suggesting the high cell concentration triggers an inhomogeneous light distribution profile within the sample, with a substantial fraction of cells exposed to limiting light and thus not receiving enough energy to drive photochemistry. Nevertheless, maximal gross photosynthesis in the high-density sample equals the diluted culture, indicating the technology tested in this work can reliably estimate photosynthetic parameters even in dense microalgae cultures (Figure 3e).

3.4. Changes in cells' light absorption capacity affect photosynthetic functionality in dense microalgae cultures.

For microalgae biomass to become a competitive alternative to the current industrial processes based on the exploitation of fossil fuels, biomass productivity at scale must still be strongly improved to compensate for the high production, harvesting and operational costs.

The main limitation is that microalgae cultures in photobioreactors are heavily limited by light availability (Perin et al., 2022), curbing light-use efficiency and biomass productivity.

The improvement of the light distribution profile in microalgae mass cultures has been a strategy long hypothesized to increase the light-use efficiency and biomass productivity at scale. Microalgae evolved in a natural environment where light is often limiting for growth, determining the evolution of large molecular complexes (i.e. pigment-binding proteins) to maximize the binding of Chl molecules and thus increasing the chances of light harvesting (Falkowski, 1994). In the past years, several research efforts were successfully devoted to the isolation of strains carrying a reduced pigment content than the corresponding parental strains, in different microalgae species (Cazzaniga et al., 2014; Kirst et al., 2012; Kirst & Melis, 2014; Perin et al., 2015; Wobbe et al., 2009). These domestication efforts were demonstrated to increase light-use efficiency and growth of microalgae in controlled lab-scale conditions (Falkowski, 1994).

However, once domesticated strains were moved to the complex cultivation environment of dense pilot plants outdoors, mixed results were obtained, with the confirmation of a growth advantage in some cases (Cazzaniga et al., 2014), but not in others (de Mooij et al., 2015). This discrepancy of growth performances has been under-investigated so far for two main reasons: i) the impact of the complexity of the light environment experienced in dense cultures in photobioreactors, that has a significant effect on the acclimation capacity of microalgae photosynthesis, as observed e.g. for domesticated *Nannochloropsis* strains (Perin, Simionato, et al., 2017) on microalgae photosynthesis has not been studied yet and ii) the available

methods to measure photosynthetic functionality prevented the collection of reliable information for dense microalgae cultures.

In this work we used four *Nannochloropsis* strains, previously isolated for a reduced pigment content and unaffected phototrophic growth (Figure 4), that already demonstrated an improved biomass productivity in lab-scale PBRs (Perin, Bernardi, et al., 2017), and measured their PI curves using the NEXTGEN-O2K technology, comparing diluted and dense cultures (Figure 5). In diluted samples, we did not observe any significant improvement in O_2 flux for all the four strains here investigated (Figure 5a and Supplementary Figure S2). Instead, in dense cultures, we observed a significant improvement in the O_2 flux with respect to the parental strain (Figure 5b and Supplementary Figure 2), that progressively increases with the reduction of the Chl content (Figure 5f).

The NextGen-O2K technology of this work enables to simulate at the lab-scale the light conditions of PBR and to estimate in a reliable way the photosynthetic functionality of microalgae strains with an optimized photosynthesis.

We successfully demonstrated that reducing the cell light absorption capacity improves the photosynthetic functionality of microalgae dense cultures, providing an explanation for the growth advantage observed in lab-scale PBRs.

4. Conclusions

The available technology for lab-scale investigations of photosynthetic functionality prevents the collection of reliable information on either the impact of natural light conditions experienced in real ecological niches or of the complex light environment of photobioreactors for microalgae industrial applications.

The biggest issue that research efforts to improve microalgae productivity in PBR are yet to solve is the huge gap of growth performances between lab- and industrial-scale microalgae cultures.

The NextGen-O2k technology represents a valuable tool to improve our knowledge on how microalgae photosynthesis responds to the complex light environment of dense PBR cultures and to assess the behavior of domesticated strains already at the lab-scale, thus speeding up the identification of robust biological targets for biotechnological optimization.

5. Materials and methods

5.1. Microalgae strains and culture conditions.

In this work we used the microalgae species *Nannochloropsis gaditana,* strain CCAP 849/5, that was purchased from the Culture Collection of Algae and Protozoa (CCAP).

N. gaditana was maintained in F/2 solid media, containing 32 g L^{-1} sea salts (Sigma Aldrich), 40 mM Tris-HCl pH 8, Guillard's (F/2) marine water enrichment solution (Sigma Aldrich) and 1% agar (Duchefa Biochemie). Microalgae cells were pre-cultured in sterile F/2 liquid media in Erlenmeyer flasks exposed at 100 µmoles of photons m^{-2} s^{-1} with 100 rpm agitation, at 22 ± 1 °C in a growth chamber. Growth curves were performed in the same conditions of pre-cultures from cells washed twice in fresh F/2 media, starting from 5 $\times 10^6$ cells mL^{-1} concentration in sterile F/2 liquid media supplemented with 10 mM $NaHCO_3$ to avoid carbon limitation.

5.2. Preparation of cells for measurements of oxygen evolution.

Cell concentration was measured with an automatic cell counter (Cellometer Auto X4, Cell Counter, Nexcelom) at the fourth day of cultivation in the growth conditions described above. Microalgae cells were collected via mild centrifugation at 3,500 g for 10 minutes at room temperature and then resuspended in fresh sterile F/2 media supplemented with 10 mM $NaHCO_3$ right before the start of oxygen evolution assessment to avoid carbon limitation during the measurement.

5.3. High resolution oxygen evolution

Oxygen evolution was measured at the fourth day of the growth curves described above. Measurements were performed using a test version of the NextGen-O2k and the PhotoBiology (PB)-Module (Oroboros Instruments, Innsbruck) with the software DatLab 7.4.0.4 (Went et al., 2022) according to the methods developed in (Vera-Vives et al., 2022). The PB light source contained a blue OSLON® LED (emitting wavelength range 439-457 nm with the peak at 451 nm, manufactured by OSRAM) attached to the window of the NextGen-O2k chamber. The oxygen concentration was assessed in 2-mL measuring chambers at 22 °C with a 2-seconds

frequency and samples were magnetically stirred at 750 rpm. Two measurements were done in parallel at each time, taking advantage of the two chambers of the instrument.

At first, the measuring chambers were filled with fresh and sterile F/2 medium, containing 10 mM $NaHCO_3$ to avoid carbon limitation during the measurement and to equilibrate the temperature at 22 °C for few minutes. Then, a fraction of medium (<10% of the chamber volume) was replaced with a suspension of *Nannochloropsis* cells to reach the desired final concentration in the measuring chamber. The chambers were then closed, and the samples were dark adapted for 10 min to assess the respiration rate before starting the measurements of the oxygen flux at increasing irradiances. After stabilization of the respiration signal, light was turned on at increasing irradiances, waiting at least 5 min at each light intensity to achieve the stabilization of the oxygen evolution rate (on average the O_2 flux trace stabilized within the first 2-3 minutes). The values of oxygen evolution rate reported in this work at each irradiance correspond to the median of 40-50 points in the stable region of oxygen flux. Respiration and photosynthesis rates at different irradiances were calculated with the software DatLab 7.4.0.4.

5.4. Determination of chlorophyll content

After evaluation of oxygen evolution, microalgae samples were further processed to extract chlorophyll molecules from *Nannochloropsis* cells, using 1:1 ratio of 100% N, N-dimethylformamide (DMF) (Sigma Aldrich), at 4 °C in the dark, for at least 24 h (Wellburn, 1994). The chlorophyll concentration was calculated, using specific extinction coefficients (Wellburn, 1994), from the absorption values at 664 nm of DMF *Nannochloropsis* extracts, collected using a Cary 100 spectrophotometer (Agilent Technologies).

5.5. Statistical analysis

In this work, we performed a statistical hypothesis testing for all the data presented. Statistical significance was assessed by t-test using OriginPro 2020 (v. 9.7.0.188) (http://www.originlab.com/). Samples size was at least 4 for all the measurements collected in this work.

6. References

Cazzaniga, S., Dall'Osto, L., Szaub, J., Scibilia, L., Ballottari, M., Purton, S., & Bassi, R. (2014). Domestication of the green alga Chlorella sorokiniana: reduction of antenna size improves light-use efficiency in a photobioreactor. *Biotechnology for Biofuels*, *7*(1), 157. https://doi.org/10.1186/s13068-014-0157-z

de Mooij, T., Janssen, M., Cerezo-Chinarro, O., Mussgnug, J. H., Kruse, O., Ballottari, M., Bassi, R., Bujaldon, S., Wollman, F. A., & Wijffels, R. H. (2015). Antenna size reduction as a strategy to increase biomass productivity: A great potential not yet realized. *Journal of Applied Phycology*, *27*(3), 1063–1077. https://doi.org/10.1007/S10811-014-0427-Y/TABLES/3

Doerrier, C., Garcia-Souza, L. F., Krumschnabel, G., Wohlfarter, Y., Mészáros, A. T., & Gnaiger, E. (2018). High-resolution fluorespirometry and oxphos protocols for human cells, permeabilized fibers from small biopsies of muscle, and isolated mitochondria. *Methods in Molecular Biology*, *1782*, 31–70. https://doi.org/10.1007/978-1-4939-7831-1_3/TABLES/2

Falkowski, P. G. (1994). The role of phytoplankton photosynthesis in global biogeochemical cycles. *Photosynthesis Research*, *39*(3), 235–258. https://doi.org/10.1007/BF00014586/METRICS

Formighieri, C., Franck, F., & Bassi, R. (2012). Regulation of the pigment optical density of an algal cell: Filling the gap between photosynthetic productivity in the laboratory and in mass culture. *Journal of Biotechnology*, *162*(1), 115–123. https://doi.org/10.1016/j.jbiotec.2012.02.021

Gnaiger, E. (2008). Polarographic Oxygen Sensors, the Oxygraph, and High-Resolution Respirometry to Assess Mitochondrial Function. In *Drug-Induced Mitochondrial Dysfunction* (pp. 325–352). Wiley. https://doi.org/10.1002/9780470372531.ch12

Jassby, A. D., & Platt, T. (1976). Mathematical formulation of the relationship between photosynthesis and light for phytoplankton. *Limnology and Oceanography*, *21*(4), 540–547. https://doi.org/10.4319/LO.1976.21.4.0540

Kirst, H., García-Cerdán, J. G., Zurbriggen, A., & Melis, A. (2012). Assembly of the Light-Harvesting Chlorophyll Antenna in the Green Alga Chlamydomonas reinhardtii Requires Expression of the TLA2-CpFTSY Gene. *Plant Physiology*, *158*(2), 930–945. https://doi.org/10.1104/PP.111.189910

Kirst, H., & Melis, A. (2014). The chloroplast signal recognition particle (CpSRP) pathway as a tool to minimize chlorophyll antenna size and maximize photosynthetic productivity. *Biotechnology Advances*, *32*(1), 66–72. https://doi.org/10.1016/J.BIOTECHADV.2013.08.018

Perin, G., Bellan, A., Bernardi, A., Bezzo, F., & Morosinotto, T. (2019). The potential of quantitative models to improve microalgae photosynthetic efficiency. *Physiologia Plantarum*, *166*(1), 380–391. https://doi.org/10.1111/ppl.12915

Perin, G., Bellan, A., Segalla, A., Meneghesso, A., Alboresi, A., & Morosinotto, T. (2015). Generation of random mutants to improve light-use efficiency of Nannochloropsis gaditana cultures for biofuel production. *Biotechnology for Biofuels*, *8*(1), 1–13. https://doi.org/10.1186/S13068-015-0337-5/FIGURES/7

Perin, G., Bernardi, A., Bellan, A., Bezzo, F., & Morosinotto, T. (2017). A mathematical model to guide genetic engineering of photosynthetic metabolism. *Metabolic Engineering*, *44*, 337–347. https://doi.org/10.1016/j.ymben.2017.11.002

Perin, G., Gambaro, F., & Morosinotto, T. (2022). Knowledge of Regulation of Photosynthesis in Outdoor Microalgae Cultures Is Essential for the Optimization of Biomass Productivity. *Frontiers in Plant Science*, *13*. https://doi.org/10.3389/fpls.2022.846496

Perin, G., Simionato, D., Bellan, A., Carone, M., Occhipinti, A., Maffei, M. E., & Morosinotto, T. (2017). Cultivation in industrially relevant conditions has a strong influence on biological properties and performances of Nannochloropsis gaditana genetically modified strains. *Algal Research*, *28*, 88–99. https://doi.org/10.1016/j.algal.2017.10.013

Perry, M. J., Talbot, M. C., & Alberte, R. S. (1981). Photoadaption in marine phytoplankton: Response of the photosynthetic unit. *Marine Biology 1981 62:2*, *62*(2), 91–101. https://doi.org/10.1007/BF00388170

Sforza, E., Simionato, D., Giacometti, G. M., Bertucco, A., & Morosinotto, T. (2012). Adjusted Light and Dark Cycles Can Optimize Photosynthetic Efficiency in Algae Growing in Photobioreactors. *PLoS ONE*, *7*(6), e38975. https://doi.org/10.1371/journal.pone.0038975

Strickland, J. (1960). *Measuring the production of marine phytoplankton* (Bull Fish).

Vera-Vives, A. M., Perin, G., & Morosinotto, T. (2022). The robustness of NextGen-O2k for building PI curves in microalgae. *Bioenergetics Communications*, *19*.

Wellburn, A. R. (1994). The spectral determination of chlorophylls a and b, as well as total carotenoids, using various solvents with spectrophotometers of different resolution. *Journal of Plant Physiology*, *144*(3), 307–313.

Went, N., Gnaiger, C., Schmitt, S., Moreno-Sanchez, R., Roach, T., & Gnaiger, E. (2022). Oxygen dependence of photosynthesis and light-enhanced dark respiration studied by high-resolution PhotoRespirometry. *Biochimica et Biophysica Acta (BBA) - Bioenergetics*, *1863*, 148832. https://doi.org/10.1016/J.BBABIO.2022.148832

Wobbe, L., Blifernez, O., Schwarz, C., Mussgnug, J. H., Nickelsen, J., & Kruse, O. (2009). Cysteine modification of a specific repressor protein controls the translational status of nucleus-encoded LHCII mRNAs in Chlamydomonas. *Proceedings of the National Academy of Sciences of the United States of America*, *106*(32), 13290–13295. https://doi.org/10.1073/PNAS.0900670106

Ye, Z. P. (2007). A new model for relationship between irradiance and the rate of photosynthesis in Oryza sativa. *Photosynthetica*, *45*(4), 637–640. https://doi.org/10.1007/s11099-007-0110-5

7. Supplementary material

Supplementary Table 1 | Estimation of photosynthetic parameters at different cell concentrations. I_{comp} and I_{sat} indicate the light compensation and light saturation points, respectively, expressed as [µmol photons·s^{-1}·m^{-2}]. R_D is the dark O2 respiration rate, expressed as [pmol·s^{-1}·10^{-6} cells], P_{gmax} is the maximal gross O2 photosynthetic rate, expressed as [pmol·s^{-1}·10^{-6} cells]. $\Phi_{(I_0\_I_{comp})}$ is the quantum yield in the range between I_0 and I_{comp} [pmol O2·m^2·µmol photons^{-1}·10^{-6} cells]. Data refer to the average ± SD of four independent biological replicates. Highlighted in yellow the data from the two cell concentrations used in this work to represent a reliable description of diluted ($5 \cdot 10^6$ cells mL^{-1}) and dense ($100 \cdot 10^6$ cells mL^{-1}) microalgae cultures.

Cell concentration (10^6 cells mL^{-1})	$\Phi_{(I_0\_I_{comp})}$	I_{comp}	I_{sat}	R_D	P_{gmax}
1	0.36 ± 0.10	14.6 ± 0.5	133 ± 59	5.28 ± 1.29	9.9 ± 1.2
2.5	0.09 ± 0.02	19.5 ± 2.3	153 ± 21	1.82 ± 0.21	4.9 ± 0.2
5	0.11 ± 0.01	12.2 ± 1.1	163 ± 27	1.31 ± 0.12	4.6 ± 0.2
10	0.1 ± 0.02	9.5 ± 1.2	149 ± 37	0.95 ± 0.16	4.3 ± 0.3
20	0.09 ± 0.01	9.9 ± 0.7	157 ± 26	0.85 ± 0.12	4.3 ± 0.2
40	0.09 ± 0.01	8.1 ± 1.0	175 ± 28	0.74 ± 0.17	4.0 ± 0.6
75	0.06 ± 0.01	10.7 ± 1.1	329 ± 288	0.62 ± 0.1	4.3 ± 1.2
100	0.05 ± 0.01	11.9 ± 1.1	597 ± 263	0.57 ± 0.09	4.3 ± 1.2

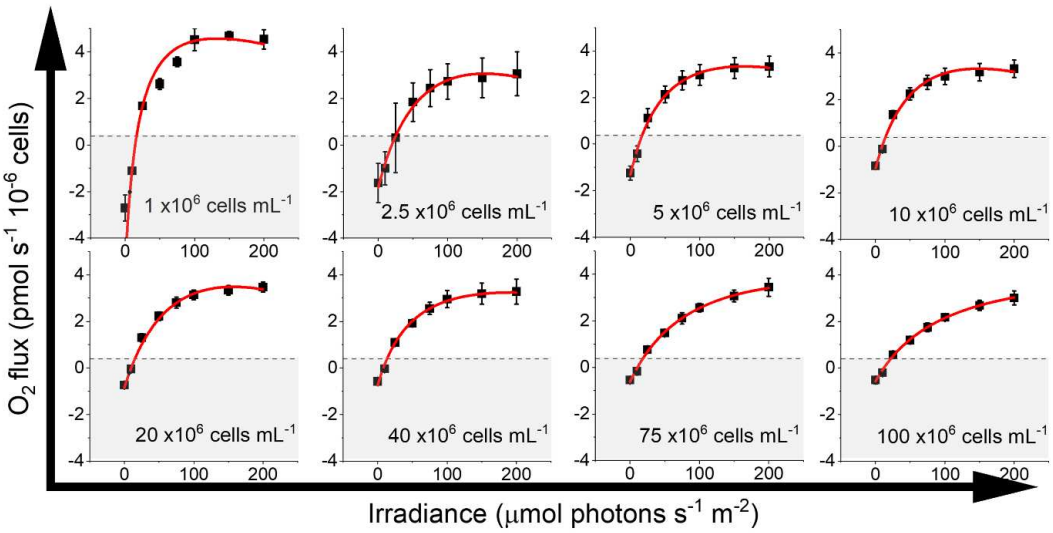

Supplementary Figure 1 | **Photosynthesis-Irradiance relationship as a function of cell concentration.** Photosynthesis is expressed as O_2 flux and it is normalized to the number of cells. Data were fitted with the equation defined in Ye (2007) using a minimum mean square error-based approach (red curves). In each panel, the area where the respiration rate is higher than photosynthesis is marked in grey. The photosynthetic parameters obtained from each curve are detailed in Supplementary Table S1. Data refer to the average ± SD of four independent biological replicates.

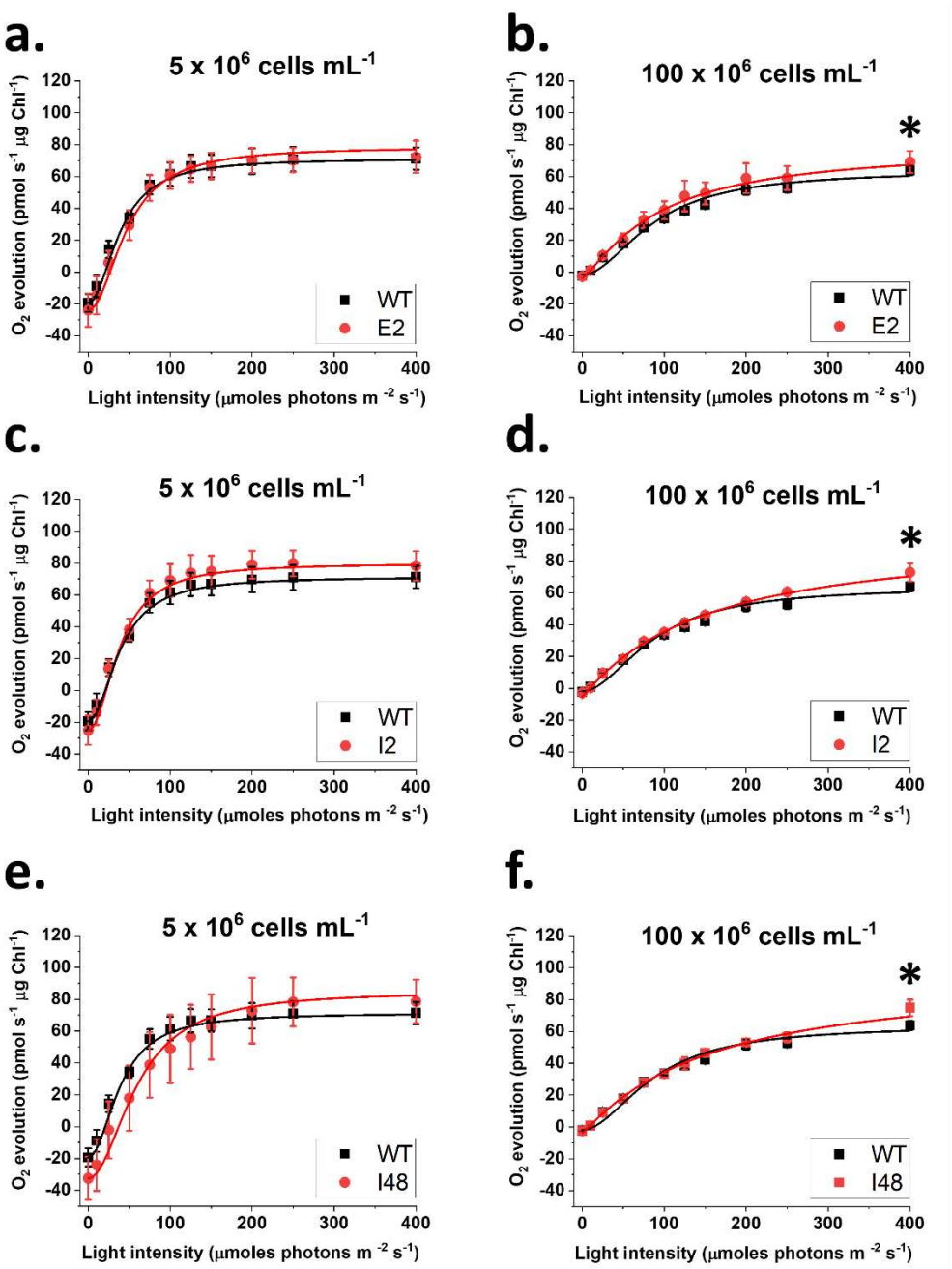

Supplementary Figure 2 | Photosynthesis-Irradiance relationship in pale green *Nannochloropsis* mutants. Photosynthesis is expressed as O_2 flux and it is normalized to the same pigment content to account for the different absorption properties of the different strains. Data were fitted with the equation defined in Ye (2007) using a minimum mean square error-based approach (red and black curves). Data refer to the average ± SD of four independent biological replicates. Asterisks indicate statistically significant differences between one mutant and the parental strain (Test-t, p-value < 0.05). A, c and e show the PI curves of strain E2, I2 and I48 (in red), respectively, compared to the WT (in black) in diluted cultures (i.e. $5 \cdot 10^6$ cells mL^{-1}). B, d and f show the PI curves of strain E2, I2 and I48 (in red), respectively, compared to the WT (in black) in dense cultures (i.e. $100 \cdot 10^6$ cells mL^{-1}).

APPENDIX IV

High-resolution photosynthesis-irradiance curves in microalgae

Antoni M. Vera-Vives[1], Giorgio Perin[1] and Tomas Morosinotto[1]

1. Department of Biology, University of Padova, Italy

This appendix was published in “Bioenergetics Communications” (2022)

Authorship statement:

The general research question and experimental design were proposed by Prof. Tomas Morosinotto and Prof. Giorgio Perin. I performed the experiments and collected all the data. I analyzed the data, wrote the first draft and revised it after the comments of Prof. Giorgio Perin and Prof. Tomas Morosinotto.

BEC BIOENERGETICS COMMUNICATIONS
Bioenerg Commun 2022.19
https://doi.org/10.26124/bec:2022-0019
Open Access

Technical Communication

Cite
Vera-Vives AM, Perin G, Morosinotto T (2022) High-resolution photosynthesis-irradiance curves in microalgae. Bioenerg Commun 2022.19. https://doi.org/10.26124/bec:2022-0019

Author contributions
Data collection was performed by AMVV. Data analysis was done by AMVV and GP. TM and GP conceived and designed the experiments. All authors wrote the manuscript.

Conflicts of interest
Tomas Morosinotto was registered as a key opinion leader by Oroboros Instruments for testing new developments of the NextGent-O2k.

Received 2022-05-05
Reviewed 2022-07-18
Revised 2022-10-12
Accepted 2022-12-13
Published 2022-12-15

Open peer review
Sabine Schmitt (editor)
Thomas Roach (reviewer)
Lijin Tian (reviewer)

High-resolution photosynthesis-irradiance curves in microalgae

Antoni M Vera-Vives, Giorgio Perin, Tomas Morosinotto*

Department of Biology, University of Padova, Italy

* Corresponding author: tomas.morosinotto@unipd.it

Summary

The rate of oxygen evolution provides valuable information on the metabolic status and photosynthetic performance of a cell, and it can be quantified by means of a photosynthesis-irradiance (PI) curve. Up to now, the construction of PI curves of unicellular organisms based on oxygen evolution has been difficult and time consuming due to the lack of sensitive instruments. Here we describe the setup of a reproducible method for constructing PI curves based on oxygen evolution using small amounts of sample in the microalga *Nannochloropsis gaditana*, easily translatable to other algal species.

Keywords – photosynthesis, microalgae, oxygen evolution

1. Introduction

Photosynthetic eukaryotic organisms rely on two organelles, chloroplasts and mitochondria, for the synthesis of the molecules fuelling their metabolism, NAD(P)H and ATP. The two organelles share common features such as membrane-bound enzymatic complexes implicated in electron transfer coupled to proton translocation and the generation of a protonmotive force driving the synthesis of ATP.

In chloroplasts, light energy fuels the electron transfer from water to $NADP^+$ to generate NADPH via photosystem II (PSII), cytochrome b_6f (Cyt b_6f) Complex and photosystem I (PSI), generating oxygen as by-product. The electron transfer is coupled to proton translocation from the chloroplast stroma into the thylakoid lumen and

establishes a transmembrane electrochemical potential, exploited by the ATP synthase for the synthesis of ATP in a process called photophosphorylation.

Photosynthetic eukaryotes contain mitochondria, where electrons are transferred from the substrates NADH and succinate to molecular oxygen O_2. In the dark, respiration is responsible for cells energy supply, but respiration also occurs in the light, when its activity is important for carbon fixation and optimal photosynthesis (Bailleul et al 2015).

In the same way that O_2 consumption is used as a proxy for quantifying respiratory activity and electron transfer through the mitochondrial electron transfer system (ETS), photosynthetic activity and the rate of electron transfer through the plastidial electron transfer system (pETS) can be quantified by the rate of O_2 evolution.

Oxygen evolution and, hence, the photosynthetic rate, depend on light intensity. At low intensities, photosynthesis is limited by the light availability and thus the energy to drive electron transfer. Therefore, in this range, the relationship between light intensity and electron transfer (and thus O_2 evolution) is linear. This linearity is lost at elevated light intensities where other factors (i.e. rate of carbon fixation) become limiting for photosynthesis and any further increase of photons does not result in a higher rate of electron transfer. On the contrary, when photosynthesis is saturated at high intensities, light excess can drive the generation of reactive oxygen species (ROS) and photoinhibition.

This relationship between light intensity and photosynthetic rate is depicted by the so-called photosynthesis-irradiance (PI) curve. Historically, the proxy for photosynthesis quantification in microalgae has been the rate of carbon fixation measured as ^{14}C-carbon assimilation (for examples see Jassby, Platt 1976; Perry et al 1981). Another proxy for PI curves is the rate of O_2 evolution, as O_2 is directly proportional to the number of electrons that move through the pETS. Compared to CO_2, which is only indirectly linked to the transfer of electrons as other metabolic pathways compete for the ATP and reducing power, O_2 is a better proxy for building PI curves. Quantification of O_2 was done first with the so-called clear and dark bottle method (Strickland, 1960), and then using low-resolution devices based on Clark-type sensors. However, these techniques have limitations due to the difficulty in precisely controlling the amount of light that reaches the sample. In addition, they usually require elevated concentrations of cells, which can cause inhomogeneity due to internal shading.

The high resolution of the NextGen-O2k with the PhotoBiology module (PB-Module) enable construction of PI curves with an unprecedented accuracy (Huete-Ortega et al 2020; Went et al 2021). The increased resolution comes from the two components of the system. First, the core O2k-FluoRespirometer is more sensitive than any of the other Clark sensor-based oxygraphs (Gnaiger 2008) commonly used in plant and algal research. This makes it possible to perform measurements of oxygraphy using a very small amount of sample, as we demonstrate in this work. Second, the PB-Module permits fine-tuning of the light intensity that reaches the sample. The combination of these two factors allow PI curves to be obtained in a fast and reproducible manner.

In this work we (*1*) analyze the ability of the NextGen-O2k to build PI curves with high resolution quickly and using low amounts of material and (*2*) titrate different cell concentrations to check for consistency and reproducibility of the measurements.

We use as a model the oleaginous alga *Nannochloropsis gaditana*, an heterokont that is gaining interest for its industrial applications.

2. Methods

2.1. Algal cultures

Nannochloropsis gaditana, strain CCAP 849/5, was purchased from the Culture Collection of Algae and Protozoa (CCAP) and maintained in F/2 solid media, with 32 $g \cdot L^{-1}$ sea salts (Sigma Aldrich), 40 mM Tris-HCl (pH 8), Guillard's (F/2) marine water enrichment solution (Sigma Aldrich), 1 % agar (Duchefa Biochemie). Cells were pre-cultured in sterile F/2 liquid media in Erlenmeyer flasks irradiated with 100 µmol photons$\cdot s^{-1} \cdot m^{-2}$, 100 rpm agitation, at 22 ± 1 °C in a growth chamber. Growth curves started from a cell-count concentration of $5 \cdot 10^6$ x$\cdot mL^{-1}$ in F/2 supplemented with 10 mM $NaHCO_3$ to avoid carbon limitation and were kept in the same growth conditions of pre-cultures.

2.2. Cell counting

Cell concentration was monitored on the fourth day of the growth curve with an automatic cell counter (Cellometer Auto X4, Cell Counter, Nexcelom) to collect the different numbers of cells needed for high-resolution respirometry. For high concentrations, cells were collected via mild centrifugation at 3500 *g* for 10 minutes at room temperature.

2.3. High-resolution respirometry

Oxygen consumption and production were measured on the fourth day of the growth curve. Measurements were performed at 22 °C using a test version of the NextGen-O2k and the PB-Module (Oroboros Instruments, Innsbruck) with the software DatLab 7.4.0.4 (Went et al 2021). The O2k-chambers were magnetically stirred at 750 rpm and the O_2 concentration of the chambers was measured at a data sampling interval of 2 seconds. The PB light source contained a blue OSLON® LED (emitting wavelength range 439-457 nm with the peak at 451 nm, manufactured by OSRAM) attached to the window of the NextGen-O2k chamber.

The 2 mL chambers were filled with growth medium containing 5 mM $NaHCO_3$ to avoid carbon limitation during the measurement and equilibrated to experimental temperature (22 °C) for a few minutes. Then, a small fraction of medium was replaced with an aliquot of cell suspension to reach the desired final concentration in the chamber. The chambers were then closed and the O_2 consumption rate at dark was monitored.

2.4. Light curve protocol

After stabilization of dark respiration, the light source was turned on at 10 µmol photons$\cdot s^{-1} \cdot m^{-2}$ until stabilization of the O_2 flow, typically 5-10 min (Figure 1). This was done recursively for the following light intensities: 10, 25, 50, 75, 100, 150 and 200 µmol photons$\cdot s^{-1} \cdot m^{-2}$. The reported values of O_2 evolution rates at each intensity correspond to the median of 40-50 points in the stable region of oxygen flow (pink regions in Figure 1A). The protocol was automated by running a DatLab 7 script, with an initial period of 600 s for measurement of dark respiration, followed by 300 s intervals at the light intensities shown above, and a final phase of dark respiration in both chambers.

2.5. Data analysis

After each experiment, the raw data were exported from DatLab and analyzed with a spreadsheet template provided by Oroboros Instruments. For building PI curves, we used the O_2 flow normalized to cell concentration expressed in million cells: pmol $O_2 \cdot s^{-1} \cdot 10^{-6}$ x = amol $\cdot s^{-1} \cdot x^{-1}$.

The data were fitted with the equation defined in Ye (2007) using a minimum mean square error-based approach with OriginPro Version 2020b (OriginLab Corporation, Northampton, MA, USA)

$$P_N = \Phi_{(I_0-I_{comp})} \times \frac{1-\beta \cdot I}{1+\gamma \cdot I} \cdot (I-I_{comp})$$

where: P_N is the net O_2 photosynthetic rate per 10^6 cells [pmol $\cdot s^{-1} \cdot 10^{-6}$ x]; $\Phi_{(I_0-I_{comp})}$ is the quantum yield in the range between I_0 and I_{comp} [pmol $O_2 \cdot m^2 \cdot$µmol photons$^{-1} \cdot 10^{-6}$ x]; β and γ are two adjusting factors (dimensionless); I is the photosynthetic photon flux density [µmol photons $\cdot s^{-1} \cdot m^{-2}$] and I_{comp} is the light compensation point [µmol photons $\cdot s^{-1} \cdot m^{-2}$]. Further three derived parameters were calculated: R_D, the dark O_2 respiration rate [pmol $\cdot s^{-1} \cdot 10^{-6}$ x]; P_{gmax}, the maximal gross O_2 photosynthetic rate [pmol $\cdot s^{-1} \cdot 10^{-6}$ x], and I_{sat}, the light saturation point [µmol photons $\cdot s^{-1} \cdot m^{-2}$]. These three parameters were derived as follows:

$$R_D = \Phi_{(I_0-I_{comp})} \cdot I_{comp} \qquad P_{gmax} = P_N + R_D \qquad I_{sat} = \frac{\sqrt{\frac{(\beta+\gamma)\cdot(1+\gamma \cdot I_{comp})}{\beta-1}}}{\gamma}$$

3. Results

3.1. Establishment of a protocol for PI curves

First tests were run with different cell concentrations, observing that $5 \cdot 10^6$ x $\cdot$mL^{-1} to $10 \cdot 10^6$ x $\cdot$mL^{-1} were sufficient to obtain traces of good quality as shown in Figure 1.

At a working cell-count concentration of $10 \cdot 10^6$ x $\cdot$mL^{-1} (corresponding to 0.8 µg Chl $\cdot$mL^{-1}, see the corresponding plot in Figure 2), the rate of dark respiration was estimated as 0.95 ± 0.16 pmol $O_2 \cdot s^{-1} \cdot$mL^{-1}. We increased light intensity progressively starting from 10 µmol photons $\cdot s^{-1} \cdot m^{-2}$. After each light increase the O_2 flux stabilized within 2-4 minutes. The light compensation point, I_{com}, (*i.e.* the point at which net photosynthesis is null) was estimated to be 9.5 ± 1.2 µmol photons $\cdot s^{-1} \cdot m^{-2}$, while saturation was reached at 149 ± 37 µmol photons $\cdot s^{-1} \cdot m^{-2}$.

From first experiments as the one reported in Figure 1, we established and automated a protocol to increase the light every 5 minutes, followed for all measurements reported hereinafter:

1) Add the sample into the chamber.
2) Wait for 10 minutes to measure dark respiration.
3) Turn light on at 10 µmol photons $\cdot s^{-1} \cdot m^{-2}$.
4) Measure for 5 minutes.

5) Increase the light to 25 µmol photons·s^{-1}·m^{-2} followed by 50, 75, 100, 150, 200 µmol photons·s^{-1}·m^{-2}, measuring for 5 minutes after each light change. These intervals were chosen as the most informative to describe the PI curve shape.
6) Wash the chambers and start next experiment.

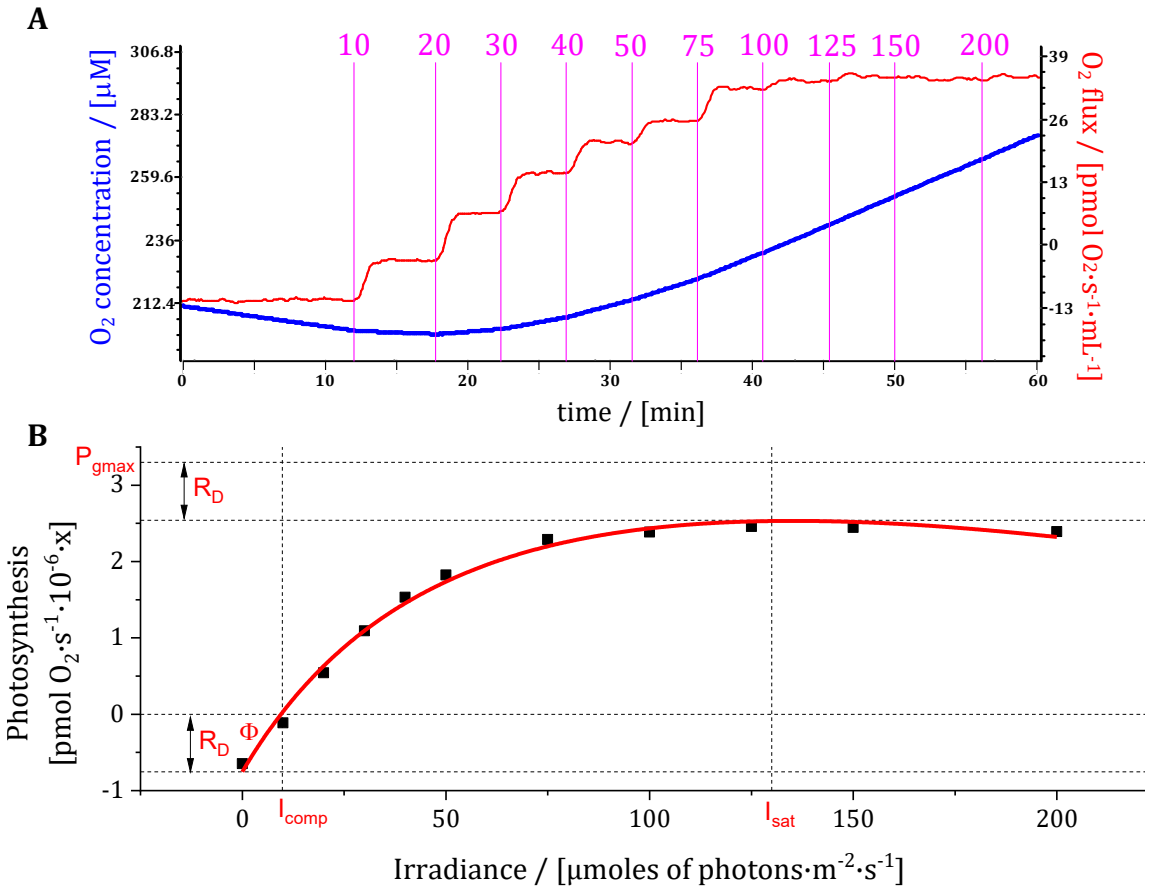

Figure 1. Construction of a PI curve. (A) Simplified diagram of a typical experiment as visualized by DatLab. After each increase in light intensity (vertical lines, values in µmol photons·s^{-1}·m^{-2}), the O_2 flux (red plot, background-corrected time-derivative of O_2 concentration in blue) first increases and then stabilizes. At high light intensities a plateau is reached. **(B)** Fitting of a PI curve to the data reported in A. Each point represents the median of 30-40 datapoints of the stable region of O_2 flux at each intensity (pink segments in A).

A complete experiment lasted less than 1 h, allowing us to perform up to 10 experiments per day, each in two replicas, in the two chambers. It is worth noting that the parameters derived from the PI curves are not influenced by the initial O_2 concentration, given every experiment starts after equilibration of the incubation medium with atmospheric oxygen (Figure 1).

3.2. Testing the effect of cell concentration on PI curves

Once we defined our experimental protocol, we performed different sets of measurements to check for the ideal range of cell concentrations. In our samples, the chlorophyll content was approx. 0.08 µg of chlorophyll per million cells. It should be

mentioned that *Nannochloropsis* cells are quite small (diameter of 2-3 µm). Working concentrations with other microalgae such as *Chlamydomonas*, that have a 10 µm diameter and thus approx. 50 times larger cell volume, should be approx. 25-50 times smaller in terms of cell count.

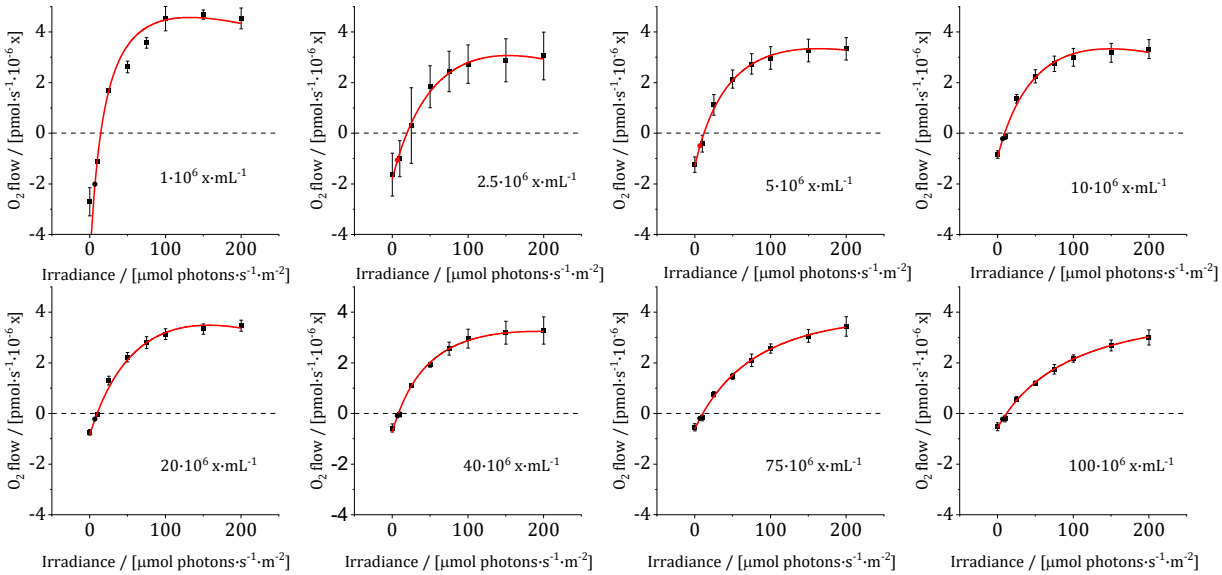

Figure 2. PI curves at cell concentrations ranging from 2.5·10⁶ x·mL⁻¹ to 100·10⁶ x·mL⁻¹. Each data point is the mean of 4 replicates, and the error bars correspond to the standard error.

We tested the following cell concentrations (10^6 x·mL^{-1}): 1, 2.5, 5, 10, 20, 40, 75 and 100. The respective PI curves are shown in Figure 2. Lower concentrations were also tested but were not retained as the low volume-specific flux was too noisy. In all considered cases, the data points followed the expected shape represented in Figure 1B and could be fitted accurately with our PI model. The values of photosynthetic parameters are reported in Table 1.

Table 1. Photosynthetic parameters at different cell concentrations. Values correspond to the mean of four replicates ± standard error. Please refer to the methods section for the description of the meaning of all parameters.

Cell concentration (10^6 x·mL^{-1})	$\Phi_{(I_0\text{-}I_{comp})}$	I_{com}	I_{sat}	R_D	P_{gmax}
1	0.36 ± 0.10	14.6 ± 0.5	133 ± 59	5.28 ± 1.29	9.9 ± 1.2
2.5	0.09 ± 0.02	19.5 ± 2.3	153 ± 21	1.82 ± 0.21	4.9 ± 0.2
5	0.11 ± 0.01	12.2 ± 1.1	163 ± 27	1.31 ± 0.12	4.6 ± 0.2
10	0.1 ± 0.02	9.5 ± 1.2	149 ± 37	0.95 ± 0.16	4.3 ± 0.3
20	0.09 ± 0.01	9.9 ± 0.7	157 ± 26	0.85 ± 0.12	4.3 ± 0.2
40	0.08 ± 0.01	8.3 ± 1.2	175 ± 29	0.64 ± 0.13	3.9 ± 0.2
75	0.05 ± 0.01	10.8 ± 1.4	329 ± 288	0.59 ± 0.1	4.2 ± 0.7
100	0.05 ± 0.01	12.2 ± 1.2	347 ± 263	0.56 ± 0.08	3.8 ± 0.6

Three groups of concentrations could be defined. First, for 1·10⁶ x·mL⁻¹ and 2.5·10⁶ x·mL⁻¹, data variability was larger, especially at low light intensities where O_2 flux per volume [pmol·s⁻¹·mL⁻¹] was low, affecting the signal-to-noise ratio. These cell

concentrations are not optimal, even though these limitations could be addressed by increasing the number of experimental replicates and prolonging sampling times.

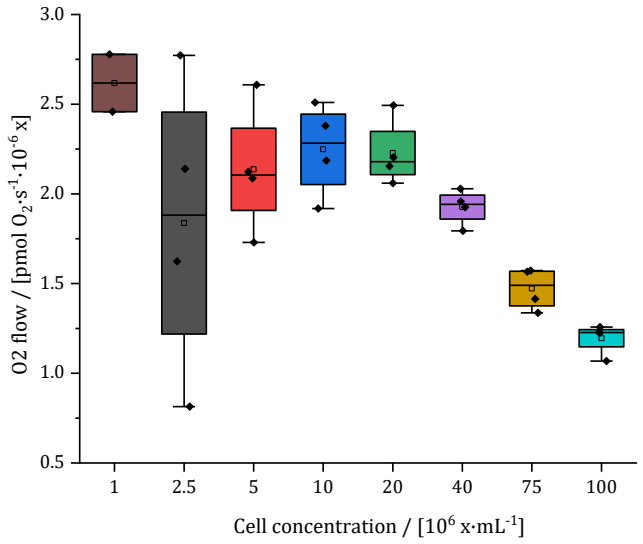

Figure 3. Comparison of O_2 flow at a mid-light intensity (50 µmol photons·s^{-1}·m^{-2}) at different cell concentrations.

Second, the cell concentration range comprised between $5{\cdot}10^6$ x·mL^{-1} and $20{\cdot}10^6$ x·mL^{-1} showed no major differences in terms of curve shape or internal variability among replicas. Since O_2 evolution was normalized to the number of cells, this consistency suggest that the measurements are stable and not influenced by the cell concentration in this range (Figure 3). This also suggests that light shading is not affecting the measurements. Concentrations within this range seem optimal for future PI curve experiments.

Last, for $40{\cdot}10^6$ x·mL^{-1} to $100{\cdot}10^6$ x·mL^{-1}, there was instead an effect due to the cell concentration, especially during the linear phase (Figure 3). The light saturation point was higher with higher concentrations, likely explained by a shading effect between cells at higher concentrations due their high optical density that caused an inhomogeneous light distribution in the sample. This hypothesis was confirmed by the observation that P_{gmax} was the same for all concentrations (Table 1). This suggests that even at high cell concentrations the value of maximal photosynthesis is correctly estimated because self-shading is not a factor anymore when light is in excess.

4. Conclusions

Our results demonstrate that the protocol developed for building PI curves of *Nannochloropsis gaditana* cultures with the NextGen-O2k is robust and reproducible. The possibility of making programmed light changes enables multiple measurements with limited time and efforts. The ideal working cell concentrations are those in the range of $5{\cdot}10^6$ x·mL^{-1} to $10{\cdot}10^6$ x·mL^{-1}, corresponding to 0.4-0.8 µg Chl·mL^{-1}. This concentration is more than 30 times lower than the one we used in the past with a classical Clark sensor (Perin et al 2015). In our conditions, a 20 mL 4 day-old culture of *Nannochloropsis* had typically a cell concentration of $25{\cdot}10^6$ x·mL^{-1} to $45{\cdot}10^6$ x·mL^{-1}. Therefore, a single measurement needed a volume of culture of 200-800 µL, less than 0.1 % of the total culture volume. Consequently, the same culture can be used for other experiments, optimizing its use. This is of particular interest for strains with a reduced growth rate. The reproducibility of our approach makes it possible to compare the photosynthetic performance of different strains and mutants under various experimental conditions.

Another major advantage of working with low concentrations is that it is possible to work in a range where self-shading effects are negligible. This is particularly important to study the effect of light intensity on the photosynthesis parameters.

Acknowledgements

This work was supported by project NextGen-O2k which has received funding from the European Union's Horizon 2020 research and innovation programme under grant agreement Nº 859770 (Oroboros Instruments).

References

Bailleul B et al (2015) Energetic coupling between plastids and mitochondria drives CO_2 assimilation in diatom. https://doi.org/10.1038/nature14599

Gnaiger E (2008) Polarographic oxygen sensors, the oxygraph and high-resolution respirometry to assess mitochondrial function. https://doi.org/10.1002/9780470372531.ch12

Huete-Ortega M, Di Marcello M, Iglesias-Gonzalez J, Gnaiger E (2020) High-resolution respirometry for chloroplast and mitochondrial bioenergetics in Chlamydomonas reinhardtii — towards biotechnology exploitations. https://doi.org/10.26124/mitofit:ea20.algaeurope.0001

Jassby AD, Platt T (1976) Mathematical formulation of the relationship between photosynthesis and light for phytoplankton. https://doi.org/10.4319/LO.1976.21.4.0540

Perin G, Bellan A, Segalla A, Meneghesso A, Alboresi A, Morosinotto T (2015) Generation of random mutants to improve light-use efficiency of Nannochloropsis gaditana cultures for biofuel production. https://doi.org/10.1186/s13068-015-0337-5

Perry MJ, Talbot MC, Alberte RS (1981) Photoadaption in marine phytoplankton: Response of the photosynthetic unit. https://doi.org/10.1007/BF00388170

Strickland J (1960) Measuring the production of marine phytoplankton. https://waves-vagues.dfo-mpo.gc.ca/library-bibliotheque/10157.pdf

Went N, Di Marcello M, Gnaiger E (2021) Oxygen dependence of photosynthesis and light-enhanced dark respiration studied by High-Resolution PhotoRespirometry. https://doi.org/10.26124/mitofit:2021-0005

Ye ZP (2007) A new model for relationship between irradiance and the rate of photosynthesis in *Oryza sativa*. https://doi.org/10.1007/s11099-007-0110-5

APPENDIX V

Acclimation of photosynthetic apparatus in the mesophilic red alga *Dixoniella giordanoi*

Nicolò Fattore[1], Simone Savio[1], Antoni M. Vera-Vives[1], Mariano Battistuzzi[1], Isabella Moro[1], Nicoletta La Rocca[1] and Tomas Morosinotto[1]

1. Department of Biology, University of Padova, Italy

This appendix was published in “Physiologia Plantarum” (2020)

Authorship statement:

My main contribution to this work was to design, perform and analyze the experiments regarding oxygen evolution and photosynthesis-irradiance relationship, and comment the draft during the revision process.

Received: 17 September 2020 | Accepted: 17 June 2021

DOI: 10.1111/ppl.13489

PHOTOBIOLOGY AND PHOTOSYNTHESIS

Physiologia Plantarum

Acclimation of photosynthetic apparatus in the mesophilic red alga *Dixoniella giordanoi*

Nicolò Fattore[1] | Simone Savio[1] | Antoni M. Vera-Vives[1] | Mariano Battistuzzi[2,1] | Isabella Moro[1] | Nicoletta La Rocca[1] | Tomas Morosinotto[1]

[1]Department of Biology, University of Padova, Padova, Italy

[2]Centro di Ateneo di Studi e Attività Spaziali (CISAS) "Giuseppe Colombo", University of Padova, Padova, Italy

Correspondence
Tomas Morosinotto, Department of Biology, University of Padova, Via U. Bassi 58/B, 35121 Padova, Italy.
Email: tomas.morosinotto@unipd.it

Edited by A. Krieger-Liszkay

Abstract

Eukaryotic algae are photosynthetic organisms capable of exploiting sunlight to fix carbon dioxide into biomass with highly variable genetic and metabolic features. Information on algae metabolism from different species is inhomogeneous and, while green algae are, in general, more characterized, information on red algae is relatively scarce despite their relevant position in eukaryotic algae diversity. Within red algae, the best-known species are extremophiles or multicellular, while information on mesophilic unicellular organisms is still lacunose. Here, we investigate the photosynthetic properties of a recently isolated seawater unicellular mesophilic red alga, *Dixoniella giordanoi*. Upon exposure to different illuminations, *D. giordanoi* shows the ability to acclimate, modulate chlorophyll content, and re-organize thylakoid membranes. Phycobilisome content is also largely regulated, leading to almost complete disassembly of this antenna system in cells grown under intense illumination. Despite the absence of a light-induced xanthophyll cycle, cells accumulate zeaxanthin upon prolonged exposure to strong light, likely contributing to photoprotection. *D. giordanoi* cells show the ability to perform cyclic electron transport that is enhanced under strong illumination, likely contributing to the protection of Photosystem I from over-reduction and enabling cells to survive PSII photoinhibition without negative impact on growth.

1 | INTRODUCTION

Organisms performing oxygenic photosynthesis exploit sunlight to fix CO_2 into biomass thanks to the activity of photosystem (PS) I and II, two multiprotein supercomplexes located in the thylakoid membranes. Both photosystems involved in oxygenic photosynthesis are composed of a core complex responsible for the charge separation and electron transfer reactions that are highly conserved among photosynthetic organisms, both prokaryotic and eukaryotic. Photosystems also include an antenna system to increase the light-harvesting capacity. Antenna proteins diverged during evolution, possibly also due to adaptation to different ecological niches. In cyanobacteria and red algae, the ability to capture light is increased by soluble protein complexes, called phycobilisomes (PBS), that bind pigments like phycocyanin and phycoerythrin. In most eukaryotes, instead, the antenna system is composed of hydrophobic light harvesting complexes (LHC) proteins, localized in the thylakoid membranes and bind chlorophyll (Chl) and carotenoids (Car). In different eukaryotic groups, the LHC themselves diversified into various subfamilies, such as LHCA/B found in green algae and plants or LHCF in diatoms (Büchel, 2015).

Photosynthetic activity is highly influenced by environmental factors like illumination intensity, temperature, CO_2, and nutrient

availability. Many environmental conditions can drive the photosystems to saturation and over-reduction, with the possible production of various Reactive Oxygen Species (ROS) causing oxidative damage of the photosynthetic apparatus (photoinhibition) (Li et al., 2009; Murata et al., 2007; Szabó et al., 2005). To thrive in highly variable environmental conditions, photosynthetic organisms evolved multiple mechanisms to modulate photosynthetic activity depending on the environmental conditions, limiting over-reduction and ROS formation. These regulatory mechanisms have different activation timescales, enabling responses to short-term and long-term dynamics of the environmental factors (Eberhard et al., 2008; Walters, 2005). The long-term acclimation response involves modulation of the composition of the photosynthetic apparatus according to irradiance intensity, regulating Chl and Car content (Falkowski & LaRoche, 1991; Walters, 2005). On a shorter timescale, photosynthetic organisms instead activate mechanisms for the modulation of light harvesting efficiency, such as non-photochemical quenching (NPQ), driving the dissipation of excess excitation energy as heat (Li et al., 2009). Strong illumination also activates the xanthophyll cycle, where zeaxanthin is synthesized from pre-existing violaxanthin, further contributing to the protection from ROS (Havaux et al., 2007). Photosynthetic electron transport is also regulated by the presence of alternative electron transport mechanisms, such as cyclic electron flow (CEF) and pseudo-cyclic electron flow (Shikanai, 2014), that were shown to be particularly important to protect PSI from over-reduction and damage (Allahverdiyeva et al., 2015; Storti et al., 2020).

All photosynthetic organisms present multiple regulatory mechanisms, a clear indication that modulation of photosynthesis is essential. On the other hand, not all mechanisms are conserved in all organisms, and interesting differences are observed in different species, possibly in correlation with evolutionary history and colonization of specific ecological niches (Alboresi et al., 2019; Goss & Lepetit, 2015; Quaas et al., 2014). The exploration of the diversity of regulatory responses in various phylogenetic groups thus represents a valuable source of information for a better understanding of their molecular mechanisms and biological role.

In this context, microalgae are particularly interesting since they are highly diverse, with more than 200,000 estimated species colonizing a wide range of ecosystems (Bleakley & Hayes, 2017). Eukaryotic algae originated from a primary endosymbiosis event approximately 1600 million years ago (Mya), which gave origin to Rhodophyta (red algae), Chlorophyta (green algae), and Glaucophyta (Gaignard et al., 2019). Diverse clades of photosynthetic organisms, including heterokontophytes, dinoflagellates, and haptophytes, originated through secondary and tertiary endosymbioses, thus further increasing the biodiversity of these organisms. Most of these latter endosymbiosis events involved phototrophic red microalgae, which thus have a central place in the evolution of photosynthetic organisms (Keeling, 2013).

Red algae (Rhodophyta) are estimated to include more than 7000 species, consisting of both micro and macroalgae (Guiry & Guiry, 2021). According to the more recent classification, the phylum Rhodophyta is divided into two subphyla, Cyanidiophytina and Rhodophytina (Yoon et al., 2006). The former includes unicellular red microalgae living in extreme environments, such as *Cyanidioschyzon merolae* or *Galdieria sulphuraria*. Rhodophytina is, instead, divided into six classes, three of them including microalgae: Porphyridiophyceae, Rhodellophyceae, and Stylonematophyceae.

Red algae present chlorophyll *a* (Chl *a*) (Gaignard et al., 2019; Gantt et al., 2003) and β-carotene as the major carotenoid (Schubert et al., 2006). Differently from other eukaryotes, red algae still present phycobilisomes as antenna proteins connected to PSII (Gantt et al., 2003; Marquardt & Rhiel, 1997; Wolfe et al., 1994). Like other eukaryotes, however, red algae also show transmembrane antennas LHC proteins, called LHCR, associated with Photosystem I (PSI) (Bhattacharya et al., 2013; Brawley et al., 2017; Neilson & Durnford, 2010). Even though structural biology allows obtaining high-resolution structural models and new information on the composition of photosynthetic complexes (Antoshvili et al., 2019; Ma et al., 2020; Pi et al., 2018), the knowledge concerning the in vivo regulation of photosynthesis in red algae is still limited (Eggert et al., 2007; Kowalczyk et al., 2013; Krupnik et al., 2013; Magdaong & Blankenship, 2018).

To increase available information on the biodiversity of photosynthetic organisms and, in particular, of the red lineage, we investigated a recently identified unicellular mesophilic red alga *Dixoniella giordanoi* (Sciuto et al., 2021) belonging to the Rhodellophyceae. We assessed the response of its photosynthetic apparatus to illumination dynamics with different timescales, investigating its acclimation to different light intensities as well as the capacity of activating NPQ response, xanthophyll cycle, and effective cyclic electron transport.

2 | MATERIALS AND METHODS

2.1 | Culture conditions

Dixoniella giordanoi was isolated from Adriatic Sea samples and identified as a new species of the genus *Dixoniella* (Sciuto et al., 2021). Here it was grown in sterile-filtered f/2 medium (Guillard & Ryther, 1962), using sea salts 32 g/L from SIGMA, 40 mM Tris HCl pH 8, SIGMA Guillard's (f/2) marine water enrichment solution ×1. Growth experiments were performed in Erlenmeyer flasks with orbital shaking, starting from a preculture at exponential phase grown at 100 μmol of photons m^{-2} s^{-1} illuminated with white LED lamps. The preculture was diluted to a final OD_{750} equal to 0.2, corresponding to approximately 0.9×10^6 cells/mL in a final volume of 30 mL. OD was measured using 1 cm length cuvettes. Constant illumination of 20, 100, and 400 μmol of photons m^{-2} s^{-1} was provided with white LED lamps. The temperature was kept at 22°C ± 1°C in a growth chamber. Algal growth was maintained for 4 days and daily monitored by cell counting. Maximal growth rates (expressed as day^{-1}) were calculated as the slope of the exponential phase of growth curves. For preliminary transmission electron microscope observations and Western blot analysis, algae were grown using f/2 medium enriched with nitrogen, phosphate and iron sources (0.75 g/L $NaNO_3$, 0.05 g/L NaH_2PO_4, and

0.0063 g/L $FeCl_3 \cdot 6H_2O$ final concentrations), in 5 cm diameter Drechsel's bottles with a 250 mL working volume and bubbling of air enriched with 5% CO_2.

2.2 | Transmission electron microscopy (TEM)

Cells were collected by centrifugation (10 min, 17,000*g*) and fixed overnight at 4°C in 3% glutaraldehyde in 0.1 M sodium cacodylate buffer (pH 6.9) and post-fixed for 2 h in 1% osmium tetroxide in the same buffer. The specimens were dehydrated in a graded series of ethyl alcohol and propylene oxide and embedded in Araldite. Ultrathin sections (80–100 nm) were cut with an ultramicrotome (Ultracut; Reichert-Jung, Vienna, Austria) and stained with lead citrate and uranyl acetate; they were then analyzed under a transmission electron microscope (Tecnai G2; FEI, Hillsboro, Oregon) operating at 100 kV.

2.3 | Pigment extraction and analysis

Chlorophyll *a* and total carotenoids were extracted from *D. giordanoi* cultures after 4 days of growth. Cells were centrifuged for 10 min at 17,000*g*. Hydrophobic pigments were extracted from centrifuged cells at 4°C using a 1:1 biomass to solvent ratio of 100% N,N′-dimethylformamide for at least 24 h under dark conditions. Pigment concentrations were determined spectrophotometrically using extinction coefficients (Porra et al., 1989; Wellburn, 1994).

2.4 | High-performance liquid chromatography pigment extraction and analysis

Pigments were extracted from *D. giordanoi* cultures after 4 days of growth. Cells were harvested by 10 min centrifugation at 10,000*g* at room temperature, and the supernatant was carefully discarded. Cells were disrupted with a Mini Bead Beater (Biospec Products). Four cycles were performed: rupture at 3500 OPM for 10 s in the presence of glass beads (150–212 mm diameter) and acetone 80% followed by 30 s in ice. The extracted pigments were then centrifuged at 20,000*g* for 10 min, and the supernatant was kept for the analyses. The content of individual carotenoids was determined using an High-performance liquid chromatography (HPLC; 1100 series, Agilent), equipped with a reversed-phase column (5 μm particle size; 25 × 0.4 cm; 250/4 RP 18 Lichrocart) as described in Färber and Jahns (1998). The peaks of each sample were identified through the retention time and absorption spectrum (Jeffrey et al., 1997).

2.5 | Phycobiliprotein extraction and analysis

Phycobiliproteins were extracted from *D. giordanoi* cultures after 4 days of growth. Cells were harvested by 10 min centrifugation at 10,000*g* at room temperature and washed twice in phosphate buffer (0.01 M Na_2HPO_4 and 0.15 M NaCl). Cell rupture was performed by three freeze–thaw cycles in liquid nitrogen in dark conditions to avoid phycobiliprotein photodegradation. Disrupted cells were resuspended in phosphate buffer (1:1), and phycobiliprotein concentrations were determined spectrophotometrically as described in Bennett and Bogobad (1973).

2.6 | SDS-PAGE electrophoresis and Western blotting

Samples were collected from cultures in the late exponential phase. Cells were disrupted with a Mini Bead Beater (Biospec Products, Oklahoma) at 3500 rpm for 20 s in the presence of glass beads (150–212 mm diameter), B1 buffer (400 mM NaCl, 2 mM $MgCl_2$, and 20 mM Tricine–KOH, pH 7.8), 0.5% milk powder, 1 mM PMSF, 1 mM DNP-e-amino-n-caproic acid, and 1 mM benzamidine. The ruptured cells were then solubilized in a buffer (×3) contained 30% glycerol, 125 mM Tris, pH 6.8, 0.1 M dithiothreitol, and 9% SDS at RT for 20 min. SDS-PAGE analysis was performed with a Tris-glycine buffer system as previously described (Laemmli, 1970) with acrylamide at a final concentration of 12%. Western blot analysis was performed by transferring the proteins to nitrocellulose (Bio Trace, Pall Corporation, Auckland, New Zealand) and detecting them with alkaline phosphatase-conjugated antibodies. The antibodies recognized the PSI subunits PsaA and PsaD (Agrisera), D2, LHCX1, VCP, and LHCII proteins (antibodies produced by immunizing New Zealand rabbits with purified spinach protein [D2, LHCII] or recombinant *N. gaditana* proteins [VCP and LHCX1]; Meneghesso et al., 2016).

2.7 | In vivo monitoring of photosynthetic parameters

Chlorophyll fluorescence was determined in vivo using Dual PAM 100 from Waltz. The parameters Fv/Fm, NPQ, and Y(II) were estimated using a light curve protocol, where the cells were stepwise exposed to increasing light intensity every 1 min, from 0 to 2006 μmol of photons m^{-2} s^{-1}, after 20 min of dark adaptation. Fv/Fm, NPQ, and Y(II) were calculated as $(Fm - F_0)/F_0$, $(Fm - Fm')/Fm'$, and $(Fm' - F)/Fm'$, respectively (Walz, 2006). Far-red light was switched on during the measurements unless otherwise stated. When actinic light was set off, NPQ was calculated only by a series of saturating pulses (6000 μmol of photons m^{-2} s^{-1}, 600 ms) every 1 min. NPQ was also estimated by incubating cells with nigericin (10 μM) for 10 min before the measure. The PSII antenna size was measured according to the fluorescence induction kinetics using a JTS-10 spectrophotometer in the fluorescence mode. Two milliliters of samples with a final concentration of 5×10^6 cell/mL were incubated with DCMU (3,4-dichlorophenyl-1,1-dimethylurea, 10 μM) for 10 min after 20 min of dark adaptation. The induction kinetics was measured upon excitation with 80 or 150 μmol of photons m^{-2} s^{-1} of actinic light at 630 nm. In the presence of this inhibitor, an average of 1 photon per

PSII center is absorbed at time *t*, corresponding to 2/3 of the fluorescence increase. This parameter was estimated to evaluate the number of absorbed photons by photosystems II, i.e. the antenna size. The electron flows were estimated, measuring P_{700} absorption at 705 nm in intact cells. The analysis was carried out exposing cells (at $\sim 5 \times 10^6$ cells/mL) to saturating actinic light (2050 μmol of photons m^{-2} s^{-1}, 630 nm) for 15 s to maximize P_{700} oxidation and reach a steady state. P_{700}^+ re-reduction in the dark kinetics were then monitored after the light was switched off. The total electron flow (TEF) was estimated measuring the P_{700}^+ re-reduction rates in untreated cells (Meneghesso et al., 2016; Simionato et al., 2013). The same procedure was repeated in samples treated with DCMU (10–80 μM) to evaluate the contribution of cyclic electron flow (CEF) and with DCMU in combination with DBMIB (dibromothymoquinone, 100–300 μM). In all cases, re-reduction kinetics of P_{700}^+ were quantified as the rate constant $1/\tau$ after fitting with a single exponential. By multiplying these rate constants the fraction of P_{700} oxidized (which was obtained by comparison with DCMU and DBMIB-poisoned cells), the number of electrons transferred per unit of time was evaluated.

2.8 | Oxygen evolution

The evolution of oxygen through increasing light intensities was measured using the O2k FluoroRespirometer (Oroboros Instruments; Doerrier et al., 2018). The measuring chambers were magnetically stirred at 750 rpm, and the oxygen concentration of the chambers was measured with a frequency of 2 s. The light source was a blue LED (emitting wavelength range 439–457 nm with the peak at 451 nm) attached to the chamber of the instrument (provided by Oroboros Instruments, manufactured by Osram Oslon). The 2 mL chambers were filled with a growth medium containing 5 mM $NaHCO_3$ and let equilibrate to experimental temperature (22°C). Then, a small fraction of the medium was replaced with an aliquot of the cell suspension to reach a final concentration in the chamber of 0.5×10^6 cells/mL. The chambers were then closed, and the oxygen consumption rate at dark was calculated. The light was turned on at 25 μmol of photons m^{-2} s^{-1} until stabilization of the oxygen flow (5–10 min). This was done recursively for the following light intensities: 25, 50, 100, 150, 200, 250, 300, 400, 500, 600, 700, 800, 900, and 1000 μmol of photons m^{-2} s^{-1}. The reported values of oxygen evolution rates at each intensity correspond to the median of 40–50 points in the stable region of oxygen flow minus the oxygen flow at dark (respiration).

3 | RESULTS

3.1 | Photosynthetic apparatus composition in *Dixoniella giordanoi*

Dixoniella giordanoi cells highlighted the presence of a single chloroplast characterized by a multilobate shape, occupying the largest part of cell volume, as typically found in red algae (Figure 1A). Within the chloroplasts, the thylakoids are unstacked for the presence of disk-shaped multiple phycobilisomes, present with an alternated arrangement on the thylakoid membranes (Figure 1B). Starch granules were visible outside of the chloroplast. Indeed, differently from green algae and plants, red algae carbohydrate reserves, called floridean starch, are found in the cytoplasm and not in the organelles (Viola et al., 2001). An eccentric nucleus with associated Golgi dictyosomes was also visible (Figure 1C). The peculiar position of Golgi bodies near

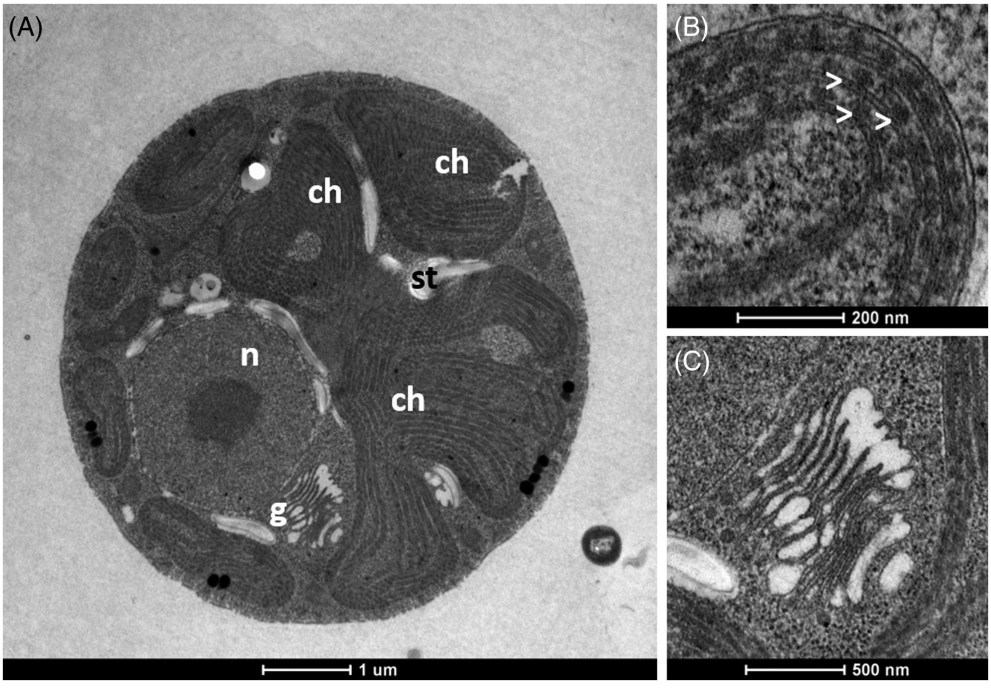

FIGURE 1 Transmission electron microscopy of *D. giordanoi* cells. (A) Complete view of a cell. Specific features and organelles are marked as n, nucleus; g, Golgi apparatus; ch, chloroplast; st, starch. (B,C) show details of thylakoids and dictyosomes of the Golgi apparatus, respectively. The white arrows indicate phycobilisomes associated with the thylakoids

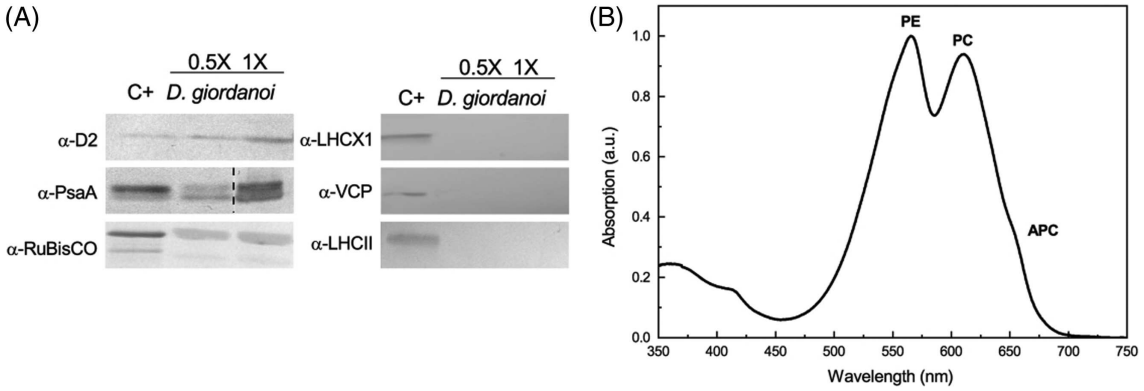

FIGURE 2 Composition of *D. giordanoi* photosynthetic apparatus. (A) Western blotting targeting different components of the photosynthetic apparatus from PSII (D2), PSI (PsaA), RuBisCO, and antenna complexes (LHCX1, VCP, and LHCII). Different dilutions of total cell extracts were loaded. The ×1 corresponds to 1 μg of Chl for each *D. giordanoi* sample, except for the case of PsaA, where 2 μg were loaded. As positive control (C+) total proteins extracted from the moss *Physcomitrella patens* were loaded for the targeting of D2, PsaA, RuBisCO, and LHCII. Extracts from *Nannochloropsis gaditana* were used as a positive control for LHCX1 and VCP. The dashed line indicates the removal of a lane not essential for the picture. (B) Absorption spectrum of isolated PBS fraction. Three absorption peaks are identified as phycoerythrin (PE), phycocyanin (PC), and allophycocyanin (APC) from their absorption maximum

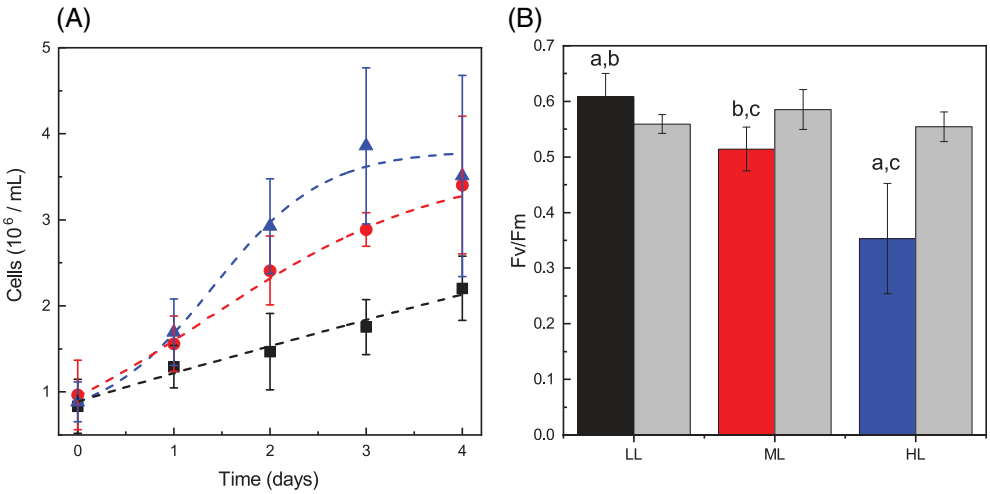

FIGURE 3 *D. giordanoi* growth under different light regimes. (A) Growth curve for *D. giordanoi* cells exposed for 4 days to LL, ML, and HL (20, 100, and 400 μmol of photons m^{-2} s^{-1}), shown as black squares, red circles, and blue triangles, respectively. The fitting of experimental data is shown as dashed lines. Average ± SD are reported (n > 4). (B) Photosystem II quantum yield quantified from Fv/Fm, of *D. giordanoi* after 4 days of growth in LL, ML, and HL (black, red, and blue, respectively). a, b, and c indicate differences statistically significant from ML, HL, and LL, respectively (one-way ANOVA, $p < 0.05$, n > 4, ±SD). Fv/Fm values after 24 h of dark recovery are represented with grey bars (n = 3, ±SD)

the outer membrane of the nuclear envelope is indeed a characteristic feature of only a few red algae genera, like *Dixoniella*, *Glaucosphaera*, and *Neorhodella* (Scott et al., 2011).

Western blot analysis performed to evaluate the composition of the photosynthetic apparatus allowed the detection of PsaA and D2 proteins, core subunits of, respectively, PSI and PSII even using antibodies raised against green algae and plants proteins, respectively, confirming the conservation of the sequences of these multiprotein complexes in photosynthetic organisms (Figure 2A). The presence of RuBisCO was also detected, corroborating the high conservation of the protein sequence. The presence of transmembrane antennas LHC protein was also tested using antibodies raised against proteins from highly divergent proteins, namely LHCX1 and VCP antenna from the heterokont *Nannochloropsis gaditana* and LHCII from plants. In neither case, there was any recognition in *D. giordanoi* samples confirming that, unlike the core complex of photosystems, antenna complexes show larger variability among the different groups of photosynthetic organisms.

Different protocols available in the literature were tested and optimized to isolate a phycobilisome (PBS) enriched soluble fraction from hydrophobic thylakoids. Even though the PBSs were not completely purified, absorption analysis of the soluble protein fraction revealed the presence of three distinct absorption peaks identifiable as typical of phycoerythrin (PE, peak at 562 nm), phycocyanin (PC, 615 nm), and allophycocyanin (APC, 652 nm), respectively (Figure 2B).

TABLE 1 Pigment composition of *D. giordanoi* cells grown under different light regimes

	LL	ML	HL
Chl *a* content (pg/cell)	1.01 ± 0.17[a]	0.57 ± 0.13[b]	0.32 ± 0.13[b]
Car/Chl ratio (pg/pg)	0.41 ± 0.03[a]	0.61 ± 0.09[b]	0.78 ± 0.08[b]
Zea/Chl *a* (mol)	0.28 ± 0.01[a]	0.43 ± 0.09[b]	0.67 ± 0.14[b]
Beta/Chl *a* (mol)	0.21 ± 0.01	0.19 ± 0.10	0.29 ± 0.06
Phycocyanin (pg/cell)	3.11 ± 0.90[a]	0.74 ± 0.25[b]	0.19 ± 0.16[a,b]
Allophycocyanin (pg/cell)	0.64 ± 0.35	0.14 ± 0.04	n.d.
Phycoerythrin (pg/cell)	1.37 ± 0.46[a]	0.28 ± 0.11[b]	n.d.

Note: Pigment composition of *D. giordanoi* cells assessed after 4 days of growth at LL, ML, and HL (20, 100, and 400 μmol of photons m^{-2} s^{-1}). Chl content per cell, Car/Chl ratio, and phycobiliproteins (phycocyanin, allophycocyanin, and phycoerythrin) content per cell are reported (n = 3). n.d., not detectable for values smaller than 0.05 pg/cell.
[a and b] indicate statistically differences from ML and LL samples, respectively (one-way ANOVA, $p < 0.05$, n = 3, ±SD).

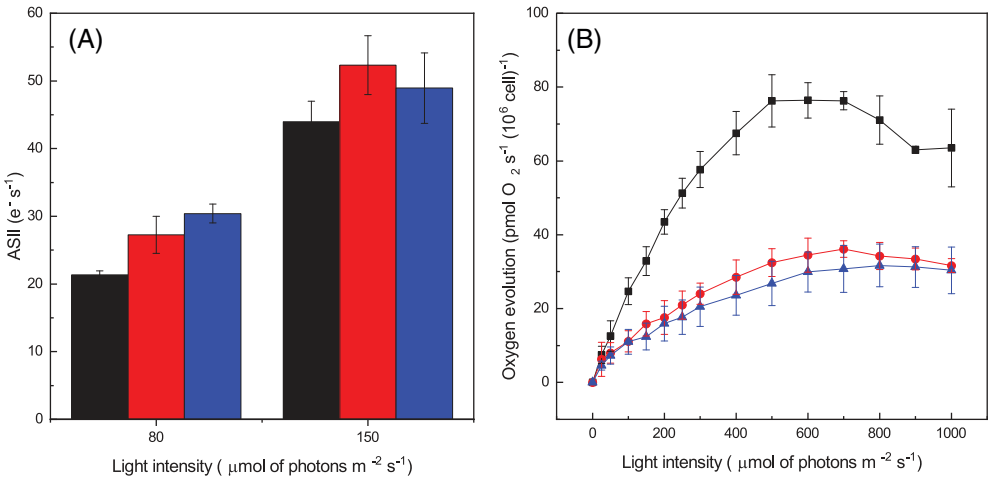

FIGURE 4 Acclimation of *D. giordanoi* cells to different light illumination. (A) Average PSII antenna size for all samples. Fluorescence measurements were taken with 10 million DCMU-treated cells in the presence of 80 or 150 μmol of photons m^{-2} s^{-1} of actinic light at 630 nm. (B) Oxygen evolution activity of acclimated cells exposed to increasing light intensity. Measurements were taken with 1 million cells. For both the pictures, LL, ML, and HL cells are represented in black, red, and blue, respectively. Data are reported as the average of three biological replica ±SD

3.2 | Response of *Dixoniella giordanoi* to growth under different light conditions

In nature, the light intensity is highly dynamic, with changes that can occur with different kinetics spanning from seconds to weeks. To cope with light variability, photosynthetic organisms evolved multiple regulatory mechanisms with different activation timescales, enabling responses to short-term and long-term variations. Here *D. giordanoi* ability to respond to different illumination was assessed by exposing batch cultures to three light intensities of 20, 100, and 400 μmol of photons m^{-2} s^{-1}, hereafter called LL, ML, and HL (Low, Medium, and High Light), respectively. Cultures exposed to LL showed the lowest growth rate, equal to 0.22 ± 0.03 day^{-1}, suggesting that this light intensity was limiting (Figure 3A). Indeed, cells exposed to ML showed faster growth (0.46 ± 0.07 day^{-1}). A further four times increase in light intensity yielded a further small increase in growth rate (0.60 ± 0.05 day^{-1}), suggesting that light saturation was reached.

To assess how the photosynthetic apparatus responded to different light intensities, the maximum PSII quantum yield was estimated by Fv/Fm. (Figure 3(B); Murata et al., 2007). PSII quantum yield was 17% and 38% lower in ML and HL compared with LL. If cells were left in the dark for 24 h, the Fv/Fm completely recovered in all cases, suggesting that the lower values were attributable to the photoinhibition of PSII experienced at ML and especially HL that is recovered, allowing enough time for damage repair.

3.3 | Acclimation of *Dixoniella giordanoi* to different illumination

Photosynthetic organisms exposed to different light regimes often respond by modulating the photosynthetic apparatus composition and functionality. Indeed, chlorophyll (Chl) content in *D. giordanoi* was strongly altered by growth under different illumination

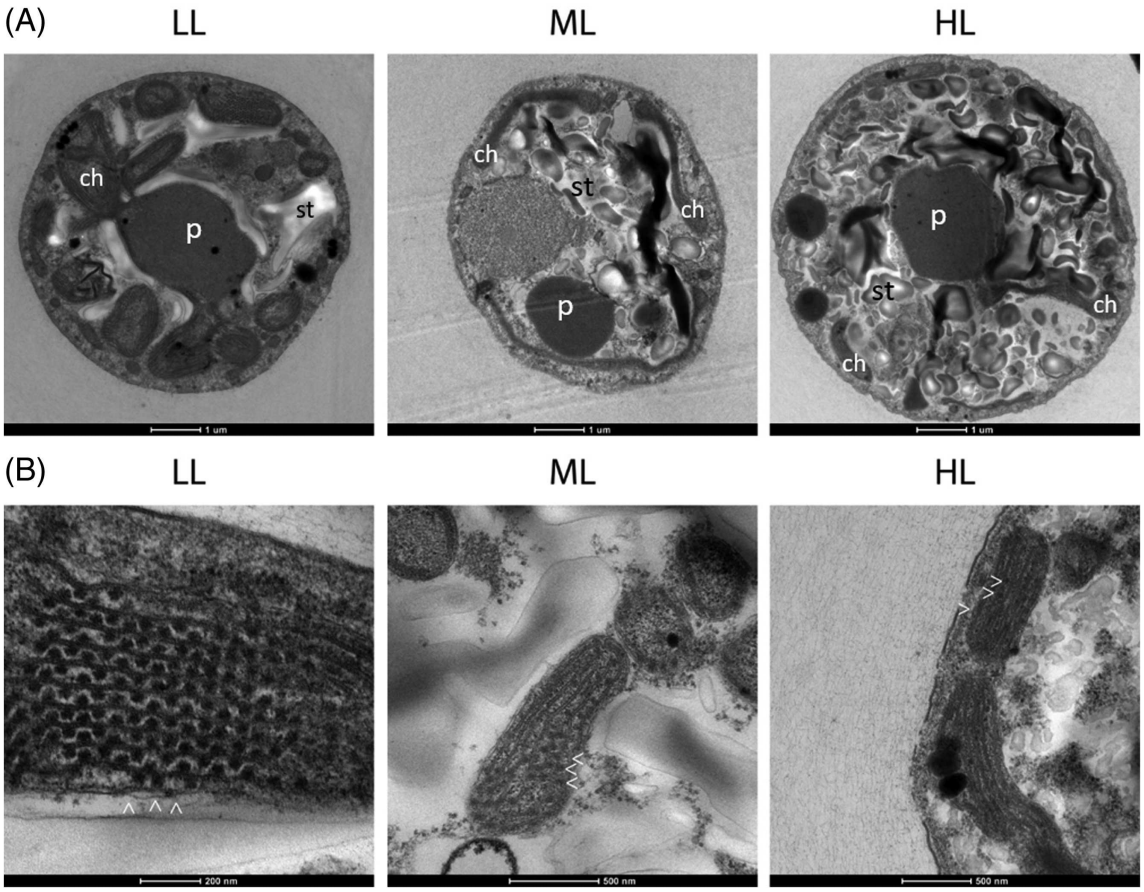

FIGURE 5 Ultrastructure of *D. giordanoi* cells acclimated to LL, ML, and HL. Panel (A) shows images of the whole cells. Specific features and organelles are marked as p, pyrenoid; ch, chloroplast lobes; st, starch. In (B) details of thylakoid membranes are shown. The white arrows indicate phycobilisomes associated with the thylakoids

regimes. Chl content was higher in LL cells with approximately 40% and 70% lower content in ML and HL, respectively (Table 1). The relative content of carotenoids, on the contrary, increased with the light intensity, as shown by the increase of Carotenoid/Chlorophyll ratio (Car/Chl), suggesting the relatively increased accumulation of these pigments with antioxidant activity. HPLC analysis showed that zeaxanthin and β-carotene are the main carotenoids in *D. giordanoi* in all light conditions. The relative content of zeaxanthin was progressively higher in cultures exposed to higher light intensity, while β-carotene remained stable.

Phycobilisomes (PBS) content was also strongly affected by light intensity, as evidenced by the decrease by 75%–80% in ML cells compared with LL for all three pigments classes: phycocyanin, allophycocyanin, and phycoerythrin. The decrease was even larger in HL cells, which showed a 95% lower content of PBS than LL acclimated cells (Table 1). Taken together, these data indicate that *D. giordanoi* showed a strong acclimation response with modulation of Chl, carotenoids, and PBS content.

The assessment of functional PSII antenna size using red light at 630 nm, thus poorly absorbed by PBS, showed no major differences between LL, ML, and HL cells, suggesting that LHC content was not significantly regulated (Figure S1; Figure 4A).

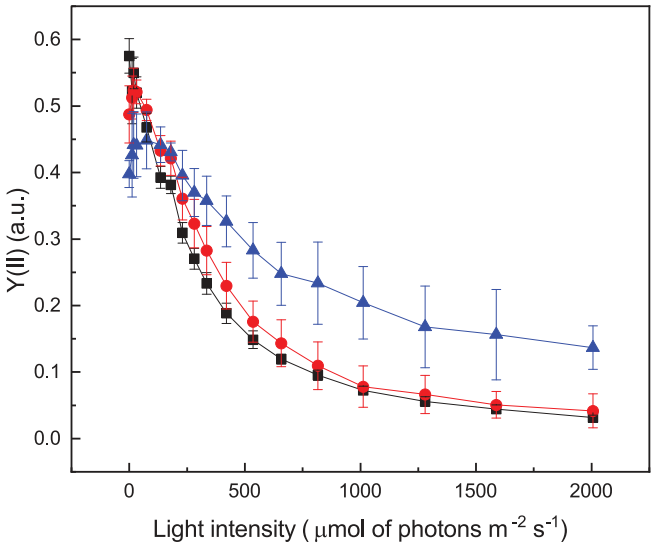

FIGURE 6 Photosynthetic regulation of *D. giordanoi* to different light intensities. Chl fluorescent kinetics were used to calculate PSII quantum yield expressed as Y(II) of acclimated cells and illuminated with a progressively stronger light. LL, ML, and HL cells are represented in black, red, and blue, respectively. During the measurements, the far-red light was switched on. Data are expressed as the average of three biological replica ±SD

Acclimation of photosynthetic activity was further assessed by measuring the oxygen evolution activity in cells exposed to increasing light intensities (Figure 4B). Comparing data measured with an equal cell concentration, with the lowest light intensities, LL cells showed a higher oxygen evolution activity compared with ML and HL, suggesting a higher light harvesting efficiency of these cells. Since blue excitation light is not well absorbed by PBS, the difference is likely underestimated. Oxygen evolution activity increased until reaching saturation at 500 μmol of photons m^{-2} s^{-1} and showed a decrease, likely because of photoinhibition, at higher light intensities. ML and HL cells instead reached saturation at higher illumination (7–800 μmol of photons m^{-2} s^{-1}), and photosynthetic activity did not decrease if the light was further increased.

All cells showed a similar oxygen evolution capacity per Chl amount (Figure S2), suggesting all cells, including HL cells have similar photosynthetic activity. This observation also suggests a similar light harvesting efficiency of Chl binding pigments, consistent with antenna size estimations (Figure S2).

The effect of light acclimation on *D. giordanoi* cell ultrastructure was assessed using transmission electron microscopy (Figure 5). Thylakoid membrane content and their organization were strongly affected by light intensity. In LL cells, thylakoid membranes were arranged in parallel arrays that included regularly spaced phycobilisomes. In ML cells and, to an even larger extent, in HL cells, thylakoids showed drastically reduced size, occupying a smaller part of cell volume, and were less organized. The number of phycobilisomes was also clearly lower in ML than in LL, and only a few were visible in HL cells. ML and especially HL cells also showed a large part of cell volume occupied by starch reserves. This indicates that an increasing fraction of carbon fixed was converted into reserve carbohydrates suggesting that photosynthetic activity was in excess in comparison to cells' ability to use light energy for growth, with other factors becoming limiting. The comparison of LL cells with ML and HL also showed a progressive reduction of chloroplast lobes volume, while the pyrenoid, containing Rubisco, remained well visible, consistent with a decrease in light harvesting efficiency while maintaining carbon fixation capacity.

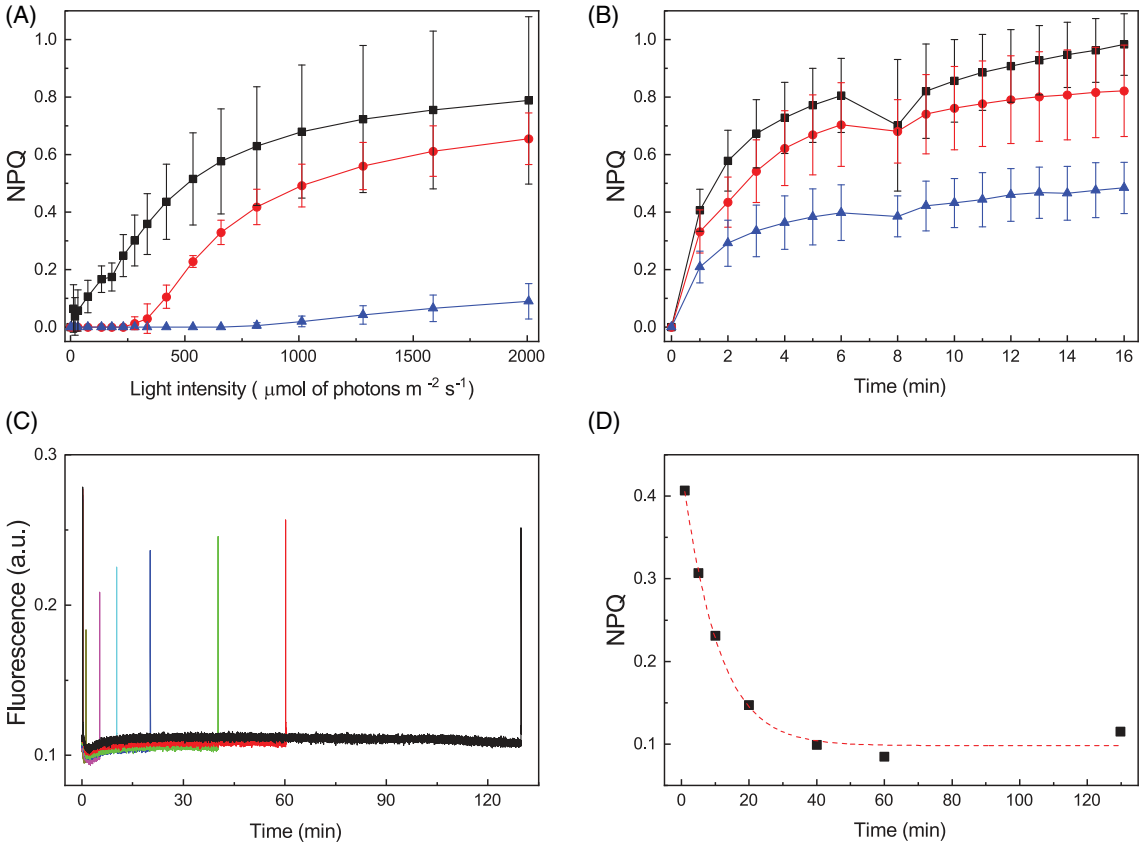

FIGURE 7 Non photochemical quenching in *D. giordanoi*. (A) NPQ was measured exposing acclimated cells to increasing light intensity. During the measurements, the far-red light was switched on. (B) NPQ of acclimated cells exposed to saturating pulses every minute with actinic light off (far-red off). For both figures, LL, ML, and HL cells are represented in black, red, and blue, respectively. Data are shown as the average of three biological replica ±SD. (C) Fluorescence traces of LL cells illuminated by a first saturating pulse followed by a second one after 1, 5 10, 20, 40, 60, or 130 min (in dark yellow, magenta, cyan, blue, green, red, and black, respectively). (D) The graph reports the kinetics of NPQ relaxation after one saturating pulse. The fitting of experimental data is shown as a dotted line

3.4 | Photosynthesis regulatory mechanisms in *Dixoniella giordanoi*

Photosynthetic organisms modulate not only the composition but also the activity of the photosynthetic apparatus in response to the illumination regimes. Photochemical capability can be deducted by measuring the effective quantum yield of PSII, Y(II), in cells illuminated with an actinic light intensity of different intensity. As shown in Figure 6, Y(II) progressively decreased with the increase of illumination because of the increased saturation of photochemical capacity. While Y(II) dropped rapidly in cells grown in LL and ML, HL cells maintained photochemical capability under strong illumination and did not show complete saturation even with the strongest illumination tested, showing that *D. giordanoi* cultures acclimated to high light can exploit a large fraction of absorbed light for photochemistry even under strong illumination.

Fluorescence measurements can also be exploited to assess regulatory mechanisms of photosynthesis and, for instance cell ability to activate thermal dissipation of excess energy quantifiable as NPQ. Figure 7 (A) shows that *D. giordanoi* LL cells can activate a measurable NPQ when exposed to illumination of different intensities, but this capacity is lower in ML cells and even further decreased in HL cells. The addition of nigericin, a molecule dissipating membrane ΔpH, does not inhibit NPQ in *Dixoniella*, suggesting the response is not pH-dependent (Figure S3).

Earlier reports showed in other red microalgae that saturating pulses alone could induce a detectable NPQ (Delphin et al., 1998). Indeed, *Dixoniella* cells simply exposed to a series of saturating pulses with the actinic light off showed the progressive decrease of fluorescence maxima and thus an apparent NPQ, that is not significantly different from the response with the light on (Figure 7(B); Figure S4). A single saturating pulse is indeed sufficient to induce an NPQ value equal to 0.4 (Figure 7B), which takes a significant over 40 min, to be relaxed (Figure 7(C,D)). Overall, the results show that an apparent NPQ is activated in *D. giordanoi*, but it has some peculiar characteristics different from those normally observed in other algae and plants.

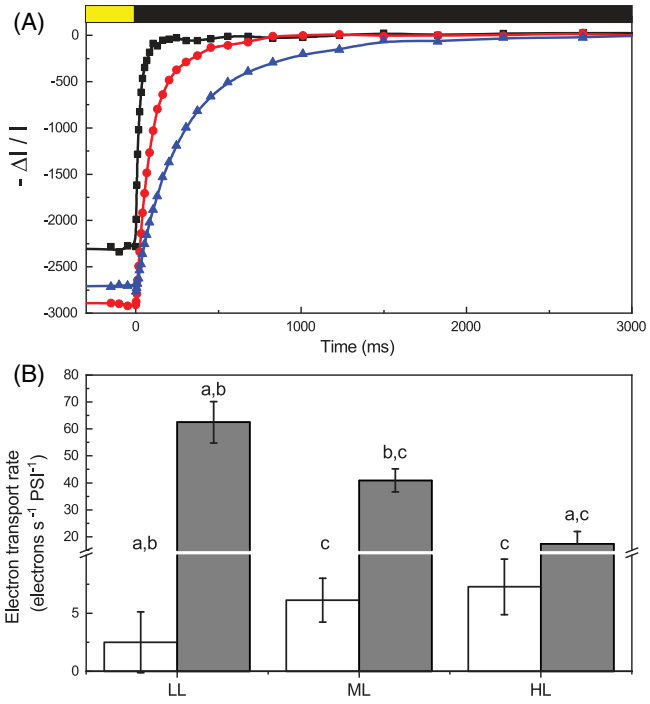

FIGURE 8 Regulation of photosynthetic electron transport in *D. giordanoi*. (A) Representative P_{700} redox kinetics from cells grown in ML. Cells acclimated to 100 μmol of photons m^{-2} s^{-1} (ML) were exposed to saturating light intensity (2050 μmol of photons m^{-2} s^{-1}) for 15 s before the dark recovery kinetics. Reduction of P_{700}^{+} after switching light off is followed by monitoring differential absorption at 705 nm. Untreated cells, cells treated with DCMU, and cells treated with DCMU+DBMIB are shown as black squares, red circles, and blue triangles, respectively. (B) Rates of cyclic electron flow (CEF, white) and total electron flow (TEF, gray) were evaluated from P_{700}^{+} reduction kinetics after illumination in LL, ML, and HL acclimated cells. a, b, and c indicate differences statistically significant from ML, HL, and LL, respectively (one-way ANOVA, $p < 0.05$, n = 3, ±SD)

3.5 | Regulation of photosynthetic electron transport

Chlorophyll fluorescence signal in intact cells primarily originates from PSII, and thus, the previous analyses are mainly indicative of its activity and regulation. PSI activity can instead be assessed by monitoring the P_{700} redox state in vivo. To this aim, cells were first exposed to actinic light inducing oxidation of PSI reaction center, generation of P_{700}^{+} that can be monitored from a differential absorption signal at 705 nm (Simionato et al., 2013). After cells were exposed to illumination for 5 min and reached steady-state photosynthesis, the light was switched off, allowing for the reduction of P_{700}^{+}. The kinetics of P_{700} reduction depends on the rate of electron transports from PSII and cytochrome b_6f to PSI and thus allows estimating the total electron flow (TEF), i.e. the sum of all the electron transport processes through PSI. The same measurements were repeated in the presence of inhibitors of PSII and cytochrome b_6f (DCMU and DBMIB, respectively) to assess the relative contribution of the linear (LEF) and cyclic (CEF) electron pathways to this total electron transport. As shown in Figure 8(A), PSII inhibition through DCMU strongly reduced electron transport, suggesting that linear electron transport through PSII and PSI is the main pathway in *D. giordanoi*, as commonly observed in various photosynthetic organisms. Treatment with both DCMU and DBMIB, thus inhibiting both PSII and Cyt b_6f, showed a further decrease in P_{700} reduction kinetics, suggesting that there is a significant contribution of cyclic electron flow around PSI to electron transport (Figure 8A). Similar experiments were repeated for cells acclimated to different conditions to assess the contribution of linear and cyclic electron transport to photosynthesis. Cells exposed to higher light intensities showed a small decrease in linear electron transport capability, but this was at least partially compensated by a relative increase of cyclic electron transport, whose activity was stronger in high light acclimated cells (Figure 8B).

4 | DISCUSSION

4.1 | Acclimation to different illumination by modulation of Chl and phycobilisomes content

Photosynthesis involves a complex set of redox reactions occurring in an oxygen-rich environment that are prone to the generation of reactive species. Many environmental parameters like temperature, irradiance, CO_2, and nutrients availability strongly influence photosynthesis requiring a continuous modulation. To thrive in such a dynamic and complex environment, photosynthetic organisms evolved multiple regulatory mechanisms to maintain photosynthetic efficiency while also protecting from the danger of over-excitation and over-reduction. Functional genomic studies with model organisms, *Arabidopsis thaliana* and *Chlamydomonas reinhardtii* in particular, allowed isolation and characterization of specific mutants resulting in the identification of several genes involved in the regulation of photosynthesis (Eberhard et al., 2008; Li et al., 2009). Mutant generation can, however, also drive to pleiotropic or compensatory effects that may impair a full understanding of biological function. A clear example can be found in the case of cyclic electron transport that depends on multiple mechanisms with significant functional overlap and where single mutants generally have mild phenotypes, leading to an underestimation of their biological relevance. On the contrary, when multiple mutations are combined, phenotypes are much more severe, showing how regulation of electron transport is indeed essential for photosynthesis (Munekage et al., 2004; Storti et al., 2020).

While all photosynthetic organisms present several regulatory mechanisms modulating activity, they are not all conserved in all species. Exploring biological diversity is thus a powerful approach to identify organisms showing specific combinations of regulatory mechanisms or unexpected features (Berne et al., 2018), complementing functional genetic studies. Algae with their large biodiversity are particularly interesting in this context since they are a source of variability that can be exploited for the understanding of the distribution of regulatory mechanisms (Shimakawa et al., 2018), motivating the analysis of under-investigated groups like the mesophilic red algae studied here.

D. giordanoi cultures under different light intensities respond to environmental conditions through the reorganization of the photosynthetic apparatus and the modulation of its photosynthetic efficiency (Figure 3B). *D. giordanoi* cells cultivated under high light intensity show a decrease in the cell Chl content and a reduction of the number of thylakoid membranes (Table 1; Figure 4), a commonly observed response (Falkowski & LaRoche, 1991; Walters, 2005). *D. giordanoi* also shows a strong modulation of the content of PBS that in HL acclimated cells decrease by 95% and become barely detectable (Table 1; Figure 5). Such modulation is much more extreme of what was observed for LHC antennas both in plants and algae that even upon exposure to extreme illumination retain a relatively large antenna system (>50%; Ballottari et al., 2007; Bonente et al., 2012; Meneghesso et al., 2016). The light-harvesting phycobilisomes are important to increase light absorption under low light intensities and, because of their presence, red algae can efficiently harvest radiation between 490 and 650 nm. This ability represents a significant competitive advantage in environments characterized by low sunlight availability, such as deep waters (Larkum, 2016). On the other hand, in case of exposition to strong illumination, the presence of PBS becomes detrimental, pushing *D. giordanoi* cells to almost remove the PBS antenna system completely.

Red algae antenna system also includes transmembrane LHC, as in other eukaryotes. The functional analysis of the antenna size (Figure 4A) and the oxygen evolution activity normalized per Chl content (Figure S2) using wavelengths poorly absorbed by PBS suggest that the LHC content is instead not significantly modulated between LL, ML, and HL cells. This suggests that acclimation response is dominated by two main responses: the modulation of the overall number of photosynthetic complexes and thus the Chl content per cell the regulation of PBS accumulation, while the LHC/reaction center ratio remains rather constant.

4.2 | *Dixoniella giordanoi* activates a peculiar fluorescence quenching as other unicellular red algae

NPQ consists of the thermal dissipation of excess energy and it is a regulatory mechanism widespread in photosynthetic organisms. Plants and many species of algae can activate NPQ thanks to specific proteins, PSBS or LHCX (Li et al., 2000; Peers et al., 2009). An NPQ mechanism with different properties is present in cyanobacteria as well, although it depends on the presence of another protein, OCP (Kirilovsky & Kerfeld, 2016). No gene encoding for these proteins has been found in red microalgae genomes sequenced so far, thus questioning the presence of an NPQ response in these organisms.

Here we show that it is possible to observe a fluorescence quenching in *D. giordanoi* (Figure 7A), but with peculiar properties compared with what is observed in plants, other eukaryotic algae, or even cyanobacteria. This response is detectable in *D. giordanoi* independently from the presence of actinic light and it is induced by the simple application of saturating flashes during the measurement (Figure 7B). A similar phenomenon was previously observed in other red algal species (Delphin et al., 1998), suggesting this is a specific feature of at least multiple species of this phylogenetic group.

The effect of the inhibitor nigericin suggests this NPQ is not dependent on the generation of a ΔpH (Figure S3). While inhibitors' activity with unknown species must be taken with caution, this hypothesis is fully consistent with the observation that quenching induced by a single saturation pulse takes at least 40 min to relax (Figure 7D). The metabolic effect of a single saturation pulse (6000 μmol of photons m^{-2} s^{-1} for 600 ms) is expected to be negligible but, even if this is not the case, any eventual ΔpH generated should be fast consumed and cannot last for several minutes. On the contrary, the long resilience of this effect must be attributed to some signaling and regulatory phenomena activated by light but independent from the metabolic effect.

Mechanistically, one possible explanation for this quenching would be the functional disconnection of some PBS from the PSII, which would cause a reduction in absorption and thus a potential decrease in fluorescence emission signal. A light-induced dissociation of PBS from PSII has been observed in the red alga *Porphyridium cruentum* by single-molecule spectroscopy (Liu et al., 2008) and, indeed, PBS mobility has been suggested to be a typical feature of mesophilic red algae, differently from extremophiles (Krupnik et al., 2013). This hypothesis would be consistent with the observation that the quenching response is smaller in HL cells, where PBS content is also reduced.

Alternative hypotheses such as an NPQ activated in the reaction center, as suggested for the extremophilic red alga *Cyanidioschyzon merolae* (Krupnik et al., 2013), or the modulation of excitation energy spillover between photosystems (Kowalczyk et al., 2013) are, however, possible.

4.3 | *Dixoniella giordanoi* accumulates zeaxanthin under strong illumination without a xanthophyll cycle

D. giordanoi, like other red algae, accumulates zeaxanthin together with β-carotene (Table 1—Schubert et al., 2006; Serive et al., 2017). However, there are no other detectable xanthophylls, and violaxanthin and antheraxanthin are missing, suggesting the absence of a xanthophyll cycle. This is consistent with findings from other red algae (Marquardt, 1998; Schubert et al., 2006; Serive et al., 2017) and with the available knowledge on red algae genomes that do not contain the genes coding for the enzymes involved in the xanthophyll cycle, violaxanthin de-epoxidase (VDE) and zeaxanthin epoxidase (ZE) (Bhattacharya et al., 2013; Coesel et al., 2008; Nozaki et al., 2007; Weber et al., 2004). Functional ZE genes have been identified in *Compsopogon coeruleus*, *Adagascaria erythrocladioides*, and *Calliarthron tuberculosum*, but they are all red seaweeds and the corresponding gene was never identified in unicellular organisms. Furthermore, these red algal ZE introduces only a single epoxy group into zeaxanthin, yielding antheraxanthin instead of violaxanthin (Dautermann & Lohr, 2017).

While the xanthophyll cycle is absent in *D. giordanoi*, data from pigment composition of cells grown under different illumination show that zeaxanthin is specifically over-accumulated in response to strong illumination, while β-carotene content remained stable (Table 1). Since the proteins potentially binding these carotenoids, LHC, are not increased in HL cells, these additional zeaxanthin molecules are likely found free in the thylakoid membranes. The accumulated zeaxanthin likely contributes to protection from an excess illumination in *D. giordanoi* cells acclimated to HL, similarly to what was observed in plants where zeaxanthin free in the thylakoid membranes is acting as an antioxidant, scavenging ROS (Havaux et al., 2007).

The xanthophyll cycle enables the modulation of zeaxanthin accumulation within minutes depending on illumination conditions. While *D. giordanoi* can still modulate the accumulation of zeaxanthin, the kinetics of synthesis/degradation is much slower. If cells acclimated to HL are exposed back to lower illumination it can be expected that they will retain the zeaxanthin, negatively impacting the light use efficiency. While the accumulation of zeaxanthin likely contributes to the protection from an excess of illumination in *D. giordanoi*, the absence of a xanthophyll cycle can represent a disadvantage when growing conditions are dynamic, impairing its fast synthesis and degradation when light intensity changes. At least in plants, it has been shown that this capacity for fast modulation of xanthophyll composition has a strong impact on photosynthetic productivity in a variable environment (Kromdijk et al., 2016).

4.4 | Cyclic electron flow in Dixoniella giordanoi is increased under strong illumination

D. giordanoi cells show a significant capability for cyclic electron flow, which is also increased in cells acclimated to HL (Figure 8). This suggests that modulation of photosynthetic electron transport is playing a role in the *D. giordanoi* response to strong illumination. In plants, cyclic electron flow is particularly important to protect PSI from over-reduction (Tiwari et al., 2016), while NPQ and xanthophyll cycle are more important for limiting damage from over-excitation to PSII (Peers et al., 2009; Tian et al., 2019). *D. giordanoi* cells show signs of PSII photoinhibition, as evidenced by the lower Fv/Fm (Figure 3B) if exposed to high or even intermediate light intensity (HL/ML). Despite this damage, however, ML and HL cells are still growing much faster than LL cells that show higher PSII activity. This suggests that PSI in *D. giordanoi* is well protected, likely with the contribution of cyclic electron transport, and capable of maintaining its activity. The loss of PSII activity is thus at least partially compensated by cyclic around PSI and this is sufficient to support a fast growth (Larosa et al., 2018).

AUTHOR CONTRIBUTION

Nicolò Fattore: Performed most experiments, analyzed the data, and wrote the article. **Simone Savio:** Performed most experiments, analyzed the data. **Antoni M. Vera-Vives:** Performed oxygen evolution measurements. **Mariano Battistuzzi:** Performed HPLC analyses. **Isabella Moro:** Performed TEM analyses. **Nicoletta La Rocca:** Analyzed the data. **Tomas Morosinotto:** Designed the research, analyzed the data, wrote the article. All authors reviewed the manuscript.

DATA AVAILABILITY STATEMENT

The data that support the findings of this study are available from the corresponding author.

ORCID

Tomas Morosinotto https://orcid.org/0000-0002-0803-7591

REFERENCES

Alboresi, A., Storti, M. & Morosinotto, T. (2019) Balancing protection and efficiency in the regulation of photosynthetic electron transport across plant evolution. *The New Phytologist*, 221, 105–109.

Allahverdiyeva, Y., Suorsa, M., Tikkanen, M. & Aro, E.-M.E.-M. (2015) Photoprotection of photosystems in fluctuating light intensities. *Journal of Experimental Botany*, 66, 2427–2436.

Antoshvili, M., Caspy, I., Hippler, M. & Nelson, N. (2019) Structure and function of photosystem I in Cyanidioschyzon merolae. *Photosynthesis Research*, 139, 499–508.

Ballottari, M., Dall'Osto, L., Morosinotto, T. & Bassi, R. (2007) Contrasting behavior of higher plant photosystem I and II antenna systems during acclimation. *The Journal of Biological Chemistry*, 282, 8947–8958.

Bennett, A. & Bogobad, L. (1973) Complementary chromatic adaptation in a filamentous blue-green alga. *The Journal of Cell Biology*, 58, 419–435.

Berne, N., Fabryova, T., Istaz, B., Cardol, P. & Bailleul, B. (2018) The peculiar NPQ regulation in the stramenopile Phaeomonas sp. challenges the xanthophyll cycle dogma. *Biochimica et Biophysica Acta - Bioenergetics*, 1859, 491–500.

Bhattacharya, D., Price, D.C., Xin Chan, C., Qiu, H., Rose, N., Ball, S. et al. (2013) Genome of the red alga *Porphyridium purpureum*. *Nature Communications*, 4, 1941. https://doi.org/10.1038/ncomms2931

Bleakley, S. & Hayes, M. (2017) Algal proteins: extraction, application, and challenges concerning production. *Foods (Basel, Switzerland)*, 6, 33.

Bonente, G., Pippa, S., Castellano, S., Bassi, R. & Ballottari, M. (2012) Acclimation of *Chlamydomonas reinhardtii* to different growth irradiances. *The Journal of Biological Chemistry*, 287, 5833–5847.

Brawley, S.H., Blouin, N.A., Ficko-Blean, E., Wheeler, G.L., Lohr, M., Goodson, H.V. et al. (2017) Insights into the red algae and eukaryotic evolution from the genome of *Porphyra umbilicalis* (Bangiophyceae, Rhodophyta). *Proceedings of the National Academy of Sciences of the United States of America*, 114, E6361–E6370.

Büchel, C. (2015) Evolution and function of light harvesting proteins. *Journal of Plant Physiology*, 172, 62–75.

Coesel, S., Oborník, M., Varela, J., Falciatore, A. & Bowler, C. (2008) Evolutionary origins and functions of the carotenoid biosynthetic pathway in marine diatoms. *PLoS One*, 3, e2896.

Dautermann, O. & Lohr, M. (2017) A functional zeaxanthin epoxidase from red algae shedding light on the evolution of light-harvesting carotenoids and the xanthophyll cycle in photosynthetic eukaryotes. *The Plant Journal*, 92, 879–891.

Delphin, E., Duval, J.C., Etienne, A.L. & Kirilovsky, D. (1998) ΔpH-dependent photosystem II fluorescence quenching induced by saturating, multiturnover pulses in red algae. *Plant Physiology*, 118, 103–113.

Doerrier, C., Garcia-Souza, L.F., Krumschnabel, G., Wohlfarter, Y., Mészáros, A.T. & Gnaiger, E. (2018) High-resolution FluoRespirometry and OXPHOS protocols for human cells, Permeabilized fibers from small biopsies of muscle, and isolated mitochondria. *Methods in Molecular Biology*, 1782, 31–70.

Eberhard, S., Finazzi, G. & Wollman, F.-A. (2008) The dynamics of photosynthesis. *Annual Review of Genetics*, 42, 463–515.

Eggert, A., Raimund, S., Michalik, D., West, J. & Karsten, U. (2007) Ecophysiological performance of the primitive red alga *Dixoniella grisea* (Rhodellophyceae) to irradiance, temperature and salinity stress: growth responses and the osmotic role of mannitol. *Phycologia*, 46, 22–28.

Falkowski, P.G. & LaRoche, J. (1991) Acclimation to spectral irradiance in algae. *Journal of Phycology*, 27, 8–14.

Färber, A. & Jahns, P. (1998) The xanthophyll cycle of higher plants: influence of antenna size and membrane organization. *Biochimica et Biophysica Acta - Bioenergetics*, 1363, 47–58.

Gaignard, C., Gargouch, N., Dubessay, P., Delattre, C., Pierre, G., Laroche, C. et al. (2019) New horizons in culture and valorization of red microalgae. *Biotechnology Advances*, 37, 193–222.

Gantt, E., Grabowski, B. & Cunningham, F.X. (2003) Antenna systems of red algae: phycobilisomes with photosystem II and chlorophyll complexes with photosystem I. In: Green, B.R. & Parson, W.W. (Eds.) *Light harvesting antennas in photosynthesis*. Dordrecht: Springer Netherlands, pp. 307–322.

Goss, R. & Lepetit, B. (2015) Biodiversity of NPQ. *Journal of Plant Physiology*, 172, 13–32.

Guillard, R.R.L. & Ryther, J.H. (1962) Studies of marine planktonic diatoms: I. *Cyclotella nana hustedt*, and *Detonula confervacea* (cleve) Gran. *Canadian Journal of Microbiology*, 8, 229–239.

Guiry, M.D., Guiry, G. (2021) Algaebase: Listing the World's Algae. Available from: https://www.algaebase.org/ [Accessed: 29 June 2021]

Havaux, M., Dall'osto, L. & Bassi, R. (2007) Zeaxanthin has enhanced antioxidant capacity with respect to all other xanthophylls in Arabidopsis leaves and functions independent of binding to PSII antennae. *Plant Physiology*, 145, 1506–1520.

Jeffrey, S.W., Mantoura, R.F.C. & Wright, S.W. (1997) *Phytoplankton pigments in oceanography: guidelines to modern methods. Monographs on oceanographic methodology*. Paris: UNESCO Publishing.

Keeling, P.J. (2013) The number, speed, and impact of plastid endosymbioses in eukaryotic evolution. *Annual Review of Plant Biology*, 64, 583–607.

Kirilovsky, D. & Kerfeld, C.A. (2016) Cyanobacterial photoprotection by the orange carotenoid protein. *Nature Plants*, 2, 16180.

Kowalczyk, N., Rappaport, F., Boyen, C., Wollman, F.-A., Collén, J. & Joliot, P. (2013) Photosynthesis in *Chondrus crispus*: the contribution of energy spill-over in the regulation of excitonic flux. *Biochimica et Biophysica Acta*, 1827, 834–842.

Kromdijk, J., Głowacka, K., Leonelli, L., Gabilly, S.T., Iwai, M., Niyogi, K.K. et al. (2016) Improving photosynthesis and crop productivity by accelerating recovery from photoprotection. *Science*, 354, 857–861.

Krupnik, T., Kotabová, E., van Bezouwen, L.S., Mazur, R., Garstka, M., Nixon, P.J. et al. (2013) A reaction center-dependent photoprotection mechanism in a highly robust photosystem II from an extremophilic red alga, *Cyanidioschyzon merolae*. *The Journal of Biological Chemistry*, 288, 23529–23542.

Laemmli, U.K. (1970) Cleavage of structural proteins during the assembly of the head of bacteriophage T4. *Nature*, 227, 680–685.

Larkum, A.W. (2016) Photosynthesis and light harvesting in algae. In: Borowitzka, M.A., Beardall, J. & Raven, J.A. (Eds.) *The physiology of microalgae*. Cham: Springer International Publishing, pp. 67–87.

Larosa, V., Meneghesso, A., La Rocca, N., Steinbeck, J., Hippler, M., Szabò, I. et al. (2018) Mitochondria affect photosynthetic electron transport and photosensitivity in a green alga. *Plant Physiology*, 176, 2305–2314.

Li, X.P., Björkman, O., Shih, C., Grossman, A.R., Rosenquist, M., Jansson, S. et al. (2000) A pigment-binding protein essential for regulation of photosynthetic light harvesting. *Nature*, 403, 391–395.

Li, Z., Wakao, S., Fischer, B.B. & Niyogi, K.K. (2009) Sensing and responding to excess light. *Annual Review of Plant Biology*, 60, 239–260.

Liu, L.-N., Elmalk, A.T., Aartsma, T.J., Thomas, J.-C., Lamers, G.E.M., Zhou, B.-C. et al. (2008) Light-induced energetic decoupling as a mechanism for phycobilisome-related energy dissipation in red algae: a single molecule study. *PLoS One*, 3, e3134.

Ma, J., You, X., Sun, S., Wang, X., Qin, S. & Sui, S.-F. (2020) Structural basis of energy transfer in *Porphyridium purpureum* phycobilisome. *Nature*, 579, 146–151.

Magdaong, N.C.M. & Blankenship, R.E. (2018) Photoprotective, excited-state quenching mechanisms in diverse photosynthetic organisms. *The Journal of Biological Chemistry*, 293, 5018–5025.

Marquardt, J. (1998) Effects of carotenoid-depletion on the photosynthetic apparatus of a *Galdieria sulphuraria* (Rhodophyta) strain that retains its photosynthetic apparatus in the dark. *Journal of Plant Physiology*, 152, 372–380.

Marquardt, J. & Rhiel, E. (1997) The membrane-intrinsic light-harvesting complex of the red alga Galdieria sulphuraria (formerly *Cyanidium caldarium*): biochemical and immunochemical characterization. *Biochimica et Biophysica Acta - Bioenergetics*, 1320, 153–164.

Meneghesso, A., Simionato, D., Gerotto, C., La Rocca, N., Finazzi, G. & Morosinotto, T. (2016) Photoacclimation of photosynthesis in the

Eustigmatophycean Nannochloropsis gaditana. *Photosynthesis Research*, 129, 291–305. https://doi.org/10.1007/s11120-016-0297-z

Munekage, Y., Hashimoto, M., Miyake, C., Tomizawa, K., Endo, T., Tasaka, M. et al. (2004) Cyclic electron flow around photosystem I is essential for photosynthesis. *Nature*, 429, 579–582.

Murata, N., Takahashi, S., Nishiyama, Y. & Allakhverdiev, S.I. (2007) Photoinhibition of photosystem II under environmental stress. *Biochimica et Biophysica Acta*, 1767, 414–421.

Neilson, J.A.D. & Durnford, D.G. (2010) Structural and functional diversification of the light-harvesting complexes in photosynthetic eukaryotes. *Photosynthesis Research*, 106, 57–71.

Nozaki, H., Takano, H., Misumi, O., Terasawa, K., Matsuzaki, M., Maruyama, S. et al. (2007) A 100%-complete sequence reveals unusually simple genomic features in the hot-spring red alga Cyanidioschyzon merolae. *BMC Biology*, 5, 1–8.

Peers, G., Truong, T.B., Ostendorf, E., Busch, A., Elrad, D., Grossman, A.R. et al. (2009) An ancient light-harvesting protein is critical for the regulation of algal photosynthesis. *Nature*, 462, 518–521.

Pi, X., Tian, L., Dai, H.E., Qin, X., Cheng, L., Kuang, T. et al. (2018) Unique organization of photosystem I–light-harvesting supercomplex revealed by cryo-EM from a red alga. *Proceedings of the National Academy of Sciences of the United States of America*, 115, 4423–4428.

Porra, R.J., Thompson, W.A. & Kriedemann, P.E. (1989) Determination of accurate extinction coefficients and simultaneous equations for assaying chlorophylls a and b extracted with four different solvents: verification of the concentration of chlorophyll standards by atomic absorption spectroscopy. *Biochimica et Biophysica Acta - Bioenergetics*, 975, 384–394.

Quaas, T., Berteotti, S., Ballottari, M., Flieger, K., Bassi, R., Wilhelm, C. et al. (2014) Non-photochemical quenching and xanthophyll cycle activities in six green algal species suggest mechanistic differences in the process of excess energy dissipation. *Journal of Plant Physiology*, 172, 92–103.

Schubert, N., García-Mendoza, E. & Pacheco-Ruiz, I. (2006) Carotenoid composition of marine red algae. *Journal of Phycology*, 42, 1208–1216.

Sciuto, K., Moschin, E., Fattore, N., Morosinotto, T. & Moro, I. (2021) Description of Dixoniella giordanoi sp. nov., a new cryptic species inside the primitive genus Dixoniella (Rhodellophyceae, Rhodophyta). *Phycologia*.

Scott, J., Yang, E.C., West, J.A., Yokoyama, A., Kim, H.J., Loiseaux De Goër, S. et al. (2011) On the genus Rhodella, the emended orders Dixoniellales and Rhodellales with a new order Glaucosphaerales (Rhodellophyceae, Rhodophyta). *Algae*, 26, 277–288.

Serive, B., Nicolau, E., Bérard, J.B., Kaas, R., Pasquet, V., Picot, L. et al. (2017) Community analysis of pigment patterns from 37 microalgae strains reveals new carotenoids and porphyrins characteristic of distinct strains and taxonomic groups. *PLoS One*, 12, e0171872. https://doi.org/10.1371/journal.pone.0171872

Shikanai, T. (2014) Central role of cyclic electron transport around photosystem I in the regulation of photosynthesis. *Current Opinion in Biotechnology*, 26, 25–30.

Shimakawa, G., Murakami, A., Niwa, K., Matsuda, Y., Wada, A. & Miyake, C. (2018) Comparative analysis of strategies to prepare electron sinks in aquatic photoautotrophs. *Photosynthesis Research*, 139, 401–411.

Simionato, D., Block, M.A.M.A., La Rocca, N., Jouhet, J., Maréchal, E., Finazzi, G. et al. (2013) The response of Nannochloropsis gaditana to nitrogen starvation includes de novo biosynthesis of triacylglycerols, a decrease of chloroplast galactolipids, and reorganization of the photosynthetic apparatus. *Eukaryotic Cell*, 12, 665–676.

Storti, M., Segalla, A., Mellon, M., Alboresi, A. & Morosinotto, T. (2020) Regulation of electron transport is essential for photosystem I stability and plant growth. *The New Phytologist*, 228, 1316–1326.

Szabó, I., Bergantino, E. & Giacometti, G.M. (2005) Light and oxygenic photosynthesis: energy dissipation as a protection mechanism against photo-oxidation. *EMBO Reports*, 6, 629–634.

Tian, L., Nawrocki, W.J., Liu, X., Polukhina, I., van Stokkum, I.H.M. & Croce, R. (2019) pH dependence, kinetics and light-harvesting regulation of nonphotochemical quenching in Chlamydomonas. *Proceedings of the National Academy of Sciences of the United States of America*, 116, 8320–8325.

Tiwari A., Mamedov F., Grieco M., Suorsa M., Jajoo A., Styring S. et al. (2016) Photodamage of iron–sulphur clusters in photosystem I induces non-photochemical energy dissipation. *Nature Plants*, 2(4).

Viola, R., Nyvall, P. & Pedersén, M. (2001) The unique features of starch metabolism in red algae. *Proceedings of the Royal Society B: Biological Sciences*, 268, 1417–1422.

Walters, R.G. (2005) Towards an understanding of photosynthetic acclimation. *Journal of Experimental Botany*, 56, 435–447.

Walz, H. (2006) *Dual-PAM-100 measuring system for simultaneous assessment of P700 and chlorophyll fluorescence*. Germany: Heinz Walz GmbH.

Weber, A.P.M., Oesterhelt, C., Gross, W., Bräutigam, A., Imboden, L.A., Krassovskaya, I. et al. (2004) EST-analysis of the thermo-acidophilic red microalga Galdieria sulphuraria reveals potential for lipid a biosynthesis and unveils the pathway of carbon export from rhodoplasts. *Plant Molecular Biology*, 55, 17–32.

Wellburn, A.R. (1994) The spectral determination of chlorophylls a and b, as well as total carotenoids, using various solvents with spectrophotometers of different resolution. *Journal of Plant Physiology*, 144, 307–313.

Wolfe, G.R., Cunningham, F.X., Durnfordt, D., Green, B.R. & Gantt, E. (1994) Evidence for a common origin of chloroplasts with light-harvesting complexes of different pigmentation. *Nature*, 367, 566–568.

Yoon, H.S., Müller, K.M., Sheath, R.G., Ott, F.D. & Bhattacharya, D. (2006) Defining the major lineages of red algae (Rhodophyta). *Journal of Phycology*, 42, 482–492.

SUPPORTING INFORMATION

Additional supporting information may be found online in the Supporting Information section at the end of this article.

How to cite this article: Fattore, N., Savio, S., Vera-Vives, A. M., Battistuzzi, M., Moro, I., La Rocca, N. et al. (2021) Acclimation of photosynthetic apparatus in the mesophilic red alga *Dixoniella giordanoi*. *Physiologia Plantarum*, 1–13. Available from: https://doi.org/10.1111/ppl.13489

SUPPORTING INFORMATION

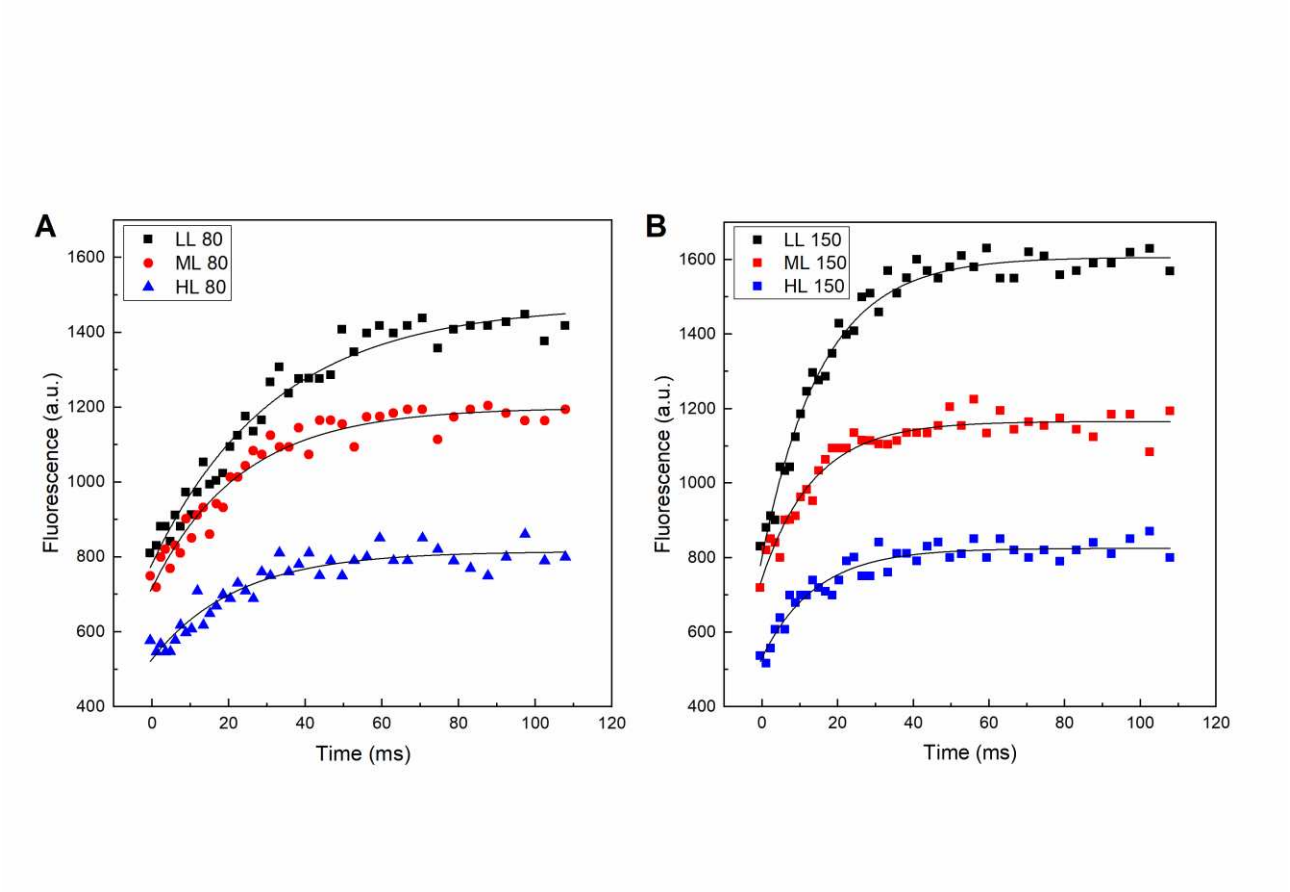

Figure S1. Modulation of the functional antenna size in PSII. Representative traces of the fluorescence kinetics of DCMU-treated cells in the presence of 80 (A) or 150 (B) µmol of photons m^{-2} s^{-1} of actinic light at 630 nm. LL, ML and HL cells are represented in black, red and blue, respectively.

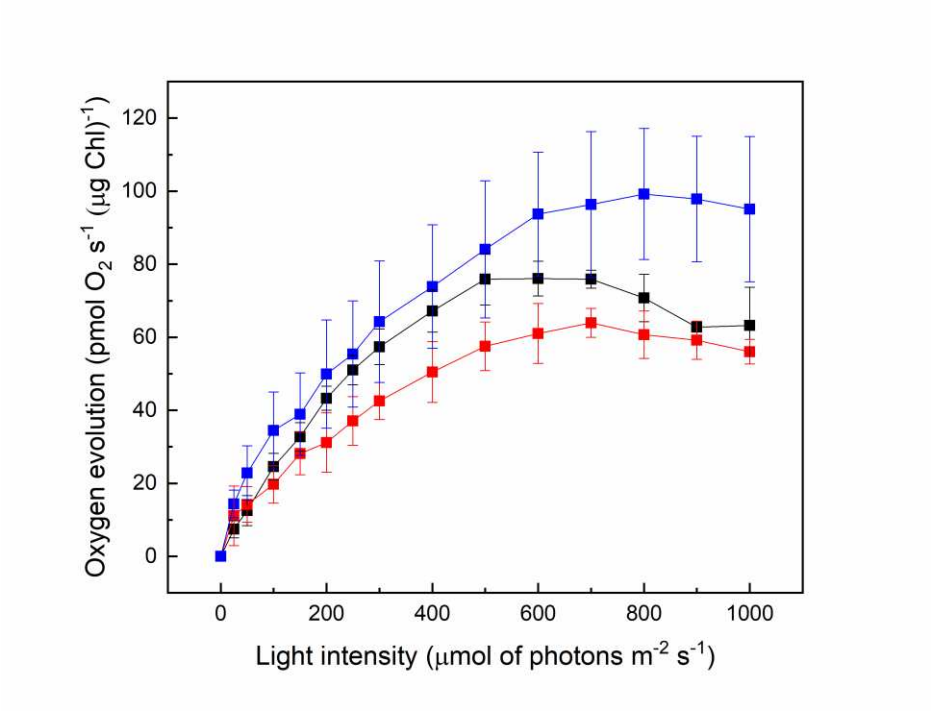

Figure S2. Oxygen evolution of acclimated cells. Oxygen evolution activity of acclimated cells exposed to increasing light intensity. Measurements were normalized with the amount of chlorophyll. LL, ML and HL cells are represented in black, red and blue, respectively. Data are reported as the average of three biological replica ± SD.

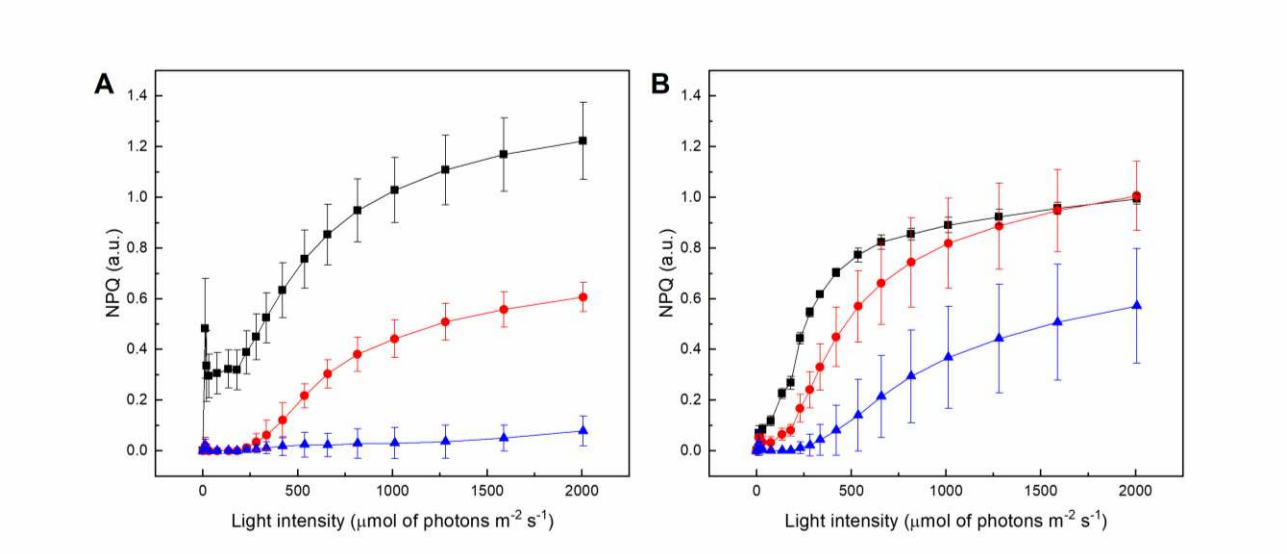

Figure S3. NPQ measurements of acclimated cells. A) NPQ of LL, ML and HL cells exposed to increasing light intensity with far-red off. B) The same measurements were taken with nigericin-treated cells. For both the pictures, LL, ML and HL cells are represented in black, red and blue, respectively. Data are reported as the average of three biological replica ± SD.

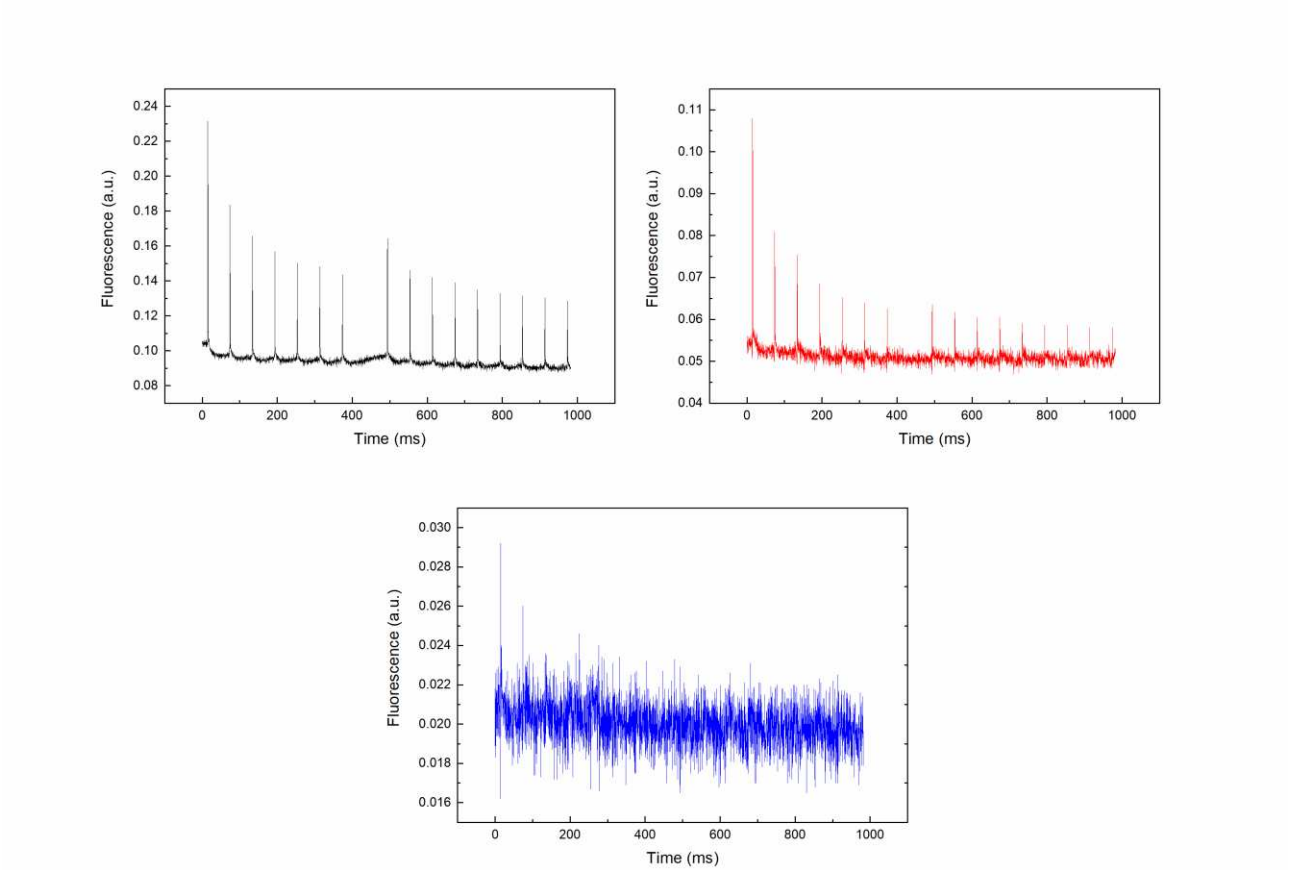

Figure S4. Fluorescence traces of *D. giordanoi* cells. The figure reports the fluorescence traces of acclimated cells exposed to a series of saturating pulses with actinic light off (far-red off). LL, ML and HL cells are represented in black, red and blue, respectively.

ACKNOWLEDGMENTS

I would first like to thank my supervisor Tomas Morosinotto for guiding me through this enthralling research project while giving me the liberty to follow my intuitions and freely explore my research interests. I would also like to acknowledge Alessandro Alboresi: his expertise and trust have been essential to get the best of myself during these years. I also thank Marco Mellon, who first introduced me to the main project, for his patience and help with the setup of the first experiments, and for his great human quality.

Thanks to the two incredible lab ~~magicians~~ technicians Anna Segalla and Alessandra Bellan, who make everything possible. Your generosity and expertise have been pivotal to conclude the experimental part of this thesis, and your bonhomie has been the key to get to the other side of this PhD journey alive.

I must declare my sincere gratitude also to all the collaborators that have been part of this journey. Most especially, to Markus Schwarzländer, Ke Zheng and other members of the Plant Energy Lab in Münster, who warmly welcomed me on each occasion that we met. Also to Libero Gurrieri, Francesca Sparla and colleagues from the University of Bologna, who were always available. I am also grateful to Michela Zottini for the availability and frequent discussions.

Thanks to the institutions and organizations that believe in science and back early career researchers through their academic journey. Thanks to the Department of Biology, who funded my scholarship and gave me the freedom to define my own research project. Thanks to the Italian Society of Plant Biology (SIBV), whose financial support allowed the international collaboration that brought to life a chapter of this thesis, and whose initiatives allowed the establishment of a nice network of young plant researchers in Italy. Thanks to the international community of researchers working with plant mitochondria, which are generous and always keen to welcome new members. The 12th ICPMB congress at Malmö opened my mind to new concepts and ideas that were pivotal to build up most of this thesis. A very honest acknowledgement to Alexandra Elbakyan and her

incorruptible commitment with open science; I cannot imagine completing this PhD journey without the existence of Sci-Hub.

Thanks to the very big list of people that formed part of the family that is the TMs lab throughout these four years: Francesca, Claudia, Eleonora, Tina, Diana, Giorgio, Mariano, Mattia, Raffaella... and a large etcetera. You provided a sociable and nice working atmosphere and made me feel like home. Special thanks to my PhD companions Francesca Bucci and Alberto Tamborrino, two amazing people who have always been available for giving scientific advice or emotional support.

Grazie a quelli che siete stati la mia familia in Italia. Il mio grande compagno di viaggio, Luca. Lara, Andrea e tutta la familia di Marina, che rimane sempre casa. I padovani, di nascita o adozione: Lello, Eca, Sara, Giulio, Manuel, Fede. I membri del lab Dell'Amico, compagni di cene e *calçotades*. Grazie per esserci, sempre.

Finalment, l'agraïment més gros és per a aquells que heu cregut en la meva aventura des del seu començament. A mumare, Victòria, a mun pare, Gaspar i a la meva germana, Maria del Mar. També als amics de Mallorca, Elisa, Claudia, Pedro, Joana, i altres, que sempre hi sou. Un gràcies especial a n'Aina que, a més de ser-hi sempre, ha fet els dibuixos que encapçalen els capítols. Sense el vostre suport incondicional no hauria assolit aquesta important fita. Vos estim a tots.